

Journal of ASTM International
Selected Technical Papers STP 1514
**Durability of Building and Construction
Sealants and Adhesives: 3rd Volume**

JAI Guest Editor:
Andreas T. Wolf



ASTM International
100 Barr Harbor Drive
PO Box C700
West Conshohocken, PA 19428-2959

Printed in the U.S.A.

ASTM Stock #: STP1514

Library of Congress Cataloging-in-Publication Data

ISBN: 978-0-8031-3426-3

Copyright © 2010 ASTM INTERNATIONAL, West Conshohocken, PA. All rights reserved. This material may not be reproduced or copied, in whole or in part, in any printed, mechanical, electronic, film, or other distribution and storage media, without the written consent of the publisher.

Journal of ASTM International (JAI) Scope

The JAI is a multi-disciplinary forum to serve the international scientific and engineering community through the timely publication of the results of original research and critical review articles in the physical and life sciences and engineering technologies. These peer-reviewed papers cover diverse topics relevant to the science and research that establish the foundation for standards development within ASTM International.

Photocopy Rights

Authorization to photocopy items for internal, personal, or educational classroom use, or the internal, personal, or educational classroom use of specific clients, is granted by ASTM International provided that the appropriate fee is paid to ASTM International, 100 Barr Harbor Drive, P.O. Box C700, West Conshohocken, PA 19428-2959, Tel: 610-832-9634; online: <http://www.astm.org/copyright>.

The Society is not responsible, as a body, for the statements and opinions expressed in this publication. ASTM International does not endorse any products represented in this publication.

Peer Review Policy

Each paper published in this volume was evaluated by two peer reviewers and at least one editor. The authors addressed all of the reviewers' comments to the satisfaction of both the technical editor(s) and the ASTM International Committee on Publications.

The quality of the papers in this publication reflects not only the obvious efforts of the authors and the technical editor(s), but also the work of the peer reviewers. In keeping with long-standing publication practices, ASTM International maintains the anonymity of the peer reviewers. The ASTM International Committee on Publications acknowledges with appreciation their dedication and contribution of time and effort on behalf of ASTM International.

Citation of Papers

When citing papers from this publication, the appropriate citation includes the paper authors, "paper title", J. ASTM Intl., volume and number, Paper doi, ASTM International, West Conshohocken, PA, Paper, year listed in the footnote of the paper. A citation is provided as a footnote on page one of each paper.

Contents

Overview	vii
Laboratory Testing and Specialized Outdoor Exposure Testing	
An Attempt at Finding a Correlation Between Environmental and Accelerated RILEM TC 139-DBS Weathering for One-Component Polyurethane Sealants Applied on Mortar	
E. Pozzi, V. Carcano, and A. Ausilio	3
Joint Sealing Systems for Pavements—A New Approach Towards a Performance Related Evaluation of Capability and Durability	
C. Recknagel and S. Pirskawetz	15
Long-Term Outdoor Weathering Study of Construction Sealants	
E. D. Bull and G. M. Lucas	38
Selective Review of Weathering Tests for Sealants and Thoughts on the Development of Novel Test Concept Based on Simultaneous Weathering and Movement	
J. M. Klosowski and P. D. Gorman	73
New Weathering Test Method for Sealants and Preliminary Experimental Results	
J. M. Klosowski and P. D. Gorman	84
Effects of Water Immersion on Building and Civil Engineering Joints and the Use of the Arrhenius Method in Predicting Adhesion Lifetime of Water-Immersed Joints	
A. T. Wolf	111
Experimental Evaluation of Ultraviolet and Visible Light Curing Acrylates for Use in Glass Structures	
B. Weller and S. Tasche	135
Relative Resistance of Silicone and Si-Hybrid Based Sealants to Alternating Periods of Accelerated Weathering and Thermo-Mechanical Movements	
D. Longo and P. Vandereecken	157
Evaluation of the Durability Potential of Silyl Terminated Polyacrylate Based Construction Sealant	
Y. Nakagawa and S. Yukimoto	165
Factors Influencing the Durability of Sealed Joints and Adhesive Fixations	
Substrate Durability Guidelines Used in Silicone Structural Attachment	
L. D. Carbarry	185
Adhesion Development of Organic and Silicone Sealants on Wet and Dry Concrete	
F. Gubbels and C. Calvet	200
Cleaning Silicone Residue from Glass	
J. M. Klosowski, E. S. Breeze, and D. H. Nicastro	217
Resistance of Adhesive Bonding of Ultra-High Performance Concrete to Hygrothermal, Corrosive, and Freeze-Thaw Cycling Environments	
R. Krelaus, G. Wisner, S. Freisinger-Schadow, M. Schmidt, S. Böhm, and K. Dilger	227
Durability by Design: New Results on Load-Carrying Silicone Bonding	
A. Hagl	254

Development of New Test Methods and Performance-Based Specifications

Evaluation of Silicone Sealants at High Movement Rates Relevant to Bomb Mitigating Window and Curtainwall Design K. Yarosh, A. T. Wolf, and S. Sitte	277
Quantification of Effect of Enforced Cyclic Movement and Regional Exposure Factors on Weatherability of Construction Sealants N. Enomoto, A. Ito, and K. Tanaka	302
Using Rheology Test Methods to Assess Durability of Cured Elastomers Undergoing Cyclic Deformation G. V. Gordon, L. D. Lower, and L. D. Carbary	313
Effect of Strain on the Modulus of Sealants Exposed to the Outdoors C. C. White, D. Hunston, and K. Tean Tan	328
Development of Accelerated Aging Test Methodology and Specimen for Bonded CFRP Systems J. Deng, J. E. Tanner, C. W. Dolan, and D. Mukai	342
Water Penetration of Cladding Components—Results from Laboratory Tests on Simulated Sealed Vertical and Horizontal Joints of Wall Cladding M. A. Lacasse, H. Miyauchi, and J. Hiemstra	359

Field Experience with Sealed Joints and Adhesive Fixation

Field Performance and Accelerated Weathering of High Performance Acrylic and Polyurethane Sealants for Tilt-Up Applications V. Demarest, A. Liss, R. Queenan, and P. Gorman	391
Author Index	413
Subject Index	415

**LABORATORY TESTING AND
SPECIALIZED OUTDOOR
EXPOSURE TESTING**

Enrico Pozzi,¹ Valerio Carcano,¹ and Antonio Ausilio¹

An Attempt at Finding a Correlation Between Environmental and Accelerated RILEM TC 139-DBS Weathering for One-Component Polyurethane Sealants Applied on Mortar

ABSTRACT: Two sets of butt joint test specimens (ISO 8339 type) with mortar substrate (ISO 13640, Method 1) were prepared without primer using eight one-component polyurethane sealants; four of low modulus (LM) type showing a movement capability of 25 % and four of high modulus (HM) type showing a movement capability of less than 12.5 % (nomenclature HM according to ISO 11600 as they show a secant modulus >0.4 MPa at 23°C and >0.6 MPa at -20°C , but the movement capability of these sealants does not comply with any of the HM classes stated by ISO 11600). All specimens were conditioned according to ISO 8339 Conditioning Method B. Afterwards the specimens were divided into two sets: the first set was exposed for 24 months in static conditions to the outdoor environment in the urban area of Milan, facing southeast at an angle of 45° . Periodically, i.e., every four months, they were evaluated by visual inspection of their exposed surface. The second set of joints was subjected to accelerated weathering according to RILEM TC 139 DBS in a light-exposure apparatus (xenon-arc type) with water spray. At the end of each RILEM cycle (eight weeks weathering plus one week thermo-mechanical cycling according to ISO 9047) the specimens were visually inspected. The authors found a good correlation between the results obtained in outdoor exposure and those observed after the RILEM durability cycling. In addition to tabulating the findings for crack density and size, the results are also presented as photographic documentation.

Manuscript received June 24, 2008; accepted for publication February 24, 2009; published online April 2009.

¹ R&D Laboratories—MAPEI Spa Via Cafiero 22-20158, Milan, Italy, e-mail: polyurethanes.lab@mapei.it

Cite as: Pozzi, E., Carcano, V. and Ausilio, A., "An Attempt at Finding a Correlation Between Environmental and Accelerated RILEM TC 139-DBS Weathering for One-Component Polyurethane Sealants Applied on Mortar," *J. ASTM Intl.*, Vol. 6, No. 4. doi:10.1520/JAI101965.

Copyright © 2009 by ASTM International, 100 Barr Harbor Drive, PO Box C700, West Conshohocken, PA 19428-2959.

KEYWORDS: RILEM TC 139 DBS, accelerated weathering, outdoor exposure, correlation, polyurethane, sealants

Introduction

The durability test method elaborated by RILEM TC 139-DBS [1] is a laboratory-based procedure that is meant to anticipate the weathering resistance of sealants for high movement joints, especially curtain wall joints, such as in anodized aluminum building façades.

According to the “Significance and Use” statement of the TC 139-DBS procedure “the correlation of the test data obtained using this experimental procedure with the behavior of a sealant subjected to actual weathering and service conditions (e.g., geographic locations, sealant orientation) on a given building is unknown. The use of this method as a predictor of the service life of a sealed joint for a given climate and location and on a given building has not been demonstrated”... “The applicability of test data therefore will be at the discretion of the users of this method and depends on their interpretation of the movement and exposure conditions of a given job site situation” [2,3].

In fact, as far as we know, until now no correlation data have been published between the RILEM test and any kind of outdoor exposure; however, it is important for the user to know the predictive value of the method in order to estimate the service life of a sealant in specific conditions.

The purpose of this study is to verify the degree of correlation between the accelerated RILEM test and outdoor degradation in static conditions carried out in the urban area of Milan, Italy.

We focused the study on one-component elastomeric polyurethane sealants sold for high and low movement construction joints on mortar or concrete substrates, for instance, joints in precast wall panels, floors, parking decks, balconies, etc.

Experimental Work

Two sets of butt joint test specimens (ISO 8339 type [4]) with mortar substrate (ISO 13640 Method 1 [5]) were prepared without primer using eight one-component polyurethane sealants: four of low modulus (LM) type showing a movement capability of 25 % according to ISO 11600 [6] and four high modulus (HM) sealants rated at a movement capability of less than 12.5 %.

Note that the nomenclature “HM” is used here in accordance with ISO 11600, class 25, as the secant moduli at 100 % extension of these sealants exceed 0.4 MPa at 23°C and 0.6 MPa at 20°C; however, the movement capability of these sealants, as rated by their manufacturers, does not comply with any of the classes stated in ISO 11600 (M).

These products are today primarily used in the United States and in Europe as elastomeric self-leveling or thixotropic sealants and often the suppliers claim to meet a movement capability of 12.5 % for them.

As shown in Table 1, Sealants No. 1, 3, 5, and 7 are laboratory prototypes or standard commercial products provided by Mapei SpA; Sealants No. 2, 4, 6,

TABLE 1—Sealants studied (M_1 : Method 1, smooth-surface mortar according to ISO 13640 up: unprimed, notation according to ISO 11600).

PU-1C Construction Sealants—Type F (ISO 11600)			
Class: 25 LM— M_{1up}			
Rheology	Number	Isocyanate Type	TiO ₂ Presence
Thixotropic	1	aromatic	Yes
	2	aromatic	Yes
Self-Leving	3	aromatic	Yes
	4	aromatic/aliphatic	Yes
Class: Not Classified—(less than 12.5) HM, M_{1up}			
Rheology	Number	Isocyanate Type	TiO ₂ Presence
Thixotropic	5	aromatic	Yes
	6	aromatic	Yes
Self-Leveling	7	aromatic	No
	8	aromatic/aliphatic	Yes

and 8 are frequently used competitive commercial European products. For these competitive products the identification of the type of isocyanate was carried out by Infrared (IR) and Nuclear Magnetic Resonance (NMR) analyses and the identification of TiO₂ presence was carried out by X-ray fluorescence analysis (XRF). All Mapei sealants contain light stabilizers and antioxidants.

A first set of test specimens (three for each type of sealant) was prepared in the laboratory, without primer, and cured and conditioned for seven weeks according to ISO 8339, Method B.

After the B cycle their tensile properties according to ISO 8339 are shown in Table 2.

Afterwards the specimens were exposed on the ground, in static conditions, to the outdoor environment of the center of Milan, facing southeast at an angle of 45° degrees for 24 months (the self-leveling sealants starting from March 2006, the thixotropic ones starting from September 2006).

Figure 1 shows the average data of temperature, relative humidity, global irradiation, and total precipitation recorded in the center of Milan during the exposure period as recorded at the Milano Duomo Meteorological Observatory.

Every four months we took a photograph of each specimen in an extended state—in order to ease the detection of defects—and we visually inspected the joints for defects—and adhesion loss according to the criteria suggested by the Recommendation of RILEM TC 190-SBJ: “Service life prediction of sealed building and construction joints”—Document: SBJ N027 [7].

The specimens were extended by 100 % for the LM25 class sealants and by 25 % for the not classified HM sealants right before taking the photograph. This is a more stringent inspection method than the one required in the RILEM TC139-DBS test protocol, which only requires an extension by 25 % for the LM 25 class sealants.

A second set of test specimens, prepared and conditioned as the first set,

TABLE 2—*Tensile properties of the sealants tested according to ISO 8339.*

		PU-1C Construction Sealants—Type F (ISO 11600)			
		Class: 25LM—M _{1up}			
		Thixotropic	Thixotropic	Self-Leveling	Self-Leveling
		No. 1	No. 2	No. 3	No. 4
Max. tensile strength	N/mm ²	0.95	0.43	0.73	0.62
Max. elongation	%	350	495	503	681
100 % modulus	N/mm ²	0.39	0.31	0.28	0.16
		Class: Not Classified—(less than 12.5) HM—M _{1up}			
		Thixotropic	Thixotropic	Self-Leveling	Self-Leveling
		No. 1	No. 2	No. 3	No. 4
Max. tensile strength	N/mm ²	1.2	0.8	0.62	1.2
Max. elongation	%	134	60	100	410
100 % modulus	N/mm ²	1.1	...	0.7	0.6

was statically exposed in a fully automated test chamber (Type Atlas XC2020 Xenon Weather-Ometer, available from Atlas Material Testing Technology, Chicago, IL 60613) having a 6500 Watt cooled xenon-arc lamp irradiating a total exposure area of 6500 cm² and water-spray capability. The test specimens were exposed to three aging cycles consisting of an accelerated weathering period and a mechanical movement exposure period. One accelerated weathering period lasts eight weeks, as defined by the RILEM TC139-DBS protocol, and is based on repeating the following cycle 672 times: 102 minutes dry period with light irradiation (65°C black standard thermometer, 60 % r.h.) and 18 minutes wet period with light irradiation and water spray. After each accelerated weathering cycle, the joints were subjected for one week to thermo-mechanical cycling (two cycles of low temperature extension and high temperature compression according to ISO 9047, Section 8, Test Procedure, First Week [8]). The amplitude of mechanical cycling was ±25 % for the LM25 sealants and ±7.5 % for the not classified HM sealants.

After each ISO 9047 thermo-mechanical cycle we took a photograph (5× magnified) of the test specimen in extension (by 100 % for the LM25 and by 25 % for the nonclassified HM sealants) and we visually inspected them for defects and adhesion loss according to the criteria suggested by the Recommendation of RILEM TC 190-SBJ: “Service-life prediction of sealed building and construction joints”—Document: SBJ N027—indicated in Table 3.

Results

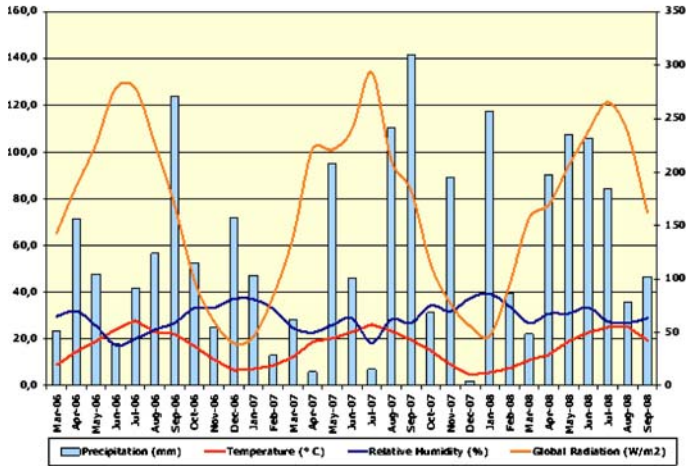
The photographic documentation in Fig. 2(a)–2(d) and Fig. 3(a)–3(d) shows the comparative aging results after the first RILEM aging cycle and after twelve months of outdoor exposure and the comparison between the appearance of

Osservatorio Meteorologico di Milano Duomo Piazza del Duomo 21 20121 MILANO Tel. +39 02 86462443
 Fax +39 02 8900829 <http://www.meteoduomo.it> e-mail:
info@meteoduomo.it P. IVA 03137140152



OMD

(a)



SISTEMA CERTIFICATO UNI EN ISO 9001:2000

(b)

FIG. 1—Analysis of monthly mean temperature, relative humidity, global radiation, and total precipitation.

TABLE 3—Evaluation criteria according to RILEM TC 190-SBJ.

Rating	Quantity of Cracks	Rating	Width of Craks
0	None, i.e., no detective cracks	0	Not visible at 10× magnification
1	Very few, i.e., some just significant cracks	1	Only visible under magnification up to 10×
2	Few, i.e., small but significant amount of cracks	2	Just visible with normal vision
3	Moderate, i.e., medium amount of cracks	3	Clearly visible with normal vision
4	Considerable, i.e., serious amount of cracks	4	Large cracks generally up to 1 mm wide
5	Dense, i.e., dense pattern of cracks	5	Very large cracks generally more than 1 mm wide

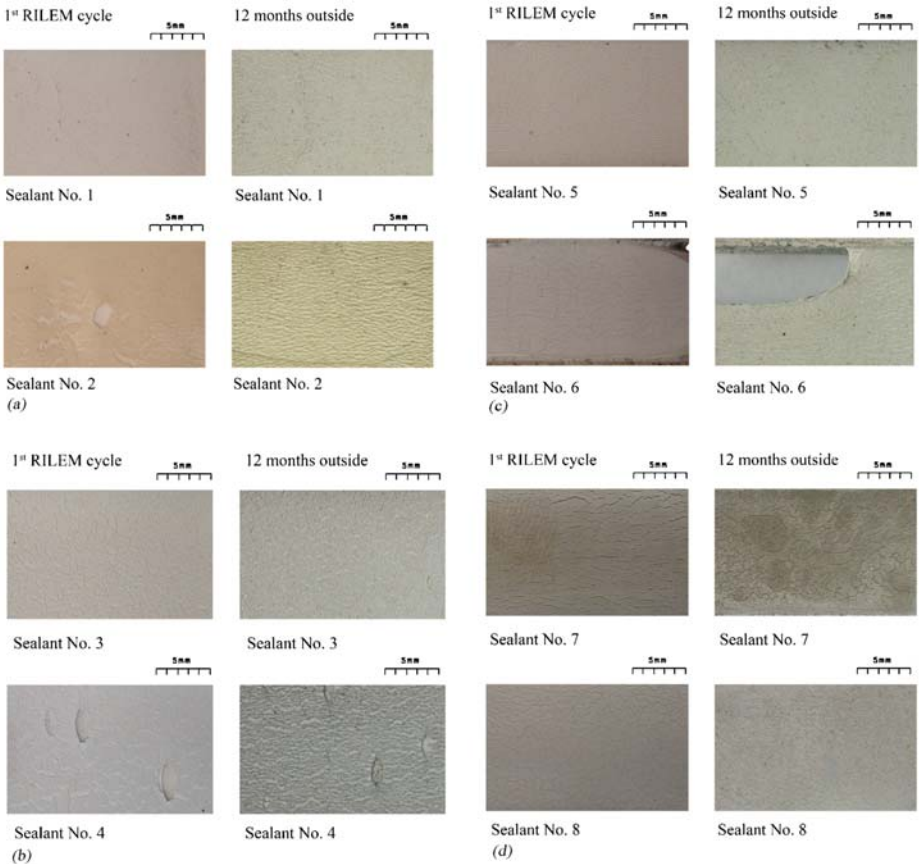


FIG. 2—(a) Appearance of joints specimens for 25 LM Sealant No. 1 and No. 2 after first RILEM aging cycle and twelve months of outdoor exposure (joints extended by 100 %). (b) Appearance of joints specimens for 25 LM Sealant No. 3 and No. 4 after first RILEM aging cycle and twelve months of outdoor exposure (joints extended by 100 %). (c) Appearance of joints specimens for HM Sealant No. 5 and No. 6 after first RILEM aging cycle and twelve months of outdoor exposure (joints extended by 25 %). (d) Appearance of joints specimens for HM Sealant No. 7 and No. 8 after first RILEM aging cycle and twelve months of outdoor exposure (joints extended by 25 %).

the specimens after the third RILEM aging cycle and 24 months of outdoor exposure.

Evaluation of Results

Tables 4 and 5 show the results of the evaluation of cracks density and size according to the criteria shown in Table 3.

Generally we observed that:

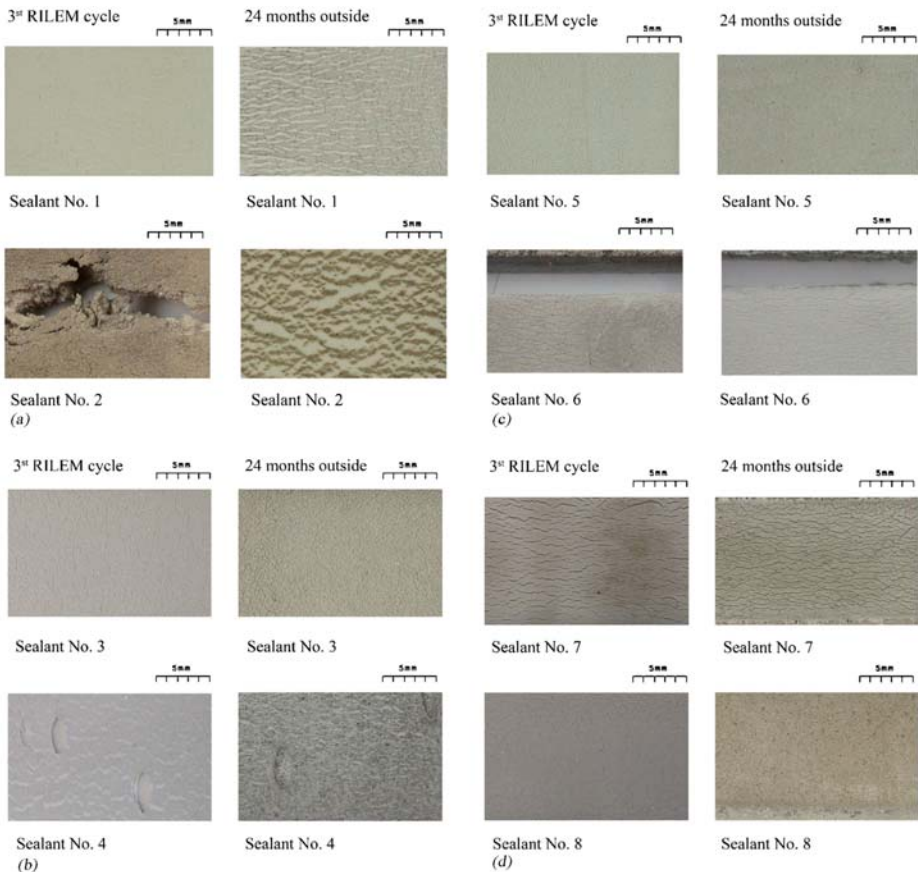


FIG. 3—(a) Appearance of joints specimens for 25 LM Sealant No. 1 and No. 2 after third RILEM aging cycle and 24 months of outdoor exposure (joints extended by 100 %). (b) Appearance of joints specimens for 25 LM Sealant No. 3 and No. 4 after third RILEM aging cycle and 24 months of outdoor exposure (joints extended by 100 %). (c) Appearance of joints specimens for HM Sealant No. 5 and No. 6 after third RILEM aging cycle and 24 months of outdoor exposure (joints extended by 25 %). (d) Appearance of joints specimens for HM Sealant No. 7 and No. 8 after third RILEM aging cycle and 24 months of outdoor exposure (joints extended by 25 %).

- More degradation is visible during summer time than winter time.
- The accelerated weathering regime gradually degrades the sealants, while the outdoor degradation of the sealants shows a seasonal dependence.

For the four self-leveling sealants we verified a fairly good to good degree of correlation between the surface degradation observed after the first RILEM cycle and twelve months outdoor exposure and between the third RILEM cycle and the 24 months outdoor exposure independently of the formulation (type of

TABLE 4—Low modulus ISO11600 PU 1C construction sealants correlation results.

		25 LM—M _{1up}						
Number	First RILEM Cycle			12 Months Outside			Correlation Degree	
	Cracking			Cracking				
	Density	Size	Remarks	Density	Size	Remarks		
Thixotropic	1	2	2	...	3	2	...	fairly good
	2	4	5	big cracks	5	4	...	sufficient
Self-Leveling	3	4	3	...	4	2	...	fairly good
	4	4	4	...	4	3	...	fairly good
		Third RILEM Cycle			24 Months Outside			
Number	Cracking			Cracking			Correlation Degree	
	Density	Size	Remarks	Density	Size	Remarks		
Thixotropic	1	3	3	...	4	4	...	sufficient
	2	5	5	cohesive failure into the bulk	5	5	...	fairly good
Self-Leveling	3	4	3	...	5	3	...	fairly good
	4	4	5	...	4	3	...	fairly good

isocyanate, presence of TiO₂). We observe that Sealant No. 8 is very stable both in artificial and outdoor exposure.

In the case of the four thixotropic sealants the degree of correlation between the first RILEM cycle and the twelve months outdoor exposure is fairly good for the low modulus Sealant No. 1 and reasonable for the low modulus No. 2; for the high modulus Sealant No. 6 it is good; however, correlation is poor for the high modulus Sealant No. 5, for which the first RILEM cycle is more aggressive than the twelve months outdoor exposure. The degree of correlation between the third RILEM cycle and the 24 months is fairly good or good for Sealant No. 2, No. 5, No. 6, and reasonable for Sealant No. 1.

Nevertheless, the comparison between Sealant No. 5 (no adhesive failure in both exposure regimes) and Sealant No. 6 (adhesive failure in both regimes) shows a clear difference in the quality of the exposure results.

In order to obtain a more objective evaluation of the cracking, which was carried out visually according to the criteria indicated in Table 3, we tried examination of the photographic documentation using image analysis based on 8-bit gray-scale images. We used the software Image PRO-PLUS 5.0.1 (supplied by Media Cybernetics Inc. 8484 Georgia Avenue, Suite 200, Silver Spring, MD 20910) in order to calculate the percentage of the area covered by cracks to the total area within a given portion of each photograph. This portion represents about 1.3 cm², that means about 21 % of the total area of the specimen. The region was the same size for all the specimens.

Examples of the black and white images obtained by the software analysis are reported in Fig. 4.

TABLE 5—High modulus ISO 11600 PU 1C construction sealants correlation results.

Not Classified—HM-M1up								
	Number	First RILEM Cycle			12 Months Outside			Correlation Degree
		Cracking			Cracking			
		Density	Size	Remarks	Density	Size	Remarks	
Thixotropic	1	4	2	...	1	1	...	Poor
	2	4	3	Beginning of adhesion failure in the peripheral region	4	3	adhesion failure	Good
	3	3	4	...	4	4	...	fairly good
Self-Leveling	4	3	3	...	3	2	...	Good
Third RILEM Cycle								
	Number	Cracking			Cracking			Correlation Degree
		Cracking			Cracking			
		Density	Size	Remarks	Density	Size	Remarks	
Thixotropic	1	4	2	...	4	2	...	good
Thixotropic	2	5	4	adhesion failure	5	4	adhesion failure	good
Self-Leveling	3	4	4	...	5	4	...	fairly good
Self-Leveling	4	3	3	...	3	2	...	good

The results obtained in the automated image analysis confirm the ratings deduced from the visual evaluation.

Conclusions

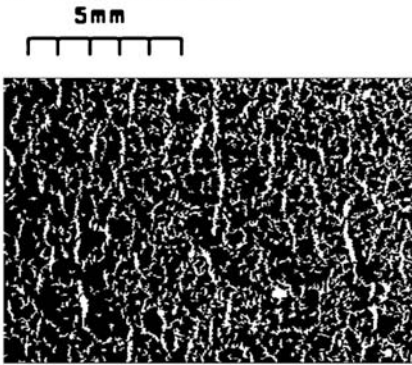
1. The systematic study carried out allowed us to demonstrate that the RILEM TC 139-DBS accelerated weathering method is a good tool for predicting the static outdoor degradation of PU sealants on mortar. A fairly good to good degree of correlation between the first RILEM cycle and the twelve months outdoor exposure was evident in six cases (Sealants No. 1, 3, 4, 6, 7, and 8) among the eight sealants evaluated. A fairly good to good degree of correlation between the third RILEM cycle and the 24 months outdoor exposure was observed in seven cases among the eight sealants evaluated.

The evaluation of the surface degradation was carried out visually as well as by software-supported image analysis.

However, since we carried out the outdoor exposure in a static manner, our results cannot be used to completely validate the RILEMTC139-DBS method.

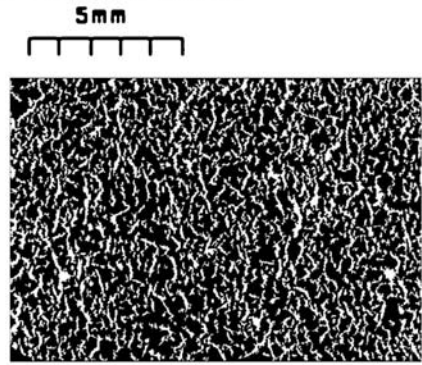
In order to reach this goal we need to carry out the outdoor exposure in a dynamic manner (with enforced movement of the joints), as recommended in RILEM TC 190-SBJ: "Service-life prediction of sealed

3st RILEM cycle

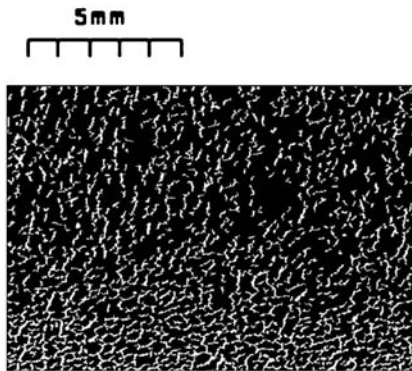


Sealant No. 3 (joint extended by 100%)
Percentage of cracks: 23%

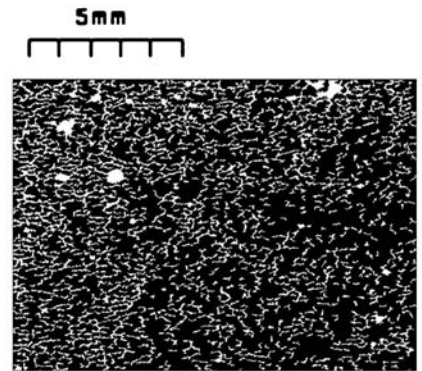
24 months outside



Sealant No. 3 (joint extended by 100%)
Percentage of cracks: 28%



Sealant No. 5 (joint extended by 25%)
Percentage of cracks: 17%



Sealant No. 5 (joint extended by 25%)
Percentage of cracks: 20%

FIG. 4—Appearance of joints specimens of Sealants No. 3 and No. 5 examined by image analysis after the third RILEM aging cycle and 24 months of outdoor exposure.

building and construction joints”-Document: SBJ N027-(edited in December 2007), which is easier to carry out than other dynamic exposure methods, such as the use of pre-cast wall panels [9] or the use of special joints holders [10–13].

In order to quantify the degree of degradation in natural and artificial weathering we will take into account the indications of Enomoto [14].

2. The systematic study carried out was also very useful for rapidly evaluating the different performance of sealants by comparing the behavior

of a sealant in accelerated weathering to that of a “benchmark” sealant of known field performance. Comparing the individual behavior of the pair of sealants, e.g., No. 1/No. 2 and No. 5/No. 6, allowed us to rapidly evaluate their different performance already after the first RILEM durability cycle, i.e., after only nine weeks of accelerated testing.

References

- [1] RILEM 139-DBS, “Durability Test Method—Determination of Changes in Adhesion, Cohesion and Appearance of Elastic Weatherproofing Sealants for High Movement Façade Joints after Exposure to Artificial Weathering,” *Mater. Struct.*, Vol. 34, 2001, pp. 579–588.
- [2] Wolf, A. T., “Durability Testing of Sealants,” *The Trouble with Sealants—Sealants Technology Conference*, Oxford Brookes University, School of Technology, 13 October 2004.
- [3] Jones, T. G. B., Hutchinson, A. R., and Wolf, A. T., “Experimental Results Obtained with Proposed RILEM Durability Test Method for Curtain Wall Sealants,” *Mater. Struct.*, Vol. 34, 2001, pp. 332–341.
- [4] Standard ISO 8339, “Building Construction-Sealants-Determination of Tensile Properties (Extension to Break),” International Standardization Organization, Geneva, 2005.
- [5] Standard ISO 13640, “Building Construction-Jointing Products-Specifications for Test Substrates,” International Standardization Organization, Geneva, 1999.
- [6] Standard ISO 11600, “Building Construction-Jointing Products-Classification and Requirements for Sealants,” International Standardization Organization, Geneva, 2002.
- [7] Document SBJ N027, Recommendation of RILEM TC 190-SBJ, “Service-Life Prediction of Sealed Building and Construction Joints, Durability Test Method-Determination of Changes in Adhesion, Cohesion and Appearance of Elastic Weatherproofing Sealants after Exposure of Statically Cured Specimens to Outdoor Weathering and Simultaneous Mechanical Cycling.”
- [8] Standard ISO 9047, “Building Construction-Jointing Products-Determination of Adhesion/Cohesion Properties at Variable Temperatures,” International Standardization Organization, Geneva.
- [9] Tanzer, J. D. and Frenkel, L. S., “Climate Driven Durability Tester,” *Science and Technology of Building Seals, Sealants, Glazing, and Waterproofing*, ASTM STP 1200, 2nd Vol., J. M. Klosowski, ASTM International, West Conshohocken, PA, 1992, pp. 29–44.
- [10] Onuoha, U. O., “Durability of One-Part Polyurethane and Polyurethane Hybrid Sealants,” *Durability of Building Sealants*, RILEM State-of-the-Art Report, A. T. Wolf, Ed., Vol. 21, 1999, pp. 235–251.
- [11] Karpati, K. K., Solvason, K. R., and Sereda, P. J., “Weathering Rack for Sealants,” *J. Coat. Technol.*, Vol. 49, No. 626, 1977, pp. 44–47.
- [12] Karpati, K. K., “Device for Weathering Sealants Undergoing Cyclic Movements,” *J. Coat. Technol.*, Vol. 50, No. 641, 1978, pp. 37–30.

- [13] Karpati, K. K., "Exposure Evaluation of Sealants with low Movement Capability," *Adhesive Age*, 1988, pp. 20–23.
- [14] Enomoto, N., Ito, K., and Tanaka, K., "Quantification of Effect of Enforced Cyclic Movement and Regional Exposure Factors on Weatherability of Construction Sealants," *C24 Building Seals and Sealants, ASTM Symposium*, Denver, CO, 26 June 2008.

Christoph Recknagel¹ and Stephan Pirskawetz¹

Joint Sealing Systems for Pavements—A New Approach Towards a Performance Related Evaluation of Capability and Durability

ABSTRACT: Joint sealants influence decisively the performance and service life of pavements although they account for only a small fraction of the total investment. Motivated by the damages observed and the resulting, increasing maintenance efforts, the Federal German Government recognizes the need for performance-evaluated joint sealing systems with improved capability (fitness-for-purpose) and durability. A literature study showed that an identification of the actual mechanical system behavior under realistic loads as well as a prediction regarding the durability (fatigue, climatic effects) of joint sealing systems are either completely lacking in most of the relevant evaluation methods or have only been incompletely addressed previously. Furthermore an imbalance between commonly used test methodologies and the actual development status of modern modified sealing materials exists, i.e., the current test methods are not effective in evaluating the performance of tailor-made products. In this paper, the authors suggest a methodology to overcome the present situation. In contrast to the existing, predominantly empirical evaluation and selection of joint sealing materials and systems for pavements, the new approach is defined by verified performance under relevant and superimposed loads. This new approach is expected to allow a more engineered joint design. In addition to the adaptation of performance-oriented material identification tests, a special focus was placed on the development and installation of a complex test facility for the investigation of the service capability and durability of joint sealing systems in building constructions in general. This paper presents an attempt at the realization of this

Manuscript received June 20, 2008; accepted for publication January 26, 2009; published online February 2009.

¹ Dipl.-Ing., Laboratory "Bituminous Materials and Sealing Technology," Federal Institute for Materials Research and Testing (BAM), Unter den Eichen 87; 12205 Berlin, Germany, e-mail: Christoph.Recknagel@BAM.de; Stephan.Pirskawetz@BAM.de

Cite as: Recknagel, C. and Pirskawetz, S., "Joint Sealing Systems for Pavements—A New Approach Towards a Performance Related Evaluation of Capability and Durability," *J. ASTM Intl.*, Vol. 6, No. 3. doi:10.1520/JAI101961.

Copyright © 2009 by ASTM International, 100 Barr Harbor Drive, PO Box C700, West Conshohocken, PA 19428-2959.

approach for pavement joints with the help of our new joint sealant test equipment utilizing a specific, adapted load function, which comprises cyclic movements (slow and fast acting), as well as crucial climatic exposures. The test data and its interpretation are discussed. For example, the actual mechanical behavior of the various joint sealing systems as well as the relevant maximum loading of cohesive and adhesive bonds can be deduced and used to differentiate between systems. Furthermore, information gained allows discrimination of products within the various joint sealing systems. The test results will also enable numerical simulations, e.g., of different joint designs or materials by finite element analysis. The fatigue behavior is detected by analysis of cycle-dependent changes of the mechanical system characteristics. The evaluation methodology further allows investigation of the degradation mechanisms of specific system failures and, thus, enables service life prediction by reproducing the performance of the complete system under realistic conditions. Constructional defects and material flaws can be activated and detected by the performance-related test methodology, thus identifying possible corrections to material selection and application procedures. The potential of the proposed evaluation methodology is discussed for several thermoplastic and reactive joint sealing systems.

KEYWORDS: pavement joints, system evaluation, system test method, superimposed loading, performance, mechanical characteristics, capability evaluation, durability evaluation, cohesive failure, adhesive failure

Introduction

A tactical arrangement of regular gaps (joints) is required in order to avoid uncontrolled cracking of rigid pavements, such as concrete pavements, when combining different pavement materials, or when connecting the surface course to technical components such as carriageway drainage or prefabricated expansion joint systems. Contrary to former strategies, nowadays these gaps are filled with special materials creating a joint sealing system. A technically successful solution for a sealed joint has to fulfill the following general requirements:

- Seal the pavement structure against penetration by water and pollutants.
- Transfer surface water to the drainage system.
- Avoid accumulation and penetration of dust and soil particles in the gap (clogging).

While the installation cost of joint sealing systems is marginal when compared to the total cost of pavement installation, the failure of joint sealing systems can cause expensive consequential damages to the pavement; (a) by erosion, (b) by cracking and rupture of pavement slabs, and (c) by bending until flexural breaks occur in the slabs (See Fig. 1). These examples emphasize the significance of capable joint sealing systems according to the requirements mentioned above.

When considering the functional principles of joint sealing systems, one quickly arrives at the conclusion that durable deformability and adhesion are

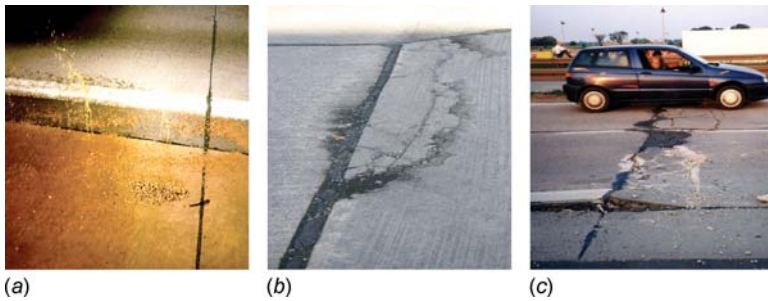


FIG. 1—Typical pavement damages attributable to incapable joint sealing systems. (Left) Water shooting out of a pavement joint during traffic loading. (Middle) Flexural breaks. (Right) Slab blow up.

the general performance characteristics to guarantee suitable fitness for purpose.

Different sealing materials and various joint sealing systems are available for this type of application. Their classification, use conditions, and installation criteria as well as their approval process based on the general evaluation and quality management requirements are specified in national and international technical standards. However, in spite of all material-based, design-related, or quality-monitoring developments that have occurred over the past 20 years, maintenance efforts in this field are still rising. For example, maintenance costs for highway pavements in Germany increased to ~ 1.64 b€ in 2007 [1]. In addition to the maintenance efforts, the associated economic loss resulting from repair- or maintenance-induced traffic interruption comes increasingly to the fore. For example, the associated economic loss by traffic interruption in Germany was ~ 1.26 b€ in 2007 [1]. These economical data reflect the corresponding feedback from the highway administrations according to which failures of joint sealing systems such as surface cracking, embrittlement and tearing (Fig. 2(a)), which result in permeable or clogged joints (see Fig. 2(b)), are still being observed in the field.

Although technical regulations and requirements published in the various joint sealant specifications as well as approval requirements and appropriate testing procedures are available, the capability and durability of joint sealing systems is dissatisfying all too often. So, what is wrong? How can improvements be achieved? What actual capability and durability has to be taken into account for a realistic maintenance strategy and cost planning? These questions motivated the authors to initiate a critical review of the testing procedures used in the evaluation of the capability and durability of joint sealing systems for pavements. A comprehensive literature review of the state-of-the-art in the late 1990s with regard to national and international regulations applying to the qualification of joint filling systems in traffic areas was conducted. The survey demonstrated that an evaluation of the actual performance of the sealing materials as well as their system behavior with current methods is possible only to a very limited extent [2]. Predominantly traditional and indirect testing methods do not emulate and reflect the actual mechanical behavior of the systems

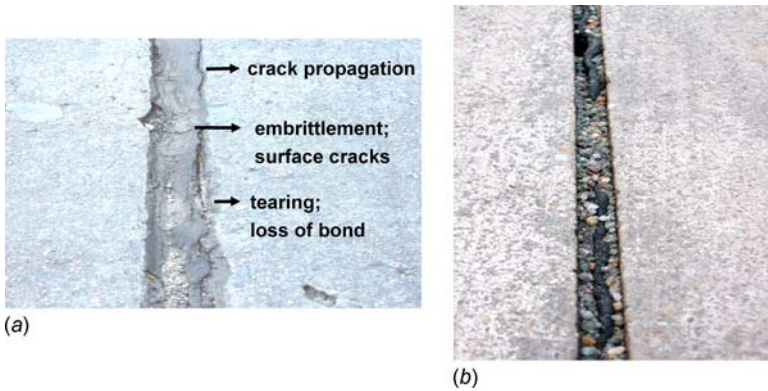


FIG. 2—Typical damages of joint sealing systems in practice. (Left) Failures of joint sealing systems. (Right) Permeable or clogged joints.

under realistic loads and provide only limited correlations to the actual in-service behavior. Methods for the prediction of durability (mechanical fatigue; climatic aging) are lacking in most regulations or they are present only in the short-term characterization of the materials. Furthermore, there is an imbalance between the current testing methodologies and the material composition of modern modified, respectively “tailor-made,” sealing products which limits their performance-oriented evaluation. In summary, the categorization, the design of sealing systems, as well as the selection of relevant sealing materials are predominantly based on historical experiences and less on methodical, performance-oriented tests. Despite these conclusions, joint sealing systems are still categorized in the existing technical regulations according to a wide range of criteria, e.g., according to their material base or their delivery form, according to installation technique or by the area of use, or according to their chemical resistance; however, also very often according to their mechanical behavior evaluated predominantly with the testing procedures described above. In summary and congruent to recent conclusions [3,4] it follows that the adaption or development of appropriate performance-related test methods can be regarded a precondition for a simplified performance-based product categorization, a suitable material selection, and optimized design of joint sealing systems for their intended use.

Methodology for an Improved Evaluation Approach

The improved approach consists of an adaptation of performance-oriented material identification tests and the verification of system performance under relevant and superimposed loads. This approach allows a more engineering-related design for joint sealing systems. Frequently used, commercially available products were investigated in the experimental section of this paper. The representative selection took into account the whole range of materials and systems approved according to the national technical regulations on joint seal-

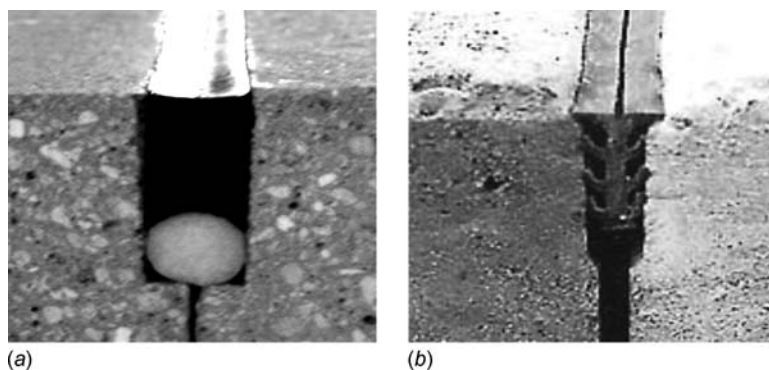


FIG. 3—Approved types of joint sealing systems for highway pavements according to the technical rules in Germany. (Left) Joint filled with sealant compound (defined by their application condition, viscoelastic properties, and curability as hot-applied plastic (PS), hot-applied elastic (ES), cold applied reactive (RS), and hot-melt bitumen strand. (Right) Joint sealing systems based on sealant profiles (gaskets).

ant systems for highway pavements in Germany. The main categories investigated and discussed in this paper are shown in Fig. 3.

According to German technical regulations the following fundamental mechanical behavior and capability requirements (see Table 1) are attributed to the different joint sealing systems.

Material Evaluation

Additional information about the material's composition and its mechanical behavior is required not only for a performance-oriented identification but also

TABLE 1—Categorization and approval requirements for joint sealing systems for high-way pavements according to German regulations.

Types of Joint Filling Systems		Attributed System Behavior	Maximum Movement Capability ^a	Durability (Minimum Service Life)
Main Category	Subcategory			
Thermoplastic sealants (hot applied)	Plastic type (PS)	Plastic	≤25 % (5 mm)	≥5 years
	Elastic type (ES)	Elastic	≤35 % (7 mm)	≥5 years
Reactive sealants (RS) (cold applied) ^b		Elastic	≤25 % (5 mm)	≥5 years
Preformed profiles (PP)		Elastic	≤30 % (6 mm)	≥5 years

^aMovements capability requirements refer to the joint width at installation of the joint filling system.

^bThese sealants are also classified as fuel-resistant.

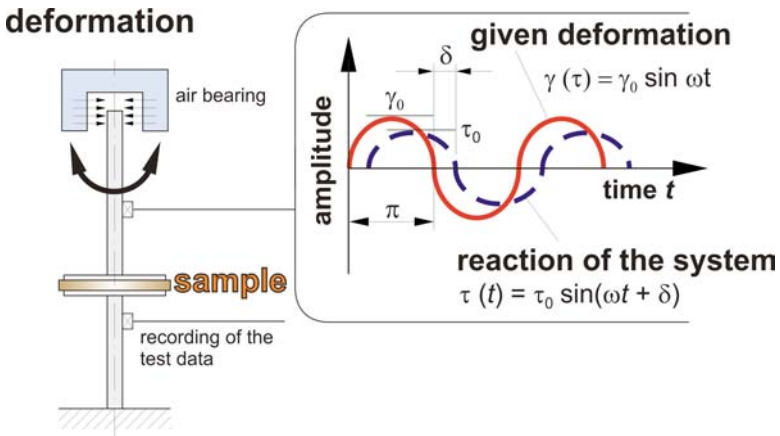


FIG. 4—Principles of dynamic mechanical material analysis by shear rheometry.

as a precondition for a material-related characterization of the joint sealing system [5,6]. In order to achieve an improved analysis of the material's composition, especially of modified and filled sealant compounds, the method of extraction of formulation constituents by solvents was adapted. Solvent extraction allows to obtain information on the content of bituminous binder (modified/unmodified) as well as the content of inorganic filler (mineral powder) and organic filler (rubber crumbs), or both. A further identification of the modified bituminous constituent was obtained by the method of size-exclusion gel permeation chromatography (GPC). This method allows separation of the molecules of the organic polymers according to their size, and results in an analytical fingerprint of the material by determination of the specific molecular weight and its distribution.

It is known from the literature, e.g., from Refs [5–7], that analysis of the dynamic mechanical behavior under temperature variation gives very useful performance-oriented material information. Therefore, we adapted the dynamic shear rheometry as a material evaluation method (see Fig. 4). With this method one obtains information on the plastic viscous (loss modulus G'' ; see Eq 2) and elastic material characteristics (storage modulus G' ; see Eq 1) and their dependency on variations in temperature (see Fig. 5), and deformation rate or frequency. The authors also consider implementation of artificial weathering (based on UV-radiation) in this test procedure. The loss angle δ (see Eq 3) is an indicator of the ability of the material to relax (relaxation indicator). This experimental tool allows the assessment of the range of plasticity (mechanical working range) between glass transition (T_g) and melting point (T_m). Thus important fundamental information for the development of a system test appropriate to the materials involved is obtained.

Dynamical-mechanical material characteristics resulting from rheometric analysis are:

Storage modulus:

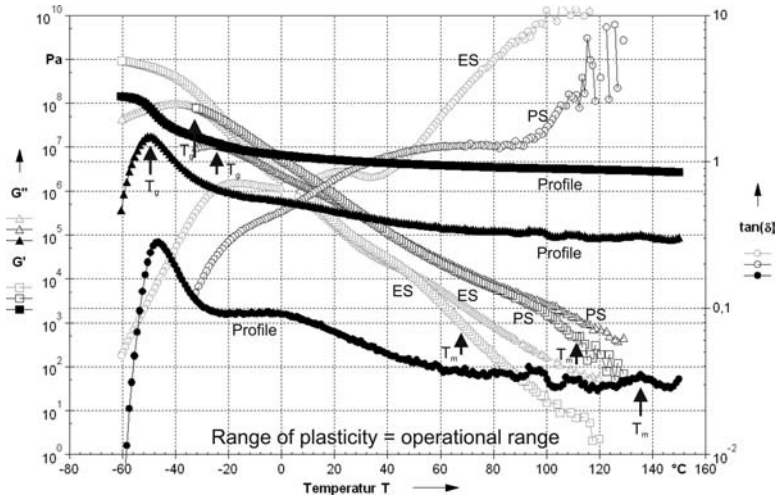


FIG. 5—Analysis of the temperature-dependent mechanical behavior (PS=red; ES =yellow; Profile=blue).

$$G' = \frac{\tau_0}{\gamma_0} * \cos \delta \text{ [Pa]} \quad (1)$$

Loss modulus:

$$G'' = \frac{\tau_0}{\gamma_0} * \sin \delta \text{ [Pa]} \quad (2)$$

Loss angle:

$$\delta = \arctan \frac{G''}{G'} \text{ [}^\circ \text{]} \quad (3)$$

System Evaluation

In addition to the optimization of material tests as part of a performance-oriented identification system, the authors placed a special emphasis on the development of a performance-related test method for joint sealing systems [8]. In order to achieve the latter goal, it was necessary to determine the significant loads exerted on joint filling systems (see Fig. 6), to transfer these loads into a practicable load function, and to define the crucial evaluation criteria for the determination of the general capability and durability of the system. Last but not least a suitable test facility had to be built.

The key loads that affect the capability and durability of the joint sealing system by activation of the internal and external aging effects can be categorized in terms of influences resulting from weather and traffic. Weather conditions induce direct climatic and indirect mechanical loads (deformation) on the joint sealing systems. Due to the strong dependency of thermo-mechanical be-

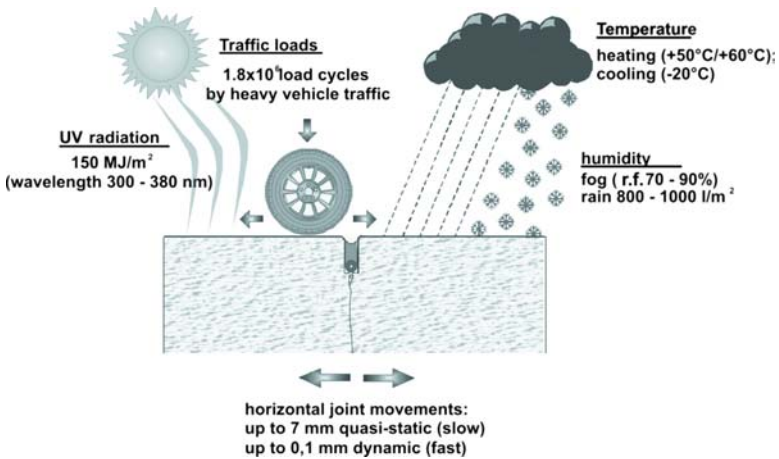


FIG. 6—Schematic representation of crucial annual loads for highway pavement joints.

havior of the different joint sealing materials on the temperature, the actual temperature variations in service are of particular importance. Temperature variation results in deformation of the joint sealing systems while simultaneously changes in their temperature-dependent mechanical behavior occur. In order to simulate the aging effects, aging by thermal exposures and UV radiation (energy impact) has to be considered. The bonding behavior of the system is substantially influenced by the ambient relative humidity or precipitation. The dynamic deformation associated with passing traffic has to be considered as a significant influence on joint sealing systems in pavements. An intensified load and an activation of aging processes (synergism) have to be expected based on the combined effect (superimposition) of the aforementioned loads. As such, a load function based on environmental conditions as experienced in service must take into account a superimposition of simultaneously acting loads.

The intensity of the load parameters shown above corresponds to the averaged climatic and service loadings in highway construction in Germany and has been used by the authors as the basis for the derivation of a representative load function adjusted to the conditions of the German highway network and one year of service. The general concept was to develop a load function representing one season with the intent to evaluate the general capability of a joint sealing system during this period of time. Cyclic repetition of this function activates the fatigue and aging behavior of the sealing system and allows qualification of its durability by proceeding until failure occurs. This failure then determines the total service life. Furthermore, in order to limit the effort and expenditure, a minimization of testing time has to be achieved. The authors suggest that all crucial loads occurring over the period of one year in service (see Table 2) can be represented by a load function acting over a period of 168 hours. The proposed acceleration appears to be an acceptable compromise between the test duration and a reasonable simulation of the relevant loading rates (e.g., for mechanical loading) and loading quantity (e.g., rain cycles or UV exposure).

TABLE 2—Control parameters of load function (simulating annual loading).

Phase	Simulated Season	Deformation		Temperature Variation	Air	Rain Cycles	UV Radiation
		Static	Dynamic		Moisture Variation		
1	Spring I	0 mm	±0.1 mm f=3 Hz	15°C	from 40 to 70 %	0	ON (100 %)
2	Summer	-1.0 mm	±0.1 mm f=3 Hz	50°C	70 %	11 × 1 min with 5 l/min	ON (100 %)
3	Autumn	0 mm	±0.1 mm f=3 Hz	15°C	from 70 to 20 %	5 × 1 min with 5 l/min	ON (100 %)
4	Winter	+4.9 mm (PS) +6.9 mm (ES) +4.9 mm (RS) +4.9 mm (PP)	±0.1 mm f=3 Hz	-20°C	...	0	OFF (0 %)
5	Spring II	0 mm	±0.1 mm f=3 Hz	15°C	20 %	0	ON (100 %)

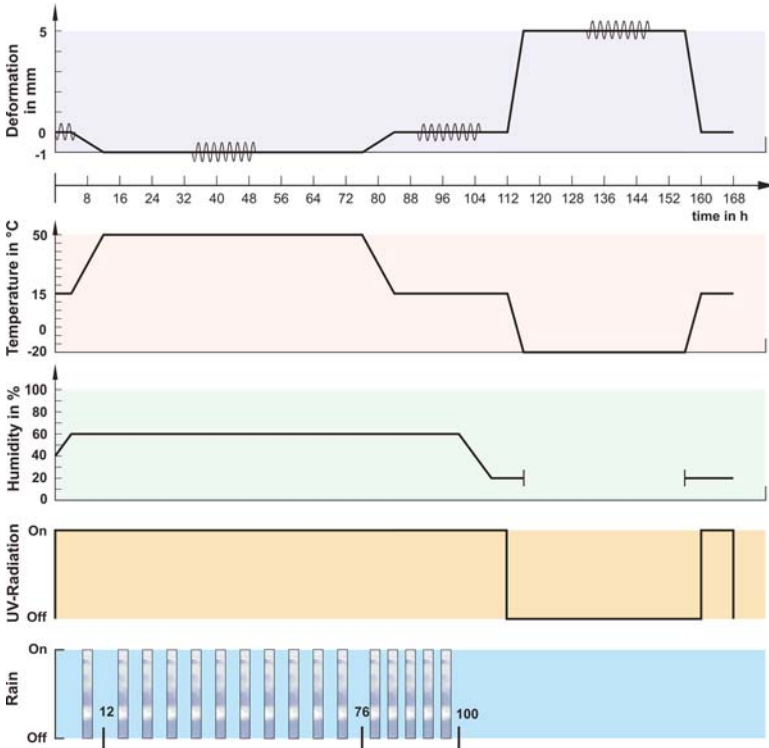


FIG. 7—Complex load function for joint sealing systems in pavements.

The mechanical load as part of the complex load function (see Fig. 7) consists of a contribution by the slow-moving (quasi-static) part of the deformation representing the annual horizontal joint movements induced by the temperature variations occurring over the course of one year. For these slow horizontal movements one has to consider not only the range of horizontal movements known by numerous measurement series in the field (≤ 3.5 mm according to Ref [8]), but also the corresponding approval requirements of the technical regulations. These approval requirements demand a horizontal movement capability (deformability) of 5 to 7 mm, depending on the joint dimensions and the category of the sealing system. In the mechanical loading function, the slow horizontal movements are superimposed with dynamic deformations of ± 0.1 mm representing traffic-induced horizontal movements of the joint. The climatic load of the complex loading function is predominantly determined by the annual maximum and minimum temperatures. For this purpose we had to take into account variations between -20°C and $+50^{\circ}\text{C}$ representing the temperature range typically observed in Germany. The temperature variation is dynamical adapted to the associated deformation state. The largest joint opening is connected with the lowest ambient temperatures and the minimum joint width is at the highest temperatures in summer conditions. That means mechanical loading under the associated temperature-depending mechanical be-

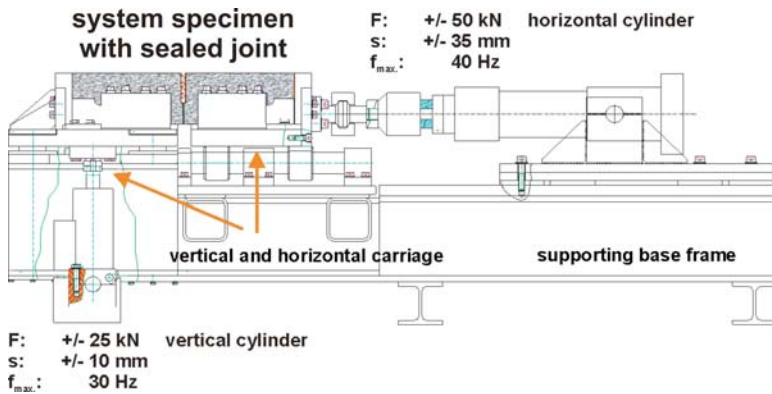


FIG. 8—Schematic representation of the mechanical loading device and its technical parameters.

havior (actual temperature depending stiffness) of the systems. Mechanical and temperature loadings follow the annual seasons beginning and ending with spring conditions. The climatic loading is associated with continuous UV irradiation during spring, summer, and autumn periods and integrated rain showers.

With regard to the load function, the following characteristics are relevant for the assessment of the performance of the joint sealing system:

- Demonstration of functional capability in terms of flexibility, cohesive and adhesive bondstrength, as well as impermeability.
- Demonstration of durability in terms of fatigue strength, long-term cohesive and adhesive bond strength (durable bond), as well as long-term impermeability (durable impermeability). A suitable system test method must have the capability of assessing these properties.

No adequate test facility could be identified based on the analysis of the existing test methods. Therefore, a test facility had to be developed that was capable of replicating the key loads in the simplified methodology discussed above. The general design principle for the test facility was to cover as wide a range of applications as possible based on a preferably universally adaptable evaluation of joint sealing systems. The test facility includes a mechanical loading device to simulate quasi-static and dynamic horizontal and vertical deformations, or a combination thereof, in order to emulate various axial and uniaxial stress conditions, or both (see Fig. 8).

The loading device is embedded in a climate chamber to simulate simultaneously the relevant climatic loads, i.e., temperature changes, rain, humidity, and UV irradiation. Both loading devices (mechanical and climatic device) are synchronized by a central control unit, thus allowing operation in single as well as coordinated, superimposed loading modes in numerous variations. In order to provide the possibility for investigations on a full size joint specimen under realistic conditions, concrete plates according to the technical specifications for

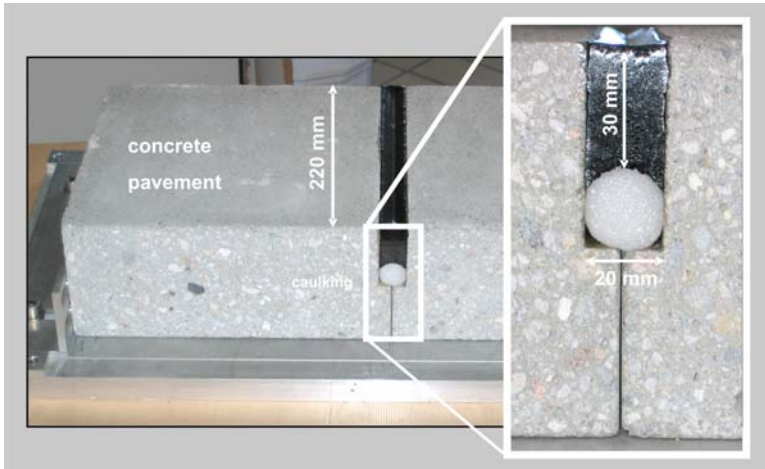


FIG. 9—Example of a full size specimen with hot-applied joint sealing system.

concrete pavements were specially prepared for the loading device (see Fig. 9). Therefore, the experimental setup is close to the actual conditions in concrete pavements.

Besides this the design conception allows also the installation of specimens with a variety of sealant contact surfaces (e.g., steel substrate, asphalt substrate, etc.).

Results of System Test and Their Interpretation

A technical check of the capability of the new test methodology as well as its applicability to joint system testing was accomplished by the investigation of in total five different joint sealing system categories for pavement joints (see Fig. 3) based on eleven different products. Due to the ongoing predominant use, a special focus was placed on sealing compounds [5,6], versus profiles, as sealant compounds are more frequently used with concrete pavements.

Each specimen was exposed to consecutive repetitions of the complex load function corresponding to the required minimum service-life duration (see Table 1) or up to the loss of performance, e.g., by cracking, breaking, or debonding. During the test, the forces (F) induced by the static and dynamic displacements as well as the climatic parameters (temperature, humidity, rain water amount, and UV energy) were measured and recorded. Basing on the mechanical data measured, additional mechanical parameters such as maximum stresses $\sigma_{A,\max}$, spring stiffness k_A of the system and work performed $W_{A,\max}$ can be calculated and discussed by normalizing the measured mechanical data to one substrate area (surface element) of the bonding surface:

$$k = \frac{F_{\max} - F_{\min}}{s_{\max} - s_{\min}} \text{ [N/mm]} \quad (4)$$

$$W = \int F * ds \text{ [N} \cdot \text{mm]} \quad (5)$$

$$\sigma_{A \text{ max.}} = \frac{F_{\text{max}}}{l * d} \text{ [N/mm}^2\text{]} \quad (6)$$

$$k_A = \frac{k}{l * d} \text{ [N/mm}^3\text{]} \quad (7)$$

$$W_A = \frac{W}{l * d} \text{ [N/mm]} \quad (8)$$

where F_{max} =load [N], l =length of the specimen's joint [mm], s =displacement [mm], d =height of the specimen's joint [mm].

The dynamically-changing (phase-dependent) evolution of $\sigma_{A;\text{max}}$ allows calculation of the key stresses within the system and at the adjacent substrates. The variation of the spring constant k_A provides information concerning the temperature-dependent stiffness of the system during the transition from season to season. This parameter should allow additional and more detailed parametric studies under the decisive load condition at low temperatures during winter with the help of numerical calculations (FEM analysis) in more detail. The parameter W_A allows information to be derived regarding the capability of partially absorbing stresses by means of dissipation (see also Ref [9]). Furthermore, the climatic parameters of moisture, radiation, temperature, and, in particular cases, the interior temperature of the sealants were recorded. Finally, a visual evaluation of adhesion quality and a test of impermeability completes the data acquisition for a comprehensive characterization of the system performance. The measured mechanical data were visualized in different graphic modes in order to describe and discuss the correlation between loading and reaction of the system. Figure 10 shows, as an example, the recorded maximum and minimum forces as well as the calculated mean force of a joint sealing system based on a hot-applied sealant of predominantly plastic type (PS) plotted versus the cycle duration time and simulated season. The first observation that can be made is a nearly symmetrical behavior of traffic-induced (tensile and compression) forces versus the neutral axis. The evolution of the mean force shows that the seasonally induced forces or stress conditions are not completely reduced (dissipated) by relaxation. Contrary to the material's categorization (predominantly plastic behavior) one can detect permanent tensile stresses, especially under winter conditions. Apparently this system shows also an elastic response even when exposed to slow displacement movements.

In the case of the hot-applied sealant of the plastic type, discussed above, the majority of mechanical loading of the system does not result from the relatively large displacements induced by seasonal climate changes but rather from traffic-induced forces. These small displacements activated by the over-rolling traffic ("traffic induced") oscillate with an amplitude of ± 0.1 mm around the mean displacement value which is determined by the annual temperature changes (please see also the top section of Fig. 7). However, despite their small

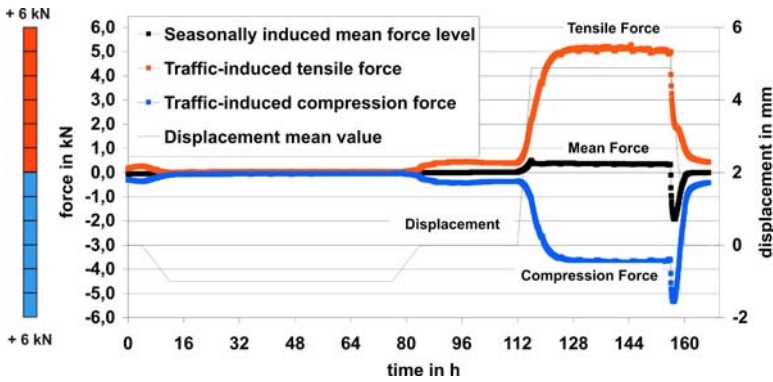


FIG. 10—Typical test results of joint sealing systems made of a hot-applied plastic sealant compound. Shown are the seasonally induced mean force (labeled “Mean force”), the traffic-induced tensile force (labeled “Tensile force”), the traffic-induced compression force (labeled “Compression force”), and the displacement mean value (labeled “Displacement”).

amplitude, these traffic-induced movements induce stresses that are approximately 15 times higher than those caused by the climatic loads. During the winter period, the joint sealing system is permanently under changing compression and tension stresses with highest loading (F_{\max} of 5.1 kN leading to $\sigma_{A;\max}$ of 0.75 N/mm²). As expected, the dynamic deformations induce a considerable elastic response. However, what is the exact mechanical behavior of the system? Are there any plasticity effects (dissipation) under these loading conditions as one would expect from the system categorization? This question will be discussed later during the interpretation of the recorded hysteresis loops. One indication of the system behavior is provided by the local peak of the compression force at the end of the cycle when the displacement returns from maximum extension to the initial state. The system does not move voluntarily from extension to its initial state without additional (and relatively high) compression forces. In summary, the forces in Cycle 1 are continuous during all simulated seasons and do not show any discontinuities indicating a capable sealing system.

Surprisingly, a similar behavior is observed also for joint sealing systems based on hot-applied sealant compounds of the predominantly elastic type (see, for example, the graph shown in Fig. 11). Contrary to their categorization, these systems show relaxation effects under seasonally induced displacements which can be seen in the graph of the mean load level.

Considerable compression forces are required in order to move the hot-applied elastic joint sealant system from the maximum induced extension to its initial state. Later the discussion of the hysteresis loops will highlight additional issues to discuss with regard to the antagonism between assigned and real mechanical behavior. Systems of this elastic categorization show generally lower force levels, with accompanying stress levels, which are approximately three times lower than those of the plastic sealant type. This behavior preserves

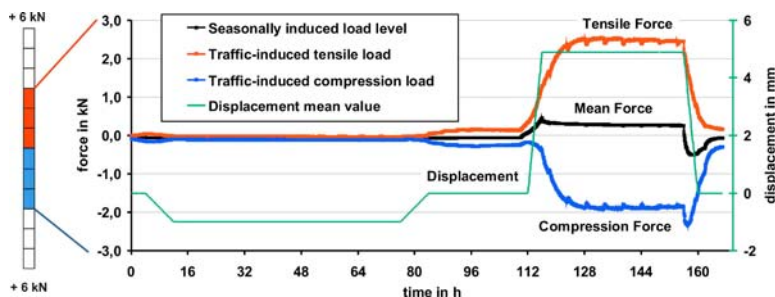


FIG. 11—Typical test result of joint sealing systems made of a hot-applied elastic sealant compound (labeling as in Fig. 10).

the cohesive and adhesive bonds and results in a considerably longer durability of the joint sealing system, as identified in the system tests.

The system studied based on a cold-applied reactive sealant (two-component polyurethane) shows a completely different mechanical behavior (see Fig. 12). Instead of observing oscillating compressive and tensile forces around the zero-force-axis (see Figs. 10 and 11), permanent compression (under simulated summer conditions) or tensile forces (under winter conditions) were measured. In other words, the seasonal deformation states dominate the system behavior. Even in this case small relaxation effects are observed; otherwise all data indicate an authentic elastic mechanical behavior. Despite the permanent stress situation, the lower stiffness of the system results in more than five times lower loading of the bond compared to PS systems and still two times less than the ES systems tested. A repetition of the complex loading cycle for more than ten times without system failure indicates the longest service life within the set of sealants tested. However, because of the permanent stress situation, we cannot exclude that mechanical damages of the seal or

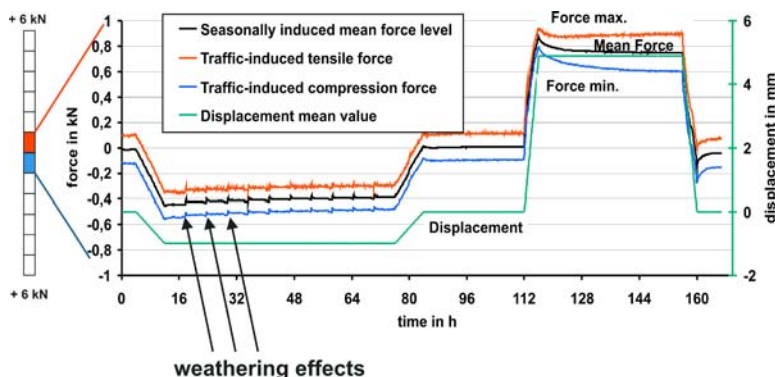


FIG. 12—Typical test result of joint sealing systems made of cold-applied reactive sealant (labeling as in Fig. 10).

imperfections, especially in the bond area, may result in rapid premature failure.

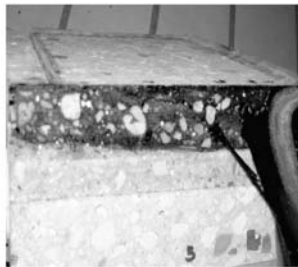
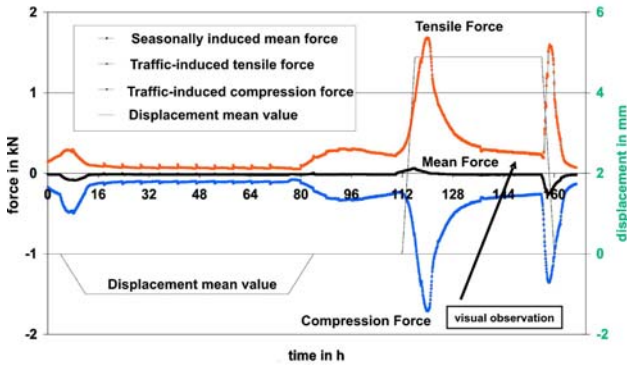
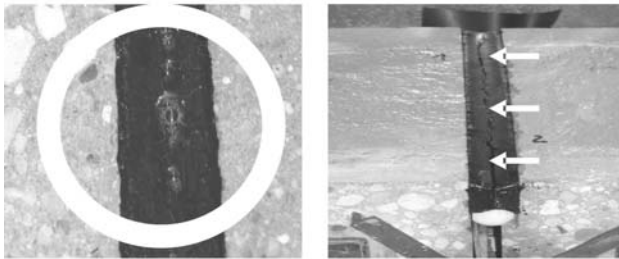
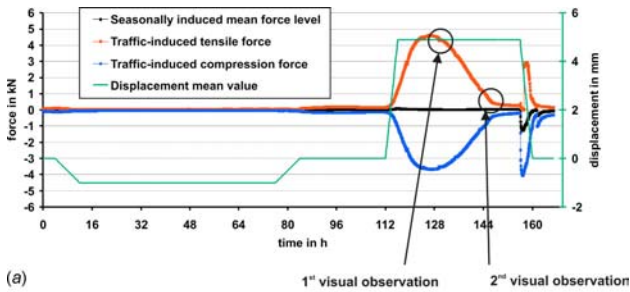
Discontinuities of the graphs provide information on failure processes. From these discontinuities the kind of failure as well as reasons for failure at the end of service life (loss of durability) can be deduced. Furthermore, the graphs also allow detection of inappropriate material selection or combination as well as design-dependent weaknesses or incorrect installation. Figure 13(a) shows a typical example of the loss of cohesion in a plastic sealant system with high filler content. Already at low displacements first internal cracks seem to have been initiated and immediately after the system went through maximum extension, water leakage occurred (see circled image in Fig. 13(a), left-hand side). The further, steep decline of the force is an indicator of the final rapid tearing (picture below Fig. 13(a), right-hand side). The test results presented in Fig. 13(b) are indicative of a system failure caused by an inappropriate primer selection (Fig. 13(b)).

Figure 14 visualizes a typical example of a fatigue failure caused by advancing loss of adhesion resulting from progressive cyclic loading which is in fact characteristic of the end of service life (durability). Illustrated are the forces observed in Cycle 5 and 6 (continuous bold lines) in comparison to those of Cycle 1 (thin lines) together with the corresponding visual appearance of the specimen. Compared to Cycle 1 a considerable and still ongoing steady decrease of the forces is detected in Cycle 5 indicating the beginning of a local loss of the adhesive bond (Fig. 14(a)). In Cycle 6 the discontinuity of the graph as well as the force level compared to Cycle 1 indicate nearly complete failure (Fig. 14(b)). Load transmission and impermeability provided by the adhesive bond are disrupted.

Comparative testing of four representative joint sealing systems based on plastic sealants (PS) revealed highly differentiated performance profiles featuring a considerable range of varying capability and of durability. Figure 15 shows the tensile stress behavior of different joint sealing systems and the associated failures.

It is obvious that the behavior of the systems based on plastic sealants PS 1 to PS 3 differ substantially from that of the system based on PS 4. The higher stiffness of these systems (PS 1–PS 3) is obviously responsible for a two to three times higher stress level. The lower stress level of system PS 4 is apparently the reason that only this joint sealing system achieved the durability requirements for the minimum service life (see Table 1). Systems PS 2 and PS 3 exhibited failures after three, respectively, four simulated annual cycles due to insufficiently durable adhesion to the substrates. System PS 1 was generally inappropriate for the intended use. It was not capable of sustaining the loads during one simulated year due to insufficient cohesive strength. It is obvious from these test results that the systems PS 1 to PS 3 do not comply with the general performance requirements. In this case, realistic application areas according to the evaluated performance must be defined for a failure-free practical use. The basis for selecting the application areas may be further system tests corresponding to the approach presented here.

After having introduced and discussed the key performance indicators, features of the investigation and the technical information about capability and



(b)

FIG. 13—(a) Failure detection; loss of cohesion bond. (Left) Appearance at first visual observation. (Right) Appearance at second visual observation. (b) Loss of adhesion caused by an inappropriate primer selection.

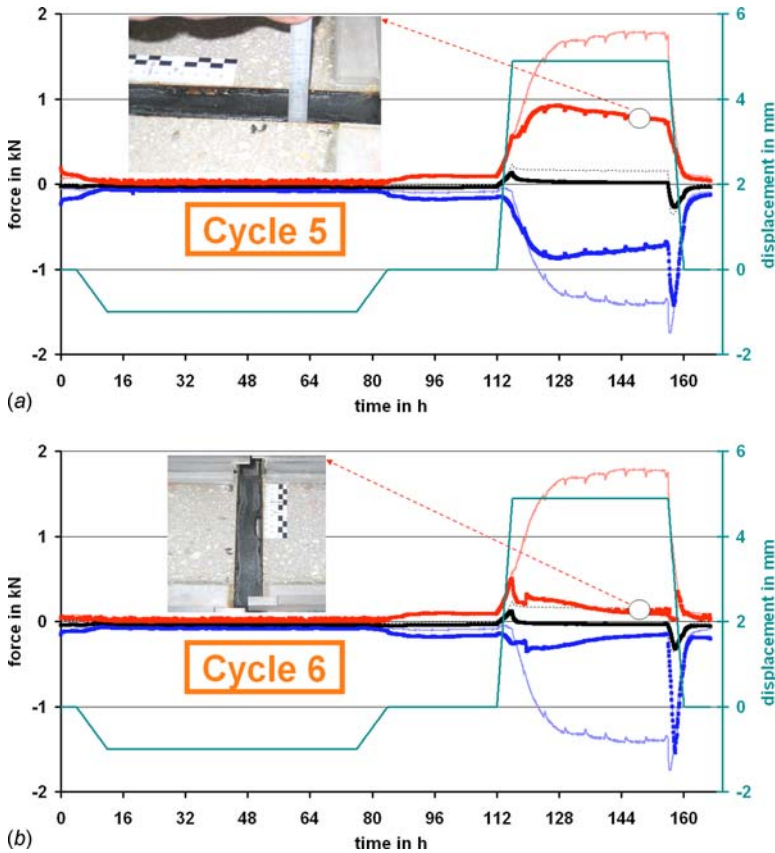
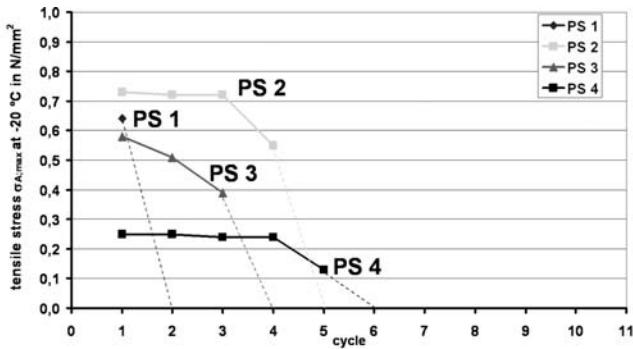


FIG. 14—(a) Typical failure at the end of system's service life (durability) indicated by the beginning of a local loss of the adhesive bond. (b) Nearly complete failure at the end of system's service life (durability).

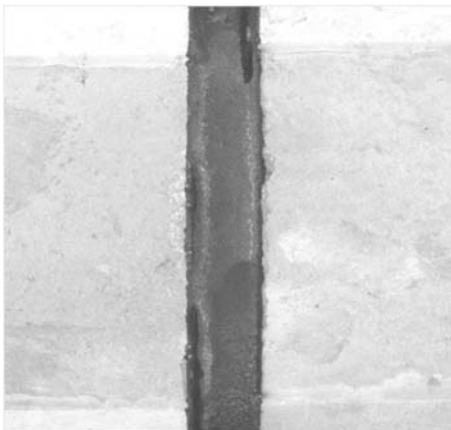
durability of joint sealing systems as derived from the discussion of annual force-deformation graphs, we now would like to introduce a tool for a physical exact characterization of the joint sealing systems that will complete the mechanical system evaluation. This supporting information can be derived from the analysis of the hysteresis curves (shape) for single dynamical deformations (see Fig. 16). From the slope of the curve, k , the stiffness of the system can be deduced. As can be seen from the hysteresis diagram shown in Fig. 16 the joint sealing system type PS 2 shows the highest stiffness. The slope of system PS 2 is approximately 35 times higher than the investigated RS 1 system and the profile system studied and still 3.5 times higher compared to system ES 2, for which the performance and durability behavior has been discussed above. A comparison of the shape and surface areas of the graphs indicates different mechanical behaviors of the various systems, whereas the shape of the hysteresis of system PS 2 indicates even differences between the tension and com-



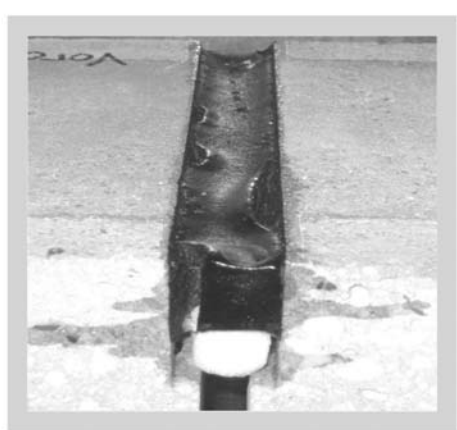
(a)



(b)



(c)



(d)

FIG. 15—Product differentiation according to capability and durability (photos show the failure situation of the tested specimen). (a) PS 1: Failure of specimen after first cycle. (b) PS 2: Failure of specimen after fourth cycle. (c) PS 3: Failure of specimen after third cycle. (d) PS 4: Failure of specimen after fifth cycle. (Note to author—please supply a, b, c, and d on photos for Fig. 15).

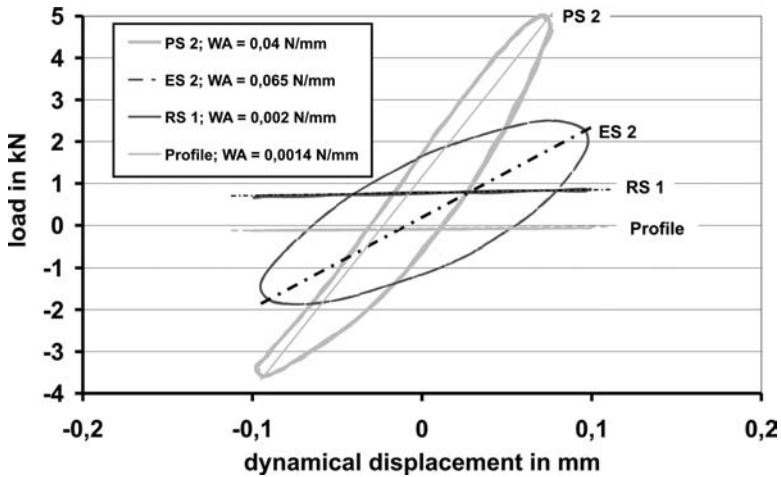


FIG. 16—Comparison of hysteresis graphs for various joint sealing systems.

pression segments. Generally speaking, systems PS 2 as well as ES 2 show viscoelastic behavior with very pronounced dissipation of the energy introduced. Surprisingly, this behavior is more pronounced in joint sealing systems based on so-called “elastic” compounds (around 1.5 times higher compared to “plastic” systems). Thus, it seems to be necessary to revise the system and product evaluation, the categorization and the associated simplified model of the system behavior. During system testing according to the new approach this mechanical behavior was visualized with the help of temperature measurements in the interior of the sealants. Repetitive cycle deformations induce heat in the joint sealing systems and with it temperature differences of $\Delta T = 7.5$ K (for system ES 2) and of $\Delta T = 5$ K (for system PS 2) compared to the surrounding temperature of -20°C were detected. The energy dissipation for the mechanical system behavior is described by the loss angle (phase shift) between loading and system reaction. This mechanical system parameter can be detected from a visualization of the dynamic loading and system response according to Fig. 17. The joint sealing system categories investigated so far, obviously with some variations depending on the specific product, show a loss angle ranging from approximately 25° for PS systems to approximately 28° for ES system and approximately 7° for the RS system and approximately 11° for the profile system.

Conclusions and Outlook

A performance-related approach was deduced from the analysis of the current state-of-the-art concerning the evaluation of joint sealing systems. The application of this approach to the evaluation of joint sealing systems was accomplished with a new system test method which incorporates the ability to vary the loading over a wide range of values and a complex load function that emu-

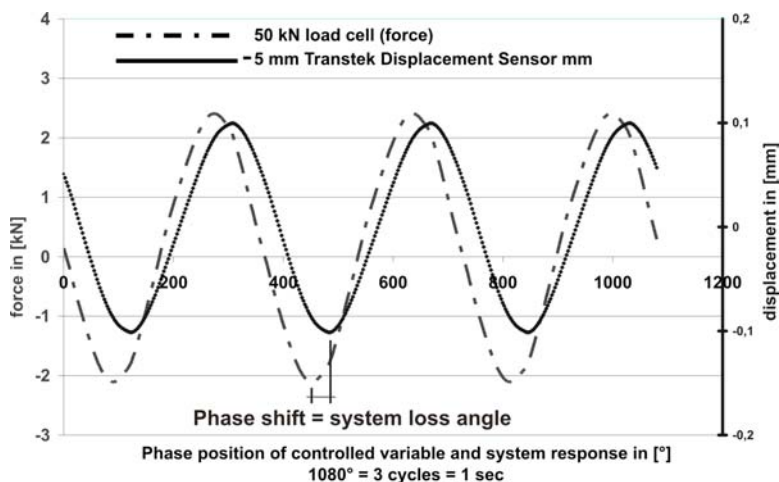


FIG. 17—Analysis of loss angle (phase shift) between loading and system reaction.

lates practical conditions. Based on the study of various joint sealing systems with different sealing products the following can be concluded from the results thus far:

- The method investigates the performance under practical loading conditions.
- The actual mechanical behavior of the system, including failure mechanisms, can be identified and used to describe the system's capability (fitness-for-purpose).
- The method reveals the system's fatigue behavior (durability).
- The structural and material effects (e.g., structural defects or material flaws) on the system behavior can be evaluated.
- The types of joint sealing systems as well as various products can be discriminated according to their capability and durability.
- The test results form the basis for further numerical investigations of material or design variation.

However, one major question remains. Can these results be correlated with actual field behavior? Observation of a field test section was started in 2002 in order to identify criteria that allow extrapolation of the laboratory behavior to field behavior. This installation comprises the joint sealing systems characterized by the new system test method discussed in this paper. Thus far, it appears that for joint sealing systems based on plastic sealant compounds the laboratory method reproduces the field behavior with a good correlation. The induced failure mechanism and the service life ranking are similar (see Table 3). This study will be continued until the year 2012.

In addition to the observation of the field test sections, the following further elements are considered for inclusion in a future evaluation program:

- Support of the system evaluation by means of numerical analysis (FEM).
- System tests under multi-axial mechanical loading.

TABLE 3—Comparison of service life predictions based on laboratory and field results.

System	Performance During System Test	Performance in the Field (added evaluation factors)
PS 1	Loss of performance at the 2nd cycle	benchmark 8 after 5 years (bad)
PS 2	Loss of performance at the 5th cycle	benchmark 6 after 5 years (unsatisfying up to middle)
PS 3	Loss of performance at the 4th cycle	benchmark 6 after 5 years (unsatisfying up to middle)
PS 4	Loss of performance at the 6th cycle	benchmark 5 after 5 years (good)

Note: Field evaluation factors: crack formation; bond behavior; tightness; embrittlement; stability. Benchmarking for field behavior: excellent=0→Dificient=10.

- Application of the testing concept to other sealing joint systems.

In summary, the results obtained on a representative choice of different products falling into the various categories of joint sealing systems for pavements indicate that the tools presented in this paper allow an improved prediction of service life, a more realistic maintenance plan, as well as cost estimation.

Acknowledgments

The authors would like to thank the German Federal Highway Research Institute (BAST) for the support received on this interesting topic. Without the partial sponsorship of BAST, such a test facility could not have been developed. Special thanks also go to our colleagues Ch. Huth (for the material testing and specimen preparation) and O. Mews for the intensive care of the test facility.

References

- [1] Federal Ministry of Transport, Building and Urban Affairs, Road Construction Report, 2007, www.bmvbs.de/Anlage/original_1034870/Strassenbaubericht-2007-barrierefreies-PDF-Dokument.pdf
- [2] Recknagel, Ch., Vater, E. J., and Mühlwinkel, R., "Overview Regarding the Status of Research and Engineering as Well as the National and International Testing Regulations for the Complex Aging Behavior of Joint Filling Systems in Pavements," Research Report 08.146 on behalf of Federal Highway Research Institute, 1997, 159 pp. (in German).
- [3] Al-Qadi, I. L., "Development of Performance Guidelines for the Selection of Bituminous Hot-Poured Crack Sealants," General overview and short report about project TPF 5 (045) of University of Illinois from 31.05.2007, see: www.ic-t.uiuc.edu, 2007.
- [4] Masson, J. F., "Bituminous Sealants for Pavement Joints and Cracks: Building the Basis for a performance-Based Specification," *3rd International Symposium on*

Durability of Building and Construction Sealants, RILEM Proceedings PRO 10, A. T. Wolf, Ed., 2000, pp. 315–328.

- [5] Recknagel, Ch., Pirskawetz, St., and Huth, Ch., “Material and System Investigations on Hot-Applied Plastic Compounds,” Research report for German Highway Research Institute (BAST), 2005, 147 pp. (in German).
- [6] Recknagel, Ch., Pirskawetz, St., Huth, Ch., and Mews, O., “Material and System Investigations on Hot-Applied Elastic Compounds,” Research report for German Highway Research Institute (BAST), 2007, 220 pp. (in German).
- [7] Masson, J.-F., Collins, P., Bundalo-Perc, S., Woods, J. R., and Al-Qadi, I. L., “Variations in the Composition and Rheology of Bituminous Crack Sealants for Pavement Maintenance,” Transportation Research Board, 84th Annual Meeting, Washington, DC, 2005, 15 pp., see: <http://irc.nrc-cnrc.gc.ca/ircpubs>
- [8] Recknagel, Ch. and Pirskawetz, St., “Development of a Complex System Test Method to Investigate the Aging Behavior of Joint Sealing Systems for Pavements,” Research report for German Highway Research Institute (BAST), 2005, 95 pp. (in German).
- [9] Worms, T., Shalaby, A., and Kavanagh, L., “Accelerated Laboratory Evaluation of Joint Sealants Under Cyclic Loads,” Paper presented at the *Annual Conference of the Transportation Association of Canada* 2005, 16 pp., see: www.tac-atc.ca/English/pdf/conf2005/s15/worms.pdf

Errol D. Bull¹ and Gary M. Lucas²

Long-Term Outdoor Weathering Study of Construction Sealants

ABSTRACT: Long-term weather resistance is an important factor to consider when selecting a sealant product for use as an exterior weatherseal for construction applications. The weathering performance of sealants used in these applications can be dependent upon sealant type, sealant chemistry, product formulation, building location, climate, and joint orientation, among other factors. This paper compares and shows the long-term performance of three construction sealant types: silicone, polyurethane, and acrylic terpolymer. Performance attributes such as toughness, flexibility, adhesion, and physical degradation (i.e., reversion, cracking, hardness, etc.) are compared after a 22 year exposure to outdoor weathering in South Florida.

KEYWORDS: durability, outdoor weathering, silicone, polyurethane, acrylic terpolymer, hardness, flexibility, adhesion, elastic recovery, toughness

Introduction

In 1983, a variety of sealant types were installed and placed on outdoor exposure racks at a weathering facility near Miami, Florida, USA. The original 1983 study was designed to serve two purposes: first, to provide shorter-term (i.e., 1–2 years) information on streaking/rundown effects of different sealants on glass and painted aluminum; secondly, to provide weathered and aged samples for longer-term durability evaluation. This paper addresses only the long-term durability aspect of the original study and is intended to review only the sealant materials, not adjacent surfaces or substrates.

Manuscript received June 17, 2008; accepted for publication February 17, 2009; published online April 2009.

¹ Technical Marketing Engineer, Momentive Performance Materials, 260 Hudson River Rd. Waterford, NY 12188.

² Principal Chemist, Sealants Technology, Momentive Performance Materials, 260 Hudson River Rd. Waterford, NY 12188.

Cite as: Bull, E. D. and Lucas, G. M., "Long-Term Outdoor Weathering Study of Construction Sealants," *J. ASTM Intl.*, Vol. 6, No. 4. doi:10.1520/JAI101946.

Copyright © 2009 by ASTM International, 100 Barr Harbor Drive, PO Box C700, West Conshohocken, PA 19428-2959.



FIG. 1—Test site, aerial view (courtesy of Atlas Materials Testing Technology LLC).

The sealants were applied to glass and painted aluminum panels at the test site and have remained in position since January 1983. The sealants have been periodically monitored over the past two decades for various performance criteria such as appearance, flexibility, hardness, and adhesion. In January 2005, after 22 years of weathering, the samples were inspected and photographed. In addition, samples of cured sealant product were cut from each individual test assembly and retained for further lab evaluation.

Test Site Location

Exposures were conducted in Miami, Florida, USA at an exposure field operated by the Atlas Weathering Services Group—South Florida Test Service (SFTS). The site is located in a rural, unpolluted environment with a general prevailing climate that provides high levels of ultraviolet radiation, humidity, and temperature in a tropical environment (see Fig. 1).

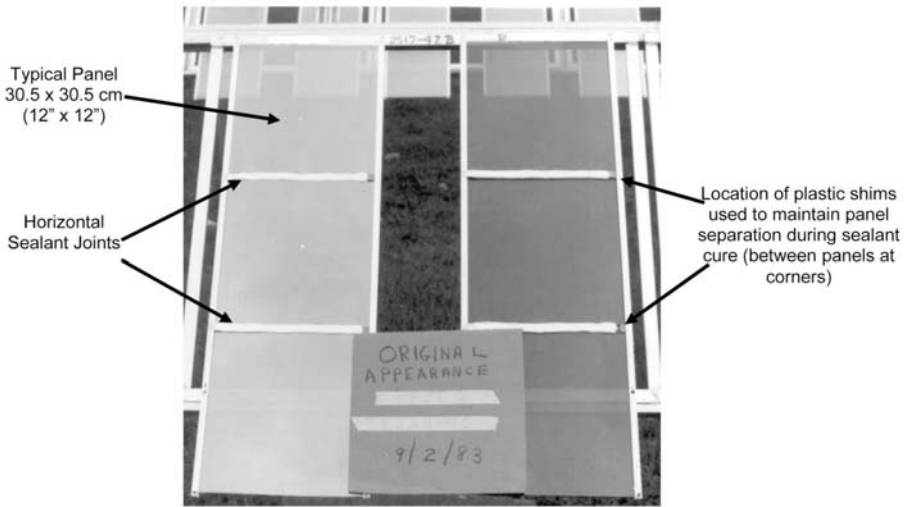


FIG. 2—Test assembly (glass panels shown).

Test Site Data

Latitude:	25° 52' North
Longitude:	80° 27' West
Elevation:	3 m (10 ft)
Average Temp, high:	Summer: 34 °C (93 °F) Winter: 26 °C (79 °F)
Average Temp, low:	Summer: 23 °C (73 °F) Winter: 13 °C (55 °F)
Avg. Relative Humidity:	78 %
Ave. Annual Rainfall:	1685 mm (66 in.)
Total Radiant Energy: ^a (295–3000 nm)	See web link below ^b 6588 MJ/m ²
Total UV: (295–385 nm)	280 MJ/m ²

^a Measured at latitude tilt angle (26° South)

^b http://www.atlas-mts.com/en/services/natural_weathering_testing/natural_weathering_testing_sites/north_america/index.shtml

Test Panel Configuration and Assembly

A series of test panels were assembled using 30.5 by 30.5 cm (12 by 12 in.) pieces of glass and painted aluminum set in aluminum channels fastened to create a supporting frame (test assembly) which was mounted to outdoor exposure racks at the test site location (see Fig. 2). The assemblies were posi-



FIG. 3—*Test assembly array at test site location.*

tioned on the racks at a 45° angle to the horizon and facing south. Each test assembly consisted of three glass (or painted aluminum) panels with two horizontal in-plane joints created between the panels (see Fig. 3). Both joints, of each test assembly, were filled with the same sealant product. All joints in all test assemblies were 1.3 cm (1/2 in.) wide and created using small plastic shims placed at the left and right edges of the panels to maintain separation. Glass thickness was 0.64 cm (1/4 in.). Painted aluminum panels used a 90° bend at the edges to provide sufficient surface length [1.91 cm (3/4 in.)] for bonding.

All glass and painted aluminum panels were cleaned prior to installation of the sealant using soap and water. After cleaning, the panels were thoroughly rinsed with water and dried. No primers were used in this study.

A polyethylene backer rod (held in place with masking tape) was used to hold the sealant in place. Once the sealants were fully cured, the backer rod was removed thus allowing the cured sealants to be exposed to the environment from both the top and bottom surfaces.

All sealants were installed using the procedures outlined by the manufacturer on the product datasheets.

In order to enhance the effects of streaking/rundown (one of the two original objectives of the study), the installed sealants were not tooled into the usual

TABLE 1—Description of sealant products.

ID #	Polymer Type, Descriptors	Manuf	Filler Type	Color
1	Silicone, 1PT, $\pm 25\%$, Ac	A	100 % fumed silica	White
2	Silicone, 1PT, $\pm 50\%$, Al	A	Calcium carbonate/fumed silica	Gray
3	Silicone, 1PT, $\pm 50\%$, Al	A	Fumed silica	Trans/Clear
4	Silicone, 1PT, $\pm 50\%$, Al	A	Calcium carbonate/fumed silica	Gray
5	Silicone, 1PT, $\pm 50\%$, Al	B	Calcium carbonate/fumed silica	Gray
6	Silicone, 1PT, $+100/-50\%$, Am	B	Calcium carbonate/fumed silica	Limestone
7	Silicone, 1PT, $\pm 25\%$, Ac	B	100 % Fumed silica	Black
8	Silicone, 1PT, $\pm 25\%$, Ac	C	100 % Fumed silica	Black
9	Silicone, 1PT, $\pm 25\%$, Ac	D	100 % Fumed silica	Black
10	Polyurethane, 2PT, $\pm 50\%$	D	Fumed silica	Black
11	Acrylic Terpolymer, 1PT, XX	D	Calcium carbonate	Black
12	Polyurethane, 1PT, $\pm 25\%$	E	Calcium carbonate/fumed silica	Limestone
13	Polyurethane, 1PT, $\pm 25\%$	F	Calcium carbonate	Gray

In this study the following abbreviated sealant descriptors are used:

1PT=single component product; **2PT**=multi-component product; $\pm 25\%$, $\pm 50\%$, $+100/-50\%$ =the manufacturer's published movement capability; **Ac**=acetoxy chemistry; sealant releases acetic acid during cure phase; **Al**=alcohol chemistry; neutral cure sealant which releases alcohol during cure phase; **Am**=aminoxy chemistry; neutral cure sealant which releases diethylhydroxylamine during cure phase; **XX**=unknown/not published.

smooth concave profile. The lack of tooling during installation of these sealant beads in 1983 was thought to be of minimal importance for the durability aspect (from a material perspective) of this study.

Description of Sealants

All sealants in this study were commercially available products sold in 1983 and marketed for use in construction applications. The sealant products used were from six different manufacturers. Twelve of the original 13 products used in this study are commercially available when this paper was prepared. Table 1 provides a brief description of the products in the study.

22 Year **Environmental Exposure History**

The data in Table 2 provided by the Atlas Weathering Services Group, South Florida Test Service Miami.

Evaluation Methods

Surface Appearance & Condition

The aged sealants were visually examined for general appearance and surface degradation (i.e., cracking, crazing, bubbling, other surface irregularity, etc., and discoloration or dirt pickup) and observations of each condition were recorded at that time. Surface irregularity descriptions are provided as footnotes to Table 3. A cursory cleaning (bucket of soapy water using a sponge to lightly clean the sealant beads including the surrounding glass and/or metal panels in the vicinity of the sealant beads) of the panels was performed to assist in visual assessment of sealant surface conditions (attempts were not made to thoroughly clean each sample). Test assemblies were cleaned and photographed prior to and after sealant cutting and removal to allow for best visual examination of the sealant surface(s).

Table 3 provides a qualitative assessment of the physical appearance and condition of the sealants. The following ratings were assigned and are tabulated in Table 3:

- For surface appearance and condition: Samples were visually and qualitatively assessed as Excellent, Good, or Poor.
- For dirt pickup: Samples were visually and qualitatively assessed as Light, Moderate, or Significant.
- For surface irregularity: Samples were visually and qualitatively assessed as None, Moderate, or Significant.
- For discoloration or color change: Samples were visually and qualitatively assessed as None, Moderate, or Significant.

Toughness

This study defines a tough sealant as being resilient, firm, resistant to gouging or probing, and flexible but not brittle. For toughness, cut samples were assessed by stretching, bending, twisting, probing, etc. Samples were assigned a score of Excellent, Good, or Poor and are shown in Table 4.

Adhesion

Sections of each sealant were physically cut out from each glass and aluminum panel test assembly and at that time the adhesion was qualitatively evaluated by hand pull and visual inspection of the joint bondline for mode of failure (cohesive or adhesive). See Figs. 4 and 5. Adhesion results are shown in Table 5.

TABLE 2—Summary of annual weathering data.

Year	Total Solar Radiation, direct @ 45°, MJ/m ²	UV Solar Radiation, direct, @ 45°, MJ/m ²	Average Ambient Temp., °F/°C	Average Black Metal Panel Temp., °F/°C	Average Relative Humidity, %	Total Time of Wetness, @ 45°, h	Total Rainfall cm / in
1983	5984.6	^a	75.2/24	93.2/34	80	4653.8	166.6/65.6
1984	5890.7	^a	75.2/24	93.2/34	79	4370.8	166.9/65.7
1985	5920.9	339.39	75.2/24	93.2/34	80	4552.3	145.3/57.2
1986	6517.7	376.21	75.2/24	95.0/35	81	5431.8	166.1/65.4
1987	5440.0	306.90	75.2/24	93.2/34	79	5239.0	122.7/48.3
1988	6146.0	292.30	77.0/25	96.8/36	86	5581.1	155.2/61.1
1989	6639.0	326.26	75.2/24	91.4/33	81	3895.9	76.7/30.2
1990	6352.1	266.51	71.6/22	89.6/32	77	3340.0	70.1/27.6
1991	6001.3	278.04	73.4/23	89.6/32	76	4085.9	105.2/41.4
1992	6233.0	305.53	73.4/23	78.8/26	77	3731.7	107.2/42.2
1993	6297.2	284.21	75.2/24	86.0/30	81	4519.5	91.7/36.1
1994	5568.0	258.90	77.0/25	78.8/26	85	5285.0	178.6/70.3
1995	6211.6	310.75	75.2/24	78.8/26	80	2775.2	135.9/53.5
1996	6681.3	287.65	75.2/24	77.0/25	71	^b	159.5/62.8
1997	6166.1	291.07	75.2/24	78.8/26	83	3207.2	111/43.7
1998	6325.7	303.48	75.2/24	78.8/26	82	3116.3	112/44.1
1999	6375.9	273.02	73.4/23	77.0/25	81	2544.4	164.8/64.9
2000	6463.5	278.03	73.4/23	78.8/26	84	3387.8	142/55.9
2001	6143.4	248.88	73.4/23	77.0/25	85	2959.2	202.9/79.9
2002	6157.0	235.71	75.2/24	78.8/26	84	5951.1	148.1/58.3
2003	5989.4	248.28	75.2/24	78.8/26	80	^c	149.4/58.8
2004	6128.9	296.51	75.2/24	78.8/26	72	^c	116.3/45.8
Averages	6165.1	290.4	74.8/23.8	84.6/28	80.2	4138.3	136.1/53.6

TABLE 2— (Continued.)

Year	Total Solar Radiation, direct @ 45°, MJ/m ²	UV Solar Radiation, direct, @ 45°, MJ/m ²	Average Ambient Temp., °F/°C	Average Black Metal Panel Temp., °F/°C	Average Relative Humidity, %	Total Time of Wetness, @ 45°, h	Total Rainfall cm / in
Totals	123 515	5263				78 628	2994.2/ 1178.8
						Total hours in 22 years (24 × 365 × 22) =	192 720
						Percent of total measured hours that samples were wet =	40.8 %
						Percent of total measured hours that samples were dry =	59.2 %

^aTest site was not measuring UV radiation at a 45° angle when the test was initiated (1983 and 1984).

^bData not available.

^cTest site stopped recording wet time hours in the beginning of 2003.

Note provided by the test site director: “The black metal panel temperatures show some variation through the years. This variation is a result of different types on panels used for this measurement throughout the years. There was/is not a “standard” black panel design type. However, there is activity in ASTM to develop a new standard for black panels which should be published soon.”

TABLE 3—Surface appearance and condition.

ID #	Sealant Type	Overall Surface Condition	Dirt Pickup	Surface Irregularity	Discoloration or Color Change	Photos
1	Silicone, 1PT, $\pm 25\%$, Ac	Excellent	Significant	None	None	13
2	Silicone, 1PT, $\pm 50\%$, Al	Excellent	Significant	None	None	14
3	Silicone, 1PT, $\pm 50\%$, Al	Excellent	Significant	None	Significant ^a	15 and 16
4	Silicone, 1PT, $\pm 50\%$, Al	Excellent	Significant	None	None	17 and 18
5	Silicone, 1PT, $\pm 50\%$, Al	Excellent	Significant	None	None	19 and 20
6	Silicone, 1PT, $+100/-50\%$, Am	Good ^b	Significant	Moderate ^b	Significant ^c	21 and 22
7	Silicone, 1PT, $\pm 25\%$, Ac	Excellent	Significant	None	Significant ^d	23
8	Silicone, 1PT, $\pm 25\%$, Ac	Excellent	Significant	None	None	24 and 25
9	Silicone, 1PT, $\pm 25\%$, Ac	Excellent	Significant	None	None	26 and 27
10	Polyurethane, 2PT, $\pm 50\%$	Poor ^e	N/A ^f	Significant ^g	N/A ^f	28 and 29
11	Acrylic Terpolymer, 1PT, XX	Poor	Light	Significant ^h	N/A ^f	30 and 31
12	Polyurethane, 1PT, $\pm 25\%$	Poor	Light	Significant ^g	None	32 and 33
13	Polyurethane, 1PT, $\pm 25\%$	Poor	Significant	Moderate	Significant	34

^aSurface of sample was white (original color was clear/translucent). The white change occurred only on the glass test assembly (i.e., color change did not occur on aluminum panel test assembly) and only on top and bottom surfaces which were exposed to the environment (i.e., color change did not occur on the sealant edges on the bond line). See Fig. 35.

^bThis sealant had numerous small surface cavities present across the surfaces on all beads on both the glass and the aluminum test assemblies. See Fig. 37.

^cThis sealant surface was permanently discolored (discoloration was not able to be removed by washing). See Fig. 36.

^dSurface of sample was white (original color was black). The white change occurred on both the glass and the aluminum test assembly and only on top and bottom surfaces which were exposed to the environment (i.e., no color change noted on bond line edges). The cause for the whiteness is unknown. See Fig. 38.

^eSamples were friable in some cases and body mass of some samples exhibited reversion (gummy). See Figs. 41 and 42.

^fAssessment not practical based on poor overall condition of remaining samples. See Fig. 40.

^gSurface cracking/crazing. See Fig. 40.

^hSurface bubbling and otherwise irregular (charcoal or pumice-like appearance). See Fig. 39.

TABLE 4—*Toughness.*

ID#	Sealant Type	Resiliency	Firmness	Flexibility	Score
1	Silicone, 1PT, $\pm 25\%$, Ac	Yes	Yes	Yes	Excellent
2	Silicone, 1PT, $\pm 50\%$, Al	Yes	Mostly ^a	Yes	Good
3	Silicone, 1PT, $\pm 50\%$, Al	Yes	Yes	Yes	Excellent
4	Silicone, 1PT, $\pm 50\%$, Al	No	Yes	No	Poor
5	Silicone, 1PT, $\pm 50\%$, Al	Yes	Mostly ^b	Yes	Good
6	Silicone, 1PT, $+100/-50\%$, Am	Yes	Mostly ^a	Yes	Good
7	Silicone, 1PT, $\pm 25\%$, Ac	Yes	Yes	Yes	Excellent
8	Silicone, 1PT, $\pm 25\%$, Ac	Yes	Yes	Yes	Excellent
9	Silicone, 1PT, $\pm 25\%$, Ac	Yes	Yes	Yes	Excellent
10	Polyurethane, 2PT, $\pm 50\%$	No ^c	No	Yes ^c	Poor
11	Acrylic Terpolymer, 1PT, XX	No ^d	N/A ^e	No ^d	Poor
12	Polyurethane, 1PT, $\pm 25\%$	Barely ^f	N/A ^e	Somewhat	Poor
13	Polyurethane, 1PT, $\pm 25\%$	No	N/A ^e	No	Poor

^aThis material could be slightly gouged if forcibly picked at.

^bDuring adhesion testing it was noted that this material was very easily gouged. See Fig. 43.

^cSealant had reverted.

^dSealant was brittle.

^eSealant was hardened.

^fSealant was very slow to return to original shape after bending.

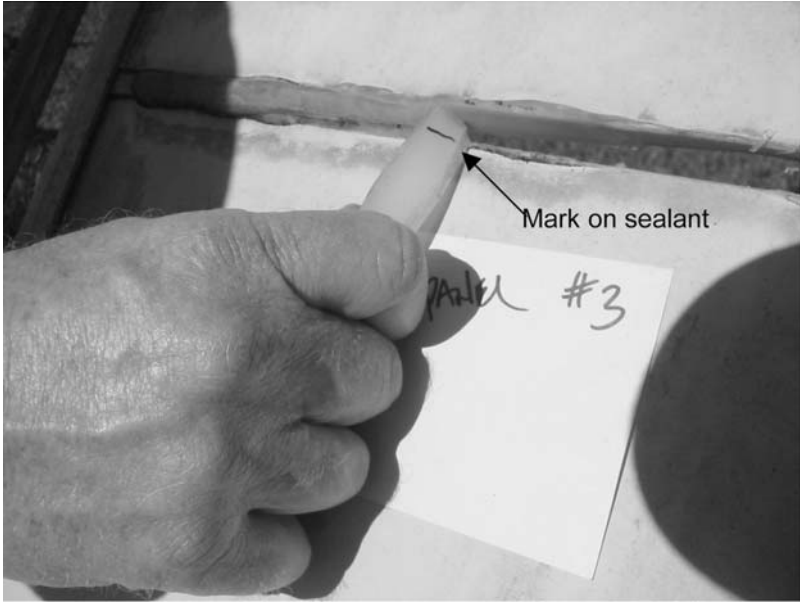


FIG. 4—Adhesion check by hand Pull, start.



FIG. 5—Adhesion check by hand Pull, during.

TABLE 5—Adhesion, flexibility, and elastic recovery.

ID#	Sealant Type	Adhesion Check Mode of Failure		Flexibility	Elastic Recovery
		Glass	Painted Aluminum		Within 5 min
1	Silicone, 1PT, $\pm 25\%$, Ac	Adhesive	Cohesive	Excellent	Yes, 100 %
2	Silicone, 1PT, $\pm 50\%$, Al	Cohesive	Cohesive	Excellent	Yes, 100 %
3	Silicone, 1PT, $\pm 50\%$, Al	Adhesive	Cohesive	Excellent	Yes, 100 %
4	Silicone, 1PT, $\pm 50\%$, Al	Cohesive	Cohesive	Poor	—
5	Silicone, 1PT, $\pm 50\%$, Al	Cohesive	Cohesive	Excellent	Yes, 100 %
6	Silicone, 1PT, +100/-50 %, Am	Cohesive	Cohesive	Excellent	Yes, 90 %
7	Silicone, 1PT, $\pm 25\%$, Ac	Adhesive	Cohesive	Excellent	Yes, 100 %
8	Silicone, 1PT, $\pm 25\%$, Ac	Not Tested	Cohesive	Excellent	Yes, 100 %
9	Silicone, 1PT, $\pm 25\%$, Ac	Adhesive	Cohesive	Excellent	Yes, 100 %
10	Polyurethane, 2PT, $\pm 50\%$,	N/A ^a	Cohesive	N/A ^b	N/A ^b
11	Acrylic Terpolymer, 1PT, XX	Adhesive	Cohesive	Poor	—
12	Polyurethane, 1PT, $\pm 25\%$,	N/A ^c	Cohesive	Good	Yes, 90 %
13	Polyurethane, 1PT, $\pm 25\%$,	Not Tested	Adhesive	Poor	—

^aAssessment not practical based on poor overall condition of remaining samples.

^bCould not perform this test due to reversion of the sealant.

^cSealant was entirely deteriorated (i.e., no physical material pieces or sample remained) and could not be evaluated.

Flexibility

Sections of each sealant were physically cut out from each glass and aluminum panel test assembly. In an effort to qualitatively assess the flexibility and/or elasticity of each sealant, the cut samples were manually bent 180° and photographed and flexibility was noted. Results of this 180° bend are shown in Table 5 as either Excellent, Good, or Poor; and defined as follows:

- Excellent—sealant able to withstand 180° bend without breaking or cracking (see Fig. 6).
- Good—sealant able to withstand 180° bend but with some cracking (see Fig. 7)
- Poor—sealant unable to withstand 180° bend without breaking (see Fig. 8).

Elastic Recovery

Immediately after each sealant was manually flexed/bent 180°, the sealant was released and the elastic recovery was noted and photographed. Elastic recovery is defined as the percent recovery to original shape within 5 min of release



FIG. 6—180° manual bend of sealant (rated *Excellent*).

from the 180° bend position. Elastic recovery results are shown in Table 5. Sealants that broke after the 180° bend test could not be tested for elastic recovery. See Figs. 9 and 10.

Adhesion, Flexibility and Elastic Recovery

Table 5 shows the results of adhesion, manual bending/flexing of the specimens, and recovery from bending/flexing.

Hardness

Sections of each sealant were physically cut out from each glass and aluminum panel test assembly. Samples were taken to lab and measured for hardness using an Exacta Model# EX200/300T hardness tester manufactured by Newage Industries, Willow Grove, PA (see Fig. 11). Sealant specimens were cut using a sharp blade to create a suitable flat surface to take readings. For each specimen, a minimum of three readings (instantaneous values) were taken and recorded. Average hardness readings are tabulated in Table 6.



FIG. 7—180° manual bend of sealant (rated Good).

Results and Observations

Survivability

Table 7 summarizes those samples which did or did not remain intact for the 22 year duration. A few sealants no longer remained in the test assembly joint, see Fig. 12.

Overall Durability Ranking

In an effort to provide a way to quantify the overall durability of these sealants, the following ranking procedure was used in this study. Only performance characteristics, deemed to have influence on weathering durability, are used (i.e., visual appearance or superficial surface conditions are not included). The following properties are thought to be fundamental requirements necessary for a product to be capable of withstanding long-term outdoor weathering for use in building construction applications: flexibility, toughness, elastic recovery, ability to maintain long-term adhesive bonding (as demonstrated on painted alu-



FIG. 8—180° manual bend of sealant (rated Poor).



FIG. 9—180° manual bend of sealant.



FIG. 10—Sealant immediately after release of 180° manual bend.



(a)



(b)

FIG. 11—Hardness tester.

TABLE 6—Hardness measurements.

ID#	Sealant Type	Initial Published Hardness ^a	22 Year Hardness Readings ^b (Type A Indenter)	Approximate Change In Hardness ^c %
1	Silicone, 1PT, $\pm 25\%$, Ac	30–35	37	+14
2	Silicone, 1PT, $\pm 50\%$, Al	22–25	32	+36
3	Silicone, 1PT, $\pm 50\%$, Al	22	31	+41
4	Silicone, 1PT, $\pm 50\%$, Al	22	62	+182
5	Silicone, 1PT, $\pm 50\%$, Al	30	17	-43
6	Silicone, 1PT, +100/-50 %, Am	15	7	-53
7	Silicone, 1PT, $\pm 25\%$, Ac	25	24	-4
8	Silicone, 1PT, $\pm 25\%$, Ac	30	23	-23
9	Silicone, 1PT, $\pm 25\%$, Ac	24	26	+8
10	Polyurethane, 2PT, $\pm 50\%$,	20–40	21	-30
11	Acrylic Terpolymer, 1PT, XX	40–50	79	+76
12	Polyurethane, 1PT, $\pm 25\%$	35–45	63	+58
13	Polyurethane, 1PT, $\pm 25\%$	38	76	+100

^aHardness (measured with Type A indenter), taken from manufacturers' published literature.

^bValues in this column represent the average hardness readings taken from a minimum of three readings per sealant sample cut-out and removed from the test site.

^cCalculated using the median value shown when published literature gives a range.

minum used in this study), and resistance to hardness change. Table 8 shows the overall durability ranking of the sealants reviewed in this study.

For ranking, the following rating system is used for Table 8:

- For toughness (see Table 4) → Excellent=3, Good=2, Poor=1
- For flexibility (see Table 5) → Excellent=3, Good=2, Poor=1
- For elastic recovery (see Table 5) → 100 % =3, 50–90 % =2, <50 % =1
- For % change in hardness (see Table 6) → 0–33=3, 34–66=2, 67–100 =1
- Ability to bond for 22 years (based on results of painted aluminum test assemblies) (see Table 5) → adhesive failure=1, cohesive failure=3

Summary of Observations

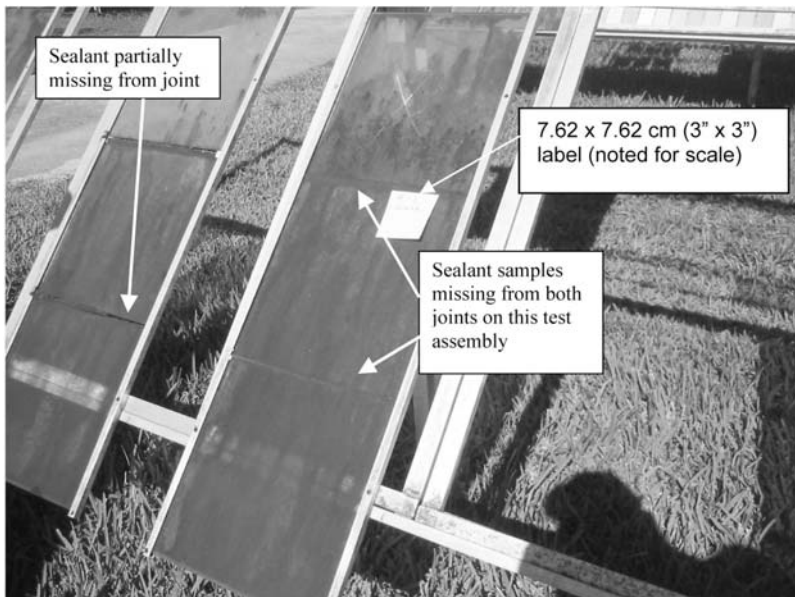
Durability and Adhesion

1. Silicone sealants outperformed the polyurethane and acrylic terpolymer sealants in durability to weathering at this test site location.
2. 100 % fumed silica filled silicone performed better than calcium carbonate/fumed silica filled silicone.
3. 100 % fumed silica filled silicone performed best of all sealant types in

TABLE 7—*Sealant survivability.*

ID #	Sealant Type	Test Assembly, Glass		Test Assembly, Painted Aluminum	
		Top Joint	Bottom Joint	Top Joint	Bottom Joint
1	Silicone, 1PT, $\pm 25\%$, Ac	Yes	Yes	Yes	Yes
2	Silicone, 1PT, $\pm 50\%$, Al	Yes	Yes	Yes	Yes
3	Silicone, 1PT, $\pm 50\%$, Al	Yes	Yes	Yes	Yes
4	Silicone, 1PT, $\pm 50\%$, Al	Yes	Yes	Yes	Yes
5	Silicone, 1PT, $\pm 50\%$, Al	Yes	Yes	Yes	Yes
6	Silicone, 1PT, +100–50%, Am	Yes	Yes	Yes	Yes
7	Silicone, 1PT, $\pm 25\%$, Ac	Yes	Yes	Yes	Yes
8	Silicone, 1PT, $\pm 25\%$, Ac	Not tested	Not tested	Yes	Yes
9	Silicone, 1PT, $\pm 25\%$, Ac	Yes	Yes	Yes	Yes
10	Polyurethane, 2PT, $\pm 50\%$	No	Yes ^a	Yes	Yes
11	Acrylic Terpolymer, 1PT, XX	Yes	Yes ^a	Yes	Yes
12	Polyurethane, 1PT, $\pm 25\%$	No	No	Yes	Yes
13	Polyurethane, 1PT, $\pm 25\%$	Not tested	Not Tested	Yes	Yes

^aApproximately half of joint remained intact and available for inspection.

FIG. 12—*Example of survivability.*

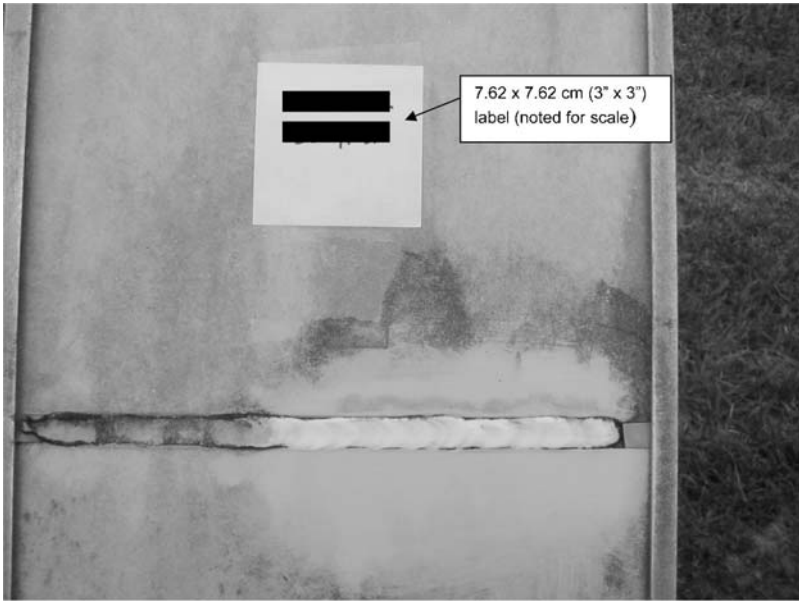


FIG. 13—Silicone sealant #1, before and after cleaning.

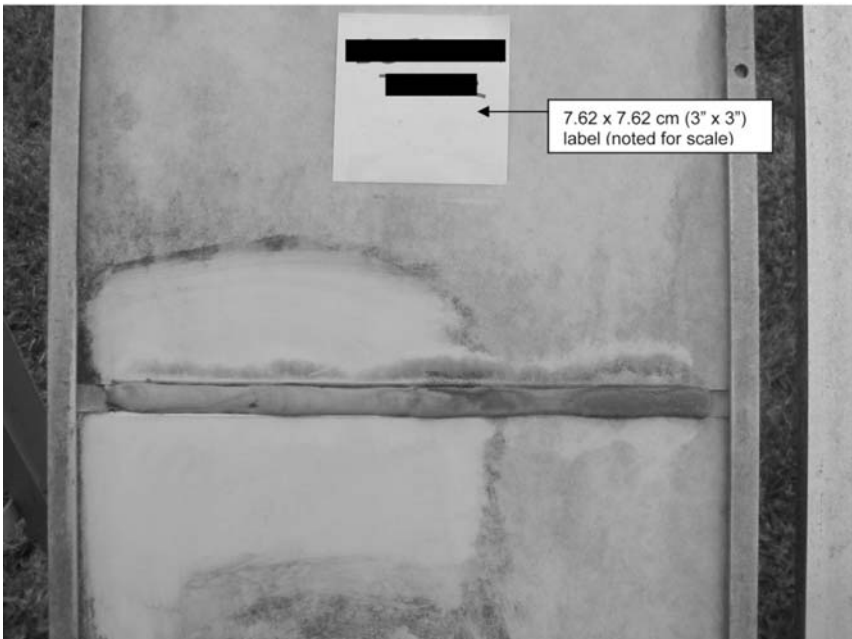


FIG. 14—Silicone sealant #2, before and after cleaning.

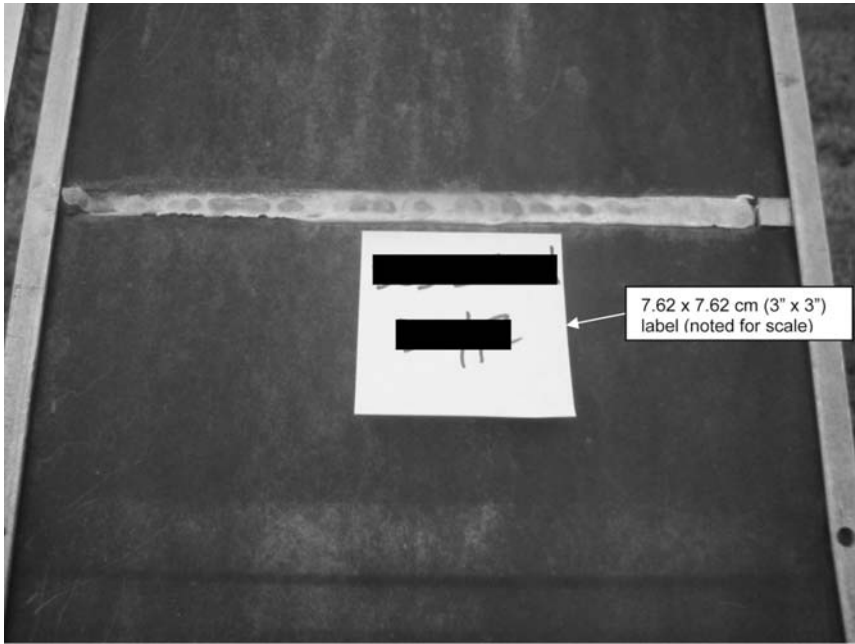


FIG. 15—*Silicone sealant #3, before cleaning.*

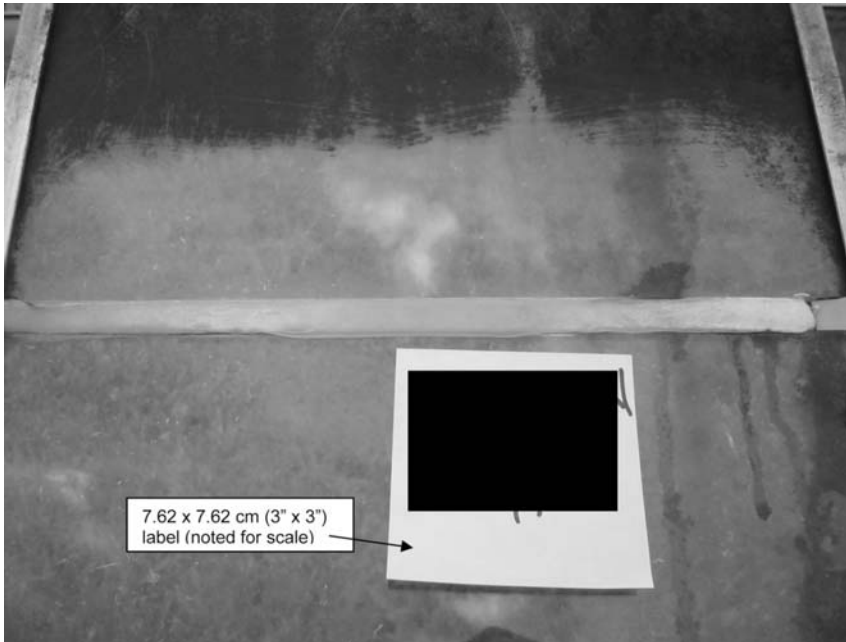


FIG. 16—*Silicone sealant #3, after cleaning.*

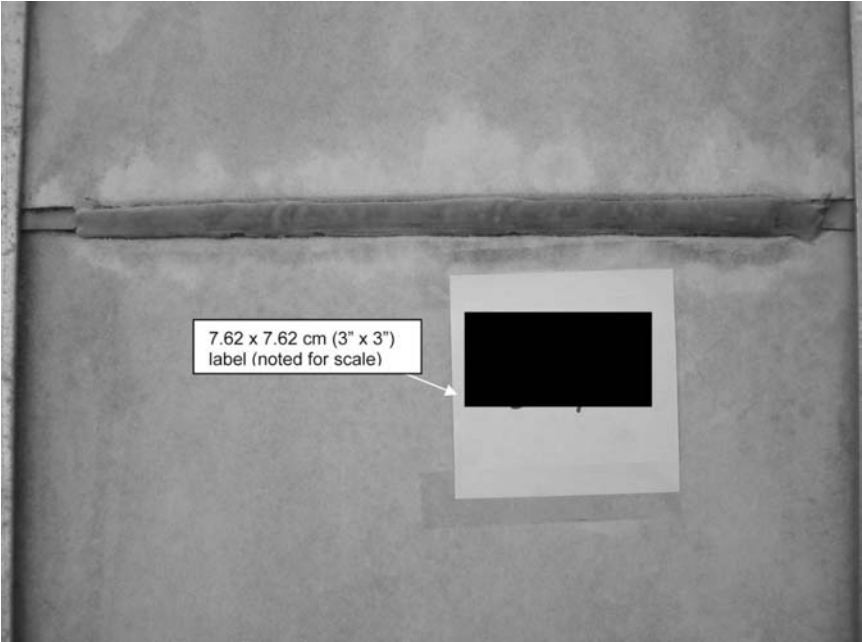


FIG. 17—*Silicone sealant #4, before cleaning.*

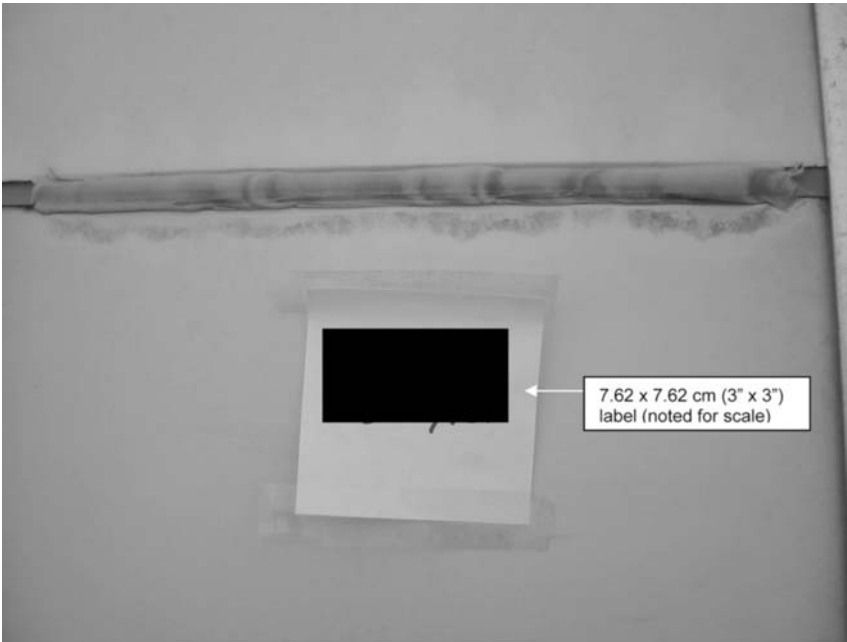


FIG. 18—*Silicone sealant #4, after cleaning.*

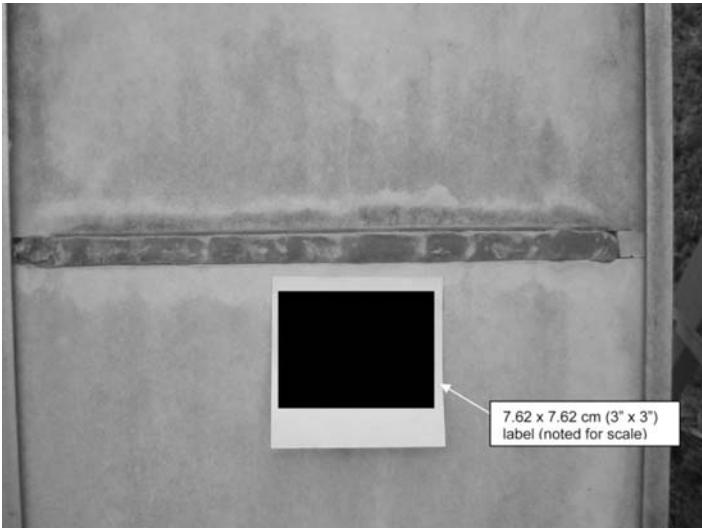


FIG. 19—*Silicone sealant #5, before cleaning.*

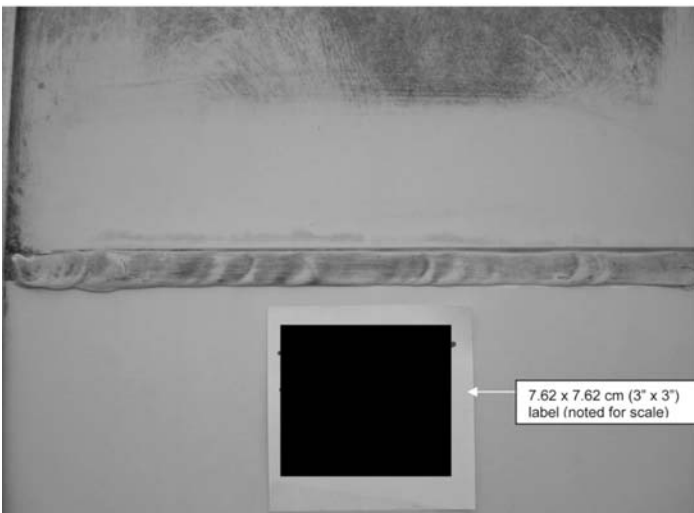


FIG. 20—*Silicone sealant #5, after cleaning.*

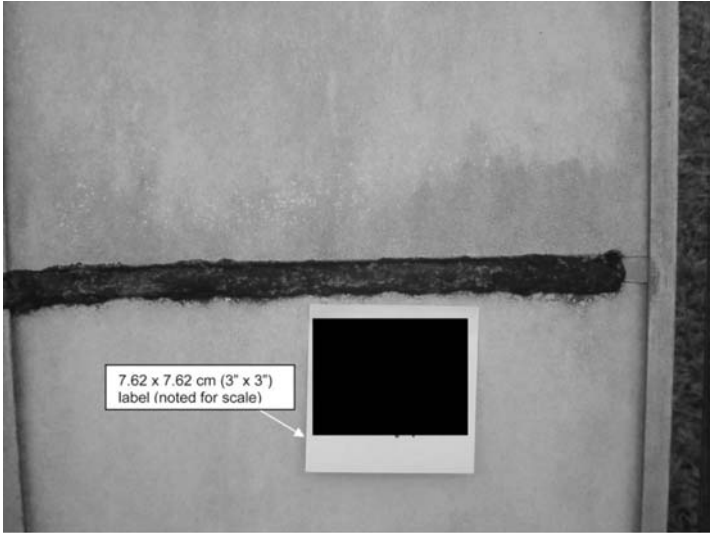


FIG. 21—Silicone sealant #6, before cleaning.

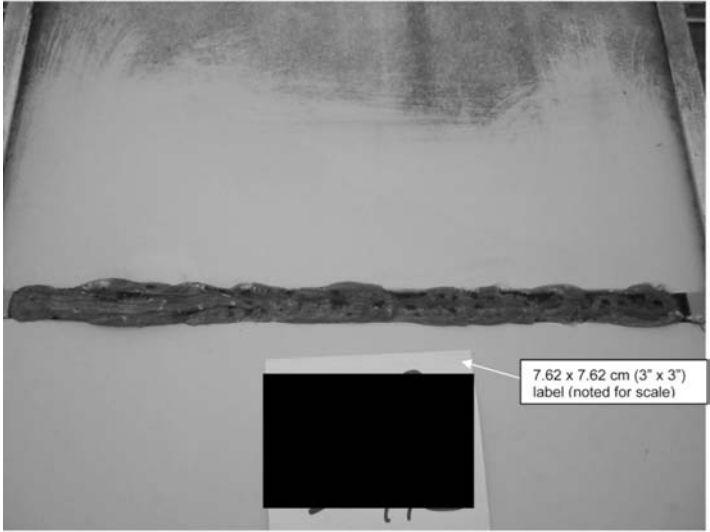


FIG. 22—Silicone sealant #6, after cleaning.



FIG. 23—Silicone sealant #7, after cleaning.

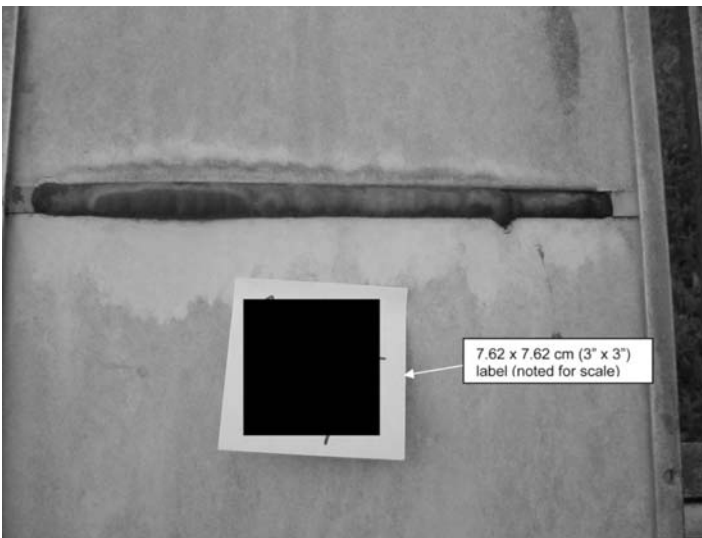


FIG. 24—Silicone sealant #8, before cleaning.

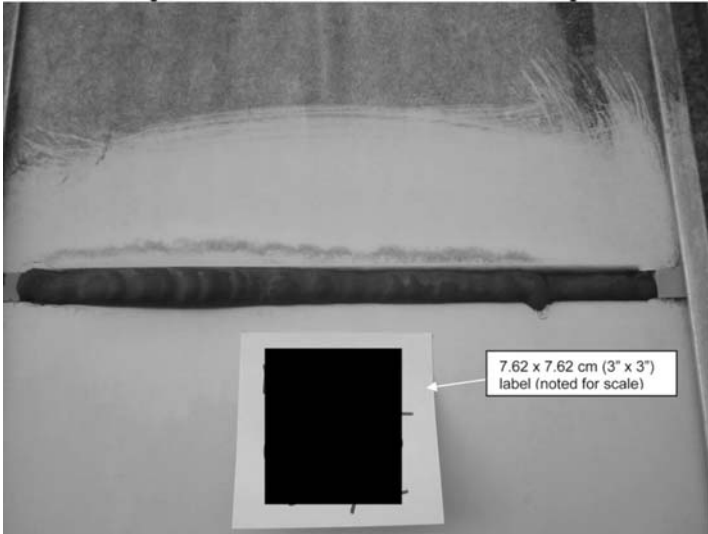


FIG. 25—Silicone sealant #8, after cleaning.

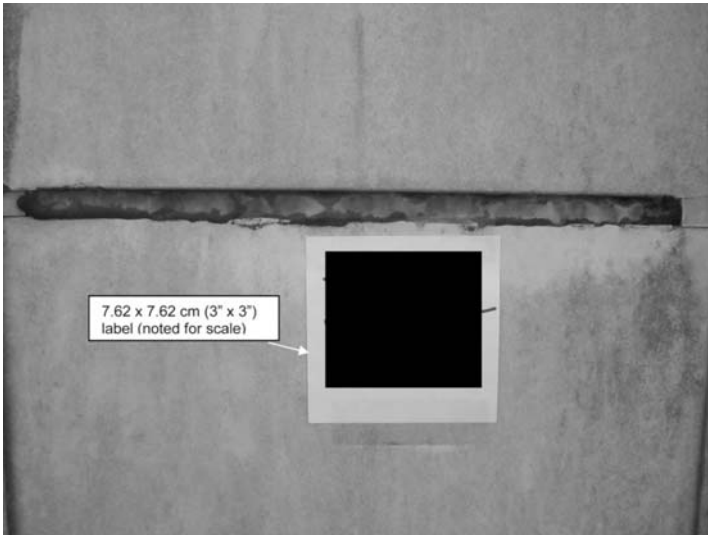


FIG. 26—Silicone sealant #9, before cleaning.

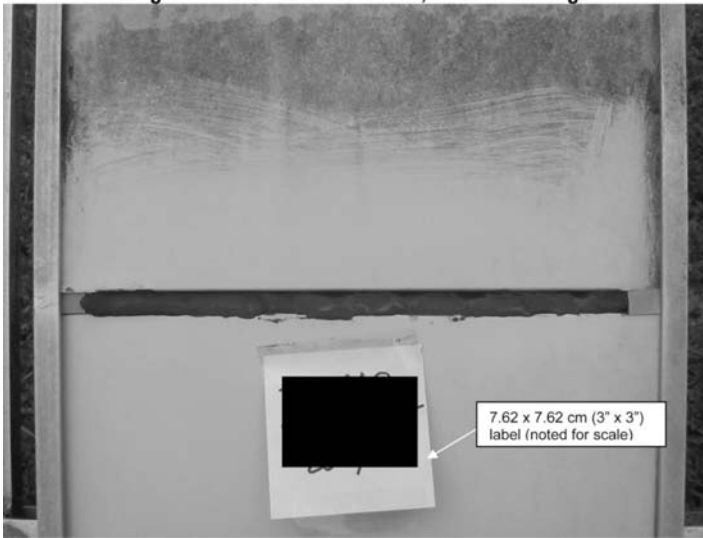


FIG. 27—*Silicone sealant #9, after cleaning.*

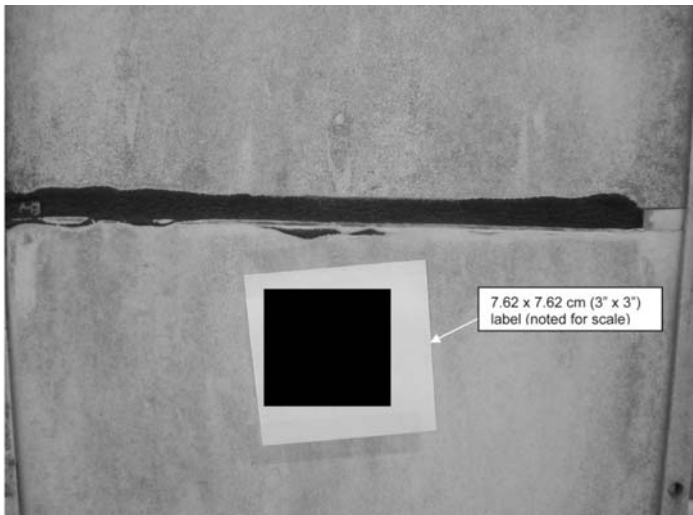


FIG. 28—*Polyurethane sealant #10, before cleaning.*

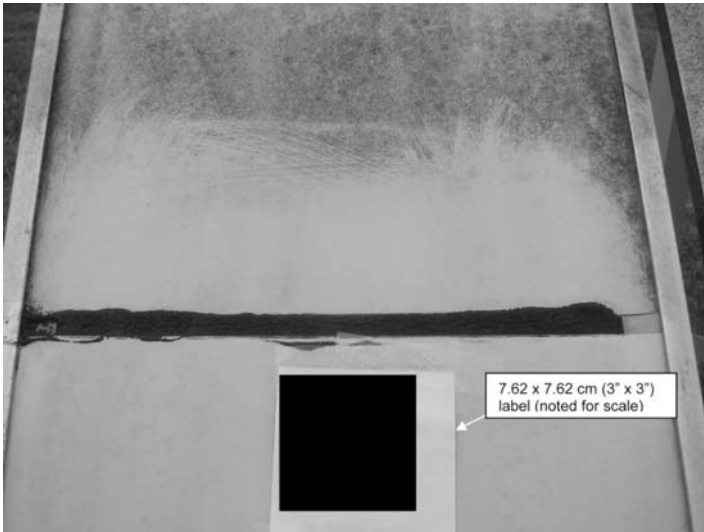


FIG. 29—Polyurethane sealant #10, after cleaning.



FIG. 30—Acrylic terpolymer sealant #11, before cleaning.

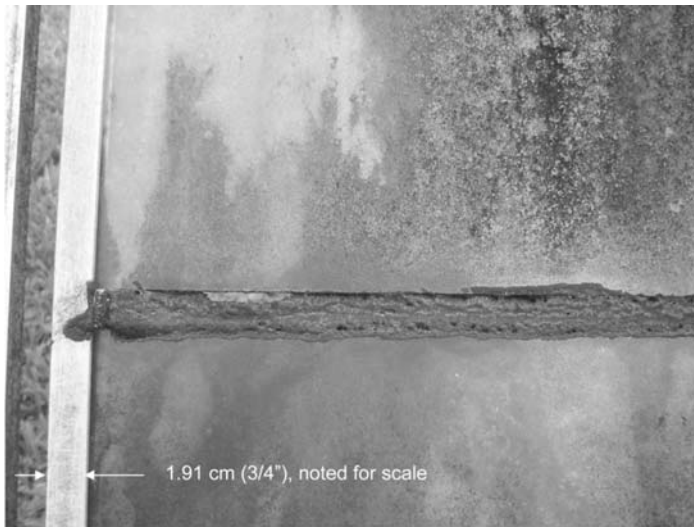


FIG. 31—Acrylic terpolymer sealant #11, close up (before cleaning).



FIG. 32—Polyurethane sealant #12, before cleaning.

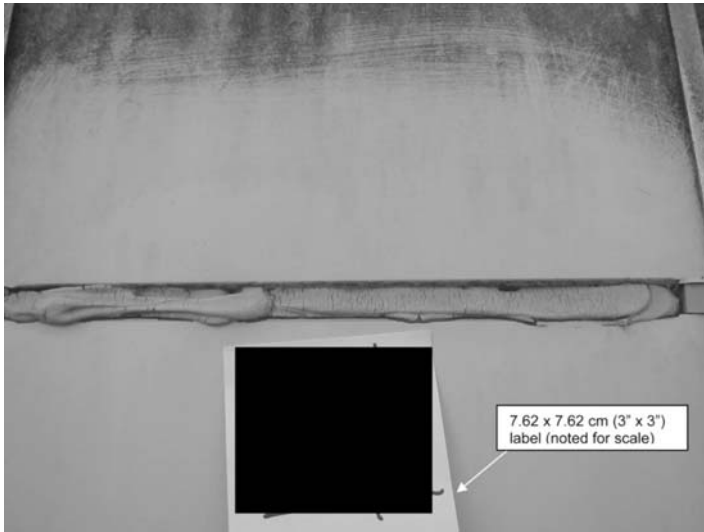


FIG. 33—Polyurethane sealant #12, after cleaning.

elastic recovery with instantaneous or near-instantaneous 100 % re-bound.

4. 100 % fumed silica filled silicone performed best of all sealant types in toughness.
5. 100 % fumed silica filled silicone showed the least percent change in hardness.
6. With the exception of one of the single component polyurethane products, all sealant products evaluated in this study demonstrated the abil-

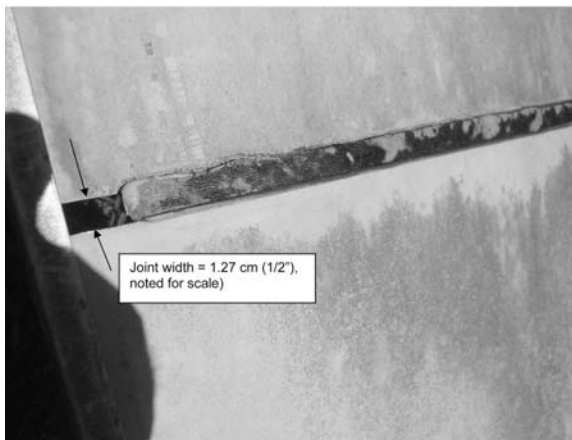


FIG. 34—Polyurethane sealant #13, surface appearance (before cleaning).

TABLE 8—Overall durability ranking.

ID#	Sealant Type	Toughness	Flexibility	Elastic Recovery	Change In Hardness	Adhesive Bond Durability	Rating Totals
1	Silicone, 1PT, $\pm 25\%$, Ac	3	3	3	3	3	$\Sigma = 15$
7	Silicone, 1PT, $\pm 25\%$, Ac	3	3	3	3	3	$\Sigma = 15$
8	Silicone, 1PT, $\pm 25\%$, Ac	3	3	3	3	3	$\Sigma = 15$
9	Silicone, 1PT, $\pm 25\%$, Ac	3	3	3	3	3	$\Sigma = 15$
3	Silicone, 1PT, $\pm 50\%$, Al	3	3	3	2	3	$\Sigma = 14$
2	Silicone, 1PT, $\pm 50\%$, Al	2	3	3	2	3	$\Sigma = 13$
5	Silicone, 1PT, $\pm 50\%$, Al	2	3	3	2	3	$\Sigma = 13$
6	Silicone, 1PT, $+100/-50\%$, Am	2	3	2	2	3	$\Sigma = 12$
12	Polyurethane, 1PT, $\pm 25\%$	1	2	2	2	3	$\Sigma = 10$
10	Polyurethane, 2PT, $\pm 50\%$	1	1	1	3	3	$\Sigma = 9$
4	Silicone, 1PT, $\pm 50\%$, Al	1	1	1	1	3	$\Sigma = 7$
11	Acrylic Terpolymer, 1PT, XX	1	1	1	1	3	$\Sigma = 7$
13	Polyurethane, 1PT, $\pm 25\%$	1	1	1	1	1	$\Sigma = 5$



FIG. 35—Silicone sealant #3, surface discoloration.

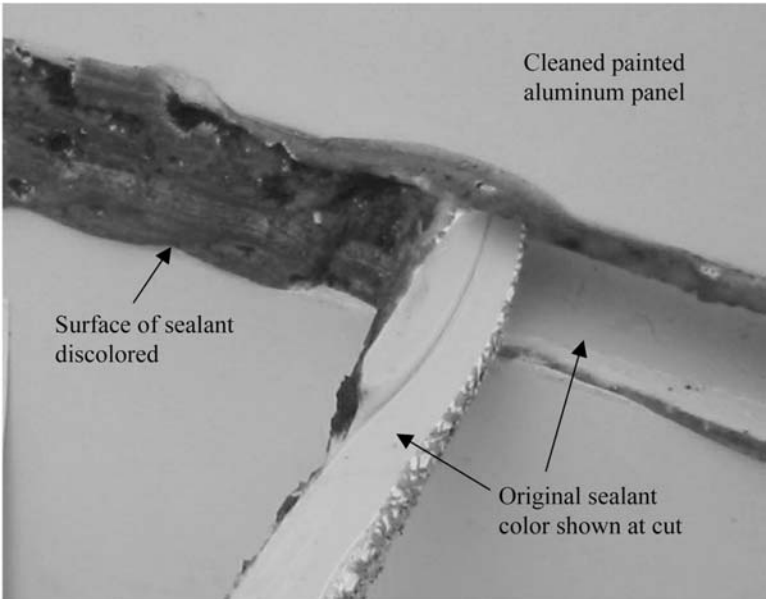


FIG. 36—Silicone sealant #6, surface discoloration.

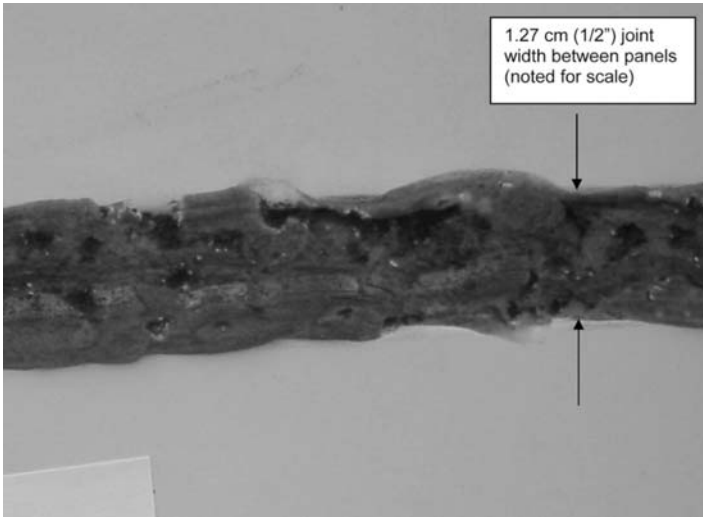


FIG. 37—Silicone sealant #6, surface cavities.

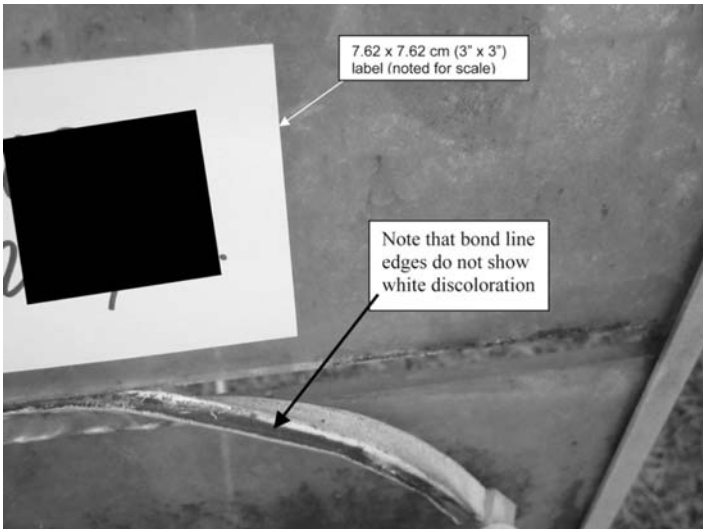


FIG. 38—Silicone sealant #7, surface discoloration.

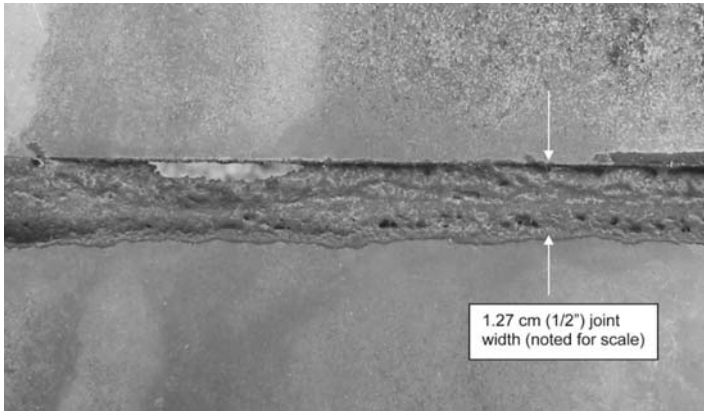


FIG. 39—Acrylic terpolymer sealant #11, degraded surface.

ity to maintain an adhesive bond to the painted aluminum substrate used in this study.

7. All three acetoxy silicones that were tested on the glass panel test assemblies lost adhesion to the 0.64 cm (1/4 in.) thick glass edges.

Surface Appearance and Cleanability

1. One polyurethane sealant evidenced very little dirt pickup.
2. The nonsilicone products exhibited the least dirt retention.
3. The general overall surface condition of the silicone products was better than the nonsilicone products.
4. 100 % fumed silica filled silicone samples were more easily cleaned to original appearance than calcium carbonate/fumed silica filled silicones.

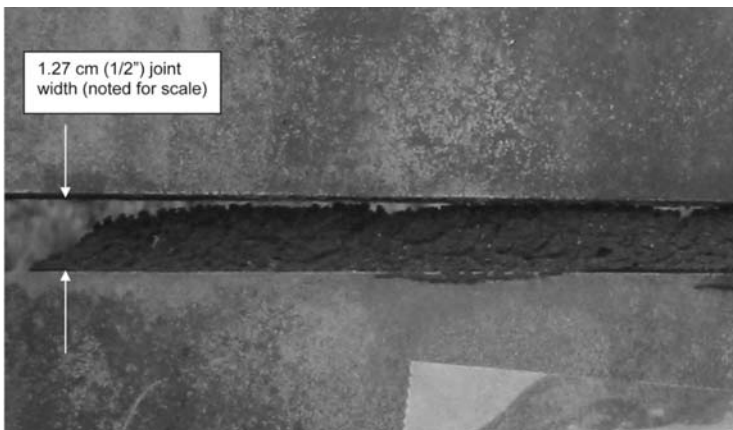


FIG. 40—Polyurethane sealant #10, degraded surface.

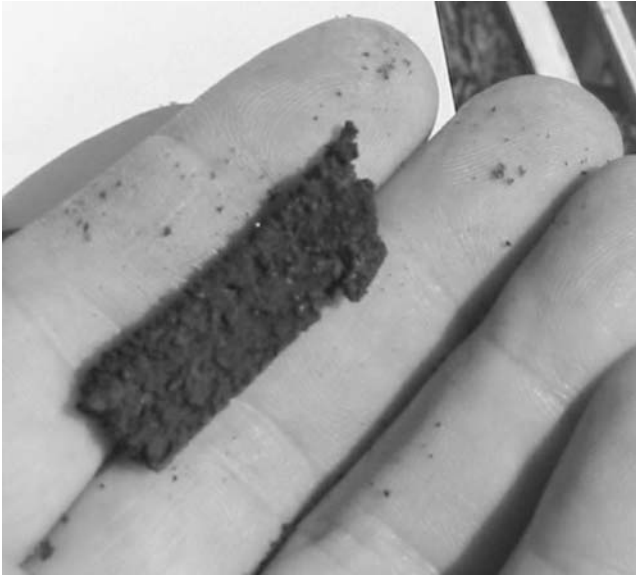


FIG. 41—Polyurethane sealant #10, degraded sealant, friable.



FIG. 42—Polyurethane sealant #10, reversion.

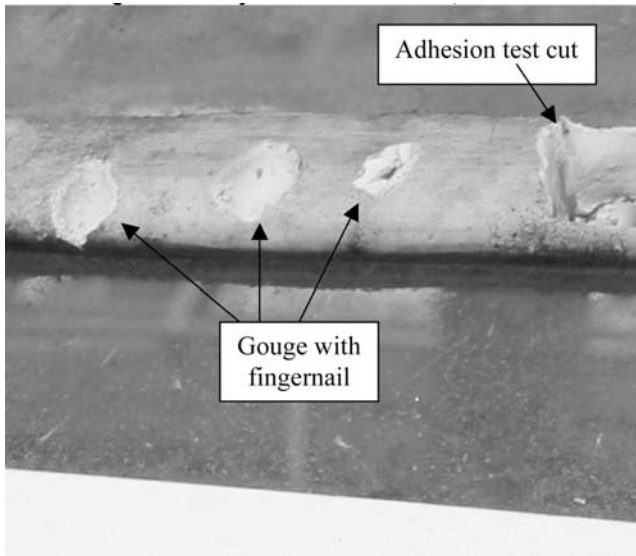


FIG. 43—*Silicone sealant #5, easily gouged.*

5. The low-modulus neutral cure silicone product showed a discolored surface that was not able to be restored back to the original sealant color by washing or cleaning.
6. The low-modulus neutral cure silicone product exhibited numerous small surface pot-hole-like cavities spread sporadically across the bead surfaces on both the glass and aluminum test panel assemblies. It is worthy of note that the glass and aluminum test panel assemblies were not located side-by-side but were separated by greater than 25 ft. No other sealants showed this phenomenon.
7. Two of the 100 % fumed silica filled silicones (one was originally black, the other clear/translucent) showed a similar white-ish surface discoloration that was not able to be restored back to the original sealant color by washing or cleaning.

Acknowledgments

The authors would like to thank Mr. James R. Brower for technical suggestions, historical information, and for originally conceiving and initiating this study.

Jerome M. Klosowski¹ and Patrick D. Gorman²

Selective Review of Weathering Tests for Sealants and Thoughts on the Development of Novel Test Concept Based on Simultaneous Weathering and Movement

ABSTRACT: This paper reviews sealant weathering test methods developed during the past 40 years and highlights the fact that repeated movement cycles were shown to be important to reproduce some of the damage seen on real buildings. The studies reviewed further demonstrate that water, sunlight (especially the UV portion), and heat are important degradation factors that act on real buildings.

KEYWORDS: accelerated testing, outdoor weathering, artificial weathering, sealants, fatigue, review

Introduction

The most substantial problem with accelerated weathering sealant tests is that present tests do not closely predict lifetimes of some sealants the way the tests are done, i.e., in a static condition. It can also take a long time to get meaningful data. In fact, most of the weathering tests recorded for sealants are not done in a joint configuration and thus do not actually test the fundamental properties, like the sealing ability of a sealant (a sealant is typically used in a joint and

Manuscript received October 14, 2008; accepted for publication September 22, 2009; published online November 2009.

¹ President, Klosowski Scientific, Inc., Chief Chemist, 3031 State Street Rd., Bay City, MI 48706-1831, Engineering Diagnostics, Inc., 106 E. 6th St., Suite 620, Austin, TX, Scientist Emeritus, Dow Corning Corporation, 2200 Salzburg Rd., Midland, MI 48686, SWR Institute, Honorary Member, 400 Admiral Blvd. Kansas City, MO 64106, FASTM, Adhesives Age Award, 110 William Street, New York, NY 10038.

² President, Gorman Moisture Protection, Inc., 2115 E. Missouri, El Paso, TX 79903-3505, ASTM C24, First Vice-Chairman, SWR Institute, Past President, 400 Admiral Blvd. Kansas City, MO 64106.

Cite as: Klosowski, J. M. and Gorman, P. D., "Selective Review of Weathering Tests for Sealants and Thoughts on the Development of Novel Test Concept Based on Simultaneous Weathering and Movement," *J. ASTM Intl.*, Vol. 7, No. 1. doi:10.1520/JAI102186.

Copyright © 2010 by ASTM International, 100 Barr Harbor Drive, PO Box C700, West Conshohocken, PA 19428-2959.

under strain and thus must be tested while under strain). The closest official method to real life is the method for artificial weathering published by RILEM [1] and introduced into ISO TC 59/SC 8, the ISO committee dealing with sealants for construction joints. This test was developed at the same time and in harmony with the new weathering practice in ASTM C24 (ASTM C1519) [2]. In each of these tests the sealed joint test specimens are weathered in a static mode but are taken out monthly when the sealant goes through cyclic movement and is examined. These new tests are an improvement but still do not exactly match the damage in real buildings and walkways. Thus the quest for an even more realistic and faster test continues.

Selective Review of Weathering Tests

In the early 1980s, this first author, in conjunction with Dr. L. Bogue Sandberg of Michigan Technological University, ran an outdoor weathering study on a static rack with ASTM C719 [3,4] type joints, comparing the outdoor-exposed samples to samples exposed in a UVF weathering machine (fluorescent UV A-340 weathering machine). One purpose of this study was to see if the UVF weathering would duplicate the outdoor weathering. The good result was that the damage (except for color change) between the accelerated weathering and the outdoor exposure was almost identical. The bad result was that sealant damage, on both the weathering rack and the artificial weathering machine, was dissimilar to the damage normally seen with the same sealant applied to real buildings. As a follow-up the outdoor part of the study was repeated. This time the condition of the sealed joint was changed from extension to compression every 3 months while on the outdoor rack. The sealant soon looked like it did on real structures. The conclusion from this study was that movement in the joint was fundamental to inflicting realistic damage to the sealant and must be part of an improved weathering test [4]. This was also noted in early weathering studies by Karpati [5–7]. The most relevant of her studies incorporated an outdoor rack where one side of a test joint was attached to a concrete beam and the other to a metal beam. Thus the joints moved with the weather and produced damage as seen on real buildings. Depending on the joint's position on the beam, the amount of movement could be varied, showing that increases in movement made huge increases in the amount of damage done. This work set the tone for almost all the work that followed.

This concept was reinforced by Jones and Lacasse in their review on the effect of movements on sealant performance [8]. This was almost certainly on the mind of Linde in the late 1980s [9] as he developed his new weathering test chamber. It had an extension/compression machine similar to that used for ASTM C719 testing, but Linde's movement apparatus was situated inside a weathering machine. The weathering machine could cool as well as heat. This was significant since a sealant could be put into extension as it cooled and became stiffer. Also, after a time in cold, the sealant could be gradually heated, taken into compression, then held at full compression at full heat for any specified time until it would again go into a chill and extension cycle. Independent of the heating/cooling and extension/compression cycles, the machine could im-

pose water, in the form of water spray or immersion, and UV radiation. Linde was studying damage to runway sealants, and this device almost identically reproduced the damage seen in the outdoor joints. The rate of joint extension or compression could be programmed to virtually any speed, especially the slow speeds where it would take 12–24 h to complete an extension or compression cycle. Jones, as part of his thesis with Hutchison, similarly exposed the sealed joint to movements while inside the weathering machine. Jones used an electrical stepper motor to move the joint that allowed him to exactly reproduce joint movement profiles previously measured on an actual building. By feeding these movement profiles into the machine, he was able to simulate whatever joint he desired, e.g., a joint in a south-facing aluminum curtain wall in London or a pavement joint between concrete slabs in Ireland. The Jones apparatus is most likely the one that gives the most realistic data [10]. The cost of these machines limited their broader use.

Since that time there have been many weathering tests with sealants including those by Beech and Beasley [11–14], Fedor and Brennan [15], Boettger and Bolte [16,17], and others. In many of these studies, generalizations are difficult to find since different generic sealant types have different degradation mechanisms. Some degrade primarily from water and heat, some from UV degradation, and some from various combinations of these. There are even variations of degradation mechanisms within generic types with subtle formulation variations relative to inhibitors, blockers, and stabilizers. Many products of the same generic type show large differences in stability.

A Karpati study [6,18,19] showed that simply accelerating the rate of cyclic movement in an indoor test gave comparable damage to sealants outdoors with comparable movement amplitudes. It was suggested (such as by Fedor [20] and Beech and Beasley [21]) that with sealants showing measurable changes, time in the UVF machine varied from about 800 up to 2600 h to achieve comparable changes to the sealants weathered in outdoor locations after 1 year. Some of these studies were also done in a machine with a xenon arc lamp radiation source, but the trend was similar and the sealants exhibited substantial changes. Damage similar to joints on buildings was only seen when there was movement while weathering.

Wolf et al. [22] attempted to summarize all this data in a 1999 overview of all the pertinent weathering studies for building sealants. In their conclusions, they report that each sealant has a specific response and a general correlation is not possible, citing the variations in climate and formulation, even within a generic type. However, they also state: “A realistic minimum accelerated weathering exposure time to provide a rough estimate of the performance after several years of outdoor exposure would be 5000 h for statically and 2000–5000 h for dynamically exposed specimens.” The authors of this paper agree with those general conclusions with one important exception. Comparing dynamic exposure in the machine and dynamic exposure outdoors, with static exposure in both the machines and outdoors for any given sealant, the acceleration factor seems to be the same. The difference is the much more severe damage done with the dynamic testing. Wolf et al. tried to determine a general number for acceleration to use as a guide in their work. The damage in sealants from those tests was measured as a modulus change or a visual change. By dividing the

TABLE 1—*Weathering machine equivalence.*

Sealants Specification Equivalent ^a	Time in Weathering Machine	
	(h)	Year
C834 std. spec. for latex	500	0.5
C920 std. spec. for elastomeric joint	250	0.25
C1311 std. spec. for solvent release	1000	1.0
C1518 std. spec. for pre-cured elastomeric silicone	2500	2.5
C1184 std. spec. for structural silicone	5000	5.0

^aUsing the typical acceleration of approximately 6; the equivalent years are noted.

machine hours into the time outdoors, based on the tests the reports produced, the acceleration factor could be as little as 4 or as high as 8 (or even 10 for a relative non-degrading northern climate with very little warm weather, lots of snow, and cloud cover). For purposes of this discussion, the authors of this paper have used an average of 6 as the typical acceleration factor (approximately 1500 weathering machine hours to be compared to 1 year in the various climates) and thus chose the length of time in a single machine cycle before property testing based on that number.

Thoughts on the Development of Novel Test Concepts

Most users of construction sealants would like the sealants to last 5, 10, or sometimes 20 years or more. This suggests that if the acceleration factor is approximately 6, the indications of a sealant's ability to perform adequately for a year outdoors would take 8–9 weeks in an accelerated weathering machine. An estimation for 5 year performance would take about 40 weeks (6000–7000 h) and 10 years for the range of 1 1/2 years, and 20 year performance estimates would take a bit over 3 years (26 000–30 000 h) to study in contemporary accelerated weathering machines (Table 1). Again, the acceleration could be 4, 6, or 8 depending on the specific sealant and the specific location of the building to be sealed. Thus the user of sealants should know that to obtain accelerated data capable of predicting longevity of a given sealant in a given area, one might need prolonged time in the weathering machines. If the weathering factor is 4 instead of 6, the time in the weathering machines might be of the order of 65 instead of 43 weeks. The reality of this is that good acceleration weathering data takes a long time. One might suggest that the short-term aspects of present specifications give the user a false sense of security and this vividly speaks to the needs of a good weathering test done over a substantial period of time.

There is yet another aspect of accelerated weathering to discuss. There have been several studies since the early 1990s showing how joint movement during cure introduced damage that further mimics what is seen in real life [23–29]. This led to an inclusion of this type of curing option in the previously mentioned RILEM published weathering test that was submitted for consideration to ISO TC 59/SC 8. The conclusion from all of the above studies is that

sealants that move during curing have lesser movement ability than sealants that are tested after they were cured with no movement. The amount of change caused by early movement varies with the sealant. The faster curing mix-on-the-job sealants show less detrimental changes. Again, the amount of damage depends on the specific sealant, and often the damage does not show the effects until after several seasons on a building (or several movement cycles).

Since all or most sealants in outdoor applications will move during the curing, it is reasonable that a good accelerated weathering test would include this phenomenon. However, a sealant could move differently each day while curing or differently according to climate, and this huge variability is difficult to regulate for a standard test method. One conclusion is that (with few, if any, exceptions) sealants in real joints might not do as well as the sealants in weathering tests since real joints will almost always move during the curing process and have compromised adhesion or joint movement ability.

There are yet more observations that come into play. It might take an expensive machine like Linde produced, with a severe cooling cycle, to obtain realistic weathering in a machine. That idea is fostered in the Fedor and Brennan study (aided by Klosowski) where sealants were adhered to aluminum sheets as in ASTM C793 [30]. The test procedure followed ASTM C793 [30] in that after UV exposure the sealant was cooled to -26°C and bent over a mandrel. The acrylic sealant studied did not show much damage from the weathering exposure but became very stiff when cold. The bending of the cold sealant over the mandrel caused the sealant to break and debond so much so that half stayed bonded and half jutted upward. In the Linde study, the sealants that stiffen severely in the cold showed adhesion failures not seen with the sealants that were not chilled. If a primary failure of a sealant is the joint extension while cooled, then test machines incapable of cold temperatures might miss this damage and give a false positive relative to the ability of this sealant to perform in a climate with potentially cold conditions. This is not a mechanism of failure for all sealants but remains a factor for some and should be included in tests that are preparing for such conditions.

Some sealants, on the other hand, seem unable to handle high heat. Some product data sheets carry the warning that the sealants are not to be used at temperatures above 70 or 80°C . The question is whether these sealants simply decompose more quickly at this higher temperature (an acceleration of processes that happens at lower temperatures) or if there are new decomposition mechanisms initiated at the higher temperatures. For bronze colored aluminum panels with thermal insulation, temperatures of 90 – 110°C are common. The artificial weathering machine that does not reach those temperatures cannot account for a major mechanism of deterioration and could therefore also produce a false positive. In essence, a test lacking in adequate extreme conditions could make a sealant look better than it is and imply that a sealant can be used in places where it should not. The converse is also true: In many climates, on lighter colored surfaces, the more extreme temperatures will not occur; and thus the test could falsely predict damage where it is not a factor.

Heat is often not the only factor, nor the key factor, in sealant deterioration. Gorman investigated over 200 jobs to study the condition of actual sealants in buildings [31]. One of his most important observations was of a urethane ap-

plied in a wall joint; the sealed joint was on the south side of a building in the southern United States, and part was painted. He observed that the unpainted section of the sealant bead had shown severe deterioration and the joint had failed, becoming tacky and viscous and exhibiting deep cracks. However, the painted part of the same joint was not viscous and had none of the deep cracking. The painted sealant had not failed. Though not measured, it was assumed the temperature was similar in both the painted and unpainted parts of the joint. The conclusion is that a primary failure mechanism was UV radiation. The assumption is that the paint protected the sealant from UV rays but not heat. In contrast, the unpainted sealant at the top of the parapet wall received even more direct sunlight and more heat and completely deteriorated with only residues of viscous material left. The sealant on the back of the parapet (the north facing wall) was in very good shape—it experienced neither high heat nor direct sunlight. The key observation was that high heat alone was not enough to cause deterioration in a sealant where such a mechanism was previously thought to be a major deteriorating factor.

This observation gave the authors hope that the common sealants used in construction would produce damage at temperatures of up to 70°C that would be indicative of the potential damage at higher temperatures (80 or 90°C), though more slowly. Also, if the weathering occurred at 70°C through two-thirds of the weathering cycle, the time in the machine would compensate for the lack of the extremely high temperatures. Assuming the Arrhenius equation holds true—where often the issue lies in there, being several degradation mechanisms occurring at any given temperature—each of the mechanisms can be accelerated at a different rate (per differing activation energy) unless there is a situation where one reaction impedes all other degradation reactions. In this case the Arrhenius equation works as long as the rate-controlling reaction is first-order. It may simply be expected that sealants intended for high temperatures in real exposure would require that weathering machines be set to duplicate those temperatures. This would necessitate at least two types of weathering studies: One study in which the machine cycles at very high temperatures (80, 90, or even 100°C if that is what is expected in some climates) and another study in which the machine cycles at more moderate temperatures (70°C) to represent the alternative lower-heat circumstances.

The primary reason for an artificial weathering study is, predictably, to accelerate real life damage to anticipate material lifespans in various climates. Obviously, faster tests would be extremely useful. The forerunner in faster testing is the work at NIST under White [32] and the correlating outdoor studies being done by Williams. These studies use an integrating sphere to generate UV radiation many times the intensity of the noonday sun but without the extreme heat that generally accompanies such a high energy output. The studies are at a stage of focusing on reciprocity and verifying that damage created is close to that of real structures. If White and Williams are successful, it will be a huge advancement in rapid weathering tests and in the science of predicting lifespans of sealants in various climates. However, the tests are likely to be costly, and there are few facilities in the world where the tests can be run.

Some may not consider these circumstances too large a drawback—providing predictive weathering data in a reasonable time frame with such a

device might be considered an acceptable business cost, such that in the future every manufacturer of reliable products would provide such data. However, the tests remain costly and the future is not so predictable. Another factor to consider in testing procedure: The report by Carbary and Bridgewater showed that different colors of the same sealant deteriorated at different rates [33]. The study Vandereecken et al. [34] investigated changes in sealant because of pigmentation. This correlates to the Gorman observation that UV blocking is fundamental to longevity in some sealants. Different colors indicate the use of different pigments, all with different UV-blocking powers (often with different amounts of chemical sunscreens as well), and thus the rate of damage induced by UV absorption can differ with sealants of different colors even within the same brand. Thus, accelerated weather data (when selling a sealant) would have to be distinct for each color. For some manufacturers this would mean dozens of tests for each sealant in the line. Such an exponential expense could be prohibitive for some small manufacturers. It should also be noted that the effect of pigmentation has also been observed in silicone sealants (adhesion of clear versus pigmented sealants).

However, the more conventional weathering test using standard accelerated weathering machines referred to above, though the required time-span is greater, are not prohibitively expensive, and thus they might be the most reasonable method of determining durability.

Lastly, this discussion includes comments on joint dimensions and substrates to be used in testing. First we will consider substrates. Since in the field a common mechanism of joint failure is loss of adhesion, this requires some serious thought. At least one frequently used sealant shows little damage from heat or cold or sunlight but stiffens so severely that it commonly loses adhesion in a relatively short time on job sites with moving joints [4]. Along with this, the adhesion is quite variable with different surfaces. The authors' experience is that hardening with age and exposure is common with many sealants. Some adhere very well to glass but not on concrete, while others do well on aluminum but very poorly on glass and concrete. When studying durability in an accelerated test, it is prerequisite to consider all common modes of failure. If in the weathering chamber the sealant adheres well to aluminum but poorly to concrete, the data generated in an accelerated test on aluminum will be of little significance to the owner of a building made with concrete panels.

Consider four of the most common reasons for a loss of adhesion. One: The sealant continues to cure and gets harder with time. The forces generated at the bond line increase as the sealant continues to stiffen until at high repeated force, the bond strength deteriorates and an adhesive failure results.

Another reason for adhesion loss is that some sealants stiffen severely in the cold, and in the cold the joint is at maximum dimensions, putting a high stress on the bond line because the stiffness of the sealant in the expanded joint. Again, the bond line sees repeated or sustained high stress, and bond fatigue leads to bond failure.

Yet another common—possibly the most common—problem is that sealants are often exposed to rain, dew, frost, or sometimes immersion. Water is an aggressive chemical and will attack the bond between sealant and substrate. With water attacking the bond, it is generally not a question of whether the

bond will deteriorate but when it will happen. This is one reason that water must be an integral part of every weathering test.

The fourth common reason is the bond failure caused by installation errors, such as failure to properly clean or properly prime or sealant applied to a moist surface and any other conditions that can exist at the job site that contribute to bond loss. In designing an accelerated weathering test, one can account for cure, UV deterioration, water damage, and even stiffening from cold, but installation errors are beyond the scope of this study.

In addition to attacking the bond line, water—in conjunction with the heat and ultraviolet radiation—will sometimes attack the polymeric backbone or cross-links of the sealant and cause depolymerization. This was shown by Leonard and Malik [35] in what they called the “frog pond test,” demonstrating how a sealant could be made to turn to paste, yet another reason why water must be part of an accelerated weathering test. The damage created by water is almost always accelerated by heat. Thus, this mode of deterioration is well accelerated in a machine.

Relative to joint dimensions and design, there is also much to discuss. A new experimental joint design was introduced to ISO TC 59/SC 8 by Enomoto, Sugiyama, and others from the Japanese Sealant Institute [36]. Their very innovative joint design has the joint $20 \times 15 \times 100 \text{ mm}^3$, different from those used with ASTM C719 test joints and ISO 8339 test joints. However, their joint is then placed in a unique fixture that has a pivot in the center; the center dimension does not change, while the ends can be extended and compressed as the fixture is squeezed at one end and then the other. For example, when one end is compressed, the other is extended and the middle remaining at 20 mm. After some exposure, the compressed end can be extended, and the extended end compressed. This is a very good design for testing a range of movements on a single joint and a huge advance in the technology of joints for testing. However, when tears start at the end, they might continue toward the center point and cause more damage from tearing than might be seen with some lesser movements in standard joints.

Conclusions

To reiterate, the authors believe there is a need for a test method that uses conventional, lower cost, and readily available accelerated weathering equipment; expands the present tests and practices to introduce joint movement, heat, water, and UV; produces a procedure predictive of building sealant durability in multiple climates; and can be performed in a reasonable time frame and at a reasonable cost. If successful, manufacturers should also be able to test the various pigmented sealants and varying formulas during product development without prohibitive cost. Users of sealants could then reasonably request such data to show the appropriateness of a sealant for a given job and a given location. This test method should utilize the key learnings gained from previous studies as outlined in this paper.

References

- [1] RILEM TC139-DBS, "Durability Test Method—Determination of Changes in Adhesion, Cohesion and Appearance of Elastic Weatherproofing Sealants for High Movement Facade Joints After Exposure to Artificial Weathering," *Mater. Struct.*, Vol. 34, 2001, pp. 579–588.
- [2] ASTM C1519, 2004, "Standard Practice for Evaluating Durability of Building Construction Sealants by Laboratory Weathering Procedures," *Annual Book of ASTM Standards*, ASTM International, West Conshohocken, PA.
- [3] ASTM C719, 2005, "Standard Test Method for Adhesion and Cohesion of Elastomeric Joint Sealants Under Cyclic Movement (Hockman Cycle)," *Annual Book of ASTM Standards*, ASTM International, West Conshohocken, PA.
- [4] Sandberg, L. B., "Comparisons of Silicone and Urethane Sealant Durabilities," *J. Mater. Civ. Eng.*, Vol. 3, No. 4, 1991, pp. 278–291.
- [5] Karpati, K. K., "Investigation of the Factors Influencing the Outdoor Performance of Two-Part Polysulfide Sealants," *J. Coat. Technol.*, Vol. 56, No. 719, 1984, pp. 32–57.
- [6] Karpati, K. K., "Laboratory Fatigue Testing of a Two-part Polysulfide Sealant Correlated to Outdoor Performance," *Durability Build. Mater.*, Vol. 5, No. 1, 1987, pp. 35–51.
- [7] Karpati, K. K., "Performance of Polyurethane Sealants on a Strain—Cycling Exposure Rack," *Mater. Struct.*, Vol. 22, No. 127, 1989, pp. 60–63.
- [8] Jones, T. G. B. and Lacasse, M. A., "Effect of Joint Movement on Seals in Sealed Joints," *Durability of Building Sealants—Report 21*, A. T. Wolf, Ed., RILEM Publications, Bagnaux, France, 1999, pp. 73–105.
- [9] Linde, S., "A New Conditioning Method for Sealants," *Proceedings Pro027: Building Joint Sealants*, A. T. Wolf, Ed., RILEM Publications, Bagnaux, France, 1998, pp. 72–77 (e-ISBN: 235158015X).
- [10] Hutchison, A. R., Jones, T. G. B., and Atkinson, K. E., "Building Joint Movement Monitoring and Development of Laboratory Simulation Rigs," *Durability of Building Sealants, RILEM Symposium Proceedings*, A. T. Wolf, Ed., E & FN Spon, London, 1999, pp. 99–116.
- [11] Beech, J. C. and Beasley, J. L., "Evaluation of Cure and Durability Aspects of Building Sealants," *Science and Technology of Building Seals, Sealants, Glazing and Waterproofing, Second Volume, ASTM STP 1200*, J. M. Klosowski, Ed., ASTM International, West Conshohocken, PA, 1992, pp. 64–73.
- [12] Beech, J. C. and Beasley, J. L., "Further Studies of Cure and Durability of Building Sealants," *Science and Technology of Building Seals, Sealants, Glazing and Waterproofing, Third Volume, ASTM STP 1254*, J. Myers, Ed., ASTM International, West Conshohocken, PA, 1993, pp. 33–50.
- [13] Beech, J. C. and Beasley, J. L., "Assessment of the Durability of Building Sealants," *Proceedings of RILEM First International Congress, From Materials Science to Materials Engineering*, Chapman & Hall (Taylor & Francis), Oxford, 1987, Vol. 3, pp. 1178–1185.
- [14] Beech, J. C. and Mansfield, C., "Prediction of the Durability of Building Sealants," *Fourth International Conference on Durability of Building Materials and Components*, Pergamon Press, New York, 1987, Vol. 1, pp. 33–40.
- [15] Fedor, G. and Brennan, P., "Correlation of Accelerated and Natural Weathering of Sealants," *The Applicator, Sealants, Waterproofing and Restoration Institute*, Kansas City, MO, Fall 1990.

- [16] Boettger, T. and Bolte, H., "Results from the University of Leipzig Project Concerning the Long-Term Stability of Elastomeric Building Sealants," *Science and Technology of Building Seals, Sealants, Glazing, and Waterproofing: Seventh Volume, ASTM STP 1334*, J. M. Klosowski, Ed., ASTM International, West Conshohocken, PA, 1998, pp. 66–80.
- [17] Boettger, T. and Bolte, H., "Studies into the Long-Term Durability of Elastomeric Building Sealants—Final Report (Dumbbell Specimens)," *Durability of Building and Construction Sealants*, A. T. Wolf, Ed., RILEM Publications, Bagnaux, France, 2000, pp. 125–149.
- [18] Karpati, K. K., "Weathering of Silicone Sealant on Strain-Cycling Exposure Rack," *Adhesives Age*, Vol. 23, No. 11, 1980, pp. 41–47.
- [19] Karpati, K. K., "Investigation of Factors Influencing the Outdoor Performance of Two-Part Polysulfide Sealants," *J. Coat. Technol.*, Vol. 56, No. 719, 1984, pp. 57–60.
- [20] Fedor, G. R., "Usefulness of Accelerated Test Methods for Sealant Weathering," *Science and Technology of Building Seals, Sealants, Glazing, and Waterproofing, ASTM STP 1200, Second Volume*, J. M. Klosowski, Ed., ASTM International, West Conshohocken, PA, 1992, pp. 10–28.
- [21] Beech, J. C. and Beasley, J. L., "Effects of Natural and Artificial Weathering on Building Sealants," *Science and Technology of Building Seals, Sealants, Glazing, and Waterproofing, ASTM STP 1243*, D. H. Nicaastro, Ed., ASTM International, West Conshohocken, PA, 1995, pp. 65–76.
- [22] Wolf, A. T., Bolte, H., and Boettger, T., "Attempts at Correlating Accelerated Laboratory and Natural Outdoor Aging Results," *Durability of Building Sealants-State-of-the-Art Report of RILEM TC 139-DBS*, A. T. Wolf, Ed., RILEM Publications, Bagnaux, France, 1999, pp. 181–201.
- [23] Lacasse, M. A. and Margeson, J. C., "Movement During Cure of Latex Building Sealants," *Science and Technology of Building Seals, Sealants, Glazing, and Waterproofing, Sixth Volume, ASTM STP 1286*, J. C. Myers, Ed., ASTM International, West Conshohocken, PA, 1996, pp. 129–145.
- [24] Brower, J. R., "Deformation of Building Sealants Due to Movement During Cure," *Science and Technology of Building Seals, Sealants, Glazing, and Waterproofing, ASTM STP 1168*, C. J. Parise, Ed., ASTM International, West Conshohocken, PA, 1992, pp. 5–8.
- [25] Karpati, K. K., "Quick Weathering Test for Screening Silicone Sealants," *J. Coat. Technol.*, Vol. 56, No. 710, 1984, pp. 29–32.
- [26] Matsumoto, Y., "The Effect of Building Joint Movements on Outside Performance of Sealants During Cure," *Science and Technology of Building Seals, Sealants, Glazing, and Waterproofing, ASTM STP 1168*, C. J. Parise, Ed., ASTM International, West Conshohocken, PA, 1992, pp. 30–44.
- [27] Margeson, J., "Effect of Joint Movement During Cure on Sealant Strength," *Science and Technology of Building Seals, Sealants, Glazing, and Waterproofing, ASTM STP 1168*, C. J. Parise, Ed., ASTM International, West Conshohocken, PA, 1992, pp. 22–29.
- [28] Flackett, D. R., "Effect of Early Joint Movement on Oxime Silicone Sealants and Comparison of Other One Part Silicone Systems," *Science and Technology of Building Seals, Sealants, Glazing, and Waterproofing, ASTM STP 1200*, J. M. Klosowski, Ed., ASTM International, West Conshohocken, PA, 1992, pp. 299–310.
- [29] Lee, T. C. P., Jones, T. G. B., and Hutchinson, A. R., "Proposed Test Procedures Incorporating Dynamic Cure," *Durability of Building and Construction Sealants*, A. T. Wolf, Ed., RILEM Publications, Bagnaux, France, 2000, pp. 297–313.
- [30] ASTM C793, 2005, "Standard Test Method for Effects of Laboratory Accelerated

- Weathering on Elastomeric Joint Sealants," *Annual Book of ASTM Standards*, Vol. 04.07, ASTM International, West Conshohocken, PA.
- [31] Gorman, P. D., "Weathering of Various Sealants in the Field—A Comparison," *Science and Technology of Building Seals, Sealants, Glazing, and Waterproofing—Fourth Volume, ASTM STP 1243*, D. H. Nicastro, Ed., ASTM International, West Conshohocken, PA, 1995, pp. 3–29.
- [32] White, C. C., Hunston, D., and Tan, K. T., "Effect of Strain on the Modulus of Sealants Exposed to the Outdoors," *J. ASTM Int.*, Vol. 6, No. 2, 2009, paper ID JAI101954.
- [33] Bridgewater, T. J. and Carbary, L. D., "Accelerated Weathering and Heat Stability of Various Perimeter Sealants," *Science and Technology of Building Seals, Sealants, Glazing, and Waterproofing: Second Volume, ASTM STP 1200*, J. M. Klosowski, Ed., ASTM International, West Conshohocken, PA, 1992, pp. 45–63.
- [34] Vandereecken, P., Wolf, A. T., Bolte, H., and Boettger, T., "FTIR Spectroscopic Investigation of the Outdoor Degradation of Polysulfide Sealants," *Durability of Building and Construction Sealants*, A. T. Wolf, Ed., RILEM Publications, Bagnaux, France, 2000, pp. 243–258.
- [35] Leonard, N. E. and Malik, T. M., "The Relation Between Rheology, Artificial Weathering and Urethane Sealant Performance," *Science and Technology of Building Seals, Sealants, Glazing, and Waterproofing: Third Volume, ASTM STP 1254*, J. C. Myers, Ed., ASTM International, West Conshohocken, PA, 1993, pp. 21–32.
- [36] RILEM Technical Committee 190–SBJ (Andreas T. Wolf), "Recommendation of RILEM TC190-SBJ: Service-Life Prediction of Sealed Building and Construction Joints—Durability Test Method: Determination of Changes in Adhesion, Cohesion and Appearance of Elastic Weatherproofing Sealants After Exposure of Statically Cured Specimens to Artificial Weathering and Mechanical Cycling," *Mater. Struct.*, Vol. 41, 2008, pp. 1497–1508.

Jerome M. Klosowski¹ and Patrick D. Gorman²

New Weathering Test Method for Sealants and Preliminary Experimental Results

ABSTRACT: A new sealant weathering test method expands on existing test methodologies. In ASTM C719, repeated movement cycles were shown to be important to reproduce some of the damage seen on real buildings. Weathering tests done previously demonstrate that water, sunlight (especially the UV portion), and heat are all important degradation factors that act on real buildings. Thus this new test combines water, heat, light, and movement acting on a sealant joint, fabricated to an ASTM C719 joint configuration, in artificial weathering machines. The joints are also subjected to identical movement in four different climates. Correlations of the damage done to various sealants in four varied U.S. climates and the artificial weathering machines are explored.

KEYWORDS: accelerated testing, outdoor weathering, artificial weathering, sealants, fatigue, silicone, urethane, acrylic

Introduction

As stated in a previous paper [1], the most substantial problem with accelerated weathering sealant tests is that present tests do not closely predict lifetimes of some sealants the way the tests are done, i.e., in a static condition. It can also

Manuscript received September 14, 2009; accepted for publication October 12, 2009; published online November 2009.

¹ President, Chief Chemist, Klosowski Scientific, Inc., 3031 State Street Rd., Bay City MI 48706–1831, Engineering Diagnostics, Inc., 106 E. 6th St., Suite 620, Austin, TX, Scientist Emeritus, Dow Corning Corporation, 2200 Salzburg Rd., Midland, MI 48686, FASTM, Adhesives Age Award, 110 William Street, New York, NY 10038, SWR Institute, Honorary Member, 400 Admiral Blvd., Kansas City, MO 64106.

² President, Gorman Moisture Protection, Inc., 2115 E. Missouri, El Paso, TX 79903–3505, ASTM C24; First Vice-Chairman, SWR Institute, Past President, 400 Admiral Blvd., Kansas City, MO 64106.

Cite as: Klosowski, J. M. and Gorman, P. D., "New Weathering Test Method for Sealants and Preliminary Experimental Results," *J. ASTM Intl.*, Vol. 7, No. 1. doi:10.1520/JAI102734.

Copyright © 2010 by ASTM International, 100 Barr Harbor Drive, PO Box C700, West Conshohocken, PA 19428-2959.

take a long time to get meaningful data. There is a need for a test method that uses conventional, lower cost, and readily available accelerated weathering equipment; expands the present tests and practices to introduce joint movement, heat, water, and UV; produces a procedure predictive of building sealant durability in multiple climates; and can be performed in a reasonable time frame and at a reasonable cost. If successful, manufacturers should also be able to test the various pigmented sealants and varying formulas during product development without prohibitive cost. Users of sealants could then reasonably request such data to show the appropriateness of a sealant for a given job and a given location.

The goal of this study is to achieve the above stated objectives; it is not to compare the durability of various sealants.

Experimental Considerations

The following will frame the present study in progress that is reported here. In the study there are five silicones, seven urethanes, and one acrylic. Some of the sealants expected to be especially UV sensitive were tested in two colors: White, which is expected to be more stable, and beige, which is expected to have less pigmentation and be less stable. Recall that in the Carbary/Bridgewater study [2] and in the Gorman study, the more neutral colors (like beige and stone) had the fastest deterioration.

The study uses two different accelerated weathering machines (UV fluorescent (UVF) and xenon arc lamp) and four outdoor locations. The outdoor locations are Southern Louisiana (hot and damp), El Paso, Texas (desert Southwest—hot, dry, and with fairly high elevation), Denver, Colorado (extreme temperature changes and high elevation), and mid-Michigan (moderate UV, often wet, and mild to cool temperatures). The UVF uses condensed water, and the xenon arc lamp uses immersion for the water exposure.

The premise of the study is to use the four most prominent deterioration factors—heat, water, UV, and joint movement—and to have the same movement on both machines and in all four weathering sites. The same movement is accomplished both outdoors and in the machines by expanding the samples by hand, blocking them open, holding them in the extended position for the desired time, then compressing them to the as-cured position for the desired time, and then putting the samples into compression. The movement cycle chosen for the outdoor samples corresponds with the start of each season (based on the seasonal calendar of the United States) so that in the Winter, the samples were extended and held open with spacer blocks (Fig. 1). On the first day of Spring, new blocks of the original dimension were inserted (Fig. 2). For the first day of Summer, however, a screw is used in a threaded substrate to bring the samples together and hold them compressed (Fig. 3). Then, on the first day of Fall, the compression is released and the original size spacer was inserted. The samples were then tested, and on the first day of Winter, they are again extended to begin another cycle.

The samples in the weathering machine (Fig. 4) change position every 2 weeks for a complete cycle of 8 weeks. Note that sealants are generally incom-

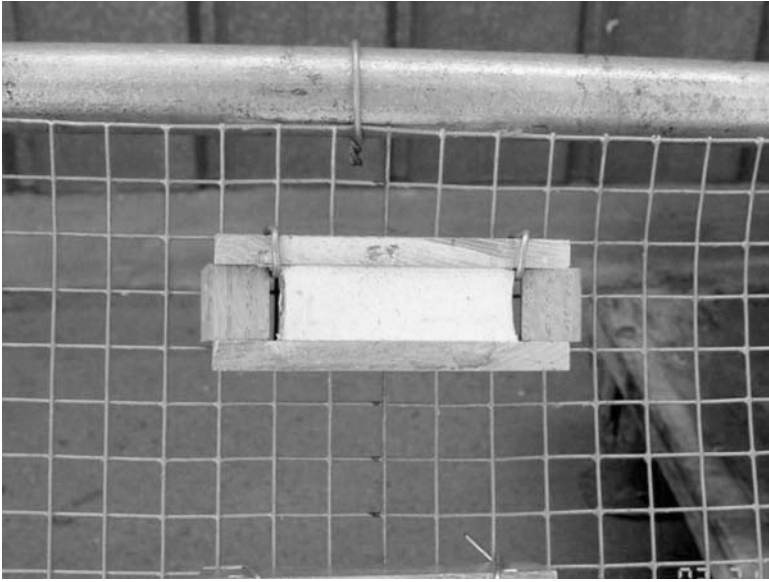


FIG. 1—*Spacer blocks in samples.*

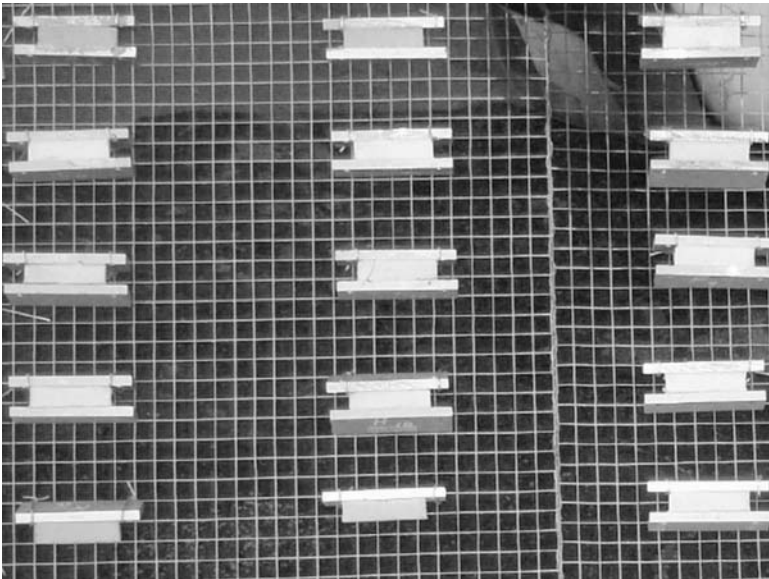


FIG. 2—*Samples in the relaxed spring and fall position.*



FIG. 3—Setting compression with screw.



FIG. 4—Two weathering machines.

pletely cured after 3 weeks of typical ASTM cure or 4 weeks of ISO curing regimes. They continue to cure as they are put into extension or compression in the weathering machines or put on the outdoor racks at the start of their exposure. If an incompletely cured sealant is taken into compression in this initial after-cure exposure, it will typically achieve a compression set, and these will then generally perform more poorly during cycling. If, after cure, the sealant is put into extension as its first after-cure exposure, it will sometimes achieve an extension set, though that is much less difficult for the sealant as it goes through subsequent extension and compression cycles. In order for as many sealants as possible to survive for correlation data, the authors began weathering in extension mode.

Outdoors the complete cycle is 1 year, changing the position each quarter. This means that samples in the weathering machines are held in a given position about one-sixth as long as those on the outdoor racks. The authors estimate peak sunlight as typically less than 2 h/day and highly damaging sunlight, less than four. Thus, a machine that reproduces the intensity of peak sunlight at 16 h/day is accelerating the UV factor close to six. This does not suggest that the acceleration of all damage is a factor of six, but rather the total radiation measured at 340 nm is approximately a factor of six.

In real conditions, water is present in many forms in the joints. There is potential for dew, which can last all night or not occur at all, and there is also the potential for rain, which is extremely variable. Water, in some form, is a likely factor on most jobs. If the machines are set for water exposure one-third of the time, it is not a huge stretch on reality and might be a two to six times acceleration compared to real exposure. However, when one adds 40°C of heat, the acceleration due to the presence of water should be at least a factor of six. Substrates temperatures are often greater than 40°C, but typical weather conditions for water exposure (such as cloud cover during rain) tend to produce an instantaneous cooling to the joint components (including how, after rain, the initial evaporation will also keep the sealant cooler than temperatures one sees on the sun heated surfaces). Thus, having 40–50°C water results in a substantial acceleration factor relative to water damage. Considering this, the UVF was set to 8 h of condensation per day at 40°C.

The xenon arc lamp uses a different cycle dictated by practicality and not science. For comparative results between the two machines relative to the damage on the outdoor racks, it would be reasonable to also use the above rationale with the xenon arc lamp, but matters are complicated in that it typically has a cycle of 102 min of UV light with heat, followed by 18 min UV light with water spray or water immersion. These machines are relatively expensive, and some believe no one would change the machine to handle the unique conditions for the occasional testing of a sealant. Because of this, the 108 min of light and heat, followed by 12 min of light, heat, and water occurring in the ASTM C1442 [3] weathering standard were used.

The heat in most of U.S. climates reaches 70°C or higher on dark surfaces. The heat is most intense during a 2–3 h span in the afternoon. As earlier mentioned, holding samples at 70°C for 16 h of the day is an acceleration factor between five and six (comparative to some climates, the acceleration is greater when considering milder climates). This can be considered a rather crude as-

sumption, as the heat transfer to the sealant is quite different between samples in a convection-controlled oven and an actual service joint. Bulk and surface temperatures show different time dependencies in such exposures. In this study the UVF machine was held at 70°C for 2–8 h cycles per day.

The most difficult consideration was the amount of movement the sealant should experience. Initially the test began with all sealants, during the first weathering cycle, opened to the maximum stated in the manufacturer data sheet. When the sealants were held for 2 weeks at the maximum extension, nearly half of the samples started to show some degree of adhesion loss. This had caused the experiment to be stopped, and the amount of movement imposed re-thought. There were three key considerations. First and foremost was that the primary purpose is not to test products to the limits suggested in their data sheets but to develop a test method. Second, the work must stress and strain the sealants sufficiently so that damage is produced in both the laboratory and at the outdoor sites so that correlations can be developed. Third, the majority of the sealants needs to be able to survive the test for several cycles to achieve desired correlations. Slight damage is difficult to compare and correlate; severe damage is much easier to compare and correlate. The most convincing reason not to use the full movement amplitude is that a sealed joint will only be exposed to the full movement over the period of 1 year. Obviously, there are locations (such as Singapore) where the diurnal and annual cycles are almost identical; however, for most locations away from the equator, the diurnal cycle is closer to 1/2 of the annual cycle amplitude.

The redesign of the test was primarily rationalized on the ideas that a sealant, when installed at the lowest temperature in the year and when the joint is fully opened, exhibits all its movement in compression and will see no extension. A sealant installed in the maximum heat of summer, when the joint is at its most closed position, will see all of its movement in extension but with no compression. If the sealant is installed at some intermediate temperature, as is most common, it will experience some combination of extension and compression. Thus, if the typical manufacturer's recommendations are followed and a $\pm 50\%$ sealant is used, it often will not see any more than a total of 50% movement. It can all be in compression, all in extension, or, most commonly, in some combination of the two. In the field it is generally not a total of 100% but a total of 50%. In the ASTM specification ASTM C920 [4], a $\pm 50\%$ sealant has to perform at $\pm 50\%$ for a total of about 100% in the ASTM C719 [5] joint movement test. Similarly, in ISO Specification 11600 [6] a sealant rated for class 25 would have to pass at $\pm 25\%$ movement in the joint movement test ISO 9047 [7]. Thus, for test development, the movement is chosen as $\pm 25\%$ for a $\pm 50\%$ sealant and $\pm 12.5\%$ for a $\pm 25\%$ sealant. The UVF is set for 8 h of UV at 0.87 W/m²/nm at 70°C, followed by 4 h of condensation at 40°C. The xenon arc lamp is set for immersion at 20°C for 18 min every 2 h, and a continuous radiation of 0.51 W/m²/nm. The compression/extension state of the joint is changed every 2 weeks starting with extension, returning to neutral, and then compression. The joint again returns to the neutral position but undergoes a physical property test after each complete 8 week cycle. In the outdoor testing, the joint configuration is changed every 3 months, and the physical properties are measured annually.



FIG. 5—Polyethylene foam backing.

Displacement at a given load was measured initially and again after each complete weathering/movement cycle. The load (stress) varies with the modulus of the sealant, varying from 0.03 N/mm^2 (3.4 g/cm^2) to 0.20 N/mm^2 (28.5 g/cm^2). The displacement at a given load is easily measured after 30 s in any laboratory with a normal stress and fatigue setup and does not require a machine that measures load at a given displacement. In the end, the tests use conventional low cost weathering machines and simple low cost testing devices.

Procedures

Samples were prepared using anodized aluminum cleaned sequentially with toluene and heptane. Each solvent was wiped on with a cotton ball and off with a paper towel. The one-part sealants were extruded directly into joints that were rectangular in cross-section, 6 mm (1/4 in.) in depth, 12 mm (1/2 in.) in width, and 50 mm (2 in.) in length. The backing material was partially closed cell polyethylene foam of rectangular cross-section (Fig. 5). The surfaces were primed or not primed according to the manufacturer's recommendations.

As stated, the one-part sealants were extruded directly into the cavity. The two-part sealants were mixed in a DAK 150 mixer³ for two 16 s mixes, with a scrape down between each mixing. These sealants were extracted from the mixing cup with a modified 10 cm³ syringe and extruded from the syringe into

³FlackTech, Inc., 1708 Highway 11, Bldg. G, Landrum, SC 29356.



FIG. 6—*Strain testing.*

the joint. This procedure was determined after several procedures were evaluated, and this seemed to yield the most air-free sealants. The sealants were cured statically for at least 3 weeks in ambient conditions.

After the samples were cured and before they were put in the weathering machines or on the weathering racks, they were tested by hanging a specific weight (Fig. 6) from the joint for 30 s and recording the strain (elongation) for a given stress. This process is then repeated after each exposure cycle. Since the authors began this procedure in the Winter months, the samples were placed on or in the respective testing locations and devices while in extension.

Results and Discussion

The experimental procedure followed the plan almost perfectly until stressing started. The original plan was to take each of the sealants to their advertised maximum movement ability. However, when the original 21 samples of the first sealant to be placed on the rack were extended, they stood overnight and then



FIG. 7—Failures after the first extension at half the rated movement.

broke adhesively, as did some of the others. The samples that broke were re-made, and the experiment continued with all samples extended to half of the rated movement instead (which is the expected movement on a typical building), and by the end of extension in the first cycle, four of the 14 sealants failed adhesively (Fig. 7). This was true in both the weathering machine and on the outdoor racks. This was an unacceptable result in some aspects since it defeated the purpose of showing the increased acceleration of the proposed new weathering test using the movement as part of the weathering cycle. In another aspect, this result showed the value of introducing movement in the weathering cycle since adhesion is a common factor in job failure; the failures that occurred would show up on the job but probably not in the standard weathering tests or tests in the standard specifications without sustained and repeated joint movement.

The manufacturers of the failed sealants were contacted, and each recommended a modification (priming or change of primer) of the joint preparation procedure. New specimens of the failed sealants were added to testing. The test development proceeded with samples of ten sealants undergoing five complete cycles in the machines and three complete cycles of the outdoor testing. In addition to the test joint samples, small slabs of each sealant were made, cured, and placed on the field test racks alongside the test joints, as well as in the UVF. These are tested for indentation (durometer) after each weathering cycle since measuring durometer from a test joint is very difficult. Also, some of the sealants underwent substantial shrinkage during cure and thus presented a concave surface, which again is not amenable to measurement with the available gauge. To compensate, flat slabs were made, cured, and weathered (statically)

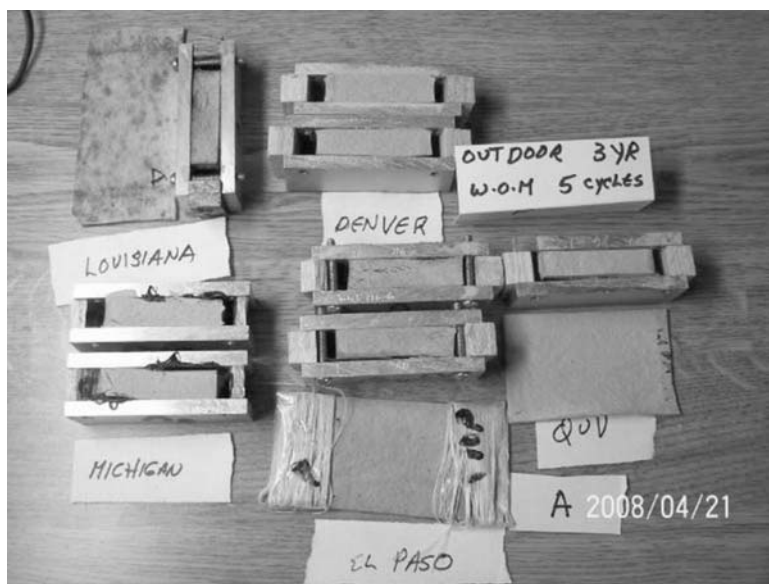


FIG. 8—Sealant A: Beige urethane one part.

so the durometer gauge could be used. However, there were no small slabs placed in the xenon arc lamp since the sample area could only accommodate a few samples and that space was used for sealant joints that would be forced into expansion and contraction, changing positions every 2 weeks.

Observations

Sealant A

With the urethane labeled Sealant A (Fig. 8), the adhesion did not withstand weathering well, which would not be seen with a static conventional weathering test. This same sealant was tested in the Sandberg study [8]. This result demonstrates that the procedure suggested here—with movement during weathering—is not just beneficial but fundamental to the user to evaluate the durability of this product. This is the first and most important conclusion of this paper. The third year of outdoor weathering, with movement, showed deep cracks progressing. This was not possible to note when the joints failed in adhesion, which almost all did. Some were repaired with an adhesive and the test continued. Adhesion loss is in fact the experience of both authors with this sealant on actual job sites. Sealants often fail primarily in adhesion, typically early in their service life. However, on the occasions where adhesion survives, cracks form and then progress through the joint over the course of several



FIG. 9—Sealant B: White urethane one part.

years. Thus, the outdoor racks, with position change each quarter, reproduced real-world experience. This was the anticipated result and indeed is what was realized.

With reference to the correlations between artificial weathering machines and outdoor racks (with the samples that survived), the only comments possible are relative to the static slabs since the joints continued to fail adhesively and thus were not able to be held in extension while weathering. With the static weathering slabs, it took about five cycles in the UVF to achieve hardness changes similar to that seen in the field over 3 years. Also note that for this particular sealant, the physical changes were similar in each of the geographic areas. The only climate-unique feature was that the Louisiana samples had considerable (approximately 50 % of the surface) mold covering and the specimen exposed in El Paso had a thin layer of dust. Similar results across climates were not expected and are not common. In terms of time-line, an estimate of the acceleration in the UVF to the outdoor damage was approximately four.

Sealant B

Sealant B in this study was also a urethane, but a slow curing one, that also resulted in cracks and creases (Fig. 9). These creases progressed through the samples in all environments. The UVF exposure was particularly hard on Sealant B, with blisters starting to form on the slab after five cycles, and cracks eventually had progressed to produce cohesive failure. This sealant was unique. When unstressed in the slab, there was a gradual hardening of the rubber with the durometer increasing from almost 100 % in the very hot climates and at

least 25 % in the more temperate climates. The perplexing observation to follow was that the sealant joints became more pliable with movement and weathering, and the strain under load increased by 100 % or more in the course of 3 years outdoors. The slabs became harder but the joints became softer. If weathering had not corresponded to joint movement, the true nature of this sealant and its rapid change in performance would never be recognized.

The UVF, after two cycles, showed joint damage and change in rubber performance comparable to that seen in 3 three years of outdoor exposure. Again, damage was comparable in each climate. This means acceleration in the UVF was about ten. The slab samples in the UVF started to bubble after five cycles. The xenon arc lamp had comparable change in rubber after 3 years, meaning an acceleration factor of approximately 6 or 6.5 when comparing this data to the rubber properties of the outdoor samples from any of the sites.

Esthetically (which may be significant for a particular job site), the white sealant appeared almost as expected, based on previous experience. The El Paso samples were covered with dust, resulting in a brown or gray appearance, tending towards dark gray. Louisiana samples were almost as dark but covered with mold instead of dust. The Denver samples were not quite as dark with dust as those exposed in El Paso. Michigan samples had approximately half of the mold of samples in Louisiana (which is to say, a quarter of the Michigan sample was covered). The UVF samples had turned from white to beige, but the xenon arc lamp samples were near white.

Sealant C

Sealant C was also white urethane (Fig. 10). In outdoor weathering, dampness is a factor of change, demonstrated by the Louisiana samples, which softened with weathering and movement and showed the greatest strain. Next in strain were the Michigan samples, and Denver and El Paso samples are comparable. All outdoor samples seemed in relatively good shape and relatively white. The wet climates of Louisiana and Michigan yielded light mold, and the dry climate samples were covered with light dust.

As to acceleration of weathering, the xenon arc lamp samples had substantial softening at three cycles—about the same as the El Paso and Denver samples. Sealant C was useful for this study since changes were substantial, but also the samples did not fail. For these climates the acceleration of the xenon arc lamp was approximately six. Note that the third, fourth, and fifth cycles of the xenon arc lamp had relatively constant data, indicating that perhaps the system was in some kind of equilibrium. Note also that the xenon arc lamp had a 102/18 cycle, with water exposure approximately 15 % of the time, much like El Paso and Denver, but different than Louisiana and Michigan. It might be that the xenon arc lamp has an acceleration of six for the Denver and El Paso areas but would not be a good device to simulate the weathering effects on the sealant unless the wet/dry time is adjusted for accuracy concerning the area of interest.

The UVF effects were unique in that the sealant turned from white to medium brown and the backside of both the sealant slab and the joint became very tacky and weak. After movement, cracks quickly propagated through the

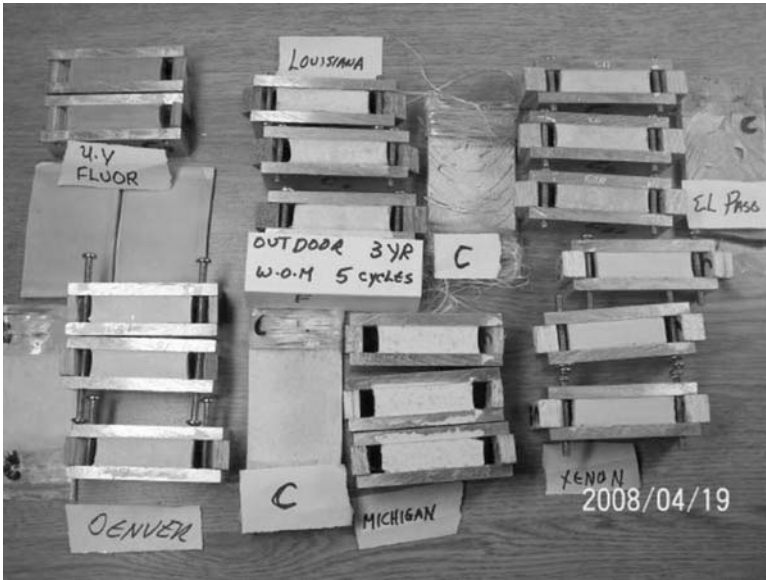


FIG. 10—Sealant C: White urethane one part.

sealant and perhaps in another cycle would have achieved total cohesive failure. Since the damage from the UVF is not indicative of results from yet-*as-seen* outdoor damage, it might be that the UVF accelerates damage to this product with a factor of 20 or more, or it might be that the device is not a good accelerating tool for the specific sealant's chemistry. An answer is only determinable with more years of outdoor exposure to find if the machine damage is eventually duplicated outdoors.

Sealant C was the esthetically "cleanest" in all locations, with El Paso showing some dust for a light gray look, and the Louisiana samples having a light gray appearance due to mold. Michigan samples had gray mold spots but were lighter than Louisiana samples. Denver had some dust, though lighter than El Paso.

Sealant D

Sealant D was a white silicone (Fig. 11). The outdoor joint samples with movement in all four locations showed no change in performance, with essentially no change in strain with the given stress. However, the 3 years of static exposure of the sealant slabs demonstrated a moderate hardening in Michigan and Denver, no change in Louisiana, and moderate softening in El Paso. The changes to date are small and might not be significant. Extending the study will provide further insight.

The joint samples in both weathering machines did reveal some slight lowering of modulus—a greater strain for the given stress. The UVF required three cycles for the softening to occur, whereas the xenon arc lamp showed such

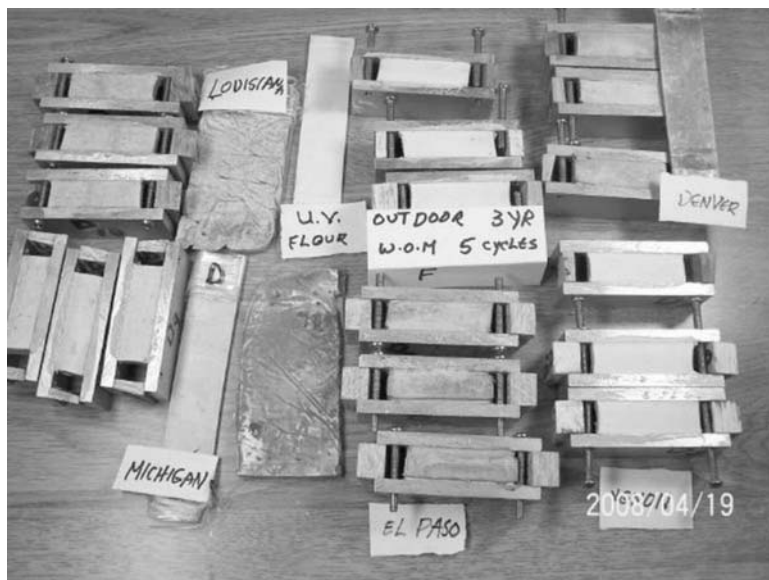


FIG. 11—Sealant D: White silicone one part.

results after the first 8 week cycle. It is interesting to note that once the change was realized, further cycles in the weathering machines did not cause subsequent change. Since there have been no definitive steady changes to note, it is not possible to define a correlation factor with this sealant—a much longer time of both outdoor and machine weathering would be needed.

Returning to esthetics, dust was a problem, more so than for urethanes A and C and less so than for urethane B. The El Paso samples had heavy coatings of dust (resulting in brownish gray coloring), followed closely by the Denver samples in similar appearance, though lighter, and the Louisiana sample was lighter and the Michigan lighter still (just a hint darker than the samples from the weathering machines).

Sealant E

Sealant E was a white urethane (Fig. 12). Hurricane Katrina affected the results for this sealant, as the Louisiana joint samples were lost after the adhesion failed. The sealant joints in the xenon arc and UVF weathering machines failed in adhesion during the first cycle, though the samples were glued back together in efforts to obtain correlation numbers relative to rubber properties. The Denver samples also failed in adhesion and were glued. All samples, joints, and slabs in all locations showed severe weather cracking and crazing. The surviving joints in Michigan, Denver, and El Paso all had similar rubber changes (softening) and nearly a doubling of strain with a given stress. The outdoor weathering of the unstressed slabs was interesting—the El Paso and Denver



FIG. 12—Sealant E: White urethane two parts.

samples softened, while the Michigan and Louisiana rubber slabs showed no change in hardness, and all outdoor samples had severe crazing.

The slab in the UVF began to bubble by the third cycle, and by the fifth cycle there was a soft froth with a Shore A durometer much too low to measure. There are no possible correlations of any kind here. To find a correlation factor to the weathering machines with this sealant, the study would have to be restarted, and a different stress-strain measuring device instead of the strain-stress device would be required. Also, the adhesively failed samples could be repaired, or the manufacturer could provide yet a better primer.

The repair of urethane sealants with failed adhesion was accomplished by wiping the surface of the substrate using two wipes with a paper towel wetted with toluene. Then commercial urethane glue was applied, the joint put back together, and held with a clamp for at least 1 week before put back into testing. The repair of the silicones was accomplished with a high strength silicone structural glazing sealant using the technique noted above. The urethane samples, in most cases, failed again in adhesion in the next weathering cycle and for the second time were instead repaired with the structural silicone mentioned above. This repair also failed in most cases.

Esthetically, the dust on the El Paso samples for Sealant E was very thick and consequently had the least crazing of the field samples. The Denver samples had less dust and very severe crazing in the intense UV. Louisiana samples had little dust but along with Michigan samples had mold to give a medium to dark gray look, but the Louisiana samples had more crazing than those in Michigan.



FIG. 13—Sealant F: White silicone one part.

Sealant F

Sealant F was a white silicone (Fig. 13). It was a very low modulus sealant and in all outdoor locations and the UVF demonstrated hardening, though in all cases was still soft and low modulus. The Denver and Michigan sealants demonstrated the hardening in the first year after cure, as did the UVF samples in the first weathering cycle. The Louisiana and El Paso sealants had this hardening during the second year of weathering. In all cases there were no further changes or other damage to be noted. The xenon arc lamp samples softened in the first weathering cycle and stayed that way. The immersion aspect of the xenon arc lamp may be the cause of the incongruent softening. Since there is no change over time to note, a correlation is not possible with Sealant F. Again, a researcher would expect to extend the study for a much longer time.

The Louisiana sample appeared almost entirely black with mold. The El Paso sample was light beige with dust, as was the Denver sample. The Michigan sample had a sprinkling of fine black mold spots—at a distance, it would look appear light gray.

Sealant G

Sealant G was a white urethane (Fig. 14). Following the manufacturer's recommendation, no primer was used. All joints failed in adhesion in the first machine cycle or the first year of outdoor weathering. None were saved. However, some data was gleaned from the weathered slabs of sealant.

The slab in the UVF became substantially softer in the first cycle and stayed that way through five cycles. The outdoor slabs either remained relatively un-



FIG. 14—Sealant G: White urethane two parts.

altered or became harder in the first year. As for the third year outdoors, there were no changes in the slabs as all changes occurred in the first year. Here as well, no correlations can be made since the changes were either minimal or did not progress with time. To determine a correlation factor, joints with durable adhesion must be made and the times of the study lengthened.

Esthetically, the Michigan and Louisiana samples had some mold, with the Louisiana sample having more crazing than the Michigan sample. The El Paso sample had a brown tint from dust, as did the Denver sample, though the Denver sample was closer to a cream color. The sample from the UVF was beige. Comparatively, this batch had a relatively “clean” appearance. However, there is no plan to rate samples relative to esthetics; it is merely noted for consideration.

Sealant H

Sealant H was a white silicone (Fig. 15). In all exposures the joint samples first softened then stiffened. Michigan, Denver, and El Paso samples all had minor softening before stiffening. They remain nearly at initial values, and it will be interesting to observe their progress in subsequent years. The Louisiana samples softened more than the others in the first year and have not yet fully recovered. One Louisiana sample lost adhesion.

The xenon arc lamp samples softened to a greater degree, much like the Louisiana samples, and after five cycles have not yet fully returned to original stiffness. Samples across all tests for Sealant H are continuing to harden and have not hit a plateau. If the span of time required for a sealant to return to its



FIG. 15—Sealant H: White silicone one part.

original strain values was used as criteria for determining an acceleration factor, then the UVF would have a factor of 2.5 relative to Michigan, nearly the same for Denver, and four for El Paso, but the Louisiana data has a variability that makes it impossible to determine a factor at this time. The xenon arc lamp has yet to yield samples which returned to original strain values, so its acceleration factor relative to the outdoor locations cannot be determined.

Judging esthetics of Sealant H, the Denver and El Paso samples were both darkened with dust. Michigan and Louisiana samples had nearly equal amounts of mold and a brown color—lighter than the dusty samples of the other locations.

Other than the one sample with an adhesion problem, there were no visible flaws in the samples, and correlations must be based on changes in rubber performance after longer exposure beyond this 3 year data.

Sealant I

Sealant I was a beige urethane (Fig. 16). All samples lost adhesion early. These were not repaired (as had been attempted with other sealants), but the study continued with the slabs. As before, only Shore A durometer and appearance were studied with the slabs. The Louisiana and El Paso samples showed a slight softening in the initial year. The Denver sample showed almost no change in the first year, and the Michigan sample hardened slightly, as did the UVF sample. However, after the first year the samples remained constant in hardness.

At the time of collecting data for this study, the Denver sample was very



FIG. 16—Sealant I: A two-part beige urethane.

clean but had some crazing of the surface, though relatively minor. The El Paso sample was coated with brown dust and had no noticeable crazing—it is possible that the heavy dust layer protected it from UV damage. The Louisiana sample was between gray and beige with visible mold and minor crazing. The Michigan sample had less mold—appearing as a peppering of gray particles—and minor crazing was present. The UVF samples became tacky but had no visible crazing.

There is no correlation of damage to be found with either the joints or slabs. Similar to the results of other sealants, in order to obtain further and more accurate data, this series would need to be redone with the adhesion tested and optimized before the start, and repairs made considering the adhesion had failed. The softening of the UVF samples is a possible indicator of long-term problems in a moving outdoor joint.

Sealant J

Sealant J was acrylic latex (Fig. 17). This sealant, like many of the others, lost adhesion quickly after the advertised movement; however, at half of the movement level, it performed quite well. At first touch it seemed hard, and it is, but a stress relaxation followed and the sealant softened somewhat. The overall trend for Sealant J was hardening with time and movement. Joints that opened to between 15 % and 20 % with a given weight after 1 month of cure would then typically open only near 5 % and often less after 1 year or more of outdoor weathering. For this sealant, correlations cannot be made for want of more precise execution in testing.



FIG. 17—Sealant J: White acrylic one part.

The hysteresis of this sealant makes sample-to-sample comparisons difficult unless the experimental technique is very carefully controlled. Specifically, the time following the release of compression or extension must be closely controlled, as the progress to the original cured position is slow and steady. This influences the strain/stress data. With durometer readings, the technique must be very precise—the time to take the measurement is controlled to the second. For each sealant the durometer was noted when measured in the first few seconds of contact. However, Sealant J showed a rapid drop as the durometer gauge was set on the sample; thus the gauge was kept in place and durometer measured at intervals. The durometer dropped approximately ten points in the 10 s that followed and approximately another ten points over the next 20 s.

Surface crazing was present and progressing slowly in the Michigan and UVF joint samples. The UVF samples were clean, as expected, and the Michigan samples were gray with dust and mold, still permitting almost full UV on the surface. The Denver samples were medium brown with dust and the crazing was less. The El Paso samples were darker with dust, and the Louisiana samples were very dark, though with mold more than dust. In each case the covering on the sealant prevented more crazing from occurring.

Accordingly, the second reason for a lack of correlation in this study is due to all or almost all field samples holding dust and dirt or growing mold, resulting in variable performances. Doubtlessly, all accelerated studies must impose extension and compression stresses to help produce crazing. In actuality, a true correlation is extremely difficult considering there are at least two deteriorating mechanisms at work: One being the hardening chemistry and the other the UV influence, which can be at least partially blocked by dust. However, the UVF



FIG. 18—Sealant K: *Beige urethane two parts.*

and the xenon arc lamp both show the same trends as the field samples, and with several more years of outdoor weathering—or the imposition of higher strains—to produce more damage, correlations would be easier to make.

Sealant K

Sealant K was a beige urethane (Fig. 18). Of 18 joint samples using this sealant, only one did not lose adhesion and even then only because it had been glued together after failing on the second yearly cycle in the same manner as detailed with other sealants. Thus, no moving joint correlations can be made to the weathering machines. Also as before, further studies require closer work with the manufacturer and a better primer.

The slabs remained in testing and a unique result occurred: The UVF slab started to bubble, near to frothing, at its center. This bubbling is inconsistent with outdoor weathering for all samples. Note, however, that the UVF samples underwent five weathering cycles in the machines, but the slabs underwent only three outdoor cycles. Sealant K could be particularly sensitive to UVA energy, and the cumulative effect of the outdoor exposure had not yet matched that of the machine. It would mean that UVF machines have a very large acceleration factor with this material.

Focusing on durometer, the UVF samples softened at first, then slowly returned to original hardness in the course of five weathering cycles—recalling that hardness could only be measured at the edges of the slab where there was no bubbling. After three years of outdoor weathering the outdoor samples show very little durometer change.



FIG. 19—Sealant L: White silicone one part.

For Sealant K, the El Paso samples were dark brown with dust and the rubber's physical change in color. The Denver samples were comparably lighter, with similar color change but less dust. Louisiana samples were more closely matched to the El Paso samples in color change but with mold growth instead of dust. The Michigan samples were lighter with less color change, less mold, and minimal dust.

Sealant L

Sealant L was a white silicone (Fig. 19). There was neither adhesion loss nor surface damage. For rubber performance, the modulus softened slightly in all outdoor samples—Louisiana the most and the machine-weathered samples even more so. The machine samples' softening occurred during the first 8 weeks of cycling, with no further change during the other five cycles tested. Until more damage or more change occurs, no correlation can be made.

For hardness, the samples in the UVF machine softened during the first cycle, further in the second cycle, experienced no change in the third cycle, then hardened in the fourth and again in the fifth cycle—some returning almost to the original hardness. Such softening was typical, but changes were small and thus elicit little confidence, added to a lack of region-specific distinctions. All regions tested exhibited similar behavior. A much longer study is needed.

Based on previous trends, esthetics were predictable. The El Paso samples were dark brown with dust; the Denver samples were the next darkest with

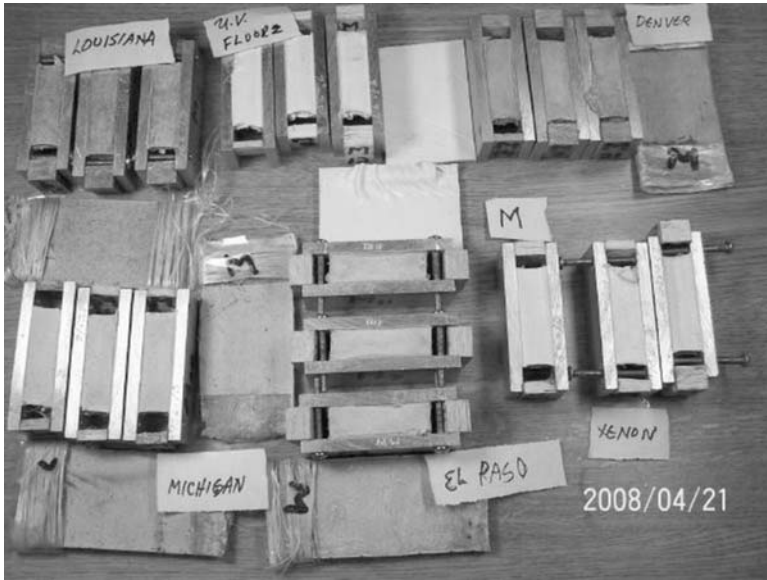


FIG. 20—Sealant M: White silicone one part.

dust. The Michigan and Louisiana samples grayed with mold, though the Louisiana samples had mold that was less evenly distributed and more easily wiped off.

Sealant M

Sealant M was a white silicone (Fig. 20). None of the samples exhibited adhesion loss or surface checking. All outdoor samples hardened, generally only from 3 % to 7 %. The UVF sample softened in the first cycle and then did not change. The xenon arc lamp samples showed no change for all five weathering cycles. There is no correlation as of yet. Hardness increased with all samples, though the outdoor samples hardened at a faster rate, meaning a negative acceleration factor, if possible.

Samples of Sealant M would have yielded the most esthetically successful results overall, except the Louisiana sample was dark gray with mold. The other locations had only negligible dust or mold.

Conclusions and Discussion

One of the primary results from this study is the realization that a second more controlled study would refine data and permit more absolute conclusions. The damage of many sealants was minor enough that the acceleration factor could not be estimated. Other sealants demonstrated a wide range between each other, with factors as low as two for some and as high as ten or 12 for others.

Excepting esthetics, the weathering machines do accelerate outdoor weath-



FIG. 21—*Laboratory.*

ering, but in the conditions used in this study, each resulted in different acceleration factors from each other. This is expected in that there was a difference in heat and water exposures in the two machines. The original plan had the two machines as identical as possible in heat exposure, water exposure, time, and cumulative UV radiation. However, the practical concerns stated earlier (the assumption that adjustments to the machines would not likely be made, as they deviate from ASTM suggested settings) prompted differences—assuring variations of acceleration factors for materials sensitive to the combined multiple variables of weathering. Some sealants also showed unique degradation in the UV weathering machine not duplicated in the xenon arc lamp or the outdoor sites in the length of this study.

Among the sealants tested were those, all of the same generic type, that performed well both outdoors and in the machines (Figs. 21 and 22). With sealants like these, correlations between outdoor and accelerated weathering need longer test periods to produce significant damage or more precise testing. On the other hand, others showed major deterioration despite the relatively short duration of the study given their intended purposes. However, some of the same generic class were still performing adequately throughout this study. This study emphasizes that there are no possible generic generalizations relative to durability, adhesion, or esthetics of a urethane. It could also be true of silicons, but longer exposures are needed for such a conclusion. It seems that generalizations in generic types relative to durability in given climates are difficult, near impossible, where the stability of a sealant depends on the concentration or types of additives, as is the case with the urethanes. Thus with such



FIG. 22—Weathering machines.

formulation-sensitive products durability needs to be studied product by product and color by color.

A significant complicating factor in the correlation of outdoor to accelerated machine testing is the variability in UV protection from dust and mold on the outdoor samples. The remedy to that is not apparent to these authors.

The next generation of this test should include more than one type of acrylic and several sealants with polyether polymeric backbones that cure with an alkoxy silane end. Fewer urethanes are recommended but should represent both contrasting levels of durability since they demonstrated largely different chemistries. There should be fewer silicones as well, and all sealants require more precise property measurements since changes in this study were at times small and slow to appear.

Some parts of the test regime need changing, such as after each year of outdoor testing and each cycle of artificial weathering, the sealants should be tested in a tensiometer, measuring stress with a given strain, instead of strain with a given stress, as in this study.

Movement during weathering was a primary factor in real-time and accelerated testing and a principal cause of the damage indicative of real job situations. This experiment proved that periodic movement is an acceptable way of achieving such, and thus a lower cost test method is possible compared to a machine that has continuous movement built into it. This study proved again that movement during weathering is necessary in any accelerated or real-time sealant tests. This study suggests that weathering without movement is not only less effective but also results in false indications of durability. This cannot be emphasized too strongly.

The degree of movement that each sealant is subjected to will be determined by the purpose of doing the durability testing. If the testing is to compare several sealants all at the same joint movements, the above test with the modifications suggested could be ideal. The results show that any amount of movement can be used in the testing, but movement ability is not separable from adhesion. This study demonstrates the real-world problem of adhesion as the primary cause of premature sealant failure with many sealants. Adhesion is highly sensitive to the degree of stress applied, which is related to the degree of strain (joint movement). The procedures outlined here are acceptable as official test methods for societies such as ASTM or ISO or for specific applications like sealants in buildings or highways. When specifying the amount of movement needed in any provision, it is critical to use the amount of movement expected on the job versus exaggerating the movement. Exaggerating the movement does not accelerate failure but instead produces failure that might not be seen in the real-world situation.

However, if the primary reason for the testing is to determine the sealant's joint movement ability as it weathers, then the suggestion is to use the Enomoto joint design (mentioned earlier) with the above machine conditions [9].

Relative to the machine conditions, for a general study, the conditions outlined in ASTM C1442 for the UVF samples would be adequate. In future studies one should consider keeping the science in tack and trying to match the total radiation in the xenon arc lamp machine to that of the UVF machine and match the total water exposure time as well.

Lastly, the goal was a fast and realistic accelerated test. This method produced realistic damage but no greater acceleration than what was seen before. However, because there were much smaller changes in the static tests (relative to time in the machines) and often lesser damage in the static condition, the cycles in the machines and outdoors could be changed to perhaps give a more accelerated weathering test. The damage was more significant and realistic when the sealants were extended and compressed. In the accelerated testing, the half of the testing time that had the sealant in the non-strained condition could be eliminated and have the sealants go from full extension to full compression without this neutral time. The one precaution is that in taking the sealant from full extension to full compression (or vice versa), the rate of sealant movement should be very slow, and no more than 3 mm/h, so as to allow sealants that have stress-relation characteristics to relax and change dimension at low and realistic stresses.

References

- [1] Klosowski, J. M. and Gorman, P. D., "Selective Review of Weathering Tests for Sealants and Thoughts on the Development of Novel Test Concept Based on Simultaneous Weathering and Movement," *J. ASTM Int.* Vol. 7, No. 1, Paper ID JAI102186.
- [2] Bridgewater, T. J. and Carbarry, L. D., "Accelerated Weathering and Heat Stability of Various Perimeter Sealants," *Science and Technology of Building Seals, Sealants,*

Glazing, and Waterproofing: Second Volume, ASTM STP 1200, J. M. Klosowski, Ed., ASTM International, West Conshohocken, PA, 1992, pp. 45–63.

- [3] ASTM C1442, 2006, “Standard Practice for Conducting Tests on Sealants Using Artificial Weathering Apparatus,” *Annual Book of ASTM Standards*, Vol. 04.07, ASTM International, West Conshohocken, PA, pp. 415–420.
- [4] ASTM C920, 2008, “Standard Specification for Elastomeric Joint Sealants,” *Annual Book of ASTM Standards*, Vol. 04.07, ASTM International, West Conshohocken, PA, pp. 146–149.
- [5] ASTM C719, 2005, “Standard Test Method for Adhesion and Cohesion of Elastomeric Joint Sealants Under Cyclic Movement (Hockman Cycle),” *Annual Book of ASTM Standards*, Vol. 04.07, ASTM International, West Conshohocken, PA, pp. 86–91.
- [6] ISO Specification 11600, International Standards Organization.
- [7] ISO 9047, International Standards Organization.
- [8] Sandberg, L. B., “Comparisons of Silicone and Urethane Sealant Durabilities,” *J. Mater. Civ. Eng.*, Vol. 3, No. 4, 1991, pp. 278–291.
- [9] RILEM Technical Committee 190-SBJ (Andreas T. Wolf), “Recommendation of RILEM TC 190-SBJ: Service-Life Prediction of Sealed Building and Construction Joints—Durability Test Method: Determination of Changes in Adhesion, Cohesion and Appearance of Elastic Weatherproofing Sealants After Exposure of Statically Cured Specimens to Artificial Weathering and Mechanical Cycling,” *Mater. Struct.*, Vol. 41, 2008, pp. 1497–1508.

Andreas T. Wolf¹

Effects of Water Immersion on Building and Civil Engineering Joints and the Use of the Arrhenius Method in Predicting Adhesion Lifetime of Water-Immersed Joints

ABSTRACT: Moisture in the form of humidity, condensation, rain, or water immersion is the most commonly encountered element of the service environment and must be considered a critical factor in determining the long-term reliability of sealed or bonded joints. Moreover, the effects of moisture are exacerbated by elevated temperature. For many polymeric systems, warm, moist environments can considerably weaken the bulk or interfacial performance properties of the jointing materials formulated with these polymers. The majority of joint failures in service environments that comprise water exposure occur by degradation of the interface(s) between sealant or adhesive, primer, and substrate. Therefore, predicting the interfacial degradation in an actual service environment is of utmost importance. This paper provides information on the current understanding of the role of water in the failures of adhesive and sealant joints and discusses the usefulness of the Arrhenius' relation in predicting the lifetime of sealed or bonded joints based on data generated at elevated temperatures. Finally, the paper suggests some guidelines aimed at improving the reliability of accelerated test and prediction procedures used in the evaluation of the durability performance of sealed or adhered joints in immersed environments.

KEYWORDS: durability, lifetime, service life, water immersion, joint, sealed, bonded, Arrhenius

Introduction

The lifetime of sealed or adhesively bonded joints can be substantially reduced by environmental stresses such as actinic radiation, elevated temperature,

Manuscript received February 26, 2008; accepted for publication July 8, 2008; published online August 2008.

¹ Ph.D., Scientist, Dow Corning GmbH, 65201 Wiesbaden, Hessa, Germany.

Cite as: Wolf, A. T., "Effects of Water Immersion on Building and Civil Engineering Joints and the Use of the Arrhenius Method in Predicting Adhesion Lifetime of Water-Immersed Joints," *J. ASTM Intl.*, Vol. 5, No. 8. doi:10.1520/JAI101721.

Copyright © 2008 by ASTM International, 100 Barr Harbor Drive, PO Box C700, West Conshohocken, PA 19428-2959.

moisture, and aggressive gases and fluids, or a combination thereof [1–3]. Moisture in the form of humidity, condensation, rain, or water immersion is the most commonly encountered element of the service environment and must be considered a critical factor in determining the long-term reliability of sealed or bonded joints. Moreover, the effects of moisture are exacerbated by elevated temperature. For many polymeric systems, warm, moist environments can considerably weaken the bulk or interfacial performance properties of the jointing materials formulated with these polymers [4].

Elastomeric sealants and adhesives are used in wet service conditions in a wide variety of building and civil engineering applications. Repetitive short-term water immersion is a common environment in many applications, such as on flat roofs, parking decks, pavements, and walkways. In these applications, standard building construction sealants and adhesives often function successfully and achieve satisfactory service lives. However, repetitive long-term or permanent immersion such as is experienced in water-retaining tanks and storage reservoirs, sewage treatment tanks, swimming pools, seawalls, culverts, embankments, and aqueducts places high demands on the jointing material and its interface with the substrate. Depending on the application, joints may be exposed primarily to load (stress), for example in an aquarium or water storage tank, or primarily to strain, for example in shallow ponds or on roofs employing evaporative cooling techniques. In some cases additional performance properties may also be required, for example, resistance to biological or chemical attack, abrasion, water flow, pressure, wet/dry cycling, etc.

The majority of joint failures in service environments that comprise water exposure occur by degradation of the interface(s) between sealant or adhesive, primer, and substrate. Therefore, predicting the interfacial degradation in an actual service environment is of utmost importance. This paper discusses the use of the Arrhenius method in predicting the degradation of adhesion resulting from water immersion at various temperatures.

Moisture Ingress into Sealed or Bonded Joints

Water may enter a joint by bulk diffusion through the adhesive or sealant, by transport (wicking) along the interface at the substrate, and by capillary action through cracks or pores in the jointing material or in the substrate [5].

The diffusion of a liquid in an elastomeric matrix can be visualized as a series of random jumps in which Brownian motion of chain segments of the polymer produces transient voids in the vicinity of the liquid penetrant, enabling it to move within the polymeric matrix (“random walk”). This type of Fickian diffusion, in which the rate of relaxation of the polymer matrix is faster than the rate of penetrant diffusion, is commonly observed in rubbery materials that display high flexibility and mobility of the polymer chains.

Water may also spread close to the interface between jointing material and substrate. For “weak” interfaces, where secondary bonding forces dominate the adhesion, failure occurs almost instantaneously as water contacts the interface. A range of other factors may enhance interfacial moisture transport, accumulation of water at the interface, and ultimately adhesive failure, for example:

- Shrinkage of the sealant or adhesive at a constrained interface may result in dilation and increased permeability of the material near the interface.
- Incomplete wetting of the substrate surface may cause nonbonded areas, where water accumulates, and from which further debonding spreads.
- Osmotic pressure and subsequent debonding may be promoted by the presence of hydrophilic sites or salts at the interface, which decrease the equilibrium vapor pressure and promote water condensation [6].
- Local inhomogeneities near the interface or a weak boundary layer with a lower crosslinking density than the bulk of the material may provide a pathway of increased moisture diffusivity [7,8].

In general, the rate of interfacial diffusion and the presence of fluid at the interface become more critical to the lifetime of the sealed or bonded joint as the strength of the interface decreases.

Moisture may also reach the interface by capillary or bulk diffusion through the substrate. This mechanism is especially important for porous or cellular substrates, such as wood, open-cell plastic foams, or concrete and masonry materials. Water may also enter the joint by capillary action through cracks or pores in the jointing material. This mechanism may be enhanced by moisture exposure itself, since moisture can also cause structural damage by inducing microcavities or crazes in polymeric materials. The formation of these structural damages can further accelerate moisture diffusion [9–11].

Effect of Water on Joints

When a joint is exposed to water, one or more of the following phenomena may occur, depending on the service conditions, and upon the type of jointing material and its state of cure [12,13]:

- Water may be absorbed in the bulk of the material, causing softening (plasticization) of the adhesive or sealant.
- For moisture-curing materials, where the cure is still incomplete at the time of water exposure, crosslinking may continue, causing an increase in modulus [14].
- The polymeric backbone of the sealant or adhesive may degrade hydrolytically, causing softening of the material.
- The bonds between the substrate, the primer (if present), and the sealant or adhesive may be impaired, resulting in adhesive failure at the interface.
- Water may physically or chemically degrade the substrate or substrate surface.

Degradation of Bulk Properties

Moisture absorbed in a polymer matrix can lead to a wide range of effects on the bulk properties of adhesives and sealants. Some effects on the polymeric materials are reversible and the material's properties can recover fully upon removal of water. Others are irreversible and result in permanent changes in

the performance of the polymeric materials. Water absorption into sealants or adhesives can cause plasticization and swelling; both phenomena are in principle fully reversible, if no other effect occurs simultaneously. By acting as an external plasticizer to the polymeric matrix, water spreads the polymer molecules apart and reduces the interactions between the polymer chains. Water acting as a plasticizer can depress the glass transition temperature of the polymer matrix and reduce the strength, modulus, and indentation hardness of the jointing material [15–17]. In this author's experience, small amounts of water may initially increase some performance properties of sealed and bonded joints, for instance, resulting in higher elongation at break and tensile strength values as well as improved practical adhesion. As suggested by Wylde [18] for epoxy adhesives and generalized by Bowditch [19], this phenomenon may be due to the relief of internal stresses within the joints due to the initial plasticization of the bulk resulting in stresses being distributed over a larger region.

Moisture can also lead to unwanted chemical reactions in the adhesive or sealant and consequently can change the bulk properties of the material in an irreversible way, for instance by causing hydrolysis [20] or further crosslinking [21], as well as by inducing cracking or crazing in the material [9,10]. In particulate-filled polymeric systems, the absorbed water can attack the polymer/filler interface and cause interfacial debonding [22,23]. With certain sealants and adhesives, the absorbed water cannot be completely removed by drying. The residual water is believed to be one that is strongly bonded to polar sites [24,25]. Water may also leach formulation constituents such as plasticizers, pigments, or fillers from the sealant or adhesive; this process then results in a loss of weight upon drying of the material [26]. For some materials, the water uptake process does not reach a saturation point and continues under disintegration of the sealant or adhesive [26]. This behavior may be observed, for example, with aqueous dispersion-polymer based materials that are not chemically cured, since such polymeric systems can be redispersed in water given sufficiently long immersion periods. For chemically cured sealants or adhesives this behavior may occur, especially at substantially elevated temperatures, as a result of chemical degradation reactions (for more information on the chemical type of sealants and adhesives as well as their bulk response to humidity exposure see, for instance, Refs. [27,28]).

Degradation of the Interface at the Substrate

As mentioned previously, in most incidences, the eventual degradation of the interface(s) between the jointing material, the primer, and the substrate is the primary reason for the failure of a joint [29]. For thin coating films it has been observed that the rate of loss of adhesion of the film to a substrate is dependent upon the rate at which water permeates through the coating to the interface [30]. In the same study, the loss of adhesion has been attributed to the accumulation of water at the interface between the coating and the substrate surface. The most convincing evidence for this hypothesis comes from studies of the adhesion of coatings and adhesives on metal oxide surfaces. In these studies, a strong dependence of adhesion strength on the relative humidity of the environment and, consequently, on the amount of adsorbed water in the coat-

ing or adhesive was noted [31–38]. Already in 1979, it has been suggested that a critical water concentration may exist in the bulk material with an associated critical ambient humidity level below which the interface is not weakened by moisture [29]. At present, the critical water concentration for a given jointing system cannot be predicted. Overall, the critical concentration of water hypothesis has not been fully substantiated yet, although experimental evidence in its favor continues to be published that also provides indications of possible causes.

Water may chemically degrade the interface by interacting with the chemical bonds that exist across the interface. Several mechanisms have been proposed to explain the degradation of interfacial adhesion due to water absorption, though no single mechanism can be applied to explain all the failure phenomena.

It is generally accepted that water reaching the interface between a sealant or adhesive and an untreated high-energy surface substrate immediately disrupts all secondary molecular interactions (van der Waals and hydrogen bonding) [1]. Gledhill and Kinloch [39] have suggested that for adhesive joints, where only secondary forces are involved in adhesion, the intrinsic stability of the interface in the presence of an absorbed liquid may be evaluated from a consideration of the thermodynamic work of adhesion. However, it should be noted that when covalent bonding, inter-diffusion, and mechanical interlocking, or a combination thereof, substantially contribute to the adhesion strength, the work of adhesion is not suitable to explain adhesive failure.

The capillary pressure forming upon water absorption in the pores and crevasses on the surface of a substrate may readily disrupt the adhesion component resulting from mechanical interlocking [1]. The durability of adhesion is generally expected to increase with the number of covalent bonds at the interface [40]. However, practical adhesion may not always be helped by chemical bonding, since the bonds force a particular orientation of the adhering molecules at the substrate surface and by doing so modify the morphology of the interfacial transition region (also termed “interphase”), which may have a negative effect on the strength of the adhesive bond [41]. Covalent bonding is generally expected to effectively reduce the space at the interface for water to reside, as well as require a hydrolysis reaction for debonding, making the occurrence of an adhesive failure in an immersed environment less likely. However, even with covalent bonding, catalysts, such as acids and bases, which may form and accumulate at the interface in the presence of water, can have a substantial effect on the rate of hydrolysis reactions. For example, a sealant or adhesive that shows excellent unprimed adhesion to stainless steel after water immersion may fail rapidly on immersed concrete or glass, due to the accumulation of alkalinity at the interface.

Degradation of the Substrate

Water may also degrade the interface by physically or chemically interacting with the substrate. Due to the multitude of construction materials and associated degradation mechanisms [42] only a few examples will be discussed here.

Concrete is the most commonly encountered substrate in building and civil

engineering applications involving elastomeric sealants and adhesives. It is also one of the most difficult substrates to adhere to [43]. Concrete can be regarded as a network of interconnected and disconnected micro-pores and micro-cracks distributed randomly in a solid matrix. Concrete durability depends largely on the ease with which liquids or gases can migrate through the hardened concrete mass. Moisture, directly or indirectly, contributes largely to the deterioration of concrete. Leaching of concrete constituents as well as moisture-induced degradation at or close to the interface with sealants and adhesives can cause loss of cohesive strength in the concrete and lead to spalling. The degradation of concrete, and more specifically reinforced concrete, by water has been discussed in detail elsewhere [42,44].

Metals are probably the second most important substrate present in building and civil engineering applications of elastomeric sealants and adhesives. Water may hydrate a metal or metal oxide surface and cause the formation of a weak boundary layer at the interface [45–48]. Electrochemical corrosion may occur in joints involving metal substrates and act as a factor that weakens the performance of a joint. Water at the interface allows formation of an electrolyte and facilitates ionic mobility, an important aspect of corrosion chemistry. Examples for aggressive corrosion have been reported for rubber/steel bonded joints exposed to seawater or salt-spray when an electrochemical potential is present [49].

Soda-lime-silica float glass is another important substrate for elastomeric sealants and adhesives. The main mechanism by which water damages float glass is by leaching glass constituents. This process results in a depletion of network modifier ions and a relative enrichment of network formers as well as the formation of a silica-rich hydrated surface layer [50,51]. The effects of water in humid air or as a liquid phase are found to be different: characteristic pits develop in humid air, while the roughness increases in a more uniform way under water [52]. The corrosion process is accentuated when corrosive gases, such as SO_2 and NO_2 , are present [53]. In humid air, swelling and formation of a gel layer are the first observed effects with alkali silicates [52,54–56]. The leaching process affects glasses more or less strongly, depending on their composition. The glass composition and the residual tin left from the float process can affect the hydrolytic stability of float glass and also sealant adhesion, although no clear trends have been observed regarding the latter [57].

Methods of Improving the Resistance of Interfacial Adhesion to Water

Limiting the presence of water at the interface slows down the processes involved in corrosion, hydrolysis, substrate hydration, and other mechanisms of joint degradation. In general, two strategies are being considered to improve the durability of adhesively bonded or sealed joints:

1. Preventing water from reaching the interface.
2. Improving the strength (durability) of the interface itself.

Preventing Water from Reaching the Interface

Considering the various pathways for water to reach the interface (migration via substrate, interface, or jointing material), the following methods of preventing or retarding moisture penetration are utilized:

Applying Barrier Coats on Porous Substrates—Primers formulated as barrier coats are commonly used to moisture-proof and strengthen the surface of porous substrates prior to applying a sealant or adhesive. The thickness and nature of the applied primer layer are generally considered important factors for the performance of joints in porous substrates exposed to water immersion.

Hydrophobing the Interface—Silane coupling agents formulated into the primer or into the sealant or adhesive form a hydrophobic poly(siloxane) network on the surface of the substrate [58,59]. For metal substrates, inhibitors may be added to retard the hydration of oxide layers at the substrate interface.

Reduction of Water Permeation by Proper Selection of the Sealant or Adhesive—Selection of the appropriate adhesive or sealant can reduce water permeation into the joint via the jointing material. Because water transport in the bulk is strongly related to the free volume of the polymeric matrix, the absorption of water may be reduced by introducing crystallinity or by increasing the crosslink density, both of which lower free volume. Water permeation can be reduced by decreasing the polymer's affinity for water, for example, by reduction of the number of polar or hydrophilic groups.

Improving the Strength of the Interface

Covalent bond formation at interfaces is a particular popular hypothesis used to explain the role of adhesion promoters and coupling agents in enhancing adhesion between dissimilar materials. Until about the early 1980s, the only justification for the covalent bonding hypothesis was the substantial amount of experimental performance data proving the effectiveness of these adhesion-promoting additives. More recently, several studies have contributed to the substantiation of the hypothesis by providing direct evidence that these bonds actually exist and are responsible for the improved performance (see Refs. [60,61]).

Organosilanes are believed to bond to metal, glass and other surfaces by forming Si-O-M bonds by condensation reaction, while the organo-group ensures reactivity with or compatibility with the polymeric matrix of the adhesive or sealant. Until recently, it was thought that reactive hydroxyl groups on the substrate surface were necessary for the bonding to occur. However, work by Debois and Zagarski [62] and Blümel [63] using FTIR and solid-state ^{29}Si NMR, respectively, indicates that alkoxy silanes can also react directly on Si-O-Si sites.

Plueddemann, who has contributed immensely to the use of silane adhesion promoters and coupling agents, including silanes with epoxy [64], methacrylate [65], styrene [66], and cationic vinylbenzyl [67] functionalities, stated in his 1982 book three conditions for maintaining bonding in the presence of water [68]:

- A maximum initial formation of M-O-Si bonds.
- A minimum penetration of water to the interface.
- Polymer structures that hold silanols at the interface.

For low molecular weight silanes the first condition can be achieved by using a suitable transesterification catalyst. The second condition can be met

by inserting a hydrophobic spacer group on the silane in order to hinder the penetration of water to the interface. The third condition is met by using tri-functional or even higher functional silanes capable of forming a network structure on the substrate surface. However, one should consider that the siloxane network structure itself remains sensitive to hydrolysis especially in the presence of acids or bases.

Prediction of Useful Lifetime Based on Temperature Dependency of Moisture-Related Diffusion and Chemical Degradation Processes

Acceleration models are usually based on the physics or chemistry underlying a particular failure mechanism. Successful empirical models often turn out to be approximations of complicated kinetics models, once the failure mechanism is better understood. However, simple models with the right response shape have generally proven to be more useful than elaborate multi-parameter models. The Arrhenius model has been used successfully for failure mechanisms that depend on chemical reactions, diffusion processes or migration processes.

The degradation of sealed or bonded joints by water-immersion proceeds faster at higher temperatures (see, for instance, Ref. [69]). This is because an elevation of temperature results in an acceleration of moisture-related diffusion and degradation processes [70]. It has long been known that the effect of temperature on the rate of chemical reactions can often be expressed by a relationship proposed by Svante Arrhenius in 1889 [71]. Therefore, the first approach usually considered when modeling a material's degradation as a function of temperature is to use the Arrhenius relationship. According to the Arrhenius rate law, the rate of a first-order chemical reaction depends on the temperature as follows [69,72]):

$$k = A \exp(\Delta E_a/RT) \quad (1)$$

where k is the reaction rate (or degradation rate) for the process, ΔE_a is the activation energy required to initiate the process, R is the ideal gas constant, T is the absolute temperature (in K) and A is a constant. The activation energy ΔE_a plays a pivotal role in determining the degradation rate and its value depends on the diffusion and failure mechanisms involved. In the past, the Arrhenius relation was often interpreted as a "rule of thumb" stating that reaction rates double for every 10 K rise in temperature. This simple rule, however, only applies, if the activation energy is about 51 kJ/mol. Obviously, the higher the activation energy is, the stronger the temperature dependence of the rate constant.

The energy of activation for diffusion is on the order of 40 kJ/mol [73] while that of thermally induced chemical reactions is likely to be 80 kJ/mol or higher. The activation energy for the hydrolysis of covalent siloxane bonds to silanols by water is 98.8 kJ/mol [68]. However, in the presence of an acidic or basic catalyst the activation energy needed for the hydrolysis reaction drops to around 25 kJ/mol [68].

The following form of the Arrhenius equation allows calculation of two specific rates of reaction, k_2/k_1 , at two temperatures, T_2 and T_1 :

$$\log(k_1/k_2) = \log k_1 - \log k_2 = \Delta E_a / (2.303R)(1/T_1 + 1/T_2) \quad (2)$$

Therefore, a plot of $\log(k_1/k_2)$ against $1/T$ produces a straight line with a slope of $\Delta E_a / (2.303R)$. The Arrhenius equation has been traditionally used in accelerated thermal or hygrothermal aging tests in the following manner: Some measure of the rate of reaction is determined at several temperatures (at least three, preferably more) and the logarithm of those rates is plotted versus $1/T$, the inverse of the absolute temperature. If the Arrhenius relationship remains valid over the whole temperature range studied, a straight line is obtained.

An alternative approach is to determine the durability time of a material, t_p , which is equal to the inverse of the reaction rate, $1/k$:

$$\log t_p = \log t_0 + \Delta E_a / (2.303RT) \quad (3)$$

Researchers often measure the time required for one of the key performance properties, for example, the tensile strength, to degrade to half its original value (half-life) at each temperature and fit their findings to the following equation [74]:

$$\log t_{1/2} = A + B/T \quad (4)$$

where $t_{1/2}$ is the half-life property, A and B are material constants, and T is the absolute temperature at which the aging experiments have been carried out.

Since a key function of structural adhesives is their load-bearing capability, while that of a sealant is maintaining adhesion under cyclic or permanent strain, researchers are often interested in assessing the durability of the adhesion to the substrate while the jointing material is under a given load (stress) or strain. However, it is important to note that placing a sealant or adhesive under constant load or constant strain generally produces quite different results for materials with viscoelastic behavior; but even more so when these materials are exposed to water immersion. When a viscoelastic jointing material is subjected to a constant stress, it will deform (creep); and the strain will increase with time. Similarly, if the material is strained and held at constant dimensions, the initial stress relaxes with time. Both creep and stress-relaxation have been described in terms of disengagements of polymer chain entanglements or breakage of hydrogen bonds. Since water may act as a plasticizer in the polymer matrix and also has an effect on hydrogen bonds, exposure to moisture may strongly accelerate creep and stress relaxation.

Typically, a sealant or adhesive placed under a given load and stress while being immersed in water will fail faster adhesively than the same material exposed to immersion without mechanical stress. The reason applied stress leads to a more rapid rate of degradation is that mechanical tension contributes to chemical bond scission. The thermal energy of activation, ΔE_a , is lowered by the potential energy of the stress, $\delta \sigma$. Thus, the familiar Arrhenius equation becomes:

$$k = k_0 \exp[-(\Delta E_a - \delta \sigma) / RT] \quad (5)$$

where σ is the stress and δ is a constant.

This equation may also be written in the corresponding Zhurkov [75] equation form:

$$\log t_p = \log t_0 + (\Delta E_a - \delta\sigma)/(2.303RT) \quad (6)$$

Thus, there is a linear relationship between the logarithm of the durability time and the stress, valid for the action of any mechanical force on any elementary chemical transformation, independent of its nature [76]. This linear relationship usually holds, however, only over a limited range of stress, where the kinetics of the process is determined largely by a single elementary event [77,78].

The Arrhenius method is particularly useful for the accelerated testing of polymeric systems as it allows short-term tests, conducted at elevated temperatures, to be used in the assessment of the effects of long-term exposures at lower temperatures. Using the general Arrhenius-type relationship for reaction rate as a function of temperature, lifetime to failure can be extrapolated for varying temperatures.

Among the limitations of this technique are that the use of a constant activation energy over the temperature range anticipated may not be valid, and that extreme extrapolation of higher temperature results to lower temperatures does not always provide an accurate result due to competing degradation mechanisms. In addition, the specific failure criterion must be directly applicable to the service conditions and the sealed or bonded joint design. Further limitations of the Arrhenius approach are that linear specific rates of change must be obtained at all temperatures used, i.e., the rate of reaction must be constant over the period of time during which the ageing process is measured, and that the mechanism of the reaction(s) involved in the aging of the material at higher or lower temperatures should not differ; otherwise, this would alter the slope of the Arrhenius plot. This is quite often the case and numerous examples of nonlinear Arrhenius behavior as a consequence of a change in mechanism can be found in the literature. Hunlett provides a detailed discussion of reasons for the deviation from the Arrhenius equation [79].

In the case of reactive sealant and adhesives, the issue of competing (degradation) reactions often leads to non-Arrhenius behavior. If there is more than one chemical reaction and those chemical reactions have different activation energies, the Arrhenius model will not correctly describe the rate of the overall chemical reaction. This is because temperature affects the two degradation processes differently, inducing nonlinearity into the acceleration function relating failure times at two different temperatures [80].

In the case of a simple one-step chemical reaction, E_a would represent an activation energy that quantifies the minimum amount of energy needed to allow this reaction to occur. However, in most applications involving temperature acceleration of a failure mechanism, the situation is much more complicated. As Escobar and Meeker [80] point out, a chemical degradation process may have multiple steps operating in series or parallel, with each step having its own rate constant and activation energy. Generally, the hope is that the behavior of the more complicated process can be approximated, over the entire range of temperature of interest, by the Arrhenius relationship. This hope can be realized, for example, if there is a single step in the degradation process that is rate-limiting and thus, for all practical purposes, controls the rate of the entire reaction. In such cases, the Arrhenius plot for the degradation results in

a linear correlation between the logarithmic failure times and the inverse absolute temperatures, indicating that the Arrhenius rate law is valid for the overall degradation process. The Arrhenius plot, therefore, is commonly used to determine if Arrhenius modeling of the temperature dependence for a single, dominant mechanism is appropriate or if methods to deconvolute the observations need to be developed. However, even in cases where a good fit with the Arrhenius relationship is observed, it is likely that more than a single-step reaction is involved in the degradation mechanism. Therefore, in most accelerated test applications, it would be more appropriate to refer to ΔE_a as “quasi-activation energy.”

Each of the Arrhenius plots generated in this way can be analyzed by fitting a straight line to the experimental values using the least-squares-method and calculating the activation energy, ΔE_a , from the slope $-\Delta E_a/(2.303R)$, where R is the gas constant. However, calculating the activation energy in this manner for an ensemble of test specimens will not yield a single theoretical value for the failure mechanism, but rather a distribution of values, reflecting the fact that a part of the population contains some defects.

Examples of Arrhenius and Non-Arrhenius Behavior and Discussion of Possible Root Causes

In an internal study, McCann used the Arrhenius method in an attempt to determine the adhesion lifetime of water-immersed, sealed joints [81]. Sealed tensile-adhesion joints similar to the one defined in ISO 8339 Building Construction—Sealants—Determination of Tensile Properties (Extension to Break) [82] were prepared in triplicate with various one- and two-part sealants and different substrates (glass, aluminum, and concrete), allowed to cured for 21 days at ambient laboratory climate, and then immersed in water kept at a constant temperature of 10, 30, 50, 70, and 90°C. Since, depending on the application, immersed joints may be additionally exposed to forces induced by loads (stresses) or strains, McCann chose two different experimental protocols. In one study, intermittent stress was applied on the joints by removing them from the water bath once per week, placing each joint under a constant tensile load for 24 hours in ambient laboratory climate, and finally placing them again (with the load removed) into the water bath. The load placed on the individual joint was determined as one-half of the load (weight) that would stretch the cured, but unaged, sealant in the tensile-adhesion joint to its advertised maximum joint movement capability, e.g., 25, 50, or 100 %. In the second study, the sealants in the tensile-adhesion joints were placed under constant strain by stretching them to their advertised maximum joint movement capability, blocking the joints with suitable spacers, and placing them in their extended state in the water bath. The time-to-failure period in the permanent strain study was determined by inspecting the specimens visually each day, while failure in the intermittent stress study was only observed while the sealed joints were exposed to the tensile stress, i.e., once per week. The time-to-failure periods were determined as averages over the individual values obtained for the triplicate specimens. By plotting the logarithm of time-to-failure versus the inverse of the

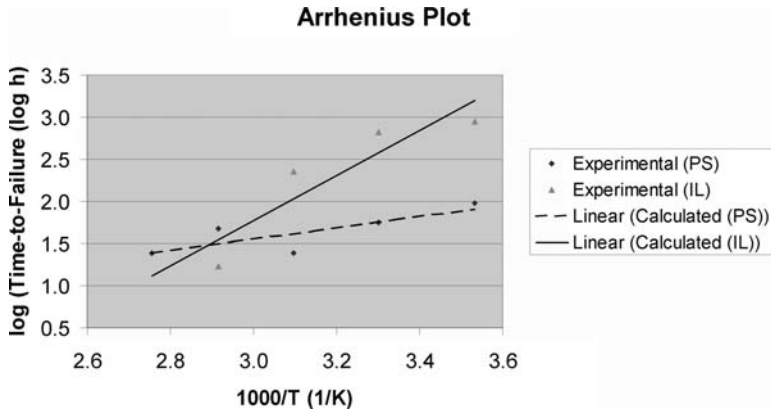


FIG. 1—Arrhenius plots for a three-part polyurethane sealant exposed either to intermittent load (stress) (IL) or to permanent strain (PS) during the water immersion.

absolute temperature and fitting a straight line to the data points using linear regression, McCann obtained Arrhenius plots of the experimental data.

Although most of the sealants exposed to constant strain would eventually stress-relax to a certain extent, placing the sealants under a constant strain proved to be considerably more damaging than the intermittent stress exposure. Figure 1 shows, as an example, the Arrhenius plots provided from this study for a three-part polyurethane sealant exposed either to intermittent stress or to permanent strain during the water immersion interval. The effect of the potential energy of the stress, $\delta\sigma$, on the overall activation energy ($\Delta E_a - \delta\sigma$) can be easily seen. Using the Zhurkov equation (Eq 6), the overall activation energy for the adhesion loss reaction under permanent strain is calculated as 12.8 (kJ/mol), while the same entity for adhesion loss under intermittent load is 51.3 (kJ/mol). However, note the poor fit of the linear regressions, reflected by coefficients of determination, r^2 , of 0.82 and 0.64 for the intermittent stress and permanent strain experiments, respectively. McCann made no effort to separate out the potential energy contribution by investigating different stress/strain ratios.

Several of the experiments conducted by McCann showed nearly perfect Arrhenius behavior. Figure 2 shows, as an example, the time-to-failure plot obtained for a medium modulus, one-part, neutral cure silicone sealant on glass exposed to intermittent stress during the water immersion period. However, several other material/substrate combinations clearly showed non-Arrhenius behavior when considering the full temperature range. Figure 3 shows, for illustration, the behavior of a low modulus, aminoxy-cure, one-part silicone sealant on aluminum substrates (with primer) when exposed to intermittent stress during water immersion. Experimentally obtained data points are shown as well as various linear regressions which are based on the inclusion of different subsets of data. The linear regression trend-lines vary dramatically; only the linear regression of all data points and the one for 10, 30, and 90°C run essentially parallel to each other. Considering the different Arrhenius

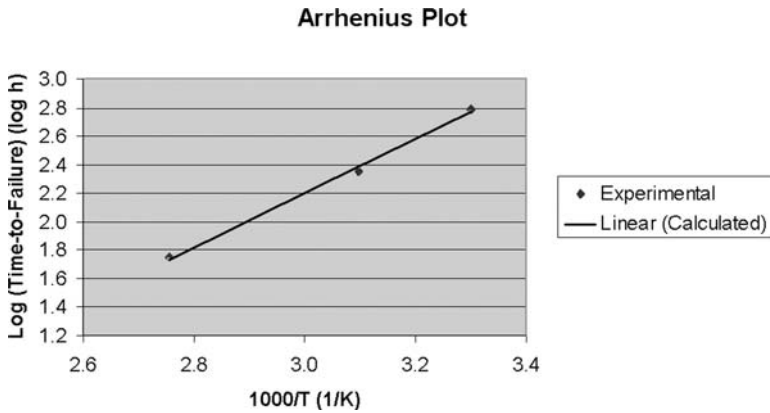


FIG. 2—Arrhenius plot for a one-part, medium modulus, neutral cure silicone sealant on glass (unprimed) exposed to intermittent stress during water immersion.

plots shown in Fig. 3, it is obvious that the linear regressions made based on all data points and on the two sets of three data points that include the low temperature (10°C) immersion result, i.e., 10/30/50 and 10/30/90, yield comparable lifetimes for immersion in room temperature (20°C) water, i.e., 1463, 1683, and 1503 h, respectively. However, a linear plot fitted to the two time-to-failure values obtained at the highest immersion temperatures, i.e., 70 and 90°C, yields a lifetime prediction of 28 219 h for immersion in 20°C water. This is approximately 15 to 20 times longer than the estimates gained by the other linear regressions!

Several possible causes of this non-Arrhenius behavior over the full temperature range exist. The most straight-forward interpretation of the data is

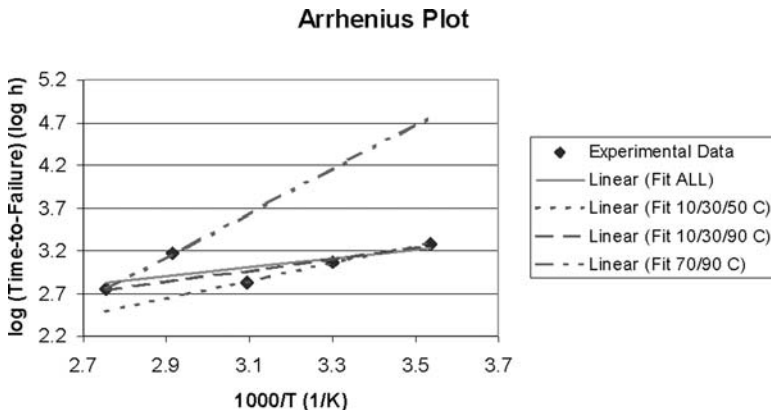


FIG. 3—Arrhenius plots (based on different subsets of data) for a one-part, low modulus, aminoxy-cure silicone sealant on aluminum (with primer) exposed to intermittent stress during water immersion.

that one either accepts the time-to-failure periods measured at 50 and 70°C as outliers or the dataset can be interpreted as suggesting two different degradation kinetics; one being in force at low to moderately elevated temperatures (10°C to less than 50°C) and another at strongly elevated temperatures (more than 50 to 90°C). However, it is interesting to note that the highest temperature immersions (70 and 90°C) are the ones that yield the longest lifetime for this sealant/substrate combination. On first sight, this finding is counter-intuitive, since one expects higher temperature immersions to result in faster degradation, not a stabilization of the system.

Interestingly, the same sealant shows almost identical non-Arrhenius behavior on glass (without primer). Calculating the overall activation energy from the slope of the linear regression obtained based on all data points yields 9.65 and 12.33 (kJ/mol) on primed aluminum and unprimed glass, respectively. For the same two substrates, linear regression fits based on low to moderate temperature data points (10, 30, and 50°C) yield 19.72 and 11.35 (kJ/mol), while for high immersion temperatures (70 and 90°C) overall activation energies of 49.54 and 51.09 (kJ/mol), each respectively, are calculated.

More surprisingly, the same sealant applied to concrete (without primer) shows nearly perfect Arrhenius behavior with an overall activation energy of 37.0 (kJ/mol) and a coefficient of determination, r^2 , of 0.97 for a linear regression based on all five data points. This behavior suggests that, indeed, two different degradation kinetics may be observed at lower and higher immersion temperatures on unprimed glass and on primed aluminum.

One potential cause for this behavior could be incomplete cure (and adhesion build-up) of the slow curing one-part silicone sealant after 21 days of conditioning in the laboratory climate on nonporous substrates (glass and aluminum), while on the porous, moisture-containing concrete substrate the sealant achieved a more complete cure within the same conditioning period. In the case of incomplete cure, elevated immersion temperatures would then first accelerate an adhesion build-up before actual degradation of the interface by hydrolysis reaction occurred. Such behavior has been observed numerous times with various sealants, where initially hot water immersion causes adhesion to improve and only over longer time periods does degradation of the adhesion occur. In any case, the various hypotheses would warrant further experimental work.

In a further internal study, Agger and colleagues also employed the Arrhenius method in their evaluation of the degradation of silicone sealant adhesion on glass during water immersion [83]. These authors prepared ten (10) tensile-adhesion specimens as defined in ISO 8339 Building Construction—Sealants—Determination of Tensile Properties (Extension to Break) per sealant sample. Specimens were cured at ambient laboratory conditions for one and two weeks, respectively, for two- and one-part sealants. Each product was tested at five different immersion temperatures, i.e., 23, 40, 55, 80, and 100°C. The immersion temperature of 100°C was maintained by boiling water under reflux in a flask with a condenser fitted to it. Every morning after the initial immersion date, the test specimens were removed from the water baths for a short period of time in order to test the adherence. This was done by placing the test specimens in a tensiometer and stretching them by 25 %. The extension was main-

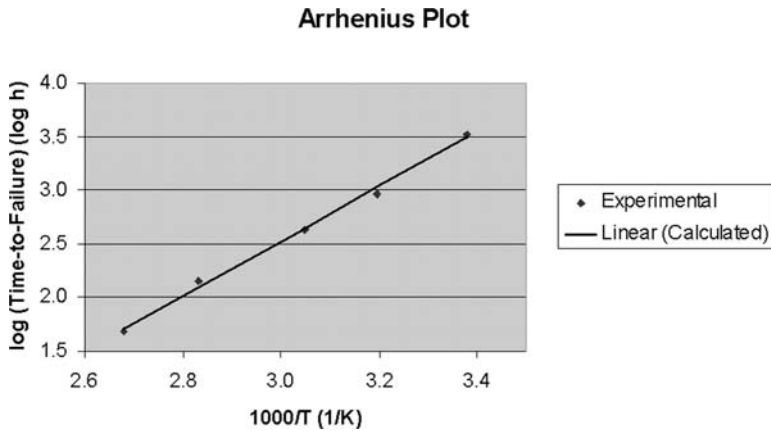


FIG. 4—Arrhenius plot for a tin-catalyzed, two-part silicone sealant on glass (unprimed).

tained for two minutes; the specimen was then removed from the tensiometer and again placed in the water bath.

One key difference to the previously mentioned study by McCann is that Agger and colleagues, rather than using the average time-to-failure periods in their evaluation of Arrhenius plots, based their assessment on the time-to-failure period for the specimen that failed last. Typically, these researchers obtained rather conclusive results, with some three to six specimens failing on the same last day, all of them in a purely interfacial mode. Agger and colleagues employed the longest rather than the average time-to-failure in order to eliminate the effects of poor specimen preparation, such as inclusion of bubbles at the interface, incomplete or improper wetting, deviations from sealed joint dimensions, surface damage during tooling, etc.

While one may argue that similar deficiencies may occur during the installation of actual service joints, their effect on the lifetime of these joints differs, due to differences in the dimensioning of the joints. For instance, edge effects in the short test joints strongly influence the performance of these specimens and amplify some of their deficiencies.

Using the last-to-fail data, Agger and colleagues observed for all but one of the sealants tested Arrhenius behavior with linear regressions providing an excellent fit to the experimental data. Coefficients of determination, r^2 , of greater 0.98 were observed for all sealants with the exception of the one slower curing one-part sealant. This sealant showed non-Arrhenius behavior and a linear regression using all data points yielded a poor fit (r^2 of 0.80). Again, for this slow curing one-part sealant it is likely that the adhesion to the substrate had not been fully developed during the two weeks conditioning period. Consequently, as mentioned before, elevated immersion temperatures would then first accelerate an adhesion build-up before degradation of the interface by hydrolysis reaction occurred.

Figure 4 shows, as an example, the excellent fit Agger and colleagues ob-

tained based on first-order degradation kinetics for a tin-catalyzed, two-part silicone sealant. The slope of the Arrhenius linear regression fit yields an activation energy of 47.22 (kJ/mol). An almost identical activation energy was observed for another tin-catalyzed, two-part silicone sealant (48.83 kJ/mol) based on the same aminosilane adhesion promoter. Note that amines and aminosilanes are known to co-catalyze condensation and hydrolysis reactions of siloxane bonds [84–86]. This finding therefore confirms the widely accepted hypothesis that hydrolysis reaction of siloxane bonds are primarily influenced by the catalyst and co-catalyst system, while the remaining ingredients in the formulation play only a minor role.

The authors of the two internal studies (McCann and Agger) did not address the sources of errors and their effect on the variability of their results. However, Agger and colleagues recorded the complete set of experimental time-to-failure periods for each specimen as a function of immersion temperature. Standard deviations calculated for the time-to-failure periods based on these datasets increase substantially with lower immersion temperatures for all sealants studied. As an example, for the most complete dataset, obtained on a two-part silicone sealant, standard deviations of 0, 1.76, 6.26, 14.77, and 58.07 days were observed for immersion temperatures of 100, 80, 55, 40, and 23°C, respectively.

Obviously, there are numerous sources of errors ranging from the preparation and cure of the specimens, over the exposure conditions (variations in experimental procedure), to the inspection of the specimens for failure (length of inspection intervals). It is, therefore, essential that the population of specimens in a study is large enough to account for this variability, as is the case in the study by Agger and his colleagues.

Furthermore, in several of the experimental examples reported in this paper, the deviation from Arrhenius behavior appears to result from incomplete cure of the sealant material. The author hypothesizes that at least some of the deviation would disappear, were the sealants allowed to completely cure. This hypothesis is also supported by the fact that deviations from Arrhenius behavior are observed for the same sealant material on certain substrates but not on others, suggesting a role of some substrates in accelerating cure (based on siloxane hydrolysis and condensation reactions) by providing moisture and catalytically acting species (alkalinity), or both. On concrete, water-content and surface pH are highly dependent on the age of the substrate and have been shown to affect initial adhesion build-up [87].

Guidelines for Improving the Reliability of Accelerated Test and Prediction Procedures

Any lifetime prediction approach based on accelerated testing involves extrapolation. This applies as well to the use of the Arrhenius method in predicting the effects of long-term exposures at lower temperatures based on laboratory data gained from short-term tests conducted at elevated temperatures. The most seriously unrealistic projections made in the past can be avoided by determining and using actual activation energies from the Arrhenius equation instead of

the “rule of thumb” that reaction rates double for every 10 K rise in temperature. Even then, accelerated tests should be designed, as much as possible, to minimize the amount of extrapolation required [88].

Clearly, it is not advisable to extrapolate the behavior of a sealed or bonded joint at room temperature from water-immersion data that have been obtained at 90 and 100°C, if the linearity of the correlation between the logarithmic failure times and the inverse absolute temperatures has not been previously demonstrated for the same sealed or bonded joint system over at least a substantial region of the full temperature range, in the above example say 40 to 100°C. High levels of an accelerating variable, such as temperature, can cause extraneous failure modes or mechanisms that would never occur at use levels of the accelerating variable.

In practice, it may often be difficult or impractical to verify the Arrhenius relationship over the entire temperature range of interest. Still, the aim of the experimental protocol must be to provide substantial evidence that the relationship holds true and the same dominant degradation mechanism prevails over the entire temperature range.

The author suggests the following guidelines for conducting accelerated hot water immersion tests and predicting lifetime data at use conditions based on the Arrhenius approach:

The experimental protocol used in the accelerated hot water immersion and in the determination of joint failure must generate the same failure mode as observed in the field. Generally, it is the experimenter’s intent to generate information about one failure mechanism using a relatively simple experimental approach. However, if more than one failure mode may occur within the range defined by the experimental protocol, the various failure mechanisms underlying these failure modes may be accelerated at different rates by an increase in temperature or mechanical stress. For example, the change of failure mode from adhesive (interfacial adhesion loss) to boundary (failure in the interphase) to cohesive (failure in the bulk) and vice versa as a function of water pick-up in the material has been widely documented (see, for instance, literature referenced by Bowditch [19]). It is, therefore, essential to verify that there is a consistent failure mode for all experimental conditions and that this failure mode is identical to the one observed in the field.

Mixed-mode failures are another type of complication, which may occur because of a gradient in cross-linking density across the substrate-adhesive interface. De Buyl and colleagues report a one part room temperature cured alkoxy silicone sealant applied in a lap-shear joint configuration to show cohesive mode of failure in the outer joint region and adhesive mode of failure in the inner region [89]. A consistent failure mode often can be achieved by selecting the experimental evaluation procedure (tensile adhesion, peel, lap shear, etc.) and by adjusting the test parameters (no load, constant load, etc.) specifically for this purpose.

In order to minimize the amount of extrapolation required in lifetime predictions based on the Arrhenius methodology, the experimental protocol must allow for long time periods to failure at low water immersion temperatures. Time to failure may vary between a few hours or days in boiling water to months or years at ambient temperature. Therefore, for very slowly failing sys-

tems, consideration should be given to accelerated aging techniques with two different stressors acting in synergy, e.g., temperature and mechanical stress. One option would be accelerated ageing tests with joint specimens exposed to different, constant loads in water immersion at different, constant temperatures, and extrapolating the results to zero mechanical load at ambient use temperature.

A further aspect of the exponentially varying failure times is the requirement that the intervals for the inspections or tests of the joint specimens for failure must be adjusted to the length of the time-to-failure periods. As an example, no accurate determination of time to failure is possible by inspecting or testing the specimen once per week, if the actual time to failure is shorter than one week. The inspection or test interval should be in the range of about 10–15 % of time to failure, i.e., if the time to failure is about one week, the test specimens should be inspected at least on a daily basis.

The use of average time to failure values provides less information than the use of the actual failure distribution. Given the impracticality of achieving defect-free test specimens, the population should be large enough to account for this variability. A minimum of six test specimens is advisable. If a single value for time to failure is to be used, the maximum failure time is a better characteristic indicator of the dominant chemical and physical degradation mechanism, or both (for a nearly perfect specimen), than the average failure time. Maximum failure times should be used to calculate quasi-activation energies for the dominant degradation mechanisms.

Despite the limitations of the Arrhenius approach, it is still capable of providing a better estimate of actual lifetime in use than test methods that rely on a single immersion temperature, such as the ETAG 002 Guideline for European Technical Approval for Structural Sealant Glazing Kits (SSGK) [90] or ASTM C1247 Standard Test Method for Durability of Sealants Exposed to Continuous Immersion in Liquids [91], if used over a sufficiently wide temperature range with a sufficient number of discrete immersion temperatures; A minimum of three immersion temperatures is recommended; however, a number ranging between four and six constitutes a better practice.

Finally, as has been pointed out by Escobar and Meeker, accelerated test programs should be planned and conducted by teams including individuals knowledgeable about the product and its use environment, the physical/chemical/mechanical aspects of the failure mode, and the statistical aspects of the design and analysis of reliability experiments.

Summary and Outlook

Hot water immersion tests in the absence or presence of an applied mechanical stress are regularly used to qualitatively evaluate the bond durability for various jointing systems exposed to different chemical and thermal conditions. The first approach usually considered when modeling a material's degradation as a function of temperature is to use the Arrhenius relationship. The paper discussed the effects of water immersion on building and civil engineering joints and the degree to which Arrhenius' law can be used to predict the lifetime of

sealed or bonded joints from data generated at elevated temperatures. Furthermore, the paper suggested some guidelines to improve the reliability of accelerated test and prediction procedures for evaluating the durability performance of sealed or adhered joints in immersed environments. The life prediction approach discussed in this paper may be applied in the determination of the durability of bonded and sealed joints in components for building, civil engineering, automotive, offshore, or other engineering applications. However, care must be taken that the failure rate is adequately defined and measured and that the temperature range over which extra—or interpolations are made is characterized in sufficient detail. Finally, the paper also showed that the degradation of a sealant's adhesion by water immersion is related to the substrate, the formulation, and the cure conditions of the sealant prior to water immersion. The Arrhenius method can be of predictive value and a useful tool in new product development only if these underlying degradation causes are well understood in advance.

References

- [1] Kinloch, A. J., *Adhesion and Adhesives—Science and Technology*, Chapman and Hall, New York, NY, 1987.
- [2] Dickstein, P. A., Spelt, J. K., Sinclair, A. N., and Bushlin, Y., "Investigation of Non-Destructive Monitoring of the Environmental Degradation of Structural Adhesive Joints," *Mater. Eval.*, Vol. 49, No. 12, 1991, pp. 1498–1505.
- [3] Nguyen, T., Byrd, E., and Bentz, D., "Quantifying Water at the Organic Film/Hydroxylated Substrate Interface," *J. Adhes.*, Vol. 48, 1995, pp. 169–194.
- [4] Comyn, J., *Polymer Permeability*, Elsevier Applied Science, London, United Kingdom, 1985.
- [5] Comyn, J., "Kinetics and Mechanism of Environmental Attack," *Durability of Structural Adhesives*, Applied Science Publishers, London, United Kingdom, 1983, pp. 85–131.
- [6] Funke, W., "Blistering of Paint Films and Filiform Corrosion," *Prog. Org. Coat.*, Vol. 9, 1981, pp. 29–46.
- [7] Comyn, J., Horley, C. C., Oxley, D. P., Pritchard, R. G., and Tegg, J. L., "The Application of Inelastic Electron Tunnelling Spectroscopy to Epoxide Adhesives," *J. Adhes.*, Vol. 12, 1981, pp. 171–188.
- [8] Allen, K. W., Alsalm, H. S., and Wake, W. C., "Strength and Failure Patterns of Metal-Metal Adhesives," *Faraday Spec. Discuss. Chem. Soc.*, Vol. 2, 1972, pp. 38–45.
- [9] Apicella, A., Nicolais, L., Astarita, G., and Orioli, E., "Effect of Thermal History on Water Sorption, Elastic Properties and the Glass Transition of Epoxy Resins," *Polymer*, Vol. 20, 1979, pp. 1143–1148.
- [10] Diamant, Y., Marom, G., and Broutman, L. J., "The Effect of Network Structure on Moisture Absorption of Epoxy Resins," *J. Appl. Polym. Sci.*, Vol. 26, 1981, pp. 3015–3025.
- [11] Brewis, D. M., Comyn, J., and Tegg, J. L., "The Uptake of Water Vapour by an Epoxide Adhesive Formed from the Diglycidyl Ether of Bisphenol-A and Di-(1-aminopropyl-3-ethoxy) Ether," *Polymer*, Vol. 21, 1980, pp. 134–138.
- [12] Anonymous, "How Moisture Affects Adhesive and Sealant Joints—Part I," <http://>

- www.specialchem4adhesives.com/, July 16, 2003.
- [13] Anonymous, "Improving the Moisture Resistance of Adhesives and Sealants—Part II," <http://www.specialchem4adhesives.com/>, July 23, 2003.
- [14] Beech, J. C. and Turner, C. H. C., "Cure of Elastomeric Building Sealants," *J. Chem. Technol. Biotechnol.*, Vol. 33A, 1983, pp. 63–69.
- [15] St. Lawrence, S., Willett, J. L., and Carriere, C. J., "Effect of Moisture on the Tensile Properties of Poly(hydroxy ester ether)," *Polymer*, Vol. 42, 2001, pp. 5643–5650.
- [16] Butkus, L. M., Mathern, P. D., and Johnson, W. S., "Tensile Properties and Plane-Stress Fracture Toughness of Thin Film Aerospace Adhesives," *J. Adhes.*, Vol. 66, 1998, pp. 251–273.
- [17] McBrierty, V. J., Keely, C. M., Coyle, F. M., Xu, H., and Vij, J. K., "Hydration and Plasticization Effects in Cellulose Acetate: Molecular Motion and Relaxation," *Faraday Discuss.*, Vol. 103, 1996, pp. 255–268.
- [18] Wylde, J. and Spelt, J., "Measurement of Adhesive Joint Fracture Properties as a Function of Environmental Degradation," *Int. J. Adhes. Adhes.*, Vol. 18, 1998, pp. 237–246.
- [19] Bowditch, M. R., "The Durability of Adhesive Joints in the Presence of Water," *Int. J. Adhes. Adhes.*, Vol. 16, No. 2, 1996, pp. 73–79.
- [20] Antoon, M. K. and Koenig, J. L., "Irreversible Effects of Moisture on the Epoxy Matrix in Glass-Reinforced Composites," *J. Polym. Sci., Polym. Phys. Ed.*, Vol. 19, 1981, pp. 197–212.
- [21] Liu, J., Lai, Z., Kristiansen, H., and Khoo, C., "Overview of Conductive Adhesive Joining Technology in Electronics Packaging Applications," *Proceedings of the 3rd International Conference on Adhesive Joining and Coating Technology in Electronics Manufacturing*, 1998, pp. 1–18.
- [22] Kasturiarachchi, K. A. and Pritchard, G., "Scanning Electron Microscopy of Epoxy-Glass Laminates Exposed to Humid Conditions," *J. Mater. Sci.*, Vol. 20, 1985, pp. 2038–2044.
- [23] Kumazawa, T., Oishi, M., and Todoki, M., "High-Humidity Deterioration and Internal Structure Change of Epoxy Resin for Electrical Insulation," *IEEE Trans. Dielectr. Electr. Insul.*, Vol. 1, No. 1, 1994, pp. 133–138.
- [24] Ivanova, K. I., Pethrick, R. A., and Affrossman, S., "Investigation of Hydrothermal Ageing of a Filled Rubber Toughened Epoxy Resin Using Dynamic Mechanical Thermal Analysis and Dielectric Spectroscopy," *Polymer*, Vol. 41, 2000, pp. 6787–6796.
- [25] Gonon, P., Sylvestre, A., Teyseyre, J., and Prior, C., "Combined Effects of Humidity and Thermal Stress on the Dielectric Properties of Epoxy-Silica Composites," *Mater. Sci. Eng., B*, Vol. B 83, 2001, pp. 158–164.
- [26] Wolf, A. T., "Environmental Degradation Factors, Their Characterization and Effects on Sealed Building Joints," *Report 21: Durability of Building Sealants, RILEM State-of-the-Art Report*, A. T. Wolf, Ed., RILEM Publications, Paris, France, 2000, pp. 41–72 (and literature cited therein).
- [27] Petrie, E. M., *Handbook of Adhesives and Sealants*, McGraw-Hill, New York, NY, 2000.
- [28] Wolf, A. T., "Construction Sealants," *Handbook of Sealant Technology*, A. Pizzi and K. L. Mittal, Eds., Taylor and Francis Group, New York, NY, 2009.
- [29] Kinloch, A. J., "Interfacial Fracture Mechanical Aspects of Adhesive Bonded Joints—A Review," *J. Adhes.*, Vol. 10, 1979, pp. 193–219.
- [30] Leidheiser, H. and Funke, W., "Water Disbondment and Wet Adhesion of Organic Coatings on Metals," *Journal of Oil Color Chemists' Association*, Vol. 70, No. 5,

- 1987, pp. 121–132.
- [31] Funke, W., and Haagen, H., “Empirical or Scientific Approach to Evaluate the Corrosion Protective Performance of Organic Coatings,” *Ind. Eng. Chem. Prod. Res. Dev.*, Vol. 17, 1978, pp. 50–53.
- [32] Linossier, I., Gaillard, F., Romand, M., and Nguyen, T., “A Spectroscopic Technique for Studies of Water Transport Along the Interface and Hydrolytic Stability of Polymer/Substrate Systems,” *J. Adhes.*, Vol. 70, 1999, pp. 221–239.
- [33] Takahashi, K. M. and Sullivan, T. M., “AC Impedance Measurement of Environmental Water in Adhesive Interfaces,” *J. Appl. Phys.*, Vol. 66, No. 7, 1989, pp. 3192–3201.
- [34] Takahashi, K. M., “AC Impedance Measurements of Moisture in Interfaces Between Epoxy and Oxidized Silicon,” *J. Appl. Phys.*, Vol. 67, 1990, pp. 3419–3429.
- [35] Wu, W. L., Orts, W. J., Majkrzak, J., and Hunston, D. L., “Water Adsorption at Polyimide/Silicon Wafer Interface,” *Polym. Mater. Sci. Eng.*, Vol. 35, No. 12, 1995, pp. 1000–1004.
- [36] Kent, M. S., Smith, G. S., Baker, S. M., Nyitray, A., Browning, J., Moore, G., and Hua, D. W., “The Effect of a Silane Coupling Agent on Water Adsorption at a Metal/Polymer Interface Studied by Neutron Reflectivity and Angle-Resolved X-Ray Photoelectron Spectroscopy,” *J. Mater. Sci.*, Vol. 31, 1996, pp. 927–937.
- [37] Kent, M. S., McNamara, W. F., Fein, D. B., Domeier, L. A., and Wong, A. P. Y., “Water Adsorption in Interfacial Silane Layers by Neutron Reflection: 1—Silane Finish on Silicon Wafers,” *J. Adhes.*, Vol. 69, Nos. 1 and 2, 1999, pp. 121–138.
- [38] Kent, M. S., McNamara, W. F., Baca, P. M., Wright, W., Domeier, L. A., Wong, A. P. Y., and Wu, W. L., “Water Adsorption in Interfacial Silane Layers by Neutron Reflection: 2—Epoxy Silane Finish on Silicon Wafers,” *J. Adhes.*, Vol. 69, 1999, pp. 139–163.
- [39] Gledhill, R. A. and Kinloch, A. J., “Environmental Failure of Structural Adhesive Joints,” *J. Adhes.*, Vol. 6, 1974, pp. 315–330.
- [40] Miller, J. D. and Hatsuo, I., “Adhesive-Adherent Interface and Interphase,” *Fundamentals of Adhesion*, L.-H. Lee, Ed., Plenum Press, New York, 1991, pp. 291–324.
- [41] Possart, W., “Modern State of Models for Fundamental Adhesion—A Review Extended Abstract,” *Adhesion and Interface*, Vol. 3, No. 1, 2002, pp. 43–51.
- [42] Moncmanová, A., *Environmental Deterioration of Materials*, WIT Press, Southampton, United Kingdom, 2007.
- [43] Petrie, E. M., “Adhesion to Concrete Substrates,” <http://www.specialchem4adhesives.com/>, May 9, 2006.
- [44] Bin Yair, M., “The Durability of Cement and Concrete in Sea-Water,” *Desalination*, Vol. 3, 1967, pp. 147–154.
- [45] Venables, J. D., “Adhesion and Durability of Metal-Polymer Bonds,” *J. Mater. Sci.*, Vol. 19, 1984, pp. 2431–2453.
- [46] Davis, G. D., Whisnant, P. L., and Venables, J. D., “Sub-Adhesive Hydration of Aluminum Adherends and Its Detection by Electrochemical Impedance Spectroscopy,” *J. Adhes. Sci. Technol.*, Vol. 9, 1995, pp. 433–442.
- [47] Kinloch, A. J., Little, M. S. G., and Watts, J. F., “The Role of the Interphase in the Environmental Failure of Adhesive Joints,” *Acta Mater.*, Vol. 48, 2000, pp. 4543–4553.
- [48] Nitowski, G. A., “Topographic and Surface Chemical Aspects of the Adhesion of Structural Epoxy Resins to Phosphorus Oxo Acid Treated Aluminum Adherends,” Dissertation, Virginia Polytechnic Institute and State University, 1998.
- [49] Stevenson, A., “The Effect of Electrochemical Potentials on the Durability of Rubber/Metal Bonds in Sea Water,” *J. Adhes.*, Vol. 21, 1987, pp. 313–327.

- [50] Hench, L. L., "Characterization of Glass Corrosion and Durability," *J. Non-Cryst. Solids*, Vol. 19, 1975, pp. 27–39.
- [51] Lombardo, T., Chabas, A., Lefèvre, R.-A., Verità, M., and Geotti-Bianchini, F., "Weathering of Float Glass Exposed Outdoors in an Urban Area," *Rivista della Stazione Sperimentale del Vetro*, Vol. 36, No. 4, 2006, pp. 5–13.
- [52] Schmitz, I., Prohaska, T., Friedbacher, G., Schreiner, M., and Grasserbauer, M., "Investigation of Corrosion Processes on Cleavage Edges of Potash-Lime-Silica Glasses by Atomic Force Microscopy," *Fresenius' J. Anal. Chem.*, Vol. 353, Nos. 5–8, 1995, pp. 666–669.
- [53] Schmitz, I., Schreiner, M., Friedbacher, G., and Grasserbauer, M., "Phase Imaging as an Extension to Tapping Mode AFM for the Identification of Material Properties on Humidity-Sensitive Surfaces," *Appl. Surf. Sci.*, Vol. 115, No. 2, 1997, pp. 190–198.
- [54] Aagard, P. and Helgeson, H. C., "Thermodynamic and Kinetic Constraints on Reaction Rates Among Minerals and Aqueous Solutions: I—Theoretical Considerations," *Am. J. Sci.*, Vol. 282, 1982, pp. 237–285, <http://www.ajsonline.org/>
- [55] Schmitz, I., Schreiner, M., Friedbacher, G., and Grasserbauer, M., "Tapping-Mode AFM in Comparison to Contact-Mode AFM as a Tool for in Situ Investigations of Surface Reactions with Reference to Glass Corrosion," *Anal. Chem.*, Vol. 69, No. 6, 1997, pp. 1012–1018.
- [56] Watanabe, Y., Nakamura, Y., Dickinson, J. T., and Langford, S. C., "Changes in Air-Exposed Fracture Surfaces of Silicate Glasses Observed by AFM," *J. Non-Cryst. Solids*, Vol. 177, 1994, pp. 9–25.
- [57] Wolf, A. T., McMillan, C. S., Stiehl, W., and Lieb, K., "Effect of Float Glass Surface Composition on Silicone Sealant Adhesion Tested After Simultaneous Exposure to Hot Water and Ultraviolet Light," *Durability of Building and Construction Sealants and Adhesives*, ASTM STP 1453, A. T. Wolf, Ed., ASTM International, West Conshohocken, PA, 2004, pp. 252–261.
- [58] Nguyen, T., Byrd, W. E., Alshed, D., Chin, J., Clerici, C., and Martin, J., "Relationship Between Interfacial Water Layer Adhesion Loss of Silicon/Glass Fiber-Epoxy Systems: A Quantitative Study," *J. Adhes.*, Vol. 83, 2007, pp. 587–610.
- [59] Nguyen, T., Byrd, W. E., Alshed, D., Chin, J., McDonough, W., and Seiler, J., "Interfacial Water and Adhesion Loss of Polymer Coatings on a Siliceous Substrate," *Mater. Res. Soc. Symp. Proc.*, Vol. 385, 1995, pp. 57–63.
- [60] Plueddemann, E. P., "Adhesion Through Silane Coupling Agents," *Fundamentals of Adhesion*, L.-H. Lee, Ed., Plenum Press, New York, 1991, pp. 279–290.
- [61] Miller, J. D. and Ishida, H., "Adhesive-Adherent Interface and Interphase," *Fundamentals of Adhesion*, L.-H. Lee, Ed., Plenum Press, New York, 1991, pp. 291–324.
- [62] Debois, L. H. and Zegarski, B. R., "Reaction of Alkoxysilane Coupling Agents with Dehydroxylated Silica Surfaces," *J. Am. Chem. Soc.*, Vol. 115, 1993, pp. 1190–1191.
- [63] Blümel, J., "Reactions of Ethoxysilanes with Silica: A Solid-State NMR Study," *J. Am. Chem. Soc.*, Vol. 117, 1995, pp. 2112–2113.
- [64] Plueddemann, E. P., "Methods of Treating Glass with Epoxy-Silanes," U.S. Patent No. 2,946,701 (to Dow Corning), 1960.
- [65] Plueddemann, E. P., Clark, H. A., Nelson, L. E., and Hoffman, K. R., "New Silane Coupling Agents for Reinforced Plastics," *Mod. Plast.*, Vol. 39, 1962, pp. 135–187.
- [66] Plueddemann, E. P., "Treated Siliceous Article," U.S. Patent No. 3,079,361 (to Dow Corning), 1963.
- [67] Plueddemann, E. P., "Cationic Unsaturated Amine-Functional Silane Coupling Agents," U.S. Patent No. 3,819,675 (to Dow Corning), 1974.
- [68] Plueddemann, E. P., *Silane Coupling Agents*, Plenum Press, New York, 1982.

- [69] Nguyen, T., Byrd, W. E., Alshed, D., Aouadi, K., and Chin, J., "Water at the Polymer/Substrate Interface and Its Role in the Durability of Polymer/Glass Fiber Composites," *Durability of Fiber Reinforced Polymer (FRP) Composites for Construction (CDCC'98), First International Conference, Proceedings*, B. Benmokrane and H. Rahman, Eds., 1998, pp. 451–461.
- [70] Nelson, W., *Accelerated Testing, Statistical Models, Test Plans and Data Analyses*, John Wiley & Sons, New York, 1990.
- [71] Arrhenius, S., "On the Reaction Speed of the Inversion of Cane Sugar by Acids," (in German), *Zeitschrift für Physikalische Chemie*, Vol. 4, 1889, pp. 226–248. (English translation available in Back, M. H., and Laidler, K. J., *Selected Readings in Chemical Kinetics*, Pergamon, Oxford, 1967).
- [72] Laidler, K. J., "The Development of the Arrhenius Equation," *J. Chem. Educ.*, Vol. 61, No. 6, 1984, pp. 494–498.
- [73] Gan, L. M., Ong, H. W. K., Tan, T. L., and Chan, S. O., "Hydrolytic Stability of Single-Package Silicone Sealant," *J. Appl. Polym. Sci.*, Vol. 32, 1986, pp. 4109–4118.
- [74] River, B. H., "Accelerated, Real-Time Ageing for Four Construction Adhesives," *Adhesives Age*, Vol. 27, No. 2, 1984, pp. 16–21.
- [75] Zhurkov, S. N., "Kinetic Concept of the Strength of Solids," *International Journal of Fracture Mechanics*, Vol. 1, No. 4, 1964, pp. 311–323.
- [76] Feller, R. L., *Accelerated Ageing—Photochemical and Thermal Aspects*, The Getty Conservation Institute, 1994, available at: www.getty.edu/conservation/publications/pdf_publications/aging.pdf
- [77] Emanuel, N. M., "Some Problems of Chemical Kinetics in Polymer Ageing and Stabilization," *Polym. Eng. Sci.*, Vol. 20, 1980, pp. 662–667.
- [78] Emanuel, N. M., and Buchachenko, A. L., *Chemical Physics of Polymer Degradation and Stabilization*, E. N. Ilyina, Ed., V. N. U. Science Press, Utrecht, 1987.
- [79] Hulett, J. R., "Deviations from the Arrhenius Equation," *Q. Rev., Chem. Soc.*, 1964, pp. 227–242.
- [80] Escobar, L. A. and Meeker, W. Q., "A Review of Accelerated Test Models," *Stat. Sci.*, Vol. 21, No. 4, 2006, pp. 552–577.
- [81] McCann, K. D., "Sealant Lifetime in an Immersed Environment," Internal Report, Dow Corning Corporation, Midland, MI, 1990.
- [82] ISO, "Standard 8339, Building Construction—Sealants—Determination of Tensile Properties (Extension to Break)," International Standardization Organization, Geneva, 2005.
- [83] Agger, J. R., Descamps, P., Iker, J., and Tilmant, G., "A Study into the Loss of Adhesion of Silicone Mastic Test Samples," Internal Report, Dow Corning S.A., Seneffe, Belgium, 1991.
- [84] Blitz, J., Murthy, R. S. S., and Leyden, D. E., "Ammonia-Catalyzed Silylation Reactions of Cab-O-Sil™ with Methoxymethylsilanes," *J. Am. Chem. Soc.*, Vol. 109, 1987, pp. 7141–7145.
- [85] White, L. D., and Tripp, C. P., "An Infrared Study of the Amine-Catalyzed Reaction of Methoxymethyl-Silanes with Silica," *J. Colloid Interface Sci.*, Vol. 227, No. 1, 2000, pp. 237–243.
- [86] Vansant, E. F., Van Der Voort, P., and Vrancken, K. C., (Eds.), *Characterization and Chemical Modification of the Silica Surface (Studies in Surface Science and Catalysis)*, Elsevier, Amsterdam, Vol. 93, 1995, pp. 560–567.
- [87] Gubbels, F. and Calvet, C., "Adhesion Development of Organic and Silicone Sealants on Wet and Dry Concrete," paper presented at *3rd International ASTM/RILEM Symposium on Durability of Building and Construction Sealants and Adhesives*,

25–26 June 2008, submitted to JAI for publication.

- [88] Meeker, W. Q., Escobar, L. A., and Lu, C. J., “Accelerated Degradation Tests: Modeling and Analysis,” *Technometrics*, Vol. 40, 1998, pp. 89–99.
- [89] De Buyl, F., Comyn, J., Shephard, N. E., and Subramanian, N. P., “Kinetics of Cure, Crosslink Density and Adhesion of Water-Reactive Alkoxysilicone Sealants,” *Int. J. Adhes. Adhes.*, Vol. 22, 2002, pp. 385–393.
- [90] EOTA, *ETAG 002 Guideline For European Technical Approval For Structural Sealant Glazing Kits (SSGK)*, European Organisation for Technical Approvals (EOTA), Kunstlaan 40 Avenue des Arts, Brussels, Belgium (Edition Nov. 1999, 1st amended: October 2001, 2nd amended: Nov. 2005).
- [91] ASTM Standard C1247 “Standard Test Method for Durability of Sealants Exposed to Continuous Immersion in Liquids,” *Annual Book of ASTM Standards*, ASTM International, West Conshohocken, PA, 1998, re-approved 2004.

Bernhard Weller¹ and Silke Tasche²

Experimental Evaluation of Ultraviolet and Visible Light Curing Acrylates for Use in Glass Structures

ABSTRACT: Adhesive joints in glass construction have been realized with one- and two-component silicones for more than 20 years. However, ultraviolet and visible light curing acrylates in glass constructions provide additional design potential due to their inherent transparency, their advantages in regard to the production process, and their increased material strength. The aging behavior of these adhesives was comprehensively examined by testing bonded joints of annealed glass and metal to gain in-depth knowledge of their durability. The study was expanded by testing full-scale samples of various glass applications.

KEYWORDS: glass, metal, light curing acrylates, structural bonds, adhesive attachment, aging resistance

Introduction

The transparency of glass enables the architect to use it as inconspicuously as possible in the construction of buildings. There are numerous examples of such applications in vertical and overhead situations, which show—in combination with unobtrusive fixations—the potential of glass for lightweight forms of construction. Glass panes and other joining members are often connected to one another or to the supporting structure by point fixations or clamping plates [1]. However, regular bolted connections are often not adequate for joining glass especially when peak stresses occur at the edge of the hole that cannot be reduced by plastic deformation. The use of adhesives for joining glass is not

Manuscript received July 22, 2008; accepted for publication August 17, 2009; published online October 2009.

¹ Professor, Dr.-Ing., Institute of Building Construction, Technische Univ. Dresden, Dresden, Saxony 01062, Germany.

² Dr.-Ing., Institute of Building Construction, Technische Univ. Dresden, Dresden, Saxony 01062, Germany.

Cite as: Weller, B. and Tasche, S., "Experimental Evaluation of Ultraviolet and Visible Light Curing Acrylates for Use in Glass Structures," *J. ASTM Intl.*, Vol. 6, No. 9. doi:10.1520/JAI101982.

Copyright © 2009 by ASTM International, 100 Barr Harbor Drive, PO Box C700, West Conshohocken, PA 19428-2959.

only appropriate to this substrate as a brittle material, but it also allows the design of simple inconspicuous details. Loads are transferred by larger contact areas with adhesive fixings, and the load transfer to the supporting components is evenly distributed throughout the entire area of the adhesive [2].

UV and VIS Light Curing Acrylates

Single-component solvent-free ultraviolet (UV) and visible (VIS) light curing acrylates are cured by radical polymerization, which is induced by light. UV radiation is, like VIS light, a part of the electromagnetic spectrum. The wavelength of UV radiation falls within a range of approximately 100 to 380 nm. This range can be divided into ultraviolet C, ultraviolet B, and ultraviolet A radiations [3]. The latter covers the range from 315 to 380 nm and plays a central role in the hardening of the acrylates. VIS light ranges from 380 to 800 nm. The curing process of adhesives is dependent on the lamp used, the lamp intensity, the lamp spacing, the wavelength of the radiation, the thickness of the radiation permeable joint, and adhesive layer thickness. The duration of the exposure required for curing acrylates is usually in the second-to-single-minute range. The duration of the manufacturing process of bonded parts using acrylates as adhesives is therefore substantially shorter than that involving commonly used silicones.

Acrylate adhesives have a rather watery consistency, i.e., a relatively low viscosity. Manufacturers of light curing acrylates restrict bond thicknesses to ensure complete curing of these adhesives. Possible bond thicknesses vary from 0.1 to 2 mm. Existing tolerances of components can therefore only be compensated for within this limited bond thickness. In this respect, these adhesives are much more suited for bonding glass surface to glass surface than glass edge to glass edge since imperfections in the glass edge that result from the manufacturing process may require a bond thickness larger than 2 mm. By comparison, suppliers of structural sealant glazing silicones generally recommend a minimum joint thickness of 6 mm to ensure proper filling of the joint [4]; however, such joints are able to tolerate much larger thermally induced movements than high modulus acrylate adhesives due to their lower modulus and elastomeric nature (Table 1).

UV and VIS light curing acrylates do not yellow or discolor under the harsh influence of UV radiation [5]. Acrylate adhesives, used either in point or linear bonded fixations, are of particular interest especially for bonding glass due to their optical clarity. The bond itself is almost invisible, leaving only the two bonded materials within the line-of-sight of the viewer. The initial tensile strength of UV or VIS light curing adhesives is about ten times higher than that of regular structural sealant glazing silicones (see Table 2). Assuming similar durability for both materials, this should allow a reduction in the required contact surface area. The aging behavior of light curing acrylates is therefore of special interest and needs to be assessed [6].

Tests on Small Bonded Specimens

The introduction of alternative adhesives in applications for structural glass construction is a protracted process, which requires numerous investigations

TABLE 1—Comparison of basic characteristics of selected acrylates.

	Adhesive ^a				
	PB 4468	PB 55727	PB 55789	PB 56422	PB 4432
Chemical base	Modified acrylate	Modified acrylate	Modified urethane acrylate	Modified urethane acrylate	Modified acrylate
Wavelength range (nm)	320–450	320–420	320–420	320–420	380–450
Color			Colorless, clear		
Viscosity (mPa·s)	7000	50 000	65 000	70 000	320
Curing time (s)	40	35	18	13	40
Coefficient of thermal expansion (K ⁻¹)			~170–50 × 10 ⁻⁶		

^aThe data shown are according to the technical literature of the adhesive manufacturer [7–11].

TABLE 2—Comparison of physical properties of silicones and light curing acrylates.

Properties ^a	SG-500 ^b	SG-20 ^c	PB 4468	PB 55727	PB 55789	PB 56422	PB 4432
Elongation at break (%)	209.68	382.80	290.43	317.48	238.00	136.00	296.40
Elongation at break (%) after 21 days of water storage ^d	281.41	304.25	291.33	269.13	216.09	132.26	281.74
Tensile strength (N/mm ²)	1.74	1.89	19.86	18.54	26.14	25.15	18.90
Tensile strength (N/mm ²) after 21 days of water storage	1.67	1.83	9.41	9.49	14.11	14.50	8.89

^aThe determination of tensile elongation parameters was carried out in accordance with Ref 12 on a dumb-bell specimen of type 5A (Fig. 1). A single specimen was tested at a rate of 5 mm/min.

^bTwo-component silicone sealant approved for structural glazing application, Sikasil[®] SG-500 [13].

^cOne-component silicone sealant approved for structural glazing application, Sikasil[®] SG-20 [14].

^dThe temperature during water storage was 45°C. The test specimens were reconditioned for 1 day in room climate and immediately tested afterwards.

and examinations relating to the aging resistance of the bonding and the entire building component when exposed to regularly occurring stresses [6,15]. Based on the test protocol defined in the European Organization for Technical Approvals (EOTA) guideline [4], the aging resistance of acrylate bonds between untreated glass (i.e., annealed glass) and metals was examined using the following seven metal surfaces: Polished-chrome brass; matt-chrome brass; powder-coated brass; turned, polished, and sanded stainless steel; and anodized aluminum. These metals and surfaces represent state-of-the-art materials for interior and exterior glass fittings. Each test was conducted in conjunction with five different light curing acrylates under environmental exposure as defined in the EOTA guideline [4]. The goal of this assessment was to collect data pertaining to the long-term stability of 35 different material combinations (MCs), resulting from seven substrates and five acrylate adhesives (Table 3). However, a test specimen deviating in type and geometry from the EOTA guideline was used. A cylindrical tensile test was applied to determine the bond strength perpendicular to the bonded joint (Fig. 2). Here, a modification of the standardized specimen in Ref 16 was used to ensure an improved application of force into the glass due to plane load application in the glass. The specimen for the determination of the shear strength (Fig. 3) was a bonded single lap joint [17]. The glass and metal substrates were cleaned extensively before bonding by following this procedure.

Standard cleaning procedure of glass substrates in the examinations:

- (a) Removal of protective plastic film,
- (b) Identification of the tin-bath glass side with UV lamp and marking it accordingly,
- (c) Rinsing of glass with tap water,
- (d) Ultrasonic bathing for 5 min in demineralized water,
- (e) Storage on lint free cloth,
- (f) Degreasing of bond surfaces with ethanol,
- (g) Ultrasonic bathing for 5 min in demineralized water,
- (h) Perpendicular storage of glass substrates and drying on lint free cloth, and
- (i) Heat chamber drying for 30 min followed by
- (j) Immediate bonding.

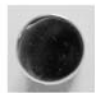


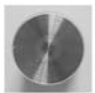
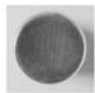
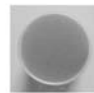
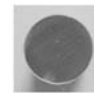
Standard cleaning procedure of metal substrates in the following examinations:

- (a) Ultrasonic bathing for 5 min in acetone,
- (b) Cleaning of the bond surfaces using acetone and lint free cloth, and
- (c) Allowance for solvent evaporation (5 min) followed by
- (d) Immediate bonding.

The tensile testing was carried out with a speed of 1 mm/min and the shear testing at a rate of 10 mm/min. Five specimens were tested and the mean value of the results was calculated for each series [6].

The strength of bonds is dependent on a variety of parameters [18]. An investigation of all parameters resulting from the various MCs, aging scenarios, methods of pre-treatments, and other factors would have required more than 10 000 test specimens. Such an extensive approach was not possible within the time limits of the project. The authors were able to reasonably reduce the num-

TABLE 3—MCs investigated.

		1	2	3	4	5	6	7
								
		B-PC, GU ^a	B-MC, GU ^b	B-PC, GU ^c	S-TU, GU ^d	S-PO, GU ^e	A-AN, GU ^f	S-SA, GU ^g
1	PB 04468	MC 11 ^h	MC 12	MC 13	MC 14	MC 15	MC 16	MC 17
2	PB 55727	MC 21	MC 22	MC 23	MC 24	MC 25	MC 26	MC 27
3	PB 55789	MC 31	MC 32	MC 33	MC 34	MC 35	MC 36	MC 37
4	PB 55779	MC 41	MC 42	MC 43	MC 44	MC 45	MC 46	MC 47
5	PB 56422	MC 51	MC 52	MC 53	MC 54	MC 55	MC 56	MC 57

^aPolished-chrome brass, untreated annealed glass (B-CP, GU).

^bMatt-chrome brass, untreated annealed glass (B-CM, GU).

^cPowder-coated brass, untreated annealed glass (B-PC, GU).

^dTurned stainless steel, untreated annealed glass (S-TU, GU).

^ePolished stainless steel, untreated annealed glass (S-PO, GU).

^fAnodized aluminum, untreated annealed glass (A-AN, GU).

^gSanded stainless steel, untreated annealed glass (S-SA, GU).

^hMC: Material combination. The numbers resulting from the combination of adhesives and materials were used to label the test specimens.

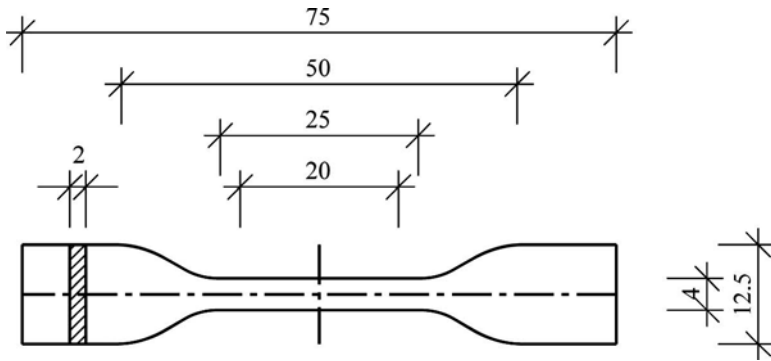


FIG. 1—Dumb-bell specimen used for comparison of physical properties of silicones and light curing acrylates (dimensions in millimeter).

ber of specimens to 3500 by using the subsequently described procedure.

Initially, an investigation of the influence of the different surfaces of the float glass (atmospheric or tin-bath side) on the tensile strength of the bond was carried out, considering the fact that the literature states different surface roughness values for the two glass surfaces [19,20]. Tin diffuses into the bath-side surface of float glass as a consequence of its production process [21]. As can be seen from Fig. 4(a), the tests showed up to 80 % higher tensile bond strength on the atmospheric side after 30 days of water immersion. The conditions of this test were as follows: Cylindrical specimens (as described above); adhesive layer thickness of 0.2 mm; immersion in 45°C warm water bath with 0.5 % (by weight) of a commercially available surfactant (standard cleaning product) added; 3, 7, 15 and 30 days of aging (immersion); and 24 h of recon-

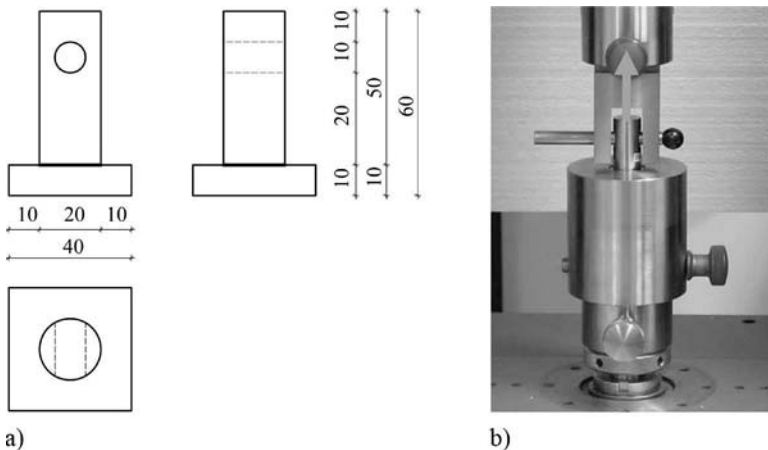


FIG. 2—Test specimen used to investigate tensile strength before and after aging: (a) schematic drawing of test specimen with dimensions in millimeter; (b) specimen placed in the testing machine.

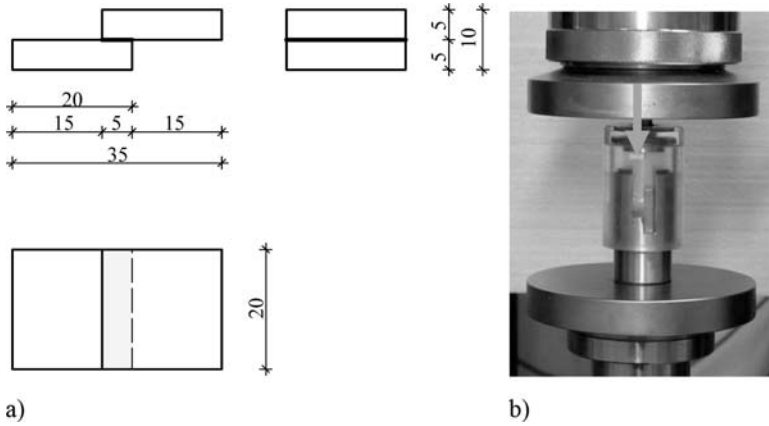


FIG. 3—Test specimen used to investigate shear strength before and after aging: (a) schematic drawing of test specimen with dimensions in millimeter; (b) specimen placed in the testing machine.

ditioning of the specimens at room climate before testing. Consequent to this initial test, all further testing was conducted only on samples where the adhesive was applied on the atmospheric side of the float glass.

In general, higher adhesive bond strength was also observed on the atmospheric glass side after 1 year of outdoor exposure. However, it should be stated that the adhesive capacity of the atmospheric side decreased significantly after 1 year of natural weathering, while the adhesive strength values for the bath side remained almost at the same level (Fig. 4(b)).

The strength of all MCs before and after 30 days of water treatment was examined in a subsequent screening. The conditions for the water treatment

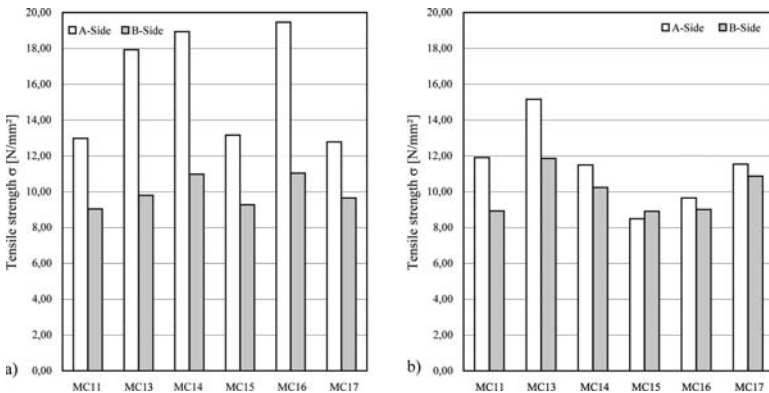


FIG. 4—Tensile strength before and after aging as determined for bath (B) and atmospheric (A) sides of the annealed glass: (a) after 30 days of water immersion; (b) after 1 year of natural weathering.

TABLE 4—Execution of aging tests in accordance with Ref 3.

Aging Scenario	Abbreviation
Bond strength at +23°C (dry)	IS ^a 23
Bond strength at -20°C (dry)	RS ^b 20
Bond strength at +80°C (dry)	RS 80
Water immersion with UV radiation—SUNTEST [®] equipment ^c	RS S
UV radiation (dry)	RS UV
Water immersion	RS WI
Humidity and sodium chloride environment	RS SC
Immersion in cleaning product	RS CP
Humidity and sulfur dioxide environment	RS SO ₂
Influence of contact materials	RS CM
Alternating climate test ^d	RS CT
Natural outdoor weathering for 1 year ^d	RS NW

^aIS: Initial strength.

^bRS: Residual strength.

^cSUNTEST[®] Cps+, Atlas Material Testing Technology LLC, Chicago, United States.

^dThese aging tests were in addition to the test protocol defined in Ref 4.

were as follows: Cylindrical specimens (as described above); thickness of the adhesive layer of 0.2 mm; and immersion in 45°C warm water to which 0.5 % (by weight) of a commercially available surfactant (standard cleaning product) had been added. By evaluating the results of these tests, the most promising combinations could be chosen for further testing [6].

The aging of the remaining 15 MCs was carried out on both types of specimens, i.e., tension and shear specimens. For these tests, a uniform thickness of the adhesive layer of 0.2 mm was used. The glass and metal substrates were cleaned by the described standard cleaning procedures and not pre-treated. Moreover, the aging scenarios recommended in the EOTA guidelines [4] were complemented by two additional tests (alternating climate test and natural weathering). The scenarios simulate indoor (heat, UV radiation, humidity, cleaning agents, etc.) and outdoor exposures (heat, cold, UV radiation, acid rain, de-icing salt, etc.), which can affect adhesive joints (see Tables 4 and 5). The initial and residual strengths after aging as well as the fracture pattern (cohesive, adhesive, mixed, or bulk failure of the bonded parts) were evaluated [22]. Furthermore, it was checked whether the residual strength remained above 75 % of the initial value prior to aging. A reduction in the bonding capacity by 25 % is allowed according to the EOTA guidelines [4] for silicone structural glazing sealants. This verification was also applied to the tested adhesives. Moreover, the characteristic load capacity at ultimate limit state was determined considering the requirements comprising temperatures of +23, -20, and +80°C.

The results of the aging tests in an abbreviated format, i.e., the tensile strengths after aging compared to the initial strengths, are presented in Table 6

TABLE 5—*Details of aging tests.*

Aging Scenario	Paragraph Number in Ref 4, Explanation of Additional Tests
Bond strength at +23°C (dry)	5.1.4.1.1, 5.1.4.1.2
Bond strength at -20°C (dry)	5.1.4.1.1, 5.1.4.1.2
Bond strength at +80°C (dry)	5.1.4.1.1, 5.1.4.1.2
Water immersion with UV radiation—SUNTEST® equipment	5.1.4.2.1
UV radiation (dry)	Storage in climatic exposure test cabinet WK11-600/40 ^a , 21 days of UV radiation (600 W), followed by reconditioning for 1 day in room climate
Water immersion	5.1.4.2.1
Humidity and sodium chloride environment	5.1.4.2.2
Immersion in cleaning product	5.1.4.2.4
Humidity and sulfur dioxide environment	5.1.4.2.3
Influence of contact materials	5.1.4.2.5, testing without UV radiation, seal assembling made of standard silicone (cure by-product: Acetic acid)
Alternating climate test	21 days of exposure based on a cycle of 4 h relative humidity of 95 %; 45°C, 4 h relative humidity of 30 % and 80°C; 4 h relative humidity of 30 % and -20°C, followed by reconditioning for 1 day in room climate

TABLE 5— (Continued.)

Aging Scenario	Paragraph Number in Ref 4, Explanation of Additional Tests
Natural outdoor weathering for 1 year	Storage of the specimens on the roof of a university building, 45° incline, direction South, installation of the specimens in the weathering rack ensures water drainage, weekly visual inspection, reporting of weather conditions provided by national weather office, after removal reconditioning for 1 day in room climate

^aWK11-600/40, Firma Weiss Umwelttechnik, GmbH, Simulation Equipment, Measuring Technology, Reiskirchen-Lindenstruth, Germany.

TABLE 6—Tensile strength after aging compared to the initial strength for several MCs.

	IS 23 (N/mm ²)	RS 80 (N/mm ²)	Verification	RS 20 (N/mm ²)	Verification
MC 14	17.50	7.20	0.41 < 0.75	17.80	1.02 > 0.75
MC 15	17.80	6.80	0.38 < 0.75	15.30	0.86 > 0.75
MC 16	17.50	5.10	0.29 < 0.75	17.10	0.98 > 0.75
MC 17	16.80	6.10	0.36 < 0.75	17.90	1.07 > 0.75
MC 26	16.30	6.90	0.42 < 0.75	19.80	1.21 > 0.75
MC 27	16.40	6.40	0.39 < 0.75	22.30	1.36 > 0.75
MC 36	15.30	8.00	0.52 < 0.75	24.60	1.61 > 0.75
MC 37	14.40	7.00	0.49 < 0.75	21.60	1.50 > 0.75
MC 56	15.00	6.50	0.43 < 0.75	22.70	1.51 > 0.75
MC 57	13.60	6.00	0.44 < 0.75	16.50	1.21 > 0.75
	IS 23 (N/mm ²)	RS S (N/mm ²)	Verification	RS UV (N/mm ²)	Verification
MC 14	17.50	10.20	0.58 < 0.75	17.40	0.99 > 0.75
MC 15	17.80	6.80	0.38 < 0.75	15.93	0.89 > 0.75
MC 16	17.50	10.30	0.59 < 0.75	21.03	1.20 > 0.75
MC 17	16.80	6.50	0.39 < 0.75	18.43	1.10 > 0.75
MC 26	16.30	10.30	0.63 < 0.75	18.73	1.15 > 0.75
MC 27	16.40	7.50	0.46 < 0.75	15.69	0.96 > 0.75
MC 36	15.30	12.40	0.81 > 0.75	20.48	1.34 > 0.75
MC 37	14.40	9.30	0.65 < 0.75	17.41	1.21 > 0.75
MC 56	15.00	14.00	0.93 > 0.75	18.67	1.24 > 0.75
MC 57	13.60	12.30	0.90 > 0.75	13.30	0.98 > 0.75
	IS 23 (N/mm ²)	RS WI (N/mm ²)	Verification	RS CP (N/mm ²)	Verification
MC 14	17.50	18.90	1.08 > 0.75	16.70	0.95 > 0.75
MC 15	17.80	13.20	0.74 < 0.75	14.30	0.80 > 0.75
MC 16	17.50	19.50	1.11 > 0.75	14.60	0.83 > 0.75
MC 17	16.80	12.80	0.76 > 0.75	16.40	0.98 > 0.75
MC 26	16.30	13.30	0.82 > 0.75	13.50	0.83 > 0.75
MC 27	16.40	10.40	0.63 < 0.75	7.90	0.48 < 0.75
MC 36	15.30	18.60	1.22 > 0.75	5.60	0.37 < 0.75
MC 37	14.40	13.20	0.92 > 0.75	1.10	0.08 < 0.75
MC 56	15.00	19.30	1.29 > 0.75	15.90	1.06 > 0.75
MC 57	13.60	14.40	1.06 > 0.75	17.80	1.31 > 0.75
	IS 23 (N/mm ²)	RS SC (N/mm ²)	Verification	RS CT (N/mm ²)	Verification
MC 14	17.50	3.98	0.23 < 0.75	21.09	1.21 > 0.75
MC 15	17.80	6.17	0.35 < 0.75	17.96	1.01 > 0.75
MC 16	17.50	9.39	0.54 < 0.75	21.94	1.25 > 0.75
MC 17	16.80	5.41	0.32 < 0.75	21.45	1.28 > 0.75
MC 26	16.30	18.78	1.15 > 0.75	20.91	1.28 > 0.75

TABLE 6— (Continued.)

	IS 23 (N/mm ²)	RS 80 (N/mm ²)	Verification	RS 20 (N/mm ²)	Verification
MC 27	16.40	7.68	0.47 < 0.75	18.01	1.10 > 0.75
MC 36	15.30	19.81	1.29 > 0.75	22.20	1.45 > 0.75
MC 37	14.40	0.57	0.04 < 0.75	20.45	1.42 > 0.75
MC 56	15.00	18.10	1.21 > 0.75	17.04	1.14 > 0.75
MC 57	13.60	8.94	0.66 < 0.75	18.39	1.35 > 0.75

Note: The italic marked rows indicate the bonding on anodized aluminum. The others are bonds on several stainless steel surfaces. Text and figures in bold indicate whether the residual strength remained above 75 % of the initial value prior to aging.

for several MCs. The tensile strengths and the shear strengths in comparison are shown in Table 7. In principle a higher reduction in the bearing capacity with aging was found for specimens under shear stresses in contrast to specimens under tensile stresses. This might be caused by the essentially more disadvantageous ratio of the linear perimeter to the square area of the adhesive joint (0.5 mm^{-1} compared to 0.2 mm^{-1} for shear and tensile specimens, respectively). Eventually the bonding is penetrated quicker and degraded by the surrounded medium. The result is a larger loss of stiffness. Furthermore, it was found that different stainless steel surfaces (MC 14: turned stainless steel; MC 15: polished stainless steel; and MC 17: sanded stainless steel) did not result in essentially different load bearing capacities of the adhesive joint. Good residual load capacities after aging were attained for bonds to anodized aluminum (see Table 6).

The shear strength did not achieve the required residual strength of 75 % for any of the MCs after exposure in the SUNTEST[®] Cps+ weathering test equipment (Fig. 5). Exposure to pure water produced a similar decrease. Other aging tests involving permanent humid exposure resulted in significantly re-

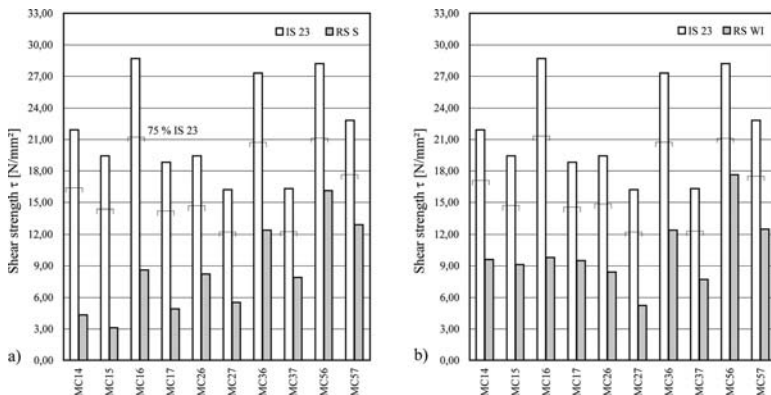


FIG. 5—Residual strength of selected MCs: (a) after 21 days of SUNTEST[®] exposure (RS S); (b) after 21 days of water exposure (RS WI).

TABLE 7—Tensile and shear strength in comparison.

	Tensile Strength			Shear Strength		
	IS 23 (N/mm ²)	RS S (N/mm ²)	Verification	IS 23 (N/mm ²)	RS S (N/mm ²)	Verification
MC 14	17.50	10.20	0.58 < 0.75	21.90	4.30	0.20 < 0.75
MC 15	17.80	6.80	0.38 < 0.75	19.40	3.10	0.16 < 0.75
MC 16	17.50	10.30	0.59 < 0.75	28.70	8.60	0.30 < 0.75
MC 17	16.80	6.50	0.39 < 0.75	18.80	4.90	0.26 < 0.75
MC 26	16.30	10.30	0.63 < 0.75	19.40	8.20	0.42 < 0.75
MC 27	16.40	7.50	0.46 < 0.75	16.20	5.50	0.34 < 0.75
MC 36	15.30	12.40	0.81 > 0.75	27.30	12.40	0.45 < 0.75
MC 37	14.40	9.30	0.65 < 0.75	16.30	7.90	0.48 < 0.75
MC 56	15.00	14.00	0.93 > 0.75	28.20	16.10	0.57 < 0.75
MC 57	13.60	12.30	0.90 > 0.75	22.80	12.90	0.57 < 0.75
	IS 23 (N/mm ²)	RS WI (N/mm ²)	Verification	IS 23 (N/mm ²)	RS WI (N/mm ²)	Verification
MC 14	17.50	18.90	1.08 > 0.75	21.90	9.60	0.44 < 0.75
MC 15	17.80	13.20	0.74 < 0.75	19.40	9.10	0.47 < 0.75
MC 16	17.50	19.50	1.11 > 0.75	28.70	9.80	0.34 < 0.75
MC 17	16.80	12.80	0.76 > 0.75	18.80	9.50	0.51 < 0.75
MC 26	16.30	13.30	0.82 > 0.75	19.40	8.40	0.43 < 0.75
MC 27	16.40	10.40	0.63 < 0.75	16.20	5.20	0.32 < 0.75
MC 36	15.30	18.60	1.22 > 0.75	27.30	12.40	0.45 < 0.75
MC 37	14.40	13.20	0.92 > 0.75	16.30	7.70	0.47 < 0.75
MC 56	15.00	19.30	1.29 > 0.75	28.20	17.60	0.62 < 0.75
MC 57	13.60	14.40	1.06 > 0.75	22.80	12.50	0.55 < 0.75

Note: Text and figures in bold indicate whether the residual strength remained above 75 % of the initial value prior to aging.

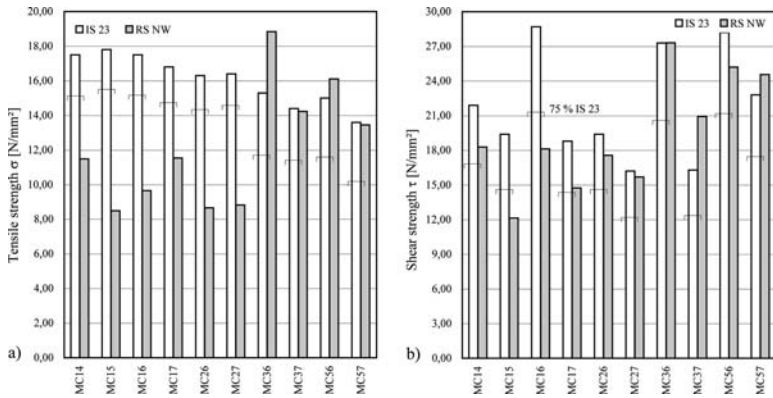


FIG. 6—Residual strength of selected MCs after 1 year of outdoor exposure: (a) tensile strength; (b) shear strength.

duced strength as well. Nonetheless, the residual capacities are still significantly higher compared to structural silicones, which possess strength values of approximately 1 N/mm². Any water impact is therefore problematic and should be avoided. The resulting construction must therefore be designed in such a way that the adhesive joint is not permanently exposed to water and the drying of the bond is ensured. A mere UV radiation yielded a hardening of the bond, which may be caused by subsequent cross-linking of the adhesive.

The influence of thermal and climatic cycling proved to be unproblematic. The results of the alternating climate test (21 days exposure based on a cycle of 4 h relative humidity of 95 % and 45 °C; 4 h relative humidity of 30 % and 80 °C; and 4 h relative humidity of 30 % and -20 °C; followed by reconditioning for 1 day in room climate) verify that short exposure to condensation water does not affect the adhesive bond if joint drying is ensured. The reduction in the strength was significant when exposed to a temperature of +80 °C (specimens immediately tested without reconditioning); however, the transferable forces are still much higher compared to silicone (see Table 6).

The acrylic adhesives show excellent performance after 1 year of outdoor exposure (Fig. 6). A higher reduction in the tensile strength was observed for the acrylates PB 4468 and PB 55727 in combination with stainless steel (MC 14, MC 15, MC 17, and MC 27) and anodized aluminum (MC 16 and MC 26). In contrast, the acrylates PB 55789 and PB 56422 showed even higher initial load bearing capacities or had only a minor reduction in tensile strength, respectively (MC 36, MC 37, MC 56, and MC 57). At this point the dependence of the bond strength on the specific acrylate used is particularly obvious.

To improve the residual capacity after 21 days of water exposure for selected MCs (MC 13, MC 15, and MC 35) under shear load Pyrosil[®]-treatment, atmospheric plasma treatment and sandblast coating (SACO) surface treatment methods on the metal surfaces were applied.

Pyrosil[®] is a pyrolytic chemical pre-treatment process that forms an amorphous silicate layer on the treated surfaces. Afterwards the surfaces are coated with silane adhesion promoters, which are normally a few micrometers thick.

Basic products are alkoxy-silanes applied on the surface by a pen-like torch. Afterwards a standard silane-based primer is applied on the created SiO_x layer. Surfaces treated with this procedure show increased adhesion and climatic consistencies [18,23,24]. The substrates were treated ten times at a feed rate of 10 cm/s. Thereafter the primer MP94E³ was applied.

The SACO[®] method⁴ connects mechanical abrasion with simultaneous coating using a chemically modified grit. The high impact energy creates very high temperatures only on the surface but causes no heating on the joining parts. Using this procedure a part of the reactive components of the grit (corundum) or of its coating is embedded in the metallic or non-metallic substrate surface. The chemical modification of the grit includes a silanisation and simultaneous adding of activators (metal powder and metallic salts). Afterwards a primer coating with a silane-based solution is applied on the surface. The SACO[®] procedure increases the adhesion behavior on the surfaces after exposure to moisture and temperature [18]. In these examinations the substrates were cleaned by the standard method, then sandblasted (RocatecTM-Pre⁵), and thereafter treated with coated grit (RocatecTM-Plus). Finally the silane adhesion promoter ESPETM SIL was applied.

At the Openair[®] plasma⁶ pre-treatment procedure, the surfaces are pre-treated by ionized gas (plasma). Gas ionizes and changes to plasma at further energy supply. After contact with material surfaces, the additionally supplied energy is transferred to the substrate and enables the subsequent surface reactions. Pre-treated surfaces display a higher wettability due to the creation of polar groups. Thereby the adhesive behavior of the surfaces and the durability of the bonding can be improved [18,25,26]. The process parameters for pre-treating the substrates by the Openair[®] plasma process were adjusted as following:

- (a) Maximal voltage of 289 V,
- (b) minimal speed of 0.6 m/min,
- (c) Diameter of vertical duct $d = 4$ mm,
- (d) Pressure of 2.5 bar,
- (e) Distance duct to surface $a = 14$ mm, and
- (f) Surface treatment for two times.

Tests executed on glass-to-glass bonds showed that a subsequent pre-treatment with the Pyrosil[®]-process after cleaning and degreasing produced the best results. In order to examine pre-treatment methods for metal substrates in glass-to-metal bonds, the glass plates were all pre-treated with the Pyrosil[®]-process.

The initial strength of the MC 35 (polished stainless steel, PB 55789) was effectively increased by pre-treating the surfaces. The least amount of strength reductions after water exposure was observed after a treatment of the metal utilizing the Pyrosil[®] or SACO process (sandblasting coat). The residual strength was significantly improved compared to standard surface cleaning

³SURA Instruments GmbH, Jena, Germany.

⁴DELO Industrial Adhesives, Windach, Germany.

⁵RocatecTM-Pre, RocatecTM-Plus, ESPETM SIL: 3M Deutschland GmbH, Neuss, Germany.

⁶Plasmatrete GmbH, Steinhagen, Germany.

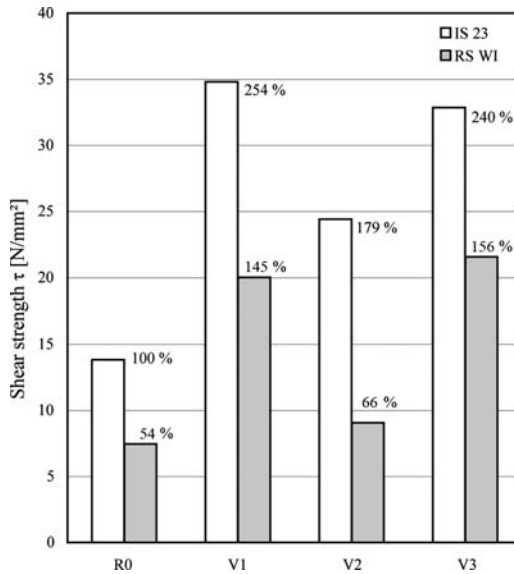


FIG. 7—Residual strength of the bonding on pre-treated polished stainless steel (MC 35) compared to standard cleaning (R0 standard cleaning, V1 Pyrosil[®] treatment based on R0, V2 atmospheric plasma treatment after R0, V3 sandblasting coat according to R0).

(Fig. 7). A prevailing adhesive failure was unavoidable however. MCs 13 and 15 showed no noticeable improvement as a result of this pre-treatment.

In summary, stainless steel and, in particular, anodized aluminum can be regarded as appropriate metal surfaces for bonds formed by acrylates. A pre-treatment of surfaces increases the residual adhesive strength.

In these examinations predominately point fixations were investigated. Because of the different temperature expansion behavior between glass, adhesive, and especially aluminum, the applicability and the parameters of linear bonding still have to be investigated.

Tests on Life-Size Structural Components

Apart from the investigation of the aging behavior on the basis of small test specimens, the load bearing behavior of bonded structural members was determined according to the guidelines and standards valid in Germany. In particular, panes bonded as part of safety glazing were examined, adhesively joined overhead glazing as well as bonded glass lamellas [5]. The tests (load bearing capacity and post breakage behavior) were conducted on non-aged elements. Homogenously bonded structural members were exposed to the outdoor weathering. These structures are regularly checked regarding VIS changes in the adhesive joint and will be tested after 5 years of outdoor weathering. The results of the bonded glass lamellas will be presented shortly hereafter. The testing comprised two different glass lamella systems. One was a single span

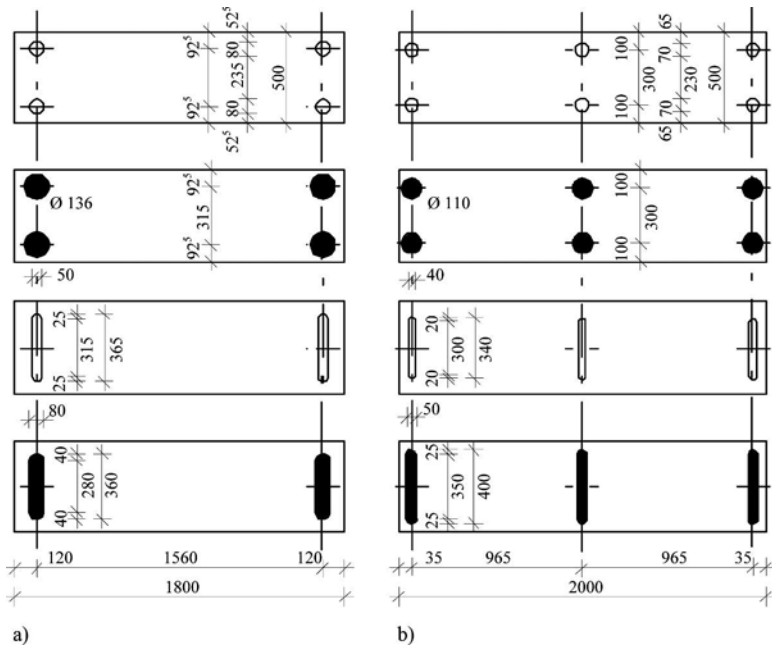


FIG. 8—Tested glass lamella systems (dimensions in millimeter): (a) single span beam; (b) two-field continuous beam. Black surfaces show the silicone bonding.

beam system (two supports at the end of the glass) and the other was a two-field continuous system (three supports over the length of the glass). Two different fixing systems, point fixation or linear joints, were examined. One UV and VIS light curing acrylate and one conventional structural sealant glazing silicone were used (Fig. 8).

The laminated safety glass (laminates made of two or more glass panes with an interlayer foil) consisted of two heat-strengthened glass panes with a thickness of $d=8$ mm with a solar control coating and a 1.52 mm thick polyvinyl butyral foil as interlayer. Compared to regular annealed glass, heat-strengthened glass has an increased breaking strength. The glass panes and high-grade steel fixings were either bonded with silicone Sikasil[®] SG 500 or acrylate PB 4432. The adhesive joints were manufactured at constant climatic conditions with a temperature of approximately 20°C and a relative humidity of 45%. The surfaces of the glass and of the high-grade steel fixings were cleaned and degreased with DELOTHEN[®] EP solvent-based cleaner⁴. The thickness of the silicone layer was adjusted to 4 mm by using a double-sided spacer tape. The thickness of the acrylate bond was set to 0.2 mm by inserted spacing wires.

The governing load combination for the bearing capacity tests resulted from tensile stress (wind suction) with simultaneously overlaid shear stress (dead load and ice load). The glass lamellas were installed horizontally into the testing device (Fig. 9). The laminated safety glass was suspended from the fixa-

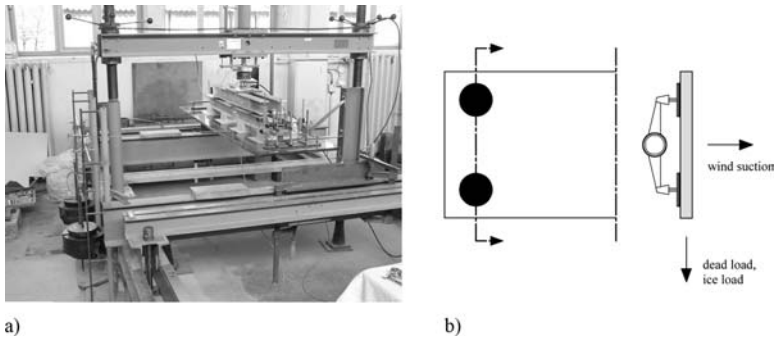


FIG. 9—(a) Governing load of the glass lamellas in the bearing capacity test. (b) The bonded joints were loaded by dead and ice loading (shear stress) as well as wind suction (tensile stress).

tion by bonding. The load was applied by the testing machine almost plane on the glazing. Hence, the bonded joints were loaded by tensile stress. Due to the horizontal test installation, the dead and ice loads were simulated at the glass edge by a rope system to generate shear stresses (Fig. 10).

Glass failure due to direct contact of glass and metal was prevented by suitable intermediate materials. The investigations at the single span beams had to be stopped due to large deformations at fourfold characteristic load. The two-field continuous beam withstood up to the eightfold of the initial load. Two of four lamellas failed due to glass breakage and in one case the metallic sub-construction broke. The glass was pulled out completely up to the polyvinylbutyral (PVB) interlayer by the bonded point fixing (Fig. 11). The bonded joints remained always intact. The maximum tensile stress of the acrylate bonding was 0.75 N/mm^2 superimposed with simultaneously acting shear stress of 0.05 N/mm^2 .

Subsequently, the lamellas were successfully tested for their residual bearing capacity after glass breakage (post breakage behavior). Loaded only with its self-weight, the broken glass pane had to remain on its supports within 24 h. This ensures the protection of accessible public areas underneath the broken glass pane.

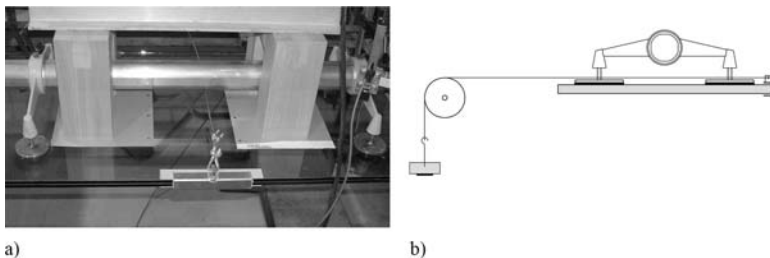


FIG. 10—(a) Detail of the load application of dead load and ice load into the glass edge. (b) Load application of dead load and ice load into the glass edge.

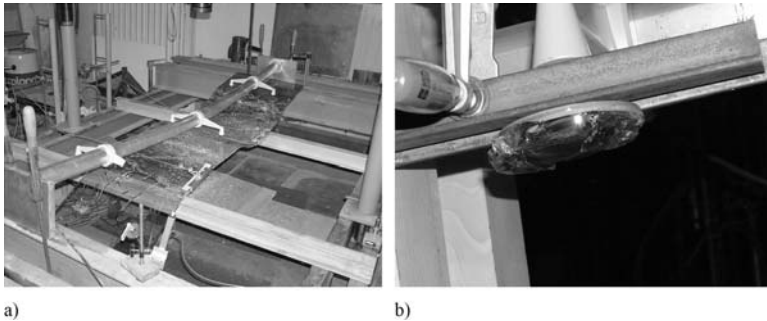


FIG. 11—(a) Two-field continuous beam failed due to glass breakage. (b) Point-fixed acrylate bonding pulled out up to the PVB interlayer.

The suitability of the examined structural elements with non-aged adhesive joints could be proven for both adhesive systems. Both types of bonded glass lamellas using acrylate are still subject to natural weathering. They will be examined after 5 years using the same approach.

Summary

The results of the small sample tests and the structural element tests generate an initial basis to evaluate UV and VIS light curing acrylates relative to the different criteria of structural glass applications exhibited under interior and exterior conditions. Continuing investigations need to focus on the improvement of the residual strength after aging and the determination of bearing capacity of adhesively bonded elements after natural weathering.

Acknowledgments

Special thanks are given to KL Beschläge Karl Loggen (Eitorf), Delo Industrial Adhesives (Windach), and the Institute of Material and Beam Technology, Fraunhofer Gesellschaft (Dresden). The testing of the full-scale specimens was technically and financially supported by Sika Services AG (Zurich) and Colt International (Berlin).

References

- [1] Weller, B., Härth, K., Tasche, S., and Unnewehr, S., *Glass in Building—Principles, Applications, Examples*, Birkhäuser, Basel, Switzerland, 2009.
- [2] Schadow, T., 2006, “Beanspruchungsgerechtes Konstruieren von Klebverbindungen in Glastragwerken [Designing Adhesively Bonded Joints to Meet Structural Requirements],” Ph.D. thesis, Technische Universität Dresden, Dresden, Germany.
- [3] DIN 5031-7, January 1984, “Optical Radiation Physics and Illumination Engineering—Part 7: Terms of Wavebands,” Beuth, Berlin.

- [4] ETAG 002, 1999, "Guideline for European Technical Approval for Structural Sealant Glazing Systems (SSGS), Part 1: Supported and Unsupported Systems," EOTA, Brussels, Belgium.
- [5] Witek, G., "Modified Acrylates Adhesives DELO-PHOTOBOND for Bonding in Glass Construction, *Glasbau2004*, Dresden, April 2, 2004, Technische Universität Dresden, Dresden, Germany.
- [6] Tasche, S., 2007, "Strahlungshärtende Acrylate im Konstruktiven Glasbau [Light Curing Acrylates in Glass Structures]," Ph.D. thesis, Technische Universität Dresden, Dresden, Germany.
- [7] DELO Industrial Adhesives, *Data Sheet DELO-PHOTOBOND[®] 4468*, Landsberg, Germany, 2005.
- [8] DELO Industrial Adhesives, *Data Sheet DELO-PHOTOBOND[®] AD VE 55727*, Landsberg, Germany, 2005.
- [9] DELO Industrial Adhesives, *Data Sheet DELO-PHOTOBOND[®] AD VE 55789*, Landsberg, Germany, 2005.
- [10] DELO Industrial Adhesives, *Data Sheet DELO-PHOTOBOND[®] GB VE 56422*, Landsberg, Germany, 2006.
- [11] DELO Industrial Adhesives, *Data Sheet DELO-PHOTOBOND[®] 4432*, Landsberg, Germany, 2002.
- [12] DIN EN ISO 527-2, July 1996, "Plastics—Determination of Tensile Properties—Part 2: Test Conditions for Moulding and Extrusion Plastics," Beuth, Berlin.
- [13] Sika Services AG, *Product Data Sheet Sikasil[®] SG-500*, Zurich, Switzerland, 2006.
- [14] Sika Services AG, *Product Data Sheet Sikasil[®] SG-20*, Zurich, Switzerland, 2006.
- [15] Wiesner, S., "Adhesive Technology in Glass Construction," *Glasbau2004*, Dresden, April 2, 2004, Technische Universität Dresden, Dresden, Germany.
- [16] DIN EN 26922, May 1993, "Adhesives—Determination of Tensile Strength of Butt Joints," Beuth, Berlin.
- [17] DELO-Standard 5, 2003, "Standard of DELO Industrial Adhesives," DELO Industrial Adhesives, Landsberg, Germany.
- [18] Habenicht, G., *Kleben, Grundlagen, Technologie, Anwendungen [Bonding, Bases, Technology, Applications]*, Springer, Berlin, 1997.
- [19] Lotz, S., 1995, "Untersuchungen zur Festigkeit und Langzeitbeständigkeit Adhäsiver Verbindungen Zwischen Fügepartnern aus Floatglas [Studies on Strength and Durability of Adhesive Connections with Annealed Glass]," Ph.D. thesis, Technische Universität Kaiserslautern, Kaiserslautern, Germany.
- [20] Peters, S., 2006, "Kleben von GFK und Glas für Baukonstruktive Anwendungen [Bonding of GRP and Glass for Structural Applications]," Ph.D. thesis, Universität Stuttgart, Stuttgart, Germany.
- [21] Schiffner, U., Langer, A., Seibold, M., Wagner, G., Hüther, R., and Bröring, K., *Fügen von Glas [Joining of Glass]*, HVG, Offenbach, Germany, 1995.
- [22] DIN EN ISO 10365, August 1995, "Adhesives—Designation of Main Failure Patterns," Beuth, Berlin.
- [23] Tiller, H.-J., Schimanski, A., Grünler, B., and Glock-Jäger, K., "Deposition of C-CVD-SiOx on Glass Surfaces—An Alternative Low Cost Process for Various Applications," *Glass Processing Days*, Tampere, Finland, June 17–20, 2005, Tamglass, Ltd., Oy, Tampere, Finland.
- [24] Weidl, R., Zobel, B., Heft, A., Pfuch, A., Gitter, U., Grünler, B., Richter, T., and Erber, C., "Atmosphärendruck C-CVD Beschichtungsverfahren—Trends und Entwicklungen" (C-CVD Deposition Methods at Atmospheric Pressure—Trends and Developments)," *Galvanotechnik*, Vol. 98, August 2007, pp. 1978–1982.
- [25] Geiß, P. L. and Wagner, A., "Adhäsion mit Plasma [Adhesion with Plasma]," *Sixth*

Praxisseminar Kleben, Jena, Germany, February 12, 2008, IFW, Jena, Germany.

- [26] Schüßler, J., "Reinigen, Aktivieren und Beschichten mit Openair[®]-Plasmatechnik von Verschiedensten Materialien" [Cleaning, Activation and Coating of Different Materials with Openair[®] Plasma], *Sixth Praxisseminar Kleben*, Jena, Germany, February 12, 2008, IFW, Jena, Germany.

D. Longo¹ and P. Vandereecken¹

Relative Resistance of Silicone and Si-Hybrid Based Sealants to Alternating Periods of Accelerated Weathering and Thermo-Mechanical Movements

ABSTRACT: Sealants used in weatherseal applications are subject to both environmental and mechanical aging during their service life. Environmental aging consists of interaction with sunlight, rain, or moisture, and other atmospheric agents such as ozone. Mechanical aging is linked to the expansion and contraction of the different substrates (glass, concrete...) due to temperature variations. In order to assess the durability of sealants, the ISO 11600 norm includes separate tests for movement capability (ISO 9047) and UV irradiation (ISO 11431) but no combinations of those tests. In 1991, the RILEM TC139-DBS "Durability of Building Sealants" was created to develop new and more adapted testing. The testing proposed by this comity, was a combination of accelerated weathering (humidity and UV) combined with thermo-mechanical cycling. This study compares the durability of silicone sealants and newly developed Si-modified organic based sealants using alternated cycles of ISO 11431 and ISO 9047 during a one year period. Results show that most Si-modified organic will show limited durability in weatherseal applications mostly because of poor UV resistance. Newly developed Si-organic based sealants tested during this work show excellent UV resistance but poor elastic recovery after compression at high temperature (70 °C). This poor elastic recovery limits their long term movement capability. However, good durability can be expected with designs leading to lower movement capability than those obtained from the ISO 11600 testing.

KEYWORDS: durability, weatherseal, resistance, silicone, hybrid, weathering, thermo-mechanical

Manuscript received May 30, 2008; accepted for publication December 12, 2008; published online January 2009.

¹ Dow Corning Europe SA, 7180 Seneffe, Belgium.

Cite as: Longo, D. and Vandereecken, P., "Relative Resistance of Silicone and Si-Hybrid Based Sealants to Alternating Periods of Accelerated Weathering and Thermo-Mechanical Movements," *J. ASTM Intl.*, Vol. 6, No. 2. doi:10.1520/JAI101912.

Copyright © 2009 by ASTM International, 100 Barr Harbor Drive, PO Box C700, West Conshohocken, PA 19428-2959.

Introduction

The successful performance of a building's exterior is frequently defined by its ability to keep rain and the elements outside, away from the building's occupants. One of the critical links in ensuring a weatherproof building is the joint sealant.

Due to their in-use functionality, those sealants are subject to both environmental and mechanical aging during their service life. Environmental aging is caused by interactions with solar radiation, heat, and moisture in the form of rain, humidity, or dew, and other atmospheric agents such as oxygen and ozone. Mechanical aging is induced by the expansion and contraction of the different substrates (glass, concrete...) due to temperature variations between night and day (diurnal cycles) or summer and winter (annual cycles). Sealant movement exposure can range from 10 to 50 % depending on the width of the joint used and the building design.

In order to assess the relative stability of sealants to environmental and mechanical factors, the ISO 11600 [1] standard includes separate tests for movement capability (ISO 9047) [2] and for resistance to ultraviolet (UV) radiation (ISO 11431) [3] but no combinations of those tests. In 1991, the RILEM TC139-DBS committee "Durability of Building Sealants" was created to develop a new and more suitable testing procedure that better reflected the actual in-service situation where the sealed joint is exposed to weathering and movement cycles [4]. The test method proposed by this technical committee was based on a combination of laboratory accelerated weathering (light, heat, and moisture) with thermo-mechanical cycling. In the present study, stabilities of sealants were assessed by exposing them to periods of laboratory accelerated weathering alternating with thermo-mechanical cycling.

In structural glazing applications, resistance of the sealant's adhesion to UV irradiation is more important than in standard weathersealing applications since the UV component of sunlight can reach the sealant/glass interface directly through the glass. For this specific application, silicone sealants outperform organic polymer based sealants. In the early 2000s, most float glass manufacturers started the commercialization of self-cleaning glasses. The effectiveness of those glasses is negatively influenced by contamination induced by silicone sealants and therefore sealants based on newly developed Si-modified organic (hybrid) polymers were increasingly evaluated for this application. Some of these Si-modified organic sealants were able to pass the requirements of ISO 11600 LM 25G.²

This study compares the resistance to weathering and thermo-mechanical movement of silicone sealants with those newly developed Si-modified organic polymer based sealants using cycles of alternating exposure to UV according to ISO 11431 [3] and thermo-mechanical cycling according to ISO 9047 [2] for an exposure duration of one year. In all weathersealing applications the sealant is exposed to sunlight and its UV component and even more so for structural glazing where the transmission occurs directly through the glass. The objective

²LM=Low Modulus; 25:±25 % movement capability according to ISO 9047; G =Glazing applications.

of this study was to evaluate the long-term behavior of sealants in weathersealing applications with UV exposure through glass.

Testing Methodology

The requirements of class ISO 11600 LM 25G do not stipulate any serious durability tests. The resistance of a sealant's adhesion on glass to artificial light and water is evaluated according to ISO 11431 [3], which comprises 500 hours of exposure to light through glass followed by 24 hours of extension at 100 %. Furthermore, the sealant's adhesion and cohesion is evaluated according to ISO 9047 [2], which comprises four thermo-mechanical cycles of 25 % compression at 70 °C followed by 25 % extension at -20 °C conducted during a period of two weeks.

However, it is generally assumed that 500 hours of artificial light exposure is less than one year exposure to sunlight in a northern location and that the four thermo-mechanical cycles of ISO 9047 [2] do not reflect the numerous diurnal and annual cycles that building joint sealants are subjected to during their service-life. Therefore, in 1991 the RILEM TC139-DBS committee "Durability of Building Sealants" was created with the objective to develop an improved testing procedure that better reflects the actual in-service situation where the sealed joint is continuously exposed to weathering and movement cycles [4].

The test procedure proposed by this committee is based on a laboratory accelerated weathering (UV radiation, heat, and moisture) alternating with thermo-mechanical cycling [4]. Although it was recognized by the RILEM committee based on previous studies that mechanical cycling during weathering was more severe than alternate weathering and movement cycles, the latter approach is generally used for simplicity reasons. In order to compare the durability of silicone sealants to that of newly developed Si-hybrid sealants, a similar testing procedure was applied in this study.

The test procedure used in this study exposed the sealant test specimen to 500 hours of fluorescent UVA-340 light, with the light exposure occurring as in ISO 11431 [3], and subsequent thermo-mechanical cycling (25 % compression at 70 °C followed by 25 % extension at -20 °C) as in ISO 9047 [2]. The complete exposure cycle of artificial light exposure and mechanical cycling lasted for about 600 h. The sealant specimen was considered as having failed if more than 20 % cohesive or adhesive failure was observed or if the elastic recovery degraded to less than 50 %, which typically meant that a "chewing gum effect" was observed. The testing was performed both for ± 20 % and ± 25 % movement exposure.

As described in the detailed procedure below, the first thermo-mechanical movement capability test is carried out only after three weeks cure and 500 h fluorescent UVA-340 exposure. This leaves enough time for the sealants to cure and build up adhesion. The method used in this study makes no attempt to emulate premature failures that can occur in buildings due to movements during the cure or due to slow adhesion build up of the sealant but focuses only the evaluation of the long term resistance aspect. It should be noted that silicone

based sealants, due to their higher water vapor permeability, generally show faster cure and adhesion build up than organic or Si-hybrid sealants.

The experimental procedure is described in detail below.

Detailed Procedure

Testing Based on $\pm 25\%$ Movement Exposure

1. Standard glass tensile/adhesion joints according to ISO 8339 [5] (12 by 12 by 50 mm³) are cured for three weeks under standard climate of 23 ± 2 °C and $50 \pm 5\%$ relative humidity.
Glass supports are 12 by 6 by 75 mm³ in dimensions.
2. The tensile/adhesion joints are placed in an artificial weathering apparatus with a fluorescent UVA-340 light source and subjected to cycles of 102 min light exposure followed by 18 min water spray (light exposure off during water spray) for a total duration of 500 h (with irradiation occurring through one of the glass supports as described in ISO 11431 [3]).
3. Test specimens are removed from the fluorescent UVA-340 apparatus and left for 24 h of reconditioning at standard climate of 23 ± 2 °C and $50 \pm 5\%$ relative humidity.
4. Test specimens are elongated by 100 % and left for 24 h under constant elongation (with the help of spacers).
5. After 24 h extension, the spacers are removed and elastic recovery is recorded after one hour of relaxation (ISO 7389) [6].
6. Test specimens are conditioned for three hours at 70 °C, and then stored compressed by 25 % for 21 h at that temperature. Samples are then conditioned for 3 h at -20 °C and then extended by 25 % during 21 h using a modification of the ISO 9047 standard [2].
7. Test specimens are then placed back into the fluorescent UVA-340 apparatus to start the second cycle (with irradiation occurring through the same glass support as in the previous cycle).
8. The test is stopped when failure (either cohesive or adhesive) of more than 20 % of the adhesion area (600 mm²) is observed or if elastic recovery falls below 50 %.

Testing Based on $\pm 20\%$ Movement Exposure

1. Standard glass tensile/adhesion joints according to ISO 8339 [5] (12 by 12 by 50 mm³) are cured for three weeks under standard climate of 23 ± 2 °C and $50 \pm 5\%$ relative humidity.
Glass supports are 12 by 6 by 75 mm³ in dimensions.
2. The tensile/adhesion joints are placed in an artificial weathering apparatus with a fluorescent UVA-340 light source and subjected to cycles of 102 min light exposure followed by 18 min water spray (light exposure off during spray) for a total duration of 500 h (with irradiation occurring through one of the glass supports as described in ISO 11431 [3]).
3. Test specimens are removed from the fluorescent UVA-340 apparatus

TABLE 1—Sealant durability for 25 % movement capability.

Sealant	Elastic Recovery	Number of Cycles	Failure
Silicone polymer base I	>90 %	>10	NF
Silicone polymer base II	>90 %	>10	NF
Silicon-polyether base	60–75 %	0–1	AF
Silicon-polyurethane base	60–70 %	0	AF
Silicon-acrylate base I	60–75 %	1–2	CF
Silicon-acrylate base II	60–75 %	1–2	CF

AF=Adhesive failure.

CF=Cohesive failure.

NF=No failure observed.

and left for 24 h of reconditioning at standard climate of 23 ± 2 °C and 50 ± 5 % relative humidity.

4. Test specimens are elongated by 60 % and left for 24 h under constant elongation (with the help of spacers).
5. After 24 h, the spacers are removed and elastic recovery is recorded after one hour of relaxation (ISO 7389) [6].
6. Test specimens are conditioned for three hours at 70 °C, and then stored compressed by 20 % for 21 h at that temperature. Samples are then conditioned for 3 h at -20 °C and then extended by 20 % during 21 h using a modification of the ISO 9047 standard [2].
7. Test specimens are placed back into the fluorescent UVA-340 apparatus to start the second cycle (with irradiation occurring through the same glass support as in the previous cycle).
8. The test is stopped when failure (either cohesive or adhesive) of more than 20 % of the adhesion area (600 mm^2) is observed or if elastic recovery fell below 50 %.

Sealants Studied

Different sealants have been tested using the above described procedure, both for ± 20 % and ± 25 % enforced movement exposure. Two silicone polymer based sealants commonly used in weatherseal applications were used as references. Different commercially available sealants based on Si-modified organic polymers were tested for comparison; conventional polyurethane and acrylic based sealants were excluded from this study. The Si-modified organic polymer based sealants tested are classified into silicon-polyether based, silicon-polyurethane based, and silicon-acrylate based (I). A new silicon-acrylate based sealant (II) for self-cleaning glass applications was also part of the evaluation program.

Table 1 shows results for 25 % movement exposure and Table 2 for 20 % movement exposure.

Tables 1 and 2 show the excellent resistance of silicone based sealants to

TABLE 2—*Sealant durability for 20 % movement capability.*

Sealant	Elastic Recovery	Number of Cycles	Failure
Silicone polymer base I	>90 %	>10	NF
Silicone polymer base II	>90 %	>10	NF
Silicon-polyether base	60–75 %	1–2	AF
Silicon-polyurethane base	60–70 %	0	AF
Silicon-acrylate base I	60–75 %	5–6	CF
Silicon-acrylate base II	60–75 %	5–6	CF

weathering and cyclic movement and their excellent elastic recovery. After ten cycles or one year of testing, the test was stopped. At that time, the silicone based sealants still showed more than 90 % elastic recovery and less than 20 % adhesive or cohesive failure.

Silicon-polyether and silicon-polyurethane based sealants on the other hand showed poor resistance to weathering and movement. Some commercially available silicon-polyether-based sealants were able to pass one cycle of the combined ISO 11431 [3] and ISO 9047 [2] exposures and would therefore probably be able to fulfill all ISO 11600 LM 25G requirements. However, even these sealants failed during the second cycle.

Silicon-acrylate based sealants do not seem to suffer from degradation induced by UV radiation and moisture; these sealants do not show adhesive failure even after five cycles (Table 2). Previous work carried out by Masaoka et al. [7] showed that sealants based on silicon-acrylate polymers could undergo 10 000 h of UV exposure under static conditions (without movement) and still show cohesive failure at the completion of the exposure. However, when exposed to 25 % movement, these sealants fail cohesively after one or two cycles. The reason for this failure is illustrated in Fig. 1. The 25 % compression test simulates the compression occurring in weathersealed buildings during hot days in summer due to glass expansion. When the compression is released the elastic recovery of the silicon-acrylate sealant is poor. In periods of glass contraction during nights and in the winter, or both, sealants will have to compensate for the joint movement and long term durability will depend on their elastic recovery capabilities. Therefore, by reducing the movement exposure occurring in weathersealing joints, either by modifying the joint design or by increasing the sealant width, the durability of the sealant could be considerably increased. Table 2 shows that if a silicon-acrylate based sealant which passes the ISO 11600 LM 25G requirements is used in an application where the imposed movement is reduced to 20 %, its durability can be considerably extended. Even with this reduced cyclic movement, these silicon-acrylate sealants still show expected durabilities at least 50 % lower than what is projected for silicone based sealants based on our testing. However, the projected life expectations for silicon-acrylate based sealants are still reasonable for their use as weatherseals in structural glazing applications.

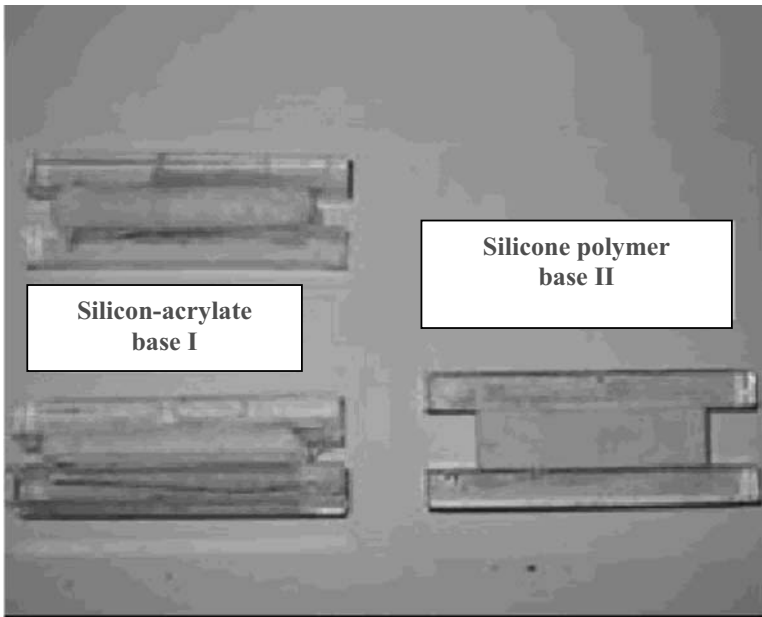


FIG. 1—Recovery of silicon-acrylate based sealants (left) and silicone based sealant (right) after 24 h 25 % compression at 70 °C following 500 h exposure to UV radiation through glass.

Summary

The durability of sealants used for weatherseal applications has been assessed using repeated alternating cycles of accelerated aging (UV/moisture/heat) and thermo-mechanical movement since it was considered that the testing needed to pass the ISO 11600 LM 25 requirements does not reflect the numerous diurnal and annual movement cycles that sealants undergo in weatherseals of structural glazing applications when exposed for 30+ years to solar radiation, temperature cycles, and moisture.

The results of this study show that most Si-modified organic sealants have limited durability in weatherseal applications mostly because of poor resistance to UV light in combination with thermo-mechanical movement. However, newly developed silicon-acrylate based sealants tested during this work show improved durability but still demonstrate poor elastic recovery after exposure to simulated weathering (UV, heat, and moisture) in combination with thermo-mechanical movement. This poor elastic recovery limits their long term movement capability. However, good durability can still be expected with joint designs resulting in lower imposed movements than those considered in the ISO 11600 Class 25 and Class 20 testing.

This study also confirms the importance of cyclic movement in combination with UV exposure for the degradation of sealants. This is highlighted by the fact that a previous study [7] showed no failure of a silicon-acrylate based

sealant after 10 000 h of accelerated UV weathering exposure without movement, while for the same sealant technology rapid degradation was observed in our study when combining the effects of accelerated weathering and cyclic movement.

References

- [1] ISO 11600:2002, "Building Construction—Jointing Products—Classification and Requirements for Sealants," International Organization for Standardization, Oct. 2002.
- [2] ISO 9047:2001, "Building Construction—Jointing Products—Determination of Adhesion/Cohesion Properties of Sealants at Variable Temperatures," International Organization for Standardization, Dec. 2001.
- [3] ISO 11431:2002, "Building Construction—Jointing Products—Determination of Adhesion/Cohesion Properties of Sealants After Exposure to Heat, Water and Artificial Light Through Glass," International Organization for Standardization, Aug. 2002.
- [4] Jones, T. G., Hutchinson, A. R., and Wolf, A. T., "Experimental Results Obtained with Proposed RILEM Durability Test Method for Curtain Wall Sealants," *Mater. Struct.*, Vol. 34, No. 5, 2001, pp. 332–341.
- [5] ISO 8339:2005, "Building Construction—Sealants—Determination of Tensile Properties (Extension to Break)," International Organization for Standardization, June 2005.
- [6] ISO 7389:2002, "Building Construction—Jointing Products—Determination of Elastic Recovery of Sealants," International Organization for Standardization, Oct. 2002.
- [7] Masaoka, Y., Nakagawa, Y., Hasegawa, T., and Ando, H., "New Durable Sealant of Telechelic Polyacrylate," *Durability of Building and Construction Sealants and Adhesives*, ASTM STP 1488, A. T. Wolf, Ed., ASTM International, West Conshohocken, PA, Vol. 2, 2006.

Yoshiki Nakagawa¹ and Sadao Yukimoto²

Evaluation of the Durability Potential of Silyl Terminated Polyacrylate Based Construction Sealant

ABSTRACT: In this paper, we discuss the durability potential of silyl terminated polyacrylate based construction sealants. The durability and performance of a silyl terminated polyacrylate (STPA) based construction sealant have been evaluated in comparison to a typical silyl terminated polyether (STPE) and a silicone sealant in order to demonstrate the potential of the STPA sealant as a high durability, high performance construction sealant that is also suitable for glazing applications. The polyacrylate backbone of STPA polymer has higher durability, especially UV stability and heat resistance, than the polyether one of STPE polymer as shown by accelerated weathering tests using carbon-arc or superhigh irradiance xenon-light sources. Adhesion of the STPA sealant on glass was retained even after 10,000 h exposure to superhigh irradiance xenon-light [180 W/m^2 (300–400 nm)]. The performance of the STPA based sealant has been compared to that of the STPE based sealant by testing according to several industrial International Organization for Standardization (ISO) and Japanese Industrial Standard (JIS) standards. The STPA based sealant conforms to a higher durability class specification than the STPE sealant, for example, the requirements of class 10030 are passed with the STPA sealant, while the STPE sealant passes only class 9030 as stipulated in JIS A 5758. Furthermore, a cyclic movement test of the STPA based sealant in a compression-extension machine shows no damage to the sealant even after 200,000 cycles of $\pm 40\%$ movement at room temperature. This performance is much better than that of sealants based on other materials, such as STPE, polyurethane, polysulfide, and silicone. These evaluations suggest a high potential of STPA based

Manuscript received September 7, 2008; accepted for publication May 26, 2009; published online August 2009.

¹ Ph.D., High Performance Polymers Division, Kaneka Corporation, 1-8 Miyamae-machi, Takasago-cho, Takasago, Hyogo 676-8688, Japan.

² High Performance Polymers Division, Kaneka Corporation, 1-8 Miyamae-machi, Takasago-cho, Takasago, Hyogo 676-8688, Japan.

Cite as: Nakagawa, Y. and Yukimoto, S., "Evaluation of the Durability Potential of Silyl Terminated Polyacrylate Based Construction Sealant," *J. ASTM Intl.*, Vol. 6, No. 7. doi:10.1520/JAI102038.

Copyright © 2009 by ASTM International, 100 Barr Harbor Drive, PO Box C700, West Conshohocken, PA 19428-2959.

sealant as durable elastomeric joint sealant, which can be used on a glass, including photocatalytic self-cleaning glass, which functions by decomposing organic materials and by providing a superhydrophilic surface.

KEYWORDS: telechelic polyacrylate, silyl terminated polyacrylate, expansion-compression cycle test

Brief History of Silyl Terminated Polyether (STPE) Sealants

Telechelic polymers with crosslinkable silyl functional groups at both ends are well known as base polymers for elastic sealants and adhesives. Crosslinkable silyl functional groups, such as the dimethoxymethylsilyl group, react with moisture in the air, generating a silanol, which condenses with another silanol formed to produce a three-dimensional polymer network.

The first telechelic polymer, a STPE for construction sealant applications, was launched in 1978 (MS Polymer®). Figure 1 shows the structure of STPE polymer. STPE polymer based construction sealants became known for their good application properties, especially high durability and nonstaining in the vicinity of the joints. STPE polymer based sealants have been applied to a large number of buildings, including famous high-rise buildings in Japan, during the past 30 years and, since 1995, enjoy a larger share of the construction sealants market in Japan than silicone and polyurethane sealants. Historical evidence proves the high durability of the STPE sealants [1].

In order to demonstrate the durability of STPE based sealants, during the inspection of a building an actual sample of STPE construction sealant was taken. The sealant had been applied 18 years ago and still provided good waterproofing function [2]. The sealant sample was sliced into 1 mm thick sheet specimens, and the appearance of the sliced specimens was checked visually. The top 2 mm layer was damaged and displayed some dirt pick-up, but the deeper layers were found not to be damaged at all (Fig. 2).

Tensile test results of the sliced specimen are shown in Fig. 3. All layers exhibit good physical properties suitable for a construction sealant. While this inspection of actual service samples clearly demonstrates the high durability of the STPE based construction sealant, STPE has still some limitations, which are their limited resistance against strong ultraviolet (UV) light and high temperatures. The UV resistance of STPE sealants is sufficient for construction applications if one tolerates a certain amount of damage to the surface of the sealant as mentioned above; however, it is insufficient for window glazing ap-

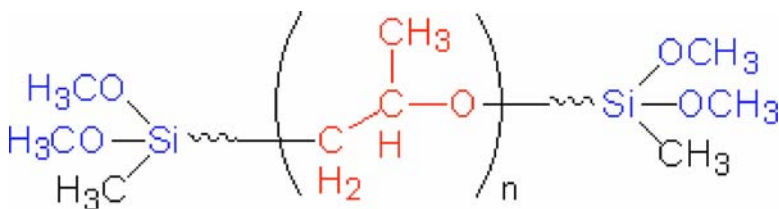


FIG. 1—Structure of STPE.

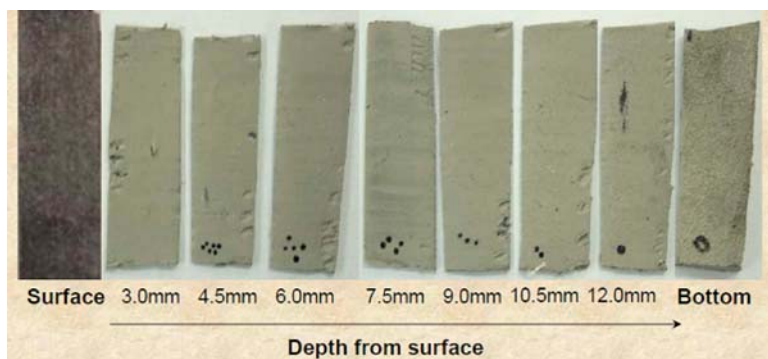


FIG. 2—Sliced specimens of 18 year old STPE based construction sealant.

plications, where the interface between the sealant and the glass, which is of key importance to adhesion, can be attacked by sunlight. The heat resistance of STPE sealants is considered to be somewhat below 100°C ; therefore STPE based sealants cannot pass the more severe durability class for construction sealants as stipulated in Japanese Industrial Standard (JIS) A 5758 [3], which requires a 100°C test condition.

Features of STPA Polymer Structure

Recently a silyl terminated polyacrylate (STPA) has been developed (Kaneka XMAP® Polymer) as a higher durability polymer for construction sealants [4–8], which allow to exceed the performance limits of STPE sealants men-

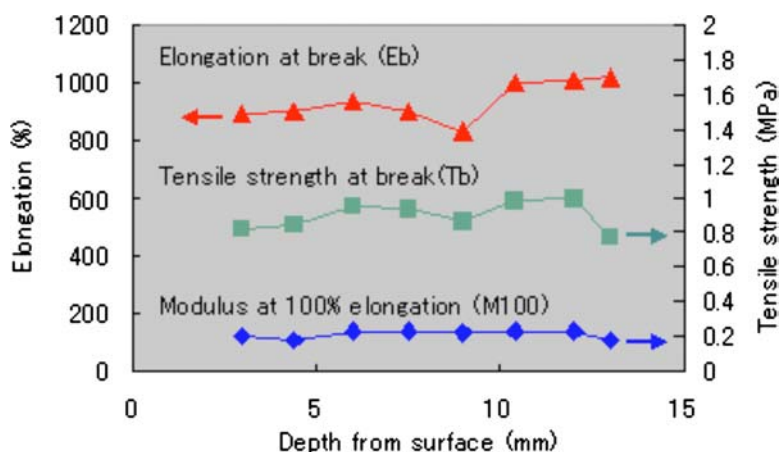


FIG. 3—Tensile test results of 1 mm thick sliced specimens of two-part STPE sealant after 18 years.

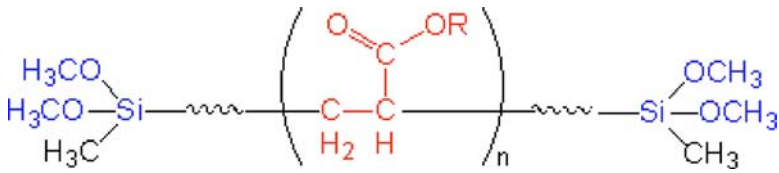


FIG. 4—Chemical structure of STPA.

tioned above. The structure of STPA is shown in Fig. 4. The backbone is a pure polyacrylate and completely consists of carbon-carbon single bonds without carrying other susceptible (weak) bonds.

There are numerous commercial products based on functional polyacrylates, which are utilized for paints, coatings, and so on. Most of these polymers have the type of structure shown in Fig. 5. It is produced by random free radical copolymerization of mainly acrylate monomer and functional acrylate monomer. As the result, the molecular weight, polydispersity, functionality, and the position of the functional groups are not controlled. On the other hand, STPA has the well-controlled telechelic structure shown in Fig. 5. The molecular weight, polydispersity, functionality, and position of the functional groups are well-controlled thanks to living radical polymerization technology. Such a well-controlled telechelic structure is considered to be very suitable as “liquid elastomeric polymer,” which is originally liquid when applied but becomes elastomeric by crosslinking, for instance, when used as a sealant base material. In the liquid form, low viscosity is required, and this is being achieved by the narrow polydispersity. In the crosslinked form, good elastomeric properties, such as high elongation, are required, and these are achieved by the well-ordered polymer network formed due to the telechelic structure.

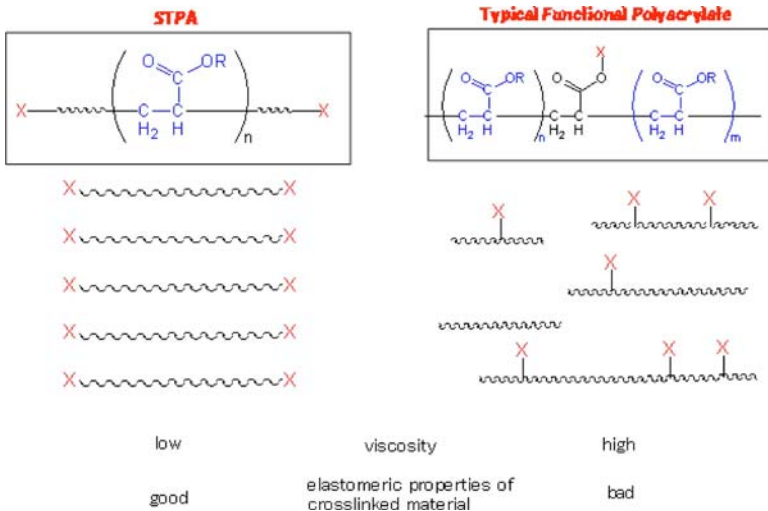


FIG. 5—Comparison between STPA and typical functional polyacrylate.

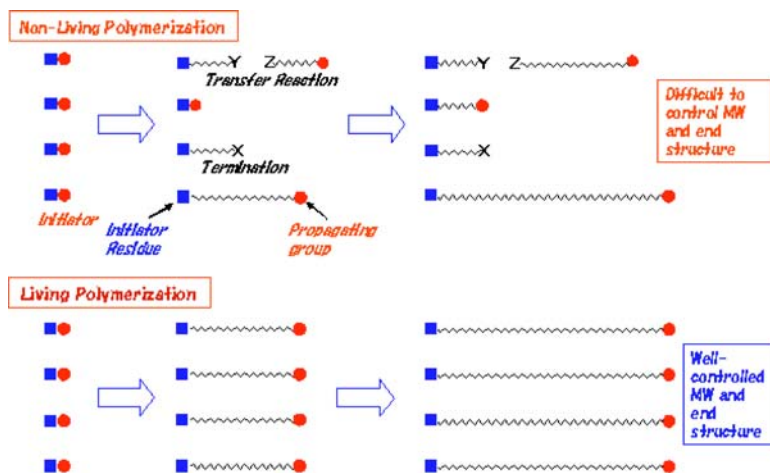


FIG. 6—Comparison between nonliving polymerization and living polymerization.

Living polymerization is an ideal technology for polymerization. Figure 6 shows a comparison between living polymerization and nonliving polymerization. Nonliving polymerization has several side reactions such as termination and transfer reactions, and the polymer produced does not have a well-controlled structure. On the other hand, living polymerization results in a well-controlled structure because of virtually no side reactions, and the consistent structure of the end-groups can be transferred into crosslinkable functional groups.

Living anionic polymerization was invented first, followed by living cationic polymerization; however, living polymerization of acrylate monomer had to wait until the invention of living radical polymerization in the middle of 1990s. Among several technologies of living radical polymerization [9,10], atom transfer radical polymerization (ATRP) [11] was chosen for producing STPA.

In order to show the differences between polymers obtained with different polymerization techniques, two polyacrylate samples, which had quite similar number average molecular weight (M_n), were prepared by ATRP and conventional free radical polymerization. Gel permeation chromatography (GPC) charts of the samples are shown in Fig. 7. While the number average molecular weights (M_n) were quite similar for these samples (21700 versus 19900), their weight average molecular weights (M_w), which correlate with viscosity, differed by more than a factor of three (24300 versus 81600).

Based on the ATRP technology, methodologies for the scaling up of the polymerization, purification, and the introduction of silyl end-functional groups were developed successfully. Furthermore, a wide variety of polyacrylate backbones, including an oil resistant grade, end-functional groups, such as thermal and UV curable ones, and formulation techniques and applications, has been developed.

The degree of functionalization of the STPA polymer with curable silyl groups is rather high, as evidenced by the high gel percentage of the cured

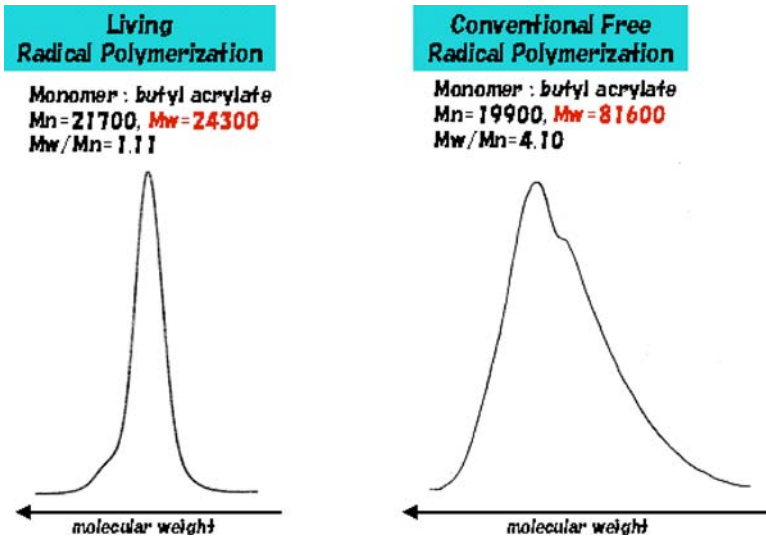


FIG. 7—GPC charts of living radical polymerization and conventional free radical polymerization.

material. The gel percentage value was measured by determining the remaining weight of cured polymer (gel) after toluene immersion. The gel content of cured STPA was 90–95 % [12].

Durability Potential of STPA Based Sealants

STPA polymer has been developed as a good sealant base material as mentioned above and has the following excellent properties [4–8,13,14]:

- (a) higher durability than STPE,
- (b) nonstaining adjacent to the joints,
- (c) higher weather resistance than STPE,
- (d) durable glass adhesion,
- (e) higher heat resistance than STPE (>150°C),
- (f) adhesion to various substrates,
- (g) paintability,
- (h) nonisocyanate,
- (i) nonsolvent,
- (j) extremely low volatile organic compound,
- (k) storage stability, and
- (l) good workability.

Some of these properties are described in the following sections.

STPA polymer can be cured by the same condensation mechanism as STPE. The methoxysilane group is hydrolyzed by atmospheric moisture in the presence of a catalyst to a silanol group; afterwards the silanol group condenses with another silanol or a methoxysilane group to form a stable siloxane group.

One silyl end-functional group has two methoxy groups so that a three-dimensional network structure can be created as a result of the crosslinking reaction.

For the formulation of a STPA based construction sealant, similar formulation techniques as for STPE can be applied, i.e., calcium carbonate fillers, plasticizers, heat stabilizers, light stabilizers, UV absorbers, silane coupling agents, and hardening catalysts may be used. Both one-part and two-part systems can be designed with STPA polymer similar to STPE, and each system may be adapted to suit the specific application. Generally the two-part system can give higher durability than the one-part system, especially in the fatigue resistance test; however, one-part sealants are easier to apply than two-part materials.

Adhesion Durability on Glass Exposed to Strong UV Irradiance

The excellent adhesion durability of STPA based one-part sealant on glass exposed to strong UV irradiance was confirmed by the following experiment. JIS 1439 H-shaped test specimens of STPA based sealant with glass and aluminum substrates were exposed for 10,000 h in superhigh irradiance xenon-light accelerated weathering equipment, in³ which the UV irradiance is three times (for 300–400 nm) as strong as in regular xenon-light accelerated weathering equipment.³ During and after the exposure period, tensile strength and failure mode were determined (Fig. 8). Even after 10,000 h, the tensile strength at break was maintained at almost the original level, and the failure mode remained cohesive in nature.

Surface Weatherability

Cured thin film specimens of 250 μm thickness made from STPA and silicone sealants were exposed in accelerated weathering equipment with open-flame carbon-arc light source sunshine weatherometer (SWOM).⁴ No change in surface appearance, such as crack formation or chalking, was observed on the surfaces of both the STPA and silicone sealant even after irradiation for 10,000 h (Table 1).

Furthermore, cured 3 mm thick sheet specimens of STPA and STPE sealants were exposed in accelerated weathering equipment with open-flame carbon-arc light source. The surface of the STPE sealant had cracks at 2160 h, but the STPA sealant showed no damage at all even after 15,500 h of weathering (Fig. 9).

Based on the results described above, the excellent weather resistance of

³Test condition: irradiation energy = 180 W/m² (300–400 nm), black panel temperature at 63°C, water spray for 18 min within 120 min weathering cycle, SUGA TEST INSTRUMENTS SX-120.

⁴Test condition: black panel temperature at 63°C, water spray for 18 min within 120 min weathering cycle.

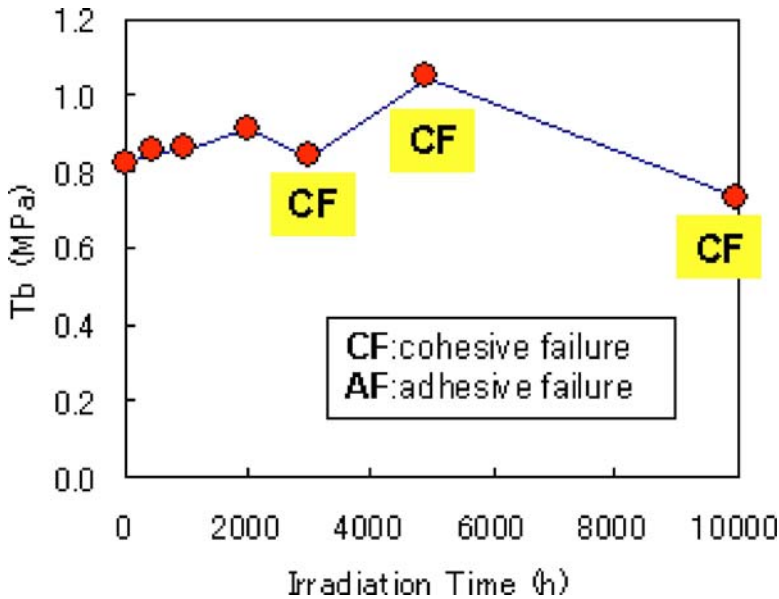


FIG. 8—Adhesion durability test on glass with exposure to strong UV irradiance in superhigh irradiance xenon-light accelerated weathering equipment (black panel temperature at 63°C, water spray for 18 min within 120 min exposure cycle, irradiation through glass).

STPA based sealant, including durable glass adhesion as glazing sealant, has been demonstrated.

Compliance with Standards

STPA based sealants are able to pass some of the more demanding standard specifications for construction sealants, such as ISO 11600, ASTM C719, and JIS A1439 [15].

For example, a STPA based one-part glazing sealant was evaluated according to class 25HM type G of ISO 11600 specification. The sealant was cured

TABLE 1—Weatherability test result of cured thin film (250 μm thickness) obtained in accelerated weathering equipment with open-flame carbon-arc light source (SWOM).

	Time (h)						
	0	300	500	1000	2000	5000	10,000
STPA sealant	NC	NC	NC	NC	NC	NC	NC
Japanese general silicone sealant	NC	NC	NC	NC	NC	NC	NC

Note: Weatherability is evaluated SWOM (Carbon-arc weathermeter). NC: no change.

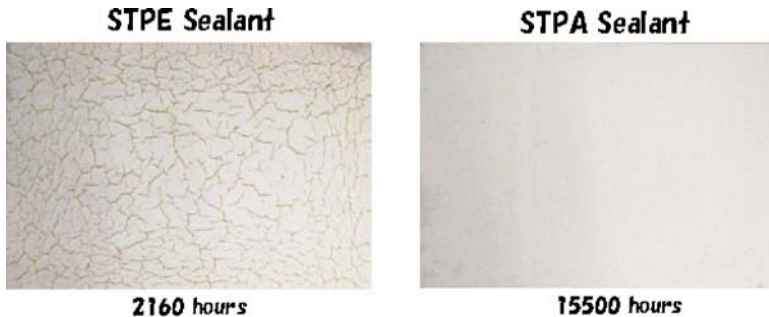


FIG. 9—Weatherability test result of cured 3 mm sheet by SWOM method.

according to Condition B of the specification. The cured sample had a high elastic recovery (70.8 % versus 60 % demanded by the specification) and no failure in 100 % expansion tests after water immersion, thermal cycle, and weathering. Detail of the specification test is shown in Table 2.

Furthermore, a STPA based one-part glazing sealant was evaluated according to ASTM C719 \pm 25 specification. The sealant passed all requirements of the specification including the thermal cycle test at cycling temperatures from -26 to 70°C . Detail of the specification test is shown in Table 3.

Japanese standards for construction sealants feature expansion-compression cycle test with a rather large number of cycles. The previous version of JIS A1439 specification, which is still considered to be important, comprises a mechanical cycling test based on 2000 cycles of ± 30 % expansion-compression amplitude with compression occurring at certain specified high temperature and expansion always occurring at -10°C . The highest class of the specification is JIS 10030, which requires 30 % compression at 100°C for 7 days, then 2000 cycles test at 23°C . Since the Japanese durable construction sealant market is dominated by two-part sealants, a STPA based two-part construction sealant was evaluated according to the JIS 10030 specification and passed all requirements without any problems observed. The STPE based two-part construction sealant is capable of passing JIS 9030 class, which implies testing at 90°C in compression but not JIS 10030 class because of its lower heat resistance.

The Japanese Architectural Standard Specification (JASS) established recently a new specification for construction sealant, class CR, which requires 6000 cycles of ± 30 % expansion-compression cycle test at room temperature after compression at a certain specified high temperature. The highest class of the specification is CR100, which requires 30 % compression at 100°C for 1 day, then followed by the 6000 cycle compression-extension movement test. A STPA based two-part construction sealant was evaluated according to the CR100 specification and passed all requirements without any problems observed.

In order to determine the limits of various two-part sealant materials, a cyclic movement test based on a much larger number of expansion-compression cycles was carried out. The movement amplitude (determined as

TABLE 2—ISO 11600 Class 25G specification test of STPA based sealant. Curing condition: $23^{\circ}\text{C} \times 28d \rightarrow (70^{\circ}\text{C} \times 3d + 23^{\circ}\text{C} \times 1d$ in water $+ 70^{\circ}\text{C} \times 2d + 23^{\circ}\text{C} \times 1d$ in water) $\times 3$ cycles. Expansion-compression cycle test condition: $\pm 25\%$ (9.0 mm \leftarrow 12 mm \rightarrow 15.0 mm).

Item	Condition	Data
Skin formation time	Initial	1:10
	After $50^{\circ}\text{C} \times 4$ week	2:00–2:30
Viscosity (Pa's)	1 rpm	2760
	2 rpm	1590
	10 rpm	498
	2 rpm/10 rpm	3.19
Viscosity (Pa's) after storage at 50°C for 4 weeks	1 rpm	3180
	2 rpm	1890
	10 rpm	684
	2 rpm/10 rpm	2.76
Cure in depth (mm)	$23^{\circ}\text{C} \times 2$ days	2.9
	$23^{\circ}\text{C} \times 7$ days	6.3
Residual tack ^a	$23^{\circ}\text{C} \times 2$ days	4
	$23^{\circ}\text{C} \times 7$ days	5
Tear strength (N/mm)		5.46
Tensile properties of dumbbell ($23^{\circ}\text{C} \times 3$ days $+ 50^{\circ}\text{C} \times 4$ days)	M50 (MPa)	0.20
	M100 (MPa)	0.37
	Tb (MPa)	0.96
	Eb (%)	560
Tensile properties of dumbbell after storage at 50°C for 4 weeks ($23^{\circ}\text{C} \times 3$ days $+ 50^{\circ}\text{C} \times 4$ days)	M50 (MPa)	0.26
	M100 (MPa)	0.46
	Tb (MPa)	1.00
	Eb (%)	510

TABLE 2— (Continued.)

Item	Condition	Data		
Test Item	Requirement	Result	Judgment	
H-shape M100 at 23°C (MPa), ISO 8339	>0.4: HM ≤0.4: LM	0.43 (NF)	HM	
H-shape M100 at -20°C (MPa), ISO 8339	>0.6: HM ≤0.6: LM	0.64 (NF)	HM	
Slip-slump, ISO 7390	5°C×24 h, vertical	≤3 mm	0 mm	Pass
	50°C×24 h, vertical	≤3 mm	0 mm	Pass
	70°C×24 h, vertical	≤3 mm	0 mm	Pass
Recovery of H-shape (%), ISO 7389	>60	70.8	Pass	
Adhesion after immersion in water, ISO 10590	NF	NF (0.35)	Pass	
Adhesion at several temp. (-20°C (25 % elongation)+70°C (25 %)), ISO 9047	NF	NF	Pass	
Weather test (500 h irradiation), ISO 11431	NF	NF (0.45)	Pass	

^aResidual tack: bad: 1 < 2 < 3 < 4 < 5 < 6 < 7 < 8: good.

Note: HM: high modulus. LM: low modulus. NF: no failure.

TABLE 3—ASTM C719±25 specification test of STPA based sealant. Curing condition: 7 days at 23°C→7 days at 38°C, 95 % RH →7 days at 23°C→7 days at 23°C in water→1 day at 23°C. Expansion-compression cycle test conditions: (1) 25 % compression at 70°C for 7 days; (2) ±25 cycle test (9.0 mm←12 mm→15.0 mm) at 23°C×10 cycles (1/8 in./h); and (3) (25 % compression at 70°C×20 h)→(25 % expansion at -26°C)×10 cycles.

	Condition	Result
ASTM C719±(25 %) test of STPA based 1part sealant	25 % compression, 70°C×7 days	Pass
	±25 % cycle test, 10 cycles	Pass
	(25 % compression, 70°C×20 h) +(-26°C, 25 % extension), 10 cycles	Pass

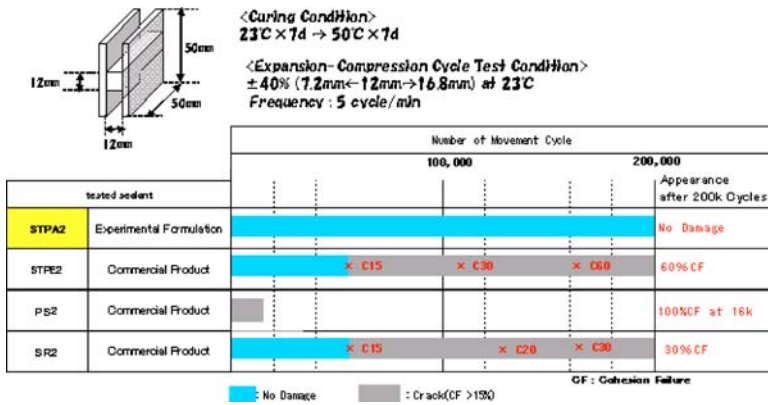


FIG. 10—Expansion-compression cyclic movement test with 200,000 movement cycles.

percentage of the expansion or compression movement versus the original joint width) was chosen as 40 %, and the test carried out at room temperature until 200,000 cycles was reached with a cycling frequency of 5 cycles/min. Cohesive failure (CF) was defined in this test as a total crack area affecting more than 15 % of the joint area. The shape of specimen (JIS H-shape), the curing and test conditions, and the results are shown in Fig. 10. The polysulfide based sealant failed with 100 % CF at 16 000 cycles. The silicone and STPE sealants showed 15 % CF at 56 000 cycles, and 30 % CF (silicone) and 60 % CF (STPE) at 200,000 cycles.⁵

The STPA based sealant exhibited excellent durability in this test as it showed no damage even after 200,000 cycles.

Nonstaining Behavior Adjacent to the Joint

Maintaining the aesthetic appearance of a sealant during aging of the building may be considered as a kind of durability, and this property is important for construction sealants. The STPE based sealants succeeded in the construction sealant market by exhibiting no staining property, which had been an issue with certain silicone sealants in the past. The STPA based sealant may be formulated to have the same no staining property as STPE sealant. A visual comparison between STPA sealant and silicone sealant for staining in the area adjacent to the joint is shown in Fig. 11. The specimens were prepared by jointing panels of artificial marble and glass with STPA and silicone sealant and exposing them outdoors for 2 years.⁶

⁵All of the compared materials, silicone, polysulfide, and STPE, are commercial products of low modulus two-part sealant in Japan.

⁶Test condition: panel angle=60°, direction=south, at Takasago, Hyogo, Japan.

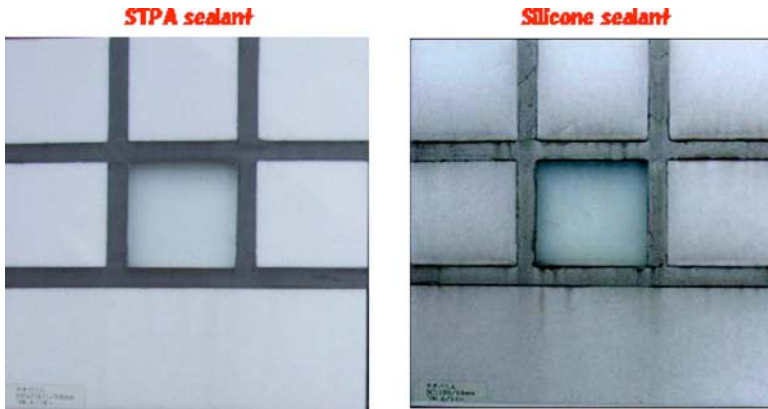


FIG. 11—Staining test results for STPA and silicone sealants. Outdoor exposure for 2 years.

TABLE 4—Oil and chemical resistance tests of cured STPA material.

Chemicals	Immersion Condition	Increased Weight (%)
10 % H ₂ SO ₄ aq	23°C, 30 days	3
Isooctane	23°C, 7 days	4
Jet fuel	23°C, 7 days	10
Antifreeze	23°C, 7 days	1
Water	23°C, 7 days	2
ASTM No.1 oil	150°C, 7 days	3
IRM 903 oil	150°C, 7 days	13

Apparent staining adjacent to the silicone sealant joint was observed, but none was observed for the STPA sealant.

Oil Resistance

One of the prominent features of STPA sealant is the excellent oil resistance at ambient or even at high temperatures. The cured material of STPA polymer is very similar to acrylic rubber, which is well known for having excellent oil and heat resistance and is used in automotive applications. Results of oil and chemical resistance test are shown in Table 4.⁷

⁷Test method of oil resistance: a piece of cured polymer (2 mm thickness) was immersed in certain oil at certain condition exhibited on Table 4; then the sample was taken out, swiped on the surface, and the weight change from the original was measured at room temperature.

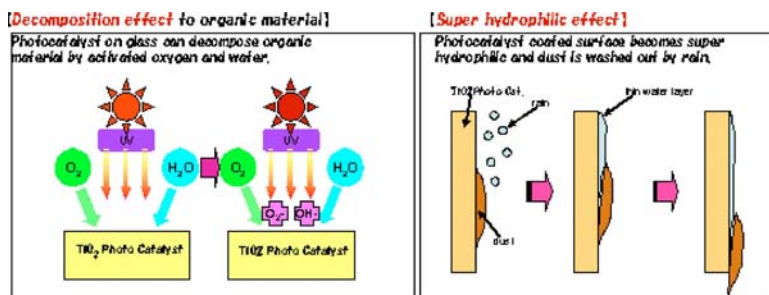


FIG. 12—Self-cleaning mechanism of photocatalytic glass (SCG).

The STPA sealant exhibited very good oil resistance against a couple of standard oils even at 150°C.

Silicone is also used for applications requiring heat and oil resistance because silicone has excellent heat resistance and low oil-swelling property; however, the latter is still higher for silicone than for STPA based materials. Actually silicone is very durable in oil at high temperature, but some oil is seeping through silicone without any seal failure occurring. On the other hand, STPA based materials can almost completely eliminate the oil penetration problem⁸

Self-Cleaning Glass Glazing Sealant Application

Since several years ago, self-cleaning glass (SCG) has been developed and introduced into the market as easy to clean and low maintenance cost glass. SCG is standard window glass coated with a photocatalytic layer, typically consisting of a titanium oxide photocatalyst. The mechanism for the self-cleaning process on glass is shown in Fig. 12. Activated by actinic UV irradiation, the photocatalytic coating on the SCG surface decomposes organic compounds in dirt particles deposited on the glass.

Furthermore, the photocatalytic surface becomes superhydrophilic with exposure to sunlight and rain (liquid water) forms a very thin layer, which washes off the dirt due to displacement from the glass surface. SCG faced a problem just at the beginning of its market development. Generally, glass glazing sealants are silicone based, so this type of sealant was also used for SCG. However, silicone sealants may release volatile silicone compounds that contaminate the surface of SCG. The silicone contamination cannot be decomposed even by the photocatalyst, and it makes the glass surface hydrophobic. As a result, SCG loses its self-cleaning function in the contaminated areas. Other sealant materials, such as polyurethane and STPE, cannot be used for this

⁸Silicone sealant was tested in the same condition for IRM 903 oil. After the test, bleeding out of the oil was observed on the surface of test piece. Such a phenomenon was not observed for STPA.

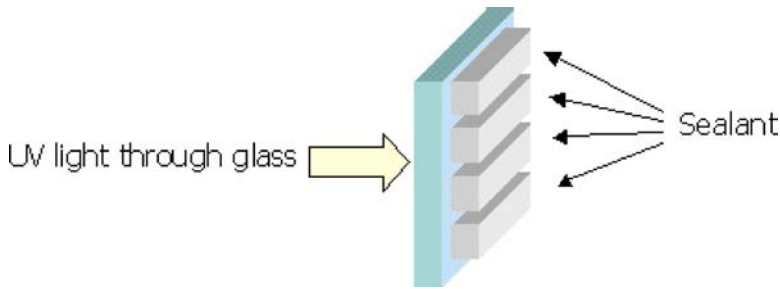


FIG. 13—Test piece.

TABLE 5—Adhesion test results after UV irradiation.

	1000 h	3000 h	5000 h	7000 h	10,000 h
Silicone	CF	CF	CF	CF	CF
STPA	CF	CF	CF	CF	CF

Note: Super Xe Weathermeter. Condition: irradiation energy=180 W/m²(300–400 nm) (approximately three times as strong as regular xenon WM). Black panel temp=63°C. Water spray condition=18 min in 120 min.

application instead of silicone because these materials do not have sufficient long-term durable adhesion on SCG when exposed to solar irradiance.⁹

UV Resistance of Adhesion on SCG

Test specimens were prepared as shown in Fig. 13, and these were cured at 23°C and ambient moisture for four weeks. The specimens were placed in an accelerated weathering equipment with a xenon-light source (Super Xenon Weathermeter) in such a manner that the adhesion interface was irradiated through the SCG. After a certain irradiation period, the test pieces were evaluated by a 180° hand peeling method (Table 5).

The tests confirmed that the STPA sealant had excellent adhesion durability on SCG under UV irradiation because it showed CF even after UV irradiation for 10,000 h.

Hydrophobic Contamination

The hydrophobic contamination test of SCG with silicone and STPA sealants was carried out by using specimens shaped like an actual window [16]. The test results after 812 days of outdoor exposure are shown in Fig. 14. The photos were taken after spraying the glass surface with water so that hydrophilicity or

⁹JASS-8-2008 shows appropriate choice of sealant materials for each type of construction application, and STPE and PU are not suitable for glass glazing use.



FIG. 14—Contamination test results on window shaped specimens (outdoor exposure for 812 days; photos taken after spraying the surface with water).

hydrophobicity of the glass surface could be observed easily. The silicone sealant specimen showed a hydrophobic contamination area along the sealant joint with a width of 15–90 mm, while the STPA sealant specimen showed no contamination at all with the whole specimen remaining hydrophilic.

Based on the results described above, the compatibility of the STPA based glazing sealant for SCG has been demonstrated very clearly. Glass manufacturers who were experiencing difficulties with contamination by silicone sealants at the early stage of SCG development certified STPA based glazing sealant as suitable glazing material, and several sealant formulators developed STPA based sealant products for this application.

Conclusion

STPA sealants were developed following the success of STPE sealants, which were shown to be durable construction sealants during the past 30 years. STPA based sealants are able to outperform STPE sealants, i.e., they have higher surface weatherability, are more durable glass adhesion under UV exposure, and are able to pass higher classes in standard specifications for construction sealant due to their better heat stability and movement capability. Therefore, STPA based sealants are considered to have a very high durability potential.

By putting these properties to practical use, STPA based SCG glazing sealant was developed to exhibit good compatibility to this type of glass.

References

- [1] Isayama, K., "A Review of Telechelic Polymers Produced by Living Polymerization Technologies for Adhesives and Sealants," *Proceedings of the World Adhesive Conference and Exposition*, April 20–23, 2008, Miami, FL, The Adhesive and Sealant Council, Bethesda, MD.
- [2] Muramatsu, E., "Silyl-Terminated Polyethers Sealant Durability Update," *Proceedings of the International Convention of the Adhesive and Sealant Council*, April 13–16, 2002, Los Angeles, CA, The Adhesive and Sealant Council, Bethesda, MD.
- [3] JIS A 5758, Japanese Industrial Standard regarding sealants for sealing and glazing in buildings.
- [4] Nakagawa, Y., "Commercialization of Telechelic Polyacrylates Prepared by ATRP," American Chemical Society, Spring Meeting, Anaheim, CA, March 29, 2004.
- [5] Nakagawa, Y., "Development of New Curable Liquid Telechelic Polyacrylate," American Chemical Society, Spring Meeting, March 29, 2004, Anaheim, CA.
- [6] Nakagawa, Y., "Development of Telechelic Polyacrylate: Features of Structure and Property," Adhesive and Sealant Council, Fall Convention, September 19–22, 2004, Pittsburgh, PA.
- [7] Masaoka, Y., Nakagawa, Y., Hasegawa, T., and Ando, H., "New Durable Sealant of Telechelic Polyacrylate," *J. ASTM Int.*, Vol. 3, No. 10, Paper ID JAI100450.
- [8] Nakagawa, Y., *Bosui Journal*, Vol. 6, 2008, pp. 32–36.
- [9] Matyjaszewski, K. and Xia, J., *Handbook of Radical Polymerization*, K. Matyjaszewski and T. P. Davis, Eds., Wiley, New York, 2002, p. 523.
- [10] Kato, M., Kamigaito, M., Sawamoto, M., and Higashimura, T., "Polymerization of Methyl Methacrylate with the Carbon Tetrachloride/Dichlorotris-(triphenylphosphine)ruthenium (II)/Methylaluminum Bis(2,6-di-tert-butylphenoxide) Initiating System: Possibility of Living Radical Polymerization," *Macromolecules*, Vol. 28, 1995, pp. 1721–1723.
- [11] Wang, J. S. and Matyjaszewski, K., "Controlled/"Living" Radical Polymerization. Atom Transfer Radical Polymerization in the Presence of Transition-Metal Complexes," *J. Am. Chem. Soc.*, Vol. 117, 1995, pp. 5614–5615.
- [12] Test method: a piece of cured polymer in a metal-net bag was immersed in toluene for 1 day, then taken out, and dried completely, and the weight change from the original was measured.
- [13] Koike, T., "Development and Performance of Glazing Sealant for Photocatalyst Cleaning Sealant," *Bosui Journal*, Vol. 6, 2008, pp. 38–41.
- [14] Kano, S., "Commercialization and Performance of Telechelic Polyacrylate Sealant," *Bosui Journal*, Vol. 6, 2008, pp. 42–45.
- [15] JIS A 1439, Japanese Industrial Standard regarding testing methods of sealants for sealing and glazing in buildings.
- [16] Tanaka, H., Makino, M., and Kusumi, A., Summaries of Technical Papers of Annual Meeting of the Architectural Institute of Japan, Vol. A-1, 2006, pp. 1109–1110.

**FACTORS INFLUENCING THE
DURABILITY OF SEALED
JOINTS AND ADHESIVE
FIXATIONS**

Lawrence D. Carbary¹

Substrate Durability Guidelines Used in Silicone Structural Attachment

ABSTRACT: This paper sets forth a procedure for evaluating substrates for durability for use in conjunction with structural silicone glazing (SSG). Lap shear and peel adhesion specimens are evaluated after exposures to various conditions using a modified ASTM C794-06, "Standard Test Method for Adhesion-In-Peel of Elastomeric Joint Sealants," and ASTM C961-06, "Standard Test Method for Lap Shear Strength of Sealants." Conditions of exposure include water, sodium hypochlorite (bleach), acetic acid (vinegar), salt fog, UV florescent accelerated weathering device (UVFI), ultraviolet light (UV) exposure, and heat. Evaluation of substrates and the interfaces are completed after tensile testing and visual surface analysis. The silicone structural glazing adhesive used in this evaluation is a high modulus high strength material intended to place the maximum load at the interface. Substrates evaluated include steel, anodized aluminum, galvanized steel, extruded rigid polyvinyl chloride (PVC), glass reinforced thermoplastic resin (fiberglass), and polyvinylidene fluoride (PVDF) painted aluminum. These evaluated substrates are tested to this procedure to show differences in performance and suggest a minimum time frame required for testing. The results and guidelines set forth in this paper provide the foundation for a practice and or a substrate specification for use in conjunction with structural silicone attachment methods.

KEYWORDS: structural silicone, lap shear, peel adhesion, durability, substrate suitability, dimensional stability

Introduction

Silicone structural glazing has been a proven method of glass attachment to aluminum curtainwalls for greater than 30 years [1]. This attachment method provides a continuous flexible anchorage of glass that is also an excellent thermal break, continuous air seal, and continuous water seal. The performance of

Manuscript received July 3, 2008; accepted for publication January 13, 2009; published online March 2009.

¹ Industry Scientist, Dow Corning Corporation, PO Box 994, Midland, MI 48686-0994.

Cite as: Carbary, L. D., "Substrate Durability Guidelines Used in Silicone Structural Attachment," *J. ASTM Intl.*, Vol. 6, No. 3. doi:10.1520/JAI102009.

Copyright © 2009 by ASTM International, 100 Barr Harbor Drive, PO Box C700, West Conshohocken, PA 19428-2959.

these systems is unmatched in performance compared to traditional glazing systems [2,3]. The flexible rubber anchorage that is used to attach glass to aluminum framing allows the differential thermal expansion between glass and aluminum on a daily basis while resisting movements induced from windloads onto the glass. Structural silicone glazing is popular on the unitized curtainwalls of the high rise buildings of today due to the excellent performance that has been documented. Structurally glazed unitized curtainwalls are found on world famous buildings such as the Petronas Towers in Kuala Lumpur Malaysia, and the Time Warner Center in New York City.

The method of structural silicone attachment shows clear advantages in the thermal performance of curtainwalls. Thermal modeling of curtainwalls is commonly done due to the building code requirements to maintain a certain thermal transmittance or U value for the façade. This is done much more often in Europe as compared to the Americas; however, the increased awareness of energy usage in the United States is making designers, owners, and contractors much more aware of the energy consumption in buildings. Due to this heightened awareness of energy conservation, additional substrates are being evaluated on curtainwalls in addition to the traditional finished aluminum and glass. As aluminum finishing processes come under scrutiny with regards to environmentally friendliness, new coatings and finishes are being developed.

When one studies the thermal performance of fenestration systems, it becomes apparent that the residential vinyl and wood windows can be more energy efficient in the supporting frame compared to an aluminum framed window system. Commercial aluminum fenestrations systems used in high rise buildings will come with thermal break systems built into the aluminum to minimize the heat transfer through the frame. There are commercial fenestration systems that use glued laminated wooden mullions to promote energy savings and interior warmth [4].

Current practice for designing structurally glazed facades is well documented within ASTM C1401-07, "Standard Guide for Structural Sealant Glazing." This comprehensive guide contains Sections 19–26 that deal specifically with Component Design Considerations. Section 23.2 states "Prior to substantial system development, the SSG system designer should verify by testing, that includes both the structural sealant and panel manufacturers, that adequate adhesion can be obtained." Herein lies the basis for the writing of this paper. Structural sealant adhesion testing to a substrate does not qualify that the substrate is suitable for the intended use. Adhesion testing to the substrate is one of many prequalification steps required for a successful system. The intent of this paper is to show that a simple adhesion test without understanding substrate durability and dimensional stability could have negative consequences regarding the success and longevity of the façade system.

Structural sealant manufacturers offer testing services as suggested above for projects, as it is in all of the parties' best interests to know the proper methods of surface preparation to get an intended structural sealant project to perform up to expectations. Expectations are no less than perfect performance for greater than 20 years without adhesion or cohesion failures, which could result in excess air and water infiltration, not to mention a life safety issue. When a new finish on an existing substrate or a new substrate is introduced to

the industry it is submitted to a sealant manufacturer for testing. A test report is returned to the submitter documenting the results. The sealant testing that is performed by responsible manufacturers will include a water immersion cycle. Some areas require a 7 day immersion in room temperature water and others require 14 days immersion in 55°C water. The test report will recommend a surface preparation appropriate to obtain optimum adhesion. The recipient of this test report now believes that the sealant manufacturer has approved this finish for structural glazing applications. Again, herein lies the intent of this paper. The substrates have to be qualified and understood with regards to durability, longevity, dimensional stability, and engineering properties in addition to a simple adhesion test in a sealant manufacturer's laboratory.

The sealant manufacturer in this test regimen did in no way certify the longevity, durability, or suitability of this new finish or substrate for the life of the project. Paints that are applied to aluminum framing members must have durability and adhesion greater than the adhesion and durability of the silicone structural glazing sealant used to attach glass to those frames. When paints are tested on aluminum, the physical properties of the aluminum frame are assumed to be constant based on standard engineering principles. Curtainwalls are specified to have maximum deflections under specified loads applied to specified spans. Aluminum, when properly protected with an anodized or painted finish, has a history of performance and is a standard in the industry. Aluminum has a known strength, modulus, thermal expansion coefficient, dimensional stability, thermal conductivity, hardness, and specific gravity. These properties are the basis of today's curtainwall frame designs and performance.

With the economic pressures to develop structures that will save energy, weight, and installation time, it is inevitable that new materials will arise in curtainwall applications. A simple adhesion test by a sealant manufacturer to obtain a proper surface preparation procedure is in no way the only criteria for use on a curtainwall for sealing and structural silicone attachment.

Structural glazing standards and specifications such as ASTM C1184-05, "Standard Specification for Structural Silicone Sealants," and EOTA ETAG 002 [5] put cured tensile specimens through durability tests. The spirit of these durability tests involves testing tensile specimens after aging in various environments, evaluating the data, and determining if the silicone product meets minimum requirements. The ETAG 002 subjects tensile samples to salt fog and SO₂ environments. The International Conference of Building Officials (ICBO) Acceptance Criteria for Structural Silicone required tensile samples to be inoculated with mold according to ASTM G21-96(2002), "Standard Practice for Determining Resistance of Synthetic Polymeric Materials to Fungi," exposed to ozone according to ASTM D1149-07, "Standard Test Methods for Rubber Deterioration—Cracking in an Ozone Controlled Environment," and immersed in various chemicals (soap solution, detergent, salt water, and ammonia) [6]. All of these test protocols involve testing a specimen that is already cured.

This paper is taking a bit of a different approach due to the inevitable additional change in surfaces and materials that the future will present. Data are presented below using lap shear and peel adhesion testing in conjunction with visual observations. The key difference here is that the substrates have undergone 500 h of aging in various environments before lap shear specimens

have been prepared. The lap shears and peels are cured for 21 days, and then tested. A duplicate set of samples are then immersed in room temperature water for seven days and tested. The intention is to determine if the substrate has durability before the application of silicone structural sealant, and if the silicone has durability to the aged substrate.

Experimental

Substrates chosen for this study are clear anodized aluminum, galvanized steel, cold rolled steel, PVDF painted aluminum, white PVC, gray PVC, and fiberglass. All of these substrates exist in fenestration applications with the exception of the unfinished cold rolled steel.

The environments that were chosen to age the substrates for 500 h are UV exposure according to ASTM C1087-00(2006), "Standard Test Method for Determining Compatibility of Liquid-Applied Sealants with Accessories Used in Structural Glazing Systems," at 50°C, 100°C oven, 6 % sodium hypochlorite solution (bleach), 5 % acetic acid solution (white vinegar), UVFL operated in accordance with ASTM C1442-06, "Standard Practice for Conducting Tests on Sealants Using Artificial Weathering Apparatus," and salt fog operated in accordance with ASTM B117-07A, "Standard Practice for Operating Salt Spray (Fog) Apparatus." A UV fluorescent artificial aging device was used in lieu of other devices as that was easily accessible to the author.

A control set of substrates was fabricated and tested at room temperature without any exposure conditioning.

Lap shear specimens were made in accordance with ASTM C961-06. All substrates tested were cut into 25 mm by 75 mm coupons for ease of testing. The dimension of the lap shear joint was 25 mm by 25 mm and the thickness was 3.4 mm. The silicone was allowed to cure for 21 days at standard lab conditions and a set of three specimens were pulled. The pull rate was 12.5 mm per minute and the peak force was recorded. The force reported for each material is an average of three specimens pulled.

The structural silicone sealant that was used was a one part material that meets ASTM C1184-05 and ASTM C920-08, "Standard Specification for Elastomeric Joint Sealants," Type S, Grade NS, Class 50, use NT, G, A, and O. This material is a one part moisture cure structural silicone material. When tested to ASTM C1135-00(2005), "Standard Test Method for Determining Tensile Adhesion Properties of Structural Sealants," it demonstrates a tensile strength of 1.2 MPa at 200 % strain and the stress at 100 % strain is 0.72 MPa.

Peel adhesion samples were made on each substrate before and after aging. The peel adhesion was a modified ASTM C794-06. The modification to the standard was that the peels were 12.5 mm in width, peels were made of aluminum screen and data were recorded at both 21 days of cure and after 7 days of water immersion. The peak peel strength is recorded in Newtons per millimetre.

Figure 1 shows both the peel adhesion specimens and the lap shear specimens during cure. Note the lap shear substrates are 25 mm by 75 mm.

Visual observations were recorded as follows in Table 1 and peel strength

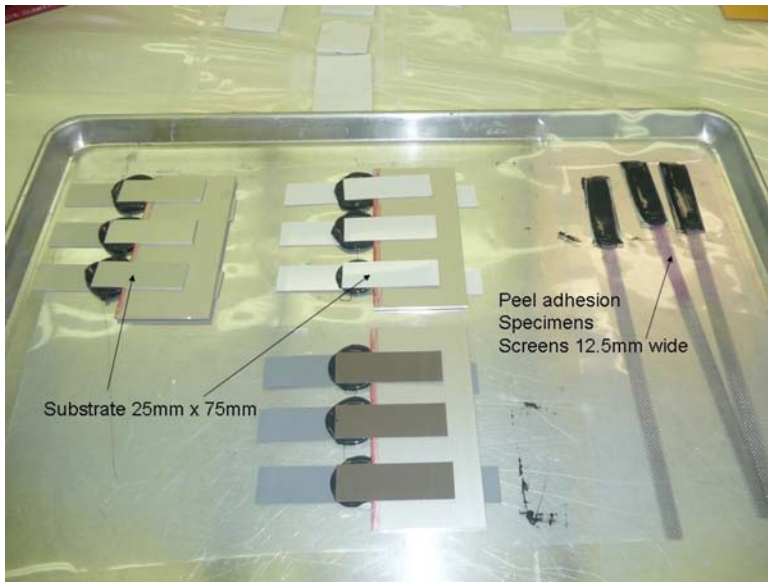


FIG. 1—Control lap shear specimens and peel adhesion specimens.

and lap shear strength are recorded in Table 2. Figure 2 shows the control data for all substrates. Figures 3–9 show the lap shear data for each substrate in each of the aging conditions.

Discussion of Results

Common construction substrates were placed in this study knowing some of the visual results. Unfinished steel and galvanized are known to degrade in environments of salt, bleach, and vinegar. It is important to show the visual and adhesion data on these substrates that are indeed perceived as being less suitable for SSG applications compared to anodized or painted aluminum. Steel is not used for silicone structural glazing applications unless a high performance coating is placed upon it. The known corrosion issues prevent its use with structural silicone due to engineering judgment. Figure 10 shows the visible corrosion noted on steel after exposure to bleach, and this type of corrosion is evident in the other environments noted in Table 1. Figure 11 shows the corrosion on a galvanized substrate after vinegar exposure.

Anodized aluminum and PVDF painted aluminum are the standards for which structural sealants are applied to support glass panels in classic SSG applications. The data of peel strength, lap shear strength on aged and unaged substrates, and the visual data presented in this study suggest that these are stable substrates. The anodized aluminum substrates had a slight tarnish after bleach water aging, but the adhesion and strength characteristics of the samples show good bonding.

Galvanized steel has been used as an adhesive attachment substrate for

TABLE 2—Peel strength in N/mm and lap shear in MPa for each substrate and exposure condition.

Substrates	Metric	Control 21 Day Cure	Control 21 Day Cure +7dH2O	UV + 7dH2O	100°C + 7dH2O	100°C + 7dH2O	Salt Fog	Salt Fog + 7dH2O	UVFI	UVFI + 7dH2O	Bleach 6.0 %	Bleach + 7dH2O	Vinegar 5.0 %	Vinegar + 7dH2O	
Galvanized	Lap shear MPa	0.95	0.95	0.80	0.90	0.84	0.83	0.60	0.47	1.12	1.31	0.51	0.32	0.88	0.81
	Peak Peel N/mm	7.00	3.85	6.48	6.13	6.30	7.00	3.50	2.98	5.60	4.38	3.68	1.05	7.53	6.48
Steel	Lap shear MPa	0.81	0.75	0.78	0.97	0.86	1.10	0.85	0.64	1.05	1.14	0.59	0.16	1.03	0.91
	Peak Peel N/mm	5.25	2.10	6.48	5.60	7.17	7.00	3.50	4.73	4.73	4.73	5.95	3.68	6.13	5.08
PVDF paint	Lap shear MPa	0.72	0.80	0.79	0.83	0.68	0.81	0.86	0.96	0.88	0.82	0.66	0.55	0.63	0.81
	Peak Peel N/mm	6.65	2.98	7.18	3.15	7.00	4.20	4.38	3.68	3.85	3.50	7.18	3.85	6.65	4.55
Anodized	Lap shear MPa	1.12	0.95	0.88	0.96	0.90	0.81	0.79	0.78	1.13	1.35	0.96	0.91	0.95	0.93
	Peak Peel N/mm	7.35	7.35	4.73	4.38	5.60	5.43	4.38	3.85	5.78	4.38	4.38	4.20	4.55	3.33
PVC 1 White	Lap shear MPa	0.96	1.14	0.94	0.94	0.38	0.29	0.89	0.86	0.12	0.03	0.88	0.88	0.82	1.01
	Peak Peel N/mm	5.25	5.25	4.73	3.68	4.38	3.50	4.73	3.50	2.98	2.45	3.85	3.50	3.85	3.85
PVC 2 Gray	Lap shear MPa	0.89	0.99	0.96	0.89	0.65	0.66	0.85	0.84	0.43	0.13	0.81	0.84	0.93	0.92
	Peak Peel N/mm	5.25	5.08	3.68	4.20	4.55	4.55	4.03	2.45	4.55	3.32	3.85	2.45	2.98	3.50
Fiberglass	Lap shear MPa	0.73	0.80	0.80	0.83	1.05	0.85	0.94	0.81	0.94	0.85	0.85	0.54	0.82	0.76
	Peak Peel N/mm	4.90	4.03	5.95	5.43	7.00	4.90	4.38	4.90	4.38	4.90	5.60	3.15	4.90	4.90

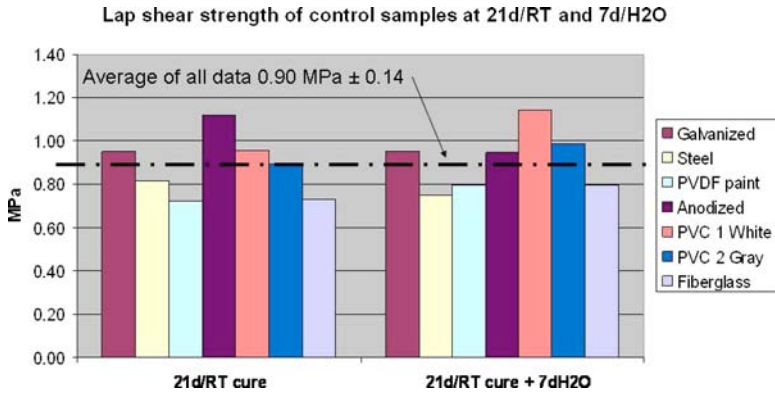


FIG. 2—Lap shear strength of control data.

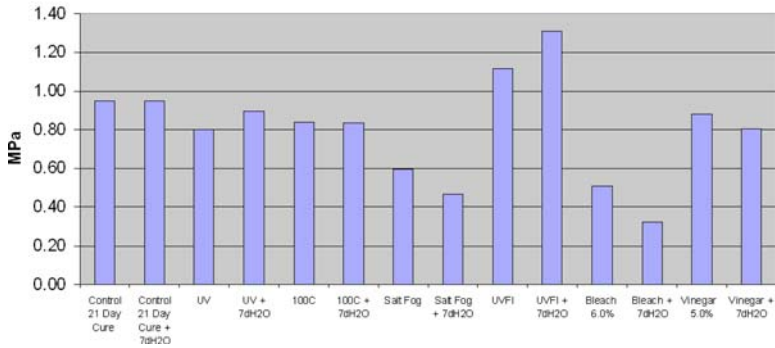


FIG. 3—Lap shear strength of galvanized through aging.

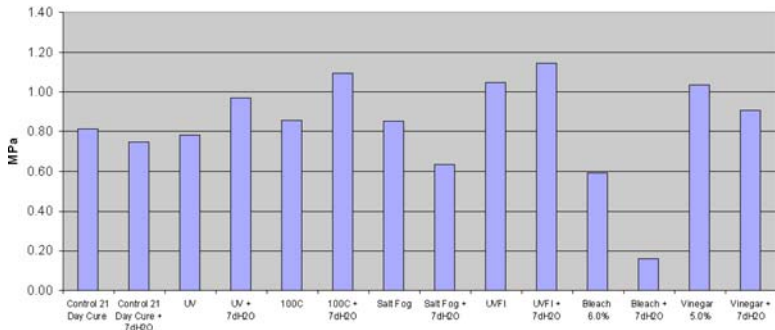


FIG. 4—Lap shear strength of steel through aging.

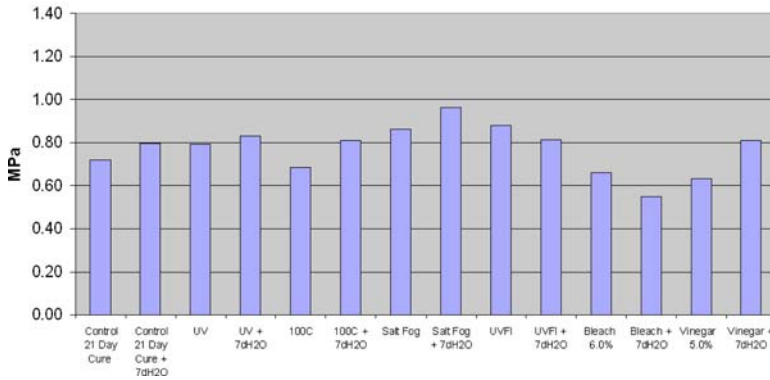


FIG. 5—Lap shear strength of PVDF paint through aging.

projects for 20 years [7] without reported failures. The UVFL aging showed some oxidation of the surface; however, the strength was not affected compared to the control. Tensile specimens fabricated according to ASTM C1135-00(2005) and then aged 2400 h in UVFL [8] on galvanized steel showed good durability based on strength retention. Note: Conditions for this referenced test in the UVFL were 4 h of UV fluorescent light at 50°C using UVB-313 bulbs followed by 4 h of condensation at 40°C. Galvanized steel is discouraged as a structural attachment substrate within 1.6 km of oceanfront due to the potential corrosion due to salt exposure. The lap shear testing in this study showed the visible increased durability of a galvanized substrate compared to a steel substrate after exposure to salt, vinegar, and bleach.

The PVC specimens were quite visually resistant to bleach, vinegar, UV, and salt fog exposures. However, the 100°C aging made the samples warp. The PVC substrates showed severe warping in the UVFL chamber and exhibited color change. This is shown in Fig.12. It was difficult to fabricate lap shears speci-

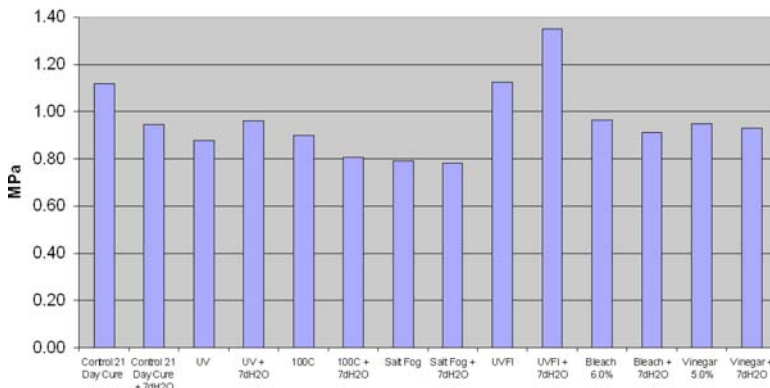


FIG. 6—Lap shear strength of anodized through aging.

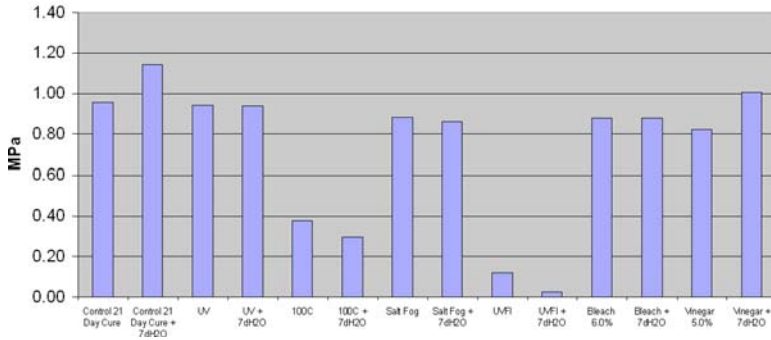


FIG. 7—Lap shear strength of PVC 1 White through aging.

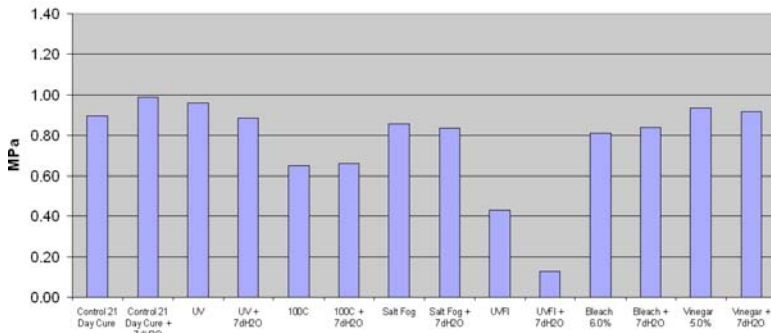


FIG. 8—Lap shear strength of PVC Gray 2 through aging.

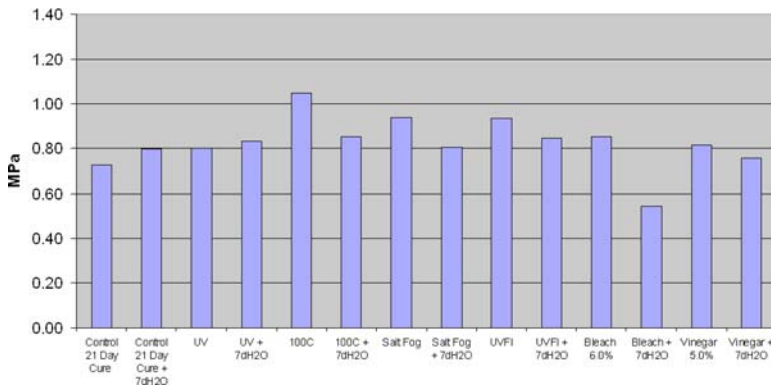


FIG. 9—Lap shear strength of fiberglass through aging.

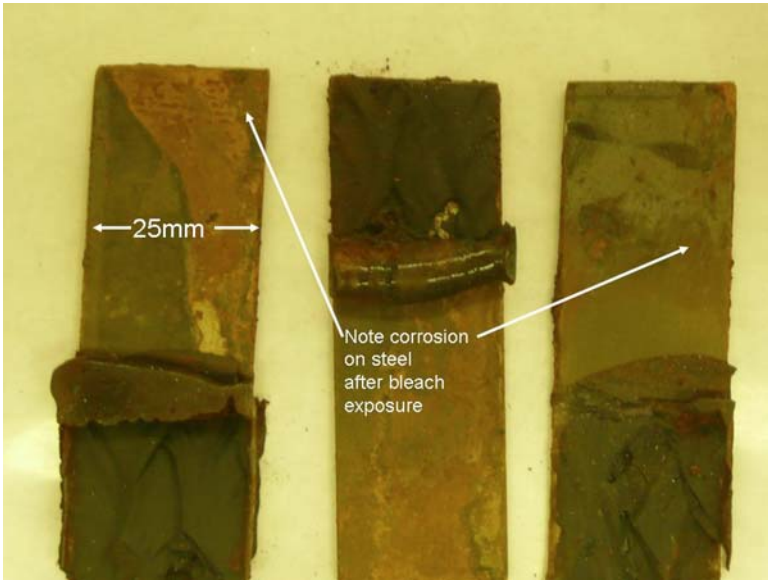


FIG. 10—Steel specimens after bleach exposure.

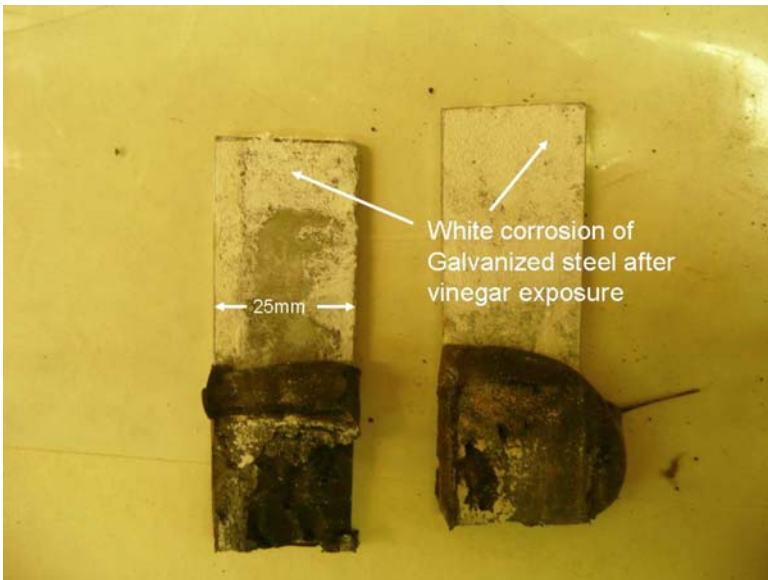


FIG. 11—Galvanized specimens after vinegar exposure.

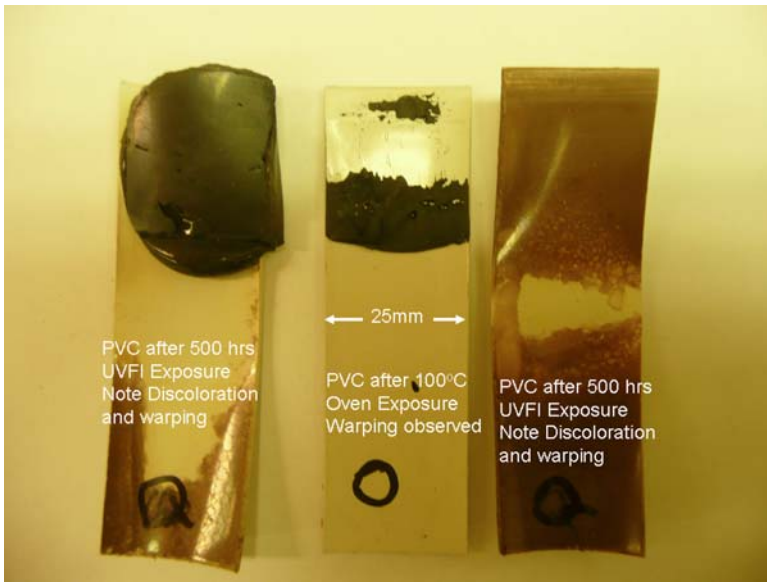


FIG. 12—PVC specimens after UVFL exposure and 100°C.

mens because the samples had an induced curve. There was also noted along a substantial loss of strength and adhesion in the lap shear specimens. Figure 12 shows an adhesion loss on the oven aged PVC specimen. Both colors of PVC showed this same trend, however, the white PVC was worse than the gray PVC. The color changed and the samples had a large dimensional instability. This noting of dimensional instability is a key signal for this short study and was an unexpected result. Designing an SSG system using this substrate would be unwise unless the designer was able to account for and mitigate any dimensional instability that could occur.

The fiberglass substrate showed excellent adhesion and strength in all but the water immersion after bleach exposure and degradation of the surface was not noted in any case. Figure 13 shows fiberglass substrate unaffected by the various conditions. When reviewing Fig. 9 to the controls noted on Fig. 2, the lap shear strength was a bit lower than the overall average and the one condition of water immersion after bleach exposure had an impact on the ultimate strength. The fiberglass substrate showed no visible effects of color change or dimensional changes through these exposures.

Figures 2–9 are the lap shear test results on the substrates. Figure 2 is shown as a control set after 21 days of cure and then 7 days of water immersion. This table is shown as it really demonstrates the variability in the ASTM C961-06 used in this lab. Please note that the average of all the control tests was $0.9 \text{ MPa} \pm 0.14 \text{ MPa}$. Adhesion was good as noted by a cohesive failure in all of these instances in the control set. Figure 2 shows that the water immersion didn't have any impact on the average lap shear strength. Upon reviewing the remaining tables it is evident that the bleach immersion of samples did show



FIG. 13—Fiberglass specimens after UV, oven, and bleach exposures and control.

some impact on the steel, PVDF, and fiberglass substrates due to the reduced strength of the lap shears.

The anodized and PVDF paint exhibited excellent results in the lap shear tests. This was expected, as these substrates are the benchmark in the industry for SSG projects. Table 1 and Figs. 7 and 8 also note the severe degradation of the PVC substrates after their aging.

Five hundred hours of artificial aging is not an undue amount of time. The aging conditions here are not a complete list of potential environments. The ICBO criteria [6] subjects cured specimens to ozone environment and cleaning chemicals. The ETAG 002 [5] subjects cured specimens to SO_2 environment and various chemicals. None of these internationally recognized standards and specifications suggests an aging of the substrates before specimen fabrication. Thus it is the intention of this paper to suggest that new substrates to the silicone structural attachment application undergo a scrutiny for durability prior to use.

Guidelines for the Use of New Substrates in Structural Silicone Attachment

An in depth analysis of data for a new substrate for structural silicone attachment is required on a substrate by substrate basis. Ensuring the long-term durability of a substrate is essential for the continued success of structural silicone attachment method. Referring to the benchmarks that are currently in place in the curtainwall industry with finished aluminum and glass, the following guidelines are provided for new substrates.

1. Physical properties of the substrate material must be documented and should include thermal conductivity, coefficient of thermal expansion,

Young's Modulus of elasticity, and hardness over the service temperature that the material is expected to perform. These data allow structural engineers to properly dimension the material and sealant joints so that the joints are not overstressed or fatigued during the service life.

2. Dimensional stability over the temperature range that the material is expected to perform. Based on the dimensional performance of the PVC tested here, oven aging and UVFL exposure should be done on substrates to show that they do not deform during their life span. Dimensional instability will cause structural sealants to deform and possibly be overstressed or put into a fatigue situation.
3. Adhesion and durability testing of structural sealants should be done using this material according to ASTM and or ETAG structural specifications before and after environmental exposure. This can show the appropriateness for the silicone substrate assembly and compare it to existing known data.
4. The material must be able to survive an exposure to the environment for which it is placed. This includes but is not limited to acid rain environments, salt spray, UV, heat, and cold.
5. The supplier of such a new material must be knowledgeable of the application of his material and the life expectancy required of that material.

This is a short study to show the effects of short-term exposure on substrates that could be used for structural silicone attachment. Changes in strength after exposures for PVDF paint and anodized specimens were not significant. This was expected due to the actual historical performance. There were changes in the galvanized and steel substrates as they were subjected to harsh environments beyond where they are expected to perform. Good engineering judgment limits the use of those materials for structural silicone attachment. This test regimen did not show degradation to the fiberglass substrate that was chosen, but did show monumental changes to the PVC substrates chosen after exposure to heat and UVFL weathering. The changes in shape and color of the PVC substrates tested here should alone exclude them from use; however, these dimensional stability and color changes were augmented with the poor adhesion and lap shear strength.

Guidelines and specifications for silicone structural attachment have not considered aged substrates or dimensional stability, and this informal testing regimen suggests that new unproven substrates should indeed be scrutinized for their durability. A simple adhesion test by a sealant manufacturer to obtain a proper surface preparation procedure is in no way the only criteria for use on a curtainwall for sealing and structural silicone attachment. Please direct any comments and questions to the author.

Acknowledgments

The author would like to thank John LaDouce of the Dow Corning Construction Laboratory for all of the work in preparing, aging, and testing the lap shears and peel adhesion specimens. A special thanks is also offered to Ron

Badour for cutting the specimens. A special thanks is also sent to Christian Kaiser for arranging the specimens in the salt fog chamber.

References

- [1] Hilliard, J. R., Parise, C. J., and Peterson, C. O., Jr., *Structural Sealant Glazing, Sealant Technology in Glazing Systems, ASTM STP 638*, ASTM International, West Conshohocken, PA, 1977, pp. 67–99
- [2] Carbary, L. D. and Albert, F. “A Thermal Modeling Comparison of Typical Curtain-wall Glazing,” *Glass Performance Days, Conference Proceedings*, Tampere, Finland, June 2007 pp. 282–286.
- [3] Carbary, L. D., “A Review of the Durability and Performance of Silicone Structural Glazing Systems,” *Glass Performance Days, conference proceedings*, Tampere, Finland, June 2007, pp. 190–193.
- [4] Fassaden Windows Catalogue, <http://www.fassadenwindows.com/> Date viewed November 19, 2008.
- [5] ETAG 002, “Guideline for European Technical Approval for Structural Sealant Glazing Systems (SSGS),” EOTA Kunstlaan 40 Avenue des Arts B -1040 Brussels.
- [6] “Acceptance Criteria for Type I Structural Silicone Glazing Sealants (Adhesive) AC45,” *ICBO International Conference of Building Officials*, April 1991, available at <http://www.icc-es.org/Criteria/> Date Viewed July 8, 2008.
- [7] Loper, W. and Obermeier, T., “Thin Stone Veneers—A Steel/Silicone Diaphragm System,” *New Stone Technology, Design, and Construction for Exterior Wall Systems, ASTM STP 996*, B. Donaldson, Ed., ASTM International, West Conshohocken, PA, 1988, pp. 137–140.
- [8] Carbary, L. D., “Structural Silicone Sealant Requirements for Attaching Stone Panels for Exterior Applications,” *Building Sealants: Materials, Properties, and Performance, ASTM STP 1069*, Thomas F. O’Connor, Ed., ASTM International, West Conshohocken, PA, 1990.

Frederic Gubbels¹ and Clementine Calvet¹

Adhesion Development of Organic and Silicone Sealants on Wet and Dry Concrete

ABSTRACT: Reliability of a sealed joint is directly related to the durability of its adhesion to the substrate. The presence of moisture on the surface of porous substrates caused by changing weather conditions prior to the application of sealants, such as the wetting of concrete by rainfall, can lead to poor sealed joint durability due to adhesion loss. In an attempt to better understand this mechanism, a method of testing adhesion of sealants on wet concrete has been developed and the effect of changes in surface conditions on sealant adhesion has been evaluated during the various drying phases identified for concrete. In the first 2 h of drying, a significant reduction of the pH at the surface is observed, which is mirrored with a reduction of the surface humidity. Both of these properties seem to have reached their plateau value within that timeframe, but in the following hours of the drying process the concrete continues to lose weight through water evaporation. Sealants based on different chemistries have been applied at various stages of the drying process ($t = 0, 0.33, 2, 8, 24, 56$ h) showing that the critical time period affecting the development of adhesion is within the first 2 h of concrete drying. This indicates that the alkalinity, surface moisture, on both, are the major factors responsible for the poor adhesion obtained on wet porous substrates and this is also the same for adhesion development of a primer on the substrate. The different sealant technologies evaluated in this program were silicones, urethanes, acrylics, silyl-terminated polyether, and silyl-terminated polyurethanes. In terms of adhesion development on wet concrete, the results highlight that the differences are more related to formulation within a sealant family than to the binder chemistry itself.

Manuscript received June 17, 2008; accepted for publication January 26, 2009; published online March 2009.

¹ Dow Corning, Rue Jules Bordet-Seneffe, Hainaut 7180 Belgium.

Cite as: Gubbels, F. and Calvet, C., "Adhesion Development of Organic and Silicone Sealants on Wet and Dry Concrete," *J. ASTM Intl.*, Vol. 6, No. 3. doi:10.1520/JAI101932.

Copyright © 2009 by ASTM International, 100 Barr Harbor Drive, PO Box C700, West Conshohocken, PA 19428-2959.

Introduction

Adhesion is one of the most important properties for both adhesives and sealants because, although the primary function of sealants is to seal, in most applications, they cannot provide this function without proper and durable adhesion to the substrates [1]. On a porous material like concrete, adhesion is mainly the result of physical-chemical interactions and mechanical interlocking. While the formation of a covalent bond is strongly recommended to prevent early failure of the seal, interlocking also enhances the strength of the interphase layer on rough surfaces. On concrete, the use of a primer is generally recommended prior to the application of the sealant for two reasons. Firstly, the primer improves the bonding by forming a bifunctional layer at the interface between the concrete and the sealant and secondly, the low viscosity of the primer ensures a deep penetration into the pores and consequently improves interlocking [2].

In the presence of an excess of water, the chemical adhesion is often impaired by the displacement of the equilibrium towards the competitive hydrolysis reaction. Due to capillary forces and surface adsorption, a wet porous substrate typically retains water for prolonged period of time [3] and thus prevents chemical bonding from occurring. Of equal importance for most sealants, unless they are of the water-borne variety, is the fact that the physical presence of water acts as a barrier against adequate wetting of the sealant and thereby reduces interlocking.

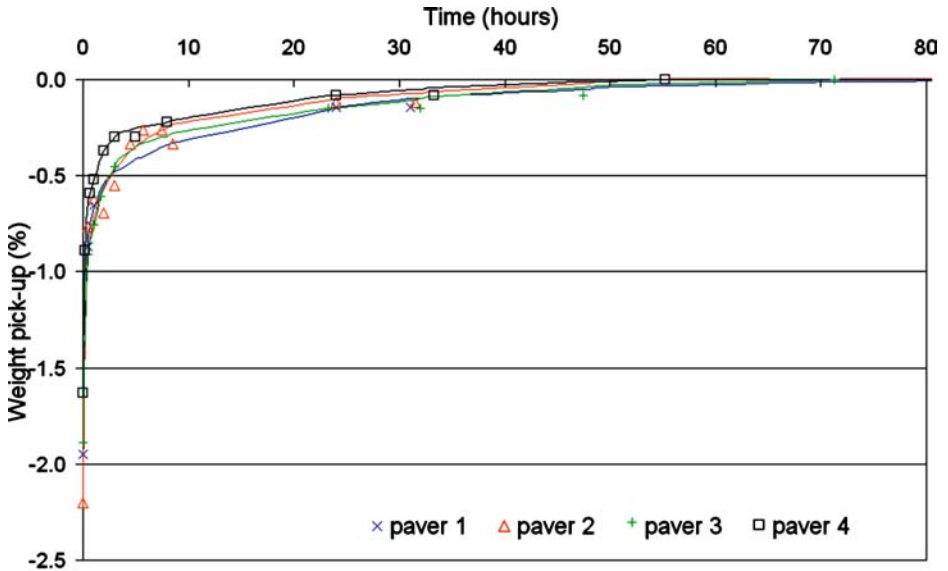
The integrity of a joint is a function of the balance between adhesion and the cohesion strengths in the substrate, in the sealant, and in the interphase. Its durability strongly depends on how these strengths evolve over time and how they degrade as a result of weathering. In many cases, degradation of adhesion strengths is responsible both for early and long-term failure. However, it is noteworthy that some poorly adhering sealant may still fail cohesively due to very low intermolecular (cohesive) strength.

In an attempt to better understand the involved mechanisms, a study of the drying phases of precast concrete has been carried out, as well as development of a method of testing adhesion of sealants on wet concrete. Additionally, the durability of adhesion on dry concrete of different sealant technologies has been studied after exposure to water immersion. The Arrhenius model has been adapted to serve the purpose of this investigation.

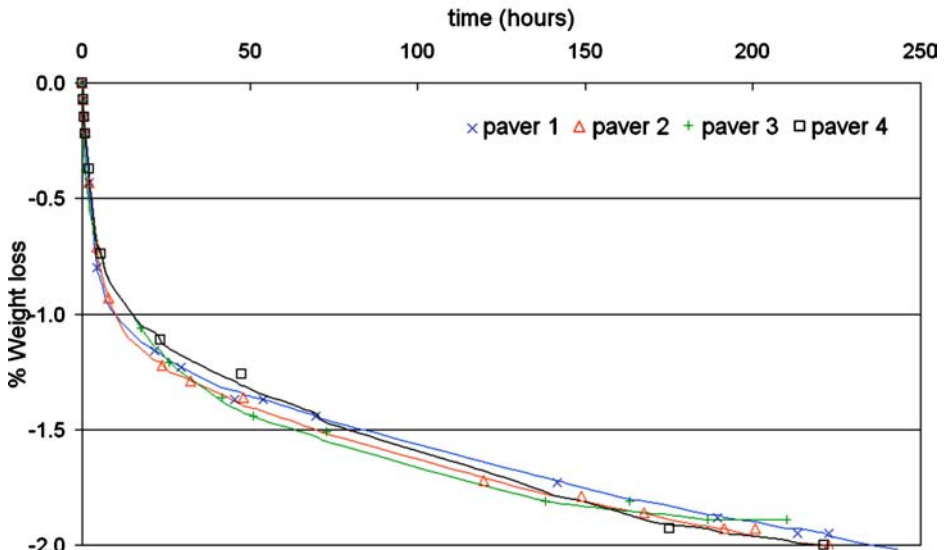
Study of Wetting and Drying Phases of Concrete

Wetting and drying phases were followed using three different testing methods developed within the frame of this study: water pick-up, tissue testing, and pH paper testing.

Kinetics of water pick-up of concrete pavers under water immersion depends on many factors, among which the hydrostatic and capillary pressures are initially driving the water ingress [4,5]. As water migrates into the paver, air has to be displaced by diffusion from deeper sections, which slows down the water pick-up process (Fig. 1(a)). During the drying phase, vapor and liquid diffusion are driving water out of the paver to equilibrate with the external



(a)



(b)

FIG. 1—Concrete pavers subjected to water immersion. (a) Wetting phase: weight pick-up during water immersion. (b) Drying phase: weight loss at 23°C 50 % RH.

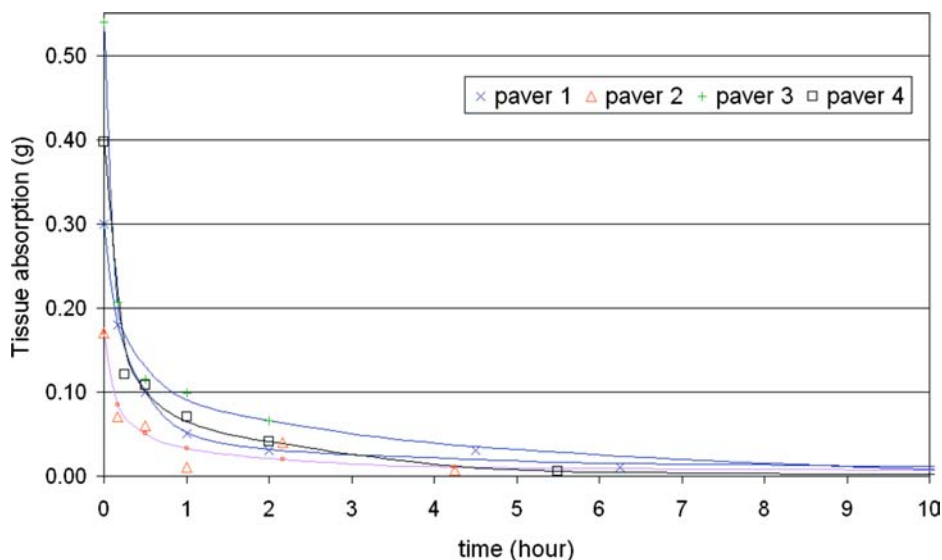


FIG. 2—Tissue testing on drying concrete pavers.

vapor pressure; i.e., relative humidity. The speed of this diffusion slows down when water comes from deeper section of the paver (Fig. 1(b)).

To distinguish surface water from in-depth water, additional testing was carried out by soaking up available surface water with a dry, preweighed, non-woven tissue that was applied with a constant load on the surface of the paver for a predetermined period of time. As can be seen in Fig. 2, this test exhibits a higher variability; however, it still highlights the fact that the majority of the water disappears from the surface within the first two hours.

In order to track alkalinity of the concrete surface, a pH paper was applied to it and the pH of the substrates was recorded over time. As can be seen in Fig. 3, the variability of this method is rather high but the trend fits relatively well with the tissue testing. The pH of the water gradually drops to reach a value of 7 after about 2 h; i.e., when water disappeared from the concrete surface. The fact that our concrete pavers exhibit a pH of 7 at the surface is indicative of a certain age of the specimen because we know that a fresh concrete surface is alkaline due to the presence of calcium oxide and hydroxide. Over time, the carbonation reaction with atmospheric carbon dioxide gradually reduces alkalinity at the surface of cementitious materials.

In this respect, X-ray photoelectron spectroscopy (XPS) may be a successful tool to explore the differences in surface chemistries between a dry and a wet concrete. As can be seen in Fig. 4(a), which compares C 1s spectra of dry and wet samples, there is a significant decrease of the carbonate content at the surface of the wet sample. This is aligned with an increase in the binding energy observed in the Ca 2p spectra indicating that CaCO₃ molecules are present in the dry sample and being replaced by CaO or Ca(OH)₂ species in the wet sample. It is likely that water is dissolving noncarbonated calcium (hydr)oxide

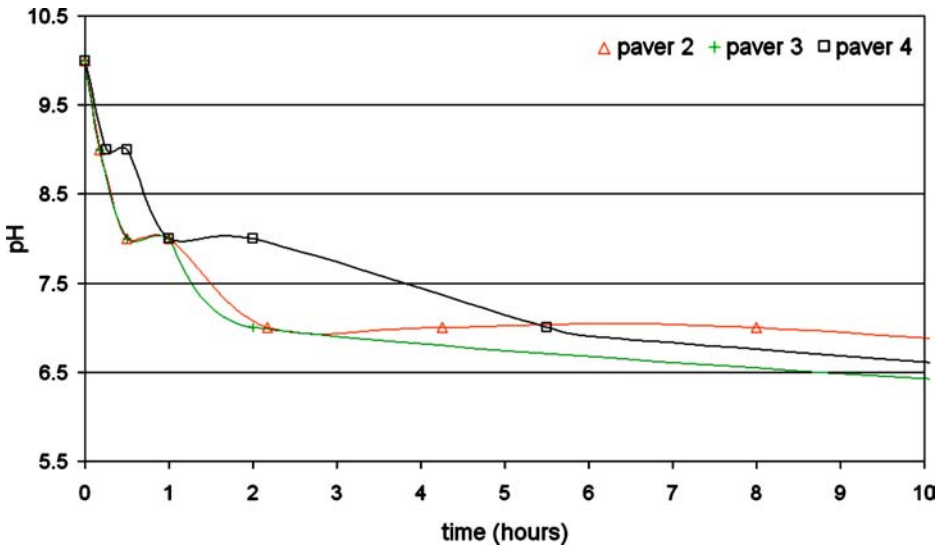


FIG. 3—*pH testing on drying concrete pavers.*

salts from the bulk of the concrete, which then diffuse to the surface of the substrate through evaporation of the water.

Based on the results of the previously mentioned testing, we defined the key wetting and drying phases as described in Fig. 5. A0 corresponds to a dry concrete paver in equilibrium with environmental moisture as it has been stored for several days at 23°C and 50% relative humidity. At A2, the paver has been subjected to 2 h of immersion, which simulates the surface of the concrete after a short rainfall, and it is noted that the paver has not yet reached saturation. At A24, i.e., after 24 h of immersion, most of the water has reached the bulk of the concrete paver, which is slowly reaching saturation and simulates a concrete surface after a heavy rain. B0 corresponds to the highest degree of water pick-up and is defined as a fully saturated wet concrete paver. B2 is the phase where humidity and alkalinity are disappearing from the surface. B8 is the time period where the speed of weight loss decreases substantially; however, the surface still shows signs of humidity. At B24 the surface is totally dry but there is still humidity in deeper sections of the concrete. At B56, the paver can be considered as fully dry, but weight pick-up continues to slowly decrease.

Results and Discussion

Table 1 summarizes the technologies of various sealants investigated in this study. Beads of sealants were extruded from the packaging and applied directly onto the surface of the drying concrete. Concrete pavers were held vertically in order to assess the ease of application of the sealant in a vertical joint. On fully wet substrates (B0), only a few sealants showed an initial adhesion to the concrete; i.e., silicone S2, silyl-polyether SPE1, solvent-borne acrylic SB ACR. and

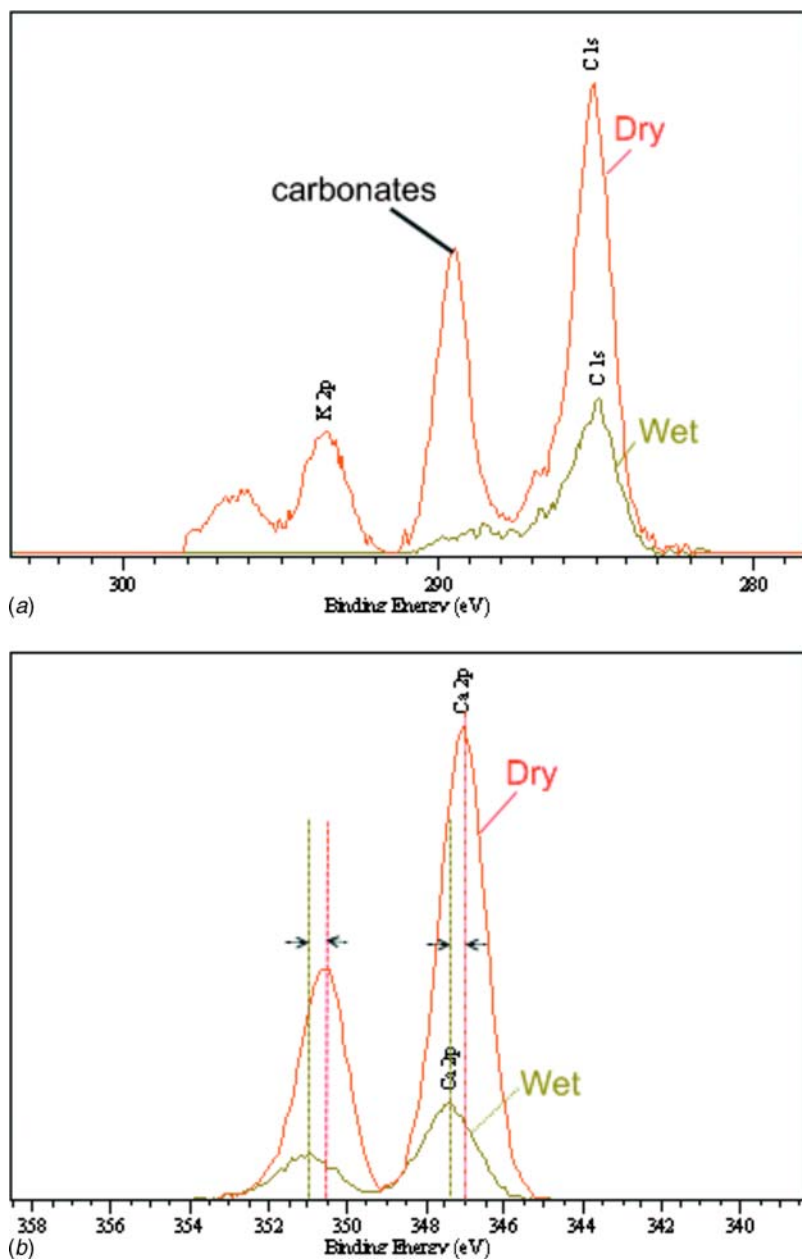


FIG. 4—(a) Comparison of C 1s spectra acquired from dry and wet concrete surfaces. (b) Comparison of Ca 2p spectra acquired from dry and wet concrete surfaces.

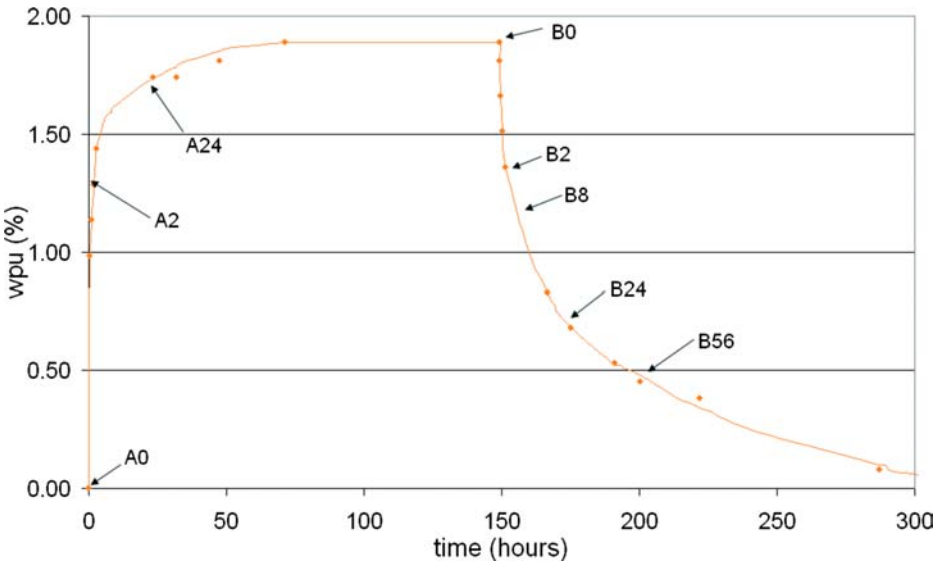


FIG. 5—Definition of the wetting and drying phases.

the silyl-acrylate SA. All other sealants were very difficult to apply and to hold on the wet surface. After 2 h of drying (B2), all sealants were showing an acceptable wetting behavior on the surface of the paver.

Table 2(a) reports the mode of failure observed over the drying period of unprimed concrete substrates as well as under water immersion aging. It can be seen that only the silyl-modified polyurethane SPUR1 is showing good adhesion to the wet substrate. This adhesion is already lost, however, when the pavers are dried for 20 min prior to the sealant application, which shows that the high level of water is boosting adhesion of the sealant. To a lesser extent this

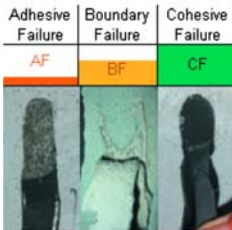
TABLE 1—Packaging, generic technologies, and chemistries of sealant benchmarked.

Generic Technology	Sealant Codes	Sealant Chemistry	Packaging
Silicones	S1	Silicone alkoxy	cartridge 300 ml
	S2	Silicone oxima	cartridge 300 ml
Urethanes	PUR	Polyurethane	cartridge 310 ml
Acrylics	SB ACR	Solvented acrylic	cartridge 310 ml
Hybrids	SPE1	Silyl polyether	cartridge 290 ml
	SPE2	Silyl polyether	cartridge 290 ml
	SPUR1	Silyl polyurethane	cartridge 300 ml
	SPUR2	Silyl polyurethane	sausage 600 ml
	SA	Silyl acrylate	cartridge 310 ml

TABLE 2—Peel adhesion testing on (a) unprimed and (b) drying concrete and after 55 °C water immersion.

	21D cure unprimed concrete						28D cure unprimed concrete		
	B ₀	B _{20'}	B ₂	B ₈	B ₂₄	B ₅₆	A ₀	1W 55 water	2W 55 water
S1	AF	AF	BF	BF	BF	BF	CF	CF	CF
S2	AF	CF	CF	CF	CF	CF	CF	AF	AF
PUR	AF	AF	AF	AF	BF	CF	AF	BF	BF
SB ACR	CF*	CF*	CF*	CF*	CF*	CF*	CF	CF*	CF*
SPE1	AF	AF	AF	AF	AF	AF	BF	AF	AF
SPE2	AF	AF	AF	AF	AF	AF	BF	AF	AF
SPUR1	CF	AF	AF	AF	AF	AF	CF	AF	AF
SPUR2	BF	AF	AF	AF	AF	AF	CF	AF	AF
SA	AF	CF	CF	CF	CF	CF	BF	AF	AF

(*) very low cohesion



(a)

	21D cure primed concrete						28D cure primed concrete		
	B ₀	B _{20'}	B ₂	B ₈	B ₂₄	B ₅₆	A ₀	1W 55 water	2W 55 water
S1	AF	AF	CF	CF	CF	CF	CF	CF	CF
S2	AF	AF	CF	CF	CF	CF	CF	CF	CF
PUR	CF	AF	AF	CF	AF	AF	AF	AF	AF
SB ACR	CF*	CF*	CF*	CF*	CF*	CF*	CF	CF*	CF*
SPE1	AF	AF	AF	AF	AF	AF	BF	AF	AF
SPE2	AF	AF	BF	CF	CF	CF	BF	BF	AF
SPUR1	AF	AF	AF	CF	CF	CF	CF	AF	AF
SPUR2	AF	AF	AF	CF	CF	CF	CF	CF	BF
SA	AF	AF	CF	CF	CF	CF	CF	AF	AF

(*) very low cohesion

(b)

phenomenon is also observed with SPUR2, which shows a boundary failure on fully saturated pavers (B0). Adhesive failure is reported when the drying period is equal to or higher than 20 min (B20'). The solvent-borne acrylic exhibits a cohesive failure mode on all pavers. However, the material stays very sticky and this material exhibits very poor cohesive qualities. It seems that 28 days are required to obtain a certain desirable cohesion in this product, but adhesion is only obtained via interlocking, which is acceptable for sealants in joints exposed to low movement. After 20 min of drying, only the silicone S2 and the silyl-acrylate SA developed good adhesion to the concrete, which was maintained for both products over the drying period. With PUR, the adhesion starts to develop only when the concrete is fully dried and adhesion after 28 days of cure remains poor, indicating that adhesion strength is relatively weak in comparison to cohesive strength, which also increases as curing time is extended. The two SPE sealants investigated exhibited very poor adhesion on wet and dry concrete when applied vertically, and a slight improvement indicated by a boundary failure observed after 28 days of cure when the sealant is applied horizontally, indicating some improvement that is induced by gravity forces. However, this weak adhesion is quickly lost during water immersion exposure. For dry concrete, adhesion increases more consistently when the sealant has been horizontally rather than vertically applied, but the differences observed may also be the result of the additional 7 days of cure with these specimens. After the first week of immersion, the silicone S1 sealant is the only sealant that maintains a robust adhesion to the substrate. This adhesion is maintained after a second week of immersion, confirming the long term stability of the bond existing between this silicone and the substrate.

As can be seen in Table 2(b), the use of a primer substantially improves adhesion development and its durability. This is especially true for all sealants based on silicon-cure technologies; i.e., silicones and silyl-modified organic hybrids. On fully wet substrate the primer acts as a barrier between the water and the sealant. Consequently the accelerating effect of water on adhesion build-up previously observed with the SPUR sealants cannot be detected once a primer has been applied to the substrate. Interestingly, the adhesion of the PUR on wet concrete (B0) has improved substantially on the primed pavers. With most sealants, the adhesive performance now seems to be controlled by the adhesion properties of the primer itself. This is confirmed by the infrared analysis of the B0 samples that showed the following. The sealant surface in contact with the concrete surface was analyzed with an attenuated total reflection Fourier transform infrared spectroscope (ATR-FTIR). All spectra are showing the presence of a C=O vibration band at 1726 cm^{-1} characteristic of the primer used. The only uncertainty lies with the silyl-acrylate sealant, which also shows an absorption peak in the same region. As can be seen the adhesion is developed on concrete after two or more hours of drying, which corresponds to the time when the alkalinity disappears from the surface. After this period a consistent adhesion is observed with the two silicones, as well as the sealants SPE2, SPUR1, SPUR2, and SA. After one week 55°C water immersion the two silicones and SPUR2 maintain good adhesion but the adhesion is lost after the second week of immersion for the SPUR2 sealant.

In order to better understand adhesion durability the Arrhenius model has

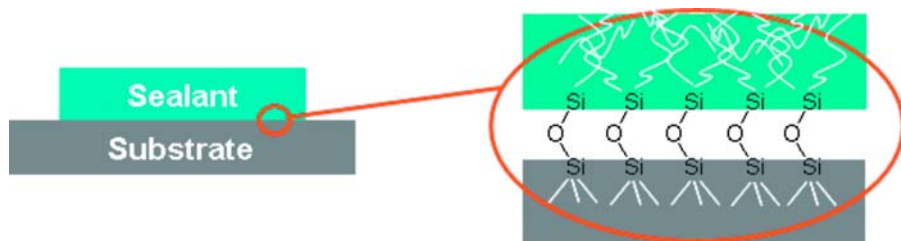


FIG. 6—Scheme illustrating chemical linkage between the sealant and the concrete.

been used and adapted to track the adhesion loss of various sealant technologies on glass and concrete [6,7]. On a nonporous substrate, adhesive failure is primarily observed when there is no chemical bonding of the sealant. Most sealant technologies are formulated with silane adhesion promoters to enhance the formation of these chemical bonds and thereby improve the durability of the joint. During cure, these silanes migrate from the bulk of the sealant to the interfaces in order to equilibrate the concentration gradient created by their consumption [8,9]. Generally, after complete cure of the sealant covalent bonds are formed with the substrate, which on glass and concrete often consists of silicate or siloxane $\equiv\text{Si}-\text{O}-\text{Si}\equiv$ bonds, as shown schematically in Fig. 6. According to the Arrhenius model, the rate of hydrolysis of these bonds depends on the activation energy of the transition complex formed.

Equation 1 describes the rate of disappearance of the chemical bonds at the interface. After mathematical integration based on the initial conditions, Eq 2 is obtained describing the number of chemical bonds present at a given time elapsed, where n_B^0 represents the number of bonds initially present after cure. For a given first-order chemical reaction, the kinetics constant k given by the Arrhenius equation (Eq 3) depends mainly on the temperature (T) and the activation energy (E_a). If we suppose that the adhesive failure occurs at a constant ratio n_B/n_B^0 of broken bonds, Eqs 3 and 2 can be combined to provide Eq 4, where the natural logarithm of time for adhesive failure is directly related to the inverse of the temperature:

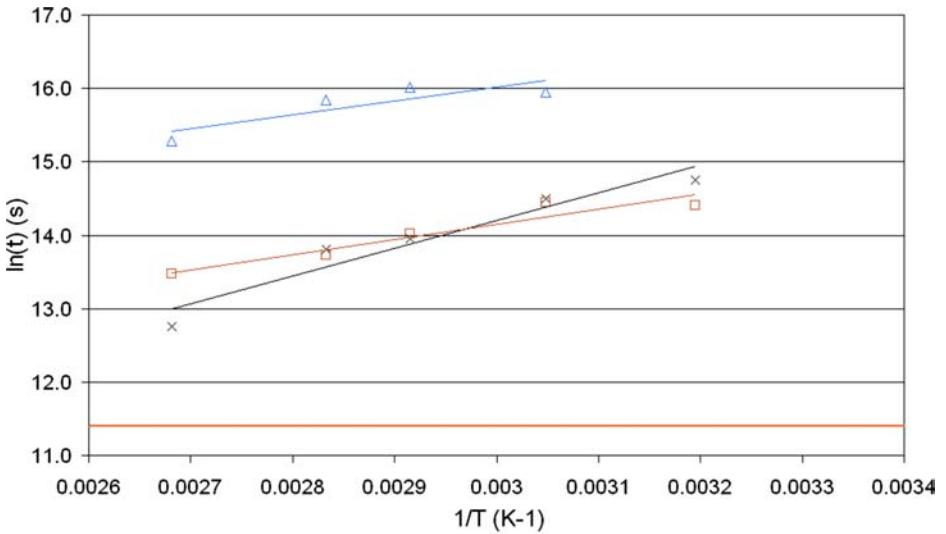
$$\frac{dn_B}{dt} = -kn_B \quad (1)$$

$$n_B = n_B^0 e^{-kt} \quad (2)$$

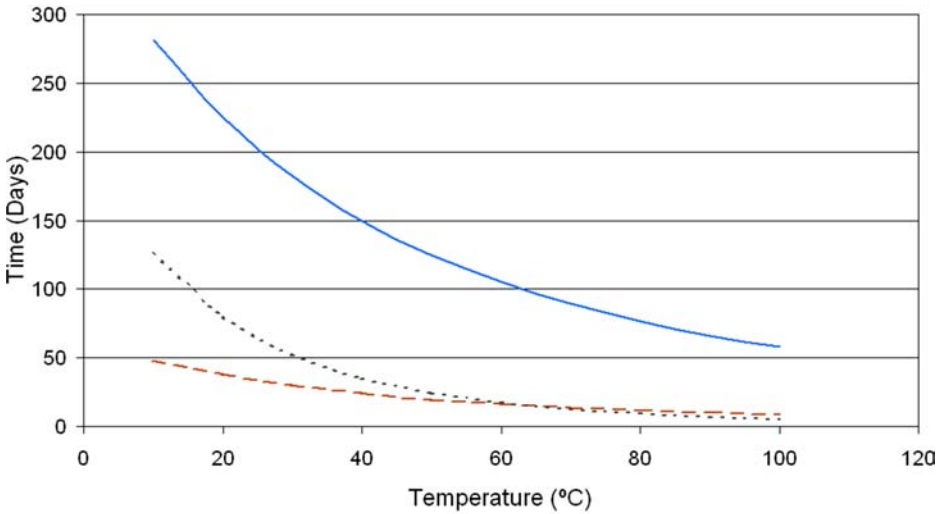
$$k = Ae^{-E_a/RT} \quad (3)$$

$$\ln t = K' - \frac{E_a}{RT} \quad (4)$$

As can be seen from the Arrhenius plot in Fig. 7(a), the adhesion of silicone on glass is very durable and temperature resistant. The linear plot of Fig. 7(b) shows that more than 50 days are required to impair adhesion at 100°C, while at room temperature adhesion is maintained for more than 250 days under



(a) × Concrete □ Concrete + Primer △ Glass



(b) — Glass - - - Primed Concrete ···· Concrete

FIG. 7—S1 silicone sealant on glass, on concrete, and on primed concrete (a) Arrhenius plot; the bottom line indicates a loss of failure after 1 day of immersion. (b) Time to observe adhesive failure mode on the substrate.

water immersion. The slope of the graphs, which is related to the activation energy, is relatively smooth, indicating a relatively low impact of temperature on the loss of adhesion. On unprimed concrete the slope is steeper, which shows that the adhesion build-up is involving a different set of chemical bonds

TABLE 3—Activation energies of various sealant technologies calculated from Arrhenius plots.

	Activation Energies (kJ/mol)		
	Glass	Concrete	Primed Concrete
S1	15.5	31.4	17.0
SPE1	63.0	57.9	—
SPUR1	54.8	44.6	—
SACR	47.3	26.0	—

and hence a different transition complex. Surprisingly, the priming of the concrete has a bigger effect on the slope of the graph than on its height. Activation energies calculated from the Arrhenius plots are reported in Table 3, which highlights that the loss of adhesion on a primed concrete is likely to occur through a similar chemical reaction mechanism as that which occurs for sealant adhered onto glass.

Figure 8 illustrates that the adhesion of hybrid systems is somewhat different than the adhesion of silicone. Interestingly, the mechanism of failure of the silyl-acrylate, and to a lesser extent the silyl-polyurethane does not strictly follow the Arrhenius law, especially at high temperatures. This suggests that more than one type of chemical bond is involved in the adhesion development and that the activation energies of these bonds are different. The slope and the height of the SPE1 sealant plot approach those of the SPUR1 sealant, which is indicative of the similarities of both systems on glass. The polyether backbone

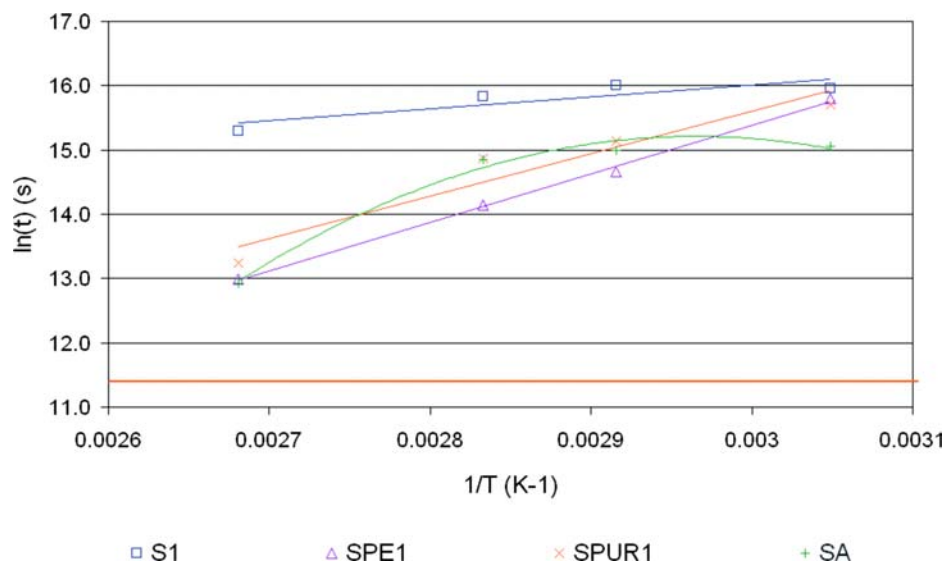


FIG. 8—Arrhenius plot of S1, SPE1, SPUR1, and SA on glass; the bottom line indicates a loss of failure after 1 day of immersion.

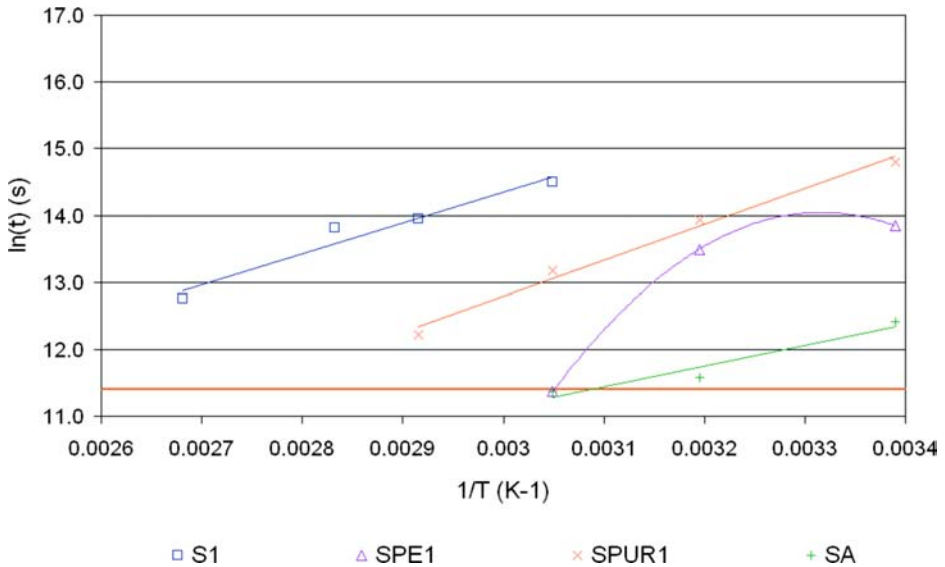


FIG. 9—Arrhenius plot of *S1*, *SPE1*, *SPUR1*, and *SA* on concrete; the bottom line indicates a loss of failure after 1 day of immersion.

present in both materials and its specific water absorption might be responsible for this similarity. The silicone product is showing a more durable adhesion that is especially notable at elevated temperatures. Figure 9 plots the adhesion failures of the same products on unprimed concrete and while silicone is again exhibiting superior adhesion durability, the slopes of plots for the various sealants are now very similar, except for the *SPE* sealant, which does not follow the Arrhenius model. This means that the sealants that are following the Arrhenius model have closer activation energies on concrete than onto glass. Both the silyl-polyether and the silyl-acrylate lose adhesion within 24 h when immersed in water at 50°C, which confirms previous data indicating that their adhesion on unprimed concrete is not durable.

Activation energies for the *SA* sealant on glass and the *SPE* sealant on concrete have been calculated based on a linear model (Table 3). These values have to be taken with care as the systems do not follow the Arrhenius law. As can be seen, the activation energies of the hybrid sealants studied are higher than that of the silicone sealant evaluated. This might be due to the fact that the hybrid sealants are formulated with tin catalysts, while the silicone studied here is based on a titanate catalyst. As shown elsewhere, tin-catalyzed silicones on glass have activation energies of hydrolysis closer to those of hybrid sealants; i.e., 47.2 and 48.8 kJ/mol [8]. This suggests that the adhesion durability of sealant formulations based on tin catalyst is more sensitive to temperature than equivalent formulations based on titanate.

As a high value of the activation energy means that temperature has a bigger influence on the rate of adhesive failure, the following rankings can be made from the systems studied.

Robustness of adhesion on glass and concrete over temperature variations:

Silicone S1 > silyl-acrylate SA > silyl-polyurethane SPUR1 > silyl
-polyether SPE1

Durability of adhesion on glass under water immersion:

Silicone S1 \cong silyl-polyurethane SPUR1 \cong silyl-acrylate SA > silyl
-polyether SPE1

Durability of adhesion on concrete under water immersion:

Silicone S1 > silyl-polyurethane SPUR1 > silyl-polyether SPE1 \cong silyl
-acrylate SA

Experimental

Water Pick-up

Water pick-up tests were carried out by immersing 30 by 30 by 4 cm³ precast concrete pavers in a 20 L bath containing distilled water. In order to study the wetting phases the pavers were weighed regularly until water saturation, i.e., until a stable weight, was measured. To study drying, saturated pavers were removed from the bath and weighed over time. After saturation, the water pick-up of the concrete pavers was between 1.6 wt % and 2.3 wt %. As concrete pavers in this study have different histories and water contents, graphs have been realigned on the saturation and dry plateaus observed on the drying and wetting curves.

Tissue Testing

A sheet of 20 by 10 cm² nonwoven tissue was weighed and then applied on a drying concrete paver that was previously saturated with water. A brick of 2.23 kg was applied on the tissue for 2 min and immediately afterwards the tissue was weighed. The measurement is expressed in grams of water absorbed by the tissue.

pH Paper Testing

A pH paper (pH measurement range: 1–14) was applied on a drying concrete paver that was previously saturated with water. If needed, a droplet of distilled water was applied on the pH paper to ensure it was completely wet.

XPS Analysis

The piece of concrete was removed from the water and bonded to a copper stub using a double-sided adhesive tape. The concrete sample and stub were immersed in liquid nitrogen to preserve the hydrated state. The sample was then transferred as quickly as possible to the sample stage, which was maintained at 0°C during analysis. XPS analysis was performed using an Axis Ultra spectrometer (Kratos Analytical). Samples were irradiated with monochromated X rays ($Al K\alpha$, 1486.6 eV) with photoelectrons analyzed from a selected area 700 μm by 300 μm , with a take-off-angle of 90°. All of the samples were initially analyzed in the survey mode (Pass Energy set at 160 eV). Data processing software was used to calculate the area under peaks representative of elements detected, which were then normalized to take into account relative sensitivity to provide relative concentrations. The samples were also analyzed in the high resolution mode (Pass Energy set at 20 eV) to determine the chemical states of the elements present at the surface from the same individual positions on each sample.

ATR-FTIR Analysis

Sealant samples have been directly applied on the golden gate of the attenuated total reflectance Fourier transform infrared spectroscope ATR-FTIR. The equipment used was a FTIR 2000 (Perkin-Elmer), accessory: MKII Golden-gate Single Reflexion ATR.

Number of scans: 15; resolution: 4 cm^{-1} ; range: 4000 cm^{-1} to 450 cm^{-1} .

Finger Peel Adhesion Testing on Wet and Dry Concrete

Wet concrete pavers were immersed 56 h prior to application of the sealant. Sealants were then applied vertically on the drying substrates according to the time defined. On primed substrates, a primer for silicones was applied vertically at the timing defined by the drying phases and left 1 h to cure prior to the application of the sealant. Directly after sealant application, a spatula was used to smooth the bead and apply a gentle pressure to favor initial wetting and grip of the sealant. Water immersion ageing has been carried out on dry concrete pavers. On these pavers, the application of the sealant and the optional primer were done horizontally. For the primed substrates, the primer was applied 1 hour prior to the sealant application. Concrete pavers were left for 28 days to cure and tested. Afterwards, they were immersed for 2 weeks in 55°C water. The test was carried out after 1 and 2 weeks. Finger peel testing was carried out using a sharp razor blade to induce a cut between the substrate and the sealant. The bead of sealant was then peeled off by hand and the mode of failure reported.

Arrhenius Testing

Tensile-adhesion joints (“H-pieces”) of 12 by 12 by 50 cm^3 dimensions were prepared in accordance to ISO 8339 [10] with glass or DIN EN 1323 [11] concrete from Rocholl GmbH, Aglasterhausen, Germany using polytetrafluoroeth-

ylene (PTFE) spacers to facilitate demolding. The non-tin side of float glass was selected using a UV lamp and cleaned with a mixture of isopropanol (IPA)/acetone 75/25 1 h prior to the application of the sealant. Dust on concrete was removed with the help of a rigid plastic brush and then cleaned with a mixture of IPA/acetone 75/25 1 h prior to the application of the sealant. Optionally, the primer was applied on concrete 1 h prior to the application of the sealant. Tensile adhesion joints according to ISO 8339 standard [10], i.e., H-pieces were left to cure in a climatic chamber for 28 days at 23 °C 50 % relative humidity (RH) prior to water immersion. For each measurement, ten H-pieces were immersed at the defined temperature in water and adhesion was gently tested every day on all (20) substrate interfaces of the ten H-piece specimens. Adhesion failure was reported when one side of the H-piece started falling apart from the sealant with a very gentle force applied by hand. The substrates were left in the water bath until all 20 substrate interfaces have shown failure. The time of failure reported in the graphs is the arithmetic mean calculated from these 20 measurements.

Conclusions

Adhesion development of various sealant chemistries has been explored on wet and dry concrete showing that for most technologies adhesion is enhanced when sealants are applied after the first two hours of drying. This indicates that the alkalinity and/or surface moisture are the major factors responsible for the poor adhesion observed on wet concrete.

This critical timing also affects the adhesion development of the primer on the substrate.

In terms of adhesion development on a wet surface, the results highlight that the differences are more related to formulation within a sealant family than to the binder chemistry itself.

On dry concrete, the adhesion development is primarily related to the sealant (binder) technology and only secondarily to the sealant formulation.

Even if it is not applicable in all circumstances, the Arrhenius model is a convenient tool to investigate the durability of adhesion and compare sealant technologies among each other.

Adhesion properties of titanate-catalyzed silicones are the least influenced by temperature variations under water immersion both on glass and concrete.

Acknowledgments

The authors are grateful to Stuart Leadley who carried out the XPS analysis. The authors would like to thank Sophie Huez and Arnaud Labrosse for their collaboration on the ATR-FTIR analysis.

References

- [1] Wolf, A. T., and Hautekeer, J., *Handbook of Adhesives and Sealants*, Vol. III, P. Cognard, Ed., Elsevier, New York (in press).
- [2] Bundies, J. F., "Two-Component Coatings on Concrete: Some Chemical and Physical Aspects of Adhesion," *Adhesion between Polymers and Concrete. Proceedings of*

- the 2nd International RILEM Symposium ISAP'99*, 1999, RILEM, Bagnaux, France, pp. 181–192.
- [3] Philip, J. R., and Devries, D. A., “Moisture movement in porous materials under temperature gradients,” *Trans., Am. Geophys. Union*, Vol. 38, 1957, pp. 222–232.
 - [4] Dullien, F. A. L., *Porous Media: Fluid Transport and Pore Structure*, 2nd Ed., Academic Press, New York, 1991.
 - [5] Adamson, A. W., *The Physical Chemistry of Surfaces*, 4th Ed., Wiley, New York, 1982.
 - [6] Parbhoo, B., O'Hare, L.-A., and Leadley, S. R., “Fundamental Aspects of Adhesion Technology in Silicones,” *Adhesion Science and Engineering, Volume II, Surfaces, Chemistry & Applications*, M. Chaudhury and A. V. Pocius, Eds., Elsevier, Amsterdam, 2002, pp. 677–711.
 - [7] Wolf, A. T., “Effects of Water Immersion on Building and Civil Engineering Joints and the Use of the Arrhenius Method in Predicting Adhesion Lifetime of Water-Immersed Joints,” presentation at 3rd Symposium on Durability of Building and Construction Sealants and adhesives, Denver, CO, 2008.
 - [8] Comyn, J., de Buyl, F., and Comyn, T. P., “Diffusion of Adhesion Promoting and Crosslinking Additives in an Uncured Silicone Sealant,” *Int. J. Adhes. Adhes.*, Vol. 23, No. 6, 2003, pp. 495–497.
 - [9] Comyn, J., de Buyl, F., Shephard, N. E., and Subramaniam, C., “Kinetics of Cure and Adhesion of Water-reactive Alkoxysilicone Sealants,” *Proceedings of the Annual Meeting of the Adhesion Society*, 2003, pp. 433–435.
 - [10] ISO8339, “Building construction. Sealants. Determination of tensile properties,” (Extension to break), International Standardization Organization, Geneva, 2005.
 - [11] DIN EN 1323, “Adhesives for tiles—Concrete slab for test,” (includes Amendment A1:1998); German version EN 1323:1996 + A1:1998 DIN-adopted European Standard/01-Mar-1999.

Jerome M. Klosowski,¹ Edward S. Breeze,² and
David H. Nicaastro³

Cleaning Silicone Residue from Glass

ABSTRACT: Silicone sealants have been used widely in the waterproofing industry because they resist deterioration. However, residue from silicone sealant (or from pre-formed silicone seals) can be difficult to remove from adjacent surfaces, if it contacts these surfaces inadvertently from improper application or fluid run-down. This article focuses on the challenge of removing silicone residue from window glass. Several of the likely sources of the silicone residue are discussed, along with the difficulty of measuring the presence of the colorless and odorless thin residue film. The testing used commercially available cleaners and digesters to attempt to remove the silicone residue. The results were mixed and largely inconclusive; however, the test methodology developed can be used for further study by additional laboratories.

KEYWORDS: sealant joint, silicone, fluid migration, glass

Introduction

The silicone polymer was developed in the 1930s. It was developed into a building sealant in the 1950s, with widespread acceptance and international use in the 1970s. Silicones are now manufactured by at least eight major manufacturers. Many silicone sealants contain silicone plasticizers that are used to increase pliability. The plasticizers lower the modulus of elasticity and allow the sealant to expand and contract more easily, resulting in greater joint movement capability and the ability to stretch with less stress on the substrate, aiding long-term adhesion. These plasticizing polymers do not react post cure with the other components of the sealant; the plasticizers remain loose within the sealant matrix and can migrate onto exterior building surfaces (fluid migration) [1].

Manuscript received June 24, 2008; accepted for publication May 26, 2009; published online July 2009.

¹ Chief Chemist, Building Diagnostics, Inc., Austin, TX 78701.

² Professional Engineer, EDI Building Consultants, Inc., Houston, TX 77057.

³ Professional Engineer, Founder and Chief Executive Officer, Building Diagnostics, Inc. and Engineering Diagnostics, Inc., Austin, TX 78701.

Cite as: Klosowski, J. M., Breeze, E. S. and Nicaastro, D. H., "Cleaning Silicone Residue from Glass," *J. ASTM Intl.*, Vol. 6, No. 7. doi:10.1520/JAI101984.

Copyright © 2009 by ASTM International, 100 Barr Harbor Drive, PO Box C700, West Conshohocken, PA 19428-2959.

The molecules in any cured sealant, including the plasticizers, are in motion. As the sealant gets warmer, the rate of movement of the molecules increases. This atomic motion is not of consequence for the atoms and molecules that have reacted and become part of the sealant system; however, the plasticizer molecules that are loose within the sealant matrix will migrate. Some of the plasticizer molecules eventually migrate to the edge of the sealant and onto or into the adjacent surfaces [2].

Plasticizers are not unique to silicone-based sealants. However, silicone sealants and their plasticizers are highly resistant to degradation when exposed to weather. The plasticizers used in other sealants tend to degrade and disappear as ultraviolet light, moisture, and heat affect them. The silicone plasticizers do not degrade within modern building life spans.

If the plasticizer is a short chain molecule, when it gets to the surface of the sealant it will slowly evaporate because of its solvent properties. These small molecule plasticizers are good for helping sealant extrusion rates but provide little value in obtaining the greater elongation and lower modulus properties that are imparted by the larger plasticizer molecules. As the molecules get larger and larger, their properties change from solvent-like characteristics, through oil-like characteristics, to grease-like characteristics; besides increasing the elasticity properties of the sealant, the larger molecules increase the propensity for dirt pickup and dirt retention ability.

Observations of Plasticizer Performance

At a macroscopic level, the plasticizers feel like a residue. The silicone residue's molecular weight and viscosity affect the dirt pickup and clean-ability. It is comparable to cleaning petroleum-based oil from the garage floor with sawdust or cat litter: If the oil is low viscosity, almost solvent-like, it will be readily absorbed into the granules, and when the granules are swept up they will take the absorbed oil. If the oil is high viscosity, almost grease-like, the absorption into the granules is very slow or non-existent, and sweeping up the grease and granule mix just spreads it around.

Now consider low molecular weight, low viscosity, silicone plasticizer residue on glass. Ambient dust hits the glass, and the residue is absorbed by the dust and gets blown away. However, if the residue is of higher molecular weight, higher viscosity (more grease-like), the dust will land on the residue but the residue will not be absorbed into the dust. Rather, the dust will adhere to the residue. The silicone plasticizer residue is colorless and invisible but the accumulation of dirt causes the window to appear to be dirty.

Typically, window washers clean the windows using detergent solutions that are applied and wiped off with squeegees. On glass with silicone residue, however, the dirt held by the residue is removed but the residue itself remains. The glass appears to be clean, but the invisible silicone plasticizer residue is still there. It then captures and holds more dust, probably at a faster rate than glass without residue. The added cost of more frequent cleaning is a concern for facility owners, managers, and maintenance personnel.

The plasticizer in some silicones may continue to migrate for many years



FIG. 1—The tangent angle of a bead of water on an oily surface at the point of contact of the water and the oily surface is typically between 90° and 110° . This angle is called the contact angle.

through bleed out, run-down, or absorption. If the silicone sealant is prone to plasticizer migration, the normal time for migration to begin to be a problem is between 1 and 2 years, based on the authors' experience. If removed from the glass, it will slowly return during a comparable period.

Residue Removal Tests

Many people have reported success at removing silicone plasticizer residue from glass as they cleaned the dust off of the glass. We polled contractors that are members of the Sealant, Waterproofing, and Restoration Institute (SWRI) to provide information on materials and methods they had used to remove silicone plasticizer residue from glass. Many responses were received including commercial products available from building supply stores and specialty products advertised for the removal of silicone. 12 of the most common recommendations received were used in this study.

It was interesting to note that most of those who reportedly cleaned the glass did not test to confirm whether the silicone plasticizer was actually removed. This type of testing is fundamental for evaluation of cleaning results. A variety of analytical testing methods were explored and contact angle was the chosen technique for this evaluation (Figs. 1 and 2).

Using only one type of glass, the contact angle for clean glass can be reproduced with reasonable consistency (surface roughness and surface energy could attempt to be unitized). Thus, it was reasoned that the silicone was re-

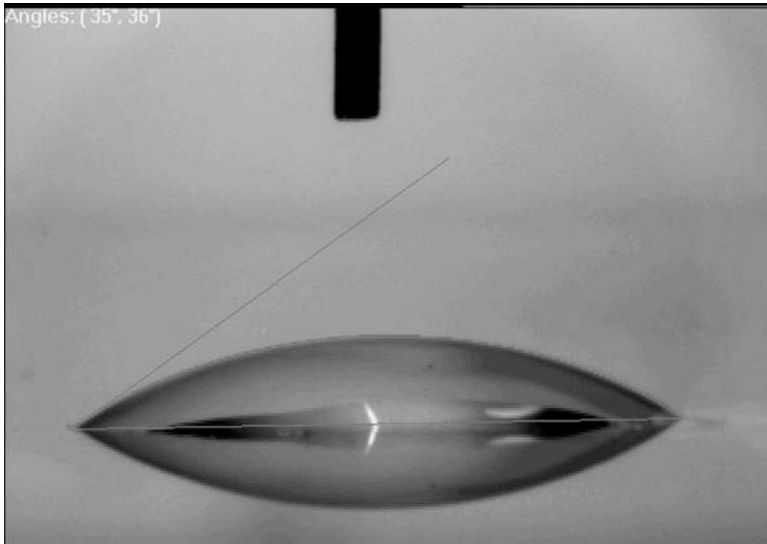


FIG. 2—The contact angle of a bead of water on very clean glass is typically between 10° and 60° , depending on the microscopic roughness of the glass surface and the surface energy of the glass.

moved from the test specimen if the contact angle after cleaning was similar to that of glass that was similarly cleaned but had never been contaminated with silicone. This holds true if any surfactant is completely removed, which may not always be the case in field application.

The study was designed to test cleaning products used in a manner consistent with the methods window washers typically use. While some manufacturers recommended that their product remain in contact with the contaminated glass for several hours or even overnight (the dwell time), this study was performed by leaving the products on the glass for a maximum of 45 min. It is our opinion this is consistent with the practices in glass cleaning using suspended scaffolding on a zone-by-zone production basis. Longer dwell times may be realized in other commercial building locations; however, this may be the subject of future study.

The most difficult silicone plasticizers to clean are generally the ones with higher viscosity; however, a range of plasticizers are in use by the silicone sealant manufacturing industry. In this study 1,000 cS kinematic viscosity (1,000 cP cm^3/g) silicone residues (trimethylsilyl ended polydimethylsiloxanes) were used to contaminate glass specimens that were then cleaned by the tested cleaners.

Experimental Method

Two sets of experiments were conducted to evaluate the effectiveness of the cleaning materials. Initially, the cleaners were tested while the glass was lying in a horizontal position. During evaluation of the findings, it was determined

that viscosity may play a role in the cleaning materials efficacy because many of the materials require extended dwell times for the silicone digesters to react; however, their viscosity did not allow for continuous wetting in a vertical position (matching the orientation of in-place building glass). Thus, the horizontal testing application would not reflect field application. A second round of experiments was conducted using glass cleaned in a vertical orientation.

A Goniometer VSA 2000 was used to measure the contact angle. This device captures video of a liquid bead on the glass surface and expands the picture 250 times and allows freezing of the picture for analysis. For this study, a bead of water was touched to the glass and allowed to spread for 5 sec., then the picture was frozen. The cross section was displayed and the contact points to the glass, the top of the bead, and the mid-point of each side were electronically marked. Software within the goniometer then calculated the contact angle of each side of the bead cross section. This procedure was repeated three times on each glass slide; the contact angle reported is the average of the six angles (two sides each of three beads). In some cases all six values for a cleaning material were similar, while in other cases the bead was asymmetrical, indicating potential inconsistencies in the cleaning.

The glass chosen for the study consisted of 2×3 in. microscope slides. Each slide was washed with commercial grade isopropyl alcohol (diluted 70 % in water). The alcohol was applied liberally and wiped off with clean commercial toweling. Each slide was cleaned twice with this technique. When thoroughly dry, some clean slides were set aside to serve as controls, and silicone plasticizer was applied to the remaining slides. The silicone fluids were liberally applied and allowed to rest on the glass up to 24 hours. The silicone fluid was then wiped off thoroughly with a paper towel, and then re-wiped with a second clean paper towel. The thorough wiping of the silicone left only a thin residue, intended to represent field conditions. To confirm the presence of silicone oil, a bead of water was applied to the surface of each slide; in each case the bead held its shape and had a very high contact angle.

The contaminated slides were labeled, and then a contaminated slide and a control slide were cleaned using the cleaner to be evaluated. The cleaner was applied to the slide and allowed to rest on the glass for 30 min during horizontal orientation testing and 45 min in vertical orientation testing. Then the glass was rinsed with flowing tap water and wiped dry with commercial cotton industrial work towels. The cleaned slides were wrapped in fresh paper towels for storage, and then the contact angle was measured on each slide (Fig. 3).

Summarizing, contact angles were measured on the following:

- Glass cleaned with alcohol.
- Glass cleaned with alcohol and then cleaned with each industrial cleaner.
- Contaminated glass cleaned with industrial cleaner.
- Contaminated glass that was wiped off, but not cleaned with industrial cleaner.

As with all strong solvent combinations, and strong acid pastes, care in handling is fundamental. This paper does not purport to address all of the safety concerns, if any, associated with their use. It is the responsibility of the

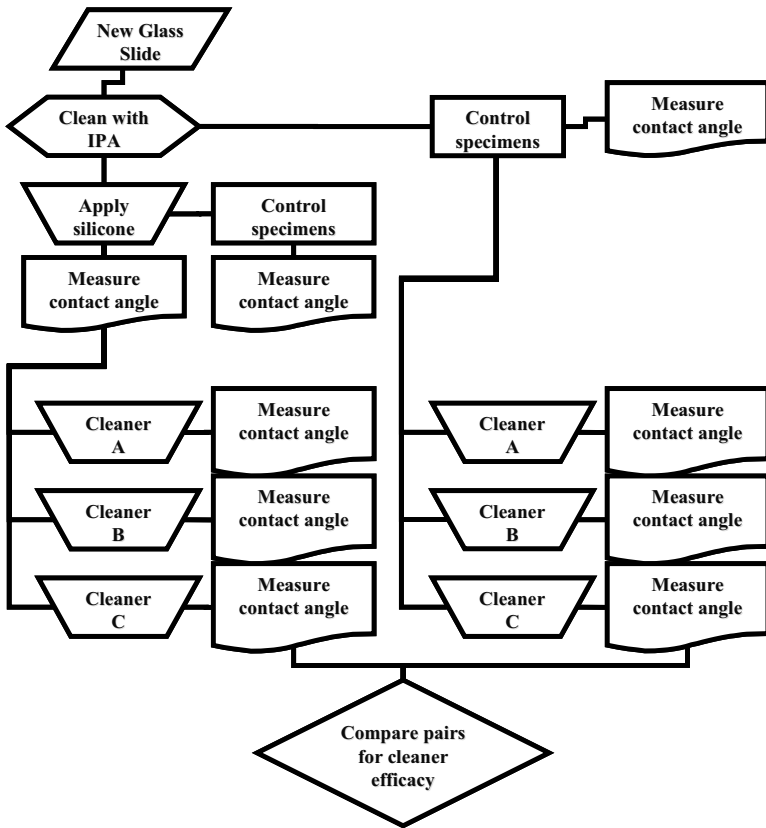


FIG. 3—Flowchart of slide evaluation.

user of any chemical to establish appropriate safety and health practices and determine the applicability of regulatory limitations prior to use.

Observations

Some of the evaluated cleaning materials consisted of solvents intended to place the silicone plasticizer back into solution and then be wiped away (often containing manufacturer’s recommendations for more than one application). Others consisted of acids intended to break apart (digest) the silicone plasticizer so that it could be removed from the surface with water.

In order to avoid advertising a single or set of products we have removed the manufacturer’s names from the sample materials tested. The cleaning solutions are grouped by viscosity, low or high. For each cleaning material, the first column represents the control sample slide that was not exposed to silicone oils but was cleaned with the tested cleaning material; the second column represents slides that were contaminated with silicone oils and then cleaned with the tested cleaning material. Therefore, a material that cleans well would have a

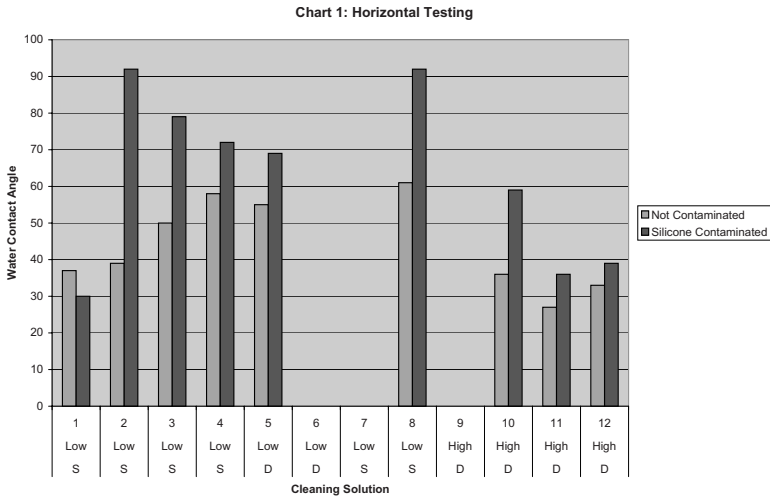


FIG. 4—Horizontal slide testing.

low value in the “Silicone Contaminated” column of Figs. 4, 5, and 6. (Note that the cleaning solution number is consistent for the material used in Figs. 4 and 5. Low/high refers to viscosity of the cleaning solution. S/D refers to solvent type or digester type cleaning solution. Samples 6, 7, and 9 were not available during our initial horizontal orientation experiments; they were received later and included in the vertical orientation experiments).

Additional evaluation of the data yielded the following charts for viscosity and solution type. Chart 3 indicates that the higher viscosity materials, on av-

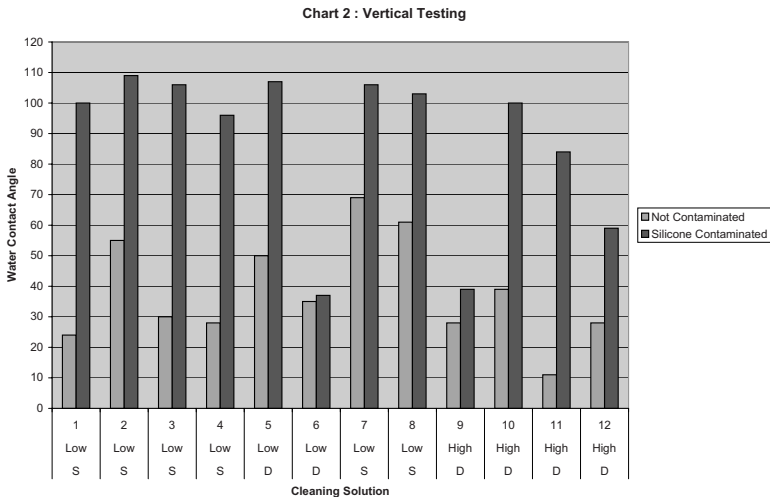


FIG. 5—Vertical slide testing.

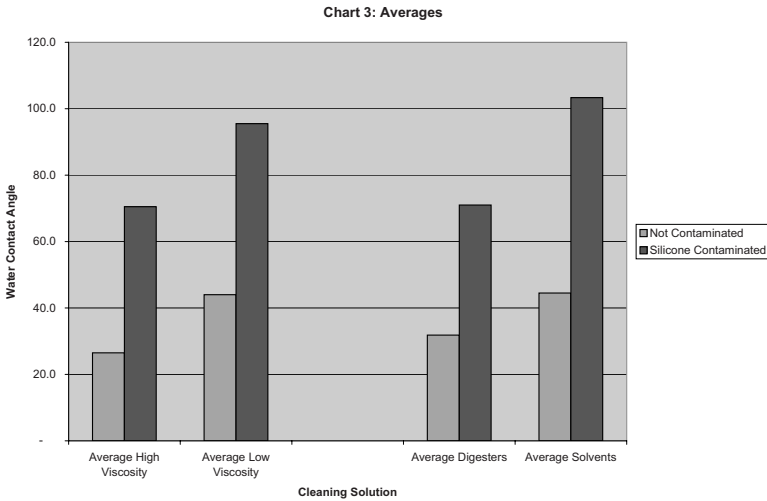


FIG. 6—Comparison: viscosity and type.

erage, cleaned more silicone residue from the glass than the lower viscosity materials. Additionally, the silicone digesters, on average, also removed more silicone residue from the glass surface than the solvent materials.

Findings

Four of the solutions evaluated consisted of high viscosity, paste- or gel-like, solutions. These products were able to be smeared on the glass in both the horizontal and vertical orientation and retained their contact with the glass without flowing off of the surface. Because each manufacturer recommended dwell times related to their product, we suspected that the high viscosity materials would fare better in the testing.

Eight of the cleaning solutions were low viscosity and ran easily from the surface, making dwell times on the vertically tested glass difficult to achieve. We found that some of these solutions were not effective on vertical or horizontal cleaned glass. One exception to this was a low viscosity solution that performed particularly well in both applications.

Error and Bias

We found some anomalies in the testing related to isolated cleaning solutions. The most disconcerting data was the variability in the values achieved with glass that was never contaminated with silicone residue. There was a low value of 11° of contact angle in one case for a material cleaned with a high viscosity cleaner.

For the 11° average, each of the three beads was nearly flat. In trying to rationalize how this glass could be giving greater wetting than non-

contaminated glass cleaned with other techniques, we considered that the cleaner may have left a surfactant (wetting agent) on the surface that caused a flatter bead than clean glass. However, if the surfactant was not somehow attached to the glass, it should wash off. Thus, this slide was rinsed with water for approximately 1 min with constant rubbing. The contact angle was measured again and there was no change. A second attempt to remove any residual surfactant was performed by rinsing the glass with acetone. After the acetone rinse, a recheck of the contact angle again showed no change.

Next, we considered that this cleaner has a pumice component; on the slides that were cleaned with scrubbing action using abrasive action, it is possible that the surface was microscopically flattened. A flatter surface would allow a flatter bead. An alternative explanation is that the pumice provided a very finely divided solid that filled in microscopic voids in the surface of the slide, resulting in a smoother surface than the other cleaned slides, and thus allowed the water to spread more.

It may be noted that the studies on uncontaminated glass exhibited widespread or inconsistent data. We reasoned that most of the contact angle differences are based on differences in the microscopic roughness on the surface; this is most dramatically illustrated by comparing the 80° contact angle on slides from one manufacturer compared to the 64° contact angle on slides from another manufacturer. This was performed prior to selecting one type of glass for each experiment. Note also that this was confirmed by repeated testing on several different glass slides from these two sources and on two different occasions.

Additional consistency in data may be achieved by the volumetric control of the water droplet, ensuring that each droplet is identical in size and proximity to the camera lens.

It is our opinion that the results shown represent the materials tested using the methods outlined. Different methods may yield varied results. Longer contact times for the low viscosity materials as well as heavier or repeated applications may also affect the cleaning results. Buffing action of the pumice-containing solutions may also improve performance.

Additional study in the future may also include measurement of surface energies of the glass surfaces for consistency between the specimen beds.

Conclusions

Each of the 12 cleaning materials evaluated advertised that they remove silicone from surfaces. We found that few were actually effective when used in this test to simulate field application. Three of the cleaners tested held promise for cleaning vertical glass. Two of these were thicker, milky or gel-like consistency, and one was a watery solvent-type material.

Variability was observed in the contact angle values achieved with glass that was not contaminated with silicone residue. There was a low value of 11° in one case only and that was when the slide was cleaned vertically with high viscosity cleaning material that also contained pumice.

Generally, the strong silicone digestants (like sulfonic acids or citrus type

acids), especially in paste consistency, allowed longer duration and constant contact when applied to vertical glass and appear to give acceptable silicone removal results. Only one of the commercial solvent (low viscosity) mixtures was effective in silicone removal under this testing scenario. From a practicable standpoint, the pastes were more easily controlled on the vertical surface of the glass and all were water soluble (miscible) and thus easy to rinse off after cleaning.

References

- [1] Andersson, L. H. U. and Hjertberg, T., "Silicone Elastomers for Electronic Applications, I. Analyses of the Noncrosslinked Fractions," *J. Appl. Polym. Sci.*, Vol. 88, 2003, pp. 2073–2081.
- [2] Andersson, L. H. U., Johander, P., and Hjertberg, T., "Silicone Elastomers for Electronic Applications. II, Effects of Noncrosslinked Materials," *J. Appl. Polym. Sci.*, Vol. 90, 2003, pp. 3780–3789.

R. Krelaus,¹ G. Wisner,² S. Freisinger-Schadow,³ M. Schmidt,⁴
S. Böhm,⁵ and K. Dilger⁵

Resistance of Adhesive Bonding of Ultra-High Performance Concrete to Hygrothermal, Corrosive, and Freeze-Thaw Cycling Environments

ABSTRACT: Ultra-high performance concrete (UHPC) with its unique material properties is suitable for the application of adhesive bonding as a joining technique. The results presented in this paper were generated as part of a research project aimed at investigating the properties of UHPC adhesive joints in terms of reliability, safety, and load bearing capacity. Fourteen adhesives were tested for strength and durability considering varying conditions of substrate surface pretreatment and different UHPC compositions. Tests under hygrothermal, freezing, and salt-spraying exposures were performed to investigate the long-term durability under different climatic conditions.

KEYWORDS: Ultra-High Performance Concrete, UHPC, UHPFRC, adhesive bonding, accelerated aging, cyclic climatic testing, freeze-thaw testing, hygrothermal testing

Manuscript received June 26, 2008; accepted for publication August 17, 2009; published online September 2009.

¹ Ph.D., Post Graduate Scientist, Former Member of Construction Materials and Chemistry, Univ. of Kassel, 34125 Kassel, Hessa, Germany.

² Graduate Scientist, Joining and Welding, Technical Univ. Braunschweig, 38106 Braunschweig, Lower Saxony, Germany. (Corresponding author), e-mail: g.wisner@tu-bs.de

³ Graduate Scientist, Construction Materials and Chemistry, Univ. of Kassel, 34125 Kassel, Hessa, Germany.

⁴ Professor, Construction Materials and Chemistry, Univ. of Kassel, 34125 Kassel, Hessa, Germany.

⁵ Professor, Joining and Welding, Technical Univ. Braunschweig, 38106 Braunschweig, Lower Saxony, Germany.

Cite as: Krelaus, R., Wisner, G., Freisinger-Schadow, S., Schmidt, M., Böhm, S. and Dilger, K., "Resistance of Adhesive Bonding of Ultra-High Performance Concrete to Hygrothermal, Corrosive, and Freeze-Thaw Cycling Environments," *J. ASTM Intl.*, Vol. 6, No. 9. doi:10.1520/JAI101990.

Copyright © 2009 by ASTM International, 100 Barr Harbor Drive, PO Box C700, West Conshohocken, PA 19428-2959.

TABLE 1—Structural properties of the UHPC composition M1BS with 1.0 vol % steel fibers in comparison to normal concrete (values given in N/mm²).

Structural Properties	M1BS (N/mm ²)	NC 30/37 ^a (N/mm ²)
Compressive strength	179	37
Tensile strength	9	~3.7
Flexural tensile strength (beams)	19.6	...
Surface tensile strength	6–8	1.5–2
Water/binder ratio	0.19	0.55
Cement content (kg/m ³)	650–835	300

^aAccording to Ref 6.

Introduction

Adhesive bonding of structural members made from ultra-high performance concrete (UHPC) is a new method for joining structural elements in the construction industry. UHPC is characterized by a very dense and homogeneous microstructure free of capillary pores resulting in a steel-like compressive strength of up to 200 N/mm², an improved surface tensile strength of about 6–8 N/mm², and a significantly improved durability. Thus UHPC is an ideal material to adopt adhesive bonding technologies to concrete.

In the past, the structural bonding technique has changed the design and construction methods in other fields of engineering such as automotive and aircraft construction. Adhesive bonding technology has a number of advantages compared to conventional joining techniques. Shear or tension stresses are transmitted from one structural element to the other over a large contact area, thus avoiding the formation of high compression or tension stress concentrations. Adhesive bonding allows for the joining of materials with different structural and surface properties while not affecting the material properties of the joining partners.

The superior material properties of UHPC are shown in Table 1 exemplarily for the concrete mixture used in building the Gaertnerplatz Bridge in Kassel, Germany [1]. This pedestrian bridge spans a river named Fulda over a length of about 140 m and was constructed with precast concrete (UHPC). Bridge slabs of the Gaertnerplatz Bridge are approximately 8–12 cm thick. This bridge is the first wide span bridge in the world consisting of load bearing structural UHPC elements being exclusively bonded together using an epoxy (EP)-based adhesive without any additional mechanical devices [2].

Adhesives based on organic polymers are widely used in the joining of assembly parts. EP and polyurethane (PUR) resins are two examples of binders used in commercially important modern civil engineering adhesives. EP resins have been used already for a long time in applications involving regular concrete surfaces. For the past two decades major applications focused on the reinforcement of existing buildings by the use of carbon fiber reinforced plastic plates [3,4]. Another adhesive technique is used in the construction of segmental bridges, where adhesives are utilized to temporarily fix precast bridge segments during the construction process [5]. However, in this application, the

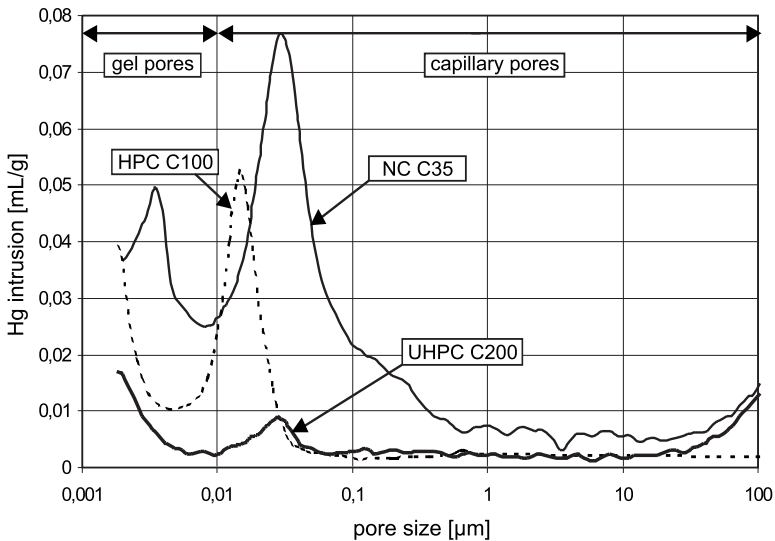


FIG. 1—Pore size distribution of UHPC compared with ordinary concrete and HPC.

adhesive acts much like a sealant and is not required to bear loads in the finished bridge. The use of adhesive technology in the load bearing joining of concrete elements could not be implemented until recently due to the inappropriate mechanical properties of ordinary concretes. In this paper, the results from a research project titled “Adhesive Bonding of UHPC Structural Members” are presented. This project was funded by the German Federation of Industrial Research Associations (Arbeitsgemeinschaft industrieller Forschung e. V. or AiF). Project partners are the University of Kassel and the Technical University of Braunschweig.

Ultra-High Performance Concrete

UHPC is a cement based material with a compressive strength of more than 150 N/mm^2 up to 200 N/mm^2 (measured on a cylinder specimen; see Table 1), which is comparable to that of steel. The high compressive strength of UHPC is achieved by a balanced mixture of different reactive and inert coarse- and fine-grained mineral fillers. In order to achieve suitable bi- or poly-modal particle size distributions, particle sizes in modern UHPC range from macroscopic grains (sand) to nanoscopic particles with diameters of less than 100 nm (micro-silica or nano-silica) [7,8]. The high packing density of the particles results in very dense concrete structures free of capillary pores. Figure 1 shows the pore size distribution of UHPC in comparison to those of regular concrete and HPC.

As shown in Table 1, the tensile strength and the surface tensile strength of UHPC are also much higher than the corresponding properties of traditional concretes, which is mainly due to the use of steel fibers as reinforcement in

UHPC [9]. In the literature this material is also referred as ultra-high performance fiber reinforced concrete. Steel fibers are introduced into the mixture in order to increase the ductility of the very dense and brittle cement matrix structure of UHPC. This technique achieves a sufficient level of safety in the design of buildings made of UHPC.

The UHPC compositions used for the experiments described in this paper are listed in Table 2. In general the mixtures can be classified as fine-grained (M1Q and M2Q) (maximum grain size of 0.5 mm) and coarse-grained mixture B4Q (maximum grain size of 8 mm). Note that the mixture M2Q contains a higher amount of cement than mixture M1Q. As shown in Table 2 each of the three mixtures was used with different amounts of steel fibers varying from 1.0 to 2.5 percent by volume. The steel fibers were of 17 mm in length and 0.15 mm in diameter. Because of the large sized aggregates, composition B4Q could be mixed only with a steel fiber content of up to 1.75 percent by volume.

Adhesives

At the beginning of the research project, 14 commercially available two-part adhesives were considered [10]. These polymer based materials were selected from adhesives that are regularly used to bond steel, light metals, wood, and glass or carbon fiber based reinforcements to concrete. After a screening process five adhesives were selected for further investigations. Table 3 shows an overview of the characteristic properties of all of the adhesives, eight of them being based on EP resins and six of them being based on PUR resins. All adhesives were classified by their density, pot life time, viscosity, and flexural strength. Five of the adhesives were filled with up to 85 mass percent of fine mineral quartz powder to improve their rheological behavior and to adapt their material properties (e.g., thermal expansion coefficient) to those of the concrete.

The mechanical strength as the cohesive behavior of the adhesive material was determined in tests on $20 \times 20 \times 80$ mm³ prisms prepared from the two-part adhesives by molding in a copper form. After 24 h the polymer prisms were demolded and further on stored for 7 days at 20°C and 65 % relative humidity. The four-point flexural bending tests on the prisms were performed in the same device as used for testing cement mortar prisms according to Ref. 11. The results of the flexural tests are shown in Table 3. Due to the high flexibility of many of the PUR adhesives, the flexural strengths could not be determined for these materials, as their plastic deformation exceeded values, where the basic theory of flexural bending is not valid at all. Adhesive No. 5 (two-part EP) showed the highest strength value of 56.4 N/mm², while adhesive No. 14 (two-part PUR) showed a value of only 16.5 N/mm².

Pretreatment of UHPC Surfaces

A well balanced combination of cohesion and adhesion is of high importance for the overall strength and durability of an adhesive joint. Adhesion between the substrate surface and the adhesive is often differentiated into molecular

TABLE 2—UHPC mixtures studied.

		M1	M2	M3	M4	M5	M6	M7	M8
Flexural tensile bending strength	N/mm ²	22.9	37.5	45.8	22.7	40.5	45.3	20.2	22.5
Steel fiber content (fibers of 17 mm length)	kg/m ³	77	134	192	77	134	192	78	136
	%	1.00	1.75	2.50	1.00	1.75	2.50	1.00	1.75
CEM I 52,5 HS-NA	kg/m ³		733			832		650	
Water	kg/m ³		161			166		158	
Sand 0/0,5	kg/m ³		1008			975		354	
Quartz powder 1	kg/m ³		183			207		325	
Quartz powder 2	kg/m ³		0			0		131	
Micro-silica	kg/m ³		230			135		177	
Basalt 2/5	kg/m ³		0			0		298.53	
Basalt 5/8	kg/m ³		0			0		298.53	
Superplasticizer	kg/m ³		28.5			29.4		30.4	
			M1Q			M2Q		B4Q	
			Fine-grained			Coarse-grained			

Note: Bold text indicates denominations of UHPC mixtures and grain size classes in Germany.

TABLE 3—Properties of the adhesives and binders. EP: epoxy; PUR: polyurethane.

Number	Type	Density (g/cm ³)	Application Temperature (°C)	Pot Life at 20°C (min)	Consistency at 20°C	Mineral Filler (mass %)	Flexural Strength (N/mm ²)
1	Two-part EP	1.60	10–25	90	Thixotropic	75.7	30.4
2	Two-part EP	1.65	8–30	40	Highly viscous	74.0	53.4
3	Two-part EP	1.50	5–35	60	Highly viscous	48.2	55.4
4	Two-part PUR	1.52	7–35	60	Highly viscous	79.3	54.5
5	Two-part EP	1.65	8–35	60	Thixotropic	79.0	56.4
6	Two-part EP	1.33	8–30	50	Thixotropic	32.6	40.4
7	Two-part PUR	Low viscous	18.0	51.5
8	Two-part PUR	1.45	10–30	30	Low viscous	35.7	10.9
9	Two-part PUR	1.50	10–35	60	Highly viscous	50.4	*
10	Two-part EP	1.33	7–35	20	Low viscous	26.1	43.2
11	Two-part PUR	1.49	7–35	35	Low viscous	27.5	24.8
12	Two-part EP	1.35	10–35	90	Thixotropic	80.5	29.7
13	Two-part EP	1.31	10–35	60	Thixotropic	42.7	42.5
14	Two-part PUR	Low viscous	48.9	16.5

Note: (*) indicates inability to perform measurement.

interactions and mechanical interlocking on rough surfaces. The specific adhesion (molecular interaction) originates from electrostatic interactions and van der Waals forces and has an effective range of only a few nanometers [12]. The mechanical adhesion depends on the surface roughness of the substrate and the wetting ability of the adhesive on the substrate; the latter property is improved by a high specific surface energy of the substrate and a low viscosity of the adhesives, allowing it to permeate into the microstructure of the substrate surface. Therefore, it is important to maximize the contact area between adhesive and substrate by increasing the surface roughness of the substrate.

Another important effect of the roughening of UHPC surfaces is the removal of a potentially weak surface layer (layer in contact to the formwork) caused by segregation of cement lime or water from the concrete (“laitance”) or by residues of form release agents used in the molding process of UHPC. The methods used for pretreatment are sandblasting or grinding of the surface of the hardened concrete or the application of a retarding agent to the surface of the fresh concrete, preventing the cement paste from hardening thus enabling easy removal of the laitance from the hardened concrete to expose the aggregates. Examples of the differently pretreated surfaces are given in Fig. 2.

Sandblasting was done manually by the use of fine-grained slag granulates. The increase in surface roughness was controlled visually. As shown in Fig. 2, by sandblasting and the application of a surface retarder, a layer about 1–2 mm thick of the UHPC surface was removed and thus single steel fibers were exposed. Embedding the exposed fibers into the adhesive can reinforce the polymer joint by improving the flexural strength as well as the ductility of the bonded specimen. If the surface was ground with a rotary diamond bur tool, a layer of approximately 1–2 mm was removed. However, in this case, the texture of the surface was smooth with microfine grooves and steel fibers were completely cut off; no fibers were exposed.

In order to evaluate the surface roughness of specimens with the different pretreatments, the topography of selected specimens with sandblasted (Fig. 3(a)), ground (Fig. 3(b)), and retarded (Fig. 3(c)) surfaces was determined in comparison to a non-modified formwork surface (Fig. 3(d)) using a stripe pattern light projection device with a height resolution of about 10 μm . Figure 3 shows the textures. From the topographical data the roughness coefficients R_a (arithmetic average of absolute height data) and R_{RMS} (root mean squared height data) were calculated [13]. R_a characterizes the surface roughness amplitude parameters based on the vertical deviations of the roughness profile from the mean line. Table 4 shows the roughness data of differently pretreated UHPC surfaces. The roughest surface texture is achieved by sandblasting ($R_a = 40.0 \mu\text{m}$). The roughness values achieved by grinding or the application of a retarding agent are lower—the latter due to the fact that a fine-grained UHPC has been tested. The roughness data calculated from the topography measurements conforms to the visual impression of the surfaces.

Selection of Adhesives and Ultra-High Performance Concrete Composition

From the list of 14 adhesives given in Table 3, five appropriate adhesives were selected in a prescreening process for evaluation in comprehensive strength

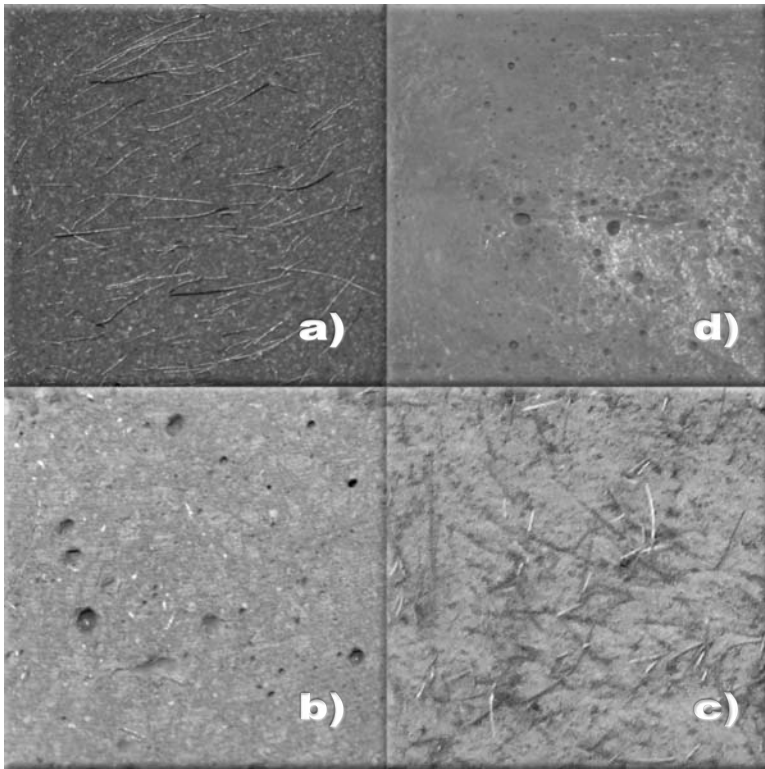


FIG. 2—Typical surface of UHPC prisms cross section of 40×40 mm² before and after modifications: Sandblasting (a), ground (b), retarder (c), and unmodified form surface (d).

and durability tests on bonded composite specimens. UHPC prisms of 40×40 mm² cross section and 160 mm length were prepared, each consisting of two halves ($40 \times 40 \times 80$ mm³). The concrete prisms were made from mixture M4. They were cast and stored according to Ref 6. After 7 days they were sawn in the center and stored for another 4 days at 20°C and 65% relative humidity. Then the sawn surfaces were pretreated (see Fig. 2) and glued together without applying any further pressure. The adhesive was allowed to cure for 7 days at 20°C and 65% relative humidity. The prisms were tested in a four-point flexural strength testing setup as shown in Fig. 4 according to Ref 11. The deformation rate was 0.02 mm/s (measured at mid span).

Results of the flexural tests on bonded prisms are shown in Table 5. The flexural tensile strengths range from 1.9 to 28 N/mm². The adhesives were classified by their fracture patterns as well. In general, three typical fracture patterns were detected: Sudden cohesive failure within the adhesive itself, sudden fracture directly at the interface between adhesive and UHPC, and a ductile failure of the concrete in a range of 3–6 mm beneath the bonded joint, which can be clearly separated from boundary failure modes because of visible fibers

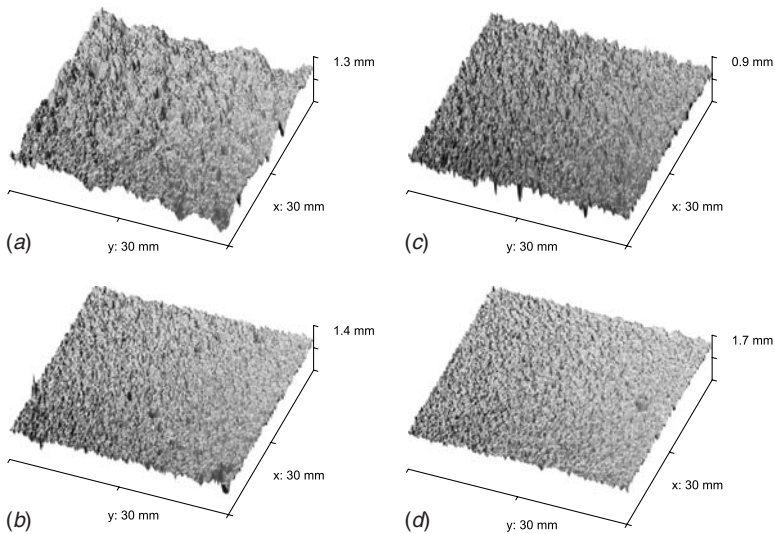


FIG. 3—Surface structures of UHPC specimens after pretreatment. (a) Sandblasted, (b) ground, (c) retarding agent, and (d) non-modified formwork surface.

pulled out of the concrete matrix. In the first two cases, respectively, the cohesive strength of the adhesive or the adhesion forces between the adhesive and the substrate were too low. The latter case is a ductile failure of the concrete under full activation of the fibers and has a fail safe characteristic. For safety reasons a ductile fracture behavior is more desirable than a high bending strength value if this is combined with sudden failure. The ductile failure mode was observed for adhesive Nos. 1, 4, and 5. Considering the processability properties of the adhesives listed in Table 3, as well as the fracture behavior and the flexural tensile strengths provided in Table 6, five adhesives, Nos. 1–5, were selected for further experiments.

In order to select the most suitable UHPC mixture, all mixtures (M1–M8) and all methods of surface pretreatment were tested in combination with the selected adhesives Nos. 1–5. In addition a non treated plain surface was included as reference. In general the specimens were prepared and stored in accordance with the procedure used for the screening tests and the same four-point flexural tensile test method was performed. Comparing the results (Fig. 5(a)–5(d)), it can be seen that the sandblasted surfaces (a) tend to result in higher strengths while ground (b) and retarded surfaces (c) are generally of lower strengths and have larger variability in the values. Unmodified surfaces

TABLE 4—Comparison of roughness data.

	Sandblasted	Ground	Retarding Agent	Smooth Formwork Surface
R_a (μm)	40.0	36.8	35.4	33.8
R_{RMS} (μm)	51.2	46.3	44.1	42.3

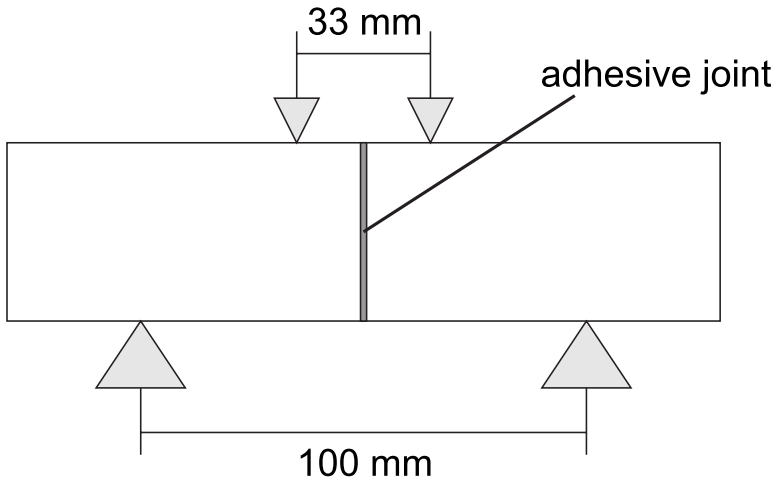


FIG. 4—Test setup for four-point flexural tensile strength experiments according to Ref 11.

(d) achieved more uniformly distributed values because of the cement rich laitance. Typically, adhesive No. 5 achieved higher strengths than the other adhesives, while adhesive No. 3 often gave the lowest strengths. To reduce the variables and influences associated with the surface treatments and adhesive materials listed in Fig. 5, the load bearing capacity of all specimens is displayed

TABLE 5—Flexural tensile strength and fracture pattern in the pretests used to select the adhesives.

Adhesive Number	Max. Flexural Strength (N/mm ²)	Fracture Pattern
12	10.2	In adhesive layer
2	21.2	In concrete
3	22.9	
6	18.7	
13	22.0	
1	17.6	Close to interface
4	16.1	in concrete
5	28.0	
10	24.4	
11	15.7	
14	10.9	
7	10.9	At interface, foaming
8	1.9	At interface
9	2.9	

TABLE 6—Combinations of temperature and relative humidity studied.

		Temp.									
		20°C		-15°C/20°C		40°C		5°C		Outdoor Exposure	
Relative Humidity	65 %	10 times: 1 day water, 3 days, ≥ 90 %, 3 days 65 %		28 freeze-thaw changes		10 times: 1 day, water, 3 days ≥ 90 %, 3 days 65 %		65 %		Under roof (180 days, 360 days)	Free (180 days, 360 days)
	(1)	(1)	(1)	(1)	(1)	(1)	(1)	(1)	(1)	(1)	(1)
	(2)	(2)	(2)	(2)	(2)	(2)

Note: (1) Short-term load (four-point-bending strength test after 56 days of exposure) (prisms). (2) Exposure under shear load (test specimen B).

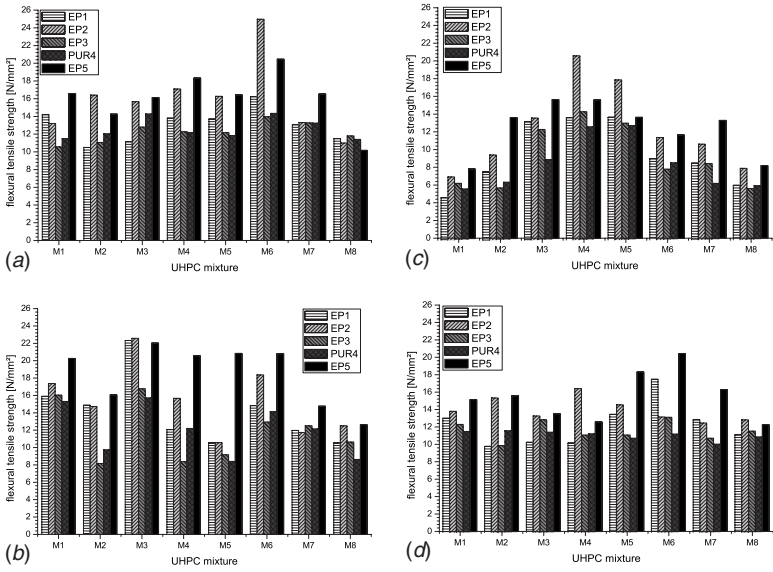


FIG. 5—Flexural tensile strengths of (a) sandblasted, (b) ground, (c) retarded, and (d) non-modified UHPC surfaces, depending on the concrete mixture and adhesive used.

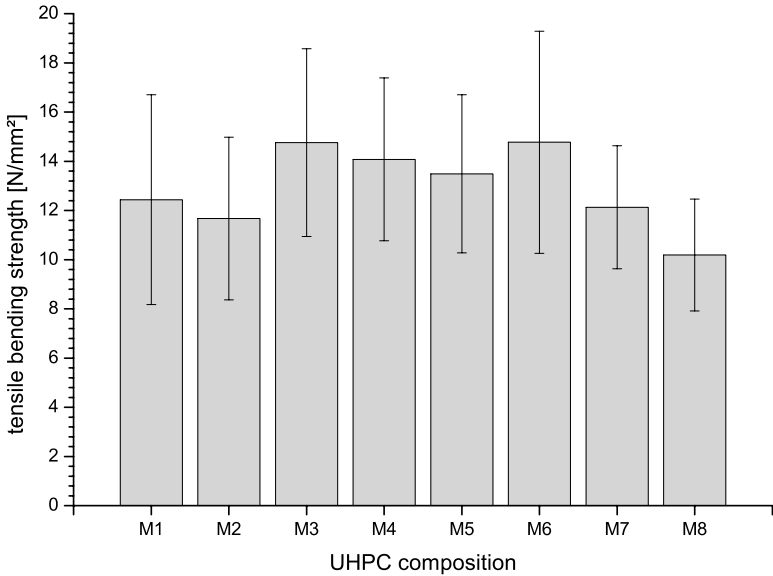


FIG. 6—Averaged flexural tensile strengths with adhesive Nos. 1–5 and all methods of surface pretreatments.

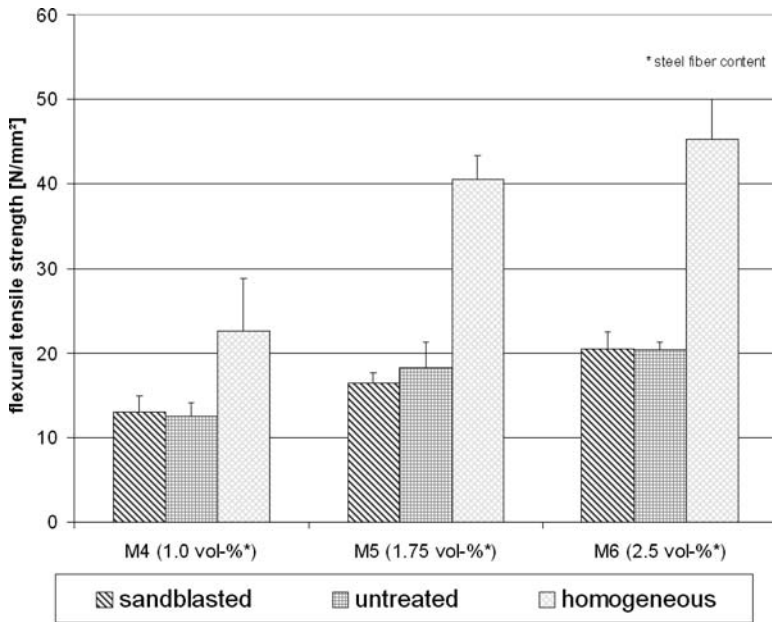


FIG. 7—Flexural bending strength of bonded prisms of UHPC mixture M2Q with increasing fiber content, bonded with adhesive No. 5, in comparison to homogeneous UHPC prisms.

for the eight different UHPC mixtures as substrate materials in Fig. 6. When comparing the mean strengths and the deviations, mixture M6 achieved the highest strengths and the fracture behavior was most often ductile. Therefore this mixture was used for further experiments on the durability of bonded UHPC specimens.

Figure 7 shows the flexural tensile strengths of bonded (adhesive No. 5) and non-bonded (homogeneous) UHPC prisms made with mixture M2Q and different steel fiber contents (mixtures M4, M5, and M6). In general, the maximal flexural bending strength of bonded prisms is about half the value observed for homogeneous prisms. For this test, UHPC prisms were cut in half and bonded on the formwork surface side with the two-part EP resin adhesive No. 5. No significant difference can be observed between prisms with no surface modification and those prepared by sandblasting before adhesive bonding. However, the influence of steel fiber content in homogenous as well as in bonded UHPC prisms is evident. As the steel fiber content is increased from 1.0 to 2.5 vol %, the bending strength nearly doubles.

Durability of Ultra-High Performance Concrete and Adhesively Bonded Joints

In service, concrete substrates as well as adhesively bonded joints are exposed to all kinds of environmental and weather conditions. Numerous test methods

involving different climates and specific environments were developed in order to predict the estimated lifetime of new materials or new material combinations within a reasonable amount of time [14,15]. In general, test specimens are exposed to a range of temperature levels and to water in all three states of phase-behavior. Corrosive chemical attack using various salts or acids is also considered as part of the exposure environment if this can be expected during the bonded component's service life [16,17].

Accelerated Aging

Material aging is a complex process driven by interior material degradation and external boundary conditions like thermal, hydrothermal, or mechanical stresses as well as corrosive attack. The process can take decades or centuries until noticeable changes occur, and most degradation processes are slow under standard conditions with low temperatures and a dry environment. A more intensive exposure to aging environments, such as elevated temperatures or higher concentrations of moisture and corrosive substances, is applied to accelerate material property changes and the degradation of strength and stiffness [18].

Standard climate conditions are suitable as reference conditions with almost no acceleration in aging. Tests at elevated temperatures on concrete parts for construction are performed at temperatures beyond 80°C, although these extreme environmental conditions do not represent usual in service aging. The glass transition temperature of most two-part EP adhesives is around 60°C. Above this temperature the mechanical properties decrease significantly. On the other hand elevated temperatures can cause a post curing effect in typical adhesives, which are usually cured at room temperature levels. Storing specimens in moisture at about 95 % relative humidity and in water is commonly used for durability testing of substrates and especially the adhesive endurance of substrates.

The rapid freezing and thawing as employed in ASTM C666 [19] is a severe durability testing method conducted in a very low temperature environment. The cycle runs 2–5 h and has a freezing cycle from +4°C down to –18°C and afterwards a warming cycle from –18 to +4°C. The test is conventionally carried out over 300 cycles. The use of salt water (typically 2 % sodium chloride in water) instead of regular water is considered as a modification of ASTM C666 when de-icing by salt is expected during service exposure. Salt-spray testing is a commonly used method for direct or indirect corrosive attack on structural materials and is performed in specially equipped salt-spray chambers. A standard concentration of about 5 % sodium chloride in the brine is conventionally used throughout various industries.

Hygrothermal Testing

Adhesive No. 5 (two-part EP) and adhesive No. 4 (two-part PUR) were chosen for the durability tests in moisture and water as well as freezing in air down to –15°C and thawing in water of 20°C according to Ref 20. After sandblasting

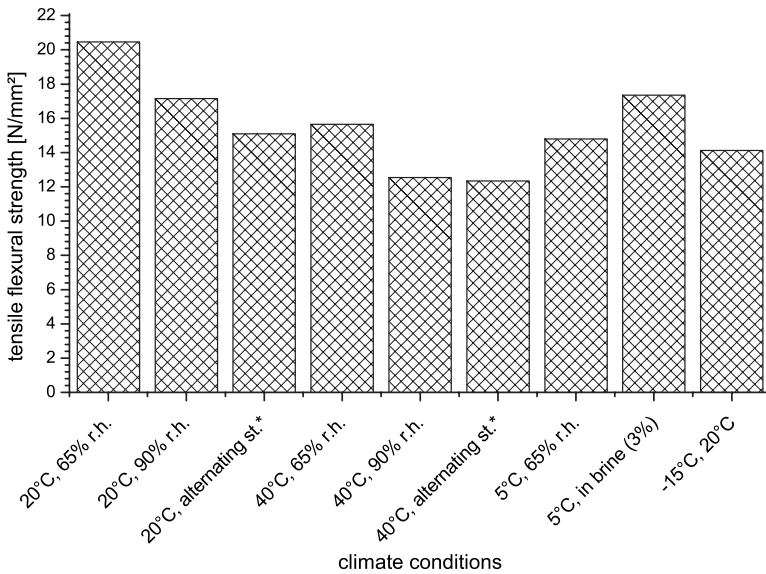


FIG. 8—Maximum flexural bending strength of bonded prisms with adhesive No. 5 after different hygrothermal exposures.

and bonding prisms on the formwork surface, specimens were stored in climatic chambers and exposed to different climate conditions. Table 6 shows the various combinations of temperature and relative humidity as well as test conditions. After 56 days (70 days with alternating cycle included), the prisms were tested with respect to their flexural tensile strength. The center-bonded prisms ($40 \times 40 \times 160 \text{ mm}^3$) used for the four-point bending tests were described earlier. During exposure to the different climates, the specimens remained without mechanical load.

Figure 8 shows the results from a completed test series conducted with adhesive No. 5 (EP). High humidity (greater than 90 % relative humidity) in combination with a temperature near the glass transition temperature range ($40\text{--}65^\circ\text{C}$) exerts a strong negative influence on the tensile flexural strength of the specimens. Fracture occurred at the interface between prism and adhesive, with the steel fibers not activated during failure. The flexural tensile strength decreased from 20.5 N/mm^2 (at 20°C and 65 % relative humidity) to 12 N/mm^2 (at 40°C and 90 % relative humidity), and all specimens failed by sudden fracture.

Permanent shear loading tests were started with simultaneous exposure to moisture and water using symmetrical specimens (test specimen type B) as shown in Fig. 9(a) and 9(b) with two adhesive layers. This specimen was made of three prisms ($40 \times 40 \times 160 \text{ mm}^3$ each). The overlap length of adhesive bonding is 80 mm on both sides with a thin adhesive layer of about 1–2 mm thickness depending on surface treatment. Permanent shear loading of the adhesive layer is achieved by mounting the symmetrical specimen in the frame of a tensile/compression machine and applying a compression load of about 20

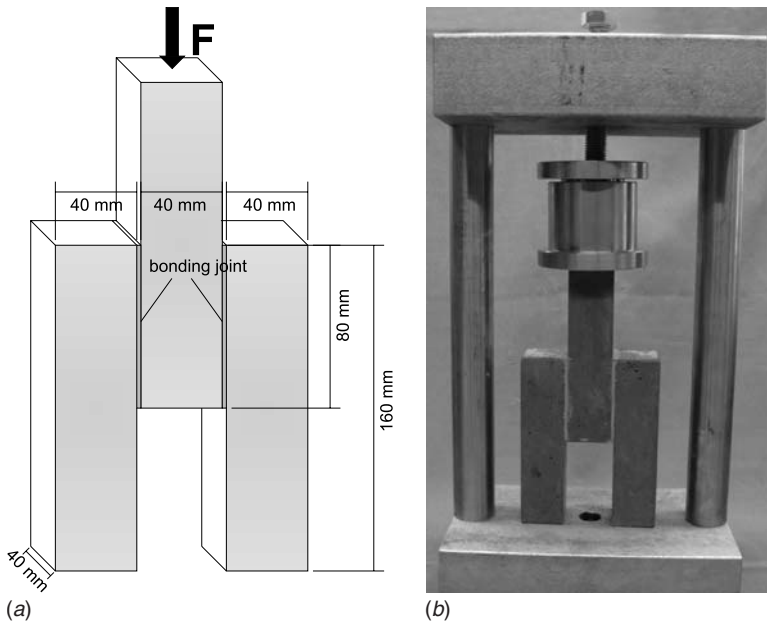


FIG. 9—Test specimen type B, dimensions and overlap (a), mounted specimen in frame (b).

KN. Table 6 shows the different climate conditions for shear tests (index 2). The first test series with adhesive No. 5 showed an obvious influence of the pretreatment by sandblasting of the UHPC substrate on the results of the shear tests. Untreated specimens failed after 14 days on average, prisms with a sandblasted surface did not fail even after 56 days. These results are shown in Fig. 10.

Combined Test Cycles

The exposure to a single aging treatment gives specific results, which help in determining a possible cause-and-effect chain. Over the past few decades, the need for a realistic assessment of different environmental aging effects has led to the development of combined testing cycles. This approach assumes that the acceleration of conventional seasonal weather conditions can be carried out in a single composite climate cycle. The Association of German Automobile Manufacturers (Verband der Automobilindustrie e. V. or VDA) established an accelerated test method for the evaluation of the endurance and durability of painted vehicle bodies as VDA 621-415 (1982-02) [21]. This method comprises a complex test cycle. First, test specimens are exposed to tropical moisture and a temperate climate followed by a subtropical hot environment, after which the freezing part of the cycle follows immediately with temperatures down to -20°C . After thawing, the specimen rests at a temperate climate for two days. After repeating this 3 day cycle, 1 day further of salt spraying completes 1 week

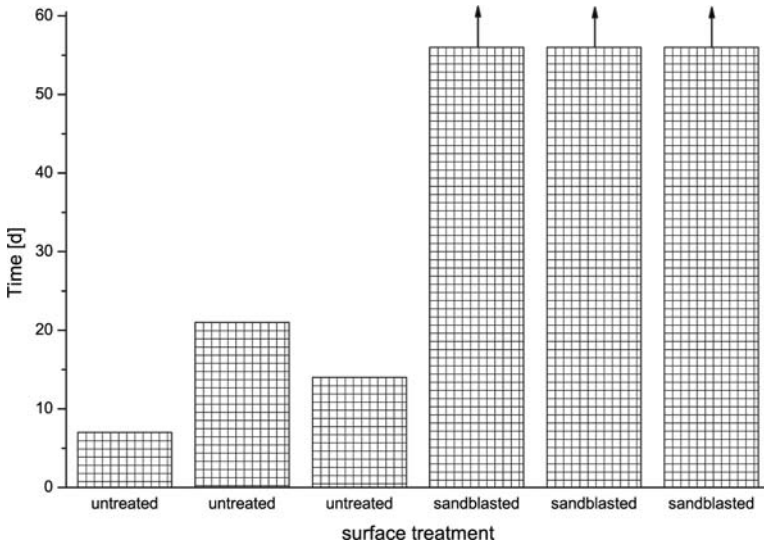


FIG. 10—Duration of permanent shear loaded specimens type B under 40°C and 90 % relative humidity. Compressive load is 20 KN. Comparison between untreated form-work surface and sandblasting before bonding with adhesive No. 5.

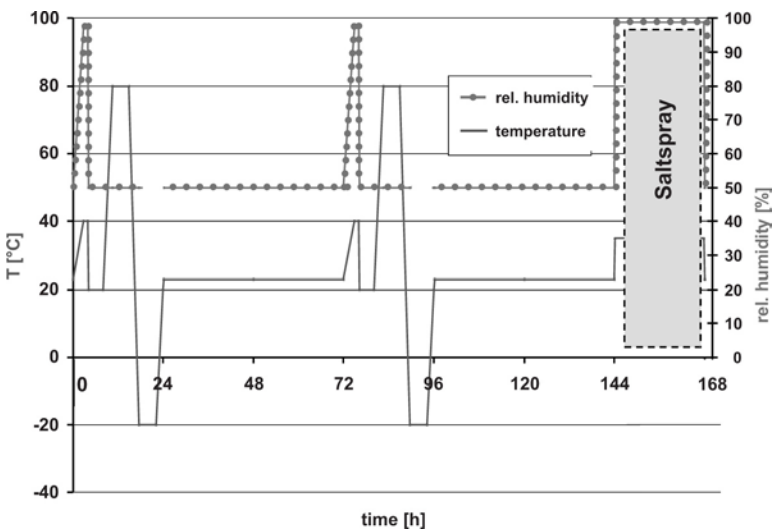


FIG. 11—Test cycle of combined changing climate and corrosive attack by salt-spray according to modified VDA 621-415 (1982-02) test method.

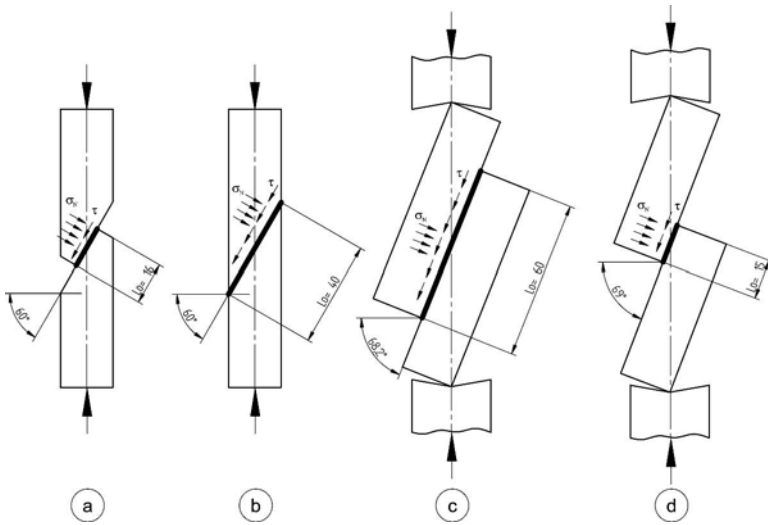


FIG. 12—Specimen geometries of different slantwise orientated joints: Prismatic specimen (a) and (b) with inclination of 60° used by Refs. 16 and 18, variable single overlap shear specimen made of cubic prisms with large overlap (c) and small overlap (d).

of cycle of accelerated aging of the modified VDA 621-415 (1982-02) (see Fig. 11 for a graphical representation of the temperature and relative humidity variations during the exposure cycle). The test procedure was adopted early on by many users of adhesive bonding since there are many similarities between paints and adhesives and the respective adhesion problems associated with all kinds of substrates.

Adhesively Bonded Specimen for Accelerated Testing

An overlap shear specimen was designed for easy modification of the glue lines, thickness of adhesive layers, or the length of overlap between parts. Figure 12 shows some specimens with differing geometries. Specimens of types 12 (c) and 12 (d) were used for the detection of the maximum shear stress of bonded joints and for determining whether the breaking pattern occurs in the concrete substrate, at the adhesive layer interface, or within the adhesive layer. These geometries were chosen because they form a very good analogy to specimens with slantwise orientated joints type 12 (a) and 12 (b). The test method was also used to determine various effects caused by overlap length and adhesive layer thickness [22,23].

The geometry of a simple single overlapped joint allowed for a great variety of positions in two directions when choosing basic prisms with a cross section of about 20 mm thickness and a width of 50 mm. The ratio of overlap as a function of length to width and the thickness of the adhesive layer were of special interest when investigating the mechanical performance of the joints. The thickness range of the adhesive layers in this investigation varied from thin

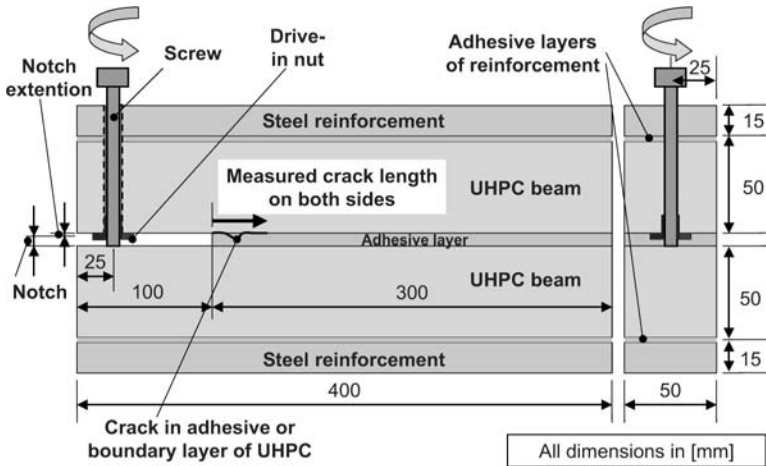


FIG. 13—MDCB specimen with outer steel reinforcements for storing in climatic chambers.

glue lines of about 2 mm to thick layers of up to 6 mm. Thick layers were of great interest because they fill larger gaps and compensate for tolerances.

A modified double cantilever beam (MDCB) specimen was designed for the prediction of the increasing crack growth in larger adhesive layers under initial stress and climatic change conditions. A compact geometry for storing in a standard climatic chamber was chosen with two adhesively bonded UHPC prisms of $50 \times 50 \text{ mm}^2$ cross section and a length of 400 mm. The adhesive layer between the UHPC substrates was 300 mm in length, which leaves a notch of 100 mm. The load was applied by extending the adhesive layer with a screw supported in a drive-in nut at a range of 25 mm measured from the open end of the notched specimen (Fig. 13). Each specimen was extended to failure at an extension of 1.2–1.6 mm (measured at the open end of the notched specimen) depending on the type of adhesive and the adhesive layer thickness. The initial crack length on both sides of the specimen was measured. A 10-week period of the modified VDA 621-415 (1982-02) climatic changing test with additional salt spray was performed while periodically measuring the increasing crack length of the prestressed specimens. An outer reinforcement made of steel bars was bonded on both sides of the specimen in order to avoid early cracking through the cross section of the UHPC prisms.

Preparation of Test Specimens

The UHPC substrate material was prepared as described earlier. Adhesive bonding was performed after a minimum storage period of 3 days at temperate climate conditions of 20°C and 50–65 % relative humidity. All different specimen geometries (short prisms for four-point bending tests, symmetrical overlap shear specimen, single overlap shear specimen, and MDCB specimen) were bonded in suitable fixtures where substrates are clamped with the appropriate

spacing and overlap position. This is due to geometrically precise forming during the hardening process. Reliable wetting on both substrates was assured through the pyramidal and amply coating with adhesive to avoid the inclusion of air into the paste-like adhesive. Adhesive material that was squeezed out from a slightly overfilled gap was removed whenever possible. A curing period of 7 days at temperate climate completed the test specimen preparation.

Specimens for accelerated aging by modified VDA 621-415 (1982-02) test method were exposed to a 10-week period and were compared with similar prepared specimens, which were tested without aging right after the curing cycle was completed. In general a non-modified formwork surface and a sandblasted surface were compared in these experiments by varying overlap length (15, 30, and 60 mm) and the adhesive layer thickness (2, 4, and 6 mm). A typical specimen mounted in a testing machine with a short overlap of 15 and 2 mm joint thickness is shown in Fig. 14. The compressive overlap shear experiments were conducted with a rate of 1 mm/min. After testing, the maximum overlap shear strength and the fracture pattern were both analyzed.

Results and Discussion

In almost every case, sandblasting as a method of surface treatment appeared to be the better preparation method for adhesive bonding when compared to the unmodified formwork surface. The abrasive treatment removes the thin weaker layer and leaves a rough but cleaned surface without any dust. In addition, the exposed steel fibers can be wetted by the adhesive and thereby improve the performance of the composite joint due to better fiber reinforcement of both materials, i.e., the UHPC and polymer adhesive.

Figure 15 shows the general performance of adhesive No. 1 on the unmodified formwork surface and the sandblasted UHPC material after 10 weeks of aging according to the modified VDA 621-415 (1982-02) test compared with not aged specimens. Thicker adhesive layers tend to perform not as well, but the effect was noticeable mostly on short and mid overlap lengths, while the long overlap exhibited less influence. The accelerated aging reduced the structural behavior in different ways, depending on surface conditions and the area exposed to corrosive attack in the salt-spray testing and freezing cracks.

In Fig. 16, the performance of adhesive No. 5 under similar conditions shows a better structural behavior than adhesive No. 1 and a lower degree of degradation when aged in the 10-week VDA aging process. The fracture pattern of these specimens mostly showed failure in the UHPC near the adhesive layer. Figure 17 shows some surface fracture pattern of non-aged and VDA aged specimens after testing. The following fracture patterns were observed:

- Failure near the adhesive on non-modified formwork surface or directly at the interface between adhesive and UHPC (Fig. 17(a) and 17(d))
- Cohesive failure within the adhesive layer (Fig. 17(f))
- Fracture within the UHPC close to the surface layer (Fig. 17(c))
- Fracture through the UHPC core material (usually this failure occurred with larger overlap lengths) (see Fig. 17(b))

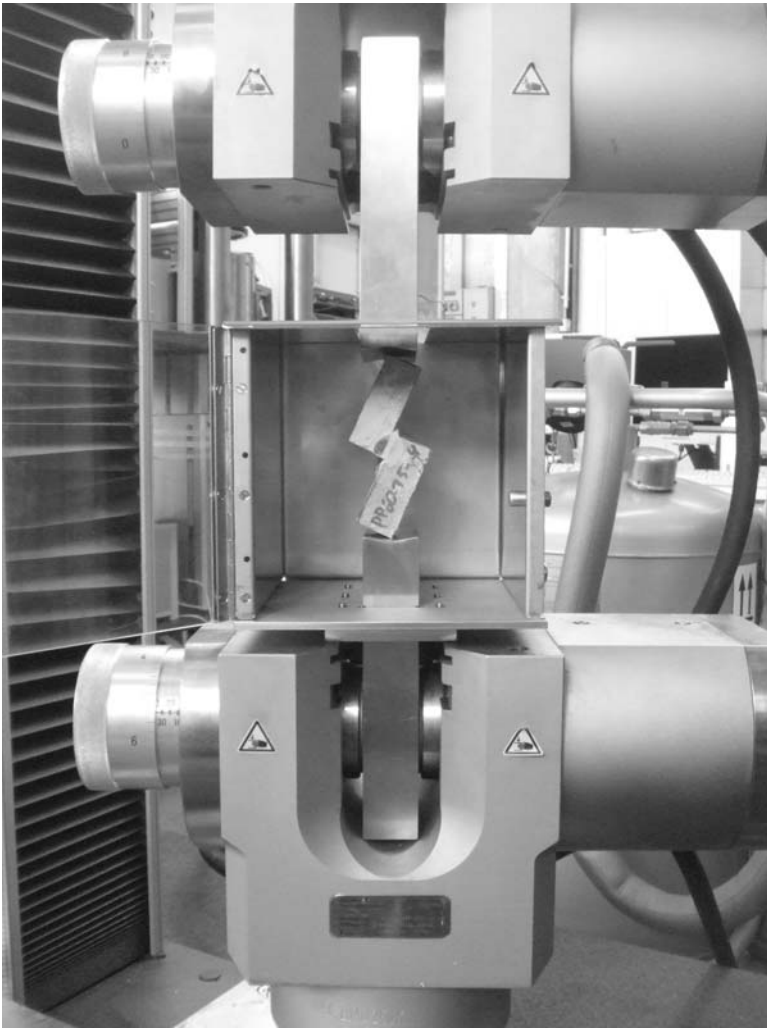


FIG. 14—Test setup for compressive overlap shear experiments. Overlap length is 15 mm with a 2 mm adhesive layer thickness.

- Fracture partly through the adhesive and UHP concrete with varying ratios (Fig. 17(e))

The steel fiber reinforcement within the UHPC material is hardly affected by the corrosive attack, although partial corrosion was observed on exposed steel fibers on the sawn prisms and especially on exposed fibers on sandblasted UHPC surfaces. The alkaline environment of the UHPC substrate protects the steel from further oxidation reaction in the UHPC core material.

The crack propagation during changing climate test and corrosive attack according to Ref 21 as observed on the MDCBs is exemplified in Fig. 18 for

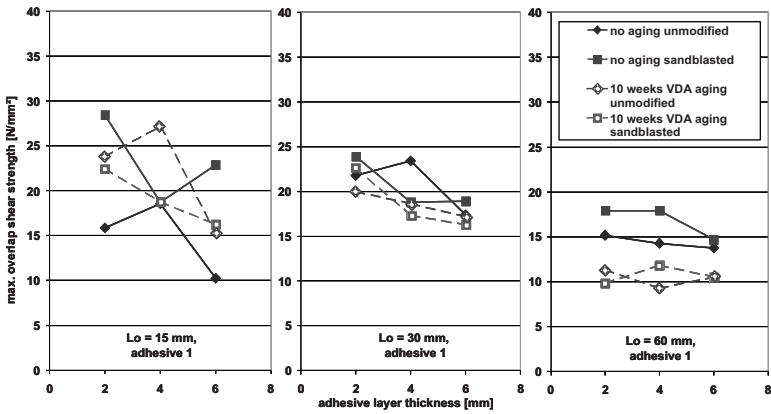


FIG. 15—Maximum compressive overlap shear strength for various overlaps and various adhesive layer thicknesses (average strength with adhesive No. 1 on sandblasted and unmodified surface).

adhesives No. 3 (EP type) and No. 4 (PUR type) and two different adhesive layer thicknesses. The initial crack length differs within a range of 5–67 mm, depending on the type of adhesive and the adhesive layer thickness. In general thicker layers provide faster crack propagation (Fig. 18(c)) than the thin adhesive layers except for the case of brittle EP on unmodified surface (Fig. 18(a)). The propagation of crack length is determined as non linear in all cases. An accelerated growth and slow down are visible in most cases due to the stress relaxation within the specimen when crack length increases. Due to their elasto-plastic properties, EP-based adhesives show a more brittle behavior than the PURs. This brittle behavior results in faster crack propagation. The cracks propagate within the boundary layer of the concrete.

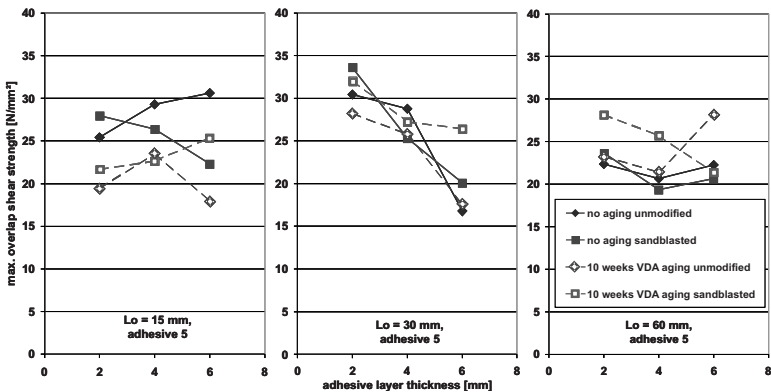


FIG. 16—Maximum compressive overlap shear strengths of 15, 30, and 60 mm overlap and various adhesive layer thicknesses (average strength with adhesive No. 5 on sandblasted and unmodified surface).

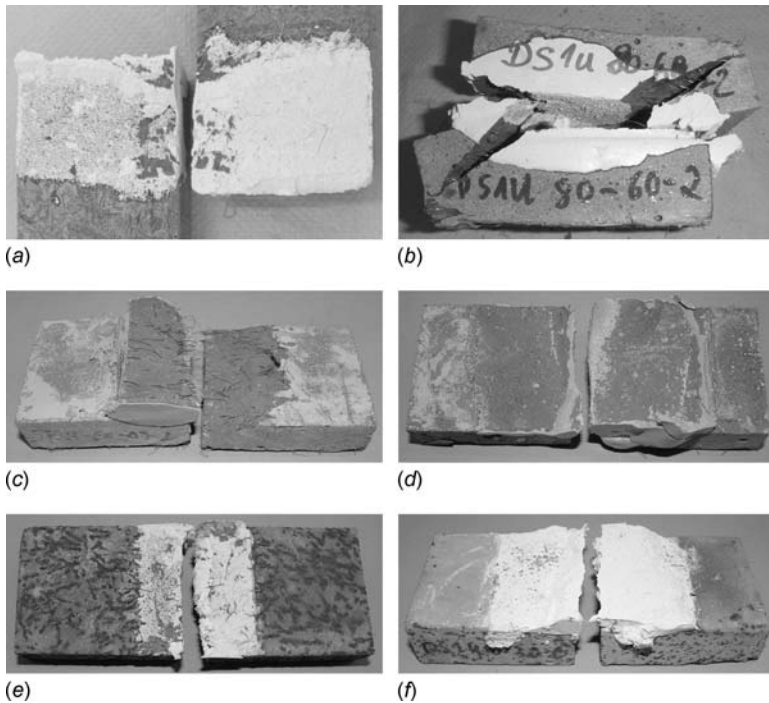


FIG. 17—Surface fracture pattern and failure of UHPC specimens after compressive overlap shear testing. Specimens with no aging treatment: (a) Adhesive failure on the unmodified concrete; (b) forced diagonal crack through huge overlapped specimen; (c) failure deep in the concrete with ductile behavior; (d) failure in the concrete boundary layer. Specimens after 10-week VDA aging: (e) Sandblasted surface with mixed fracture pattern; (f) cohesive failure through mid overlap length.

Summary and Outlook

Comprehensive experiments were carried out to explore the characteristics of adhesive joints considering various UHPC mixtures, surface pretreatments, and adhesives. According to the results of the initial prescreening experiments, the number of adhesives was reduced from 14 to 5. One UHPC mixture was identified for use in further investigations. Various surface pretreatments were evaluated quantitatively depending on their roughness coefficients. The experiments for predicting the durability of the adhesively bonded UHPC were performed with a single overlap shear geometry in a combined test method of climatic changes with freeze-thaw cycling and corrosive attack using salt spray. The VDA 10-week accelerated weathering period decreased the bonding performance in almost every case. Adhesives with a poor durability showed a decrease in strength of 50 % or more. Structural adhesives suitable for the application in civil engineering, such as adhesive No. 5, show a decrease of less than 25 %, depending on the bonding geometries. Specimens with short overlap and concentrated stresses over a small area typically caused a larger variance in

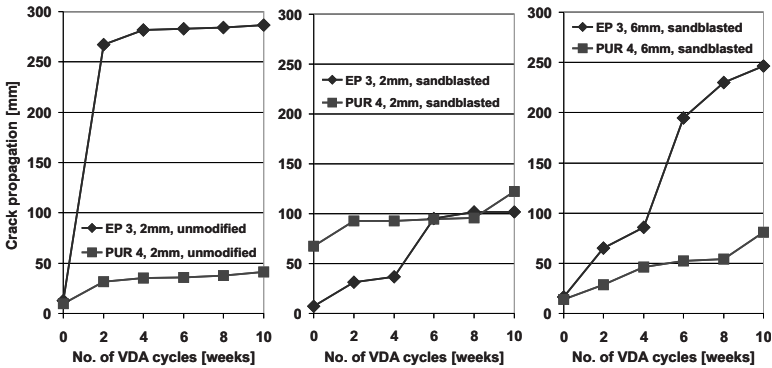


FIG. 18—Crack propagation after initial cracking in MDCB testing and storing under climatic change according to modified VDA 621-415 (1982-02) measuring both sides and averaged, adhesives No. 3 (EP) and No. 4 (PUR), adhesive layer thicknesses of 2 and 6 mm bonded on unmodified and sandblasted UHPC surface.

results due to imperfections in the manufacturing process. The aging procedure exceeded the glass transition temperature (T_g) of the tested two-part adhesives. This leads to an additional acceleration of the aging effects. On the other hand, elevated temperatures could cause a post curing effect on the adhesives, which are commonly designed for hardening at room temperature.

A great variation in fracture pattern was observed; however, the most critical case of adhesive failure at the interface to the substrate could easily be avoided by bonding on mechanically pretreated UHPC surfaces. Hygrothermal environmental conditions such as extended periods of storage in water or exposure to moisture under various temperature levels were started, and some results for shorter exposure periods of 56 days were provided in this paper. These results emphasize the need for a necessary pretreatment of the UHPC formwork surface prior to adhesive bonding. Further experimentation is ongoing and investigations into the effect of the initial conditions of the UHPC substrates prior to bonding (in particular the water content) have been started in order to create a basis for guidelines and specifications for adhesive bonding on less preconditioned construction sites under varying climates. Most critical for polymer adhesive applications are very low temperatures below $+4^\circ\text{C}$ because of poor wetting performance and imperfect curing reactions of the adhesives. To avoid undesirable interruptions in the Winter season at the construction sites, a non-polymeric adhesive based on the same chemistry as the UHPC substrate should be considered. Further experiments will be carried out to evaluate the durability of UHPC adhesive joints under stress and hygrothermal conditions.

Acknowledgments

The writers would like to thank Professor Dr. Schulz from the University of Applied Sciences in Frankfurt/Main, Germany for his support in the topo-

graphic surface measurements. The research presented here is sponsored by the German Federal Ministries of Economics and Labor (BMWA) and of Education and Research (BMBF) and promoted by the German Federation of Industrial Research Associations AiF (Arbeitsgemeinschaft industrieller Forschung e. V.) as part of the research project DVS 08.001/AiF 00.235 Z. The writers would like to express their thanks for this promotion and support.

References

- [1] Fehling, E., Schmidt, M., Teichmann, T., Bunje, K., Bornemann, R., and Midden-dorf, B., "Development, Durability, and Structural Design of Ultra High Performance Concretes (UHPC)" (German title: Entwicklung, Dauerhaftigkeit und Berechnung Ultrahochfester Betone, UHPC), *Research Report, Structural Materials and Engineering*, No. 1, Kassel University Press GmbH, Kassel, Germany, 2005; <http://www.upress.uni-kassel.de/online/frei/978-3-89958-108-9.volltext.frei.pdf>. (The original German title was translated into English without the permission of the copyright holders. The given translation is only intended to easily obtain the topic of the publication.)
- [2] Schmidt, M., Krelaus, R., Teichmann, T., Fehling, E., and Herget, E., "Glueing of UHPC Elements at the Gaertnerplatzbridge in Kassel," *BFT Int. Concr. Plant Precast Tech.*, Vol. 73, No. 10, 2007, pp. 12–22.
- [3] Clarke, J. L., "Strengthening Concrete Structures with Fiber Composites," *Proc. Inst. Civil Eng., Struct. Build.*, Vol. 156, 2003, pp. 49–50.
- [4] Stöcklin, I. and Meier, U., "Strengthening of Concrete Structures with Prestressed and Gradually Anchored CHRP Strips," *Fifth Conference on Fiber-Reinforced Plas-tics for Reinforced Concrete Structures (FRPRCS-5)*, Cambridge, UK, C. J. Bur-goyne, Ed., Thomas Telford Publishing, London, 2001, pp. 291–298; <http://www.icevirtuallibrary.com/content/chapter/frprcsv1.20399.p0004.0030;jsessionid=pnrgdj918nk.z-telford-01> (Last accessed 12 Sept. 2009).
- [5] Rombach, G., "Precast Segmental Bridge Construction—International Examples and Fields of Application in Germany," *Concr. Plant Precast Tech.*, Vol. 72, No. 2, 2006, pp. 50–52.
- [6] DIN 1045-2:2008-08, 2008, "Concrete, Reinforced, and Prestressed Concrete Structures—Part 2: Concrete—Specification, Properties, Production and Conformity—Application Rules for DIN EN 206-1," Beuth Verlag GmbH, Burg-grafenstraße 6, 10787 Berlin, Germany; <http://www.beuth.de> (Last accessed 12 Sept. 2009).
- [7] Geisenhanslüke, C., "Influence of the Granulometry of Fine Particles on the Rhe-ology of Cement Pastes," Ph.D. Thesis, University of Kassel, 2008, *Structural Ma-terials and Engineering Series*, No. 13.
- [8] Schmidt, M., Stephan, D., Krelaus, R., and Geisenhanslüke, C., "The Promising Dimension in Building and Construction: Nanoparticles, Nanoscopic Structures and Interface Phenomena," *Cement International*, Vol. 5, No. 4, Verlag Bau +Technik GmbH, Düsseldorf, Germany, 2007, pp. 86–100 (part 1), Vol. 5, No. 6, 2007, pp. 72–85 (part 2).
- [9] Tatnall, P. C., "Fiber-Reinforced Concrete," *Significance of Tests and Properties of Concrete and Concrete-Making Materials, STP 169D*, Chap. 49, J. F. Lamond and J. H. Pielert, Eds., ASTM International, West Conshohocken, PA, 2006, pp. 578–590.

- [10] Freisinger, S., Wisner, G., Krelaus, R., Schmidt, M., Boehm, S., and Dilger, K., "Structural and Semi-Structural Adhesive Bonding of UHPC by Modifying the Surface and Close-to-Surface Layers," *Proceedings of the Second International Symposium on Ultra High Performance Concrete*, Kassel, Germany, 2008, Kassel University Press GmbH, Kassel, Germany, 2008, pp. 275–282; http://www.uni-kassel.de/upress/publi/abstract_en.php?978-3-89958-376-2 (Last accessed 12 Sept. 2009).
- [11] DIN EN 196-1:2005-05, 2005, "Methods of Testing Cement—Part 1: Determination of Strength," (German version EN 196-1:2005) Beuth Verlag GmbH, Burggrafentraße 6, 10787 Berlin, Germany; <http://www.beuth.de/> (Last accessed 12 Sept. 2009).
- [12] Habenicht, G., *Adhesive Bonding* (German title: Kleben), 6th ed., Springer Verlag, Heidelberg, New York, 2009. (The original German title was translated into English without the permission of the copyright holders. The given translation is only intended to easily obtain the topic of the publication.)
- [13] Momber, A. W. and Schulz, R.-R., *Surface Treatment of Concrete* (German title: Handbuch der Oberflächenbearbeitung Beton), Birkhäuser, Boston, 2006. (The original German title was translated into English without the permission of the copyright holders. The given translation is only intended to easily obtain the topic of the publication.)
- [14] Schutz, R. J., "Organic Materials for Bonding, Patching, and Sealing Concrete," *Significance of Tests and Properties of Concrete and Concrete-Making Materials, STP 169D*, Chap. 54, J. F. Lamond and J. H. Pielert, Eds., ASTM International, West Conshohocken, PA, 2006, pp. 625–630.
- [15] Nmai, C. K., "Freezing and Thawing," *Significance of Tests and Properties of Concrete and Concrete-Making Materials, STP 169D*, Chap. 15, J. F. Lamond and J. H. Pielert, Eds., ASTM International, West Conshohocken, PA, 2006, pp. 154–163.
- [16] Thomas, M. D. A. and Skalny, J., "Chemical Resistance of Concrete," *Significance of Tests and Properties of Concrete and Concrete-Making Materials, STP 169D*, Chap. 24, J. F. Lamond and J. H. Pielert, Eds., ASTM International, West Conshohocken, PA, 2006, pp. 253–273.
- [17] Franke, L., Deckelmann, G., and Schmidt, H., "Behavior of Ultra-High Performance Concrete with Respect to Chemical Attack," *Proceedings of the Second International Symposium on Ultra High Performance Concrete*, Kassel, Germany, 2008, Kassel University Press GmbH, Kassel, Germany, 2008, pp. 453–460; http://www.uni-kassel.de/upress/publi/abstract_en.php?978-3-89958-376-2 (Last accessed 12 Sept. 2009).
- [18] Muehlbauer, C. and Zilch, K., "Experimental Investigation of the Long-Term Behavior of Glued UHPC Joints," *Proceedings of the Second International Symposium on Ultra High Performance Concrete*, Kassel, Germany, 2008, Kassel University Press GmbH, Kassel, Germany, 2008, pp. 561–568; http://www.uni-kassel.de/upress/publi/abstract_en.php?978-3-89958-376-2 (Last accessed 12 Sept. 2009).
- [19] ASTM Standard C666/C666M-03(2008), "Test Method for Resistance of Concrete to Rapid Freezing and Thawing," ASTM International, West Conshohocken, PA; <http://www.astm.org/Standards/C666.htm> (Last accessed 12 Sept. 2009).
- [20] Bunke, N., "Testing of Concrete; Recommendations and Notes as a Supplement to DIN 1048, Section 3.3: Tensile Strength," (German title: Prüfung von Beton, Empfehlungen und Hinweise zu DIN 1048, Abschnitt 3.3 Zugfestigkeit), *Issue 422*, Deutscher Ausschuss für Stahlbeton (DAfStb) [German Committee for Steel-Reinforced Concrete], Berlin, Germany, 1991. (The original German title was translated into English without the permission of the copyright holders. The given translation is only intended to easily obtain the topic of the publication.)

- [21] VDA 621-415 (1982-02), 1982, "Testing of Corrosion Protection of Vehicle Paint by Alternating Cycles Test" (German title: Prüfung des Korrosionsschutzes von Kraftfahrzeuglackierungen bei zyklisch wechselnder Beanspruchung), Verband der Automobilindustrie e. V. (VDA), Munich, Germany. (The original German title was translated into English without the permission of the copyright holders. The given translation is only intended to easily obtain the topic of the publication.)
- [22] Rehm, G. and Franke, L., "Bonding of Concrete Structures in Civil Engineering" (German title: Kleben im konstruktiven Betonbau), *Issue 331*, Deutscher Ausschuss für Stahlbeton [German Committee for Steel-Reinforced Concrete], Berlin, Germany, 1982. (The original German title was translated into English without the permission of the copyright holders. The given translation is only intended to easily obtain the topic of the publication.)
- [23] Hranilovic, M., "Failure Criteria for Structural Joints," *Proceedings of the RILEM International Symposium on Adhesion Between Polymers and Concrete—Bonding, Protection, Repair*, Aix-en-Provence, France, 1986, H. R. Sasse, Ed., Chapman and Hall, London, 1986, pp. 650–660, ISBN 0412290502.

Anneliese Hagl¹

Durability by Design: New Results on Load-Carrying Silicone Bonding

ABSTRACT: In the year 2000, the Herz-Jesu church in Munich, Germany was finalized featuring a glass façade with advanced bonded load-carrying structures. The façade was stiffened in such a way that wind- and dead-loaded glass elements were joined to stainless steel channels by a two-component silicone adhesive for load transfer. Durability aspects related to this type of bonding were already presented by the author at the previous symposium in 2003. The technical questions raised by the design of the Herz-Jesu church initiated detailed research investigations within Germany concerning the application of complex bonding geometries for structural engineering purposes. These studies comprised experimental and theoretical activities which were focused on the mechanical properties of two-component silicone adhesives as well as on the behavior of various bonding geometries resulting from the use of L- and T-type steel elements. In the context of these research activities, attention was also paid to different aspects directly or indirectly related to durability issues. Regarding adhesive material behavior, tensile, compression, and shear tests were performed on aged and unaged specimens in order to analyze the impact of an aggressive environment. Several degradation modes were induced into the specimens in a systematic manner in order to evaluate the load-bearing capacities and failure mechanisms of the different bonding geometries and in order to assess the behavior in the view of partial failure. This paper presents an overview of the obtained experimental results complemented by detailed finite element analysis results. Former results obtained for the U-type bonding geometry are reviewed in the light of new experimental findings. Furthermore, bonding geometries like the T-type bonding are assessed in a similar

Manuscript received June 26, 2008; accepted for publication December 12, 2008; published online January 2009.

¹ Managing Director, A. Hagl Ingenieurgesellschaft mbH, Munich, Bodenseestr. 217, D-81243 Munich, Germany, e-mail: a.hagl-ingenieure@t-online.de, www.a-hagl-ingenieure.de

Cite as: Hagl, A., "Durability by Design: New Results on Load-Carrying Silicone Bonding," *J. ASTM Intl.*, Vol. 6, No. 2. doi:10.1520/JAI101956.

Copyright © 2009 by ASTM International, 100 Barr Harbor Drive, PO Box C700, West Conshohocken, PA 19428-2959.

way as previously done for the U-type bonding geometry. Finally, the paper concludes by directly comparing all investigated bonding geometries with respect to durability aspects.

KEYWORDS: structural glazing, bonding design, durability design, joint geometry, FE analysis

Nomenclature

- BSL = baseline
- ETAG = European Technical Approval Guideline
- FE(A) = finite element (analysis)
- FRD = front region disabled
- L_f = length of flange
- PFC = parallel flange channel
- SRD = side region disabled

Introduction

Beyond architectural highlights—clearly visible in Fig. 1—the Herz-Jesu church in Munich, Germany, offers also highly sophisticated technical solutions from a civil engineering point of view. One of the highlights related to the glass façade of this building is the extensive use of load-bearing U-type bonding joints based on a two-component silicone structural adhesive. The bonding connects horizontal and vertical glass beams to attachment fittings for the provision of load transfer in order to ensure the structural integrity of the entire glass façade (see Fig. 2). References [1,2] present additional details of this special design.

The horizontal glass beams are intended to primarily counteract wind loads acting on the façade. Façade dimensions are 19.00 m by 16.00 m (62.3 ft by 52.5 ft) in one direction (front face) and 47.04 m by 16.00 m (154.3 ft by 52.5 ft) in the other direction (side face). The wind loads change in time but are typically approximated by quasi-static loads; i.e., inertia effects of the façade structure are assumed to be small compared to other load sources.² A wind load sizing hypothesis based on German regulations had to be taken into account regarding the required strength of the structural bonding.

The main function of the vertical glass beams consists of keeping the horizontal glass beams in position in order to ensure structural integrity of the façade framework. The nature of the related loads is dictated mainly by dead loads of both horizontal and vertical glass beams; i.e., constant loads are acting

²This assumption neglects inertia dominated cases like bomb blast loading and related high speed phenomena.

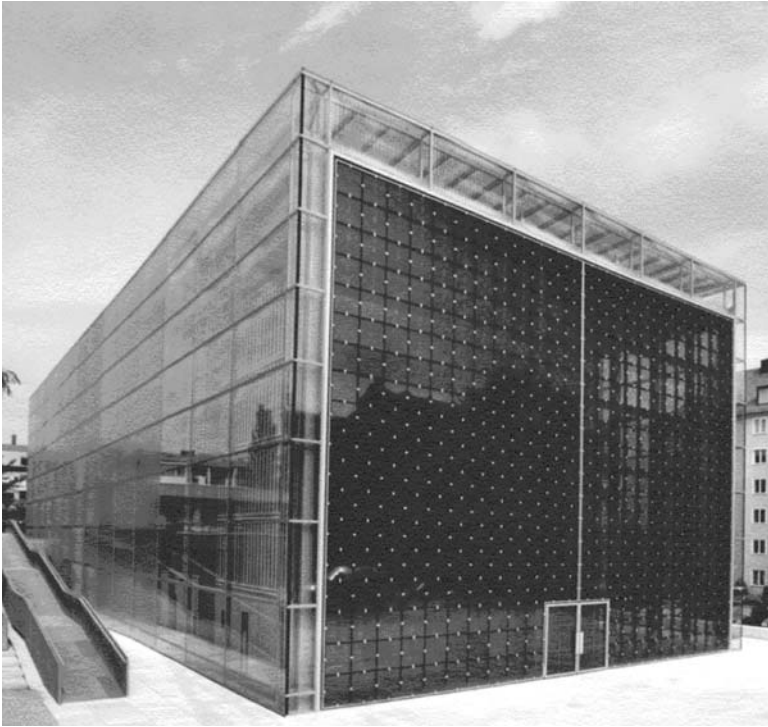


FIG. 1—Glass façade of Herz-Jesu church, Munich.

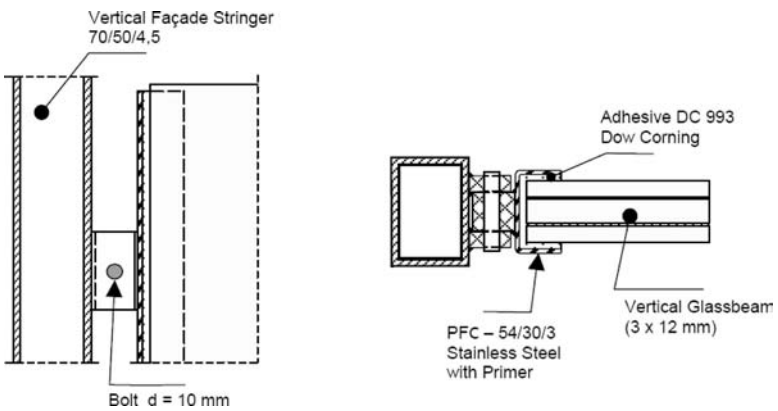


FIG. 2—Bonding design and glass façade of Herz-Jesu church.



FIG. 3—Glass façade in the year 2008.

during the service-life on the structural bonding. Thus, for designing and sizing of the structural bonding, the potential for creep had to be accordingly anticipated.

The Herz-Jesu church building was finalized in 2000. Although inspected regularly in detail, neither global nor local defects related to the structural bonding were observed until now. Figure 3 shows the façade in the year 2008. Only minor optical deficiencies were observed based on material incompatibility and cracks with respect to locally applied sealing material of high stiffness³ (see Fig. 3, right).

In Ref [2], durability aspects of structural bonding geometries as used in the glass facade of the Herz-Jesu church were discussed in detail. Table 1, which is mainly based on the outcome of Ref [3], presents an overview of major important topics for joint durability. In view of the glass façade design process or more general building design processes, some of these key issues can be favorably resolved while others might be determined by requirements other than durability.

Taking into account the considerations listed in Table 1, this paper is intended to mainly address issues regarding joint design and stress distributions. These areas of interest are illustrated by some experimental results which were aimed at baseline physical properties of a two-component silicone adhesive certified and typically applied for structural glazing. The conclusions can be easily extended to other adhesive materials in case they fulfill the following two conditions: they show a certain level of incompressibility, which is the case for all elastomeric materials, and the adhesive bonding layers have a comparable thickness leading to a certain geometric similarity. The main objective of this paper is to extend the knowledge of special joint configurations as used in the structural bonding of façade components of the Herz-Jesu church. This will be achieved first, for the U-type joint design, by considering not only fully func-

³Fast curing mortar according to the manufacturer's description.

TABLE 1—*Parameters affecting joint durability.*

Environment	The arrangement of bonded structures inside the glass façade is favorable regarding the effects of external humidity and temperature.
Adhesive type	The selection of silicone adhesive is dominated by structural glazing requirements.
Adherents	The selection of glass beams resulted from façade design; stainless steel channels were selected for reduced corrosion sensitivity.
Adherent surface pretreatment	The cleaning of glass surfaces was performed with a special cleaning agent, additionally priming of channel surfaces.
Moisture/Stress/ Temperature	Effects of moisture, stress and temperature are determined mainly by bonding geometry; careful consideration of bonding design is required.

tional bonding, as in the previous papers by the author, but also some degraded bonding configurations and second, by investigating other bonding geometries, such as T-type, L-type, and E-type joint designs. In the following section the paper introduces first some adhesive material test results which will form the foundation for experimental and numerical results in the remaining sections.

Adhesive Material Test Results

Although silicone adhesives differ from a chemical point of view from other elastomeric materials with respect to their inorganic Si-O backbone, they share a lot of mechanical peculiarities with—chemically speaking—more conventional elastomeric materials such as organic rubbers. Typical characteristics are, for instance, the large elastic deformations known as hyperelasticity, the Mullins effect, the near-perfect incompressibility, and the non-viscous damping behavior. An adequate comprehensive description of this complex mechanical behavior of elastomeric materials for general applications is still the aim of extensive research activities around the world and is outside the scope of this paper. Nevertheless, appropriate assumptions and approximations allow a beneficial use of the current knowledge by accordingly reducing the required complexity of material description for civil engineering purposes. In view of the glass façade of the Herz-Jesu church, wind and dead loads are the main parameters for sizing which allow for a quasi-static material modeling approach, thus skipping time-dependent phenomena such as viscoelasticity. Furthermore, it is assumed that the critical load cases are not governed by a cyclic loading scheme with previously experienced stress states, in order to neglect the Mullins effect. As a result of these approximations, representative material tests can

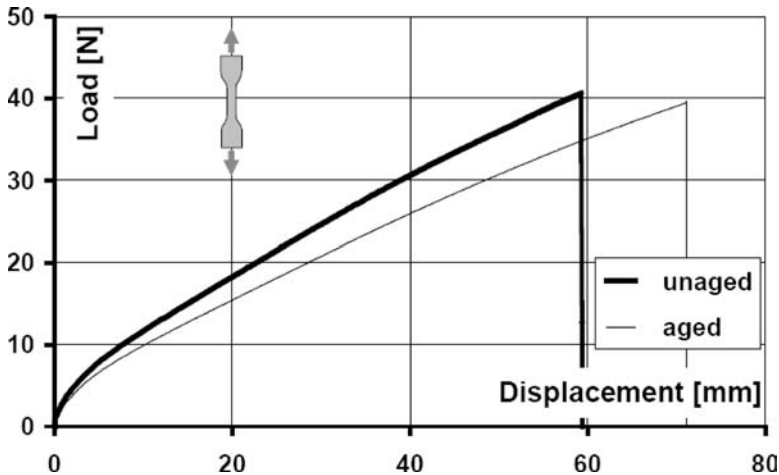


FIG. 4—Comparison of tension tests: aged versus unaged conditions⁴ [7]. Representative specimen results selected from ten specimens (unaged) and five specimens (aged).

be reduced to quasi-static load conditions. Furthermore, hyperelastic material laws available in commercial finite element (FE) codes such as Mooney-Rivlin or Ogden can be applied favorably for related numerical investigations. For the adhesive behavior, the numerical results in this paper are based on a strain energy function of the Mooney-Rivlin kind [4]. The coefficients were derived from tensile dog-bone test results and shear tests of ETAG 002 H-type specimens [5]. For the description of the almost incompressible behavior of the adhesive, results of Ref [6] were used.

Generally, test procedures were adopted from the European guideline ETAG 002 [5], where applicable. Figure 4 shows the results of a tensile test comparing aged with unaged specimens of the standard dog-bone type. The aged specimens were exposed to artificial aging according to the following procedure [7], assessed to be more challenging than ETAG 002:

- 3 days at 80°C (dry)
- 10 days at 45°C in de-mineralized water with cleaning agent (5 %)
- 3 days at 80°C (dry)
- 10 days at 45°C in de-mineralized water with simultaneous UV radiation $50 \pm 5 \text{ W/m}^2$
- 1 day at 23°C (dry, baseline laboratory conditions)
- 8 days at 45°C in salt-water (50 g salt/L) with simultaneous UV radiation $50 \pm 5 \text{ W/m}^2$
- 2 days at -30°C (dry)
- 1 day at 23°C (dry) prior to testing.

With respect to the experimental results shown in Fig. 4, the strength of the specimens was obviously not affected by this procedure, but a modification in the elastic behavior, i.e., in effective stiffness (and flexibility respectively), is visible. The aged specimens show a somewhat softer behavior.

A similar test campaign comparing aged and unaged behavior was per-

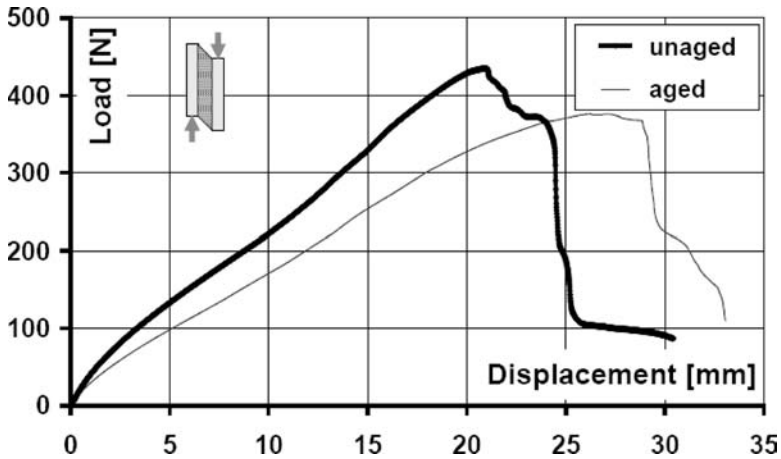


FIG. 5—Comparison of shear tests: aged versus unaged conditions⁵ [7]. Representative specimen results selected from five specimens each.

formed with specimens exposed to shear. The same artificial aging procedure as presented above for the tensile tests was applied to the specimens. Figure 5 shows the experimental shear results confirming the previous observations in tension that aging leads to lower stiffness. Contrary to the tensile tests, the maximum load of the aged specimen in shear is slightly reduced compared to the unaged counterpart. Nevertheless, as will be shown later, the importance of shear strength is lower than the importance of tensile strength for the investigated bonding geometries when studied in the undamaged state of the U-type bonding.

The presented results are related to a baseline test environment under laboratory conditions at 23°C for both unaged and aged specimens. Tension and shear tests were performed additionally at high and low temperatures in order to study the impact of temperature on strength. Figure 6 demonstrates the impact of temperature on the tensile test results. Regarding strength, a clear trend is visible, with lower temperatures leading to higher maximum loads and vice versa. Regarding elastic behavior, no unique trend is visible for the three temperature levels investigated. While stiffness values are very similar for medium and high temperatures, the test at low temperature shows a substantially higher stiffness.

Figure 7 shows the corresponding results for shear loading. Concerning strength characteristics, the trend of increasing maximum loads for decreasing temperatures, already identified by the tensile test results, is confirmed. Regarding the elastic behavior, similar stiffness values are obtained for all investigated temperature levels. Figures 8 and 9 present a compilation of all results including additional statistical information for both tension and shear (using a database of at least five specimens for each test configuration).

In addition, creep tests were performed within the framework of the tensile test campaign. A constant tensile loading was applied to the specimens for a duration of 105 days. The loading was adjusted to a load level obtained by

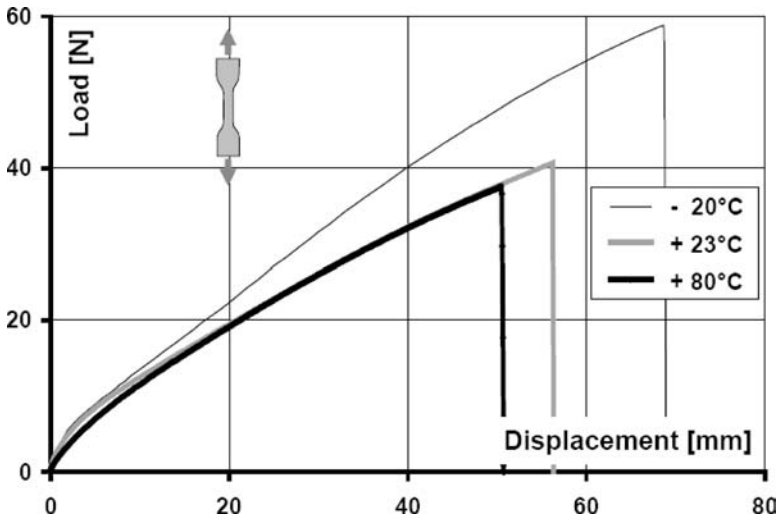


FIG. 6—Comparison of tension tests at different temperatures [7]. Representative specimen results selected from ten specimens (23°C) and five specimens (other).

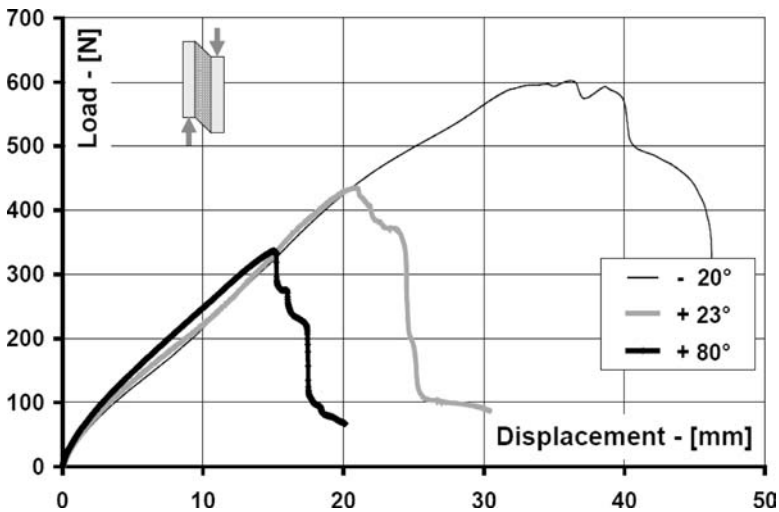


FIG. 7—Comparison of shear tests at different temperatures [7]. Representative specimen results selected from five specimens each.

extension of such kind of specimens to 20 % of the maximum strain of baseline test conditions.⁴ Figure 10 presents comparisons of regular specimens with those exposed to creep loading prior to tensile testing. As can be clearly iden-

⁴Nominal 50 mm/min.

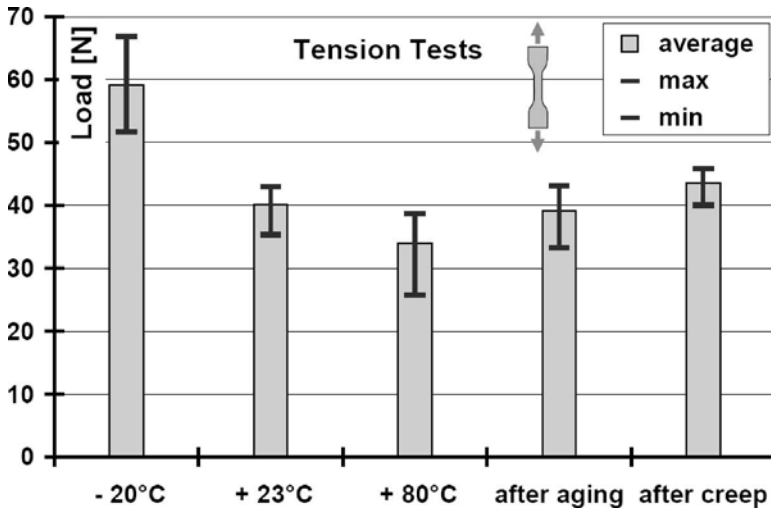


FIG. 8—Overview of tensile test results: all specimens.

tified in Fig. 10, there is a similar behavior of both sets of specimens concerning stiffness and maximum loads in the highly loaded regime. Differences in the low to medium level can be explained by the Mullins effect due to the cycle of creep loading, unloading including recovery for 24 h and strength testing afterwards. For the tested conditions, there is only limited impact on the highly loaded adhesive facilitating the consideration of creep loading in the design process significantly.

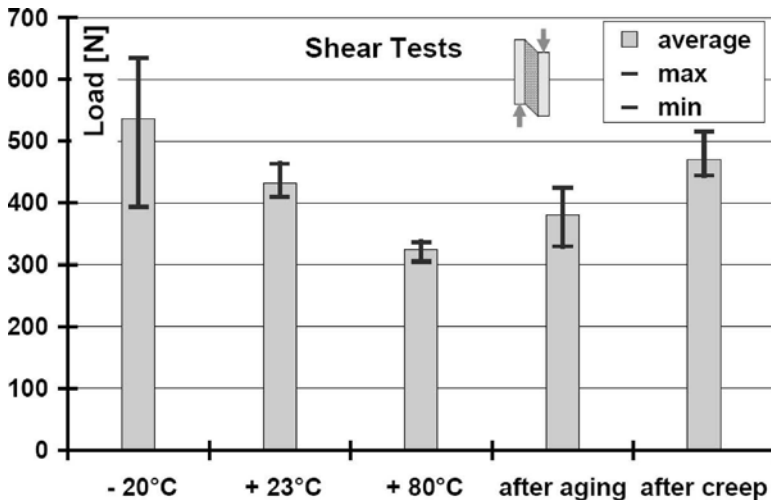


FIG. 9—Overview of shear test results: all specimens.

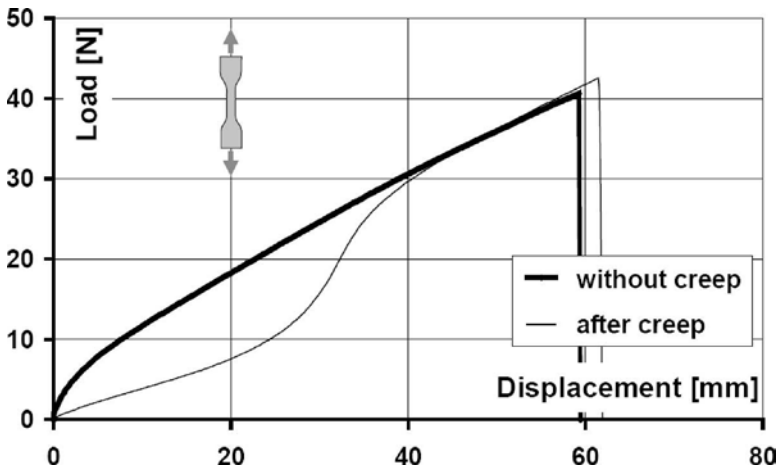


FIG. 10—Comparison of tension tests, without and after creep loading [7]. Representative specimen results selected from ten specimens (baseline) and five specimens (creep).

The experimental results presented above were used to allow the assessment of the impact of various environmental parameters on joint strength for structural engineering purposes. With respect to the scope of this paper, special importance is seen in the determination of the impact of aging on maximum loads showing almost no effects on tension specimens and a minor degradation for shear specimens. Compression tests are of less interest because on the one hand, elastomeric materials are assumed not to fail under pure compression loads for representative load levels, and on the other hand, it is difficult to design appropriate compression tests without running into problems with respect to buckling and friction. For future applications, other test parameters might be of interest as well such as high speed loading; e.g., for analysis of a bomb blast.

U-type Bonding Geometries without and with Degradation

Since the beginning of the consideration of the U-type bonding geometry, focus was put on physical insights into the failure mechanisms observed under tensile loading. Recalling the issues in Table 1, one key element for joint durability is joint stress; thus, knowledge of stress and related failure is also important for assessing durability aspects of the joint design. Other load cases are less critical because either they are easier to understand or they are less important regarding strength issues.

Shear loading is an example for simple mechanical behavior. In the case of shearing the glass components relative to the steel framework, pure shear assumptions for each part of the bonding allow one to estimate stiffness and strength of the entire bonding with adequate accuracy. For sizing purposes, design values of shear stress and shear strain can be compared with shear test data obtained, for instance, on ETAG specimens. Low shear stiffness and miss-



FIG. 11—U-type bonding test configurations.

ing stiffening effects lead to low shear stresses beneficial for thermal loading cases.

The case of compression loading of the bonding is an example of a less critical case concerning strength issues. In this case, the primary load path is established by compression of the adhesives in the front region of the U-type bonding. Based on engineering practice, it is widely accepted that elastomeric materials do not fail under high compression loads experienced in the framework of conventional civil engineering applications.

When analyzing tensile results obtained with specimens of the U-type bonding geometry, as used in the glazing of the Herz-Jesu church, significant differences were observed in comparison to tensile H-type ETAG specimens. Based on theoretical and numerical test results, it was hypothesized that the specimens of the U-type bonding fail stepwise (see Refs. [1,7]), which can be explained by the fact that front and side regions of the U-type bonding are acting in different manners. Numerical predictions revealed a highly stressed front region evoked by the almost perfect incompressibility of the applied silicone adhesive in combination with an effective suppression of the lateral contraction of the silicone. The hereby required constraining of the adhesive is caused by relatively stiff components surrounding the bonding area such as the glass body or the steel channels in addition to the small portion of free, i.e., unconstrained, adhesive surface. The nearly incompressible material responds to this loading primarily by high effective stiffness in tension. The related high stress levels induce material damage already at low load levels in the front region. The impact of this deterioration mechanism can be identified as a significant drop of stiffness, as seen in the experimental results. As tensile loading continues, loads are shifted from the front region to the side regions until the side regions finally fail due to the shear strength limits.

Since the publication of the 2003 symposium paper this hypothesis was experimentally investigated by the analysis of degraded U-type bonding geometries as presented in Ref [8]. Degradation was emulated by preventing the adhesive from adhering with the help of an inserted polyethylene foil. Two types of degradation were studied: one with the side regions disabled (SRD) and one with the front region disabled (FRD), as shown in Fig. 11. Figure 12 presents experimental results comparing the fully operational bonding (BSL) with degradations in the side and front regions. At first glance, the behavior of the BSL configuration can be understood as a superposition of the SRD and FRD configurations. The dominant role of the front region for small displace-

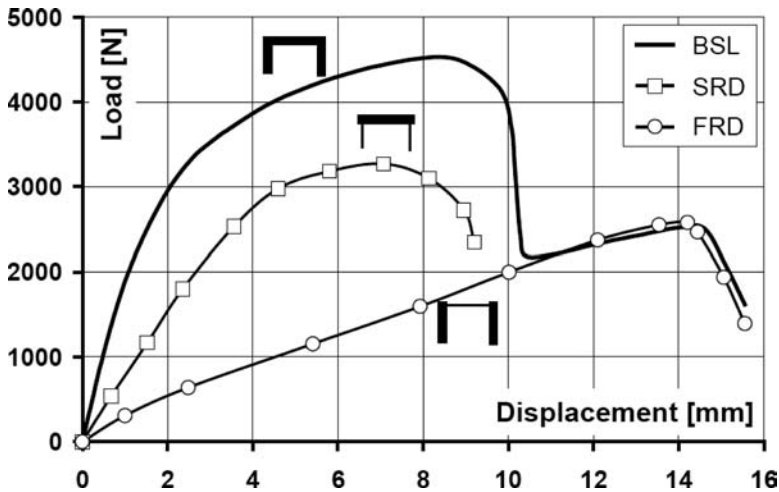


FIG. 12—U-type bonding geometry: test results. Averaged results obtained from five specimens for each configuration.

ments is clearly visible when one compares the BSL case with the SRD case, both featuring a fully operative front region at the beginning of the test and both showing high initial stiffness. The behavior at large displacements is easily identified as guided by shear loading when the BSL case is compared with the FRD case. The conclusion drawn from these results is that the hypothesized failure mechanism, beginning at the front region and finally propagating towards the side regions, is clearly confirmed by these experiments.

What are the consequences of these findings with respect to joint design, strength, and durability? First, the failure mechanism which occurs stepwise can be utilized in tailoring a dedicated safety concept of the bonding. It is desirable that after experiencing an overload condition, bonding strength is not completely lost; rather, a certain amount of mechanical integrity should still be preserved until repair will be performed. Such a safety concept might be based on the activation of the load-bearing capability of the side regions in case of front region failure. This approach leads to design rules for the sizing of the side regions which depend on the demanded strength levels after partial failure of the front region due to overload. Second, the side regions also effectively encapsulate and shield the highly loaded adhesive regions at the front of the U-type bonding which is beneficial to the long-term durability of the joint. It is worth mentioning that the geometry of the side regions not only affects the stress levels at the exposed surfaces but also the diffusion of aggressive environmental media into the adhesive.

In order to assess the loading of the side region and the related impact on durability, stress distributions in U-type bonding geometries were investigated using finite element analysis. In these studies, maximum principal stresses are considered as representative stress level indicators for the silicone adhesive [9]. Maximum principal stresses of the finite elements are evaluated along the bond-line at three different levels within the bonding thickness: in the vicinity

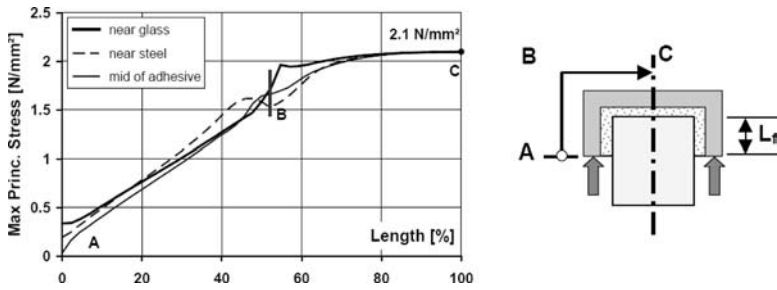


FIG. 13—Maximum principal stress distributions in U-type bonding for load transfer via flanges (1 N/mm²=1 MPa).

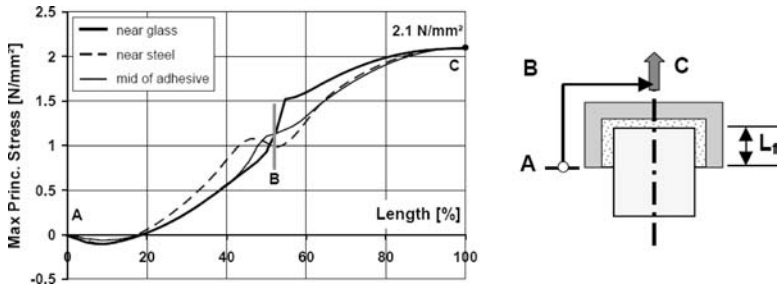


FIG. 14—Maximum principal stress distributions in U-type bonding for load transfer via symmetry axis (1 N/mm²=1 MPa).

of the interface to steel, in the vicinity of the interface to glass, and in the center of the bonding. In this context, it should be noted that the use of averaged element stresses avoids stress singularities in the corner region expected from theory. However, the stress levels obtained by averaging with respect to the element volume are assumed to be lower than those directly related to the interface.⁵ Figure 13 presents two-dimensional FEA results based on plane strain states for the baseline configuration with fully operational bonding starting from the end of the flanges (0 % bonding length) towards the symmetry axis in the front region (100 % bonding length). Special locations along the bond-line are

- A: end of flange
- B: corner
- C: center of adhesive.

It should be noted that the corner of the bonding geometry (location B) is located at approximately 52 % along the length of the bond-line for all investigated adhesive cross-sectional levels in the figure.

⁵In addition, one should note that in the numerical model, the interfaces are geometric boundaries with stepped properties, while in nature, interfaces at least of the glass surfaces show a different behavior on the micro-scale level [10].

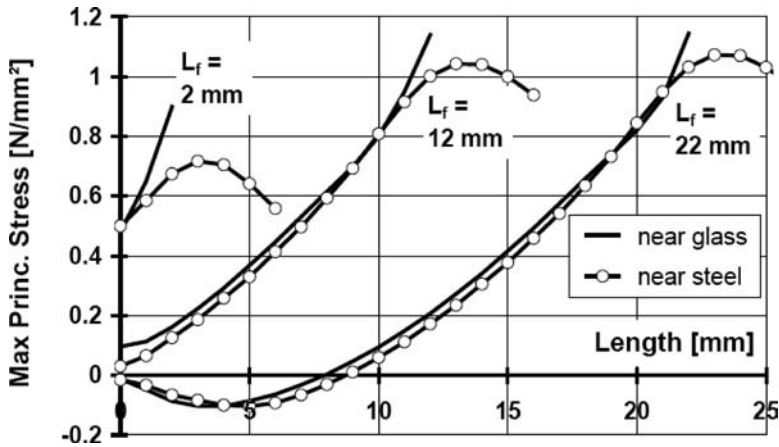


FIG. 15—U-type bonding: maximum principal stress distributions for different flange length ($1 \text{ N/mm}^2 = 1 \text{ MPa}$).

Two different load transfer attachments were analyzed: one with loads transmitted to the flanges (Fig. 13) and one with loads transmitted along the symmetry axis of the front region of the U-type joint configurations (Fig. 14). The first configuration is often used in specimen testing while the latter one represents a typical case occurring in actual service. The load levels of the numerical models were chosen in such a way that a stress level of approximately 2 MPa is achieved in the front region. The selection of this limit value is based on experimental findings; see also Ref [9].

The following conclusions can be drawn based on the findings which were shown in Figs. 13 and 14:

- In the front region, the highest stress levels are experienced near the interface to glass.
- In the side region, the highest stress levels are primarily experienced near the interface with steel.
- Stress levels in the side region are generally lower for the configuration with load transfer along the symmetry axis; a situation which is assumed to be more favorable for durability. It should be noted that the difference in the stresses resulting from the different load introduction locations is due to flexibility of the PFC element given by thickness and material (the presented studies are based on stainless PFC elements of 3 mm thickness).
- By adjusting the loading in the FEA model to the limit stress level, a different total load is obtained for both load transfer configurations; this result is again related to the flexibility of the PFC element.

In the next step, parameter studies were performed by varying the length of the flange L_f from 22 mm (baseline value) down to 2 mm for the smallest flange length. Figure 15 shows the stress levels calculated for the side region near the interfaces to glass and steel. In this figure, the stress level curves span across the bonding length defined by abscissa values from 0 mm corresponding

to the location of the exposed edge of the adhesive in the side region to the interior edges of the glass pane and the steel profile. For a flange length of 12 mm, the stress level curve near the glass interface spans across 12 mm towards the glass edge, while the corresponding curve near the steel profile interface spans across 17 mm (12 mm flange length plus 5 mm bond thickness). The results shown in Fig. 15 lead to the following conclusions:

- The variance of stress levels between glass side and steel side is small. Typically the glass side shows slightly higher stress values.
- The curves for flange lengths of 12 mm and 22 mm are very similar when applying a shift of 10 mm which corresponds to the difference in the bonding geometry. Thus, it can be concluded that for these bonding geometries, the loading in the interior of the U-type joint is quite similar. The stress levels, calculated for the 2 mm flange length, differ which is caused by the close vicinity of the bonding corner.
- The curves for 12 mm and 22 mm flange lengths show small stress levels at the exposed adhesive surface; this is beneficial for durability. For the 12 mm flange length case, stress levels immediately increase inside the bonding, while for the 22 mm flange length case, stress levels are negative up to approximately 8 mm bond length.
- If a representative penetration depth of an aggressive environmental medium is known in advance in addition to a related allowable stress level, an optimized flange length can be approximately calculated by horizontally shifting the 22 mm curve in such a way that it passes the allowable stress level at the bond-line length related to the penetration depth. This horizontal shift then determines the enlarging or shortening of the flange for an optimized configuration.

Nevertheless, the size of the flange also affects other characteristics such as the failure characteristics in an overload situation. In this case, additional design guidelines might have to be considered as well.

T-type Bonding Geometries without and with Degradation

Similar to the U-type bonding, experiments have been performed for the T-type bonding with degradation (FRD) and without degradation (BSL) [11]. Figure 16 presents the results obtained for a fully operational T-type bonding and a bonding intentionally degraded in the front region. The overall behavior shows substantial similarities to the U-type bonding without and with failed front region. As for the U-type bonding, the front region in the T-type bonding causes high bonding stiffness and loads at the beginning of the tensile test, but is also subjected to early failure after 4 mm to 6 mm displacement. After the failure of the front region, the curves generated for non-degraded and degraded specimens are almost coincident, indicating that loads are transmitted mainly by shear for large displacements. These findings confirm that the conclusions reached for the U-type bonding in terms of the failure mechanics, i.e., that the failure starts in the front region; can also be applied to T-type bonding geometries. Furthermore, it is assumed that these statements do not only hold for U-type and T-type bonding geometries, but for all bonding geometries with

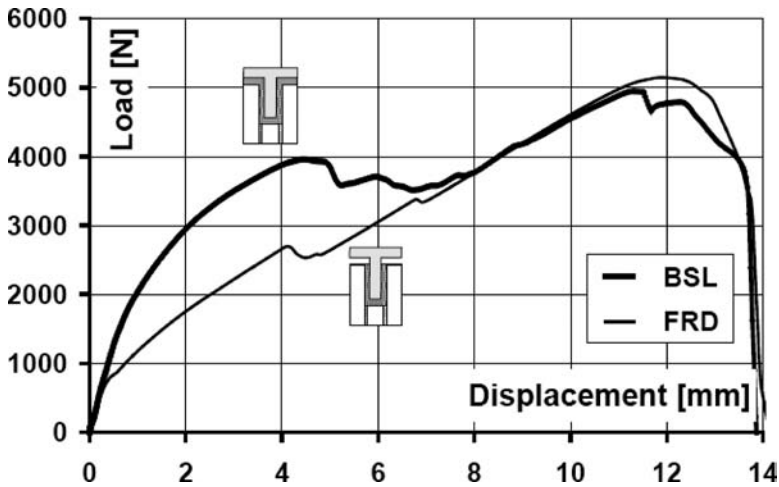


FIG. 16—*T*-type bonding: test results [7]. Averaged results obtained from five specimens for each configuration.

horizontal (i.e., perpendicular to the tensile load axis aligned) front regions and vertical (i.e., parallel to the tensile load axis aligned) side regions. This assumption leads to the following conclusions:

- Bonding areas perpendicular to the tensile load axis and thus subjected to tension stresses lead to higher overall joint overall stiffness. The level of stiffness increase depends on the level of suppression of the lateral contraction.
- Due to the high stiffness of these bonding areas, local loads and stress levels will increase very rapidly with growing displacements. Thus, failure of the bonding will also start in this area.
- If bonding areas perpendicular to the tensile load axis start failing, load transfer will increasingly be established via shear by the bonding areas parallel to the applied tension loads.
- Therefore, the maximum load capacity can be expected to exceed the load level at which failure starts. The related margin depends on the bonding geometry, as shown for instance in Fig. 16. Thus, post-failure characteristics can be tuned by design means.

The last four statements are fundamental concerning the general mechanical behavior of these joints. When one additionally takes into account the durability aspect, a fifth conclusion should be added, stating that for favorable durability behavior, the bonding areas perpendicular to the tensions loads should be encapsulated, as explained below. In a similar manner as for the U-type bonding geometries, maximum principal stress levels⁶ are shown for T-type bonding geometries in Fig. 17. In contrast to the U-type bonding geometry, high stress levels are observed in the vicinity of the freely exposed bonding

⁶In this case, only load transfer along the symmetry axis is considered.

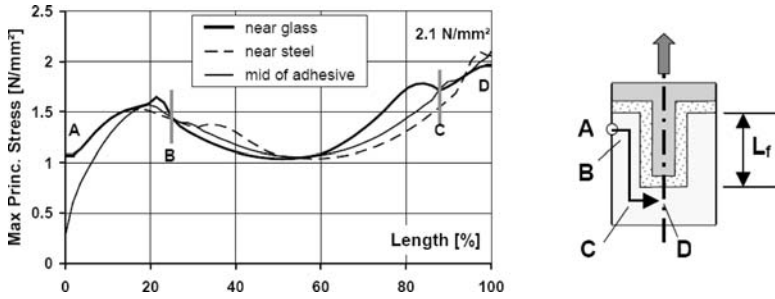


FIG. 17—Maximum principal stress distribution in T-type bonding, $L_f=35$ mm ($1 \text{ N/mm}^2=1 \text{ MPa}$).

surface (label A) giving the T-type bonding geometry a very low ranking with respect to durability aspects. Furthermore, a variation of the length of the flange does not significantly alter stress levels in the area critical for the fully operative bonding (see Fig. 18). Results for two T-type bonding geometries are shown differing significantly in the length of the flange. Nevertheless, the stress levels at the freely exposed bonding surface are quite similar. Obviously, the behavior of these two different bonding geometries changes in case of failure of the front region caused by overloading or due to environmental attack of aggressive media. In these situations, the size of the flange will define the remaining maximum load capacity and will lead to different load-bearing and durability characteristics.

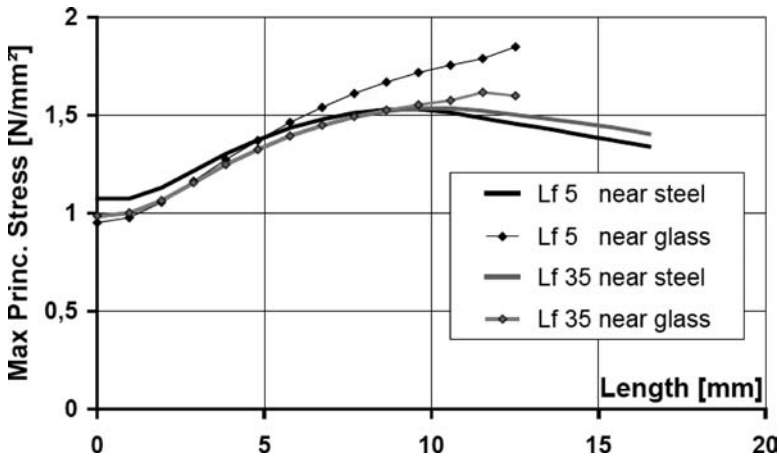


FIG. 18—T-type bonding: maximum principal stress distributions for different flange lengths ($1 \text{ N/mm}^2=1 \text{ MPa}$)

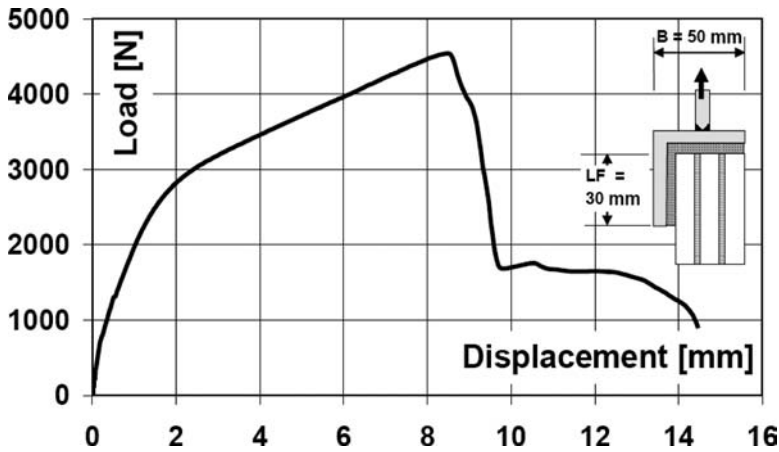


FIG. 19—*L*-type bonding: test results [7]. Averaged results obtained from five specimens for each configuration.

Other Bonding Geometries of Interest: L- and E-types

U-type and T-type bonding geometries can be considered as baseline geometries which can be used for the derivation of conclusions for other geometries; for example, L- and E-type bonding geometries. The L-type bonding geometry can be interpreted as a modification of a U-type bonding geometry by eliminating one of the two side regions. Figure 19 presents experimental results for this bonding geometry, confirming close relationship between U-type and L-type bonding geometries. The mechanical characteristics are very similar; thus, a similar test campaign with degraded bonding was not taken into account. In the view of durability, L-type bonding geometries are assumed to be less favorable than U-type bonding geometries as one of the two exposed surfaces of the bonding geometry is located at the highly loaded front region. Depending on whether this side of the bonding is exposed to environmental attack, the highly loaded front region might fail faster due to these conditions. In this case, the size of the side region will determine the actual load capacity.

Figure 20 shows the stress levels for front and side regions in the usual way, confirming the above-mentioned statements. While the stress distribution with respect to the side region is qualitatively in good agreement with the side region of the U-type bonding geometry, the stress distribution in the front region and especially at the exposed surface shows similarities with the front region of the T-type bonding geometry.

Thus, it can be concluded that the exposed surface at the front region (label C) is the weak point of the L-type bonding with respect to durability in case both surfaces are exposed in the same way to the environment. Otherwise, it is recommended, if possible, to place the side region of the L-type bonding geometry towards the more aggressive environment in order to shield the highly loaded front region.

The E-type bonding geometry can be considered as an extension of the

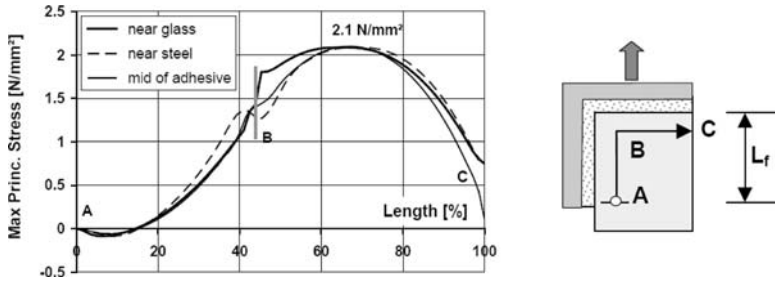


FIG. 20—Maximum principal stress distribution in L-type bonding, $L_f=30$ mm ($1 \text{ N/mm}^2=1 \text{ MPa}$).

U-type bonding geometry by adding the inner flange or alternatively as an extension of a T-type bonding geometry by adding two outside flanges. For the E-type bonding geometry, no experimental tests were performed. Nevertheless, it can be hypothesized that the mechanical behavior is similar to a superposition of U-type bonding and T-type bonding. In terms of durability aspects, the E-type bonding geometry is assumed to correspond to U-type bonding geometries. These assumptions are supported by Fig. 21 showing the stress distributions for the E-type bonding geometry. The stress distribution obtained with respect to the outer side region is in qualitative agreement with that of the U-type bonding geometry, while the inner flange loading is in qualitative agreement with the corresponding behavior of the T-type bonding geometry.

Summary and Conclusions

This paper outlines two topics of high importance for structural joint durability. First, the jointing material itself was in the focus of research activities. Tensile and shear tests were performed for unaged and artificially aged specimens. Furthermore, corresponding tests were performed for unaged specimens at different temperatures. Finally, creep behavior was also tested within the

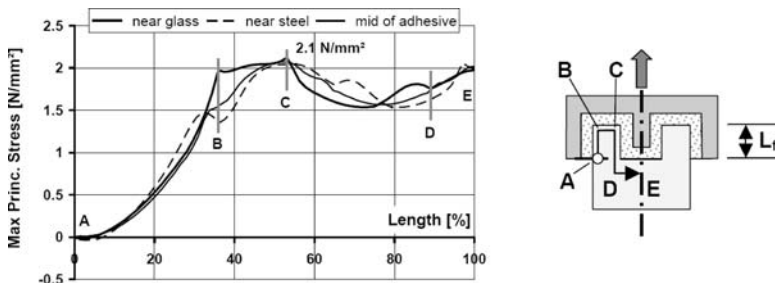


FIG. 21—Maximum principal stress distribution in E-type bonding, $L_f=22$ mm ($1 \text{ N/mm}^2=1 \text{ MPa}$).

framework of the tensile tests. The experimental results are summarized as follows:

- Regarding tension tests, aging leads to increased flexibility but no significant changes in strength are visible.
- Regarding shear tests, aging leads to increased flexibility and to reduced strength.
- Regarding tension tests, increasing temperatures lead to increased flexibility, but no clear trend is visible for strength.
- Regarding shear tests, increasing temperatures lead to increased flexibility and to reduced strength.
- Regarding tension tests, creep does not show significant impact on flexibility and strength at higher loads.

As not all experimental results show unique trends, additional test activities in this field are recommended. In addition, other adhesive materials should be investigated as well in order to broaden the experimental database.

As a second step, different bonding geometries were analyzed with respect to durability issues, working with the hypothesis that the maximum principal stress level in the vicinity of the exposed bonding surface is a measure for durability. This assumption is based on the concept that the environmental impact of aggressive media and solar radiation is related to the penetration depths into the adhesive. The highest impact of environmental effects is expected at the exposed bonding surface. In addition, it is supposed that an attenuation of these effects appears with increasing depth from this surface. For aggressive media, this assumption is guided by the physical principles of diffusion into the adhesive, while for radiation, physical principles of absorption of the radiation seem applicable for the adhesive. Although it is quite difficult to quantify the impact of these mechanisms on material strength in terms of exact numbers, this approach allows the derivation of design rules for different bonding geometries such as U-type, T-type, L-type, and E-type bonding designs which were numerically and, in part, also experimentally analyzed. Furthermore, the design considerations can be generalized to a class of bonding geometries with planes parallel and perpendicular to the tensile load axis. Regarding durability it can be concluded that:

- Bonding geometries with all exposed surfaces located only at the end of side regions are expected to show good durability properties in the context of applied stress.⁷ Examples are U-type bonding geometries and E-type bonding geometries.
- Bonding geometries with at least one free surface located at a front region are expected to show lower durability properties in the context of applied stress. Examples are T-type bonding geometries and L-type bonding geometries. One should note that these statements hold true for

the fully operative bonding. The situation of post-failure behavior is not treated in this paper with the exception of the presentation and discussion of experimental results for degraded bonding geometries.

⁷An adequate flange length L_f is assumed.

Acknowledgments

The author would like to thank the building owner—Erzdiözese München und Freising, Erzbischöfliches Baureferat—for unconditional support of the advanced design of the Herz-Jesu Church, Munich. Furthermore, the author would like to thank Dow Corning GmbH for their outstanding technical support provided during the design of the façade as well as in the related research phase.

References

- [1] Hagl, A., "Synthesis of Glass and Steel: The Herz-Jesu Church in Munich," *Stahlbau*, Vol. 71, No. 7, 2002, pp. 498–506. (Original title: Synthese aus Glas und Stahl: Die Herz-Jesu Kirche in Muenchen.)
- [2] Hagl, A., "Durability by Design: Load Carrying Silicone Bonding, Herz Jesu Church, Munich," *Durability of Building and Construction Sealants and Adhesives*, ASTM STP 1453, A. T. Wolf, Ed., ASTM International, West Conshohocken, PA, 2004.
- [3] Kinloch A. J., (Ed.), *Durability of Structural Adhesives*, Elsevier Applied Science Publishers Ltd., London, 1983.
- [4] Crisfield, M. A., *Non-linear Finite Element Analysis of Solids and Structures*, Advanced Topics, Vol. 2, John Wiley & Sons, London, 1997.
- [5] European Organization for Technical Approvals, "ETAG 002 Guideline for European Technical Approval for Structural Sealant Glazing System (SSGS)—Part 1 Supported and Unsupported Systems," www.eota.be/pdf/ssgs-fin-am3.pdf.
- [6] Wolf, A. T., and Descamps, P., "Determination of Poisson's Ratio of Silicone Sealants from Ultrasonic and Tensile Measurements," *Performance of Exterior Building Walls*, ASTM STP 1422, P. G. Johnson, Ed., ASTM International, West Conshohocken, PA, 2002.
- [7] University of Applied Sciences Munich, FB02, "Structural Bonding in Glass Constructions," *Research Report*, BMBF (Federal Ministry of Education and Research) Project, AIF-Nr.: 1755X04, 2007. (Original title: *Geklebte Verbindungen im Konstruktiven Glasbau*.)
- [8] Hagl, A., "Understanding Complex Adhesive Behavior: Case Study U-type Bonding Geometry," *Challenging Glass Symposium*, Bos Louter Veer, Eds., Delft University of Technology, May 2008.
- [9] Hagl, A., "Pointwise Bonding with Silicones," *Stahlbau*, Vol. 77, No. 11, 2008, in press. (Original title: *Punktuelles Kleben mit Silikon*.)
- [10] Habenicht, G., "Bonding: Basics, Technology, Applications," Springer, Berlin, 1997. (Original title: *Kleben: Grundlagen, Technologie, Anwendungen*.)
- [11] Hagl, A., "Sizing of Bonding—Structural Bonding with Silicone," *Glass in Glass Construction V Conference*, Germany, Muenchen, March 2007. (Original title: *Klebung bemessen—Tragende Verklebungen mit Silikon*.)

**DEVELOPMENT OF
NEW TEST METHODS AND
PERFORMANCE-BASED
SPECIFICATIONS**

Kenneth Yarosh,¹ Andreas T. Wolf,² and Sigurd Sitte³

Evaluation of Silicone Sealants at High Movement Rates Relevant to Bomb Mitigating Window and Curtainwall Design

ABSTRACT: Silicone sealants have a long history of successful use in high performance windows and curtainwalls, such as structural glazing systems. With the recent threat of terrorist attacks, there has been an increased use of windows designed to mitigate the impact of bomb blasts. Due to the high strength and durability characteristics of silicone sealants, structural silicone sealants have been utilized in new bomb blast mitigating window designs. Effective bomb blast mitigating window designs allow the window system to withstand a moderate bomb blast without causing significant injury to building occupants from the blast itself or flying glass shards. The occupants are protected because laminated or filmed glass, which can withstand the blast, is attached in the framing with a silicone sealant. Silicone sealants provide unique benefits to these window designs due to their strength properties and their ability to anchor the laminated glass in the framing during a blast situation. In this paper, three commercially available high strength structural silicone sealants are evaluated at applied load velocities (movement rates) up to 5.0 m/s. These elevated load velocities are intended to simulate loads encountered during a bomb blast. Sealant joints are fabricated to evaluate the sealant in tension, shear, and combined tension and shear loads. Sealant joints are also exposed to accelerated weathering (heat, water, and artificial light through glass). Results show that the sealant strength values

Manuscript received June 20, 2008; accepted for publication November 18, 2008; published online December 2008.

¹ Associate Scientist, Dow Corning Corporation, Midland, MI, 48686-0994.

² Ph.D., Senior Scientist, Dow Corning GmbH, 65201 Wiesbaden, Hessia, Germany, e-mail: Andreas.Wolf@DowCorning.com (Corresponding author).

³ Industry Specialist, Dow Corning GmbH, 65201 Wiesbaden, Hessia, Germany.

Cite as: Yarosh, K., Wolf, A. T. and Sitte, S., "Evaluation of Silicone Sealants at High Movement Rates Relevant to Bomb Mitigating Window and Curtainwall Design," *J. ASTM Intl.*, Vol. 6, No. 2. doi:10.1520/JAI101953.

Copyright © 2009 by ASTM International, 100 Barr Harbor Drive, PO Box C700, West Conshohocken, PA 19428-2959.

increase substantially at elevated rates of applied load. The paper discusses the effect of joint configuration, load velocities, and accelerating weathering on the performance and durability of the silicone sealants tested.

KEYWORDS: bomb blast, silicone, sealant, movement rate, loading rate, high speed, window, curtainwall

Introduction

The increased threat of terrorist attacks over recent years has highlighted the need for enhanced physical security features to be incorporated into building façades [1]. Historically, the majority of serious injuries or fatalities in blast events sustained by building occupants and the general public in and around the buildings were caused by high-velocity glass fragments originating from the building's exterior window systems that were fragmented by the forces of the bomb blast (see, for instance, Refs. [2–6]). Figure 1 shows, as an example, the glazed curtain wall of a building adjacent to the Australian Embassy damaged by the Sept. 16, 2004 bomb blast in Jakarta, Indonesia. Nine persons were killed and more than 170 injured in this bomb blast. It is estimated that in a bomb attack up to 80 % of injuries and fatalities are attributable to flying glass shards and falling debris. For example, in the April 19, 1995 bombing of the Alfred P. Murrah Building in Oklahoma City, 40 % of the survivors within the building cited glass as contributing to their injuries. Within nearby buildings, laceration estimates ranged from 25 to 30 % [2].



FIG. 1—Glazed curtainwall damaged by bomb blast (note the remaining shards of glass) (Source: Associated Press).

In addition to posing a hazard to humans, glass fragments can contaminate the work place and cause business disruptions after a bomb blast event. For example, following the 1993 Bishopsgate bombing in the City of London, United Kingdom, the whole air conditioning and ducting system in the building had to be replaced as no other efficient means of removing the contamination was deemed viable [7].

Due to the hazardous behavior of regular glazing systems in bomb blast events, there is a clear conflict between the need to construct secure facilities on the one hand and the importance of designing warm, open, and welcoming buildings such as embassies, hotels, or office blocks on the other. This has led to a renewed effort in the design of transparent facades that mitigate injuries and structural damage from blast loads and has prompted an increase in the use of bomb blast mitigating glazing designs globally during the past decade, especially in new construction for government, institutional, and some high profile commercial buildings. Furthermore, existing window designs, which were not originally designed to withstand bomb blast, also have been retrofitted with specially developed protective films bonded by silicone sealants to the frame [8,9]. In summary, the primary objective of the various blast-mitigating protective glazing systems is to protect people in and around buildings by minimizing the quantity and hazard of broken glass and blast-induced debris.

Despite the amount of research that has taken place into the fracture behavior of architectural glazing under blast loads, this remains a field in which science is still evolving and the levels of expertise vary greatly. One of the greatest difficulties lies in anticipating the interactions between the high-speed dynamic behaviors of the various materials involved in these glazing systems. Various factors, such as momentum transfer, natural period of vibration, dynamic increase in material strength, aspect ratio, energy adsorption, and load path, need to be carefully considered for a balanced design. One of the key materials is the structural sealant, whose proper use and selection is critical to the performance of protective glazing systems.

In this paper, three commercially available high strength structural silicone sealants which are currently marketed for bomb blast mitigating window designs are evaluated in high speed testing to simulate loads imposed on the sealant joint during a bomb blast. Sealant joint designs similar to those used in current bomb blast mitigating windows are tested in tension as well as shear and results are analyzed to determine mechanical performance parameters at high loading rates that are useful for optimum sealant joint design.

The performance of a window system is the result of the interaction of all of the components of the system based on their attributes, including design, materials, and construction. The information provided in this paper is intended to help the designer of these systems to better understand the characteristics and behaviors of silicone sealants for bomb-blast mitigating window designs.

Bomb Blast Characteristics

When a high explosive, such as trinitrotoluene (TNT), is detonated a rapid decomposition of the condensed phase material occurs, resulting in the release

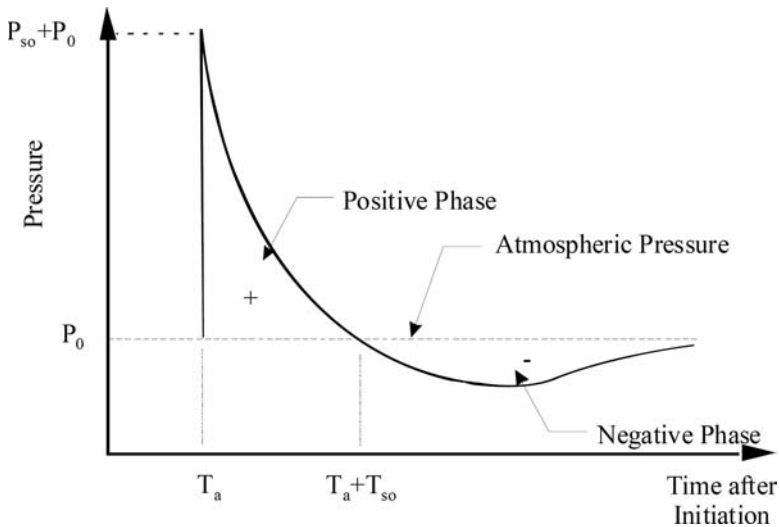


FIG. 2—Blast pressure as function of time at a given location (T_a : Time of blast pressure arrival, T_{so} : Time of first return to atmospheric pressure, P_0 : atmospheric pressure, P_{so} : maximum blast pressure).

of a gas at extremely high temperature and pressure. Typically the pressure at the origin of the detonation is of the order of 20 GPa. The sudden release of a gas at high pressure results in an outward directed pressure wave in the air with an extremely steep pressure rise. This shock wave, consisting of highly compressed air, is traveling radially outward from the source at supersonic velocities (up to 10 000 m/s at the explosion origin) [10]. As the shock wave expands, the pressure decreases rapidly with distance (as a function of the cube of the distance). However, when it meets a surface that is in line-of-sight of the explosion, it is reflected and, for planar surfaces, typically amplified by a factor of 8–12. The amplification factor may be much higher for geometrically complex structured building surfaces at which double or even triple reflections occur [11]. The magnitude of the reflection factor is a function of the proximity of the explosion, the topology of the building envelope, and the angle of incidence of the shock wave on the building surface. It is not uncommon for a building structure in the path of the pressure wave to be subjected to blasts with peak pressures of the order of hundreds, if not thousands, of kilopascal (kPa). As the detonation wave passes over a given point, the pressure initially rises almost instantaneously to its peak, followed by a rapid, i.e., exponential, decay (see Fig. 2). The positive pressure phase has a very brief span of existence, measured in milliseconds. Late in the explosive event, the shock wave becomes negative, creating suction. While the negative pressure phase can have a longer duration (typically at least twice as long as the positive pressure phase), it is limited to the maximum negative pressure of one atmosphere (100 kPa), and, therefore, represents only a small fraction of the initial positive impulse. The positive phase of the pressure trace is generally simplified to an

equivalent triangular pulse and for engineering calculations only two parameters, the peak pressure and effective duration, are used to characterize the load. The duration of the positive blast pressure phase is directly related to blast damage. For a given value of peak air blast pressure, damage increases as duration increases, because the air blast forces act for a longer period [12]. Alternatively, peak pressure and positive phase impulse are used to describe a blast wave. The positive phase load impulse is the integrated pressure load over time, from the pulse arrival time (T_a) to the time when the pressure first returns to atmospheric pressure ($T_a + T_{so}$), or the area under the pressure duration curve between those two time intervals.

Bomb Blast Mitigating Glazing Design

Any attempt to design glazing that minimizes bodily injury and property damage during a bomb blast requires an understanding of the fracture behavior of architectural glazing subjected to blast loading. Traditional window glass design methodology, which assumes that loads act quasi-statically with durations measured in seconds or longer periods, is not suitable for designing blast mitigating windows.

It is important to emphasize the principal differences between static, dynamic, and short-duration dynamic loads. Static loads, such as gravity loads, are assumed to act on a building structure for long periods of time and are not time dependent. Dynamic loads, such as induced by earthquakes or wind gusts, have strong time dependencies and their durations are typically measured in tenth of seconds up to several seconds. Short-duration dynamic loads, such as those induced by explosions or debris impact, are pulse loads with a duration that is about 1000 times shorter than the duration of a typical earthquake. In addition to their short-duration dynamic nature, air blast pressure loadings tend to have much larger magnitudes than wind and snow loadings that typically govern window glass design.

The damage potential of explosive blasts lies in their ability to deliver kinetic energy to the glass pane. Under static loading the glass pane reacts by bending, i.e., the deformation occurs while the load is acting on the glass pane. Dynamic wind or seismic loading increase relative slowly when compared to the structure's natural frequency. When resisting the acceleration from such slow dynamic forces, the strain distribution is similar to the one observed under static loading; therefore, such situation can be treated in a quasi-static approach. However, if the positive phase duration of the blast pressure is shorter than the natural period of vibration of the glass pane, the response is described as impulsive. In this case, most of the deformation of the glass pane will occur after the blast loading has diminished. The dynamic air blast pressure loading associated with an explosion excites higher vibration modes in a window glass pane and causes much higher stresses and deflections than a quasi-static loading having the same magnitude of pressure [5].

Figure 3 shows qualitatively the relative amplitude-frequency distribution for different dynamic loads acting on a building. In this figure, for nonoscilla-

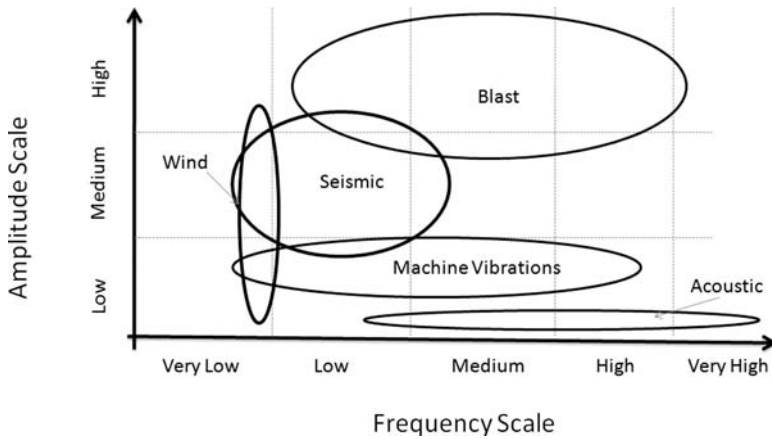


FIG. 3—Qualitative amplitude-frequency distribution for different dynamic loads acting on a building (adapted from Ref [13] and modified by authors).

tory pulse loads, such as blast load, frequency is to be considered the inverse of pulse duration.

The best protection from a bomb is standoff distance since the loading associated with a given bomb decreases rapidly with increasing standoff distance. Therefore, typically a perimeter wall is constructed at the property boundary to restrict access to the site and to achieve a certain minimum standoff distance. However, the building's façade is often its first and only defense against the effects of a bomb. The manner in which a façade responds to blast loading substantially affects the behavior of the building's structure. Typically, the design philosophy is to focus on the post-damage behavior with the aim of having the building and its cladding components standing or attached long enough to evacuate every person and to protect occupants from injury or death resulting from flying debris.

Generally, the least hazardous post-damage behavior is achieved when the window units are composed of laminated or filmed glass. For a range of blast pressures and impulses, failed laminated or filmed glass panes retain the shards of glass, thereby limiting the extent of flying debris. Even when cracked by blast pressure, the outer glass layers of a laminated glass pane remain bonded to the inner plastic interlayer rather than forming free-flying shards, so long as the blast does not exceed the postulated maximum peak pressure and impulse used in dimensioning the blast mitigating glazing system [14–16]. For the laminated or filmed glazing system to be effective, the glass must remain attached to the suitably enhanced mullions or window frame. This is typically accomplished by means of a sufficiently strong structural silicone sealant. For laminated glass, retaining the glass pane may also be achieved by a sufficiently deep rebate. Standard glazing bites with gaskets will not restrain fractured laminated glass under air blast pressure loading and the entire glass pane may be pulled out from the rebates and dislodged from the frame as the glass deflects. On the other hand, the use of very deep bites with gaskets might restrain the blast-

resistant glazing, but could lead to other problems such as thermal breakage in annealed laminated glass [5].

Maximum protective performance is achieved by securely bonding the glass pane to its frame or mullions by means of a structural silicone sealant, thus enabling the cracked laminated or filmed glass to behave as a ductile membrane that bulges inwards, assuming an external explosion event. If the impact-absorbing interlayer or film remains intact and the fixation of the glass pane is maintained, the glazing prevents blast pressures from entering the building and at most a fine glass dust is detached from the surface of the inner laminated glass pane. Most of the causes of injury are thereby removed.

Stretching the laminated glass polyvinyl butyral (PVB) interlayer beyond the limit of its ductility (ca. 200 % at room temperature) causes it to tear. Even after tearing has commenced, the laminated glass pane will continue to offer some blast resistance until the opening is substantial. This is because as it deforms and ruptures, the applied blast pressure will diminish over time so that the residual blast pulse, which does eventually enter the interior of the building, will be less than the full pulse [17].

The ability of laminated or filmed glass to absorb and dissipate blast energy is well proven, both in tests and actual terrorist bomb explosions [5,7,8]. However, in order to effectively utilize the membrane capacity of laminated or filmed glass and to transfer the blast load to the window frame or mullions, the glazing must be securely adhered to its supporting structure. Silicone sealants provide unique benefits to these window designs due to their inherent strength properties, resulting in their ability to anchor the glazing in the framing during a bomb blast event. However, the silicone sealant is only one component of a glazing system. A glazing system that meets the testing and code requirements for bomb-blast resistant glazing must successfully integrate the frame or mullion and its anchorage, glass or other glazing materials, protective film or interlayer, and silicone sealant into a system capable of transferring the sustained forces to the structural building slabs. Various recommendations and standards dealing with the testing, classification, and guidance for installation have been developed (see, for example, Refs. [18–26], and the discussion of International and European Standards in Ref [27]).

The most commonly used performance specifications for bomb blast mitigation in the United States are the GSA (Government Services Administration) Levels C and D [18]. The GSA levels are defined in terms of (1) an overpressure, and (2) an impulse (integrated pressure duration product). Level C specifies a peak pressure of 27.6 kPa and an impulse loading of 193 kPa·ms, while Level D specifies a peak pressure of 69.0 kPa and an impulse loading of 614 kPa·ms. The behavior of the glazing under the given pressure impulse conditions is then classified in terms of the breakage mode with the classification ranging from Category 1 (no break) to Category 5 (high hazard). The intent of these criteria is to reduce, but not necessarily eliminate, the potential hazards, recognizing that not all windows will survive a bomb attack.

However, it is important to note that terrorist bombing is a very low probability event. Most of the time during their service life, bomb-blast resistant windows and façades must provide their regular function, which is to protect the building and its inhabitants from the exterior environment while allowing

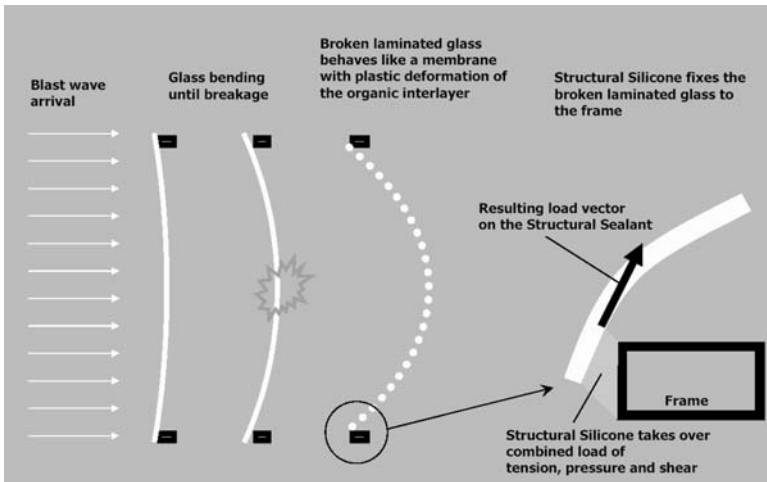


FIG. 4—Schematic model of window behavior upon impact of blast load.

light to enter the building and its occupants to visually observe the outside world. Furthermore, since one cannot predict if and when a building will be exposed to a blast event, all materials used in the building façade must have durability characteristics that will allow them to withstand the blast regardless whether the building just has been completed or already has been in use for the past 10 or 20 years. Silicone sealants excel in their long-term elasticity, adhesion and durability; properties that are important for the proper functioning of a façade, both during regular weather exposure as well as during a bomb-blast event [28].

Behavior of Bonded Architectural Glazing Subjected to Bomb Blast Loading

When a window glazed with a laminated or filmed glass that is bonded to the frame successfully passes air blast pressure loading, the following stages can be observed (as shown schematically in Fig. 4):

1. The glass pane deforms elastically and stores some of the impacting blast energy.
2. The glass pane(s) fracture(s), and the fracture dissipate(s) the stored energy.
3. The film or interlayer remains bonded to the glass shards as it deforms (stretches) in an elastoplastic manner and the deformation dissipates most of the impacting blast energy, causing the filmed or laminated glazing to deflect considerably (300 to 400 mm is not uncommon for larger glazing sizes).

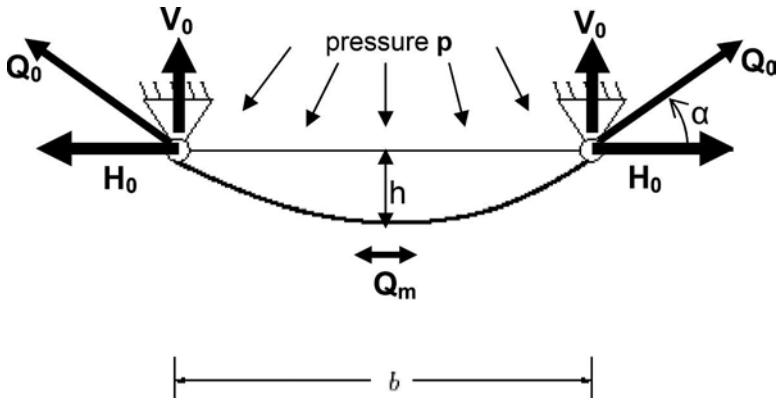


FIG. 5—Two-dimensional model for the laminated glass membrane deformation.

4. The frame and support system (mullions) deform and dissipate the remaining blast energy.

The overall design philosophy for bomb blast mitigating windows requires the laminated or filmed glass to break as this consequently allows the interlayer or film to stretch, causing the large-scale dissipation of blast energy. Because of this successful energy dissipation less load is transferred into the structural frame.

In order for a blast-mitigating window to fail properly, the glazing must be held in place long enough to develop sufficient stress to cause glass failure. Fundamental to the behavior of the window or curtainwall is the ability of the laminated or filmed glass to remain attached to the frame or mullions. The silicone sealant, essential for retaining the glazing, is first compressed by the glass bearing against the frame or mullions, and then subjected to a complex triaxial state of superimposing bending, shear, and tensile stresses as the glazing is crazed and deformed. Since the deformation process occurs within a few milliseconds, giving rise to stresses in the silicone sealant close to its performance limits, it is of importance when selecting products in the design of blast-mitigating glazing systems to know the response of silicone sealants to high strain rates and high stress loads.

Some of the deformation conditions that the silicone sealant experiences can be approximately derived from actual blast tests on laminated or filmed glass. In a simplistic (quasi-static) approach, the maximum force acting on the sealant at the center of the long edge of the glass pane can be estimated by replacing the three-dimensional membrane with a two-dimensional cross section represented by a flexible "rope" fixed between two points under constant load (see Fig. 5). In this model, the load is acting perpendicular on the rope at any point along its length. Simple static considerations allow derivation of the line load and its perpendicular components at the fixation points and at the center of the membrane, as follows:

$$H_0 = p \left(\frac{b^2}{8h} - \frac{h}{2} \right) \quad (1)$$

$$V_0 = \frac{p \cdot b}{2} \quad (2)$$

$$Q_m = p \left(\frac{b^2}{8h} + \frac{h}{2} \right) \quad (3)$$

$$Q_0 = \sqrt{H_0^2 + V_0^2} = Q_m \quad (4)$$

$$\alpha = \arctan(V_0/H_0) = \arctan \frac{4bh}{b^2 - 4h^2} \quad (5)$$

where

b = Span (m)

h = Deformation of the membrane in the middle (m)

p = Pressure load (kPa)

H_0 = Horizontal line load on fixation (N/mm)

V_0 = Vertical line load on fixation (N/mm)

Q_m = Tension line load in the middle of the membrane (N/mm)

Q_0 = Resulting line load on fixation (N/mm)

α = Directional angle of resulting load Q_0

Obviously, a more sophisticated approach should be based on finite-element (FE) or computational fluid dynamics (hydro-codes) modeling considering the silicone sealant as a hyper-elastic material attached to the glass plate edges. However, for the purpose of deriving the key experimental parameters for sealant testing, only the simplistic approach is considered here.

Kranzer and colleagues report pressure and displacement versus time histories measured on laminated glass panes (two panes of 3-mm thick float glass laminated with 1.52-mm thick PVB film) exposed to blasts generated by high explosive field charges or pressurized air releases in shock tubes [29]. The glass area loaded by the blasts was $1.0 \times 0.8 \text{ m}^2$ and the blast impulses were designed to take the laminated glass to the point when the glass pane just crazes (referred to as the Break Safely/No Hazard level). Under these conditions, center pane displacements of around 15 mm and maximum center pane velocities of 4.9 to 7.5 m/s were measured using a noncontact, laser-optical displacement measurement technique.

Laminated glass can be made from preprocessed glass panes (annealed, heat strengthened, or fully tempered) of different structural strength (and post-breakage behavior). Furthermore, many secondary effects, such as the age of glass, scratches at the glass surface, the adherence of the laminate to the glass surface, the stiffness of mounting, the moment on the support, dry or wet

glazing, ambient temperature and humidity, etc., result in changes of the window's resistance to explosive blast [29,30]. In general, however, for laminated glass with a size of $1.0 \times 0.8 \text{ m}^2$ made from two float glass panes with an individual thickness of up to 6 mm and laminated with PVB film of up to 2.28-mm thickness, the Break Safely/No Hazard Level is achieved for a displacement ratio $h/b < 0.03$. However, much higher displacement ratios, in the range of $h/b \sim 0.2$, may be observed for high impact implosions, taking the laminated glass to GSA/ISC performance levels of 3 or 4.

Considering the above experimental blast testing information, and using Eqs 4 and 5, typical deflection angles of 4° to 40° and typical line loads in the range of 60–160 N/mm were estimated for a laminated glass of $1.0 \times 0.8 \text{ m}^2$ size. Using a range of 5 to 20 milliseconds for the positive pressure phase and the typical displacement ratios given above (h/b ratios of 0.03 to 0.2), maximum center pane velocities for successful blast tests, i.e., without the pane dislodging, are estimated to fall in the 4 to 30 m/s range. Considering the post-breakage ductility of the laminated glass at high strain rates [31], an estimate for maximum movement rates on the sealant ranged between 1 and 15 m/s. However, it should be emphasized that the cornerstones of this range represent an attempt at a conservative “educated guess;” a better defined range should be derived from direct experimental measurements.

Behavior of Silicone Sealants at High Strain Rates Relevant for Bomb Blast Mitigating Window Designs

Overview of Test Program and Sealants Tested

Three commercially available high strength structural silicone sealants, which are currently marketed for bomb blast mitigating window designs, were selected for evaluation.

Sealant A is a two-component (alkoxy cure) silicone sealant used for structural glazing applications. Sealant A complies with ASTM C1184 Specification for Structural Silicone Sealant [32].

Sealant B is a two-component (alkoxy cure) silicone sealant used for structural glazing applications. Sealant B complies with ASTM C1184 and ETAG 002 Guideline for European Technical Approval for Structural Sealant Glazing Kits [33], EN 13022 Glass in Building—Structural Sealant Glazing [34], and GB 16776-2005 Structural Silicone Sealants for Building [35].

Sealant C is a one-component neutral cure (alkoxy) silicone sealant used for structural glazing applications. Sealant C complies with ASTM C1184, ETAG 002, EN 13022, and GB 16776-2005.

Table 1 provides an overview of the test program. Different test specimens, described below, were exposed to tension, compression and shear tests as well as tests with combined tension and shear loads. Furthermore certain tension tests with glass substrates were performed after artificial aging. Movement rates of 50 mm/min (v_1), 0.5 m/s (v_2), 1.0 m/s (v_3), 2.5 m/s (v_4), and 5.0 m/s (v_5) were selected. Each test series comprised between three and six replicate specimens.

TABLE 1—Overview of test program.

Load	Test Specimen (Cross-sectional area)	Sealant	Movement Rates				
			0.00083 m/s	0.5 m/s	1.0 m/s	2.5 m/s	5.0 m/s
Tension	Type H0 (12 mm by 12 mm)	A	X	X	X	X	X
		B	X	X	X	X	X
		C	X	X	X	X	X
	Type HW after UV—Exposure (12 mm by 12 mm)	A	X
		B	X
		C	X
Compression	Type HS (12 mm by 6 mm)	B	X	X	X	X	X
	Type HL (24 mm by 12 mm)	B	X	X	X	X	X
	Type H0 (12 mm by 12 mm)	A	X	X	X
		B	X	X	X
		C	X	X	X
	Shear	Type M (12 mm by 12 mm)	B	X	X	X	X
Tension & Shear	Type L	B	X	X	X	X	X

The test specimens were assembled and allowed to cure for 28 days at ambient laboratory conditions ($23 \pm 3^\circ\text{C}$ and $50 \pm 10\%$ r.h.). The specimens were then shipped to an external, independent test laboratory for high speed testing [36], and prior to testing were conditioned at ambient laboratory conditions for a minimum of 24 hours. In total, the specimens were conditioned (cured) for a minimum of 40 days prior to the testing.

Test Specimen Configurations

Silicone sealant properties and constitutive response are often derived from specimens in which the stress fields remain parallel during uniaxial loads. Actual sealed joints in blast mitigating windows or curtainwalls, however, are exposed to extremely complicated stress fields that are still difficult to model based on the constitutive behavior of the sealant. Furthermore, the simple specimens used in deriving the constitutive response do not take adhesion or joint geometry into account; these factors need to be considered in the mathematical modeling of the actual joints. As an interim step, the authors of this paper considered various specimen configurations that mimic actual sealed joints in blast mitigating window and curtainwall designs.

Specimen Type H0 (Tension and Compression Tests)—Test specimens were fabricated as tensile adhesion joints (*H*-pieces) as described in ASTM C1135 Test Method for Determining Tensile Adhesion Properties of Structural Sealants [37] and ETAG 002 Guideline for European Technical Approval for Structural Sealant Glazing Kits with a sealed joint of dimensions 12 by 12 by 50 mm³ (width by height by length) between two (mill-finished) aluminum sub-

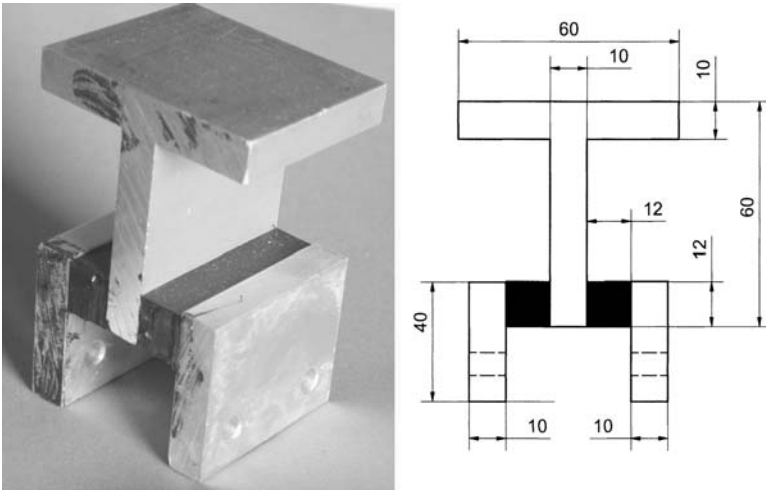


FIG. 6—Configuration and dimensions of specimen Type M (dimensions given in millimetres).

strates of dimensions 40 by 5 by 50 mm³ (width by height by length).

Specimen Type HW (Tension)—Test specimens of Type HW were of the same configuration as Type H0, however, with one of the (mill-finished) aluminum substrates replaced by a float glass plate of dimensions 40 by 6 by 50 mm³ (width by height by length).

Specimen Type HS (Tension)—The tension test specimens of Type HS were similar to those of the Type H0, however with a smaller cross-sectional area, i.e., with a sealed joint of dimensions 12 by 6 by 50 mm³ (width by height by length) between two (mill-finished) aluminum substrates of dimensions 40 by 5 by 50 mm³ (width by height by length).

Specimen Type HL (Tension)—The tension test specimens of Type HS were similar to those of the Type H0, however with a larger cross-sectional area, i.e., with a sealed joint of dimensions 24 by 12 by 50 mm³ (width by height by length) between two (mill-finished) aluminum substrates of dimensions 40 by 5 by 50 mm³ (width by height by length).

Specimen Type M (Shear)—The configuration of specimen Type M is shown in Fig. 6. The specimen configuration comprises two symmetrically arranged joints, each having sealed joint dimensions of 12 by 12 by 50 mm³ (width by height by length) between two (mill-finished) aluminum substrates.

Specimen Type L (Combined Tension and Shear)—The configuration of specimen Type L is shown in Fig. 7. The specimen configuration comprises a U-shaped joint holding two L-shaped sealed joints between two (mill-finished) aluminum substrates.

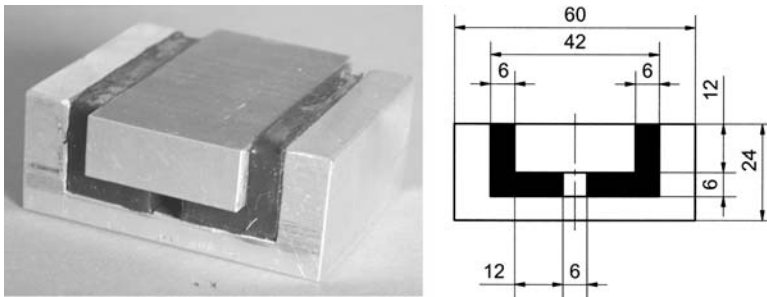


FIG. 7—Configuration and dimensions of specimen Type L (dimensions given in millimetres).

Artificial Accelerated Weathering

Prior to the tension tests, specimens of Type HW were subjected to artificial accelerated weathering according to ETAG 002, Clause 5.1.4.2.1. In this procedure, test specimens are exposed to 1000 hours of immersion in hot demineralized water with a water temperature of $45 \pm 1^\circ\text{C}$ while simultaneously undergoing irradiation by artificial light (UV, VIS, IR) through the nonimmersed upper glass plate. Immersion and light exposure was carried out in a Heraeus Xenon Test 250 T accelerated weathering device. At the beginning and the end of the weathering, the intensities of the global (300–800 nm) and ultraviolet (UV) (300–400 nm) radiation were determined. The global intensity fell from 440 W/m^2 (initial) to 437 W/m^2 (final), the UV intensity from 27.3 W/m^2 to 26.9 W/m^2 (note that ETAG002 and ISO 11431 [38], referenced in the ETAG, stipulate an irradiance at the surface of the test specimens between wavelengths of 290 nm 800 nm of $(550 \pm 75)\text{ W/m}^2$). After the test specimens were removed from the chamber they were conditioned for about 48 hours at ambient laboratory conditions prior to performing the tension tests.

Mechanical Test Procedure

The tension, compression, and shear tests at the low movement rate ($v = 50\text{ mm/min}$) were performed using a conventional, screw-driven 10 kN mechanical test machine (Zwick GmbH & Co., Ulm, Germany). For higher movement rates ($v_2 = 0.5\text{ m/s}$ to $v_5 = 5\text{ m/s}$) a 20 kN servo-hydraulic mechanical test machine (Zwick REL 1856 with a clamp speed range of 1 to 10 m/s) was used. All machines were fitted with precision strain gage load cells for continuous operation at maximum dynamic loading. Different adapters were fabricated to mount the specimens in the test equipment (see Fig. 8).

In tests with higher movement rates (v_2 to v_5) the striking cylinder of the testing machine was accelerated up to the required speed before making contact with the receptor on the specimen holder. The impact of the striker against the receptor caused an elastic compression wave (incident wave) to propagate along the specimen holder. Therefore, in the tension tests a conical attachment

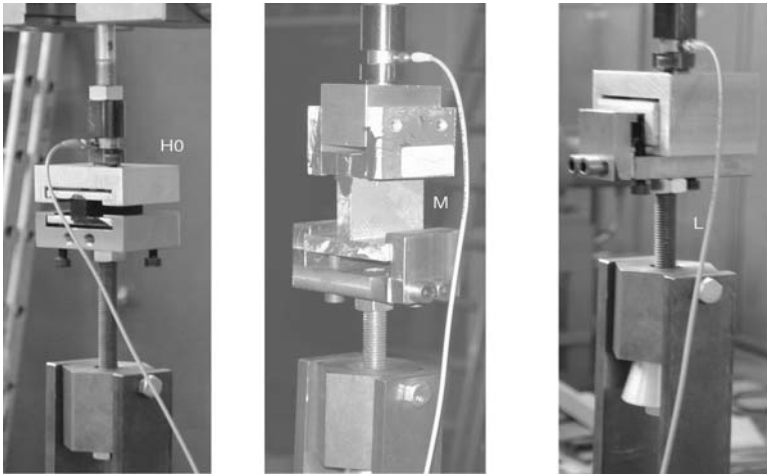


FIG. 8—Adaptors used for mounting the various specimens in the test equipment (shown from left to right: adaptors for specimens H0, M, and L).

was used as a receptor to minimize vibrations induced by the impact in the test specimen, as the vibrations, which increased with higher movement rates, interfered with the measurement of the force signal. The amplitude, frequency and damping behavior of these vibrations depended on the test setup including the adapter used and the specimen type, especially its mass, stiffness, and damping characteristics. The tensile responses of the silicone sealants were measured to the point of fracture of the specimens. The experimental setup allowed for a constant movement rate in all tension tests until rupture of the specimen occurred.

In the compression tests the striking cylinder decelerated towards the end of the test, however, the experimental setup was such that it always achieved a displacement of about 9 mm after making contact with the test specimen holder.

The ambient conditions during the test were $20 \pm 2^\circ\text{C}$ and $50 \pm 5\%$ relative humidity. The load-displacement histories were recorded by digitally measuring the signals of force $F(t)$ and displacement $x(t)$. Fast piezoelectric quartz load-cell devices were used to measure the forces at higher movement rates (v_2 to v_5). A fast noncontact optical displacement sensor was employed in the compression tests with higher movement rates (v_2 and v_3). The maximum sampling rate was 15 kHz (used at $v_5 = 5$ m/s) and the sampling rate was adjusted such that the load-displacement curves within time intervals down to below 10 ms were represented by a minimum of 100 measurement values.

The measured data were evaluated to determine the maximum stresses, σ_{\max} and τ_{\max} , and the corresponding strains ϵ_{\max} and γ_{\max} , in tension or shear, respectively, at maximum loads F_{\max} . The stresses and strains were related to the actual values of the cross-sectional area (width (W) by height (H) by length (L)) determined for each test specimen with an accuracy of ± 0.1 mm.

Tensile/shear strength:

TABLE 2—Tension test results for H0 specimen configuration at various movement rates.

Sealant	Mean Stress and Strain	50 mm/min	0.5 m/s	1.0 m/s	2.5 m/s	5.0 m/s
A	stress σ_{\max} [MPa]	1.41	2.37	2.79	3.13	3.46
	strain ε [%] at $F=F_{\max}$	72	100	155	174	180
B	stress σ_{\max} [MPa]	1.38	2.16	2.36	2.74	2.85
	strain ε [%] at $F=F_{\max}$	91	170	155	193	177
C	stress σ_{\max} [MPa]	1.02	1.90	2.06	2.25	2.44
	strain ε [%] at $F=F_{\max}$	141	214	218	235	238

$$\sigma_{\max} = F_{\max}/(W \cdot L) \quad \tau_{\max} = F_{\max}/(W \cdot L) \quad (6)$$

Strain at maximum load:

$$\varepsilon_{\max} = x_{\max}/H \times 100 \% \quad \gamma_{\max} = x_{\max}/H \times 100 \% \quad (7)$$

The maximum loads in the compression tests were given by the limits of loading devices $F_{\max} = 10$ kN and 20 kN, respectively. In this case stresses $\sigma_{50 \%}$ at strains of $\varepsilon = 50 \%$ were evaluated:

Compressive stress at $\varepsilon = 50 \%$:

$$\sigma_{50 \%} = F_{50 \%}/(W \cdot L) \quad (8)$$

Results

In general the specimens failed 100 % cohesively unless otherwise stated below. For a few specimens, imperfections due to air entrapment (bubbles) during mixing and application as well as insufficient mixing (streaking) were observed.

Tension Tests—Table 2 and Fig. 9 provide a summary of the tension test results obtained with specimen Type H0. Figure 10 shows, as a representative sample, the individual stress-strain curves measured for Sealant A at the different movement rates.

Test results for specimen Type HW were obtained after accelerated ETAG 002 weathering for all sealants at a movement rate of 5 m/s. Table 3 and Fig. 11 show a comparison of these test results with those obtained for the (unweathered) H0 specimens.

The fracture behavior of Sealant A specimens was completely cohesive in the sealed joint. For some specimens of Sealants B and C partially adhesive failure was observed between the sealant and the substrate (aluminum or glass).

For Sealant B, the effect of sealed joint cross section on the tension test results was investigated for all movement rates. Table 4 and Fig. 12 summarize the results obtained for specimen Types HL and HS in comparison to Type H0. Due to the smaller sealed joint volume the results for the specimen Type HS were considerably more affected by vibrations induced by the striker than those obtained for specimen Types HL and H0. The superimposed vibrations did not

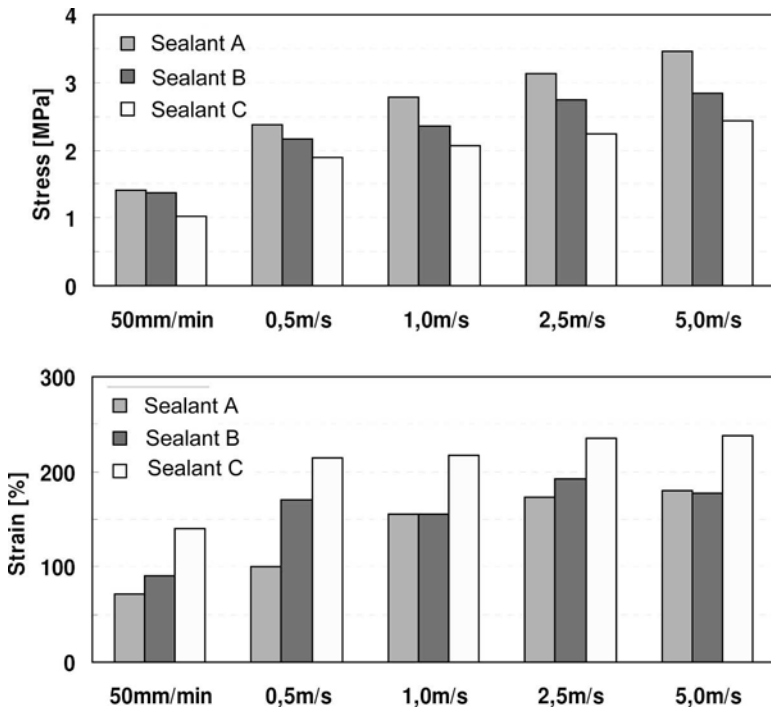


FIG. 9—Tension test results obtained with specimen Type H0.

allow a meaningful analysis of stress maxima for movement rates >1 m/s, although the stress-strain curves showed a clear trend towards increased tensile strength for higher movement rates.

Shear Test—Table 5 summarizes the results of the shear tests carried out on Sealant B using specimen Type M.

Combined Tension and Shear Test—Table 6 summarizes the results of the combined tension and shear test carried out on Sealant B using specimen Type L.

Compression Test—Table 7 summarizes the results of the compression test carried out on all sealants using specimen Type H0.

Discussion

The three silicone sealants studied all toughened and also appeared to stiffen with increasing movement rates. The toughening of the sealants results from a simultaneous increase in maximum strength and strain, which translates into substantially increased fracture energy, which corresponds to the area under the stress-strain curve. For a well-balanced blast mitigating window design, the

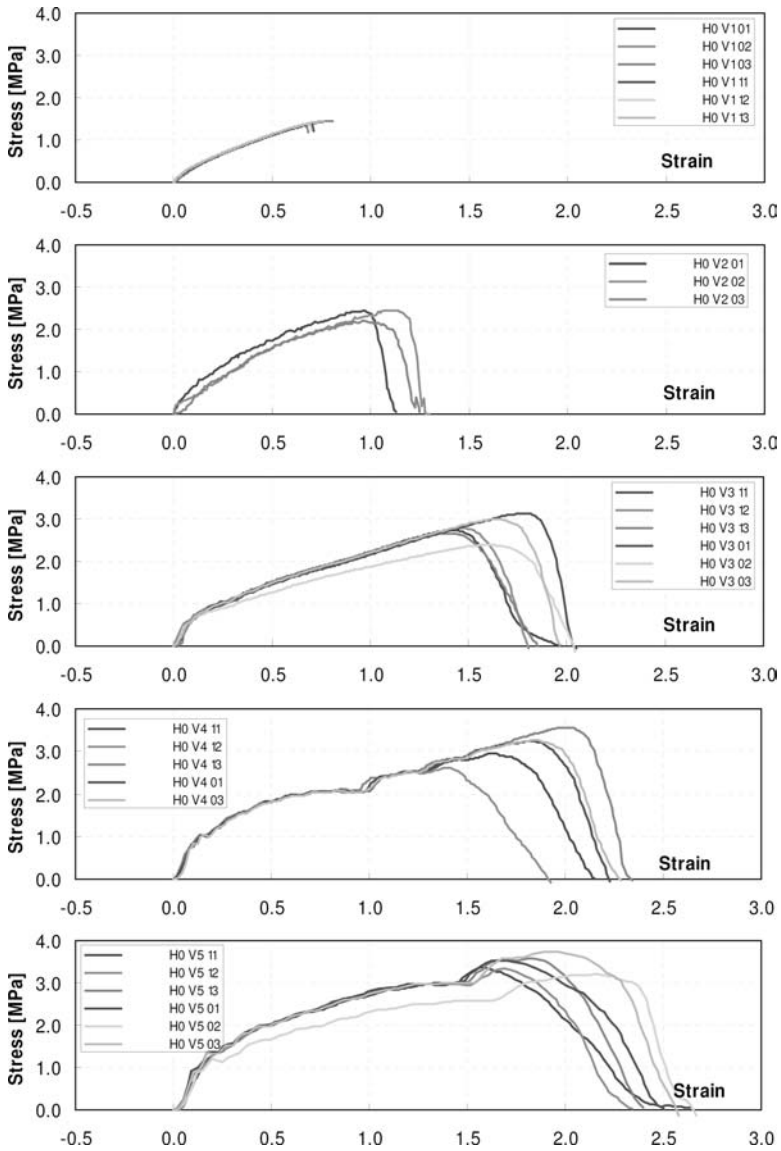


FIG. 10—Individual stress-strain curves measured for Sealant A at the different movement rates.

increased toughness results in greater blast capacity, assuming the silicone sealant represents the weakest link in the performance chain of the design.

In tension, both tensile strengths and corresponding strains increase by a factor of about 2 to 2.5 for all three sealants with an increase in movement rate from 50 mm/min to 5.0 m/s (see Tables 2 and 4 and Figs. 9 and 12). In the

TABLE 3—Tension tests results for H0 (unweathered) and HW (weathered) specimen configurations at a movement rate of 5 m/s.

Sealant	Mean Stress and Strain	H0 (Unweathered)	HW (Weathered)
A	stress σ_{\max} [MPa]	3.46	2.89
	strain ε [%] at $F = F_{\max}$	180	126
B	stress σ_{\max} [MPa]	2.85	2.46
	strain ε [%] at $F = F_{\max}$	177	168
C	stress σ_{\max} [MPa]	2.44	2.36
	strain ε [%] at $F = F_{\max}$	238	217

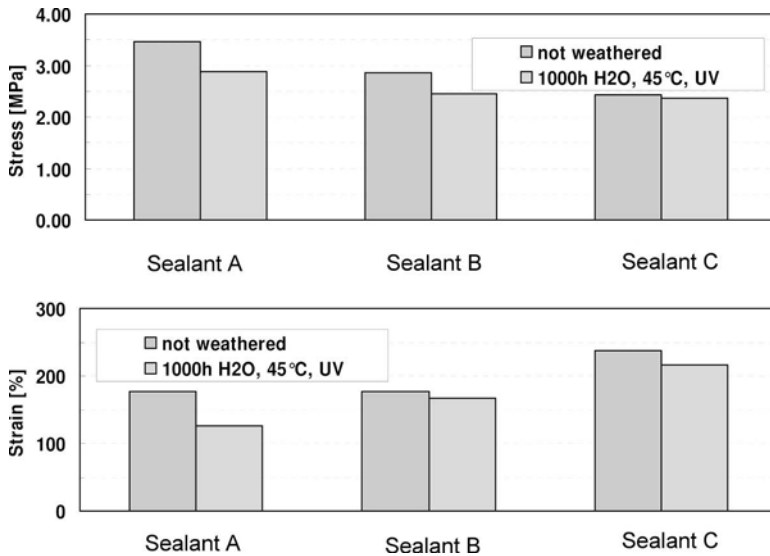


FIG. 11—Tension tests results for H0 (unweathered) and HW (weathered) specimen configurations at a movement rate of 5 m/s.

TABLE 4—Tension test results for Sealant B for different specimen configurations (H0, HL, and HS) at various movement rates (effect of sealed joint sizes).

Geometry	Mean Stress and Strain	50 mm/min	0.5 m/s	1.0 m/s	2.5 m/s	5.0 m/s
H0	stress σ_{\max} [MPa]	1.38	2.16	2.36	2.74	2.85
	strain ε [%] at $F = F_{\max}$	91	170	155	193	177
HL	stress σ_{\max} [MPa]	1.36	1.91	2.30	2.50	2.95
	strain ε [%] at $F = F_{\max}$	69	148	135	159	171
HS	stress σ_{\max} [MPa]	1.40	2.12	2.38
	strain ε [%] at $F = F_{\max}$	55	64	35

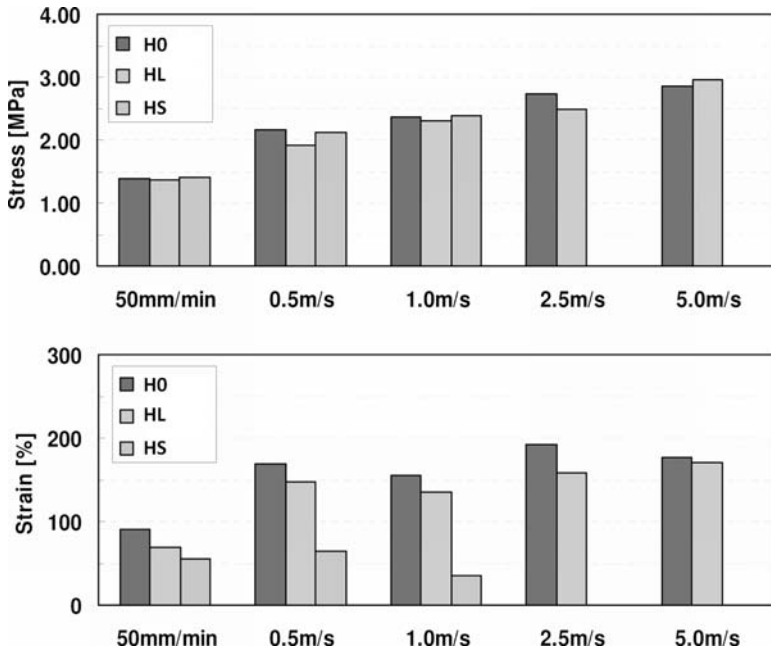


FIG. 12—Tension test results for Sealant B for different specimen configurations (H0, HL, and HS) at various movement rates (effect of sealed joint sizes).

TABLE 5—Shear test results for Sealant B obtained with specimen configuration M at various movement rates.

Geometry	Mean Stress and Strain	50 mm/min	0.5 m/s	1.0 m/s	2.5 m/s	5.0 m/s
M	stress τ_{max} [MPa]	0.64	1.46	1.74	2.09	2.22
	strain γ [%] at $F = F_{max}$	111	210	210	230	234

TABLE 6—Shear test results for Sealant B obtained with specimen configuration L at various movement rates.

Geometry	Mean Stress and Strain	50 mm/min	0.5 m/s	1.0 m/s	2.5 m/s	5.0 m/s
L	Force F_{max} [N]	2411	3384	3867	4717	5201
	Displacement u [mm] at $F = F_{max}$	3.7	6.1	7.5	7.3	7.6

TABLE 7—Mean compressive stress σ_{50} % [MPa] at strain $\varepsilon=50$ % obtained with specimen configuration H0 at various movement rates (50 mm/min to 1.0 m/s).

Sealant	50 mm/min	0.5 m/s	1.0 m/s
A	4.26	8.04	10.70
B	4.04	4.79	5.12
C	2.50	3.56	3.77

shear experiment on Sealant B, a corresponding increase in shear strength by a factor of 3.5 and strain by a factor of 2.1 is observed (see Table 5). Furthermore, in the combined shear and tension experiment carried out on Sealant B, increases in the force and displacement by factors of 2.2 and 2.1, respectively, were measured over the range of movement rates (see Table 6).

Earlier studies on the strain rate sensitivity of silicone sealants were limited to much slower movement rates (0.01 to 125 mm/min) in tension (see, for example, Ref [39] as an early study), but had found similar results.

In compression, the increase in strengths with movement rates showed a stronger dependency on the formulation of the sealants than the corresponding increases in tension, shear, or in combined load. As can be seen from Table 7, the strengths at 50 % compression increased by a factor of 2.5, 1.3, and 1.5 for Sealants A, B, and C, respectively, with an increase in movement rate from 50 mm/min to 5.0 m/s.

As can be seen from Fig. 10, an increase in movement rate typically also appeared to result in an increase in Young's modulus of the sealant.

The relation between microstructure and constitutive response of rubbers is well understood (see, for example, Ref [40]), and can be summarized as follows. The viscoelastic nature of amorphous rubbers (such as silicones above glass transition and crystallization temperatures) derives from the mobility of the polymer chain on the atomic scale (rotations between molecular units) and on the macroscopic scale (straightening of the chain between cross-links). The strain rate sensitivity reflects the timescale required for these polymer chain reorientations to take place. At low strain rates the polymer chains have sufficient time to reorientate themselves and the storage modulus of the rubber is low. At high strain rates, the deformation of the polymer chains is restricted to bending and stretching of the chemical bonds, and the storage modulus of the rubber can increase by up to three orders of magnitude.

Accelerated weathering according to ETAG 002 does have an effect on mechanical properties and adhesion of the sealants. A decrease in strengths (–3 to –17 %) and strains (–5 to –29 %) at maximum load in relation to nonweathered specimens is observed. Furthermore, while specimens of Sealant A all failed cohesively, some specimens of Sealants B and C displayed partial adhesive failure.

The geometry of the sealed joint has little effect on the maximum stress levels achieved, however, a thinner glueline (specimen Type HS) results in lower strains at maximum force.

Summary

Bomb blast mitigating window designs are clearly growing in popularity in response to increased terrorist risks. These window designs are complex with many variables affecting their performance. One essential component needed to develop a successful bomb blast mitigating window system is the silicone sealant. Only a silicone sealant can reliably meet the demands of these systems: strength to anchor the laminated or filmed glass in the frame, flexibility, long-term adhesion and proven structural glazing durability. Testing of silicone sealant in a manner simulating bomb blast conditions in terms of movement rates shows an increase in tear energy (toughness) and often also in Young's modulus. By providing data on the behavior of silicone sealants at high movement rates, a design professional is armed with information needed to innovate, model, and develop systems, which will perform successfully and hopefully save lives.

References

- [1] Elliott, C. L., Mays, G. C., and Smith, P. D., "The Protection of Buildings Against Terrorism and Disorder," *Proceedings of the Institution of Civil Engineers (ICE), Structures and Buildings*, Vol. 94, No. 3, 1992, pp. 287–297.
- [2] Hinman, E. E., Durkin, M. E., and Osteraas, J. D., "Preliminary Analysis of Casualties Resulting from the Oklahoma City Bombing," Report No. FaAA-SF-R-96-12-20, Project No. SF23049, prepared for: The Blast Injuries Study Group, Oklahoma State Department of Health, Oklahoma City, OK, prepared by: Failure Analysis Associates, Inc., Menlo Park, CA, 20th Dec. 1996.
- [3] Norville, H. S., Harvill, N., Conrath, E. J., Shariat, S., and Mallonee, S., "Glass-Related Injuries in the Oklahoma City Bombing," *J. Perform. Constr. Facil.*, Vol. 13, No. 2, 1999, pp. 50–56.
- [4] Norville, H. S., Smith, M. L., and King, K. W., "Survey of Window Glass Broken by the Oklahoma City Bomb on April 19, 1995," Glass Research and Testing Laboratory, Texas Tech University, Lubbock, Texas, 1995; Norville, H. S., Swofford, J. L., Smith, M. L., and King, K. W., "Survey of Window Glass Broken by the Oklahoma City Bomb on April 19, 1995," Revised, Glass Research and Testing Laboratory, Texas Tech University, Lubbock, Texas, 1996.
- [5] Norville, H. S. and Conrath, E. J., "Considerations for Blast Resistant Glazing Designs," *J. Archit. Eng.*, Vol. 7, No. 3, 2001, pp. 80–86.
- [6] Stewart, M. G. and Nethertona, M. D., "Security Risks and Probabilistic Risk Assessment of Glazing Subject to Explosive Blast Loading," *Reliab. Eng. Syst. Saf.*, Vol. 93, No. 4, 2008, pp. 627–638.
- [7] Chegwin, R., "Fragment Retention Window Film in the Oil and Gas Industry," *Business Briefing: Exploration & Production: The Oil & Gas Review*, 2004, pp. 46–48.
- [8] Lin, L. H., Hinman, E., Stone, H. F., and Roberts, A. M., "Survey of Window Retrofit Solutions for Blast Mitigation," *J. Perform. Constr. Facil.*, Vol. 18, No. 2, 2004, pp. 86–94.
- [9] Grosskopf, K. R., "Protective Window Safety Films: A Case Study in ASTM All-Hazard Building Code Standards," *J. ASTM Int.*, Vol. 2, No. 7, 2005, Paper ID JAI12893, available online at www.astm.org (visited 2008-06-06).

- [10] Zukas, J. A. and Walters, W. P., Eds., *Explosive Effects and Applications*, Springer-Verlag, Berlin and New York, 1998, Chapter 4.
- [11] Slater, J. E., Ritzel, D. V., and Thibault, P. A., "Development of Computational Methods and Conduct of Experimental Tests for Blast Loading Analysis," *Structures Under Shock & Impact III, The Built Environment*, Vol. 8, P. S. Bulson, Ed., Wessex Institute of Technology, and Mott MacDonald Group, UK, 1994, pp. 383–392.
- [12] Kinney, G. F. and Graham, K. J., *Explosive Shocks in Air*, 2nd ed., Springer-Verlag, Berlin and New York, 1985.
- [13] Ettouney, M. M., "Is Seismic Design Adequate for Blast?," *Society of American Military Engineers National Symposium on Comprehensive Force Protection*, Charleston, SC, Nov. 2001; and Ettouney, M. M., Smilowitz, R., and Daddazio, R., "Comparison Between Design Requirements of Earthquake and Blast Events," Paper T210-1, *Structural Engineering World Wide* (CD-ROM), Elsevier Science Ltd., Oxford, England, 1998.
- [14] Smith, D. C. and Hadden, D., "Blast Hazard Mitigation Through the Use of Performance-Specified Laminated Glazing Systems," *Glass Processing Days Conference Proceedings*, J. Vitkala, Ed., Tamglass Oy, Tampere, Finland, June 2003, pp. 419–422; available online at: <http://findarticles.com/> (visited 2008-06-04).
- [15] Hadden, D. and Lee, A., "The Role of External Façade in Protecting Building Occupants Against Terrorism and Impacts," Hong Kong Productivity Council (HKPC), *Professional Services Development Assistance Scheme, Materials Science and Technology in Engineering Conference 2005*, available online at: www.hkpc.org/hkiemat/mastec05_program_notes/Ir.Dr.%20Andy%20LEE_a.pdf (visited 2008-06-04).
- [16] Smilowitz, R. and Tennant, D., "Curtainwall Systems and Blast Loading," *Glass Magazine*, Vol. 47, No. 9, 1998, pp. 47–51.
- [17] Hadden, D., "Overview of Blast Mitigation Design Measures, Note 1-Structure and Facades," Arup Security Consulting, 13 Fitzroy Street, London, UK; available for download at: http://www.arup.com/_assets/_download/download250.pdf (visited 2008-06-04).
- [18] GSA-TS01-2003, *U.S. General Services Administration Standard Test Method for Glazing and Window Systems subject to Dynamic Overpressure Loadings*, U.S. General Services Administration (GSA), Washington, DC, 1st Jan. 2003, available for download at: <http://www.protectiveglazing.org/resources/GSA%20TEST%20Method.pdf> (visited 2008-06-04).
- [19] *ISC Security Design Criteria for New Federal Office Buildings and Major Modernization Projects*, The Interagency Security Committee, Washington, DC, 2001.
- [20] ASTM Standard F1642, 2004, "Standard Test Method for Glazing and Glazing Systems Subject to Airblast Loading," *Annual Book of ASTM Standards*, ASTM International, West Conshohocken, PA.
- [21] ASTM Standard C1564, 2004, "Standard Guide for Use of Silicone Sealants for Protective Glazing Systems," *Annual Book of ASTM Standards*, ASTM International, West Conshohocken, PA.
- [22] EN 13541, "Glass in Building, Security Glazing, Testing and Classification of Resistance Against Explosion Pressure," European Committee for Standardization (CEN), 36 rue de Stassart, B-1050 Brussels, 2001; available online at: <http://www.cen.eu/cenorm/homepage.htm> (visited 2008-06-04).
- [23] EN 13124-1, "Windows, Doors and Shutters, Explosion Resistance, Test Method, Part 1: Shock Tube," CEN, 36 rue de Stassart, B-1050 Brussels, 2001; available online at: <http://www.cen.eu/cenorm/homepage.htm> (visited 2008-06-04).

- [24] EN 13124-2, "Windows, Doors and Shutters, Explosion Resistance, Test Method, Part 2: Range Test," CEN, 36 rue de Stassart, B-1050 Brussels, 2004; available online at: <http://www.cen.eu/cenorm/homepage.htm> (visited 2008-06-04).
- [25] ISO 16933, "Glass in Building—Explosion-Resistant Security Glazing—Test and Classification by Arena Air-blast Loading," International Standardization Organization, Geneva, 2007.
- [26] ISO 16934, "Glass in Building—Explosion-Resistant Security Glazing—Test and Classification by Shock Tube Loading," International Standardization Organization, Geneva, Switzerland, 2007.
- [27] Johnson, N. F., "International Standards for Blast Resistant Glazing," *J. ASTM Int.*, Vol. 3, No. 4, 2006, Paper ID JAI12892, available online at www.astm.org (visited 2008-06-04).
- [28] Wolf, A. T., "Durability of Silicone Sealants, Durability of Building Sealants," RILEM Report 21, A. T. Wolf, Ed., RILEM Publications, Bagneux, France, 1999, pp. 253–273.
- [29] Kranzer, C., Gürke, G., and Mayrhofer, C., "Testing of Bomb Resistant Glazing Systems Experimental Investigation of the Time Dependent Deflection of Blast Loaded 7.5 mm Laminated Glass," *Glass Processing Days Proceedings*, J. Vitkala, Ed., Tamglass Oy, Tampere, Finland, 2005, pp. 497–503; available online at: <http://findarticles.com/> (visited 2008-06-04).
- [30] Haldimann, M., "Fracture Strength of Structural Glass Elements—Analytical and Numerical Modeling, Testing and Design," Ph.D. Thesis No. 3671, Polytechnic Institute of Lausanne, Switzerland, 2006.
- [31] Bennison, S. J., Sloan, J. G., Kristunas, D., Buehler, P. J., Amos, T., and Smith, C. A., "Laminated Glass for Blast Mitigation: Role of Interlayer Properties," *Glass Processing Days Proceedings*, J. Vitkala, Ed., Tamglass Oy, Tampere, Finland, 2005, pp. 494–496; available online at: <http://findarticles.com/> (visited 2008-06-04).
- [32] ASTM Standard C1184, 2005, "Specification for Structural Silicone Sealant," *Annual Book of ASTM Standards*, ASTM International, West Conshohocken, PA.
- [33] ETAG 002, *Guideline for European Technical Approval for Structural Sealant Glazing Kits*, Edition Nov. 1999, 1st amended: Oct. 2001, 2nd amended: Nov. 2005, European Organization for Technical Approvals (EOTA), 40 Avenue des Arts, Brussels, Belgium.
- [34] EN 13022, Part 1, "Glass in Building—Structural Sealant Glazing: Glass Products for Structural Sealant Glazing Systems for Supported and Unsupported Monolithic and Multiple Glazing," CEN, 36 rue de Stassart, B-1050 Brussels, 2006; available online at: <http://www.cen.eu/cenorm/homepage.htm> (visited 2008-06-04).
- [35] GB 16776, "Structural Silicone Sealants for Building," Standardization Administration of China (SAC), 2005; available online at [CSSN-China Standards Information Center: http://www.cssn.net.cn/index.jsp](http://www.cssn.net.cn/index.jsp) (visited 2008-06-04).
- [36] Krüger, G., "Mechanical Tests on Structural Silicone Joints at Higher Load Velocities Up to 5 m/s, Client Confidential Test Report," MPA University of Stuttgart, Otto-Graf-Institute, Department Light Weight Construction, Glass Construction, Facades, 70569 Stuttgart, Germany (July 25, 2007).
- [37] ASTM Standard C1135, 2005, "Test Method for Determining Tensile Adhesion Properties of Structural Sealants," *Annual Book of ASTM Standards*, ASTM International, West Conshohocken, PA.
- [38] ISO 11431, "Building Construction—Jointing Products—Determination of Adhesion/Cohesion Properties of Sealants after Exposure to Heat, Water and Artificial Light through Glass," International Standardization Organization, Geneva, Switzerland, 2002.

- [39] Karpati, K. K., "Mechanical Properties of Sealants: II. Behavior of a Silicone Sealant as a Function of Rate of Movement," *J. Paint Technol.*, Vol. 44, No. 569, 1972, pp. 58-65.
- [40] Ferry, J. D., *Viscoelastic Properties of Polymers*, 2nd ed., John Wiley & Sons, New York, 1970.

Noriyoshi Enomoto,¹ Akihiko Ito,² and Kyoji Tanaka³

Quantification of Effect of Enforced Cyclic Movement and Regional Exposure Factors on Weatherability of Construction Sealants

ABSTRACT: This paper presents information on the weatherability of construction sealants based on a newly developed test specimen design that allows simultaneous exposure of the sealant to forced compression and extension movement in a single specimen. In this study, exposure to cyclic movement and weathering is carried out simultaneously. Furthermore, an evaluation method for surface cracks induced by weathering is presented that allows an assessment of the overall “degree of degradation,” a single number characterizing the state of degradation of the sealant surface. In order to study the effects of the extent of extension and compression as well as the regional exposure factors on the degree of degradation, twelve sealants were exposed to outdoor weathering for four years at three exposure sites, located in the northern, central, and southern areas of Japan. The evaluation of surface cracks was carried out according to the rating provided in ISO 4628-4, with the modification that new rating criteria were introduced to evaluate minute cracks. A mathematical equation determining the “degree of degradation” was obtained for each sealant, which is based on a component reflecting aging under static condition and another component reflecting the dynamic conditions induced by mechanical movement and regional exposure factors. This equation provides a reasonable relationship between the experimental observation and calculated degradation over the exposure period.

Manuscript received July 2, 2008; accepted for publication November 18, 2008; published online January 2009.

¹ Sunstar Engineering Inc., Yamanashi, Japan.

² Auto Chemical Industry, Co., Ltd., Ibaragi, Japan.

³ Tokyo Institute of Technology, Yokohama, Japan.

Cite as: Enomoto, N., Ito, A. and Tanaka, K., “Quantification of Effect of Enforced Cyclic Movement and Regional Exposure Factors on Weatherability of Construction Sealants,” *J. ASTM Intl.*, Vol. 6, No. 2. doi:10.1520/JAI101949.

Copyright © 2009 by ASTM International, 100 Barr Harbor Drive, PO Box C700, West Conshohocken, PA 19428-2959.

KEYWORDS: sealant, weatherability, regional factor, joint movement, out-door exposure

Introduction

A construction sealant is a material used to maintain the waterproof and airtight functions of a joint over the long term, and the weatherability of the sealant is an important performance criterion for maintaining these functions. Although the degradation of sealants in the outdoors proceeds by UV irradiation, heat, water, and many factors in general, the dynamic movement to which the sealant is exposed in actual joints accelerates the degradation.

The quantification of the surface degradation on a particular exposure site [1] was reported by using the newly devised test specimen [2].

The purpose of this study is to evaluate the extent to which the geographic location of exposure influences the surface degradation by carrying out the exposure test at three different sites in Japan.

Experimental Procedures

Sealants and Tested Sealants

Eight sealants, commercially available in Japan (see Table 1), which are conforming to JIS A 5758 [3] and are tested in accordance with JIS A 1439 [4], were used to carry out the exposure test.

The configuration of the test specimen that enabled exposure of the sealant to continuous degrees of extension and compression in a single specimen is shown in Fig. 1.

TABLE 1—*Sealants tested.*

Sealant	Mark	Physical Properties ^a		
		50 %M. (N/mm ²)	Tensile Strength (N/mm ²)	Elongation (%)
2 part Silicone	SR-2	0.14	0.81	1170
2 part Polyisobutylene	IB-2	0.11	0.38	490
2 part Modified Silicone (General Purpose type)	MS-2 (GP)	0.15	0.49	650
2 Part Modified Silicone (Stress Relaxation type)	MS-2 (SR)	0.12	0.43	480
1 part Modified Silicone	MS-1	0.12	0.56	560
2 part Polysulfide	PS-2	0.14	0.40	550
2 part Polyurethane	PU-2	0.15	0.53	570
1 part Polyurethane	PU-1	0.14	1.03	950

^aPhysical Properties: based on JIS A 1439.

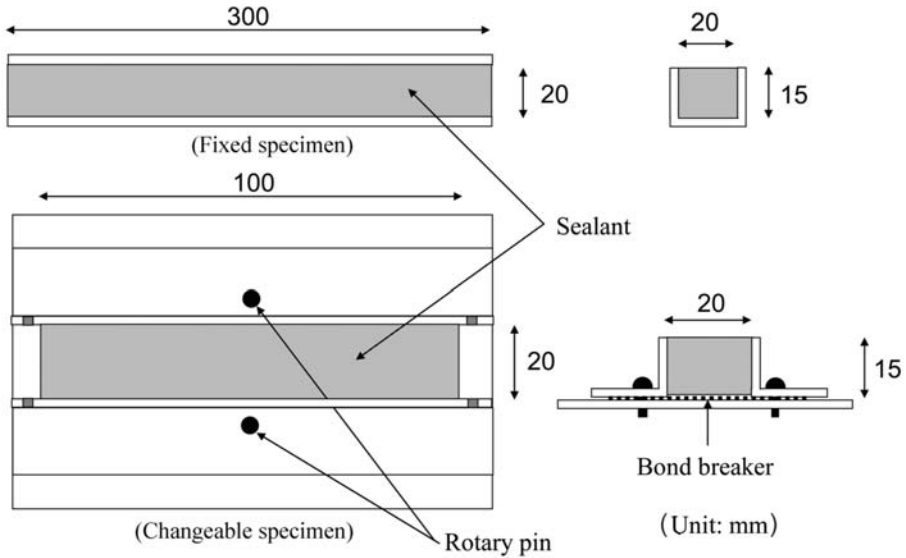


FIG. 1—Test specimen.

Outdoor Exposure Conditions

The exposure test was carried out at three sites in Japan. The exposure conditions and a summary of the weather indicators at the exposure sites are given in Tables 2 and 3, respectively. The test specimens were exposed to both static and dynamic conditions, i.e., the static condition was without any movement and the dynamic condition exposed the specimen to extension and compression cycles that were periodically reversed once every month. The evaluation of surface degradation on the specimen was determined at four locations on the sealant surface, i.e., for the statically exposed specimens at $\pm 0\%$ movement amplitude, and for the dynamically exposed specimens at $\pm 1.5\%$, $\pm 15\%$, and $\pm 25\%$ movement amplitude. The center of the dynamically exposed specimen was undergoing a movement of $\pm 1.5\%$ due to the offset between the rotary pin and the edge of the specimen.

TABLE 2—Exposure conditions.

Location of Exposure	Term of Exposure	Direction/ Angle	Interval of Extension/Compression Exchange	Position of Evaluation
North			None (Static)	$\pm 0\%$
Central	Oct. 1, 2002 ~ Sept. 31, 2006	South/45°	Twice/week (Dynamic)	$\pm 1.5\%$ $\pm 15\%$
South				$\pm 25\%$

TABLE 3—Summary of weather indicators.^a

		North	Central	South
Temperature (°C)	Max.	33.6	28.8	33.1
	Min.	-25.5	-2.1	13.5
	Ave.	6.6	14.2	23.7
Accumulated total solar radiation (0° · M/Jm ²)		16,962	20,345	22,694
Accumulated precipitation (mm)		3,994	7,156	8,392

^aTerm: Oct. 1, 2002 to Sept. 31, 2006.

Evaluation

Determination of Degradation

The determination of the degradation was based on the rating scheme provided in ISO 4628-4 [5] with additional rating criteria introduced to determine the influence of minute surface cracks (see Tables 4 and 5 as well as Fig. 2).

Evaluation of Degree of Degradation

The degree of degradation (*QS*-value) is based on the product of the rating of Quantity (*Q*) and Size (*S*) of cracks as shown in Eq 1. The approximate relationship between the *QS*-value and the surface condition is indicated in Fig. 3. The digital photos of the cracked sealant surfaces given in Fig. 4 illustrate the effectiveness of the *QS*-value to assess the state of degradation of the sealant.

$$QS(t) = Q(t) \times S(t) \quad (1)$$

where *QS*(*t*) is the *QS*-value after *t* months, *Q*(*t*) is the rating of *Q* after *t* months, and *S*(*t*) is the rating of *S* after *t* months.

TABLE 4—Crack rating index of quantity.

Rating	Quantity of Cracks (<i>Q</i>)
0	None
0.5 ^a	Trace
1	Very few
2	Few
3	Moderate
4	Considerable
5	Dense

^aNewly introduced rating.

TABLE 5—Crack rating index of size.

Rating	Size of Cracks (S)
0 ^a	Not visible × 100 magnification
0.3 ^a	Only visible under magnification up to × 50
0.5 ^a	Only visible under magnification up to × 30
1	Only visible under magnification up to × 10
2	Just visible with normal corrected vision
3	Clearly visible with normal corrected vision
4	Large cracks generally up to 1 mm wide
5	Very large cracks generally more than 1 mm wide

^aNewly introduced rating.

Test Results

The changes in the QS-value for the different sealants are provided in Fig. 3. A summary of the test results is given below.

1. Although the degree of degradation increases with an increase in the extent of extension and compression, the degree to which this change occurs with an increasing extent of extension and compression depends on the type of sealant.
2. The two-part silicone sealants did not show surface degradation for any of the test conditions.

Discussion

Model of QS-Value Change

A three-dimensional model (response surface) of the QS-value as a function of exposure time and extent of extension and compression was generated from the test results as shown in Fig. 5.

Based on Fig. 6, the equation for the QS-value can be stated as shown in Eq 2.

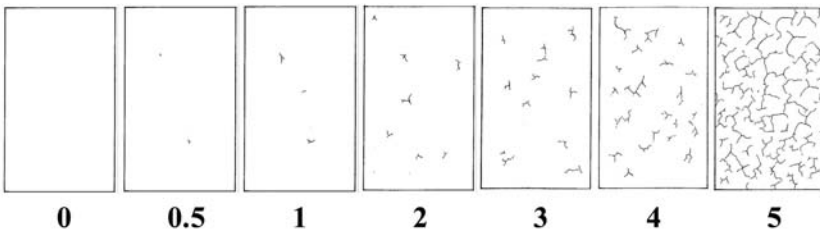


FIG. 2—Crack patterns for quantity.

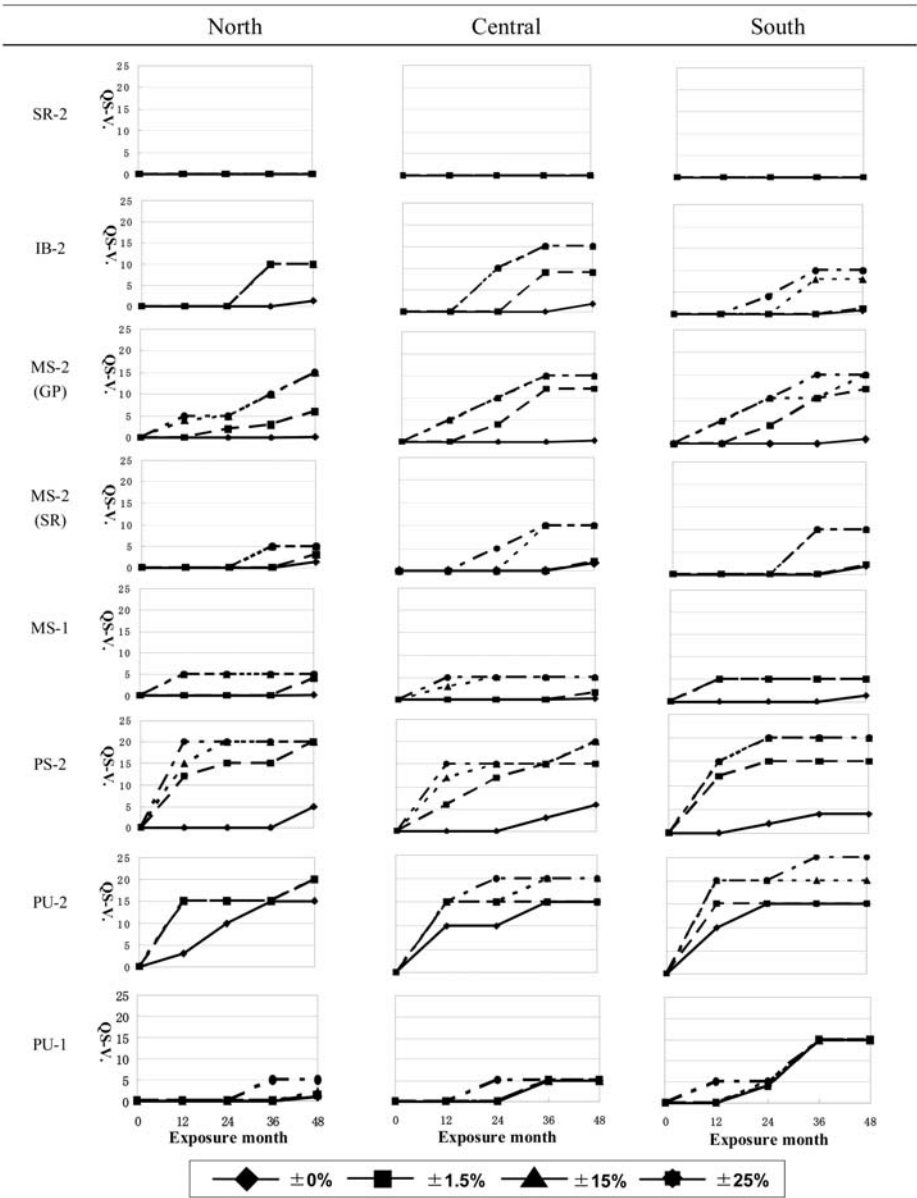


FIG. 3—Change of QS-value of sealants.




QS value	State of Degradation
25	 Serious Degradation
20	
15	 Medium Degradation
10	
5	 Slight Degradation
0	
	Little Degradation

FIG. 4—Surface degradation condition rating.

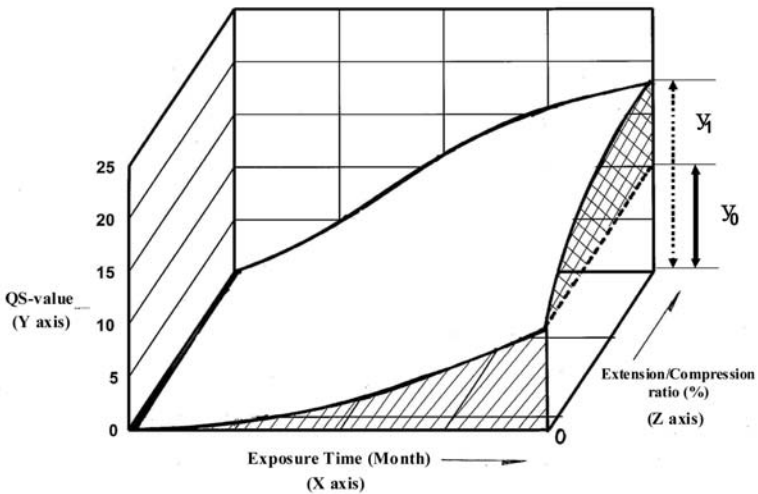


FIG. 5—Response surface model of dependency of QS-value on exposure time and degree of extension/compression.

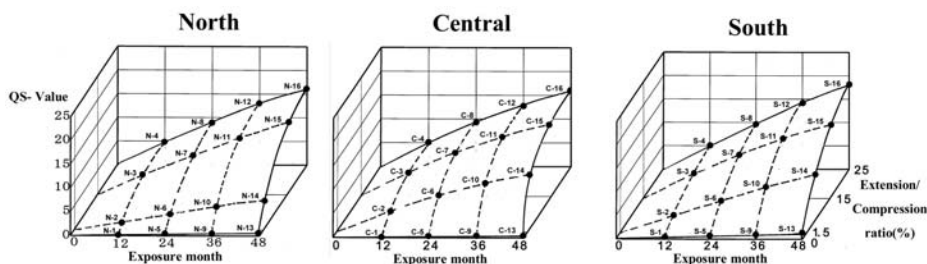


FIG. 6—Model of QS-value change in each exposure site.

$$QS(\varepsilon \cdot t) = QS_0(t) \times B = (a \cdot t^b) \times (1 + c \cdot \varepsilon^d) \tag{2}$$

where $QS(\varepsilon \cdot t)$ is the QS-value at ε % after t months, $QS_0(t)$ is the QS-value under static condition after t months, t is the exposure duration (in months), ε is the extent of extension and compression ratio, and a , b , c , and d are constants.

Dependency of QS-Value on Geographic Exposure Location

The changes of QS-value with exposure location can be approximated by Eq 3, in which the factor R provides a relative comparison between the specific exposure site and the central (reference) site. The relative comparison factor is calculated by dividing the QS-value of the specific exposure site by the QS-value of the central (reference) site as shown in Eq 4 and Fig. 6.

The equation of the central site derived for each sealant is given in Table 6, and the relative comparison factors of the specific exposure sites are shown in Fig. 7.

TABLE 6—Equation of each sealant at central site.

Sealant	Equation for $QS(\varepsilon \cdot t)$
SR-2	$QS(\varepsilon \cdot t) = (0 \cdot t^{1.0}) \times (1 + 0 \cdot \varepsilon^{1.0})$
IB-2	$QS(\varepsilon \cdot t) = (0.04 \cdot t^{4.0}) \times (1 + 2.2 \cdot \varepsilon^{0.5})$
MS-2(GP)	$QS(\varepsilon \cdot t) = (0.006 \cdot t^{3.0}) \times (1 + 27.4 \cdot \varepsilon^{0.3})$
MS-2(SR)	$QS(\varepsilon \cdot t) = (0.04 \cdot t^{4.0}) \times (1 + 0.3 \cdot \varepsilon^{0.9})$
MS-1	$QS(\varepsilon \cdot t) = (0.06 \cdot t^{4.0}) \times (1 + 5.4 \cdot \varepsilon^{0.4})$
PS-2	$QS(\varepsilon \cdot t) = (0.4 \cdot t^{0.6}) \times (1 + 1.5 \cdot \varepsilon^{0.3})$
PU-2	$QS(\varepsilon \cdot t) = (1.3 \cdot t^{0.7}) \times (1 + 0.07 \cdot \varepsilon^{0.7})$
PU-1	$QS(\varepsilon \cdot t) = (0.2 \cdot t^{0.9}) \times (1 + 0.003 \cdot \varepsilon^{2.2})$

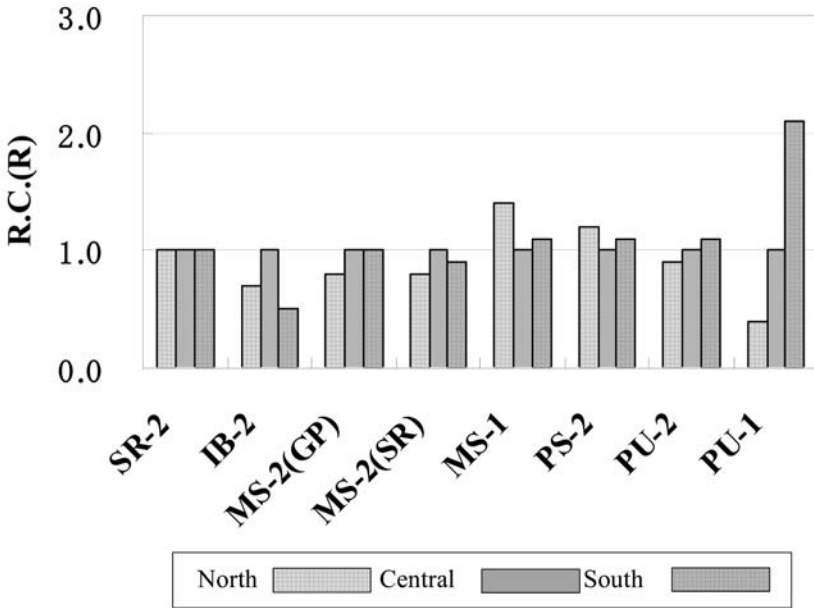


FIG. 7—Relative comparison factor for each sealant.

$$QS(\varepsilon \cdot t) = R \times \{(a \cdot t^b) \times (1 + c \cdot \varepsilon^d)\} \tag{3}$$

where R is the relative comparison factor.

$$R = \text{Average of } QS\text{-value}_{[each\ site]} / QS\text{-value}_{[central\ site]} \tag{4}$$

Relationship between Observation and Calculation

The relationship between observed QS -values and those calculated are shown in Fig. 8.

Conclusions

The following conclusions can be drawn from this study:

1. The equation for the QS -value of each sealant shows a reasonable correlation between the experimental observation and the calculated value for each exposure site.
2. Although the one-part polyurethane sealant shows a dependency of the degradation on the location of the exposure site (which matches the commonly held opinion that degradation is affected by the exposure location), the surface degradation of the other sealants does not show many differences between exposure locations.

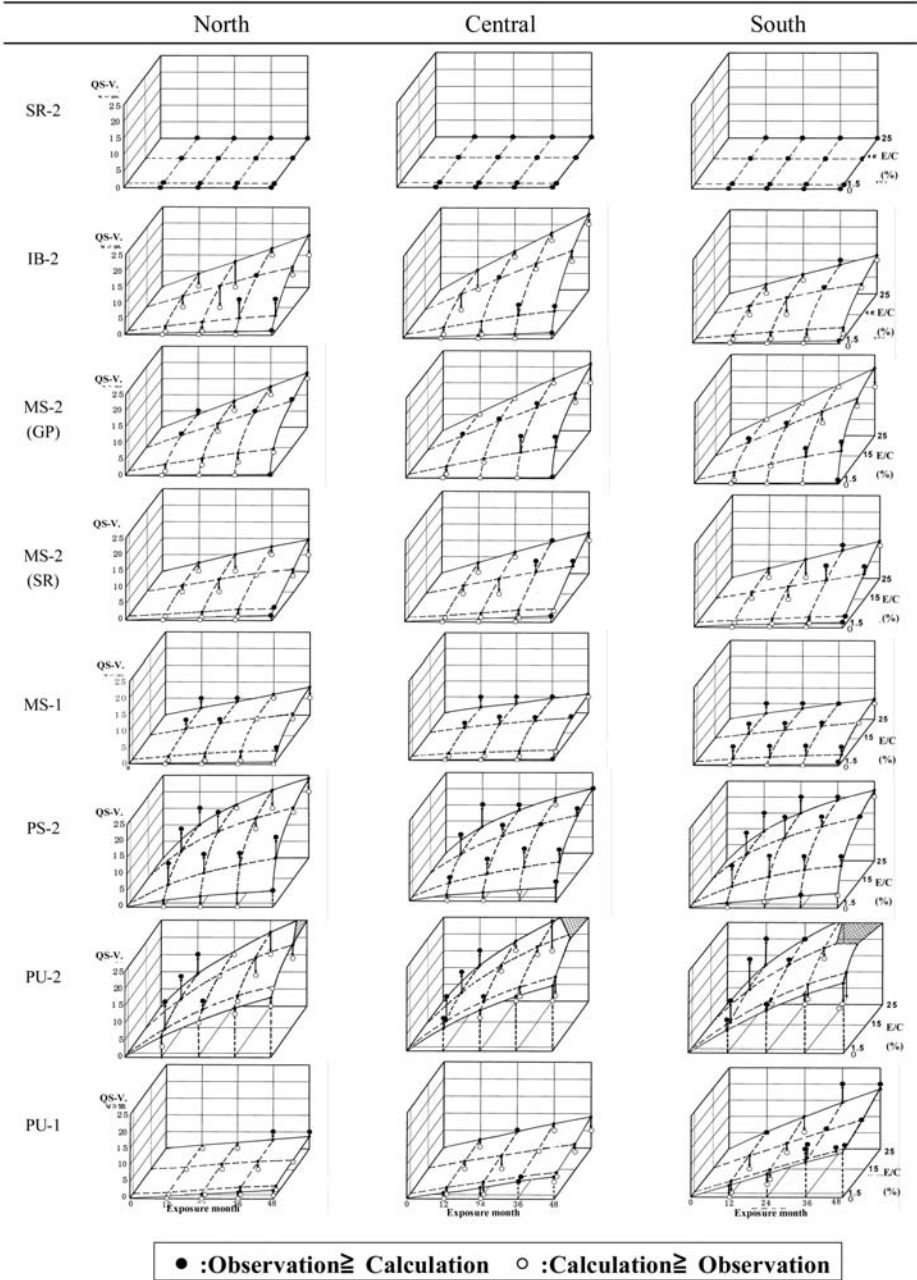


FIG. 8—Relationship between observation and calculation.

References

- [1] Enomoto, N. and Tanaka, K., "Quantification of Effect of Dynamic Movement for Weatherability of Construction Sealants," *Durability of Building Materials & Components*, 2008, pp. 713–720.
- [2] Enomoto, N. and Tanaka, K., "New Test Specimen and Method for Evaluation of Weatherability of Sealants," *Architectural Institute of Japan*, 2006, pp. 17–22.
- [3] JIS A 5758:2004, "Sealants for Sealing and Glazing in Buildings," Japan Industry Standard.
- [4] JIS A 1439:2004, "Testing Methods of Sealants for Sealing and Glazing in Buildings," Japan Industry Standard.
- [5] ISO 4628-4:2003, "Paints and Varnishes—Evaluation of Degradation of Coatings—Designation of Quantity and Size of Defects, and of Intensity of Uniform Changes in Appearance—Part 4: Assessment of Degree of Cracking."

Glenn V. Gordon,¹ Loren D. Lower,¹ and Lawrence D. Carbary¹

Using Rheology Test Methods to Assess Durability of Cured Elastomers Undergoing Cyclic Deformation

ABSTRACT: The current measurement test method to assess elastomeric sealant durability is ASTM C719. This method requires a minimum of five weeks of curing and conditioning before being subjected to ten movement cycles at room temperature and then ten movement cycles at variable temperatures. This method is a fine predictor of sealant movement capability for products used in moving joints in commercial construction applications. ASTM E1886 suggests that building assemblies be subjected to 9000 cycles of wind pressure. Sealant materials are typically used to anchor glazing assemblies into frames, and the choice of the correct sealant is critical to passing the test criteria specified in ASTM E1866. Rheological instruments have the capability to characterize the dynamic mechanical behavior of elastomeric materials undergoing oscillatory (cyclic) deformation under controlled test conditions and, therefore, provide a laboratory tool for assessing durability. Cyclic testing can be conducted under controlled strain (deformation) conditions at frequencies that simulate joint movement due either to thermal expansion differentials or seismic events, or under controlled stress (load) that model hurricane-force wind loads or design pressures. An immediate stress-softening response was observed from controlled-strain experiments at 15 % movement that was ascribed to the Mullins effect; however, three of the four cured silicone sealants exhibited a modest recovery over the remaining four days of cyclic testing. Under controlled-stress cycling at 0.138 MPa for 150 minutes at 0.5 Hz, the silicones exhibited ultimate deformations well below their rated movement capabilities. The results from both types of

Manuscript received June 23, 2008; accepted for publication January 26, 2009; published online March 2009.

¹ Dow Corning Corporation, 2200 W. Salzburg Road, Midland, MI 48686-0994.

Cite as: Gordon, G. V., Lower, L. D. and Carbary, L. D., "Using Rheology Test Methods to Assess Durability of Cured Elastomers Undergoing Cyclic Deformation," *J. ASTM Intl.*, Vol. 6, No. 3. doi:10.1520/JAI101975.

Copyright © 2009 by ASTM International, 100 Barr Harbor Drive, PO Box C700, West Conshohocken, PA 19428-2959.

rheology test methods did not reveal outward signs of fatigue and suggest which elastomeric materials will perform better under the drastic cycling that occurs in ASTM E1866 and ASTM C719 testing.

KEYWORDS: cycling, deformation, durability, elastomers, movement, rheology, rheometry, sealant, silicone

Introduction

Durability evaluation of sealant-materials is a science unto itself. The existing assessments of sealant durability include the ASTM C719-93 “Standard Test Method for Adhesion and Cohesion of Elastomeric Joint Sealants under Cyclic Movement (Hockman Cycle)” [1], “JIS-A 5758 Sealing Compounds for Sealing and Glazing in Buildings” [2], and “ISO 9047:2003 Building construction—Jointing products—Determination of adhesion/cohesion properties of sealants at variable temperatures” [3]. These methods use a block of sealant approximately 12 mm by 12 mm by 50 mm extruded between two parallel plates made from a selection of available substrate material(s). The sealant is allowed to cure and the adhesion and cohesion properties are evaluated after extension and compression cycles. For example, ASTM C719 requires a minimum of five weeks of curing and conditioning before being subjected to ten movement cycles at room temperature and then ten movement cycles at variable temperatures. These methods are used by the global industry to assess movement capability of high performance sealants. Other custom assessments of durability use the same joint design and will subject the specimens to conditions that are specified in structural glazing specifications such as the European Organization for Technical Approval (EOTA) ETAG 002 Guideline for European Technical Approval for Structural Sealant Glazing Systems [4] and ASTM C1184-00a Standard Specification for Structural Silicone Sealants [5]. These specifications assess the properties of structural sealants after aging in environments such as salt fog, water immersion, heat, cold, hot water, and SO₂ environments by comparing the stress-strain properties and adhesion to control samples.

After Hurricane Andrew blew by South Florida in 1992, the destruction and devastation that occurred prompted the development of glazing standards for the hurricane-prone areas in the United States. ASTM E1886-02 “Standard Test Method for Performance of Exterior Windows, Curtain Walls, Doors, and Impact Protective Systems Impacted by Missile(s) and Exposed to Cyclic Pressure Differentials” [6] proposes that building assemblies be subjected to a total of 9000 cycles of wind pressures after the glazing is impacted with specified flying debris, simulating hurricane conditions. This full-scale test requires the proper glazing, frame design, and structural attachment of the glazing. The spirit of the test is to ensure that the glazing remains in the frame after being impacted during a hurricane. When the glazing remains in the frame after the impact event, the interior of the building is protected from the windblown debris and rain damage that can occur.

ASTM E1886 requires the sealants, framing system, and glazing system to harmoniously perform for the duration of the test. This harmonious performance has several times been a study in trial and error. There is no sealant

durability test that really predicts the performance of a sealant in this full size assembly. This paper is an attempt to take a different approach to determining a method that can predict sealant performance undergoing either strain- or stress-dependent movement cycles.

Rheology, the study of the deformation and flow of matter, provides test methods to determine material functions that describe the viscous or elastic response of a material. For example, a rheology test method was applied to examine the temperature dependence of the dynamic tensile properties of various sealants as a diagnostic tool in durability assessment [7]. Building upon this data, an attempt is made to further understand the use of this tool to predict durability of elastomeric materials.

Rheometry

Two types of rheometers used as laboratory research tools have historically been commercially available: controlled-strain or controlled-stress instruments. In the former, strain—represented by γ for shear deformation—is defined as the input test parameter and stress σ is the output response based on the geometry of the test material; in the latter, a force (or load) is the controlled parameter and the corresponding deformation is measured. The current state-of-the-art instrumentation allows for both types of control from a single instrument, handles a wide range of samples, and provides a footprint that requires minimal laboratory space.

Rheological instruments have the capability to characterize the stress-strain behavior, transient properties such as creep and stress relaxation, and dynamic mechanical behavior of elastomeric materials undergoing oscillatory (cyclic) deformation. The modes of deformation include tensile, compression, bending, torsion, and shear. Therefore, rheometry would appear a suitable test method overall for characterizing the properties of cured elastomers including sealants and adhesives.

Rheometers capable of oscillatory testing provide a tool for assessing the durability of a material in terms of fatigue resistance. Cyclic testing can be conducted under (1) controlled strain (deformation) at low frequencies to simulate joint movement due to thermal expansion differentials or at intermediate frequencies (1 to 10^3 Hz) corresponding to seismic events, and (2) controlled stress at frequencies that model hurricane-force wind loads or design pressures. Although a sinusoidal waveform, shown schematically in Fig. 1, is the default standard for defining a dynamic deformation cycle, arbitrary waveforms can be programmed in some instruments including the (1) triangular waveform in ASTM C719, (2) square waveform found to relate to real joint movements at constant temperature [8], and (3) trapezoidal waveform being recommended in current RILEM durability test methods [9]. A sinusoidal waveform may also be viewed as a suitable representation of both daily and monthly temperature cycles. Figure 1 depicts an output sinusoidal response lagging the input pulse if the material being tested was not completely elastic.

A rheological instrument [10] can be accessorized or lend itself to be custom-modified to expose a test specimen to a controlled (oxidizing, inert, or pressurized) atmosphere either at a constant temperature or a dynamic range

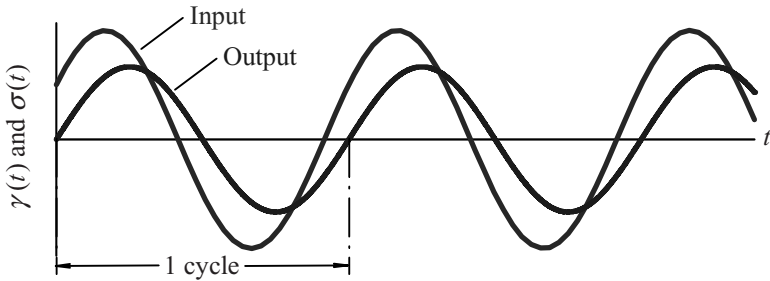


FIG. 1—A sinusoidal waveform used in cyclic testing in shear deformation mode where the output response will lag the input pulse if the test material was not completely elastic.

anywhere from -170°C to 1000°C , controlled humidity between 5°C to 80°C , total immersion in fluid media, or ultraviolet or visible radiation energy. Rheometers that accommodate disposable geometry fixtures provide the option of defining a desired size for the test specimen, constructing substrates from different materials, or allowing test specimens to be cured off-line. Using smaller fixtures will shorten the time required to fully cure and condition one-part RTV sealants, for example.

Experimental

Materials

Table 1 summarizes the four moisture curing materials used for this work: a pair of one-part RTV and a pair of two-part structural silicone sealants. The listed movement capability that ranged from 12.5 % for the two-part sealants to 50 % was determined following ASTM C719. Each test specimen was allowed to cure in situ, to optimize material-substrate contact with the rheometer plate fixtures, at ambient conditions (23°C and 40 % RH) for one week under static conditions. For future considerations and in the event that proposed standard testing parameters are established [11], rheometers can also be used to cure specimens under dynamic conditions while simultaneously measuring its change in rheological properties over time.

TABLE 1—Description of moisture curing silicone sealants.

Sealant Designation	Type	Si Cure Chemistry	Rated Movement Capability, %	Shear Modulus, MPa
A	One-part	Acetoxy	25	0.4
B	One-part	Alkoxy	50	0.7
C	Two-part	Alkoxy	12.5	1.5
D	Two-part	Alkoxy	12.5	1.4

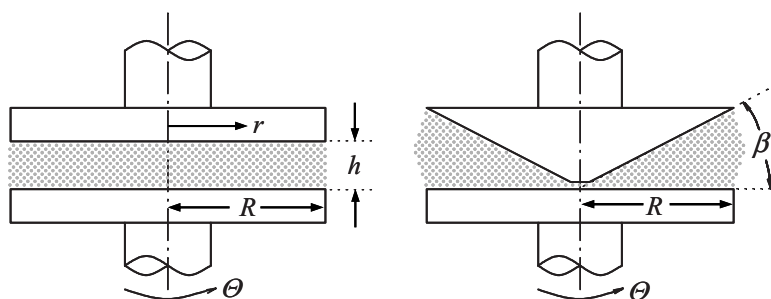


FIG. 2—Schematic diagrams for parallel-plate (left) and cone-and-plate (right) geometries with a plate radius R .

Using dimensions defined by the rheometer fixtures described in the next section, full cure of the 8-mm diameter test specimens under ambient conditions (22°C , 40 % RH) was predicted to be 73 ± 25 h and 81 ± 10 h for the one-part RTV sealants A and B, respectively. This was based on preliminary in-house experiments using (1) rheometry to monitor the modulus build up to an asymptotic (full cure) value using small-amplitude deformation (1 % strain), and (2) cure-in-depth measurements of one-part RTV sealants. After the seven-day cure period, the environmental test chamber for the rheometer was engaged to compartmentalize the test setup and the cured sealant was allowed to equilibrate at 25°C for 24 hours. A preliminary stress-strain test was conducted to approximate the shear modulus of the elastomer (Table 1).

Instruments

Rheometers—TA Instruments (New Castle, DE) Advanced Rheometric Expansion System (ARES) controlled-strain and AR550 controlled-stress rotational rheometers were used to conduct post-cure dynamic deformation experiments. The full-scale torque was $200 \text{ mN}\cdot\text{m}$ and $50 \text{ mN}\cdot\text{m}$ for the ARES and AR550, respectively. In dynamic testing mode, the frequency range capability of the ARES and AR550 was 10^{-5} to $500 \text{ rad}\cdot\text{s}^{-1}$ ($10^{-5.8}$ to 80 Hz) and $10^{-3.2}$ to $250 \text{ rad}\cdot\text{s}^{-1}$ (10^{-4} to 40 Hz), respectively. The ARES was equipped with a forced (air or N_2) convection oven while the AR550 used a controlled convection/radiant-heating environmental chamber.

Plate Geometries—Rotational rheometers are typically accessorized with two different plate geometries shown schematically in Fig. 2. Plate geometry fixtures with a radius R of 4 mm were used to impose a shear deformation, represented in Fig. 2 by the angular displacement Θ , on the test specimens based on the instrument design specifications, the modulus of rigidity of the cured sealants, and the testing parameters. The parallel-plate fixture was the primary geometry used. It had the advantage of allowing for a gap h between the plates, corresponding to the specimen thickness, to be specified, which can be useful if a certain aspect ratio of the test specimen is desired. In this work,

the thickness of the sealant test specimens was approximately 1.5 mm. An autotension capability allowed the gap to be adjusted automatically during the cure cycle to compensate for forces generated as a result of volume shrinkage from leaving reaction by-products. The ARES was equipped with plates constructed from stainless steel whereas a stainless steel upper plate and aluminum bottom plate was utilized with the AR550. Both rheometers had the option of using disposable plate fixtures constructed from different materials.

A cone-and-plate geometry was used in controlled-strain experiments with the ARES rheometer to validate the results obtained with the parallel plates. The cone angle β was 0.0999 radians and the cone tip was truncated to a gap of 0.044 mm. This truncation gap needed to be maintained regardless of temperature, which, unlike the parallel plate geometry, did not permit the thickness of the test specimen to be varied.

Discussion

Shear Deformation

The parallel-plate geometry imposes a torsional deformation; the strain on the material varies from zero at the center to a maximum at the rim (edge) of the moving plate. Therefore, the deformation geometry is defined by plate radius R and the gap h between the plates such that the maximum shear strain on a test specimen arising from an angular displacement Θ relative to its initial state of rest is

$$\gamma_R = \frac{R}{h} \Theta \quad (1)$$

This is not the case for the cone-and-plate geometry where, for cone angles $\beta < 6^\circ$, the variation in shear strain across the plate radius is less than 1 % [12] such that the following approximation holds

$$\gamma = \frac{\Theta}{\beta} \quad (2)$$

The mathematical relationship between γ and joint movement can be derived following the schematic diagram in Fig. 3. A unit volume originally at rest, represented by the solid line, is deformed by shearing its top surface resulting in a change of shape denoted by the dotted line. Noting that the bottom surface remains fixed, shear strain is the ratio of the change in shape defined by the displacement Δ to the height of the unit volume h

$$\gamma = \Delta/h \quad (3)$$

If joint movement can be defined as $m \times 100\%$, then geometrically according to the Pythagorean theorem

$$[(1 + m)h]^2 = h^2 + \Delta^2 = h^2 + (\gamma h)^2 \quad (4)$$

$$(1 + m)^2 h^2 = (1 + \gamma^2) h^2 \quad (5)$$

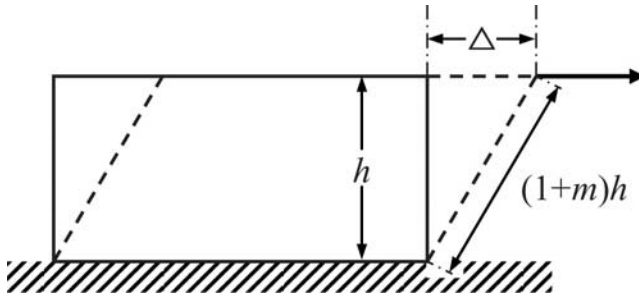


FIG. 3—Schematic diagram for a unit volume in shear deformation.

$$m = \sqrt{1 + \gamma^2} - 1 \quad (6)$$

For example, a 15 % movement corresponds to a shear strain of 56.8 %.

Controlled-Strain Cyclic Deformation

A method for evaluating the fatigue properties of structural silicone glazing materials was recently proposed by Carbery et al. [13] to simulate shear deformation typical in curtainwall designs due to daily thermal movement differentials. The proposed test method subjected specimens, prepared according to the ASTM C1135-00 “Standard Test Method for Determining Tensile Adhesion Properties of Structural Sealants” [14], to 36 500 cycles of 15 % movement at a frequency of five cycles per minute. A total of nine (one- and two-part) silicone sealants representing movement capabilities from 12.5 to 50 % were investigated. The results from ASTM C1135 tensile adhesion testing before and after the fatigue test revealed a modulus reduction for each sealant.

Figure 4 reproduces some of the results from Ref [13] in terms of the 25 % secant modulus. In general, the trend suggested that sealants with a higher initial modulus ($t=0$) exhibited a larger modulus reduction (approaching 40 %) compared to the lower modulus elastomers (~ 20 % reduction). Nevertheless, it was evident that this approach, which produced only two data points from each experiment, provided no degrees of freedom in proposing an appropriate fatigue mechanism that was not linear with time (or number of fatigue cycles).

A test protocol was set up for the ARES controlled-strain rheometer to follow the deformation history described in Ref [13]. From Eq 6, a shear strain of 56.8 % using a dynamic frequency of 0.083 Hz was defined. For each sealant listed in Table 1, more than 10^4 data points of the stress response, starting approximately 12 s after starting the test, were collected over more than five days of cycling. Figure 5 shows the results obtained using the parallel-plate geometry where, for the purpose of clarity, only every 300th data point was plotted.

All four sealants exhibited an overall shear stress reduction ranging, as listed in Table 2, from 10 % for the one-part alkoxy Sealant B to 17 % for the one-part acetoxy Sealant A. This reduction was consistent with the 25 % secant modulus data plotted in Fig. 4; however, the results in Fig. 5 revealed more

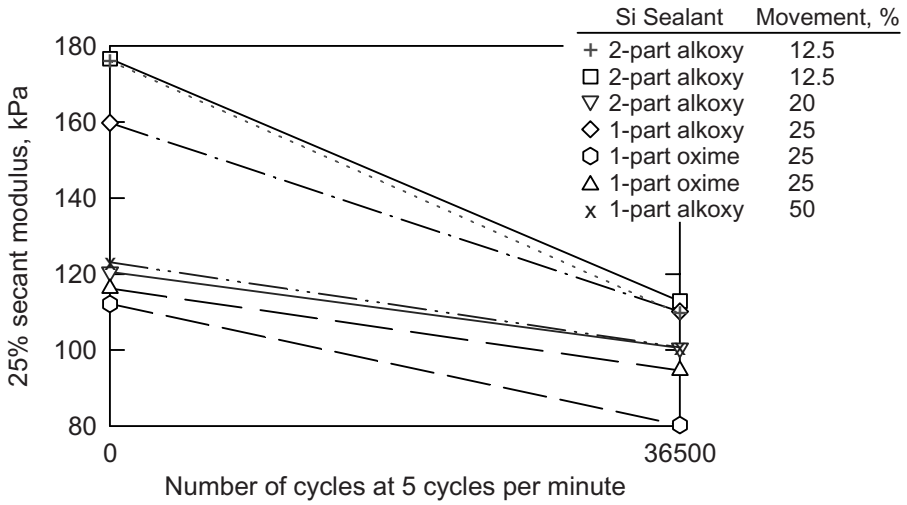


FIG. 4—Effect of cycling at 15 % shear movement on the 25 % secant modulus from ASTM C1135 testing reported in Ref [13].

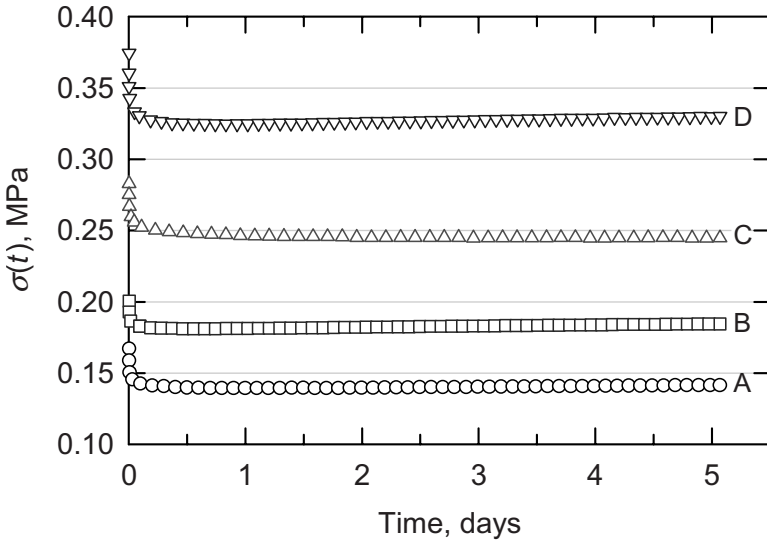


FIG. 5—Effect of cycling at 56.8 % torsional strain (15 % movement) on the stress response for four cured silicone sealants (Table 1) at 25°C. Data edited for clarity by plotting every 300th point.

TABLE 2—Sealant response to 0.083 Hz sinusoidal deformation of 56.8 % shear strain at 25°C.

Silicone Sealant	Shear stress (MPa)				
	Initial	Minimum (time, h)	1 - Minimum/Initial, %	Final (5.1 days)	1 - Minimum/Final, %
Parallel plate					
A	0.167	0.139 (23)	17	0.142	1.5
B	0.200	0.181 (18)	9.7	0.184	1.9
C	0.283	0.245 (122)	14	0.245	N/A
D	0.375	0.325 (20)	13	0.330	1.6
Cone-and-plate					
B	0.179	0.164 (15)	8.5	0.167	1.6
D	0.271	0.236 (8)	13	0.249	5.2

aspects to the stress response. First, the majority of the stress/modulus reduction occurred within the first 24 hours of cycling at 57 % shear strain. This strain-induced stress-softening phenomenon with successive cycling is typical in filled systems and has been referred to as the Mullins effect [15]. This effect was attributed to polymer chains, having reached its limit of extensibility, detaching from the filler surface or slipping on the filler surface [16]. The Mullins effect has been closely related to the mechanical fatigue of elastomers and, consequently, has received a lot of attention in addressing the durability and service life of these systems. To be consistent with the experimental protocol in Ref [13], the test specimens were not preconditioned by imposing a strain greater than 57 % to remove the Mullins effect. Therefore, the stress-softening response in Fig. 5 was not unexpected, noting that shear is the least damaging such that the Mullins effect is small relative to other types of deformation [17].

More noteworthy was the subsequent stress recovery observed for the remainder of the test period in three of the four sealants, which is listed in the last column of Table 2. Relative averages for the standard deviation (0.006 %) and range (0.13 %) of the actual strain data over each five-day test period could not account for a significant contribution to the observed stress recovery. To determine if this response was a consequence of torsional (nonuniform) deformation, two of the sealants were tested at uniform shear strain using the cone-and-plate geometry where similar trends were observed as well (Table 1 and Fig. 6). Hence, it would appear that some sealants are able to exhibit a modest recovery during the remaining four days of cyclic deformation. While noting that the magnitude of the Mullins effect depends in part on the sealant formulation, White and Hunston [18] also observed recovery from the Mullins effect given sufficient periods of time between repeated loading cycles. For future considerations, it may be revealing to investigate both the effects of cycling frequency and strain amplitude on the rate of recovery from the Mullins effect.

Another issue of concern was the nonlinear mechanical response of sealants. Figure 7 shows the stress-strain profile for two sealants tested using the cone-and-plate geometry and a dynamic frequency of 0.083 Hz. A deviation from a linear correspondence (given by each straight line) was evident well

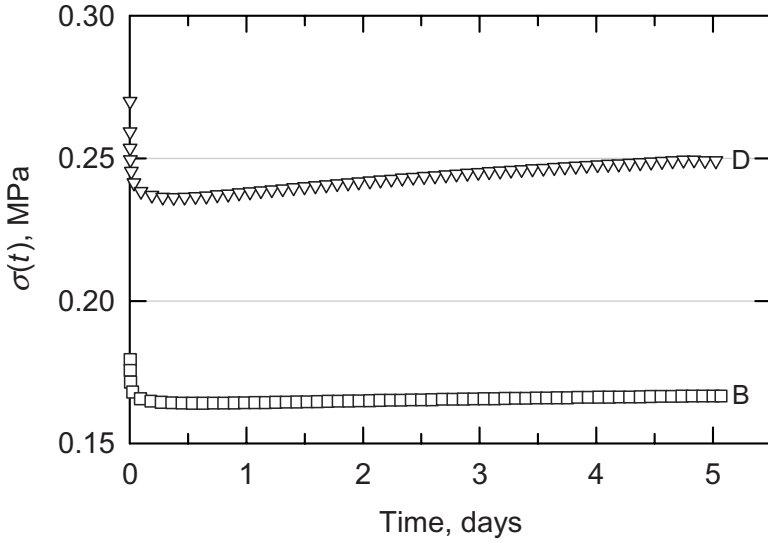


FIG. 6—Effect of cycling at 56.8 % shear strain (15 % movement) on the stress response for two cured silicone sealants (Table 1) at 25°C using the cone-and-plate geometry. Data edited for clarity by plotting every 300th point.

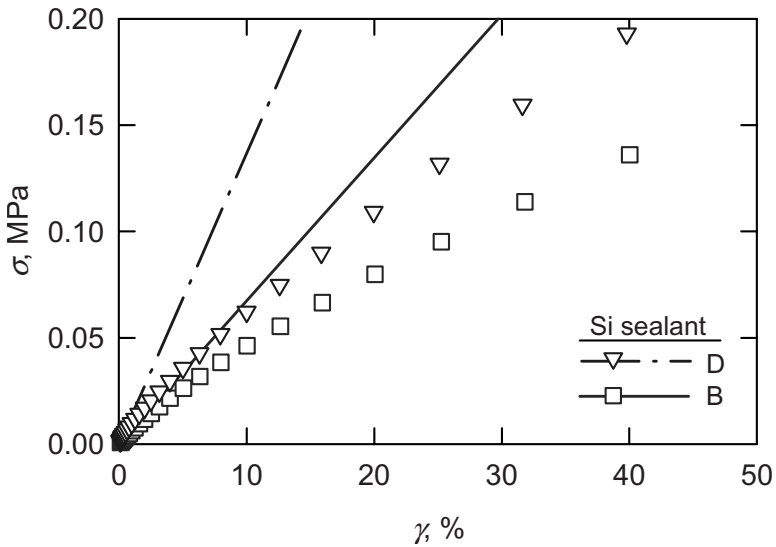


FIG. 7—Stress-strain response in dynamic shear deformation for two cured sealants at 25°C.

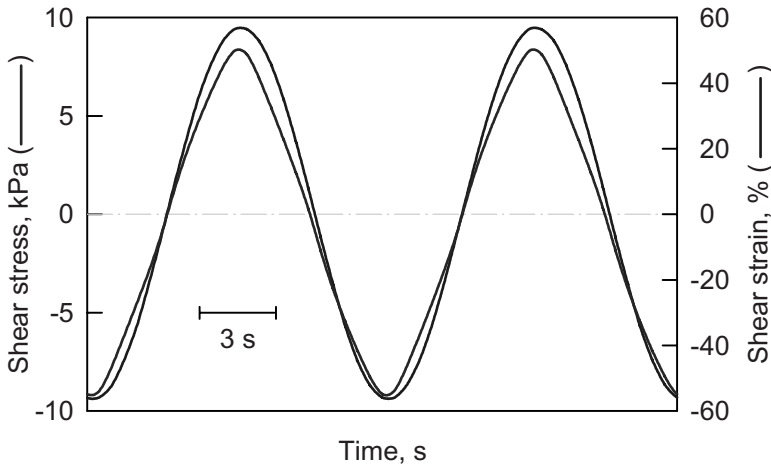


FIG. 8—Waveform of the stress response relative to the input sinusoidal strain of Sealant D using the cone-and-plate geometry.

below the 57 % shear strain applied during the cycling testing. A sinusoidal waveform cannot be expected from a nonlinear response to a sinusoidal input. An example is shown in Fig. 8 for Sealant D, where the input and output waveforms were monitored using the RheoChart software accompanying the Waveform & Fast Data Sampling Option with the ARES rheometer. A distorted output waveform was evident relative to the input sinusoidal waveform. Therefore, no attempt was made to decompose the dynamic response into its elastic (storage) and viscous (loss) modulus components [19].

Controlled-Stress Cyclic Deformation

The ASTM E1886 test method evaluates the performance of entire fenestration designs and impact protective systems after missile impact by subjecting the unit to static pressure differentials to determine its ability to remain unbreached during a windstorm. Eight loading sequences are used to generate 4500 positive and 4500 negative air pressure cycles, where the duration of each cycle shall not be less than 1 s and not more than 5 s. The applied air pressure is anywhere from 20 to 100 % of the design pressure under service load conditions.

Rheometry can be utilized as a screening tool to characterize the performance of any sealant or adhesive component in a fenestration design or an impact protection system that is subjected to a controlled-load cyclic deformation. Therefore, a test protocol was constructed using the following test parameters after the sealant test specimen was cured between the parallel-plate fixtures and subsequently equilibrated at 25°C: (1) a stress amplitude of 0.138 MPa (20 psi) equivalent to the specified design pressures of silicone sealants; (2) an oscillatory frequency of 0.5 Hz that simulated the fastest oscillation cycle specified in ASTM E1886; and (3) a total of 4500 cycles (as drawn in Fig.

1, one oscillation cycle corresponds to a test specimen experiencing a maximum deformation amplitude once each in the positive and negative direction).

Figure 9 plots the measured deformation profiles of the controlled-stress experiments at 25°C in terms of movement following Eq 6. After an equivalent of 2.5 h of oscillatory stress cycling at 0.138 MPa (round 1), each sealant was allowed to recover for a period of 24 h before undergoing a second round under the same set of test conditions. In general, the results from the first round (unfilled symbols) were consistent with the sealant modulus listed in Table 1 (lower modulus \approx more movement). The deviation from a 1:1 correlation—particularly with respect to Sealants C and D—infers that the sealants have distinct stress-strain profiles, which may be a function of multiple variables including formulation and cross-link density.

The ultimate movement observed for each sealant was significantly less than its rated capability (Table 1) as well as the magnitude used for the controlled-strain cyclic testing. In these controlled-stress experiments, there appeared to be minimal to no distortion in the output sinusoidal waveform as visually observed from the waveform display feature of the AR550 Advantage Instrument Control software.

Overall, the more rigid the sealant, the faster was its response to a steady-state strain. After a 24-hour recovery period, the initial response to a second round of oscillatory stress (dotted symbols) revealed that complete recovery from the initial round was not achieved. Nevertheless, the ultimate movement did not vary significantly to that from the initial round and, more importantly, no obvious signs of fatigue were observed.

Summary

The potential of rheology test methods as a screening tool to isolate and evaluate the mechanical durability of the elastomeric silicone sealant component in building assemblies undergoing cyclic deformation was demonstrated. In absence of other artificial degradation pulses, the stress reduction observed in sealants undergoing controlled strain sinusoidal deformation at five cycles per minute was attributed to the Mullins effect. The stress-softening phenomenon occurred within the first 24 hours of cycling; however, three of the four sealants subsequently exhibited signs of recovery during the remainder of the testing period lasting at least four more days.

Under controlled-load cyclic testing at its design load of 0.138 MPa, the sealants exhibited an ultimate deformation within the 2.5-h test cycle well below its rated movement capability with no apparent signs of fatigue. Therefore, these sealant materials tested should be acceptable in an impact-resistant assembly if the frame remains rigid and the stresses induced from the design wind pressures are transferred to the fully cured and adhered sealant joints.

A next step to further characterize the sealants is to ascertain that the cyclic strains or stresses imposed upon the sealants in real systems are quantified properly so that the rheology test methods presented can better assess the performance and durability of an individual material.

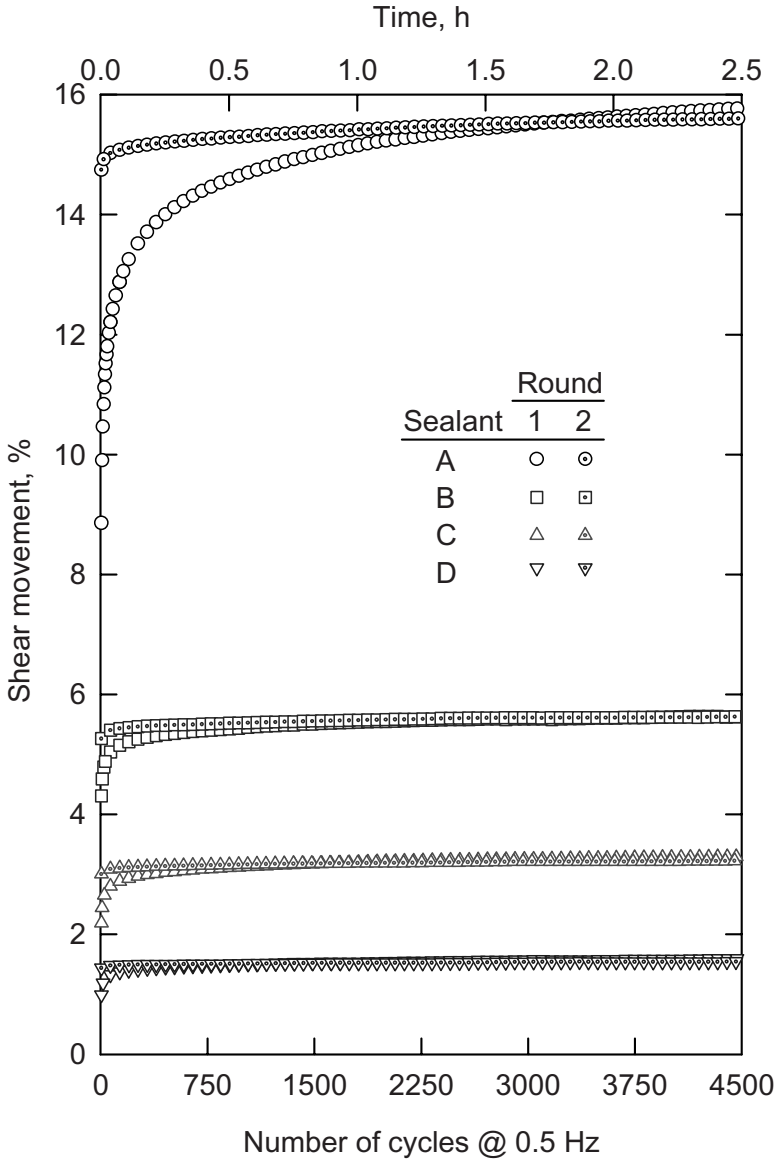


FIG. 9—Deformation response to a controlled-stress oscillation of 0.138 MPa at a frequency of 0.5 Hz and 25°C. Each sealant was allowed to recover for 24 hours before being subjected to a second round. Data edited for clarity by plotting every 12th point.

References

- [1] ASTM Standard C719-93 (Reapproved (2005)), "Standard Test Method for Adhesion and Cohesion of Elastomeric Joint Sealants under Cyclic Movement (Hockman Cycle)," *Annual Book of ASTM Standards*, ASTM International, West Conshohocken, PA, 2007.
- [2] Japanese Industrial Standards Committee JIS-A 5758, "Sealing Compounds for Sealing and Glazing in Buildings," JISC Standards Department, Ministry of International Trade and Industry, Tokyo, Japan, 1992.
- [3] International Standard Specification ISO 9047:2003, "Building Construction—Jointing Products—Determination of Adhesion/Cohesion Properties of Sealants at Variable Temperatures," International Organization for Standardization, Genève, Switzerland, 2003.
- [4] European Organization for Technical Approval ETAG 002, "Guideline for European Technical Approval for Structural Sealant Glazing Systems," EOTA, Brussels, Belgium, 2001.
- [5] ASTM Standard C1184-00a, "Standard Specification for Structural Silicone Sealants," *Annual Book of ASTM Standards*, ASTM International, West Conshohocken, PA, 2007.
- [6] ASTM Standard E1886-02, "Standard Test Method for Performance of Exterior Windows, Curtain Walls, Doors, and Impact Protective Systems Impacted by Missile(s) and Exposed to Cyclic Pressure Differentials," *Annual Book of ASTM Standards*, ASTM International, West Conshohocken, PA, 2007.
- [7] Gutowski, W., Russell, L., Cerra, A., and Petinakis, S., "New Opportunities in Sealant Diagnostics Through Dynamic Mechanical Analysis and Micro-Specimen Testing," *Durability of Building Sealants: Proceedings International RILEM Symposium*, A. T. Wolf, Ed., E & FN Spon, London, 1999, pp. 81–98.
- [8] Jones, T. G. B., Hutchinson, A. R., and Lacasse, M. A., "Effect of Movement Waveforms on the Experimental Performance of Newly Sealed Joints," *Proceeding, 3rd International RILEM Symposium Durability of Building and Construction Sealants*, A. T. Wolf, Ed., RILEM, France, 1999, pp. 211–227.
- [9] Wolf, A., "RILEM TC190-SBJ: Development of Recommendations on Novel Durability Test Methods for Wet-Applied Curtain-Wall Sealants," *Mater. Struct.*, Vol. 41, 2008, pp. 1473–1486.
- [10] NETZSCH DMA 242C product brochure, NETZSCH-Gerätebau GmbH, Selb/Bavaria, Germany; TA Instruments Rheometers 2008 product brochure, TA Instruments, New Castle, DE; Perkin Elmer DMA 8000 2007 product brochure, Perkin Elmer, Waltham, MA; Physica MCR product brochure, Anton Paar GmbH, Graz, Austria.
- [11] Wolf, A. T., "Progress Towards the Development of a Durability Test Method for Sealants," *Durability of Building Sealants*, A. T. Wolf, Ed., RILEM, France, 1999, pp. 365–380.
- [12] Walters, K., *Rheometry*, Chapman and Hall, London, 1975, p. 60.
- [13] Carbary, L. D., Bull, E. D., and Mishra, S. S., "Development of a Practical Method to Evaluate the Fatigue Properties of Structural Silicone Glazing Adhesives," *J. ASTM Int.*, Vol. 4, 2007, Paper ID JAI100403.
- [14] ASTM Standard C1135-00, "Standard Test Method for Determining Tensile Adhesion Properties of Structural Sealants," *Annual Book of ASTM Standards*, ASTM International, West Conshohocken, PA, 2007.
- [15] Mullins, L., "Effect of Stretching on the Properties of Rubber," *J. Rubber Res.*, Vol.

16, 1947, pp. 275–289.

- [16] Clement, F., Bokobza, L., and Monnerie, L., “On the Mullins Effect in Silica-Filled Polydimethylsiloxane Networks,” *Rubber Chem. Technol.*, Vol. 74, 2001, pp. 847–870.
- [17] Beatty, M. F., “The Mullins Effect in a Pure Shear,” *J. Elast.*, Vol. 59, 2000, pp. 369–392.
- [18] White, C. C., and Hunston, D. L., “Issues Related to the Mechanical Property Characterization of Sealants,” *J. ASTM Int.*, Vol. 1, 2004, Paper ID JAI11607.
- [19] Ferry, J. D., *Viscoelastic Properties of Polymers*, Wiley, New York, 1980.

Christopher C. White,¹ Donald Hunston,¹ and Kar Tean Tan¹

Effect of Strain on the Modulus of Sealants Exposed to the Outdoors

ABSTRACT: The effects of applied strain on sealants exposed to outdoor weathering were examined for two sealant formulations, Sealants A and C. Both static and dynamic strain was applied to the sealants during the summer in a Gaithersburg, MD outdoor location. Both sealants exhibited a reversible change in equilibrium distance. Stress relaxation studies on all samples revealed that, for Sealant A, two mechanisms affected modulus change; exposure without applied strain increased the modulus while additionally applied strain decreased the modulus. Only one mechanism that decreased the modulus was found for Sealant C. A 7 % dynamic strain and a 25 % static strain were observed to produce equivalent modulus changes in both systems.

KEYWORDS: sealant, strain, modulus, outdoor weathering, characterization

Introduction

Sealants are expected to seal gaps between dissimilar materials in the building envelop that change dimension with changes in either temperature (differential thermal expansion coefficients) or humidity (wood frame construction). The ability of a sealant to maintain its physical integrity, thus maintaining a seal as the gap dimensions change, is a critical function of the sealant. The time dependent response to applied strain is critical in the in-service environment and yet is often neglected in the test methods employed to evaluate the sealant.

The current evaluation methods for sealants are either threshold-based or based on long-term exposure outdoors. The most typical example of a threshold-based test is the ASTM Standard Test Method for Adhesion and Cohesion of Elastomeric Joint Sealants under Cyclic Movement (Hockman Cycle) (ASTM C719). In this test, the sealant is exposed to a series of environmental

Manuscript received June 19, 2008; accepted for publication November 18, 2008; published online December 2008.

¹ National Institute of Standards and Technology, Building and Fire Laboratory, 100 Bureau Dr., Stop 8615, Gaithersburg, MD 20899-8615.

Cite as: White, C. C., Hunston, D. and Tan, K. T., "Effect of Strain on the Modulus of Sealants Exposed to the Outdoors," *J. ASTM Intl.*, Vol. 6, No. 2. doi:10.1520/JAI101954.

Copyright © 2009 by ASTM International, 100 Barr Harbor Drive, PO Box C700, West Conshohocken, PA 19428-2959.

stresses, such as exposure to elevated temperature, immersion in water, and cyclic mechanical testing, each conducted in sequence. At the end of the serial exposures, the sealants are evaluated visually for failure in adhesion or cohesion. ASTM C719 based testing has been effective in creating a minimal-performance threshold; however, it does not have the ability to predict in-service performance or differentiate between products that perform above this minimal threshold.

Typical commercial outdoor exposures are performed with no strain on the sealant. If strain is included in the outdoor exposure experiment, a static strain is developed using gage blocks to strain the sealant to a set tension level or clips for a set compression value. These strains do not reflect the dynamic strain that occurs in the in-service environment on the sealant.

There are several examples of outdoor weathering devices that impose strain on the sealant that are constructed of two materials with dissimilar coefficients of thermal expansion. Upon thermal change, these devices impose a strain on the sealant. Examples include unplasticized polyvinyl chloride (PVC) and steel [1], wood and aluminum [2], concrete and aluminum [3], and steel and aluminum [4] devices. Manually operated devices have also been used to create cycling effects [5]. Results from these devices have indicated that joint movement is a predominate factor in sealant failure [6]. From these limited results, it is clear that imposed strain on the sealant is a critical part of the exposure environment.

These studies illustrate that applied strain strongly affects the response of the sealant [7]. What is not clear is what the expected response of the sealant would be under long-term exposure to a dynamically or static applied strain. Additionally, a modulus characterization of the sealant was used to track the changes in the sealant. Changes in the time dependent modulus can be specifically attributed to molecular level mechanisms [8].

In previous studies, the sealant was evaluated both before and after exposure by visual inspection [6]. While useful for determining cracking and morphological changes, such evaluation does not anticipate the fundamental changes of the sealant that occur at the molecular level.

An additional complication is the nonlinear viscoelastic nature of the sealant. The sealant responds to deformation by dissipating (viscous) or storing (elastic) the resulting stress that is imparted to the sealant during the applied strain. The viscoelastic response is both time- and strain-dependent. To separate this time and strain dependence and to characterize the viscoelastic nature of the sealant, stress relaxation experiments were performed to evaluate the sealant both before and after exposure.

Experimental

Characterization

Sealant specimens for two formulations (A and C) were fabricated by our industrial partners (see Acknowledgments) according to ASTM C719 a commonly referenced industrial standard. Sealant A exhibits a reversible stable dimen-

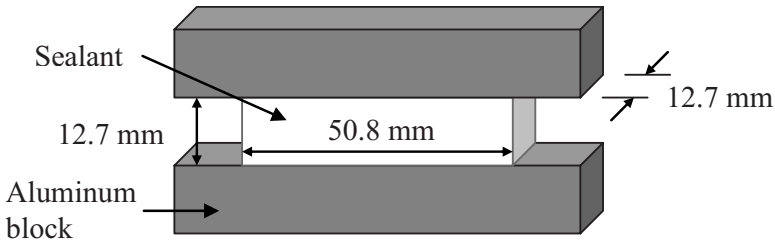


FIG. 1—Illustration of the ASTM C719 sealant sample size employed in these studies.

sional change when exposed to applied strain, while Sealant C does not exhibit a dimensional change when exposed to applied strain. The specimen geometry is shown in Fig. 1. Fabrication involved bonding a sealant sample ($W = 50.8$ mm, $B = 12.7$ mm, and $H = 12.7$ mm) between two aluminum blocks with dimensions of 76.0 by 12.7 by 12.7 mm. The fabricated specimens were subjected to tension tests by pulling the metal beams apart in a direction perpendicular to their longitudinal axis and to compression tests by pushing them together in the opposite direction. One limitation of this geometrical system is that the sealant is constrained at the point where it attaches to the metal bars so that it cannot deform laterally (perpendicular to the imposed load) when it is either stretched or compressed. Consequently, the deformations are not uniform throughout the sample and the modulus calculated from these tests will be somewhat different from that obtained in a tension experiment. Nevertheless, the wide acceptance of this geometrical system makes it a useful starting place, and as long as an identical geometry is used for all tests, comparisons should be meaningful.

The stress-relaxation experiments were conducted on either a Model 1125 Instron machine with computer control² or a custom load-displacement apparatus described elsewhere [9]. The main difference between these two machines for the purposes of this study is that the custom apparatus can characterize up to 30 samples simultaneously. The sealants were soft and thus a rigid loading fixture was used so that the crosshead displacement could be obtained as sample deformation with no correction for machine compliance. Deformation is defined in terms of the extension ratio, $\lambda = \{1 + (\Delta/H)\}$, where Δ is the displacement and H is the sample height. The stress, σ , is defined as $\{L\lambda/WB\}$, where L is the load and W and B are the sample width and thickness, respectively. These expressions assume that the samples were incompressible, which is generally an acceptable assumption for elastomers. The specimens were loaded rapidly (100 cm/min, cross-head speed) up to a given extension ratio, λ , and maintained that value while the load was monitored as a function of time.

²Certain commercial materials and equipment are identified in this paper in order to specify adequately the experimental procedure. In no case does such identification imply recommendation or endorsement by the National Institute of Standards and Technology, nor does it imply necessarily that these items are the best available for the intended purpose.

The time required to load a specimen was less than 1 s, so the first data point was not obtained until after 5 s to avoid transient effects associated with loading. An apparent modulus, E_a , was calculated using a relationship based on a statistical theory of rubber-like elasticity [8,10].

$$E_a(t, \lambda) = \frac{3L(t)}{WB(\lambda - \lambda^{-2})} \quad (1)$$

The modulus is termed apparent because of the assumptions used in the derivation of the equation and the complications discussed above with regard to the constraints on the specimen.

The standard uncertainties for the measurement of specimen dimensions and displacements were ± 0.5 mm and ± 0.01 mm, respectively. In all but one case, the standard uncertainties in the stress measurement and modulus determination were ± 2.7 % and ± 5 %, respectively. For experiments that were completed in minutes, such as the stress-strain tests, the uncertainty in the load measurement produced by zero drift was ± 0.1 N. The stress relaxation tests, however, required measurements over 10 to 20 h and, under these conditions, the uncertainty in the load measurement associated with zero drift increased to ± 0.4 N.

Instrumentation

A custom-built, outdoor exposure device to impose dynamic strain on the sealant, based on the differential coefficient of thermal expansion between the PVC pipe and wood, was used in this study. The details of this apparatus are found elsewhere [11], but a short summary is included here. This device imposes a strain on the sealant sample based on the relative expansion of the PVC pipe relative to the wood frame to which the PVC pipe is attached. The applied strain is designed to be ± 25 % of the sealant joint height based on the expected temperature range in Gaithersburg, MD. There are two versions of this apparatus, one that imposes a compression strain on the samples with increasing temperature and one that imposes a tensile strain on the samples with increasing temperature.

Experimental Design

All 30 sample replicates for Sealants A and C were characterized with a tensile stress-relaxation experiment (strain of $15 \text{ \%} \pm 0.2 \text{ \%}$) prior to exposure. Following the characterization, four samples of Sealants A and C were placed in the outdoor custom dynamic strain devices in the early spring of 2007. Additional sample sets of three replicates of Sealants A and H were placed in the same exposure environment with gage blocks to impart static 0, 5, 10, 20, and 25 % tensile strains and clips to impart 5, 10, 20, 25, and 30 % compressive strains; these replicates were placed in the same outdoor environment as the dynamically strained samples. All specimens were monitored over the summer (May 10–September 1). In the fall (September 1), the samples were removed from the

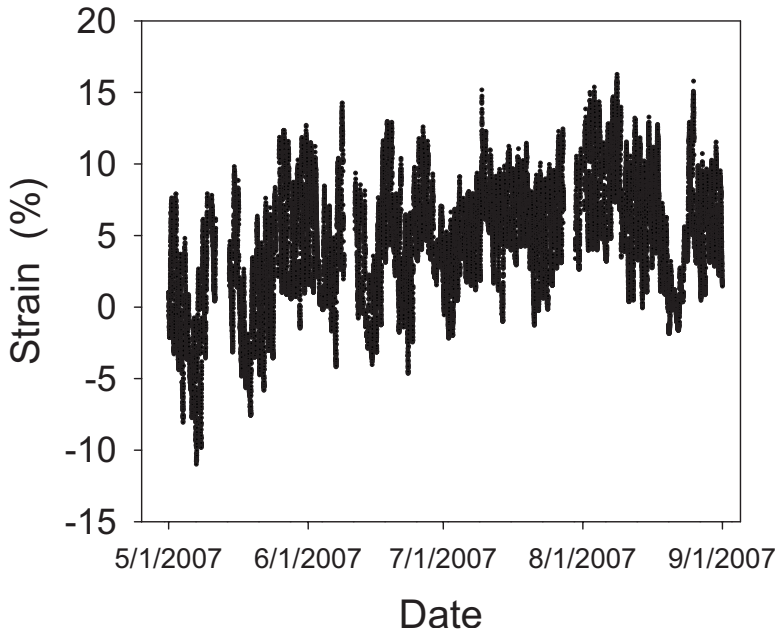


FIG. 2—Plot of the strain versus date for the summer exposure (May 10–September 1) of the dynamically strained samples.

testing fixtures, forced into their original configurations, and characterized again by stress-relaxation experiments.

Results and Discussion

Dynamically Strained Samples

During the summer, the dynamic strain on the samples was recorded and is shown in Fig. 2. In this figure, the average strain was 7 % with peaks of 16 % strain based on a zero-point strain of a warm day, May 10.

Sealant A shows deformation upon removal from the testing fixtures as shown in Fig. 3. The dynamically strained Sealant A samples showed a significant compressive or tensile set when first removed from the testing apparatus. After the samples were forced into their initial pre-exposure sample dimensions for a period of ten days (using gage blocks or clips), both replicates that experienced either tension or compression were stable at the sample dimensions observed prior to exposure.

Stress-relaxation tests on these samples, shown in Fig. 4, reveal an interesting pattern. The baseline data for samples that did not experience summer exposure are shown as circles. The samples that experienced no strain during exposure (squares) increased in either modulus or stiffness with no change in curve shape. This finding most likely represents a change in the molecular

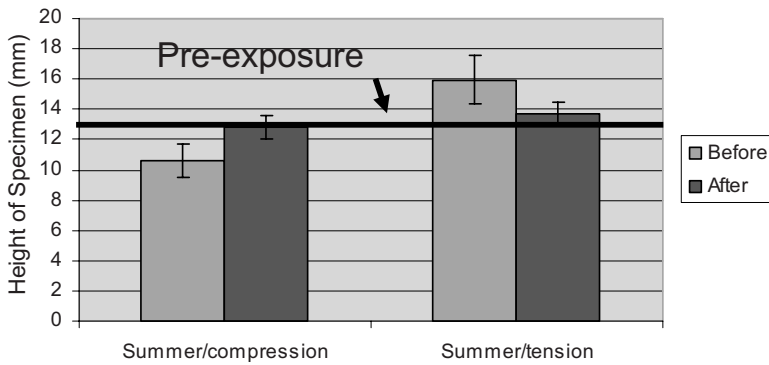


FIG. 3—Width of Sealant A immediately after removal from dynamic outdoor exposure on September 1 (before) and after ten days of forced return to the dimensions prior to exposure (after).

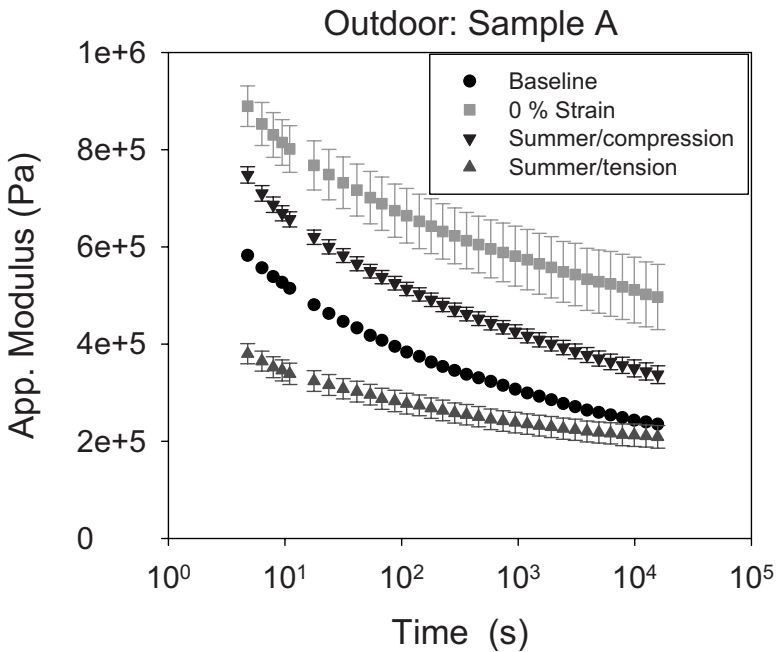


FIG. 4—The stress-relaxation modulus for Sealant A shown for prior to any exposure (Baseline), after exposure with no strain (0 % strain), after exposure to dynamic compression (shown in Fig. 2) (Summer/compression), and after exposure to dynamic tension (shown in Fig. 2) (Summer/tension). The points represent the mean values and the error bars are the relative standard uncertainty.

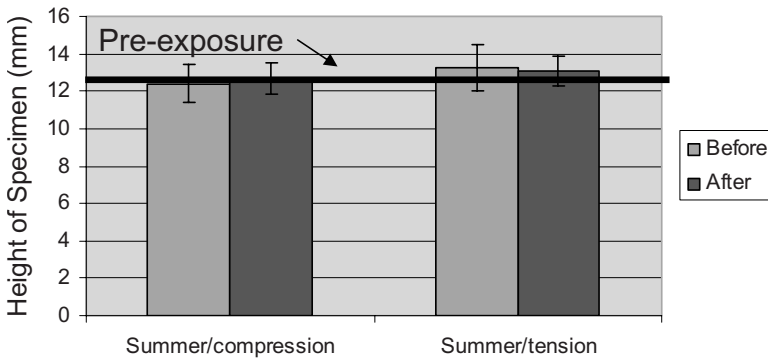


FIG. 5—Width of Sealant C immediately after removal from outdoor exposure on September 1 (before) and after ten days of forced return to the dimensions prior to exposure (after).

weight between cross-links. The samples that experienced compression during the summer (inverted triangles) have a modulus lower than the zero-strain samples, but greater than the baseline, again with the same curve shape. The samples that experienced tension during the summer decreased in the modulus and had a much flatter curve shape compared with the baseline samples. This finding suggests that the sealant responded differently to exposure with or without strain, and the type of strain (compressive or tensile) also had an effect.

Sealant C had more dimensional stability as shown in Fig. 5 than Sealant A shown in Fig. 3. Both before and after exposure, the dimensions of the Sealant C did not differ within the experimental uncertainty. Again, after exposure, the sealant was forced back into the pre-exposure sample dimensions and maintained for ten days.

The stress-relaxation data for Sealant C (Fig. 6) revealed that with just exposure and no strain, the sample modulus decreased, but was not significantly different within the experimental uncertainty. The samples that experienced dynamic compression during exposure showed a decrease in the modulus that was statistically different from both Sealant C samples with exposure and no strain or Sealant C without exposure. The samples that experienced tension during the summer showed larger decreases in the modulus. This result suggests that for Sealant C, there is a single mechanism that affects modulus change, but the introduction of both strain and the type of strain has a significant effect on the resulting modulus.

Statically Strained Samples

The Sealant A samples that were statically strained in both compression and tension during exposure also exhibited a change in dimensions consistent with the results from the dynamically strained Sealant A samples. The degree of dimensional change in both tension and compression is proportional to the extent of the static strain as shown in Fig. 7 (before treatment). Again, these samples were removed from exposure and forced back into the pre-exposure

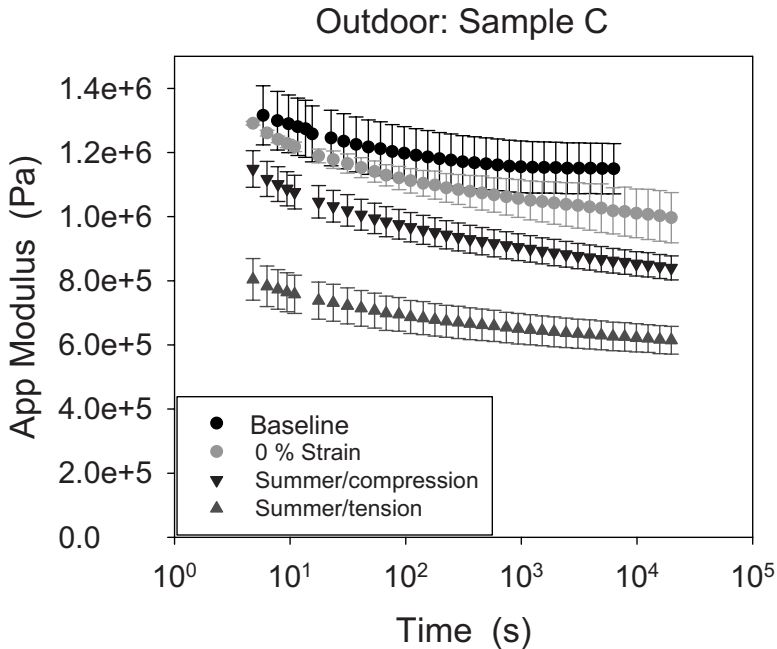


FIG. 6—The stress-relaxation modulus for Sealant C shown for prior to any exposure (Baseline), after exposure with no strain (0 % strain), after exposure to dynamic compression (shown in Fig. 2) (Summer/compression), and after exposure to dynamic tension (shown in Fig. 2) (Summer/tension). The points represent the mean values and the error bars are the relative standard uncertainty.

sample dimensions for ten days. All samples, from both static tension and compression, were returned into the pre-exposure sample dimensions (dotted line) after treatment (Fig. 7).

Results of the stress-relaxation tests on the Sealant A samples exposed to tension are shown in Fig. 8. The data are similar to the dynamically strained data from Fig. 4. The 5 %-strain data are intermediate between the no exposure and exposure with no strain values. Again, these data have a similar curve shape. The 10 %-static strain with exposure data is virtually identical to the no-exposure, no strain data, suggesting that a 10 % static-tensile strain decreases the modulus as much as the exposure increased the modulus. For values of greater strain, such as 20 and 25 % tension, the rate in change of modulus decreases as can be seen in the shallower slope of the stress relaxation curve over time. The 25 % static-strain data, with a value below baseline, had an almost identical curve shape and value to the dynamically strained tension sealant. This finding suggests that a dynamic strain of 7 % tension produces the same amount of molecular change monitored by a change in the complex modulus similar to a 25 % static-strained sample.

The compressively strained Sealant A samples are shown in Fig. 9. In this figure, all values for the statically and compressively strained samples had a

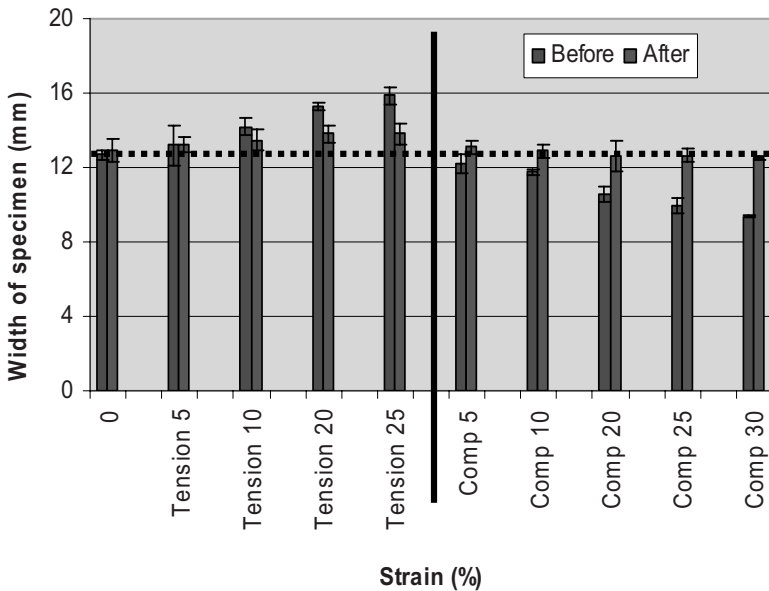


FIG. 7—Width of Sealant A immediately after removal from static outdoor exposure on September 1 (before) and after ten days of forced return to the dimensions prior to exposure (after).

modulus greater than either the samples with no exposure or the dynamically strained (compression) samples. This result suggests that the static-compressive strain on the samples, up to 30 %, was insufficient to produce an effect on the modulus similar to the 7 % dynamic-compressive strain.

The Sealant C samples again had more dimensional stability when removed from static strain (Fig. 10). Again, the dimensional changes were proportional to the degree and direction of the static strain with the larger strains producing larger changes in sample dimensions. All of these Sealant C samples were able to return to their pre-exposure sample dimensions after ten days under original conditions.

The stress-relaxation data for the statically strained Sealant C samples are shown in Fig. 11. Consistent with the dynamically strained Sealant C samples, the modulus values decreased with the addition of either strain or exposure. Both the 5 and 10 % static tensile-strain values are intermediate between the zero strain and the dynamically strained values. The static strains of 20 and 25 % produced results similar to the dynamically strained Sealant C results. There was no apparent change in curve shape in these results, again consistent with the dynamic data.

The stress-relaxation data for the compressively strained Sealant C samples are shown in Fig. 12. The modulus values of 5 and 20 % compressive strain were comparable to the modulus value of exposure with no strain. The 25 % compressive strain modulus was analogous to the modulus value of the dynamic compression for Sealant C. This finding suggests that a dynamic strain

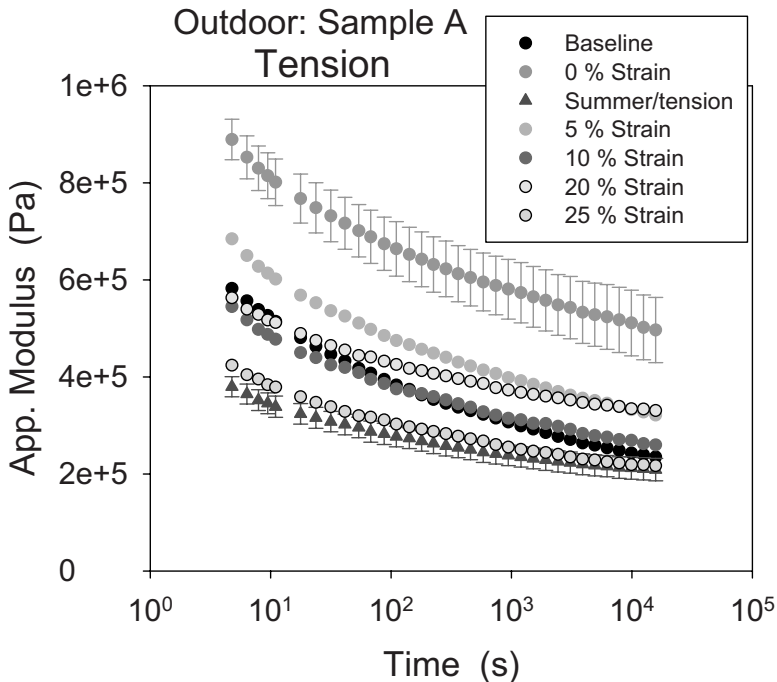


FIG. 8—The stress-relaxation modulus for Sealant A shown for prior to any exposure (Baseline), after exposure with no strain (0 % strain), after exposure to static tension of several levels (5, 10, 20, 25 % strain). Also shown is the stress relaxation data for dynamic tension (Summer/tension) from Fig. 4. The points represent the mean values and the error bars are the relative standard uncertainty.

of 7 % compression produces a similar decrease in the modulus as a static compressive strain of 25 %. Again, the decrease in modulus is much smaller in compression than in tension.

For both Sealants A and C, a static strain of 25 % tension produced a similar change in the modulus value to the dynamic-strained samples with an average 7 % strain. This result suggests that even a small dynamic strain creates a much more aggressive strain compared with a long-term static strain. If the sealant had a viscous response on the order of days, it could relax applied strain in a matter of days; consequently, a static strain could be relaxed by lowering the internal stress within the sealant. A dynamic strain would be much more difficult for the sealant to relax by either molecular reorganization or network reformation due to a faster timescale of the applied strain in comparison with the viscous dissipation of the sealant.

Summary

Two sealant formulations (A and C) were exposed to outdoor weathering either with static tensile or compressive strain or with dynamic strain. The dynamic

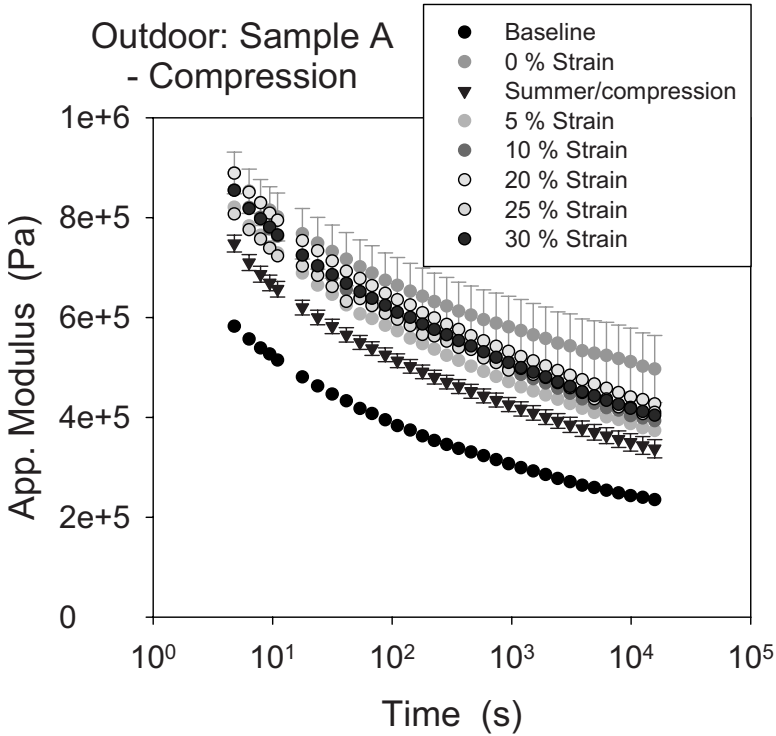


FIG. 9—The stress-relaxation modulus for Sealant A shown for prior to any exposure (Baseline), after exposure with no strain (0 % strain), after exposure to static compression of several levels (5, 10, 20, 25 % strain). Also shown is the stress relaxation data for dynamic compression (Summer/compression) from Fig. 4. The points represent the mean values and the error bars are the relative standard uncertainty.

strain on the samples was produced by an instrument composed of two different materials with different coefficients of thermal expansion. The resulting changes in the complex modulus were quantified with stress-relaxation experiments. One of the formulations, Sealant A, exhibited significant dimensional changes in response to the applied strain. These dimensional changes were reversed by maintaining the samples at the pre-exposure sample dimensions for ten days. Sealant A also exhibited two apparent mechanisms that affected the modulus. Exposure with no strain produced an increase in the modulus. With the addition of strain to the exposure, either a reduction in the modulus was observed or a decrease in the modulus and a change in the curve shape were noted.

For Sealant C, a greater degree of dimensional stability was observed, but it also was able to return to pre-exposure sample dimensions within ten days under original conditions. The stress-relaxation data for Sealant C revealed a single mechanism that affected the complex modulus as all exposures either with or without strain exhibited a decrease in the modulus. The decrease in the

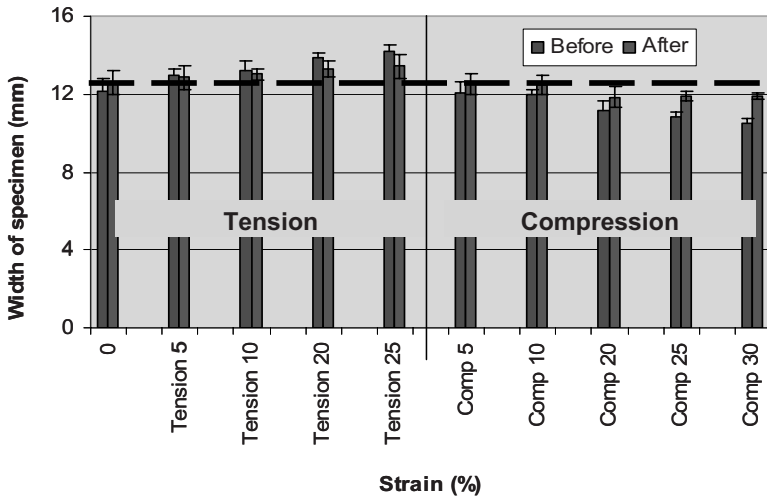


FIG. 10—Width of Sealant C immediately after removal from static outdoor exposure on September 1 (before) and after ten days of forced return to the dimensions prior to exposure (after).

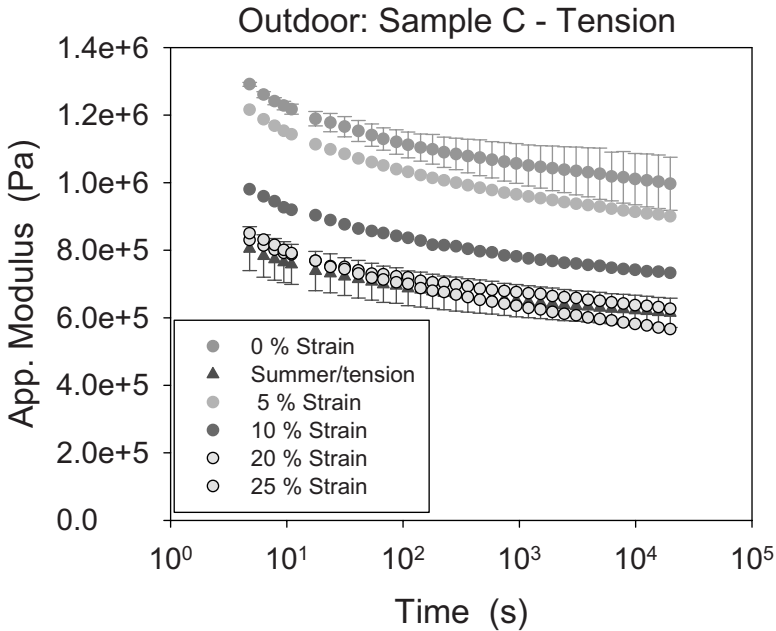


FIG. 11—The stress-relaxation modulus for Sealant C shown for prior to any exposure (Baseline), after exposure with no strain (0 % strain), after exposure to static tension of several levels (5, 10, 20, 25 % strain). Also shown is the stress relaxation data for dynamic tension (Summer/tension) from Fig. 6. The points represent the mean values and the error bars are the relative standard uncertainty.

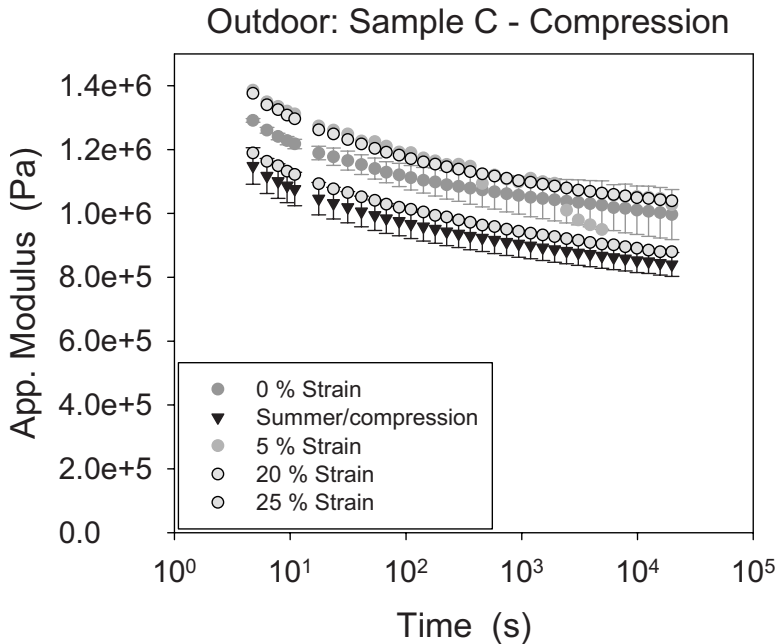


FIG. 12—The stress-relaxation modulus for Sealant C shown for prior to any exposure (Baseline), after exposure with no strain (0 % strain), after exposure to static compression of several levels (5, 10, 20, 25 % strain). Also shown is the stress relaxation data for dynamic compression (Summer/compression) from Fig. 6. The points represent the mean values and the error bars are the relative standard uncertainty.

modulus was greater for the tensile-strained samples compared with the compressive-strained samples for both static and dynamic applied strains.

Acknowledgments

Support from an industry/government consortium entitled the Service Life Prediction of Sealant Materials, centered at National Institute of Standards and Technology (NIST) was critical to the completion of this project. Assistance from DAP, BASF, Dow Corning, Kaneka Texas, SIKA, Solvay, Tremco Wacker, and Rohm & Haas was greatly appreciated. The Department of Housing and Urban Development, through the Partnership for Advancing Technology for Housing program, provided essential financial support for these efforts.

References

- [1] Onuoha, U. O., "Durability of One-Part Polyurethane and Polyurethane-Hybrid Sealants," *Durability of Building Sealants*, A. T. Wolf, Ed., RILEM Publications, Bagneux, France, 1999, pp. 235–251.

- [2] Brown, N. G., *Assessment of Joint Sealants Outdoor Exposure in Cyclic Movement Testers*, Highett, Ed., CSIRO Division of Building Research, Victoria, Australia, 1965, pp. 16–22.
- [3] Burstrom, P. G., “Durability and Aging of Sealants,” *Durability of Building Materials and Components, ASTM STP 691*, P. J. Sereda and G. G. Litvan, Eds., ASTM International, West Conshohocken, PA, 1980, pp. 643–657.
- [4] Karpati, K. K., Solvason, M. R., and Sereda, P. J., “Weathering Rack for Sealants,” *J. Coat. Technol.*, Vol. 49, No. 626, 1977, pp. 44–47.
- [5] Lacasse, M. A., “Advances in Test Methods to Assess the Long Term Performance of Sealants,” *Science and Technology of Building Seals, Sealants, Glazing and Waterproofing, ASTM STP 1254*, J. C. Myers, Ed., ASTM International, West Conshohocken, PA, pp. 5–20.
- [6] Wolf, A. T., Ed., *Durability of Building Sealants*, RILEM Publications, Bagneux, France, 1999.
- [7] Wolf, A. T., Ed., *3rd International RILEM Symposium on Durability of Building and Construction Sealants*, RILEM Publications, Senefte, Belgium, 2000.
- [8] Ferry, J. D., *Viscoelastic Properties of Polymers*, 3rd ed., John Wiley & Sons, Inc., New York, 1980.
- [9] White, C., Embree, E., and Buch, C., “Design, Development and Testing of a Hybrid in-situ Testing Device for Sealant,” *Rev. Sci. Instrum.*, Vol. 76, 2005, p. 045111.
- [10] Taylor, C. R., et al., “Nonlinear Stress Relaxation of Polyisobutylene in Simple Extension,” *Trans. Soc. Rheol.*, Vol. 20, No. 141, 1976, p. 1076.
- [11] White, C. C., Tan, K. T., O’Brien, E. P., and Hunston, D. L., “Design, Fabrication and Implementation of Thermally-Driven Outdoor Testing Devices for Building Joint Sealants,” unpublished.

J. Deng,¹ J. E. Tanner,² C. W. Dolan,³ and D. Mukai⁴

Development of Accelerated Aging Test Methodology and Specimen for Bonded CFRP Systems

ABSTRACT: Determining long-term behavior of bonded CFRP systems requires developing an accelerated aging test method for CFRP applications. This paper examines the development of test methodology and specimen for both flexure and direct tension behavior of bonded CFRP materials using a specimen submerged in a water bath subject to elevated temperature. Test results of three commercial CFRP systems are presented. A discussion of accelerated aging is included in the developmental effort.

KEYWORDS: accelerated aging, CFRP, bond strength, flexural strength, tensile strength, strength reduction factor, durability

Introduction

In recent years, fiber-reinforced polymer (FRP) composites have been increasingly used in various fields such as aerospace, automotive, athletic, recreational equipment, military, and infrastructure facilities. Glass, carbon, and aramid fiber polymers are currently the three most commonly used advanced polymer composite materials. Compared to glass and aramid fiber polymers, carbon fiber polymers exhibit superior resistance to harsh environmental exposure and fatigue load, making it more practical for civil engineering applications [1–3]. A

Manuscript received July 24, 2008; accepted for publication January 13, 2009; published online March 2009.

¹ Structural Engineer at Magnusson Klemencic Associates, Seattle WA, Formerly Ph.D. Candidate at University of Wyoming, e-mail: jd@mka.com

² Assistant Professor, Civil and Architectural Engineering, University of Wyoming, e-mail: tannerj@uwyo.edu

³ HT Person Professor, Civil and Architectural Engineering, University of Wyoming, e-mail: cdolan@uwyo.edu

⁴ Associate Professor, Civil and Architectural Engineering, University of Wyoming, e-mail: dmukai@uwyo.edu

Cite as: Deng, J., Tanner, J. E., Dolan, C. W. and Mukai, D., "Development of Accelerated Aging Test Methodology and Specimen for Bonded CFRP Systems," *J. ASTM Intl.*, Vol. 6, No. 3. doi:10.1520/JAI101976.

Copyright © 2009 by ASTM International, 100 Barr Harbor Drive, PO Box C700, West Conshohocken, PA 19428-2959.

great deal of research, including laboratory tests and short-term field applications, has identified that externally bonded CFRP composite systems could efficiently improve load carrying capacity [4–6]. The short-term behavior of CFRP composites has been studied, and construction specifications for bonded repair have been developed under NCHRP Project 10-59A [7]. Despite this research, the long-term performance of CFRP applications is not fully quantified and durability issues remain unanswered. The lack of real-time test data has made it difficult for investigators to completely understand the deterioration mechanism of FRP bonding in composite systems. This knowledge is necessary for establishing a uniformly accepted durability assessment criterion for externally bonded CFRP applications. Lack of a uniform test method and variability of CFRP systems further complicates this situation.

Moisture and temperature are commonly regarded as two predominant factors affecting the bond performance of FRP composite systems [8–11]. Lefebvre et al. [8] investigated adhesion loss at interfaces between adhesive and inorganic substrates. The adhesive was air-cured at room temperature with a high relative humidity. They found a critical relative humidity (RH) value, which was an intrinsic property of the adhesive. When the environmental RH was higher than the critical RH, some permanent changes in the internal state of the material took place and an abrupt adhesion drop occurred. RH values exceeding the critical threshold humidity resulted in moisture accumulation at the bond line. Ultimately this resulted in a loss of adhesion between the adhesive and substrate. Au et al. [9] used interface fracture toughness as the quantification parameter of CFRP-adhesive resin-concrete systems to investigate bond deterioration mechanisms by peel and shear testing accelerated by moisture conditioned specimens. They obtained a similar conclusion as Lefebvre, that there existed a threshold value of moisture accumulation beyond which the fracture toughness could decrease by 60 %. Malvar et al. [10] conducted three separate investigations to evaluate short-term effects of temperature, moisture and chloride content on the CFRP adhesion using pull-off tests and had strength reduction results similar to Lefebvre's results.

Karbhari and Engineer [11] investigated short-term environmental exposure effects on the bond performance between composite laminates and the concrete substrate. They concluded that the use of low T_g resin systems resulted in deterioration and loss of efficiency of the CFRP retrofit. The selection of appropriate resin systems was critical to successfully retrofitting and rehabilitating infrastructure applications. Further research performed by Abanilla and Karbhari [12–14] indicated that moisture uptake and other environmental factors could appreciably deteriorate the strength characteristics at the matrix and interface levels. They reported that increasing the number of CFRP layers of samples increases the rate of degradation at the matrix and interface levels and concluded that exposure to aqueous solutions results in deterioration in interlaminar and intralaminar characteristics. Toutanji and Gomez [15] studied the effect of harsh environmental conditions such as wet/dry cycling using salt-water on the performance of FRP-bonded concrete beams and on the interfacial bond between the fiber and the concrete. A pronounced bond strength reduction in specimens subjected to wet/dry cycling was observed; furthermore, fibers did not break but rather the adhesive resin debonded at the fiber-

TABLE 1—*Properties of CFRP materials.*

Composite System	Reinforcement Type	Tensile Modulus (ASTM D638) MPa	Tensile Strength (ASTM D638) MPa	Ultimate Rupture Strain (ASTM D638)
A	Unidirectional fabric	234 500	3793	1.5 %
B	Unidirectional fabric	227 000	3793	1.67 %
C	Pre-cured laminate	165 000	3100	1.69 %

concrete interface. They postulate that the strength reduction may be attributed to deterioration in the interface and the bond between the fiber and the concrete.

In practical applications, engineers are concerned with how to select an appropriate CFRP composite system under specific environmental conditions and make proper predictions regarding service life. Accelerated aging has long been used to determine the suitability of new materials for structural engineering applications to characterize long-term behavior. In CFRP bonding applications, accelerated aging is typically attempted by increasing the temperature or concentration of conditioning agents to speed up chemical or physical processes in an effort to study changes in bond strength [16]. The objective of this study is to investigate the effects of elevated temperature water baths on bond strengths of externally bonded CFRP concrete beams, and to develop a conservative accelerated aging test specimen for bonded CFRP systems. Three commercial CFRP composite systems were bonded to saw-cut plain concrete beams and exposed to different elevated temperature water baths. These specimens were tested at regular intervals by three-point bending and direct tension tests.

Materials, Specimens, and Test Methods

Three commercial CFRP composite systems (A, B, and C) were supplied by manufacturers. CFRP System A consists of unidirectional fabric sheet and a two-part adhesive resin with a mixture ratio 2.9 to 1.0 by mass. CFRP System B consists of unidirectional fabric sheet and adhesive resin system which is composed of primer, putty, and saturant, The mix ratio is 100 to 30 (Part A to Part B) by mass for primer, 100 to 30 (Part A to Part B) by mass for putty and 100 to 34 (Part A to Part B) by mass. CFRP System C consists of precured plate laminate and a two-part adhesive resin, Part A and Part B with a mixture ratio 3 to 1 by volume. According to the technical specifications of manufacturers, the general properties of the above CFRP materials and adhesive resins are listed in Table 1 and Table 2.

The concrete beams used in this study were supplied by Rocky Mountain Prestress, Denver, CO, with dimensions of 100 by 100 by 380 mm (4 by 4 by 15 in.) and 28-day compressive strength 70.9 MPa (10 130 psi). The cement used was Type I and the ratio of cement: sand: coarse aggregate (pea gravel)

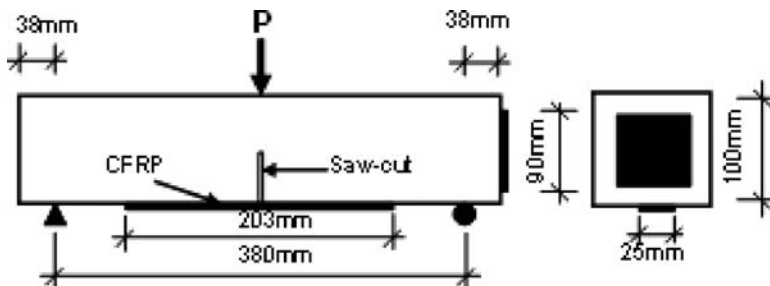
TABLE 2—*Properties of Adhesive resins.*

Composite System	Adhesive Resin	Glass Transition Temperature T_g (°C)	Tensile Modulus (ASTM D638) MPa	Ultimate Rupture Strain (ASTM D638)
A	Resin A	85	1724	3 %
B	Resin B			
	Primer	77	717	40 %
	Putty	75	1800	7 %
	Saturant	71	3040	3.5 %
C	Resin C	62	4482	1 %

was 1:2.07:2.30 by weight and the water/cement ratio was 3:2.

Prior to applying the CFRP, a 50 mm (2 in.) deep saw cut was made at mid-span of each beam to maximize environmental exposure at the point of flexural failure. Next, CFRP fabric or laminate strip with dimensions 200 mm by 25 mm (8 in. by 1 in.) was bonded to the beam using adhesive resin of each system. This external reinforcement was centered on the tension side of the flexural specimen as shown in Fig. 1. The development length of the CFRP bonding system is supported by the findings of other investigators. Chajes et al. [4] tested different development lengths of FRP by performing force-transfer tests. An approximate 90 mm (3.5 in.) effective length could develop the failure load of the CFRP, beyond which no further increase in failure load could be achieved. Dai [17] conducted a comprehensive literature review on effective development length of FRP externally bonded concrete applications and summarized that an appropriate development length should range from 75 mm (3 in.) to 200 mm (8 in.). The 200 mm long CFRP strip used in this study had a development length of 100 mm (4 in.) on each side. A 90 mm by 90 mm (3.5 in. by 3.5 in.) fabric square was bonded to one end of the concrete beam for Systems A and B for a direct tension test. For System C, the size of the laminate square is 50 mm by 50 mm (2 in. by 2 in.). Both flexural and tension testing are available from a single specimen.

The surface preparation of concrete is another important factor affecting the ultimate strength. The bonding surface must be sound, free from dust, chlorides, and other contaminants. Sandblasting, water jet, mechanical abra-

FIG. 1—*Specimen configuration and dimensions.*

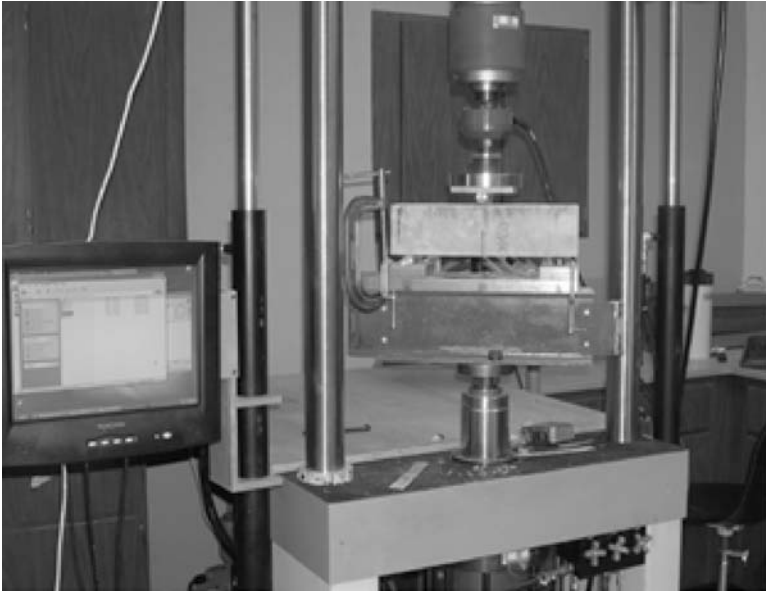


FIG. 2—*Three-point bending test setup.*

sion, and needle gun chiseling are common methods to increase strength of FRP composite system [18–20]. The concrete surface preparation can remove weak material, surface laitance, and other contaminants. The roughened concrete surface effectively increases the contact area and mechanical interlocking between adhesive and concrete. In this study, after 28-day standard curing, all the concrete beams were dried and sandblasted to a minimum ICRI profile of 3 [7], and cleaned using compressed air. CFRP strips and squares were applied to the prepared surface according to the manufacturer's specification.

After curing 14 days in ambient conditions, CFRP System A, B, and C specimens were placed into steel tanks filled with water at elevated temperatures ranging from 30°C to 60°C. Commercial heaters were installed in each tank to maintain a constant temperature within $\pm 4^\circ\text{C}$. The top of these tanks were sealed with plastic sheets and covered with 50 mm (2 in.) thick insulating foam board. The sides of each tank were surrounded by 150 mm (6 in.) thick insulation to maintain constant temperature. The maximum and minimum water temperatures in each tank were recorded daily using a commercial thermometer whose sensor was immersed in each tank. Before testing, the specimens were removed from tanks and immediately placed into a room temperature water bath for one day to cool. After cooling for one day, the specimens were allowed to air-dry for one day in the laboratory.

A three-point bending test setup modified from ASTM C78-02 [21] was used for flexural testing to determine flexural strength of CFRP composite specimens. The specimens were loaded using a servo-controlled Instron 1332 testing machine with a 45 kN (10 kip) load cell as shown in Fig. 2 (www.instron.com).

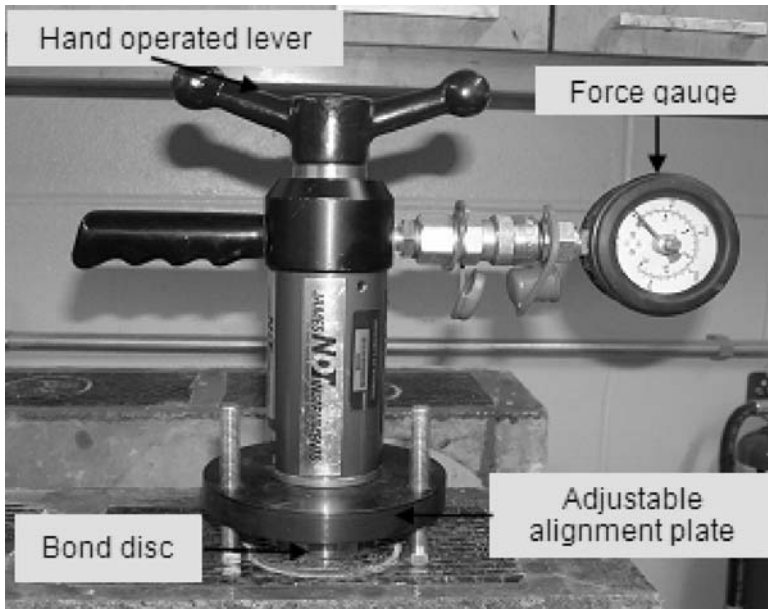


FIG. 3—James 007 Bond Test apparatus, James Instruments Inc., Chicago, IL.

Load was applied at a constant rate of 0.84 mm/min (0.033 in./min) to cause failure in three to five minutes.

After beam flexural testing, the half of the specimen with a CFRP square bonded on the end was tested in direct tension to evaluate the tensile strength of CFRP systems based on ASTM D4541-02 [22]. The CFRP square was cored 2.5 mm (0.1 in.) deep with a 50 mm (2 in.) diameter coring bit. A James Instruments bond testing apparatus (Fig. 3) was used to test the tensile bond strength between the CFRP composite and concrete substrate (www.ndtjames.com). A quick setting adhesive resin was prequalified to ensure that adhesive bond strength was greater than tensile bond strength of the concrete substrate and CFRP composite. The observed failure modes were recorded along with the tensile strength results.

In this study, flexural strength from three-point bending tests and direct tension tests were used as a baseline measurement to quantify the degradation of exposed specimens. The exposed specimens were submerged in elevated water baths for up to 18 months. Groups of three specimens were evaluated for exposure times of twelve months or less and the number of specimens was increased to five for 18 months of exposure.

Test Results

Adhesive bonding between CFRP and concrete is affected by both the flexural and tensile strength. The strength and failure mode are related to the following five parameters: (1) mechanical properties of CFRP materials; (2) adhesive

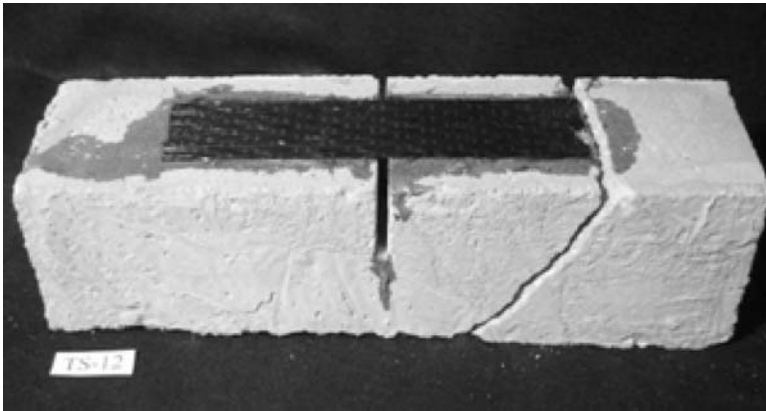


FIG. 4—Flexure-shear failure mode.

strength; (3) concrete strength; (4) concrete surface pretreatment; and (5) effective length of FRP bonding. Currently many different definitions of failure modes exist in CFRP research [23,24]. The research team defined five failure modes in this study listed below and shown in Fig. 4–8.

1. Flexure/shear failure in concrete: Diagonal crack initiated at the end of the CFRP on one end of the specimen; CFRP remains intact and fully attached to the concrete specimen (Fig. 4).
2. Substrate failure: Cohesive failure with rupture surface through concrete paste and aggregate. Concrete remains adhered to CFRP composite (Fig. 5).
3. Adhesive failure: Adhesive failure with rupture surface between CFRP and concrete surface. CFRP failure surface is clean or covered with thin layer of adhesive (Fig. 6).
4. Mixed failure mode: A combination of substrate and adhesive failure (Fig. 7).
5. Composite delamination: CFRP composite splits between laminations. Laminates remain adhered to concrete (Fig. 8).

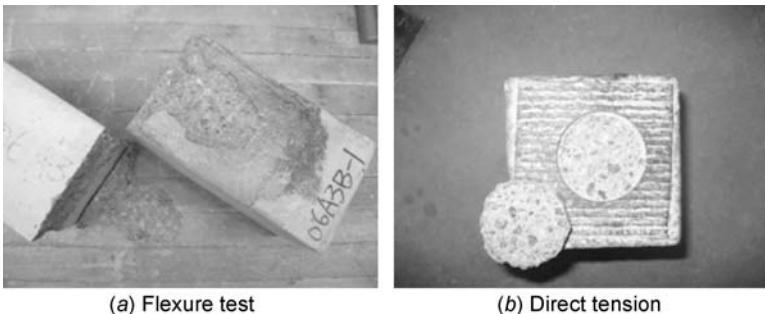


FIG. 5—Substrate failure mode. (a) Flexure test. (b) Direct tension test.

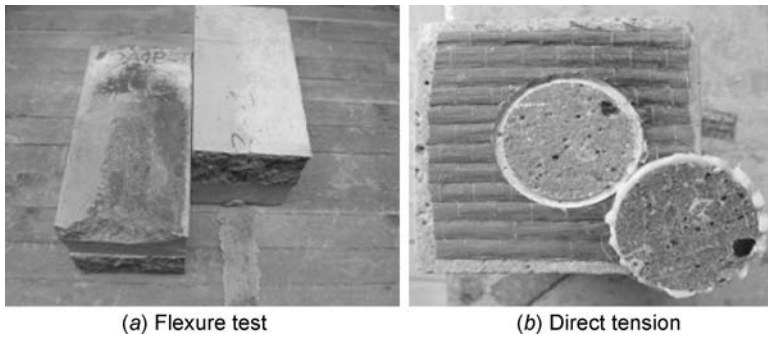


FIG. 6—Adhesive failure mode. (a) Flexure test. (b) Direct tension test.

In this study, Failure Mode 1 is undesirable because it does not identify the adhesive bond strength. The specimen geometry, concrete strength, and CFRP length were selected to ensure Failure Mode 2 through 5 [25]. For three-point bending testing, Failure Mode 2 depends on the concrete strength and bond strength between CFRP composite and adhesive resins, while Failure Modes 3, 4, and 5 depend primarily on the bond strength which is a function of the adhesive strength. An ideal externally bonded composite is stronger than the substrate concrete throughout the life of the structure and minor flaws in the adhesive are not fatal to the system [16]. The heterogeneities from a variety of materials involved in this interface complicate evaluating the bond strength. For externally bonded CFRP applications, the interface between CFRP and concrete substrate is often the weakest zone.

Control specimens were tested for flexural and tensile strength after curing for 14 days in air conditions. Additionally, a number of control specimens were air cured and tested at the conclusion of exposure testing. The investigators designed the specimens to fail in a substrate mode. Conditioned specimens tested later in the program failed by mixed-mode or adhesive failure indicating a loss of strength due to the accelerated aging protocol. A natural log curve was fit to each set of test results based on the 60, 180, 365, and 550 day test results;

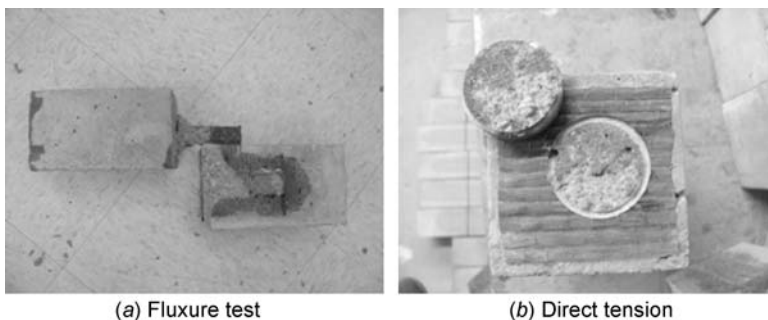


FIG. 7—Mixed failure mode (a) Flexure test. (b) Direct tension test.

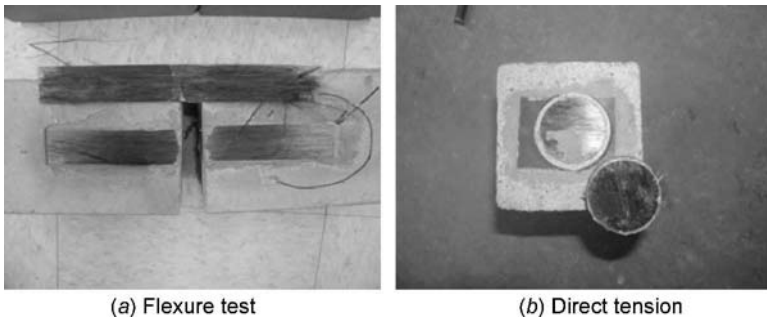


FIG. 8—Composite delamination failure mode. (a) Flexure test. (b) Direct tension test.

this type of curve is consistent with the Arrhenius equation for strength degradation.

The three-point bending test and direct tension test results of CFRP System A versus time are shown in Fig. 9 and Fig. 10, respectively. Strength in flexure tests rapidly decreases during the first two months of exposure at elevated temperatures and then begins to stabilize after twelve months of exposure. Two months of exposure to different elevated temperature results in a reduction of tensile strength of 30 % to 50 % at different temperatures. With the exception of 30°C the same trend is observed in direct tension test results. After six months of exposure the 30°C test results decreased rapidly also.

When compared to the bending test results, direct tension tests show a larger variance. Three possible factors are attributed to this increased variation: test time, potential water exposure or damage during coring, and bond flaws

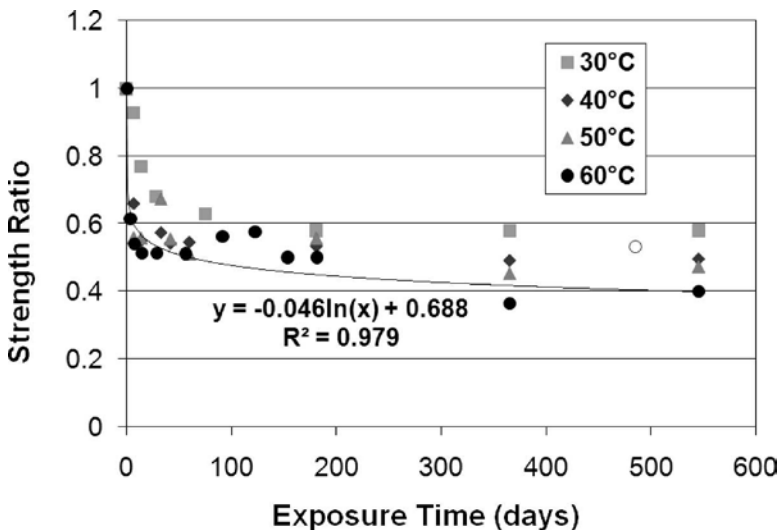


FIG. 9—Failure load ratio versus time for beam tests for CFRP System A.

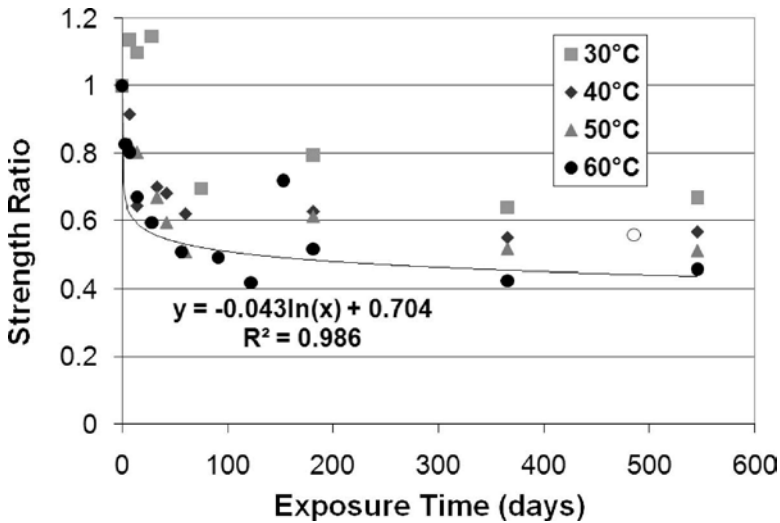


FIG. 10—Failure load ratio versus time for direct tension tests for CFRP System A.

between adhesive and concrete surface. Direct tension tests were performed two days after the flexural bond tests. An automated coring and testing process may decrease the coefficient of variation of the direct tension test results. Flaws or voids between adhesive and concrete surface will have less of an effect on a flexural test and a larger effect on the direct tension test [16]. Thus, a larger coefficient of variation would be anticipated from a tension test versus flexural tests.

The observed failure modes also change as the strength ratio decreases. Before exposure, a substrate failure is observed for both bending and direct tension tests. The failure modes change into adhesive or mixed-mode failure for bending tests and mixed failure for direct tension tests after exposure times of two months or longer. A 35 % decrease in strength was observed after submersion in water at 30°C and a 55 % strength degradation was observed after submersion at 60°C.

Test results of CFRP System B are shown in Fig. 11 and Fig. 12 for bending and direct tension tests, respectively. Exposure to a 60°C water bath results in a 35 % degradation of bending strength in the first two months that tends to stabilize after six months exposure to the same conditions. At higher temperatures, the flexural strength degradation is worse and stabilizes at a lower value. Direct tension test results show a similar degradation trend at the same temperature intervals. As observed in System A, test results of direct tension tests have a larger variation than flexural tests. The strength degradation is higher for flexural specimens than direct tension specimens for the same exposure conditions. As with CFRP System A, the failure modes change from substrate shear/interfacial failure mode to interfacial failure mode for flexural tests. Direct tension tests also change from substrate failure to interfacial or mixed failure modes.

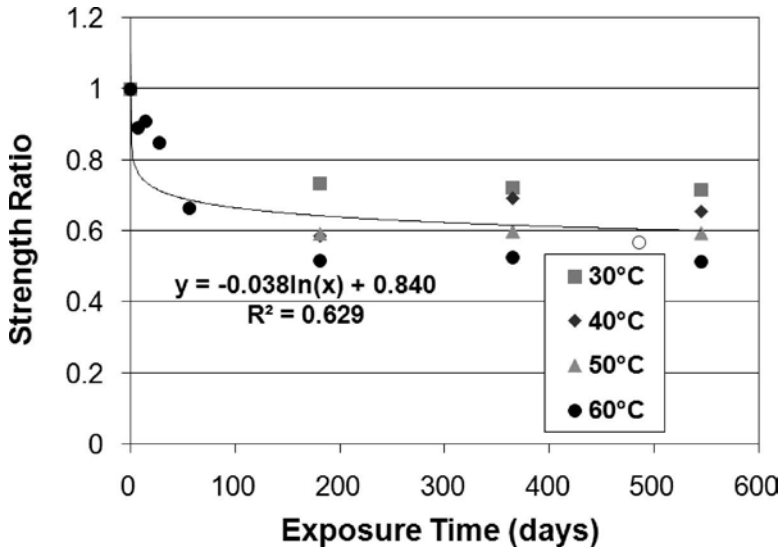


FIG. 11—Failure load ratio versus time for beam tests for CFRP System B.

Other investigators [8,15,26] report similar losses and suggest this loss can be partially recovered after drying. To evaluate this theory further, five beam specimens of Composite A and B Systems were removed from the 60°C water bath tanks at 16 months exposure, and placed in a dry environment for two months. After drying, these beam specimens were tested. Test results are presented by an open circle in Fig. 9 to Fig. 12. Compared to the specimens with

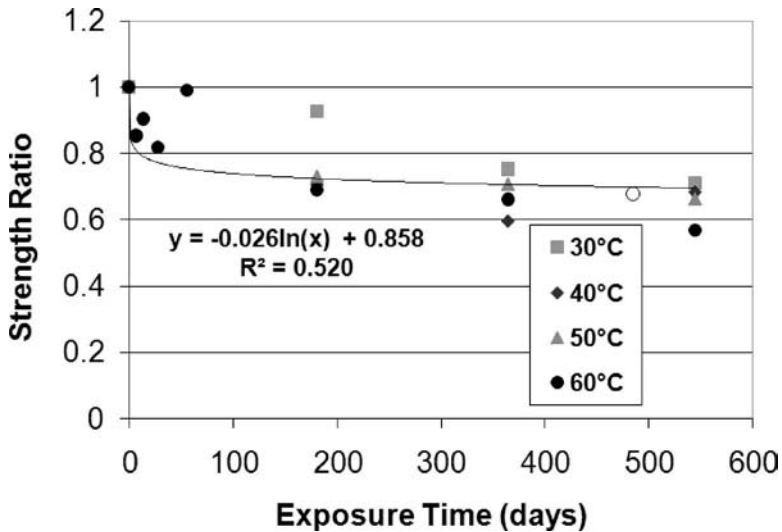


FIG. 12—Failure load ratio versus time for direct tension tests for CFRP System B.

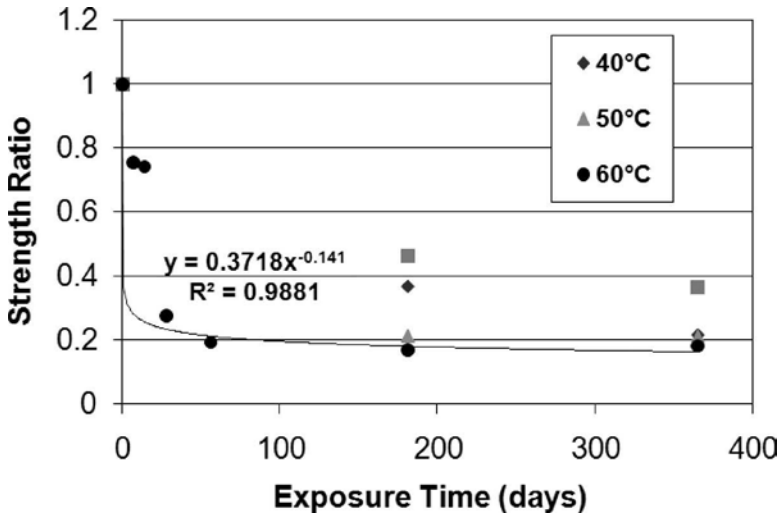


FIG. 13—Failure load ratio versus time for beam tests for CFRP System C.

18 months of continuous exposure at 60°C, the flexural strength of dried specimens showed a 5 to 15 % flexural strength recovery. These tests imply that only a partial strength recovery is possible after drying.

CFRP System C test results are shown in Fig. 13 and Fig. 14 for flexural and direct tension tests, respectively. These test results indicate that exposure at 60°C water bath over 28 day leads to a 100 % reduction of flexural and tensile strength, and the corresponding failure mode is composite delamination as

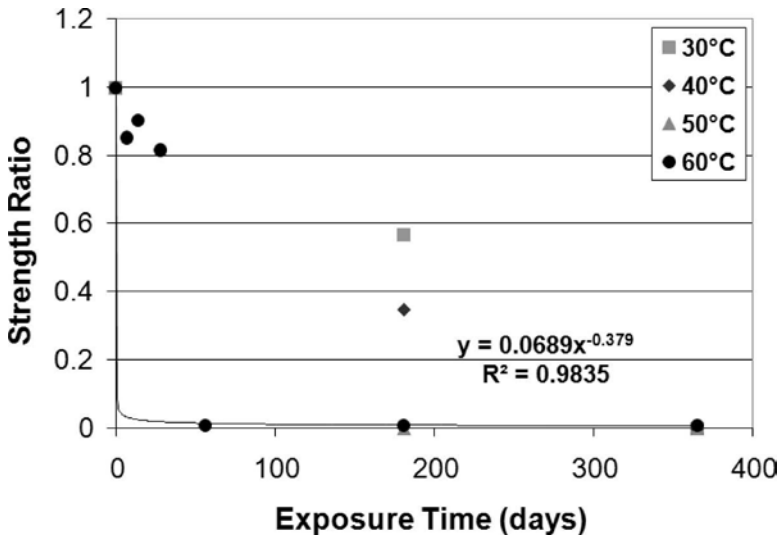


FIG. 14—Failure load ratio versus time for direct tension tests for CFRP System C.

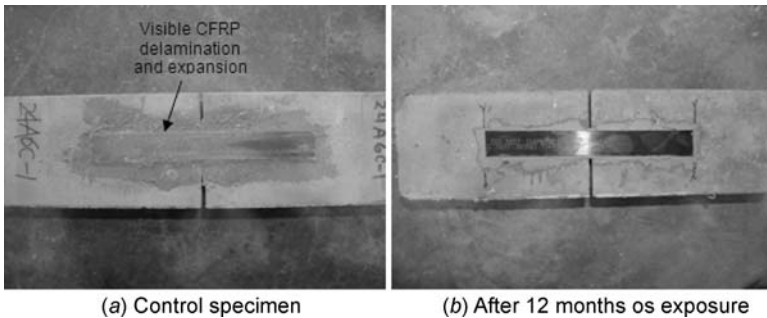


FIG. 15—Comparison of CFRP System C Specimens before and after exposure. (a) Control specimen. (b) After twelve months of exposure.

shown in Fig. 15. The degradation was so severe in this epoxy system that a power curve was used to keep strength ratio positive. The flexural beam strength of the plain concrete prisms with the saw cut and without CFRP was approximately 20 % of the control strength. Consequently, once the strength ratio of the CFRP flexural specimens drops below 20 % it is equivalent to zero additional strength from the CFRP. After six months of exposure, CFRP System C specimens at 50°C and 60°C lost nearly all the flexural strength due to FRP material. Specimens subjected to 30°C and 40°C exposure degrade 50–65 %. Twelve month exposure results indicate that CFRP System C lost all bond strength at 40°C and nearly all bond strength at 30°C. Direct tension test results show the same trend as flexural tests. Eighteen month tests were unnecessary since visual deterioration of CFRP material (Fig. 15) confirmed measured test results of 100 % loss of bond strength.

Using the curve fit data for each system, an extrapolation of the strength ratio for periods between one to five years is plotted in Fig. 16. Although direct tension test results are higher, there is more variation in these data. An appropriate strength ratio for System B based on flexural results would be between 0.55 and 0.6. System A would have a knock down factor between 0.35 and 0.4 based on this extrapolation. For practical purposes System C has no remaining strength after exposure.

Five main theories of adhesion contribute to bond strength: mechanical interlock; adsorption; diffusion; chemical bonds; and electrostatic forces [27]. Mechanical interlock occurs when the liquid adhesive penetrates the roughened concrete surface and then solidifies to enhance bond strength by forcing material failure in the adhesive. The irregularities, concrete surface pores, or any rough surfaces improve the bond strength. Water absorption into the adhesive decreases epoxy stiffness and dramatically decreases bond strength between the epoxy matrix and concrete. This leads to a lower T_g , a lower modulus of elasticity, and an increase in the creep rate. All of the above factors accelerate the adhesive bond failure, and the adhesive becomes more sensitive to increases in temperature. Water uptake is a thermodynamic property that depends on the sensitivity of the material to absorption, inherent water content, and relative vapor pressure. Submerging the specimen provides the highest

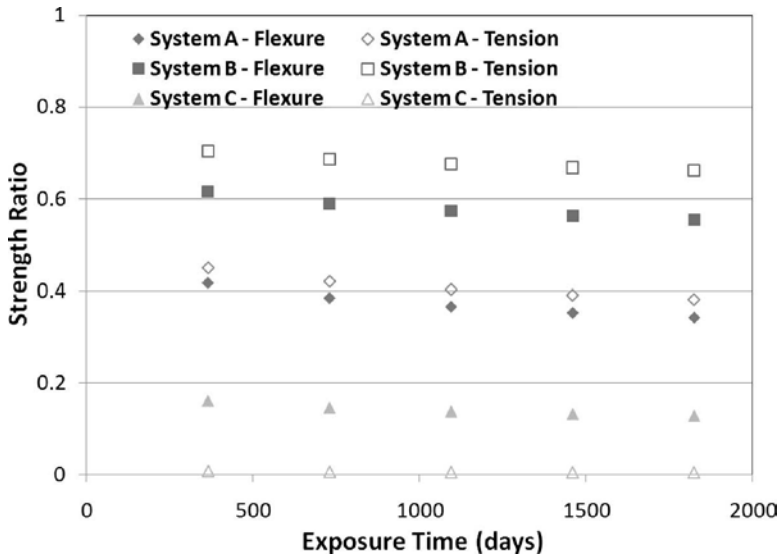


FIG. 16—Extrapolation of data for time periods between one and five years.

vapor pressure and maximum absorption. Elevated temperature accelerates the absorption rate. The absorption has a direct impact on the chemical bond.

Conclusions

Three commercial CFRP external application systems are considered in this study to evaluate strength degradation of CFRP specimens submerged in elevated temperature water baths. The accelerated aging in this study directly results in a rapid strength reduction, but different composite systems exhibit different strength losses. In terms of the test results, the failure load ratio for direct tensile strength is generally higher than that of flexural tests, which is in agreement with other investigators [28]. Although direct tension tests show higher variation than flexural tests, the degradation trend from direct tension tests is generally consistent with those observed in the flexural tests. Test results from the 18 month samples indicate that strength degradation of CFRP external application systems is closely related to water present at the bond line, exposure temperature, and inherent properties of the CFRP composite systems. No CFRP rupture failure or concrete shear failure was observed after 18 months exposure at the highest temperature for CFRP System A and B. For CFRP System C, composite delamination failure occurred, which indicates that the composite of CFRP System C experienced 100 % strength degradation and should not be used when exposed to moisture and elevated temperatures.

Based on the test results and above analysis, the following conclusions are drawn:

- An effective adhesive will develop the strength of the concrete substrate;
- After environmental exposure, bond between adhesive and concrete surface is often the weakest zone for externally applied CFRP;
- Water and temperature are two key variables that affect the bond performance of CFRP;
- Different composite systems exhibit different bond performance when subject to submersion in elevated temperature water baths, and the bond performance appears related to the composition of CFRP and adhesive materials;
- Selection of CFRP composite systems should be based on the specific service environment and mechanical and chemical properties of CFRP and adhesive materials;
- Using elevated temperature water baths as an accelerated aging method is conservative for CFRP composite applications in a wet environment, but may be too harsh for a completely dry environment; and
- Two months of submersion in elevated temperature water baths is a conservative predictor of accelerated aging.

Since the mechanical and chemical composition of commercial CFRP composite systems vary, additional data on the long-term bond performance of CFRP composite systems must be developed experimentally on a product-by-product basis at various field conditions.

To fully understand accelerated aging of externally bonded CFRP applications without testing each resin individually, researchers must develop an understanding of mechanical and chemical bond properties of the CFRP system and the influence of water content and temperature on bond. Further research may provide a logical categorization of CFRP composite systems based on better defined mechanical and chemical properties of adhesive materials and different environments. Presently the proposed strength reduction factor for durability is the strength ratio of specimens submerged in water at 60°C for 60 days, which provides a lower bound durability strength reduction factor for CFRP applications. Investigators are looking into tests at different relative humidity ratios and wet/dry conditioning.

Acknowledgments

The authors gratefully acknowledge the funding support of National Cooperative Highway Research Program under Project No. NCHRP 12-73. The opinions expressed in this paper are those of the authors and not of NCHRP.

References

- [1] Bank, L. C. and Gentry, T. R., "Accelerated Test Methods to Determine the Long-Term Behavior of FRP Composite Structures: Environmental Effects," *J. Reinf. Plast. Compos.*, Vol. 14, 1995, pp. 558-587.
- [2] Byars, E. A., Waldron, P. W., Dejke, V., and Demis, S., "Durability of FRP in Concrete: Deterioration Mechanisms," *Proceedings, FRP Composites in Civil Engineering*, Vol. II, Elsevier, Hong Kong, Dec. 2001, pp. 1517-1525.

- [3] Byars, E. A., Waldron, P. W., Dejke, V., and Demis, S., "Durability of FRP in Concrete: Current Specifications and a New Approach," *Proceedings, International Journal of Materials and Product Technology*, Vol. 19, Nos. 1–2, 2003, pp. 40–52.
- [4] Chajes, M. J., Finch, W. W., Januszka, T. F., and Thomson, T. A., "Bond and Force Transfer of Composite Material Plates Bonded to Concrete," *ACI Structural Journal*, Vol. 93, No. 2, March-April, 1996, pp. 209–217.
- [5] Toutanji, H. A. and Gomez, W., "Durability Characteristics of Concrete Beams Externally Bonded with FRP Composite Sheets," *Cem. Concr. Compos.*, Vol. 19, 1997, pp. 351–358.
- [6] Grace, N. F. and Singh, S. B., "Durability Evaluation of Carbon Fiber-Reinforced Polymer Strengthened Concrete Beams: Experimental Study and Design," *ACI Structural Journal*, Vol. 102, No. 1, Jan.-Feb. 2005, pp. 40–53.
- [7] *NCHRP Report 514: "Bonded Repair and Retrofit of Concrete Structures Using FRP Composites—Recommended Construction Specifications and Process Control Manual,"* 2004.
- [8] Lefebvre, D. R., Takahashi, K. M., Muller, A. J., and Raju, V. R., "Degradation of Epoxy Coatings in Humid Environments: The Critical Relative Humidity for Adhesion Loss," *J. Adhes. Sci. Technol.*, Vol. 5, No. 3, 1991, pp. 221–227.
- [9] Au, C. and Buyukozturk, O., "Peel and Shear Fracture Characterization of Debonding in CFRP Plated Concrete Affected by Moisture," *J. Compos. Constr.*, Vol. 10, 2006, pp. 35–47.
- [10] Malvar, L. J., Joshi, N. R., Beran, J. A., and Novison, T., "Environmental Effects on the Short-Term Bond of Carbon Fiber-Reinforced Polymer (CFRP) Composites," *J. Compos. Constr.*, Vol. 7, No. 1, Feb. 2003, pp. 58–63.
- [11] Karbhari, V. M. and Engineer, M., "Effect of Environmental Exposure on the External Strengthening of Concrete with Composites-Short-Term Bond Durability," *J. Reinf. Plast. Compos.*, Vol. 15, No. 12, 1996, pp. 1194–1216.
- [12] Abanilla, M. A., Li, Y., and Karbhari, V. M., "Durability Characterization of Wet Layup Carbon/Epoxy Composites Used in External Strengthening," *Composites: B* 2006, Vol. 37, No. 1–2, 2006, pp. 200–212.
- [13] Abanilla, M. A., Li, Y., and Karbhari, V. M., "Interlaminar and Intralaminar Durability Characterization of Wet Layup Carbon/Epoxy Composites Used in External Strengthening," *Composites: B* 2006, Vol. 37, No. 7–8, 2006, pp. 650–661.
- [14] Karbhari, V. M. and Abanilla, M. A., "Design Factors, Reliability, and Durability Prediction of Wet Layup Carbon/Epoxy Composites Used in External Strengthening," *Composites: B* 2006, Vol. 38, No. 1, 2007, pp. 10–23.
- [15] Toutanji, H. A. and Gomez, W., "Durability Characteristics of Concrete Columns Confined with Advanced Composite Materials," *Composite Structures*, Vol. 44, 1999, pp. 155–161.
- [16] Dolan, C. W., Ahearn, E. A., Deng, J., Tanner, J. E., and Mukai, D., "Durability and Accelerated Ageing Testing of CFRP Repair System," *4th International Conference on FRP Composites in Civil Engineering, (CICE2008)* 22–24 July 2008, Zurich, Switzerland.
- [17] Dai, J. G. "Interfacial Models for Fiber Reinforced Polymer (FRP) Sheets Externally Bonded to Concrete," Ph.D. Dissertation, Hokkaido University, Japan, 2003.
- [18] Toutanji, H. and Ortiz, G., "The Effect of Surface Preparation on the Bond Interface between FRP Sheets and Concrete Members," *Composite Structures*, Vol. 53, 2001, pp. 457–462.
- [19] Lorenzis, L. D., Miller, B., and Nanni, A., "Bond of Fiber-Reinforced Polymer Laminates to Concrete," *ACI Mater. J.*, Vol. 98, No. 3, May-June 2001, pp. 256–264.
- [20] Li, W. W., Yan, Z. L., Cao, Z. L., and Pan, J. L., "Effect of Concrete Surface Rough-

- ness on the Bonding Performance between the CFRP and Concrete,” *Journal of Shenzhen University Science and Engineering*, Vol. 24, No. 1, Jan. 2007.
- [21] ASTM Standard C78-02, “Standard Test Method for Flexural Strength of Concrete (Using Simple Beam with Third-Point Loading,” *Annual Book of ASTM Standards*, ASTM International, West Conshohocken, PA.
- [22] ASTM Standard D4541-02, “Standard Test Method for Pull-Off Strength of Coatings Using Portable Adhesion Testers,” *Annual Book of ASTM Standards*, ASTM International, West Conshohocken, PA.
- [23] Karbhari, V. M., “Characteristics of Adhesion between Composites and Concrete as Relate to Infrastructure Rehabilitation,” *27th International SAMPE Technical Conference*, 9–12 Oct. 1995.
- [24] Teng, J. G., Chen, J. F., Smith, S. T., and Lam, L., “Behaviour and Strength of FRP-Strengthened RC Structures: A State-of-the-Art Review,” *Proceedings of the Institution of Civil Engineering—Structures and Buildings*, Vol. 156, No. 1, 2003, pp. 51–62.
- [25] Gartner, A. L., “Development of a Flexural Bond Strength Test to Determine Environmental Degradation of Carbon Fiber-Reinforced Polymer (CFRP) Composites Bonded to Concrete,” MS Thesis, University of Florida, March 2007.
- [26] Abanilla, M. S., Li, Y., and Karbhari, V. M., “Durability Characterization of Wet Layup Graphite/Epoxy Composites Used in External Strengthening,” *Composites, Part B: Engineering*, Vol. 37, No. 2–3, April 2005/March 2006, pp. 200–212.
- [27] Horiguchi, T. and Saeki, N. “Effect of Test Methods and Quality of Concrete on Bond Strength of CFRP Sheet,” *Non-Metallic (FRP) Reinforcement for Concrete Structures, Proceedings of the 3rd International Symposium*, Vol. 1, Oct. 1997.
- [28] Mays, G. C. and Hutchinson, A. R., *Adhesives in Civil Engineering*, Chapter 2, Cambridge University Press, Cambridge, U.K., 1992.

Michael A. Lacasse,¹ Hiroyuki Miyauchi,² and J. Hiemstra³

Water Penetration of Cladding Components—Results from Laboratory Tests on Simulated Sealed Vertical and Horizontal Joints of Wall Cladding

ABSTRACT: Considerable work has focused on the deterioration of jointing compounds used to seal building joints; less emphasis has been placed on understanding the consequences of seal failure, particularly in respect to watertightness. Jointing products are subjected to different climate effects; some induce aging in the sealant that in time leads to deficiencies. Deficiencies may also come about from design faults or improper installation. Water entry at deficiencies may lead to a number of different deteriorating effects on the building fabric that may induce failure of other envelope components or premature failure of the joint sealant. Joints are also subjected to substantial wind driven rain loads, in particular atop multi-story buildings. The approach taken in this study focuses on determining the fault tolerance of joint systems of a simulated wall panel when subjected to watertightness tests that emulate heightened wind-driven rain loads. Vertical and horizontal joints of 20 mm width and sealed with a one-component polyurethane product were subjected to water spray rates ranging between 1.6 and 6 L/(min·m²) and pressures of up to 2 kPa. Faults introduced to the sealed joint and representative of deficiencies through which water could penetrate consisted of cracks of 2 to 16 mm long introduced along the sealant to substrate interface. For specific crack lengths, the crack size related to the degree of joint extension, the extension reaching a maximum of 10 % of joint width. Rates of

Manuscript received July 28, 2008; accepted for publication April 8, 2009; published online June 2009.

¹ Senior Research Officer, Ph.D., P. Eng., National Research Council Canada, Institute for Research in Construction, Ottawa, Canada.

² Assistant Professor, Dr. Eng., Department of Architectural Engineering, Chungnam National University, Daejeon, Republic of Korea.

³ Technical Assistant, National Research Council Canada, Institute for Research in Construction, Ottawa, Canada.

Cite as: Lacasse, M. A., Miyauchi, H. and Hiemstra, J., "Water Penetration of Cladding Components—Results from Laboratory Tests on Simulated Sealed Vertical and Horizontal Joints of Wall Cladding," *J. ASTM Intl.*, Vol. 6, No. 6. doi:10.1520/JAI102048.

Copyright © 2009 by ASTM International, 100 Barr Harbor Drive, PO Box C700, West Conshohocken, PA 19428-2959.

water entry across the joint were determined for cracks of different lengths and size and the nature of water entry at deficient joints in which cracks were introduced was also examined. Results on vertical joints indicated that water readily enters open cracks in relation to the crack size, quantity of water present at the crack, and pressure across the opening. Water may also penetrate cracks of nonextended “closed” joints.

KEYWORDS: fault tolerance, joint deficiencies, sealant failure, watertightness, water penetration, testing

Introduction

Overview

Considerable work has focused on the deterioration of jointing compounds used to seal building joints, either to determine suitable methods to evaluate loss in their pertinent physical or chemical characteristics or establish test methods to evaluate their expected long-term performance. Less emphasis has been placed on understanding the consequences of seal failure along joints, in particular in respect to the expected loss in air and watertightness at the joint.

Jointing products are subjected to a number of climatic effects, some of which induce aging in the sealant that in time may lead to openings or deficiencies along the joint. Deficiencies may also come about from design faults or improper installation. Indeed, deficiencies due either to the effects of aging or from lack of attention to details or installation practice are inherent to any jointing system.

Joints are also subjected to substantial wind-driven rain loads atop multi-story buildings, in particular those located along an exposed coastline. Water entry at deficiencies along joints may lead to: leakage to the interior living space resulting in the formation of mold; moisture uptake by moisture sensitive components in the wall assembly, such as corrosion prone metal substrates or rot sensitive wood components; the premature loss in adhesion of the sealant. To what extent are joints, having small deficiencies through which water enters, vulnerable to water leakage when subjected to a substantial rain event, such as a typhoon, as might be experienced in Japan, or a severe thunderstorm or hurricane as in North America? Indeed, what wind-driven rain loads might be associated with a typhoon or hurricane and how often do these occur in a given climate? In other words, what risk might there be of water entry for any location, given a specific building height, façade type, and joint configuration and inherent deficiencies in the jointing system? How fault tolerant is the façade jointing system?

As an initial step, it is useful to briefly review the incidence and nature of failure at joints and thereafter, gain some insight into the nature of climate loads atop buildings subjected to wind-driven rain and loads associated with typhoon, hurricane, and storm events.

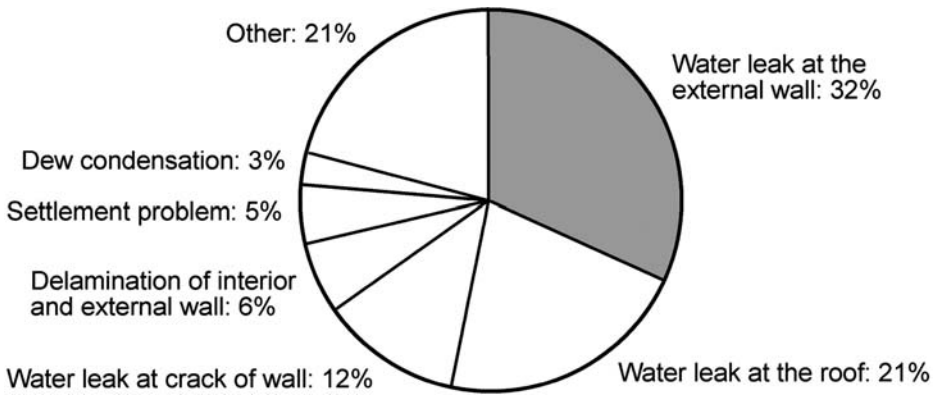


FIG. 1—Investigation of defects and complaints of building work in Japan [5].

Defects in Buildings Envelopes and Jointing Systems

Few comprehensive surveys have been published on the incidence of failure in building joints; there is literature that is of some value, notably that from survey work carried out in the U.K. [1], the results of which are reportedly [2] emulated by a similar work in Japan [3]. The highlights of the survey conducted in 1990 in the U.K. indicated that 55 % of joints failed within less than ten years, and only 15 % lasted more than 20 years.

In North America, interestingly, little has been published on this topic although there is information on individual buildings, specifically that published by Huff [4] who provides examples of two surveys, one of which was carried out on a newly constructed eleven-story building and the other, on a twin eighteen-story condominium in Long Beach, CA. In the latter case, a 5.6 % failure rate was detected in the EIFS cladding joints based on 1, 5, and 10 % sampling rates. Interestingly Huff [4] determined from this that the failure rate remained constant irrespective of the sample size.

The former example [4] of the eleven-story building had a total of ca. 10700 m (35 000 ft) of jointing product installed. The survey was conducted on two of 24 grid locations representing an 8.3 % sampling rate. From this study, 14 adhesive failures were detected on one grid section, and 20 on the other, yielding an average of 17 failures per grid section. Based on this information an estimate of the number of failures in adhesion of the entire building was 408 whereas, following a survey of the entire building 427 adhesive failures were uncovered (i.e., a 0.2 % failure rate). The author notes that although the failure rate appears small, there are nonetheless 427 failure locations that represents, based on an average length of failure of 50 mm (2-in.), approximately 21.6 m (71-ft) of product that has failed and through which water can enter.

An investigation of defects and complaints of execution of constructed works in Japan was reported by the Building Construction Society of Japan, results for which are summarized in Fig. 1 [5]. The results indicate that 65 % relate directly to water leakage, of which 44 % can be attributed to water leakage of the wall system and of this proportion, 32 % of the defects are due to

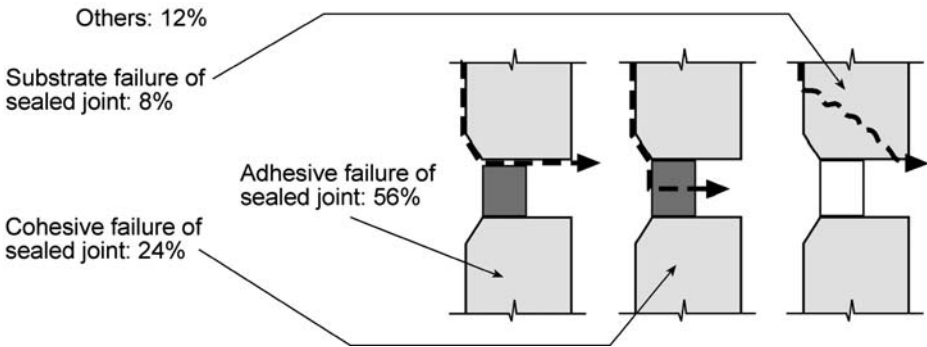


FIG. 2—Cause of failure of sealed joint in Japan [6].

leakage at the exterior of the wall, that is, at the jointing system. Hence, based on the results of this study, it is evident that a considerable proportion of defects accrue from water leakage alone. Thus understanding the nature of wind-driven rain is important when assessing the loads to which the building envelope is subjected. Additionally, considering the relatively high portion of defects attributable to jointing systems suggests that attention be placed not only on the nature of failure at joints but also, the consequences of failure.

In respect to the nature of failure at joints, the Building Construction Society of Japan reports on the different types of failure of jointing products, as summarized in Fig. 2 [6]. The greatest proportion of failures can be attributed to failure due to adhesion (56%), whereas, the proportion of failures in cohesion is reported as 24% [6].

This may broadly suggest that when attempting to determine the significance of jointing product failures on the watertightness of joints, defects such as those that accrue due to adhesion failure should first be investigated as these are perhaps the more likely to occur in building joints.

In general then, deficiencies in building façade joints are inherent in any façade jointing system even those for which proper installation procedures have been conscientiously followed. These deficiencies would typically be adhesive in nature and could lead to leakage across the wall joint. However, given that openings exist along joints, water leakage evidently can only occur if water is present at the opening and if there are forces driving water through these deficiencies. The presence of water on the façade is in part a function of the climate loads, specifically, the intensity of wind driven rain, that varies, not only in relation to the basic climate parameters of wind speed and rainfall intensity, but also in respect to the height and width of the building, and orientation of the building to the prevailing direction of the driving rain. Features on the façade such as overhangs and balconies necessarily affect local deposition of water on the façade, such features shielding the façade from direct rainfall. Once water is deposited on the façade, it migrates downwards, the concentration of water being determined by different vertical and horizontal features that form part of the cladding proper [7]. In this paper, some basic information

TABLE 1—Characteristic wind speeds and related velocity pressures for different categories of tropical cyclonic events.

Category	Wind Speed (km/h)	Velocity Pressure ^a (Pa)
WEAK TROPICAL STORM		
Speeds/velocity pressures	42–69	82–224
Gust speeds/pressures	64–103	198–515
SEVERE TROPICAL STORM		
Speeds/velocity pressures	69–103	224–515
Gust speeds/pressures	105–151	550–1080
Category 1 HURRICANE/MINIMAL TYPHOON		
Speeds/velocity pressures	105–132	515–840
Gust speeds/pressures	153–193	1130–1850
Design wind pressure/speed for Southern Coastal U.S.	113	581 (12 psf)

^a P_v (Pa) = $1/2 \rho v^2$; ρ_{air} = ca. 1.2 kg m^{-3} ; v (ms^{-1}).

relating to wind speed and rainfall intensity during key climate events is given such that these can be related to test loads used in assessing wall and cladding weathertightness performance.

Characteristics of Climate Loads

Wind driven rain is necessarily characterized by two basic climate parameters: wind or wind speed, and rainfall intensity, the latter parameter typically referred to as the rainfall rate and reported in mm/h. Wind driven rain events are associated with tropical cyclonic events such as tropical storms, typhoons (in the Western Pacific), and hurricanes (in the Eastern Atlantic). Table 1 provides the range of wind speeds and related velocity pressures in relation to different categories of tropical cyclonic events.

The values provided in Table 1 are those that occur at a height of 10 m, the height at which meteorological data are collected. Thus these would suffice for estimating the wind loads for a residential building of three stories or less. Wind loads atop buildings of greater height can be estimated by using the following equation for velocity pressure, q_z , given in ASCE-7 [8]:

$$q_z (\text{Nm}^{-2}) = 0.613 [2.01 (z/z_g)^{2/\alpha}] K_{zt} K_d V^2 I \quad (1)$$

where z = height above ground (m); z_g = 213.36 m (atmospheric boundary layer reference height); and assuming, $\alpha=7$ and $\alpha=11.5$ for exposure categories B and D, respectively, and I (Importance factor); K_{zt} (topographic factor); K_d (wind directionality factor) = 1.

For example, using this relationship, and assuming wind velocities at 10 m consistent with the range of speeds associated for a severe tropical storm (i.e., 69–103 km/h), information on velocity pressures at different building heights for different exposure categories such as urban (Exposure Category B) and flat,

TABLE 2—Velocity pressures at different building heights associated with severe tropic storms for buildings subjected to ASCE Exposure Categories B (urban, suburban) and D (flat, unobstructed).

Height (m)	Story ^a	Velocity Pressure (Pa)	
		Exposure Category B	Exposure Category D
10	3	183–417	258–587
30	10	250–571	313–711
75	25	326–742	367–834
150	50	398–904	413–941

^aEstimate assuming a 3-m story height.

open terrain (Exposure Category D) can be estimated as given in Table 2. The information is important because it shows that the pressures are not linearly proportional to the height but vary exponentially in height, thus the severity of the wind can be significantly more important atop tall buildings as compared to low-rise structures. This may be self-evident, however, it bears directly on the risk to water entry through small openings in exposed joints of tall buildings as the risk to entry is itself proportional to the pressure difference across the joint.

Rainfall Intensity during Storms—An example of the amount of rainfall that can occur during a typhoon is provided in Fig. 3 [9] that shows the temporal

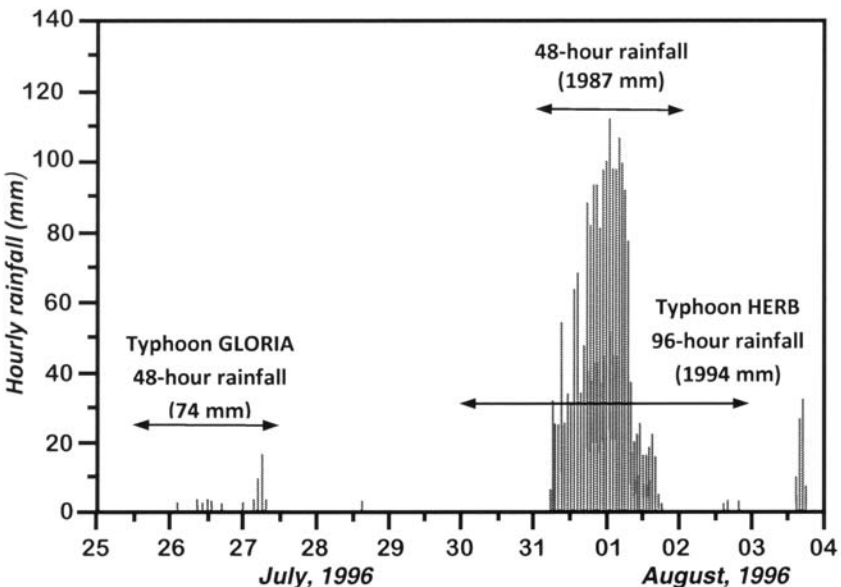


FIG. 3—Temporal rainfall variation during Typhoon Gloria and Herb, 1996 [10].

variation in rainfall intensity for an occurrence of two typhoons in Taiwan in 1996. Taiwan receives an annual rainfall of 2500 mm of which 80 % of the annual rainfall occurs in May to October and especially during typhoons. Rainfall intensity during some typhoons may exceed 100 mm/h and 1000 mm over a 24-h period with the recorded maximum one-hour and 24-h rainfall before 1996 being 300 mm and 1672 mm, respectively [9]. As can be seen in Fig. 3, the recorded 96-h rainfall for Typhoon Herb was accompanied by heavy rain that reached 1994 mm over this period, the bulk of the rain falling in a 48-h period (1987 mm) with maximum rainfall rates attaining values in exceedence of 110 mm/h.

Relating Test Conditions to Weather Parameters—A summary of extreme wind-driven rain (WDR) conditions in relation to the return period in years is provided in Table 3 for different locations across the United States including: Boston, MA, Miami, FL, Minneapolis, MN, Philadelphia, PA, and Seattle, WA [11]. Information on rates of wind-driven rain ($L/(\text{min}\cdot\text{m}^2)$) and driving rain wind pressures (DRWP) are given as average extreme hourly values. The DRWP is the velocity pressure exerted on a surface (e.g., wall) normal to the wind direction during rain. The analysis from which these values were determined also indicated that the wind driven rain values provided for Miami, FL would be overestimated for shorter return periods (i.e., ≤ 10 years), and underestimated for the longer return periods (≥ 20 yrs); the extent of under or over estimation has not yet been determined as this would require a more detailed analysis of the effects of tropical cyclonic activity on the wind-driven rain and driving rain wind pressures.

In the United States, design wind pressures are derived from information based on a 1 in 50-year return period [12]. With reference to this return period, extreme WDR conditions in Miami, FL indicate a water deposition load of $3.9 L/(\text{min}\cdot\text{m}^2)$ and a DRWP of 553 Pa, whereas in comparison, Seattle, WA provides for much reduced WDR loads; $0.3 L/(\text{min}\cdot\text{m}^2)$ and a DRWP of 198 Pa. It should be emphasized that these values represent extreme values associated with each individual driving rain parameter and are unlikely to occur coincidentally.

This implies that testing at conditions in which both extremes are used would subject a specimen to an event that would have a much heightened return period as compared to the return period associated with a particular extreme WDR parameter. Typically, for nontropical cyclonic events, at heightened rates of wind-driven rain, the corresponding DRWP are lower than those of the extreme values shown in the table and likewise, rates of WDR are lower when extreme values of DRWP are evident.

However, what is evident from this information is that tests undertaken at the 700 Pa level and $3.4 L/(\text{min}\cdot\text{m}^2)$ adequately represent expected extremes for the different locations of the United States provided in Table 3. The WDR rates at which tests were conducted (i.e., 0.8, 1.6, and $3.4 L/(\text{min}\cdot\text{m}^2)$) may be slightly higher than that provided in Table 3 for Seattle and Boston; however, the threshold value for WDR rate of $0.8 L/(\text{min}\cdot\text{m}^2)$ is reflected in values given for Minneapolis at a 1 in 10-year return period ($0.76 L/(\text{min}\cdot\text{m}^2)$), Philadel-

TABLE 3—Summary of extreme WDR values.

Location	BOS		MIA		MSP		PHL		SEA	
Return Period	WDR, L/(min-m ²)	DRWP, Pa	WDR, L/(min-m ²)	DRWP, Pa	WDR, L/(min-m ²)	DRWP, Pa	WDR, L/(min-m ²)	DRWP, Pa	WDR, L/(min-m ²)	DRWP, Pa
2	0.40	197	0.883	121	0.45	105	0.466	122	0.167	109
5	0.483	247	1.85	259	0.633	134	0.6	172	0.2	137
10	0.55	280	2.48	351	0.766	153	0.7	206	0.233	156
20	0.617	311	3.1	439	0.833	171	0.783	238	0.266	174
30	0.65	329	3.45	490	0.95	182	0.85	256	0.266	185
50	0.70	352	3.88	553	1.033	195	0.9	279	0.3	198
100	0.75	383	4.483	638	1.15	212	1	310	0.316	216

BOS=Boston, MA; MIA=Miami, FL; MSP=Minneapolis, MN; PHL=Philadelphia, PA; SEA=Seattle, WA.

phia at a 1 in 20 year return period ($0.78 \text{ L}/(\text{min}\cdot\text{m}^2)$), and every other year in Miami (1-in-2 yr: $0.88 \text{ L}/(\text{min}\cdot\text{m}^2)$). It is cautioned that for Miami, FL the values provided are likely an overestimate of WDR.

Overview of Approach

The question of fault tolerance in jointing systems has not yet been broadly explored and the approach taken in this study provides some fundamental information on the nature of water entry at joints. In this paper, information is provided on results from a laboratory study on the weathertightness of vertical and horizontal joints of a simulated wall system when subjected to water penetration tests in which test conditions emulate heightened wind-driven rain loads. An account of the experimental program is provided that includes a summary of the approach, and a description of the test apparatus, specimen, methods, and parameters. Thereafter, results of watertightness tests on both vertical and horizontal joints are given in terms of the rates of water entry across the sealed joint in relation to simulated wind-driven rain loads. The discussion focuses on the nature of entry through openings of deficiencies of the jointing product and the function of the backer rod in providing a watertight seal.

Approach and Description of Test Apparatus, Specimen, and Methods

Approach

The fault tolerance of simulated vertical and horizontal panel joints was assessed in a laboratory study in which the degree of watertightness of defective joints was determined by subjecting the joints to a range of simulated wind-driven rain loads, loads that were consistent with those that might be found atop tall buildings in a severe storm event. The joints were 20 mm wide and consisted of a one-component polyurethane product and closed cell backer rod. Small deficiencies (cracks), ranging in size between 2 and 16 mm in length, were purposely introduced in the jointing product, thus permitting water to pass through these openings. The joint was extended up to a maximum of 10 % of joint width so that the nature and size of the crack could be varied. Consequently, joints with cracks of varying length and size were subjected to water spray rates ranging between 1.6 and $6 \text{ L}/(\text{min}\cdot\text{m}^2)$ and pressures of up to 2 kPa. The watertightness tests were carried out using a purposely developed test apparatus described in detail in the subsequent section.

Test Apparatus

The water penetration tests were carried out using a recently developed test apparatus (Fig. 4) in which both the quantity of water applied to the surface of the test specimen and the air pressure difference across the assembly were automatically regulated. An elevation view of the test frame of the Mini-Dynamic Wall Testing Facility (m-DWTF) is shown in Fig. 5; a vertical sectional

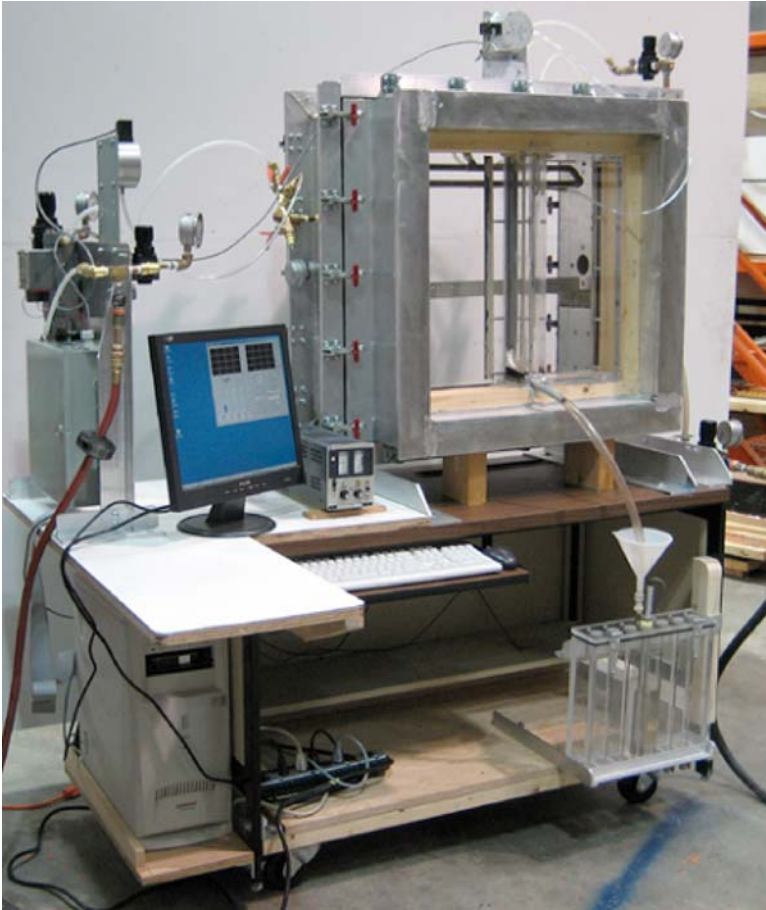


FIG. 4—Mini-Dynamic Wall Testing Facility configured for testing vertical joint.

view of the same apparatus is given in Fig. 6. Other basic components of the apparatus including the air and water pressure control systems, data acquisition and control systems, and the PC-based central processing unit are illustrated in Fig. 5. The automated setup permits acquiring information on spray rate, pressures differentials, and water collection rates in real-time over the course of a test sequence.

The water spray attachment (rack or individual nozzle) is located on the test frame; the rate of water supplied to the spray attachment is monitored from a flow sensor (Kobold; Model DPM-1170N2F300). The supply water is drained through an opening at the base of the test frame. Likewise, a drain is provided at the base of the test specimen (Fig. 5) to remove water leakage that accumulates in the space just beyond the interior plane of the jointing system. This water may also be collected in a calibrated vessel (Fig. 6) in which is

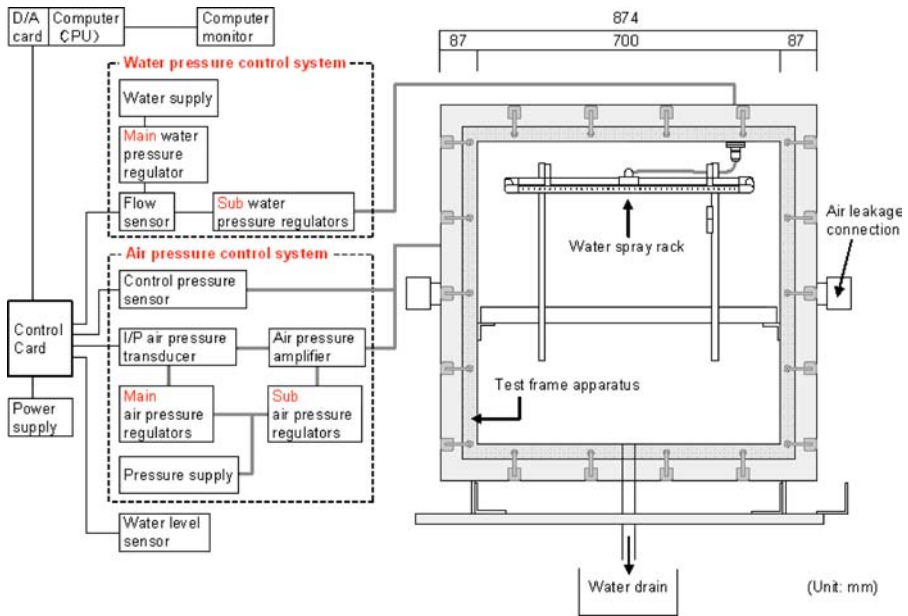


FIG. 5—Test frame apparatus of Mini-Dynamic Wall Testing Facility.

placed a water level sensor (Intempco; Model LTX20RP-B-3). This permits determining the rate of water collection in the container and hence establishing the rate of leakage through the jointing system.

Air pressure sensors (Druck, Model LPM1110) are located in the test frame portion as well as in the test specimen portion; the pressure in the test frame measures the driving pressure across the entire joint, whereas the pressure sensor located in the test specimen measures the pressure in the space between the weather seal (exterior portion of joint) and the air seal, or the inside of the joint. There is an adaptor to the test frame that permits connecting to an air leakage test device; thus, the air leakage of the test assembly can also be determined using a laminar flow element (Meriam; Model 50MW20-1) coupled to a pressure sensor (not shown).

Hence the basic wind-driven rain parameters at a panel joint can be replicated (i.e., rain deposition, pressure differential) using this apparatus and the conditions at the joint thus simulated in a reproducible manner.

Test Specimen

The configuration of the vertical and horizontal joint are illustrated in Fig. 7 and Fig. 8, respectively. The overall size of the test specimen was 610 mm by 610 mm (Fig. 7). The vertical or horizontal joint was located at the middle of the specimen (width 20 mm; depth 15 mm) that was sealed with a one-part

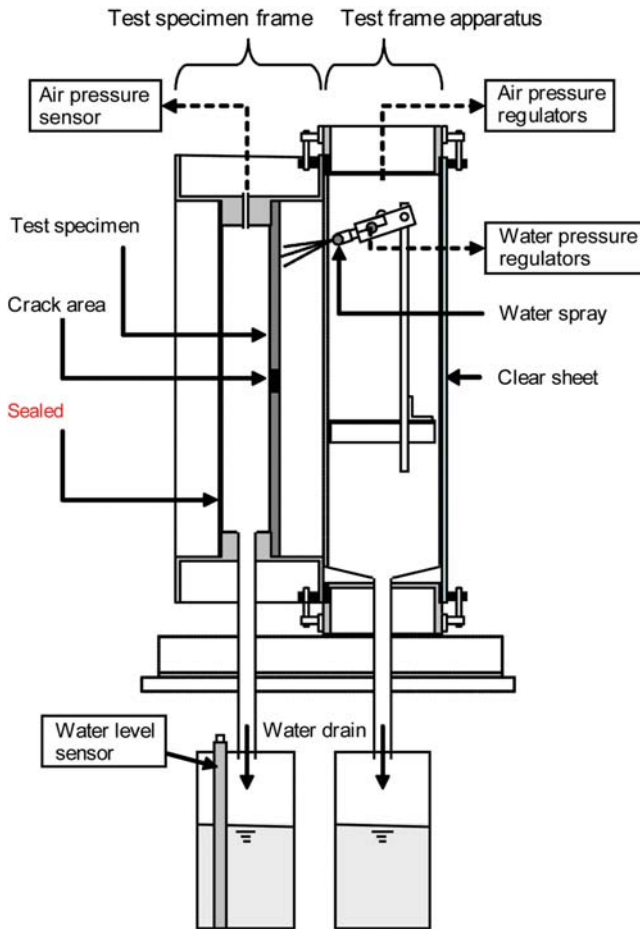


FIG. 6—Vertical sectional view of Mini-Dynamic Wall Testing Facility.

polyurethane sealant⁴ (white; no primer). The sealant was applied to a closed-cell polyethylene backer rod having a diameter of 25 mm and cured in laboratory conditions (20°C; 35 % RH) for two weeks before initiating the test. The crack introduced in the jointing product was located approximately at mid-length of either the vertical or horizontal joint. The panel assembly, and substrate to which the sealant was applied, was made of transparent acrylic sheathing; this permitted visual observation of water penetration along the joint in different test conditions over the course of the investigation. One portion of the panel assembly was fixed to the test frame (Figs. 7 and 8; fixed

⁴ISO 11600-F-25LM; ASTM C920, Type S, Grade NS, Class 35, Use NT, M, A, G, and 1; Canadian Specification CAN/CGSB-19.13-M87, Classification MCG-2-25-A-N.

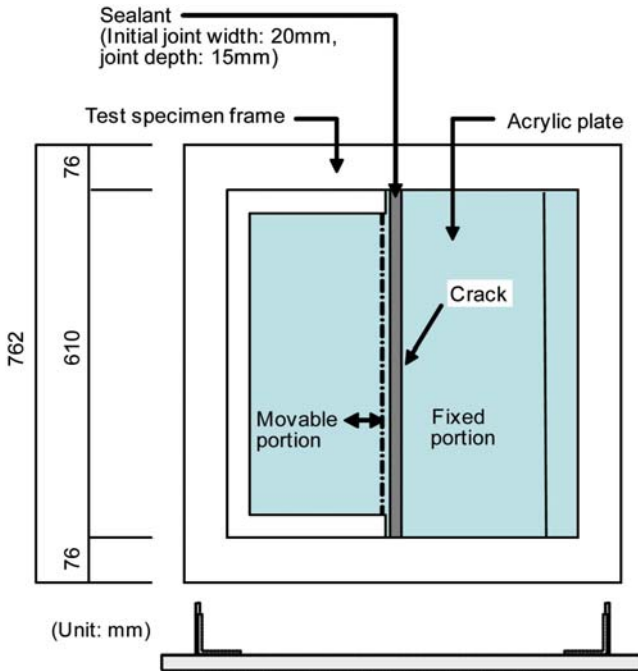


FIG. 7—Front elevation of test specimen showing 20 mm vertical joint and nominal degree of movement of transparent acrylic panel.

portion), the other was moveable thus permitting the width of the joint to be changed up to a maximum of approximately 25 % of a joint of 20 mm in width (i.e., ca. 5 mm).

Test Parameters

An overview of possible test parameters is provided in Table 4. Not all parameters given in Table 4 were tested in this study; as an initial test series reported in this paper, rates of water leakage across a deficient joint were evaluated in relation to simulated wind-driven rain loads (i.e., water deposition rate and pressure differential). The degree of deficiency of the joint was dependent on the degree of joint displacement (i.e., movement in extension) and specific “crack characteristics,” such as crack location (adhesion) and crack length. Essentially, and as will be discussed in a subsequent section, the size of the crack opening in the deficient joint and through which water might penetrate, is a function of the degree of joint extension and crack length.

However, the notional list of possible test parameters permits considering those results that might be obtained from, for example, testing joints: of different width and depth (or varying W/D ratios); with backer rods of varying size or type; in compression as opposed to expansion; having different types of cracks

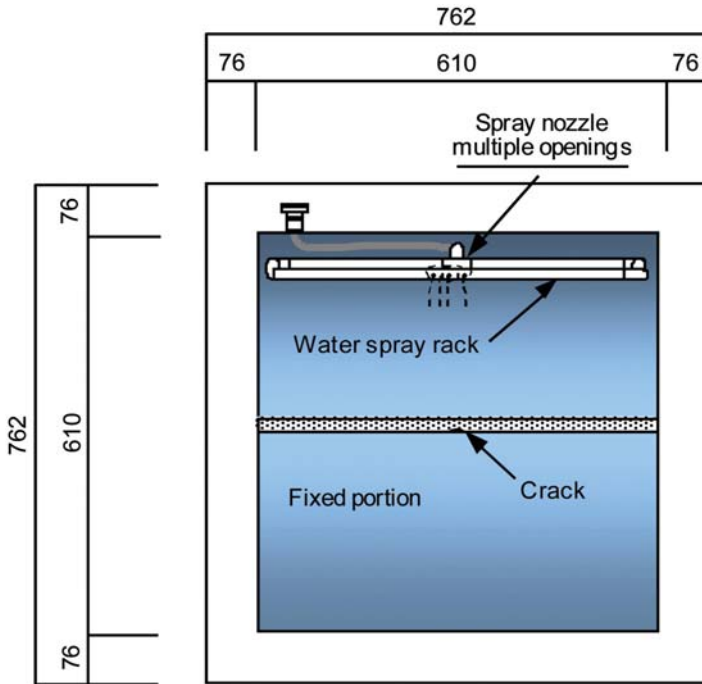


FIG. 8—Front elevation of test specimen showing horizontal joint, location of crack in joint.

TABLE 4—Experimental parameters.

Environmental parameters		
1. Water deposition rate	1.6, 3.4, 4.0, 6.0 L/(min·m ²)	
2. Pressure differential	Static pressure: (0, 75, 150, 500, 1000, 2000 Pa)	
Building (façade) condition		
3. Joint characteristics	Cross section type	Single joint
	Joint orientation	Linear vert. or horiz. joint
4. Jointing product	Type	Working joint
	Joint width	20 mm
	Joint depth	15 mm
	Backer rod	Yes (25 mm)
5. Movement	Wall movement type	Expansion/Compression
	Movement ratio	0 %, 2.5 %, 5 %, 10 %
6. Crack characteristics	Crack condition	Yes/No
	Crack location 1	Linear joint
	Crack location 2	Adhesion failure
	Crack length	No crack, 2, 4, 8, 16 mm

TABLE 5—*Rainfall area.*^a

Flow Rate L/min	L/min-m (width)	Deposition Rate L/(min-m ²)
0.088	0.88	1.6
0.187	1.87	3.4
0.22	2.2	4
0.33	3.3	6

^aWidth 0.1 m, height 0.55 m

(i.e., adhesive at the interface of the sealant and substrate as compared to a crack along center of joint); and cracks of increased size as compared to that evaluated in this study.

The different water deposition rates to which the specimens were subjected are provided in Table 4 and the corresponding rates of water flow necessary to produce these rates are given in Table 5. On the vertical joint, the “rainfall area,” was the area over which water was deposited to ensure a uniform rate over the crack (i.e., 0.1 m wide by 0.55 m high).

Test Methods

The water penetration test method is summarized in Fig. 9. The quantity of water deposition on the surface of the specimen and the air pressure difference across it was controlled according to the prescribed parameters as provided in Table 6 for tests on vertical joints, and Table 7 for those on horizontal joints. Testing undertaken at 4.0 L/(min-m²) was consistent with the requirements of the Japanese Institute of Standards A 1414-1⁵ [13] whereas those completed at 3.4 L/(min-m²) replicated conditions specified in the ASTM E331-00⁶. Testing at the other two spray rates (i.e., 1.6 and 6 L/(min-m²)) permitted subjecting the crack opening to a broader range of water deposition rates perhaps consistent with that found on the exterior of tall buildings.

The rate of water deposition (L/(min-m²)), pressure differential (Pa), and rate of water leakage (L/min) was recorded automatically by the data acquisition system. The behavior of water leakage was verified by visual observation, as depicted in Fig. 9. Figure 9 provides a horizontal sectional view of the vertical joint test specimen at the crack location. Transparent acrylic plates were used to form the panel face, and the face and sides of the joint, thus permitting observation of water entry at the crack location. The eye icon in Fig. 9 indicates the position of the observer in relation to that of the crack location in the vertical joint.

The back of the specimen was sealed with an adhesive tape (Fig. 9) permit-

⁵JIS A 1414-1: Water-Spray rate 0.4 L/(min-m²), Maximum test-pressure: 2303 Pa, Minimum test-pressure: 49 Pa.

⁶ASTM E331-00: Water-spray minimum rate of 3.4 L/(min/m²), Test-pressure of at least 137 Pa.

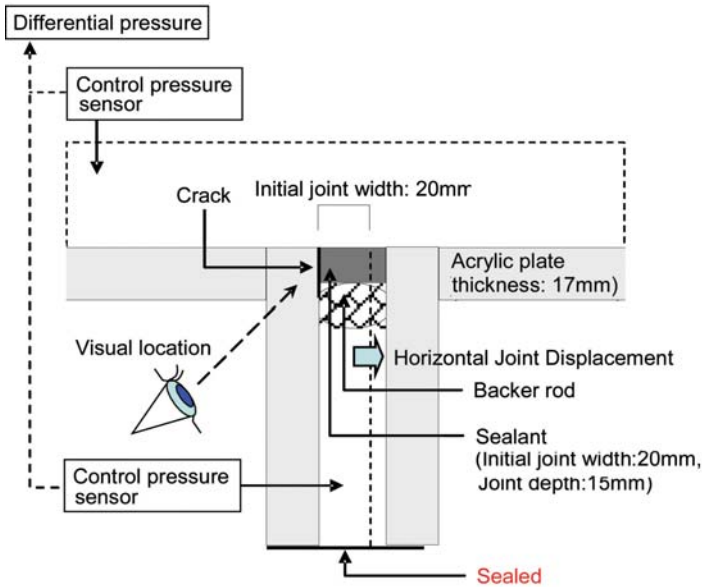


FIG. 9—Horizontal sectional view of the vertical joint test specimen at crack location; the eye icon indicates the position of the observer in relation to that of the crack location.

ting control of pressure differences across the joint. The joint strain to the prescribed displacement was adjusted with a clamp. Tests were carried out over a period of ten minutes for each test parameter.

Results from Laboratory Tests on Sealed Vertical Joints

Crack Width Related to Joint Movement and Crack Length

The nature of the degree of crack opening is illustrated in Fig. 10 and a representative photograph of the different crack lengths when not extended, and

TABLE 6—Test matrix for water penetration tests on vertical joints.

Crack Length (mm)	Joint Displacement (mm)				Quantity of Water L/(min-m ²)			
					1.6	3.4	4	6
No crack (0)	0	0.5	1	2	6 ^a
2	0	0.5	1	2	6 ^a	1 ^b	6 ^a	6 ^a
4	0	0.5	1	2	...	1 ^b	6 ^a	...
8	0	0.5	1	2	...	1 ^b	6 ^a	...
16	0	0.5	1	2	6 ^a	1 ^b	6 ^a	6 ^a

^aSix tests at: 0, 75, 150, 500, 1000, 2000 Pa.

^bOne test at: 150 Pa.

TABLE 7—*Test matrix for water penetration tests on horizontal joints.*

Crack Length (mm)	Δ -Joint Displacement (mm)				Quantity of Water L/min			
					0.088	0.187	0.22	0.33
2		1	2	6 ^a	6 ^a	
4	0	0.5		6 ^a	6 ^a	6 ^a	6 ^a	
8	0	0.5	1	2	6 ^c	1 ^b	6 ^a	...
16	0	0.5	1	2	6 ^a	...

^aSix tests at: 0, 75, 150, 500, 1000, 2000 Pa.

^bOne test at: 150 Pa.

^cSix tests only at Δ of 1 mm.

when extended by 0.5, 1, and 2 mm is given in Fig. 11. As is evident from the photograph, the greater the degree of joint extension, the more apparent the crack opening size. This is more evident in the case of the 16 mm and longest crack length shown in Fig. 11 (displacement 2 mm; joint width 22 mm).

The results obtained from joint movement at prescribed displacements and the relation to crack width and crack length is shown in Fig. 12. There is a linear relationship between joint displacement and crack opening (width) for the largest crack length. For shorter crack lengths, this relationship approaches linearity. As well, when the joint is displaced, the longer crack lengths provide for a broader crack opening. Hence, as might be expected, the largest crack openings occur for 16 mm crack lengths at a joint displacement of 2 mm (10 % joint width).

Water Penetration Test Results for Vertical Joint

A summary of the results from water penetration tests on the vertical joint is provided in Fig. 13. In this summary, the degree of water penetration is given in terms of water leakage (L/min) as a function of pressure difference across the test specimen (Pa) for 16 test conditions for which the crack length was 2, 4, 8, and 16 mm and the joint displacement (Δ) varied from 0 to 2 mm ($\Delta = 10\%$ joint width).

Quantity and Pattern of Water Leakage—The quantity and pattern of water leakage is very complex because the parameters affecting leakage are interrelated. However, in general, greater rates of water leakage occurred through cracks in the sealed joint, given either higher water deposition rates on the specimen surface or higher pressure differentials across the specimen.

The pattern of water leakage and the effect of the backer rod on water entry across the joint are characterized in Fig. 14. Specifically, when the diameter of the backer rod (nominal size 20 mm) was greater than the joint width, water flowed downwards along the gap between sealant and backer rod which is illustrated as Type "A" water leakage in Fig. 14. Whereas, when the rod diameter was less than the joint width, i.e., when the joint was extended from its original width of 20 mm, water flowed from the opening across the gap at the

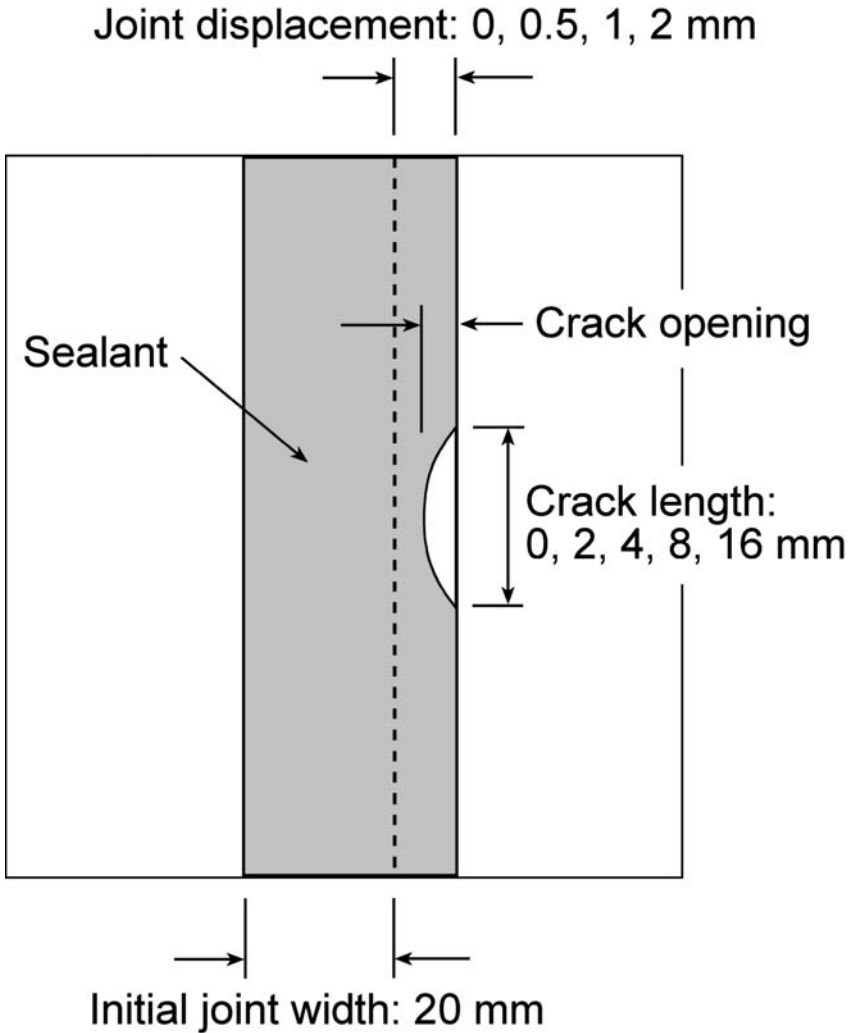


FIG. 10—Sealed joint condition.

substrate-backer rod interface, towards the back of the joint; this pattern of water leakage is illustrated as Type “D” in Fig. 14. When the rate of water entry was less than or equal to the drainage capacity along the gap, water flowed down the gap as in Pattern “B,” (Fig. 14), whereas, if the rate of entry exceeded the drainage capacity along the gap, excess water flowed up the gap as in Pattern “C” (Fig. 14).

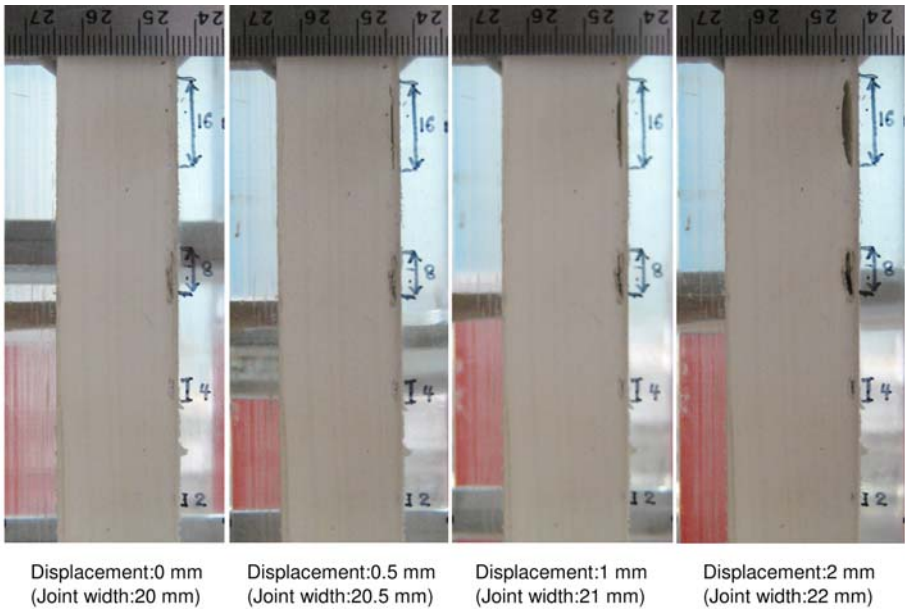


FIG. 11—Crack opening of vertical sealed joint.

Discussion of Water Penetration Results for Vertical Joint

The discussion focuses on two principal aspects that affect water leakage across deficient vertical joints, specifically, the influence of joint displacement and crack length, and the effect of the backer rod. Each is dealt with in turn.

Influence of Joint Displacement and Crack Length—Given the presence of a crack, at no joint displacement (0 mm), water leakage nonetheless occurred. Additionally, and excluding results obtained with no joint displacement (0 mm), the longer the crack length and the greater the joint displacement, the greater the rate of water penetration. Hence, the crack length and joint displacement provided a multiplicative effect on water leakage rates. As well it can be observed that at the largest joint displacement, water readily penetrated the joint, even at low pressure conditions. From this, it follows that the greatest water penetration rate (0.05 L/min) occurred at the maximum test joint extension (2 mm), largest crack length (16 mm), and highest test pressure differential (2000 Pa).

Some additional observations from the results include the following:

- The greater the driving pressure across the joint, the greater the rate of water penetration.
- When the crack length is “small” (e.g., ≤ 2 mm), regardless of the rate of water deposition at the crack location, at the low pressures, there are few differences in the rate of water penetration across the joint.
- However, given the “small” crack lengths, at high pressure differences

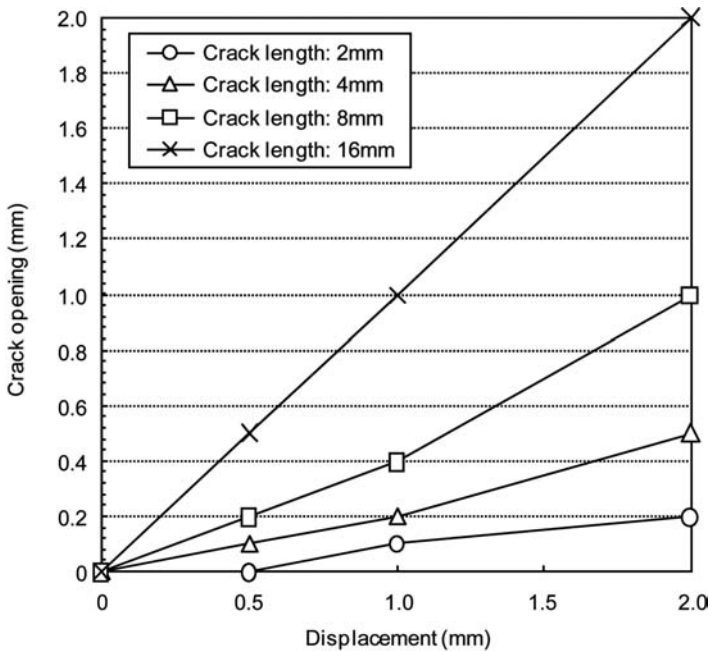


FIG. 12—Relationship between vertical joint displacements and crack opening.

across the joint, increases in the rate of water penetration are evident for corresponding increases in the rate of water deposition at the crack location.

- When the crack length is large (e.g., 16 mm), the higher the rate of water deposition at the crack, the greater the rate of water leakage.
- At larger joint displacements (i.e., 5 and 10 %) and for low water deposition rates at the crack (i.e., $1.6 \text{ L}/(\text{min}\cdot\text{m}^2)$), even at high pressure differences, the increase in the rate of water leakage with increase in pressure difference are not as significant as compared to leakage rates achieved at more substantial water deposition rates; hence occlusion of the opening with water is a factor that affects gross water entry rates.

Effect of Backer Rod—The closed-cell polyethylene backer rod acted as a gasket providing a secondary barrier to water entry at the joint. When leakage occurred at the crack, and given that the backer rod was compressed, water leakage was arrested beyond the position where the backer rod interfaces with the substrate; this typically occurred in conditions of no joint extension or when the extension was no greater than 0.5 mm. However, when the joint was extended (e.g., 1 and 2 mm) and the width of the backer rod was then smaller than the extended joint width, the rod no longer acted as a gasket. It is to be noted that the backer rod (nominal diameter 25 mm) once compressed in the 20 mm joint did not recover its size upon extension of the joint. Hence the degree of compression set of the rod affected its capability to seal the jointing

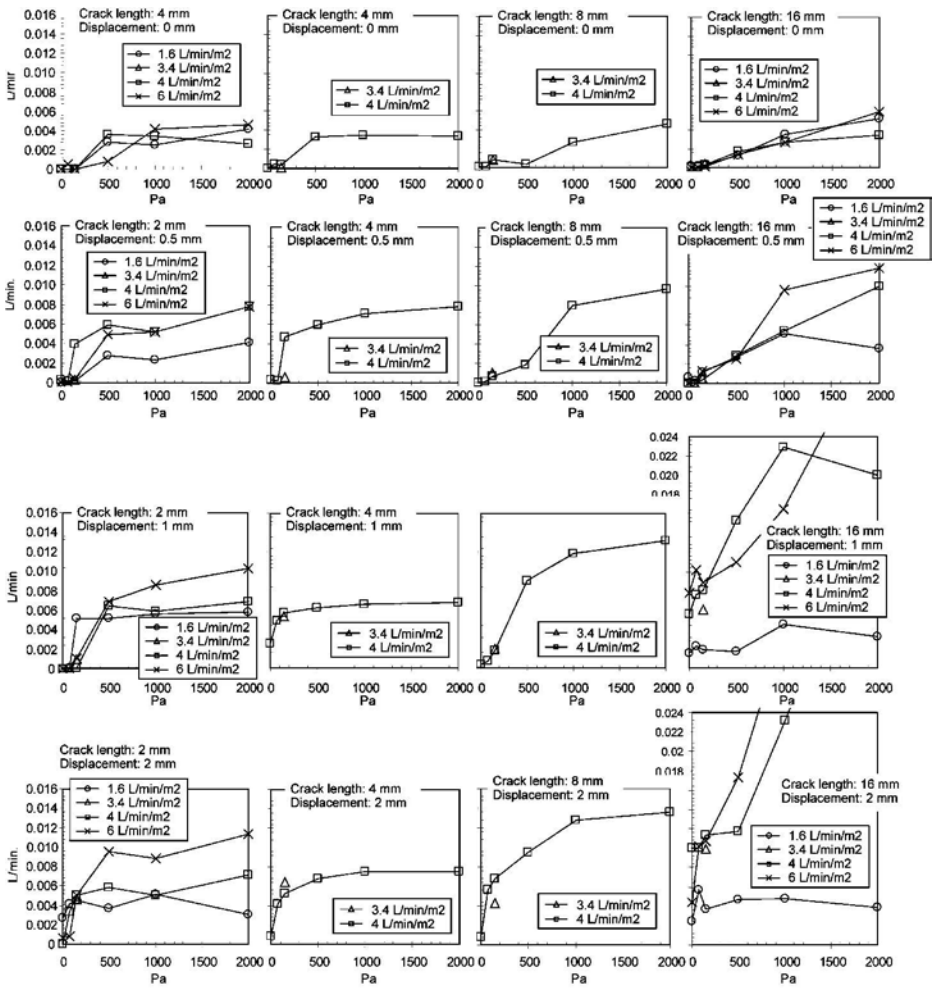


FIG. 13—Water penetration test results for vertical joint. Variation in water leakage rates (L/min) in relation to pressure different across specimen (Pa) for 16 test conditions for joints having crack length deficiencies of 2, 4, 8, and 16 mm and joint displacements (Δ) of 0 to 2 mm ($\Delta = 10\%$ joint width).

product. It appears critical to consider the diameter of backer rod and its degree of compression in a joint to help avoid water leakage should a fail-safe system be of interest.

There may also be consideration as to whether an open or closed-cell backer rod would greatly affect water leakage when the rod is sufficiently compressed to arrest the flow of water; it is expected that an open-cell rod would deter water entry but perhaps not as effectively as a closed-cell backer rod. However, such a notion would have to be evaluated from results of further testing.

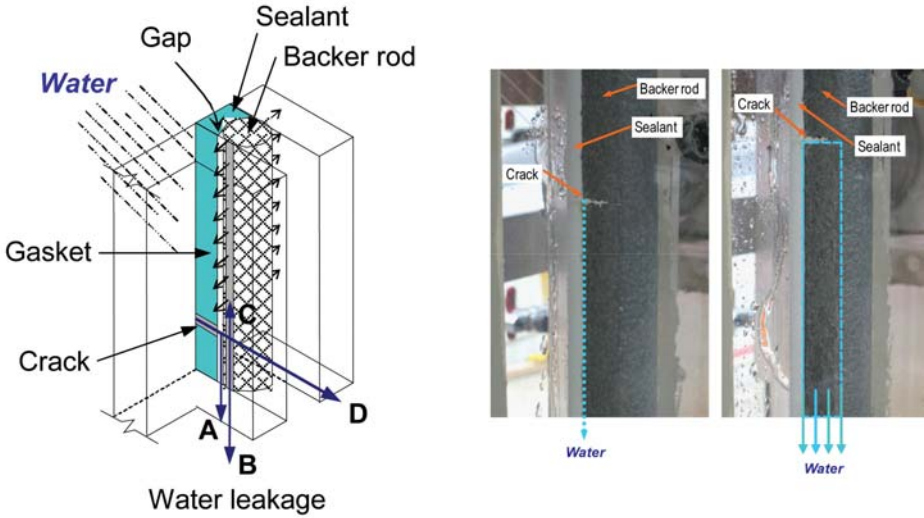


FIG. 14—Characterization of water leakage of vertical joint.

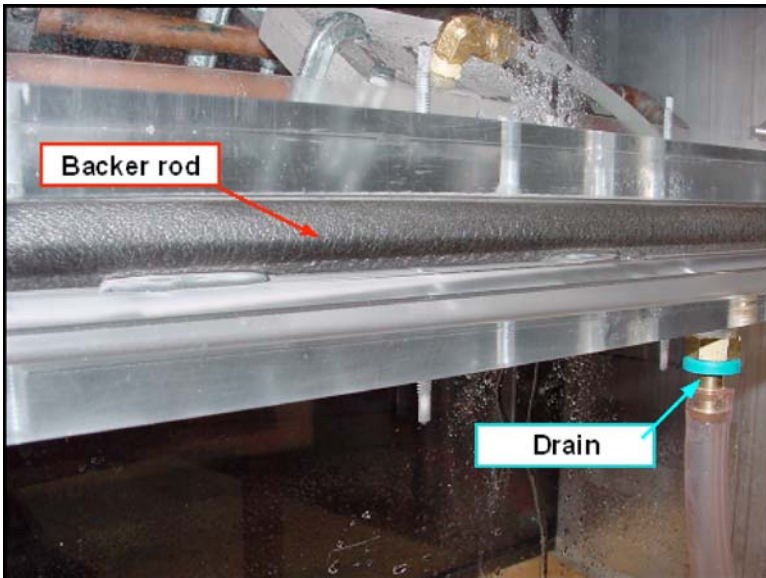


FIG. 15—View of horizontal joint from “interior” side showing backer rod between adjacent joint faces and accumulation of water on horizontal surface.

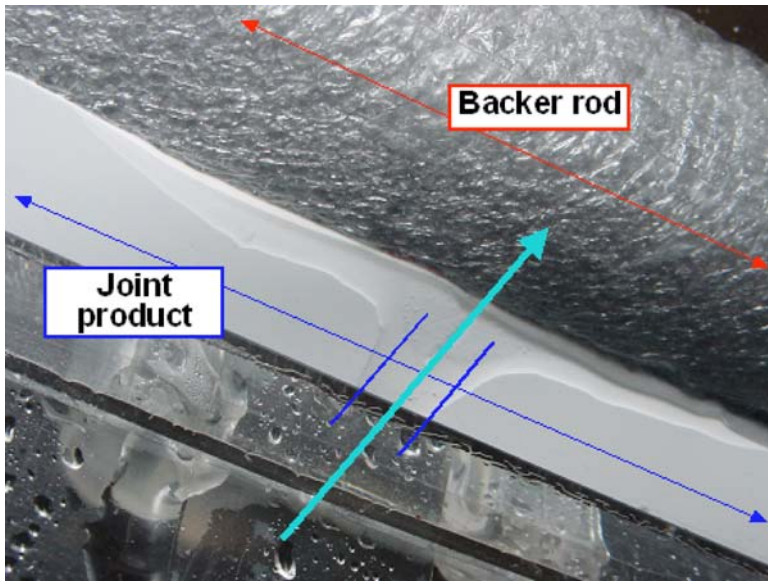


FIG. 16—View of underside of horizontal joint showing backer rod and location of crack (16 mm) opening along jointing product; arrow shows direction of water leakage across joint.

Water Penetration Test Results for Horizontal Joint

Evidence of water penetration at the horizontal joint is given in Fig. 15 and Fig. 16. A view of water entry along the interior side of the joint is shown in the photo of Fig. 14; water is seen to be pooling on the surface of the interior of the joint but ultimately made its way to the drainage opening. A photo (Fig. 16) at the underside of the joint at the crack location shows the path for water leakage through a crack opening of length 16 mm.

A summary of the results from water penetration tests on the horizontal joint is provided in Fig. 17. In this summary, the degree of water penetration is given in terms of water leakage (L/min) as a function of pressure difference across the test specimen (Pa) for ten test conditions. Results for water leakage for crack lengths of 4, 8, and 16 mm are given at joint displacements varying from 0 to 2 mm (10 % joint width). The range of scale for water leakage rate varies by three orders of magnitude, from a low of ca. 0.0018 L/min used for assessing water leakage across joints with no displacement, to a high of 0.2 L/min for joints having displacements of 2 mm.

Some key observations from water penetration tests on deficient horizontal joints are:

- Water leakage occurs when joints are “closed” (i.e., $\Delta=0$); even under low pressure differentials;
- Water leakage is pressure dependent; higher rates of leakage are obtained at higher pressure differences;
- A heightened degree of leakage can occur, up to ca. 1.6 L over a 10 min

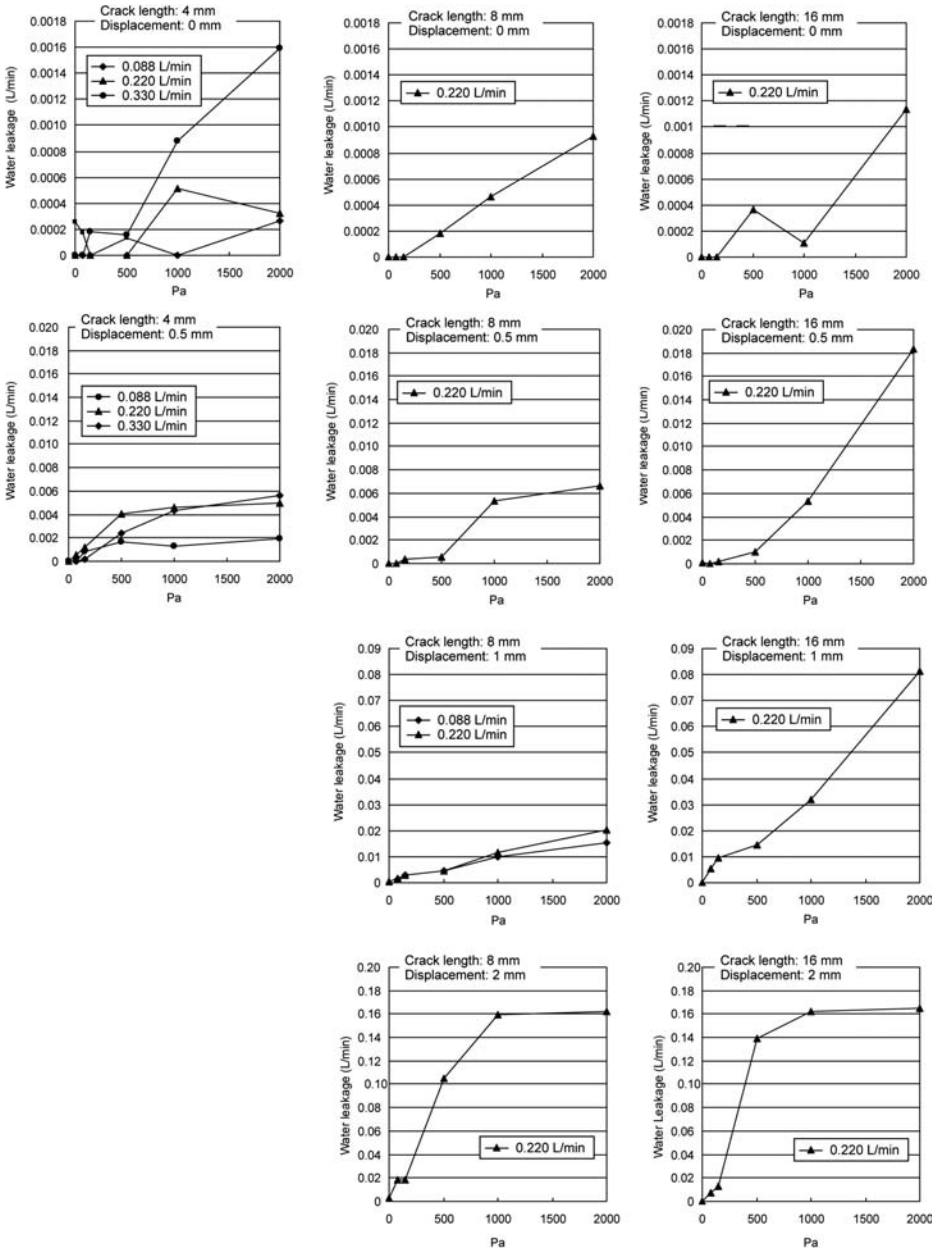


FIG. 17—Water penetration test results for horizontal joint. Variation in water leakage rates (L/min) in relation to pressure different across specimen (Pa) for joints having crack length deficiencies of 4, 8, and 1 mm and joint displacements (Δ) of 0, 2.5, 5, and 10 % joint width.

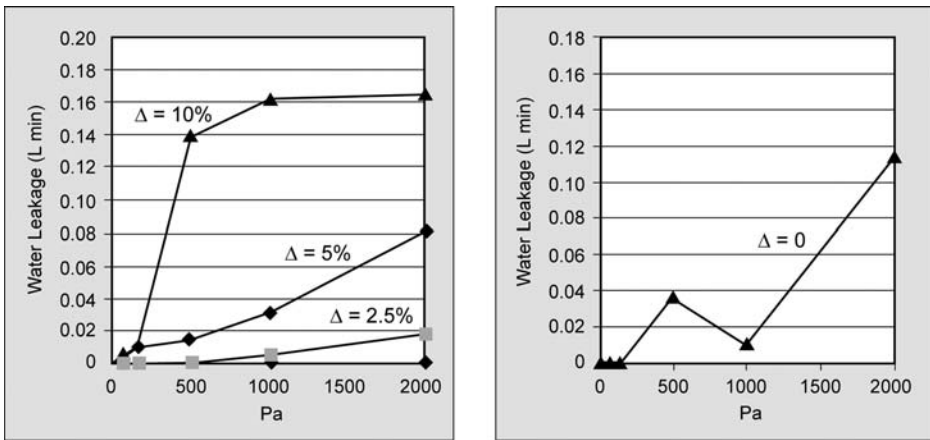


FIG. 18—Variation in water leakage as a function of pressure difference and joint displacement for a joint with crack length of 16 mm (a) results for displacement of 0, 2.5, 5, and 10 % joint width; (b) results for no displacement.

interval; this was estimated from the maximum leakage rates of greater than 0.16 L/min obtained for a crack length of 16 mm and 10 % joint opening at 1 kPa and 2 kPa driving pressures.

- Water leakage rates for a crack length of 16 mm are dependent on the crack opening size.

The final observation is more clearly evident from information provided in Fig. 18; the variation in water leakage as a function of pressure difference across specimen and joint displacements of 0, 2.5, 5, and 10 % are given for a joint having a crack length deficiency of 16 mm. The adjoining Fig. 18(b) provides results for no displacement given that these are not readily apparent from that provided in Fig. 18(a). It is evident that as the crack length increases there is a corresponding increase in the rate of water leakage at the opening. For example, at the 1 kPa pressure difference, there is a ca. fifty-fold increase in water leakage rate between a joint displacement of 2.5 % (0.5 mm) and a closed joint (no displacement), and five-fold increase in leakage rate, for increases in joint displacement from 2.5 % to 5 % and from 5 % to 10 %, respectively.

Additionally it can be seen that for the smaller crack opening sizes (i.e., $\Delta=0, 2.5, 5\%$; 0, 0.5 mm, 1 mm), rates of water entry increase with corresponding increases in pressure difference across the specimen; this suggests that the openings are completely occluded with water and the air pressure is driving water through these openings in increasing amounts and in proportion to the pressure difference. Whereas at the largest crack opening ($\Delta=10\%$; 2 mm), the leakage rate reaches a maximum at 1 kPa pressure difference (0.162 L/min) and at 2 kPa there is only a small increase in leakage rate as compared to that obtained at 1 kPa ($<2\%$ to 0.165 L/min). This suggests that at 1 kPa pressure level, the maximum leakage rate has been reached for the given water deposition rate and crack opening size; in this instance, the opening is no longer completely occluded with water hence air pressure cannot

drive additional water through the opening and no additional rate of entry is possible at these test conditions. Such findings mirror those found for the vertical joint.

At water deposition rates at which the comparatively smaller openings are occluded, the larger openings are less readily filled but nonetheless this may occur intermittently given the erratic nature of water migration over openings. For larger openings, there are likely instances in which these openings will intermittently fill with water and thereafter, these water “plugs” would be ejected by the pressure differential across the opening.

Comparison between Water Penetration Test Results of Vertical and Horizontal Joints

A comparison was made between water leakage through deficient vertical and horizontal joints as shown in Fig. 19. The results reflect leakage rates of joints subjected to a water deposition rate of 4 L/(min·m²). The Y-axis provides the rates of leakage (L/min) across the horizontal joint; that of the X-axis for the vertical joint.

Results have been organized in terms of different crack lengths; cracks of 16 mm length are shown as circular data points, 8 mm as square points, and 4 mm as triangular points. The dotted lines delineate the outer boundary of the data and the oblique line joining points 0.0001 and 1 L/min on the plot indicates when the values of horizontal and vertical leakage rates are equal. A point falling beneath this line indicates that the leakage rate through the defect at the vertical joint is greater than the rate through the defect in the horizontal joint at the given test condition.

It is apparent from this plot that there can be substantial increases in leakage rate of either vertical or horizontal joints and up to an order of magnitude difference.

The following was also evident:

- Overall, it is more likely that vertical joints will leak at higher rates than horizontal joints (ca. 59 %); as well, this was most prevalent at reduced water leakage rates (i.e., <0.005 L/min) where 81 % of the data points were those of the vertical joint having a greater leakage rate than that of the horizontal joint; on the other hand,
- At large crack openings (i.e., crack lengths of 8- and 16 mm, displacement of 1 and 2 mm) there is a greater chance (ca. 75 %) that the rate of water leakage at the horizontal joint will be more severe than that of the vertical joint;
- Clearly the rate of water leakage depends on the nature of the crack opening (i.e., crack length and width); horizontal joints appear to be more susceptible to water leakage for joints having larger defect sizes.

Conclusions

1. For vertical joints evaluated in this study:
 - There exists a linear relationship between crack width and joint dis-

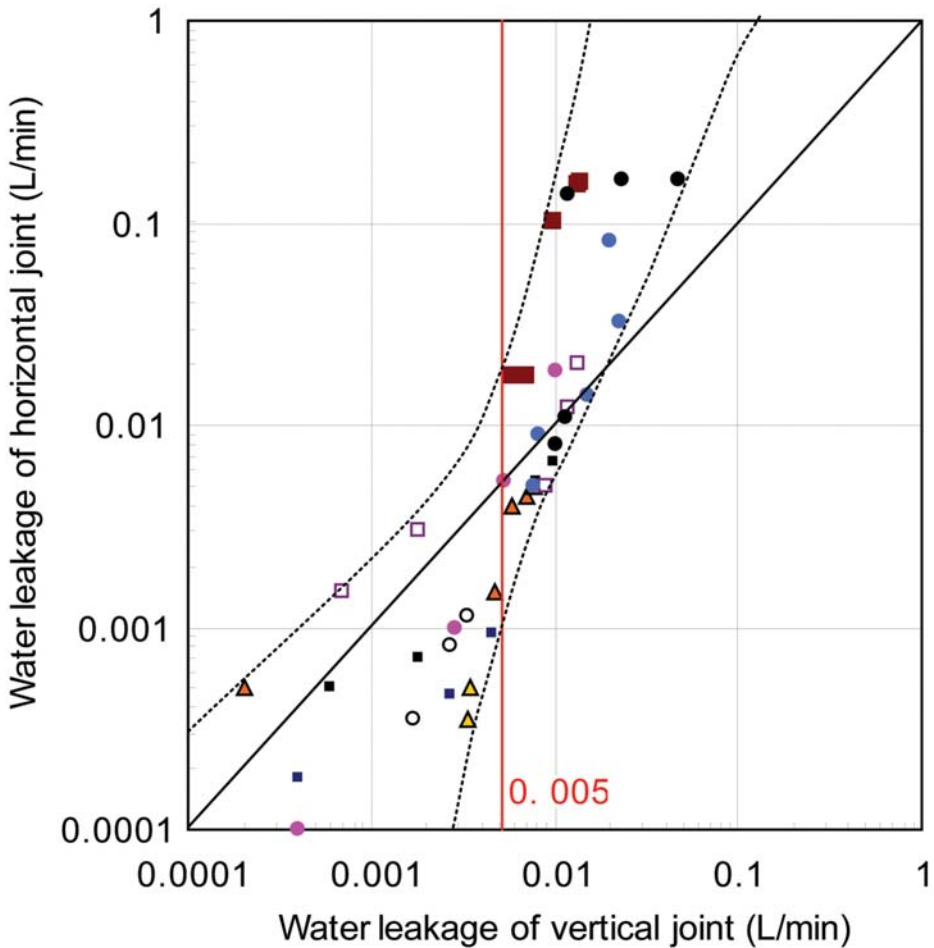


FIG. 19—Comparison of water leakage (L/min) at vertical and horizontal joint deficiencies.

placement for cracks introduced in a sealant at the sealant-substrate interface; as well,

- Larger crack lengths induce greater crack widths and crack sizes in extended joints;
 - The size and shape of the backer rod affects the nature of water leakage across the vertical joint.
2. For both vertical and horizontal joints evaluated in this study:
- The crack length and joint displacement provide a multiplicative effect on water leakage rates;
 - If a crack exists in a sealed jointing system, even if the joint displacement is 0 mm, water may penetrate the opening at the crack;
 - The higher the quantity of water deposition on or air pressure differ-

ential across the specimen, the greater the rate of water leakage of the jointing system.

3. Additionally, it may be suggested that if the crack length in a joint of an actual building is known or verified from a field inspection, an estimate of the rate of water leakage can be calculated by using the information given above and provided information is also given on the expected climate loads impinging on the façade.

It should be borne in mind that estimates provided in this initial series of tests only offer a gross approximation of leakage across a deficient joint and are based on the limited number of tests and test variations. The movement of water through small openings will be affected by the tortuosity of the leakage path and the nature of the materials along which it flows. Hence, other factors such as the type of sealant, backer rod, and substrate material to which the jointing product is adhered may affect water entry. For example, a deficient joint of sealant installed on a concrete substrate is not likely to comport itself in exactly the same manner as suggested by results on the leakage through cracks reported in this study when considering the idealized test conditions. Nonetheless, these studies offer some initial measure of the degree of water penetration at deficient joints—additional studies using the same approach would help elucidate the likely variations in leakage rate across a deficient joint that would arise given for example, different sealant and substrate materials or crack location and crack size.

Acknowledgments

That portion of this work on vertical joints was conducted over the course of a ten month visiting researcher work term at the Institute for Research in Construction (IRC), National Research Council Canada, in Ottawa. The authors are indebted to the Tokyo Institute of Technology, Japan, for having provided funding to Dr. Miyauchi for his stay at the IRC, and to the IRC for their support to the research conducted by Dr. Miyauchi and Dr. Lacasse.

References

- [1] Woolman, R. and Hutchinson, A. R., Eds., *Resealing of Buildings—A Guide to Good Practice*, Butterworth-Heinemann, Oxford, U.K., 1994, 169 pp.
- [2] Wolf, A. T., “Improving the Service Life of Sealed Cladding Joints Through a Total Quality Management Approach,” *3rd International RILEM Symposium on Durability of Building and Construction Sealants*, Fort Lauderdale, FL, 2–3, February 2000, A. T. Wolf, Ed., RILEM Publications, pp. 45–59.
- [3] Chiba, R., Wakimoto, H., Kadono, M., Kawakubo, F., Koji, H., Karimori, M., Hirano, E., Amaya, T., Sasatani, S., and Hosokawa, K., “Improvement System of Waterproofing by Sealants in Japan,” *Proceedings on International Conference*, Kyoto Kokusai Hotel, May 1992, Japan Industry Sealant Association, Tokyo, Japan, pp. 175–199.
- [4] Huff, D., “Non-Destructive Testing of Installed Weatherproofing Sealant Joints,” *ASTM STP 1453*, ASTM International, West Conshohocken, PA, pp. 335–345.

- [5] Building Constructors Society (Kenchikugyo Kyokai), *Manual of Defect and Complaint Prevention Technology in Building Work (Revised Edition)*, Japan, vol. 7, 1995.
- [6] Building Constructors Society (Kenchikugyo Kyokai), *Failure in Building Construction Sealant*, Japan, vol. 1, 2002.
- [7] El-Shimi, M., White, R., and Fazio, P. "Influence of Facade Geometry on Weathering," *Can. J. Civ. Eng.*, vol. 7, 1980, pp. 597–613.
- [8] ASCE Standard ASCE/SEI 7–05, "Minimum Design Loads for Buildings and Other Structures," prepared by the Structural Engineering Institute of the ASCE, American Society of Civil Engineers, 388 pp.
- [9] Jan, C.-D. , "Debris Flow Hazards Mitigation in Taiwan," International Sabo Association, www.sabo-int.org/projects/taiwan.html (accessed 10 July, 2008), 2004.
- [10] Jan, C. D. and Chen, C. L., "Debris Flows Caused by Typhoon Herb in Taiwan," *Debris-Flow Hazards and Related Phenomena* (Chapter 21), M. Jakob and O. Hungr, Eds., Praxis Publishing Ltd., Chichester, England, 2005, pp. 539–563.
- [11] Cornick, S. M. and Lacasse M. A., "An Investigation of Climate Loads on Building Facades for Selected Locations in the US," *J. ASTM Int.*, vol. 6, 2009, pp. 1–17.
- [12] Mehta, K. C. and Delahay J. M., *Guide to the Use of the Wind Load Provisions of ASCE 7–02*, American Society of Civil Engineers, ASCE Press, Reston, VA, 2004, 142 pp.
- [13] Japanese Industrial Standard (JIS) A1414–1, "Building (Architectural) Performance Testing of Panel Components—Part 1: General."

**FIELD EXPERIENCE
WITH SEALED JOINTS AND
ADHESIVE FIXATION**

V. Demarest,¹ A. Liss,² R. Queenan,³ and P. Gorman⁴

Field Performance and Accelerated Weathering of High Performance Acrylic and Polyurethane Sealants for Tilt-Up Applications

ABSTRACT: To demonstrate the suitability of high performance acrylic sealants to low rise industrial construction applications, a laboratory prepared high performance acrylic sealant was compared to a commonly used, commercially available two part polyurethane sealant. The centerpiece of this comparison is an exterior exposure in El Paso, TX, in which the two sealants were professionally installed in alternating joints around the perimeter of a tilt-up warehouse. The sealants were also subjected to a battery of laboratory tests, including tensile testing, sealant specification testing, paintability, and accelerated weathering in both xenon arc and fluorescent UV devices. The 3 year El Paso exposure results, in combination with the laboratory, weathering, and application test results, demonstrate the performance advantages of the high performance acrylic sealant and highlight its inherent suitability for use in low rise industrial applications such as tilt-up warehouses.

KEYWORDS: acrylic sealant, polyurethane sealant, tilt-up, durability, crazing, accelerated weathering

Manuscript received August 1, 2008; accepted for publication May 26, 2009; published online September 2009.

¹ Group Leader, Rohm and Haas Company, now a wholly owned subsidiary of The Dow Chemical Company, Spring House, PA 19477.

² Scientist, Rohm and Haas Company, now a wholly owned subsidiary of The Dow Chemical Company, Spring House, PA 19477.

³ Senior Scientist, Rohm and Haas Company, now a wholly owned subsidiary of The Dow Chemical Company, Spring House, PA 19477.

⁴ Owner, Gorman Moisture Protection, El Paso, TX 79903.

Cite as: Demarest, V., Liss, A., Queenan, R. and Gorman, P., "Field Performance and Accelerated Weathering of High Performance Acrylic and Polyurethane Sealants for Tilt-Up Applications," *J. ASTM Intl.*, Vol. 6, No. 8. doi:10.1520/JAI102053.

Copyright © 2009 by ASTM International, 100 Barr Harbor Drive, PO Box C700, West Conshohocken, PA 19428-2959.

Introduction

Perceptions of acrylic sealants in the construction industry have largely been formed by contractors' experience with low-to-mid-performance formulations. Nonspec and ASTM C834-05 [1] compliant formulations were the first acrylic sealants to be introduced into the market and contractors collectively purchase huge volumes of these products every year for use in a variety of applications with minimal movement requirements. However, despite contractors' lack of familiarity, high performance acrylic sealants with $\pm 25\%$ joint movement capability are widely available. These products fully comply with ASTM C920-05 [2], have the excellent weathering characteristics of acrylic chemistry, and have the added benefit of soap and water cleanup.

High performance polyurethane sealants are commonly used to seal exterior joints in low rise industrial buildings constructed of block, brick, and tilt-up panels. Although these sealants have been used for many years, they are not without problems. Commonly encountered issues include surface crazing and chalking caused by UV degradation, sealant burn-through in thin cross sections, variable coatability, dirt pickup on coated joints due to plasticizer migration, and the need for solvent cleanup.

ASTM C834-05 compliant acrylic sealants are frequently used to seal interior joints in low rise tilt-up buildings. Although high performance acrylic sealants are readily available, they are rarely used to seal the exterior joints of these buildings. Despite the limitations listed above, contractors continue to use polyurethane sealants instead of high performance acrylic sealants. One of the reasons for this is that there is a general lack of knowledge about high performance acrylic sealants and how they compare to sealants based on alternative chemistries. Another is the lack of performance history of high performance acrylic sealants in commercial construction applications. To begin to fill these voids, a comprehensive study was undertaken to compare the performance of a high performance acrylic sealant to a commonly used two part polyurethane sealant.

Experimental Methods

Sealants

A high performance acrylic sealant and a high performance polyurethane sealant, both conforming to the ASTM C920-05 Class 25 specification, were chosen for this evaluation.

The polyurethane sealant was specified by the moisture-proofing contractor as part of a commercial restoration project. A two part polyurethane was chosen due to the low humidity in El Paso and the extended cure times required for one part polyurethanes under these conditions. The specific product selected was not the contractor's first choice-product selection was dictated by availability at the local distributor. However, the product selected is commonly available and widely used. The contractor has had extensive experience with this product

TABLE 1—*High performance acrylic sealant formulation.*

Ingredient	Pounds/100 gal
Acrylic latex (63 % solids) ^a	567.6
Water	20.8
Surfactant	11.0
Ethylene glycol	8.2
Dispersant	3.0
Biocide	1.4
Thickener	5.9
Mineral spirits	32.2
Adhesion promoter	0.4
Calcium carbonate	536.4
TiO ₂	17.7

^aAcrylic latex from The Dow Chemical Company, Midland, MI 48674.

and has found that it crazes more than other commercially available polyurethanes upon weathering. However, in his experience, this crazing has not led to complaints or call backs.

A laboratory prepared acrylic sealant, based on a commercially available binder, was chosen for comparison. A laboratory prepared sealant (Table 1) was used instead of a commercially available sealant so that the authors could control the formulation and understand the relationship between formulation ingredients and exterior performance. A plasticizer free formulation was chosen to minimize sealant dirt pickup. Since contractor application preferences were unknown at the time that the sealant was formulated, no attempt was made to optimize the viscosity, toolability, or open time of the formulated material that was sent to El Paso.

Tilt-Up Warehouse Exposures

A tilt-up warehouse in El Paso, TX, was renovated in the Spring of 2005. As part of this renovation, the failing 20 year old sealant used in the original construction was removed and replaced with the acrylic and polyurethane sealants described above. To directly compare performance, these two sealants were applied in alternating joints around all four elevations of the warehouse, for a total of 62 joints. The sealants were applied by a moisture-proofing contractor with over 60 years in the business using two applicators with over 48 combined years of experience in the field. One applicator installed all of the polyurethane sealant, and the other installed all of the acrylic sealant.

The warehouse was constructed of concrete tilt-up panels with a decorative aggregate surface finish (Figs. 1 and 2). The aggregate finish is made up of a large aggregate embedded in a soft friable concrete mortar. Because of the size of the aggregate, the aggregate layer is roughly 3/4 in. (19 mm) deep. Although it would have been preferable, from an adhesion point of view, to install the sealants against the underlying concrete panels, it was not possible to do so



FIG. 1—El Paso, TX, tilt-up warehouse used for exposure of high performance acrylic and polyurethane sealants.



FIG. 2—Example of a prepared joint 1 in. (25 mm) wide. The underlying concrete slab and exposed aggregate surface layer are readily visible.

because of the depth of the aggregate layer. In both the original installation and in the retrofit described below, the sealants were installed flush with the building exterior and against the aggregate layer.

The joints for the replacement sealants were formed by cutting out the old sealant, widening the joints where necessary, and then smoothing the inner edges of the joints with a grinder (Fig. 2). The dust generated by the grinding process was cleaned off with a blower, and the joints were brushed off prior to the application of the sealant. The resulting joints varied from 1/2 in. (13 mm) to over 1.5 in. (38 mm) in width (Fig. 2). A closed cell backer rod was used for all sealant applications and was carefully inserted so that it remained convex and untwisted. The sealant was applied with a bulk loading gun. Since much of the application was done on a ladder, the applied joint lengths were generally limited to 4–6 ft (1.2–1.8 m) at a time. Each section of sealant was tooled immediately after application. Although tilt-up buildings in the El Paso area are often painted, the warehouse used for the current exposure was not top-coated due to its decorative aggregate finish.

During the initial construction of the warehouse, the tilt-up panels were welded together at built-in weld plates, theoretically limiting the movement of the panels relative to one another. However, movement indicators attached to representative joints at the roofline indicated that some joints exhibited substantial movement while others exhibited none. Measured movements ranged from 14 to 22 % (total) of the initial joint widths, substantially below the 50 % total movement capabilities of the applied sealants. The contractor felt that the amount of movement measured in these joints, and the variable nature of the movement, was typical for tilt-up construction in the El Paso area.

Applicator comments about the use of acrylic sealants were noted throughout the installation process and reported below. To assess application quality, sealant adhesion, and sealant cure, small sections of sealant were periodically cut and pulled from representative joints. To assess aesthetics, durability, and functional performance, the sealants were visually inspected and photographed at irregular intervals over a period of 3 years. Sealant dirt pickup, gloss, and crazing were visually assessed and readily captured in photographs. Sealant chalking was gauged by rubbing the sealant surfaces with an index finger and assessing the amount of white residue transferred from the sealant to the finger. Sealant softening and tack were subjectively gauged by digging at the sealant joints with a finger nail and pressing with fingertips.

Accelerated Weathering

In addition to the warehouse exposures described above, the durability of the two sealants was also evaluated using standard accelerated weathering procedures and ASTM C1519-04, Standard Practice for Evaluating Durability of Building Construction Sealants by Laboratory Accelerated Weathering Procedures.

Weathering of Plaques in Xenon Arc and Fluorescent UV Weathering Apparatus—Specimens for accelerated weathering were laid up as $5 \times 1\frac{1}{2} \times \frac{1}{8}$ in.³ ($127 \times 38 \times 3.2$ mm³) thick wet plaques on 3×6 in.² (76×52 mm²) aluminum panels. The specimens were cured for 3 days at $23 \pm 2^\circ\text{C}$, 50 ± 5 %

relative humidity, and then placed in either the xenon arc or fluorescent UV accelerated weathering apparatus, following the procedures described below. Changes in sealant surface appearance (e.g., crazing, pitting, and chalking) were monitored periodically over a minimum of 2000 h. Changes in sealant color, as measured by changes in $L^*a^*b^*$ [3], were measured as a function of time in the fluorescent UV apparatus using a Minolta CR-231 portable Chroma Meter color analyzer.⁵

Procedure for Exposure in Xenon Arc Light Apparatus—An Atlas Ci65A Xenon Weather-Ometer⁶ was equipped with daylight filters conforming to ASTM Practice G155 [4]. The exposure cycle was 102 min of light followed by a wet period of 18 min light with water spray. The irradiance was set to $0.51 \text{ W}/(\text{m}^2 \cdot \text{nm})$ at 340 nm and the chamber air temperature to 45°C . The uninsulated black panel temperature was measured at 68°C .

Procedure for Exposure in Fluorescent UV Apparatus—A QUV Accelerated Weathering Tester (model QUV/basic) from Q-Lab⁷ was equipped with fluorescent UVA-340 lamps that comply with the spectral power distribution specifications in ASTM Practice G154 [5]. The exposure cycle consisted of 8 h of UV exposure at an uninsulated black panel temperature of 60°C , followed by 4 h of wetting by condensation at an uninsulated black panel temperature of 50°C . Irradiance was not controlled.

ASTM C1519-04 [6] *Durability*—Three aluminum H block specimens, as described in Test Method C 719-93 [7], were made for each of the two sealants tested. The acrylic sealant specimens were cured for 1 week at $23 \pm 2^\circ\text{C}$, $50 \pm 5\%$ relative humidity, followed by 2 weeks at 50°C . The two part polyurethane sealant was mixed immediately prior to sample preparation with a paddle mixer and following the manufacturer's instructions. The resulting specimens were cured for 3 weeks at $23 \pm 2^\circ\text{C}$, $50 \pm 5\%$ relative humidity. Following cure, the specimens were placed into either a xenon arc or fluorescent UV weathering apparatus. After 4 weeks the specimens were subjected to six room temperature cycles of $\pm 25\%$ cyclic movement at a rate of 1/8 in. (3.2 mm)/h. They were then evaluated for overall appearance and amount of adhesive or cohesive failure. The cycle of weathering followed by joint movement is an ongoing process, and the test will continue until significant failures have occurred. Results to date, through a total of five cycles, are reported.

Exterior Exposure in Static Joints—Channels for static joint exposures were fabricated by nailing pine strips to a plywood base to form a series of $\frac{3}{4} \times \frac{1}{2} \times 30$ in.³ ($19 \times 13 \times 762$ mm³) channels. To prevent degradation of the sub-

⁵Konica Minolta Sensing Americas, Inc., Ramsey, New Jersey 07446, USA. The Minolta Model CR-231 Chroma Meter color analyzer has a 25 mm diameter measuring area, 45° illumination angle, and 0° viewing angle. Illuminant: D65. Color measurement according to ISO 7724. Color-coordinates: CIELAB.

⁶Atlas Material Testing Technology, Chicago, Illinois 60613, USA. The Ci65A Xenon Weather-Ometer has a 6500 W water cooled xenon arc lamp and a total exposure area of 11 000 cm².

⁷Q-Laboratory Corporation, Cleveland, Ohio, 44145, USA.

strate, the wood was first primed and then painted with a high quality exterior paint. After the paint was dry, the channels were filled with sealant. The sealants were tooled flat and flush with the tops of the channels and then cured for 4 weeks under ambient conditions. To assess sealant coatability and the appearance of overcoated sealants, half of each sealant was coated with a 38 pigment volume concentration (PVC)⁸ all acrylic elastomeric wall coating (EWC). The coating was brush applied in two coats to the sealant and channel surfaces at a combined coating weight which resulted in a calculated final dry film thickness of 20 dry mils (0.5 dry mm). The first coat was dried for 24 h before the application of the second coat, and several additional days elapsed before the EWC coated channels were taken outside for exposure. The filled and coated channels were exposed horizontally in a south-45° direction at the Spring House Farm in southeastern PA. After 1 year of exterior exposure the channels were brought back into the laboratory, and the coated and uncoated sealants were assessed for dirt pickup, crazing, and chalking.

Laboratory Testing

To complement the exterior and accelerated exposures described above, three key ASTM C920-05 tests were run. These included adhesion, joint movement testing, and hardness. Adhesion to concrete mortar was tested according to ASTM C794-06 [8], with dry adhesion being tested after the initial 3 weeks of cure and wet adhesion after additional 1 week of water soak. Joint movement to concrete mortar, at $\pm 25\%$, was tested according to ASTM C719-93 (2005). Hardness was tested as per ASTM C661-06 [9].

Tensile properties were also measured as a general indicator of sealant performance. Samples for tensile testing were laid up as 1/8 in. (3.2 mm) thick wet plaques on PTFE foil covered aluminum panels and cured as below. Dumb-bell shaped specimens, with a gauge length of 0.725 in. (18.4 mm), were cut from the dried plaques and tested on a model H10K-S Tinius Olsen⁹ tensile tester. Tensile testing was done at 2 in. (51 mm)/min and at $23 \pm 2^\circ\text{C}$ and $50 \pm 5\%$ relative humidity. Elongation to break, maximum stress, and stress at 25 % elongation were measured and reported as the mean \pm standard deviation of three measurements. The stress at 25 % elongation was also measured at 0.2 in. (5.1 mm)/min and 0.02 in. (0.51 mm)/min to assess the strain rate sensitivity of the two sealants.

In the four laboratory tests described above, the acrylic specimens were cured for 1 week at $23 \pm 2^\circ\text{C}$ and $50 \pm 5\%$ relative humidity, followed by 2 weeks at 50°C . The polyurethane specimens were cured for 3 weeks at $23 \pm 2^\circ\text{C}$ and $50 \pm 5\%$ relative humidity.

⁸PVC is the fractional volume of a pigment in the total volume solids of a dry paint film.

⁹Tinius Olsen Testing Machine Co., Inc., Horsham, PA 19044, USA.

Results and Discussion

Tilt-Up Warehouse Exposures

Early Observations—The applicator found that the acrylic sealant needed to be handled somewhat differently than the polyurethane sealants that he was used to working with. As mentioned earlier, the acrylic sealant sent to the job site was not optimized for application properties. The applicator, in fact, found that the acrylic sealant was lower in viscosity than the polyurethane sealant and had a shorter open time. The lower viscosity made the acrylic sealant easier to gun but more difficult to tool since it offered less resistance to the tooling implements. The shorter open time meant that the acrylic sealant needed to be tooled more frequently and after shorter application lengths. Since the applicator was aware that the acrylic sealant would shrink more than the polyurethane sealant, there was some attempt to apply the acrylic sealant at slightly greater application depths. However, this process was not optimized or quantified in this exposure series. At the end of each day, the applicator of the acrylic sealant used soap and water to remove residual sealant from his tools. The applicator of the polyurethane sealant used toluene.

After 24 h the polyurethane sealant was still tacky and glossy and had picked up a fair amount of dirt. The tack and gloss, however, decreased over the succeeding days. The acrylic sealant skinned to a smooth, nontacky surface in less than 1 h and picked up much less dirt than the polyurethane sealant in the first 24 h. From the pieces of sealant pulled from the joints, it was determined that the polyurethane sealant cured through in 5–7 days and that the acrylic sealant took closer to 30 days. From these pulled pieces it was also found that the cured acrylic sealant is slightly harder and stiffer to the touch than the cured polyurethane sealant.

Longer Term Observations—As determined visually and in comparative photographs, the dirt pickup of the two sealants after 1, 2, and 3 years is comparable. Dirt pickup, as might be expected, varies from elevation to elevation. However, from a distance, and from any elevation, the acrylic and polyurethane sealants look similar. After 3 years and at a distance of 20 ft (6 m), the acrylic and polyurethane sealants on the east side of the building (Fig. 3) are indistinguishable. Closer views of the two sealants on the north side of the building (Fig. 4) also reveal a similarity in overall appearance. On more detailed inspection, however, differences between the two sealants become apparent. A close-up comparison of the two sealants on the east elevation of the warehouse (Fig. 5) reveals considerable crazing of the surface of the polyurethane sealant but no apparent crazing of the acrylic sealant. This is a trend seen throughout the warehouse exposure—after 3 years of exposure, the polyurethane sealant exhibits considerable crazing in all vertical joints in all elevations. The acrylic sealant, in contrast, exhibits no visible crazing on any of the vertical joints.

The polyurethane sealant also exhibits severe crazing in all vertical and horizontal parapet joints (Fig. 6). This crazing was readily apparent after 2 years of exposure and has become significantly more pronounced during the third year of exposure. In addition, the polyurethane sealant in one of the corner parapet joints has developed crazes that extend several millimeters into



FIG. 3—View of the east elevation of the El Paso warehouse with an acrylic sealant joint on the left and a polyurethane sealant joint on the right.

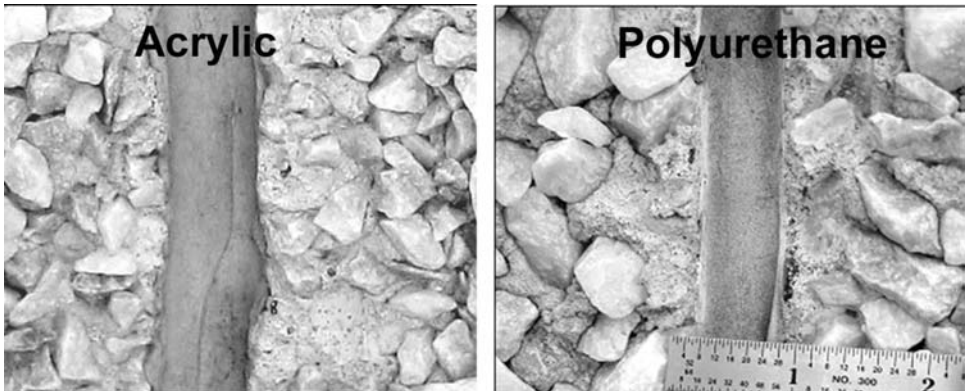


FIG. 4—Closer views of the sealants on the north elevation of the El Paso warehouse. The acrylic sealant is on the left; the polyurethane sealant is on the right.

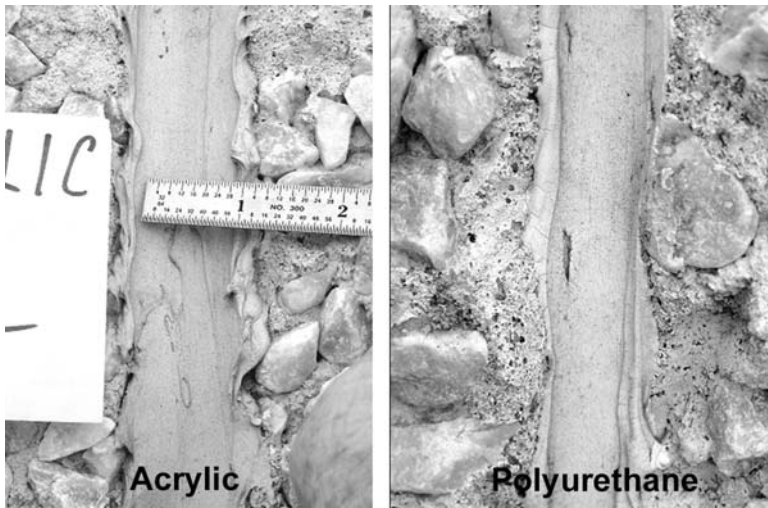


FIG. 5—Detailed views of the sealants on the east elevation of the El Paso warehouse. The acrylic sealant, on the left, exhibits no surface crazing. The polyurethane sealant, on the right, exhibits fine surface crazing.

the sealant bead and which may be compromising the functional performance of the sealant. The acrylic sealant, after 3 years of exposure, exhibits slight surface crazing or wrinkling in the horizontal joints at the top of the parapet (Fig. 7) but no visible degradation in any of the vertical parapet joints. This crazing or wrinkling was not present after 2 years of exposure. The greater degradation of the sealants in the parapet joints is due to the fact that these sealants are subjected to harsher exposure conditions than those installed at ground level. Sealants installed vertically around the interior of the parapet see reflected UV from the light colored roofing material; those installed in the horizontal joint at the top of the parapet see direct and continuous exposure to the sun.

The polyurethane sealant chalks markedly after 2 and 3 years of exterior exposure, as measured by transfer of white residue from the sealant surface to the inspector's index finger. Chalking is particularly severe in the parapet joints. The acrylic sealant, in contrast, chalks little in either the vertical or the parapet joints. The polyurethane sealant also softens noticeably during exposure, particularly in the parapet joints where the exposure conditions are most severe. The acrylic sealant does not change noticeably in hardness during exposure.

When sealant samples were pulled from representative joints to test for adhesion, both sealants pulled out easily due to substrate failure within the friable concrete mortar in the decorative aggregate surface layer. However, the mortar is holding up adequately for the joints experiencing movement, and no joint failures have been noted to date. Functional performance of both of the applied sealants appears to be intact, with the possible exception of the polyurethane sealant in the parapet corner joint noted above.

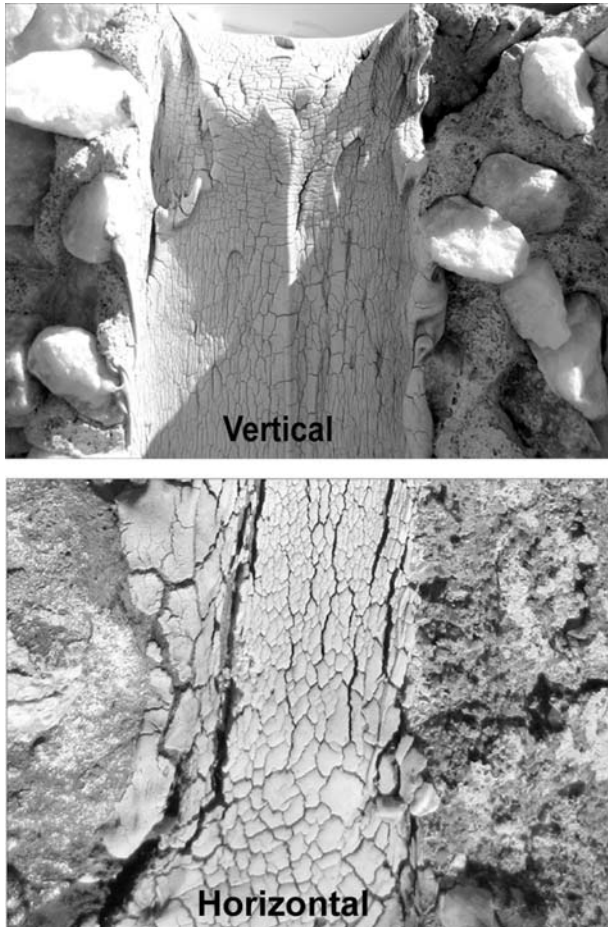


FIG. 6—Polyurethane sealant in a vertical joint in the warehouse parapet (top) showing surface crazing and chalking. Polyurethane sealant in a horizontal corner parapet joint (bottom) showing severe and deep crazing.

Accelerated Weathering

To assess their usefulness in predicting real world weathering results, the sealants exposed in the El Paso warehouse exposure were also subjected to several accelerated weathering tests. Results are presented in Tables 2–4 and in Figs. 8–11.

Weathering of Plaques in Xenon Arc and Fluorescent UV Weathering Devices—The results of the accelerated weathering of sealant plaques exposed in the xenon arc and fluorescent UV weathering devices are detailed in Table 2 and in Figs. 8 and 9. In the fluorescent UV, the polyurethane sealant plaque starts to craze after approximately 500 h and exhibits severe crazing after 2200 h (Fig. 8). These crazes extend as far as 1 mm into the bulk of the specimen. The

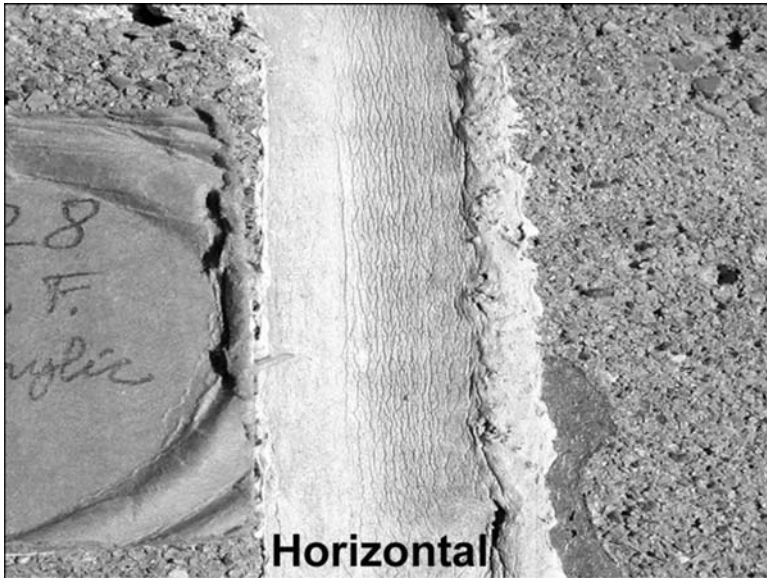


FIG. 7—Acrylic sealant in a horizontal parapet joint showing slight surface wrinkling or crazing.

acrylic sealant plaque, in contrast, exhibits no visible flaws after an extended exposure period of 6400 h in the fluorescent UV (Fig. 8). The polyurethane sealant in the xenon arc device looks similar to that in the fluorescent UV, exhibiting significant crazing after 2200 h. The acrylic sealant plaque exhibits no visible flaws in the xenon arc device after a comparable exposure period. Although there was no attempt to quantify crazing as a function of exposure time, the accelerated weathering results for both the acrylic and polyurethane sealants are consistent with the appearances of these two sealants after exterior exposure in El Paso. The early crazing of the polyurethane sealant plaque after accelerated weathering is similar to the crazing seen on the vertical joints of the polyurethane sealant after 3 years in El Paso. The deep crazing of the polyurethane sealant plaque after longer periods of accelerated weathering is consistent with the appearance of the polyurethane sealant in the parapet joints after 3 years in El Paso.

TABLE 2—Accelerated weathering results.

Sealant	Weathering Apparatus	Hours	Visual Appearance
Polyurethane	Fluorescent UV	2200	Severe crazing
Acrylic	Fluorescent UV	2200	No flaws
Acrylic	Fluorescent UV	6400	No flaws
Polyurethane	Xenon arc	2200	Severe crazing
Acrylic	Xenon arc	2200	No flaws

TABLE 3—ASTM C1519-04 durability results.

Sealant	Weathering Apparatus	Cycles	Hours	Failure ^a	Visual Appearance
Polyurethane	Fluorescent UV	5	3916	0.35 in. ² (226 mm ²) C at interface	Fine surface crazing
Acrylic	Fluorescent UV	5	3916	None	No flaws
Polyurethane	Xenon arc	5	3571	1.25 in. ² (806 mm ²) C at interface	Severe crazing; up to 3 mm deep
Acrylic	Xenon arc	5	3571	None	Slight crazing

^aFailure is reported as the total area of cohesive plus adhesive failure over three specimens. C=cohesive failure.

TABLE 4—*Appearance of sealants after 1 year of exterior exposure in static joints.*

Sealant	Coating	Dirt Pickup ^a	Crazing ^a	Chalking ^a
Polyurethane	No	80	70	30
	Yes	67	NA	NA
Acrylic	No	63	100	85
	Yes	83	NA	NA

^aQualitative scale where 100 represents no change from the initial appearance.

The polyurethane sealant softens during accelerated weathering in both the fluorescent UV and the xenon arc. This phenomenon was not quantified due to the fact that the sealant plaques used for weathering are too thin for reliable hardness measurements. However, the softening is pronounced, and the weathered polyurethane sealant after 2200 h feels gummy and significantly less tough than when it was originally exposed. This observation is consistent with the softening of the polyurethane sealant in the parapet joints in El Paso. The hardness of the acrylic sealant appears to change little during accelerated weathering.

In addition to general weathering, sealant color change was also evaluated as a function of exposure time in the fluorescent UV (Fig. 9). During the first 1500 h of exposure the polyurethane sealant yellows and darkens, as measured by changes in L^* and b^* . After 1500 h this trend is reversed as the sealant starts to chalk and, as a consequence, lighten. The color change of the polyurethane sealant during accelerated weathering was not noted in the El Paso warehouse exposure presumably because it was obscured by early dirt pickup. However,

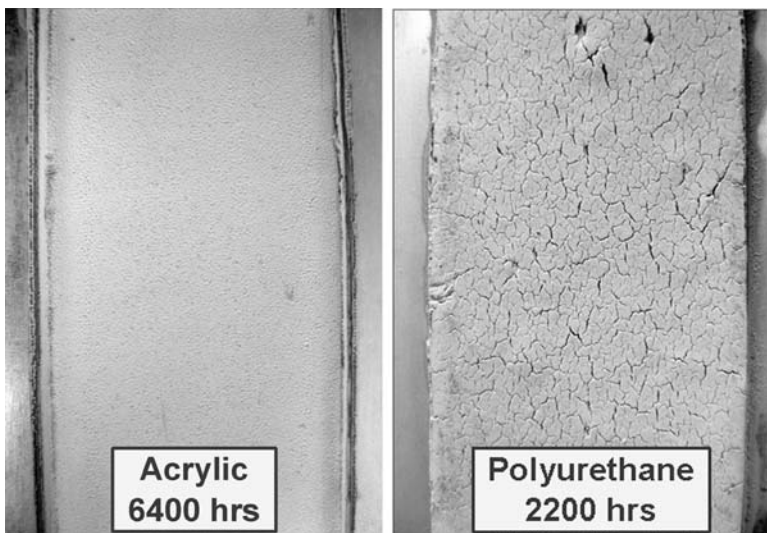


FIG. 8—*The acrylic sealant after 6400 h in the fluorescent UV apparatus (left) and the polyurethane sealant after 2200 h (right). Plaque width is 1.5 in. (38 mm).*

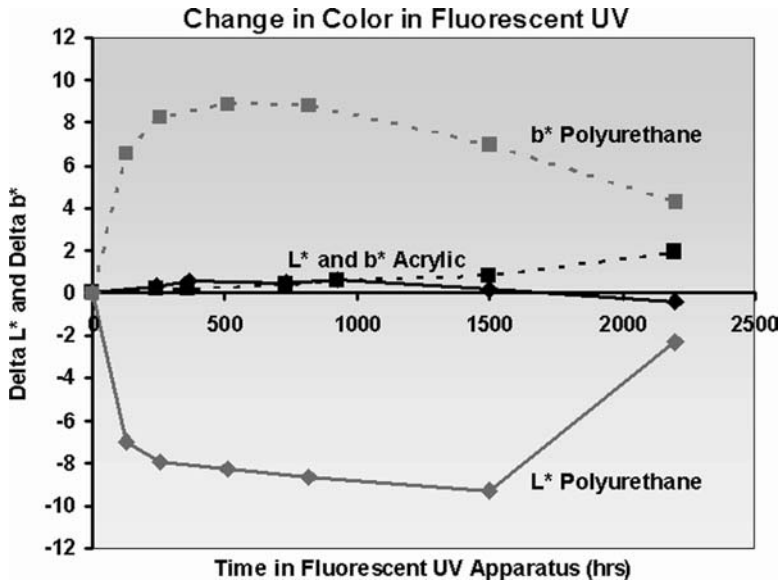


FIG. 9—Change in sealant color during accelerated weathering in the fluorescent UV apparatus.

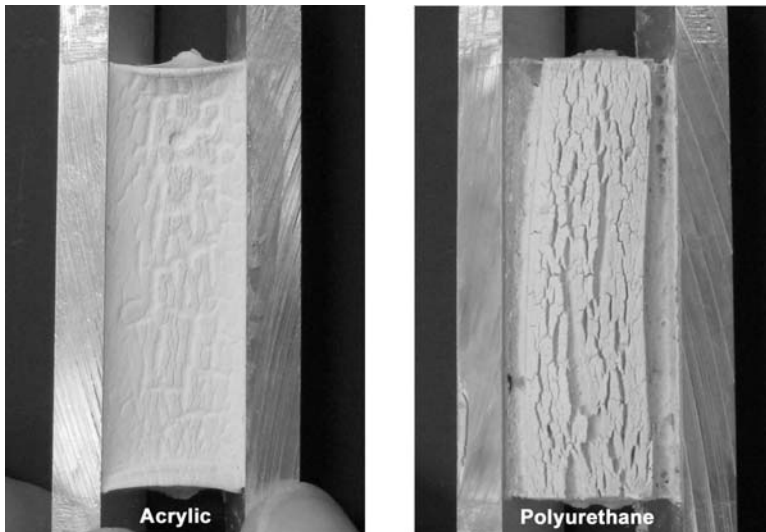


FIG. 10—Photograph of the acrylic sealant (left) and the polyurethane sealant (right) after 3571 h of weathering in the xenon arc device and five cycles of $\pm 25\%$ cyclic movement. Sealant joint dimensions are $0.5 \times 0.5 \times 2$ in.³ ($12 \times 12 \times 51$ mm³), and the sealants are slightly flexed to show crazing and loss of adhesion.

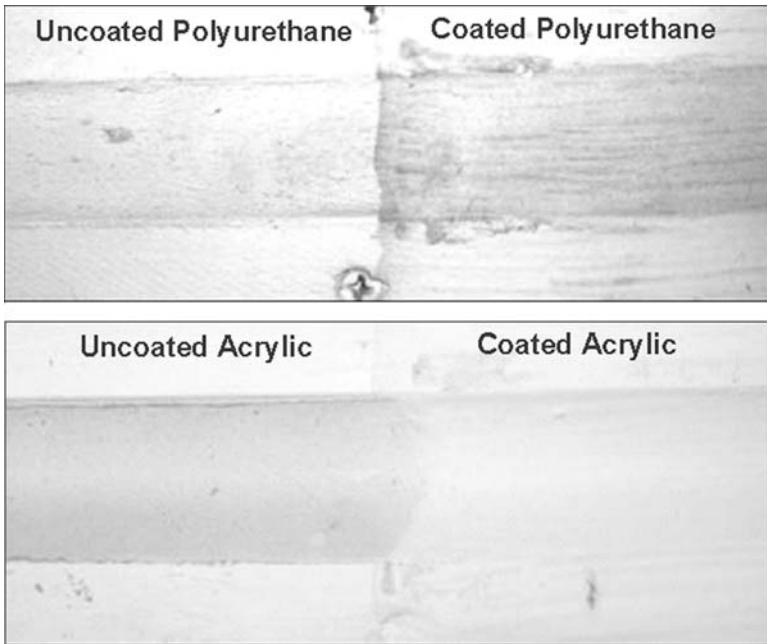


FIG. 11—Polyurethane sealant (top) and acrylic sealant (bottom) in painted wood channels. The sealant on the left hand side of each channel is unpainted. The sealant on the right hand side of each channel is coated with an EWC. The channel width is 3/4 in. (19 mm).

the chalking of the polyurethane sealant seen during accelerated weathering is consistent with the chalking observed in the field. The color of the acrylic sealant remains essentially unchanged after exposure in the fluorescent UV, and chalking after 2200 h is insignificant. This lack of chalking is likewise consistent with observations of the acrylic sealant after 3 years of exterior exposure in El Paso.

ASTM C1519-04 Durability—The results of ASTM C1519-04 durability testing are reported in Table 3 and in Fig. 10. After five cycles and 3916 h of weathering in the fluorescent UV, the ASTM C1519 polyurethane sealant H block specimens exhibit fine surface crazing and have a total of 0.35 in.² (226 mm²) cohesive failure at the interface with the aluminum substrate. Under the same conditions, the acrylic sealant specimens exhibit no surface degradation and no adhesive or cohesive failure. After five cycles and 3517 h in the xenon arc apparatus, the ASTM C1519 polyurethane sealant H block specimens are severely crazed, with the crazes extending up to 3 mm into the bulk of the specimens. The specimens also have a total of 1.25 in.² (806 mm²) cohesive failure at the substrate interface (Fig. 10). The acrylic sealant specimens exhibit slight surface crazing after xenon arc weathering but show no signs of adhesive or cohesive failure (Fig. 10).

The ASTM C1519 polyurethane sealant H block specimens weathered in

the fluorescent UV (Table 3) show substantially less surface degradation after 3916 h of exposure than the plaques of polyurethane sealant weathered for 2200 h in the fluorescent UV (Table 2). The faster surface degradation of the polyurethane sealant plaques may be due to the thinner cross section of the plaques and to the greater impact of heat and moisture on bulk sealant properties. Or it may be that the heat capacity of the H block specimens is higher than that of the plaques, resulting in less condensation during fluorescent UV exposure and less overall exposure to surface wetting. The greater degradation in the thin cross sections is consistent with the installer's observations that some polyurethane sealants in the field tend to "burn-through" or degrade when applied in thin cross sections or over backer rod that has been installed at an insufficient depth.

The ASTM C1519 polyurethane sealant H block specimens weathered in the xenon arc apparatus (Table 3) generally look similar to the plaques of polyurethane sealant weathered in the same device (Table 2). Both develop a dense network of cracks. However crack depths vary from roughly 1 mm in the exposed plaques to as much as the 3 mm in the ASTM C1519 H block specimens. The greater crack depths in the ASTM C1519 H block specimens are likely due to the longer exposure time (3571 h vs 2200 h) and to the repeated cycles of ± 25 % joint movement that are part of the ASTM C1519 durability test.

The degradation of the ASTM C1519 polyurethane sealant H block specimens is significantly greater after weathering in the xenon arc device than it is after weathering in the fluorescent UV (Table 3). This may be due to the broader spectrum of irradiance of the xenon arc light source or to the fact that specimens in the xenon arc see prolonged exposure to significantly higher temperatures than they do in the fluorescent UV. A comparison of accelerated to exterior weathering of the polyurethane sealant indicates that testing according to ASTM C1519 in the xenon arc apparatus (Fig. 10) generally predicts the worst of the UV degradation seen in the El Paso exposure (Fig. 6).

The ASTM C1519 acrylic sealant H block specimens weathered in the fluorescent UV look similar after 3916 h of exposure to the plaque of acrylic sealant weathered for 6400 h in the fluorescent UV. Neither exhibits any signs of surface degradation and the accelerated thin film degradation of the polyurethane sealant does not happen to the acrylic sealant. The lack of degradation after both accelerated fluorescent UV exposures is consistent with the lack of degradation of the vertical acrylic sealant joints after 3 years of exterior exposure in El Paso.

The ASTM C1519 acrylic sealant H block specimens weathered in the xenon arc apparatus exhibit a slight amount of surface crazing, while the plaque of acrylic sealant weathered in the same device has none. This is likely due to the longer exposure of the ASTM C1519 specimens (3571 h vs 2200 h) and to the repeated cycles of ± 25 % joint movement. The fact that the ASTM C1519 acrylic sealant H block specimens craze slightly after xenon arc weathering but not after similar times of fluorescent UV weathering may be due to the full daylight spectrum of the xenon arc lamp or to a greater exposure to elevated temperatures. Testing according to ASTM C1519 in the xenon arc apparatus (Fig. 10) predicts the slightly greater crazing of the acrylic sealant in the horizontal parapet joints in El Paso (Fig. 7).

The ASTM C1519 polyurethane sealant H block specimens soften significantly after weathering in the xenon arc apparatus but do not appear to soften after weathering in the fluorescent UV. The softening after xenon arc exposure is consistent with that seen after thin plaque weathering and after exposure in the parapet joints in the El Paso warehouse. The fact that noticeable softening of the polyurethane sealant only occurs on specimens which exhibit substantial surface crazing suggests that there is a connection between these two phenomena.

Exterior Exposure in Static Joints—The results of the Spring House Farm exposure in static joints are summarized in Table 4 and in Fig. 11. The uncoated polyurethane sealant picks up relatively little dirt but crazes and discolors upon exposure. This discoloration is consistent with that seen in the fluorescent UV exposure—initial yellowing followed by whitening due to chalking. The uncoated acrylic sealant shows no signs of degradation but picks up more dirt than the polyurethane sealant. These dirt pickup observations differ from the El Paso data, which indicate that the two sealants are very similar in appearance after 1, 2, and 3 years of exterior exposure. The reduced dirt pickup of the polyurethane sealant in the static joint relative to the exterior joints in El Paso may be due to the fact that the sealant exposed in the static joint was cured for several weeks prior to exposure, thus eliminating the early high tack, high dirt pickup phase of the polyurethane cure. The increased dirt pickup of the acrylic sealant in the static joint relative to the exterior joints in El Paso may be due to the different climate of the southeast PA exposure or to the fact that the static joints were exposed horizontally, which allows for less run-off and self-cleaning than do the vertical tilt-up joints in the El Paso exposure.

The EWC appears to be compatible with both the polyurethane and the acrylic sealants, with no apparent debonding at the coating/sealant interface. The EWC coated polyurethane sealant exhibits substantial dirt pickup. This, presumably, is due to plasticizer migration from the polyurethane sealant into the EWC. The EWC coated acrylic sealant exhibits very little dirt pickup due to the lack of plasticizer in the acrylic formulation.

Laboratory Testing

Standard laboratory tests were performed as part of a routine comparison of the two sealant binders and to augment the exterior and accelerated weathering data. Results are presented in Table 5 and Fig. 12.

Adhesion and Joint Movement Performance—The acrylic sealant has excellent wet and dry peel adhesion to mortar, with no adhesive failure and peel strengths substantially higher than the 5 lbf (22.2 N) required by ASTM C920-05. The polyurethane sealant also passes ASTM C920-05 peel adhesion requirements but with somewhat lower peel strengths. The acrylic sealant passes $\pm 25\%$ ASTM C719-93 joint movement testing on concrete mortar with no adhesive or cohesive failure. The polyurethane sealant unexpectedly fails this test in the first room temperature cycle. Since the manufacturer's technical data sheet (TDS) clearly indicates that this sealant passes $\pm 25\%$ joint movement testing to mortar, the premature failure noted in this evaluation may be due to the fact that these sealants were tested without the use of primer. The adhesion and

TABLE 5—Adhesion, joint movement, hardness, and tensile properties.

Properties	Acrylic	Polyurethane
Adhesion to mortar (ASTM C794-06)		
Dry, lbf (N)	24 (106) C	8 (35) C
Wet, lbf (N)	15 (66) C	10 (44) C
±25 % joint movement to mortar (C 719-93)	Pass, no failure	Fail, 1st RT cycle
Durometer hardness (ASTM C661-06)	29±2	16±2
Tensile properties at 2.0 in./min (5.1 cm/min)		
Stress at 25 % elongation, psi (MPa)	36±1 (0.25±0.01)	13±1 (0.09+0.01)
Maximum stress, psi (MPa)	143±1 (0.99±0.01)	84±3 (0.58+0.02)
Elongation to break (%)	647±9	297±12

joint movement properties in Table 5 and in the polyurethane TDS are consistent with the El Paso warehouse exposures where mortar adhesion is excellent and where the joint movement capabilities of the sealants are clearly adequate for the movement encountered.

Hardness and Tensile Properties—The acrylic sealant has substantially greater elongation than does the polyurethane sealant, a property generally associated with higher performance and greater joint movement capability. The measured hardness and stress values of the acrylic sealant are also higher than those of the polyurethane sealant but well within the ranges that are typical for

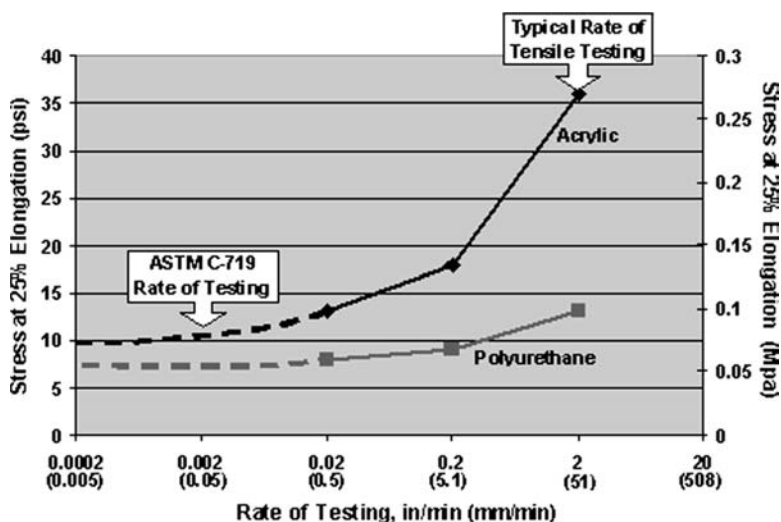


FIG. 12—The effect of rate of testing on stress at 25 % elongation of the acrylic and polyurethane sealants.

ASTM C920-05 Class 25 formulations. These measured differences are apparent in the field, where samples of acrylic sealant pulled from a joint are slightly harder and stiffer than pulled samples of the polyurethane sealant.

When comparing the tensile properties of sealants based on different chemistries, it is essential to do so with an understanding of the differing viscoelastic natures of these chemistries. Acrylic sealants are typically more viscoelastic than are more heavily cross-linked sealants based on reactive chemistries such as silicones and polyurethanes. Because of this, the mechanical properties of acrylic sealants are more strain rate dependent than are those of sealants based on reactive chemistries. When deformed quickly (such as at the rates typically found in the laboratory), acrylic sealants are often harder and stiffer (with higher stress or modulus values) than their reactive chemistry counterparts. However, when deformed slowly (such as at the rates typically encountered outside), the properties of acrylic sealants fall in line with those of alternative chemistries.

The differences in the strain rate response of the tested acrylic and polyurethane sealants are illustrated in Fig. 12, where stress at 25 % elongation (a measure of sealant stiffness) is plotted against the rate of tensile testing. Tensile measurements are generally done at rates of testing which are convenient for generating data in a timely manner. ASTM D412-06a, the commonly referenced "Standard Test Methods for Vulcanized Rubber and Thermoplastic Elastomers—Tension" [10] specifies that tensile testing be done at 20 in. (508 mm)/min. The author's laboratory routinely uses 2 in. (51 mm)/min for tensile testing as a more reasonable compromise between timely data generation and real world deformation rates. However, both of these testing rates are several orders of magnitude greater than the rate of deformation in ASTM C719-93 joint movement testing (2×10^{-3} in. (5×10^{-2} mm)/min) and the rates of joint movement likely to be encountered in exterior low rise masonry buildings ($2-5 \times 10^{-4}$ in. ($5-13 \times 10^{-3}$ mm)/min) [11,12]. These high rates of tensile testing over emphasize the differences in mechanical properties between strain rate independent elastomeric sealants and more strain rate dependent viscoelastic sealants.

When the rate of sealant testing is reduced from 2.0 in. (51 mm)/min to a more appropriate rate of 0.02 in. (0.5 mm) /min, the stress of the acrylic sealant at 25 % elongation converges on that of the polyurethane sealant, minimizing the perceived differences between the two sealants.

Conclusions

The El Paso warehouse exposure provides a unique, side by side, comparison of a high performance acrylic sealant to a commercial two part polyurethane sealant. After 3 years of exterior exposure the polyurethane sealant continues to function as a sealant, with good adhesion and adequate joint movement capability for the application. However, the polyurethane sealant exhibits considerable crazing, chalking, and softening as the result of exposure, and the function of at least one sealant joint appears to have been compromised by crazing

through to the underlying backer rod. Accelerated weathering data generally support these observations.

After 3 years of identical exposure, the acrylic sealant also continues to perform as a sealant, with good adhesion and adequate joint movement capability. The acrylic sealant has comparable dirt pickup to the tested polyurethane sealant and better exterior durability (i.e., little crazing and no chalking or softening). Laboratory test results and accelerated weathering data support and confirm these results. The lack of plasticizer in the acrylic sealant formulation eliminates plasticizer migration and dirt pickup of coatings applied over the sealant joint. Feedback from the moisture-proofing contractor suggests that the properties of the wet acrylic sealant require minimal adjustment for optimal application and that the water cleanup of the acrylic sealant is a distinct advantage from convenience, safety, and environmental points of view.

The data presented herein represent the results of 3 years of exterior and laboratory testing of a high performance acrylic sealant and a commercial two part polyurethane sealant. The results, of course, pertain to the sealants tested and are not necessarily representative of the performance of all high performance acrylic and polyurethane sealants. Certainly there are commercial urethane products on the market, which will out perform the product tested in this evaluation. However, the combined results of this side by side comparison clearly demonstrate the adhesion, durability, and aesthetic benefits of the tested acrylic sealant. While these results cannot necessarily be extrapolated to all high performance acrylic sealants, they do suggest that these products can be highly suitable for use in low rise industrial applications such as tilt-up warehouses.

References

- [1] ASTM Standard C834-05, 2005, "Standard Specification for Latex Sealants," *Annual Book of ASTM Standards*, ASTM International, West Conshohocken, PA.
- [2] ASTM Standard C920-05, 2005, "Standard Specification for Elastomeric Joint Sealants," *Annual Book of ASTM Standards*, ASTM International, West Conshohocken, PA.
- [3] McLaren, K., "The Development of the CIE 1976 (L*a*b) Uniform Colour-Space and Colour-Difference Formula," *J. Soc. Dyers Colour.*, Vol. 92, 1976, pp. 338-341.
- [4] ASTM Standard G155-05a, 2005, "Standard Practice for Operating Xenon Arc Light Apparatus for Exposure of Non-Metallic Materials," *Annual Book of ASTM Standards*, ASTM International, West Conshohocken, PA.
- [5] ASTM Standard G154-06, 2006, "Standard Practice for Operating Fluorescent Light Apparatus for UV Exposure of Nonmetallic Materials," *Annual Book of ASTM Standards*, ASTM International, West Conshohocken, PA.
- [6] ASTM Standard C1519-04, 2004, "Standard Practice for Evaluating Durability of Building Construction Sealants by Laboratory Accelerated Weathering Procedures," *Annual Book of ASTM Standards*, ASTM International, West Conshohocken, PA.
- [7] ASTM Standard C719-93, 2005, "Standard Test Method for Adhesion and Cohesion of Elastomeric Joint Sealants Under Cyclic Movement (Hockman Cycle)," *Annual Book of ASTM Standards*, ASTM International, West Conshohocken, PA.

- [8] ASTM Standard C794-06, 2006, "Standard Test Method for Adhesion-in-Peel of Elastomeric Joint Sealants," *Annual Book of ASTM Standards*, ASTM International, West Conshohocken, PA.
- [9] ASTM Standard C661-06, 2006, "Standard Test Method for Indentation Hardness of Elastomeric Sealants by Means of a Durometer," *Annual Book of ASTM Standards*, ASTM International, West Conshohocken, PA.
- [10] ASTM Standard D412-06a, 2006, "Standard Test Methods for Vulcanized Rubber and Thermo-Plastic Elastomers-Tension," *Annual Book of ASTM Standards*, ASTM International, West Conshohocken, PA.
- [11] Elfring, W. H. and Rosano, W. J., "Climate and Performance of Elastomeric Wall Coatings," *Science and Technology of Building Seals, Sealants, Glazing and Waterproofing*, ASTM STP 1200, J. M. Klosowski, Ed., ASTM STP, West Conshohocken, PA, 1992, pp. 245–259.
- [12] Evans, R. M., *Polyurethane Sealants, Technology and Application*, Technomic Publishing Company, Inc., Basel, 1993.

Overview

Introduction

The Third ASTM International Symposium on Durability of Building and Construction Sealants and Adhesives (2008-DBCSEA) was held on June 25–26, 2008 in Denver, Colorado. It was sponsored by the ASTM International Committee C24 on Building Seals and Sealants in cooperation with the International Union of Laboratories and Experts in Construction Materials, Systems and Structures (RILEM). The symposium was held in conjunction with the standardization meetings of the C24 Committee. With presentations from authors representing six countries in North America, Europe, and Asia, the symposium was a truly international event.

The symposium brought together architects, engineers, scientists, researchers and practitioners. One of the stated goals of the symposium was to transfer new ideas, gained from laboratory research and field work, to the study of sealant and adhesive durability and the development of new products and test methods. Of course the symposium did not provide all of the answers. However, it did provide an excellent forum for international experts to discuss their experiences in durability testing and assessment as well as in the application of building and construction sealants and adhesives. Perhaps the greatest value of these symposia lies in these discussions and in the dissemination of the resulting information.

The current series of ASTM symposia on Durability of Building and Construction Sealants and Adhesives is a continuation of tri-annual symposia that were inaugurated by the RILEM Technical Committee 139-DBS Durability of Building Sealants in 1994. Today, this continuing series of symposia provides the best scientific forum globally in the building and construction industry for peer-reviewed papers on all aspects of sealant and adhesive durability. Furthermore, data presented at those symposia over the past 15 years have been the single most important factor influencing ASTM International and ISO standards as well as RILEM technical recommendations related to construction sealant durability.

The increased utilization of sustainable construction practice, i.e., designing for durability by utilizing building science and life cycle analysis as its foundation, as well as mandatory government regulations, such as the European Construction Products Directive, have elevated the importance of the durability and service life performance of building and construction sealants and adhesives. All products, not just those involved in safety-critical applications, must demonstrate the durability of their fitness for purpose. Life cycle costing considerations increasingly drive investment decisions toward products and systems with longer service life cycles and lower maintenance costs.

Against a background of national and international efforts to harmonize testing and approval of building materials and structures, ASTM International and RILEM have been looking for ways of bringing together the experience of international experts gathered in the application and testing of building and construction sealants and adhesives.

As with most scientific disciplines, substantial advances often occur through a series of incremental steps by individual laboratories, each contributing pieces of the puzzle, rather than in giant leaps. This is also the case for the papers presented at the ASTM International Symposium on Durability of Building and Construction Sealants and Adhesives (2008-DBCSA). Many of the papers reflect progress reports on on-going research. At the 2008-DBCSA symposium, we saw several examples of the steady progress being made by leveraging these scientific advances into a new generation of test methods.

This book contains 19 papers presented at the symposium and two papers submitted only for publication in the proceedings, all of which were previously published by the Journal of ASTM International (JAI). JAI is an online, peer-reviewed journal for the international scientific and engineering community. Publication in JAI allows rapid dissemination of the papers as soon as they become available, while publication in this Special Technical Publication (STP) is intended to provide easy access to the condensed information in a single volume for future reference. The contributions condensed in this STP volume represent state-of-the-art research into sealant and adhesive durability and reflect the varying backgrounds, experiences, professions, and geographic locations of the authors. The following major themes are evident in this collection:

- Laboratory Testing and Specialized Outdoor Exposure Testing
- Factors Influencing the Durability of Sealed Joints and Adhesive Fixations
- Development of New Test Methods and Performance-Based Specifications
- Field Experience with Sealed Joints and Adhesive Fixations

Below is a short overview of the papers that were published in JAI in the above four categories.

Laboratory Testing and Specialized Outdoor Exposure Testing

While our understanding of the factors influencing the durability of sealed joints and adhesive fixations has progressed substantially over the past decades, there is still much to be learned. Various laboratory accelerated tests have been developed over the years to generate durability data and to duplicate the failure modes occurring in field exposures with the intent to predict the service life of sealed joints and adhesive fixations in less than real time. However, sealants and adhesives have been reported to fail prematurely in the field even though they may have performed satisfactorily when evaluated with these laboratory test protocols. Extensive research efforts are underway to develop laboratory accelerated test protocols that

provide better correlation with actual outdoor exposure and in-field service performance. A number of papers therefore focus on this topic.

In their paper, **Pozzi, Carcano, and Ausilio** report on an attempt at finding a correlation between environmental and accelerated RILEM TC139-DBS weathering for one-component polyurethane sealants applied on mortar. Half of the set of specimens is exposed for 24 months in static conditions (no movement) to the outdoor environment in the urban area of Milan, Italy, while the other half is subjected to accelerated weathering according to the RILEM TC139-DBS procedure in a light-exposure apparatus (xenon-arc type) with water spray and intermittent periods of thermo-mechanical cycling. Based on the visual inspection of the surface changes that occurred in both sets of specimens, the authors find a good correlation between the results obtained in outdoor exposure and those observed after the RILEM durability cycling. The results demonstrate the importance of achieving an appropriate mix of synergistically acting aging factors in the artificial weathering protocol. Potentially even better correlation may have been expected, if the outdoor weathering was also carried out with simultaneous enforced movement in order to induce cyclic fatigue deformation on the specimens. The authors plan such evaluations for the future.

Joint sealants decisively influence the performance and service life of pavements although they account for only a small fraction of the total investment. Motivated by the damages observed and the resulting, increasing maintenance efforts, the Federal German government recognizes the need for performance-evaluated joint sealing systems with improved capability (fitness for purpose) and durability. In contrast to the existing, predominantly empirical evaluation and selection of joint sealing materials and systems for pavements, **Recknagel and Pirskawetz** suggest a methodology aimed at verifying performance under superimposed mechanical and climatic loads. The fatigue behavior of the joint sealants is detected by analysis of the cycle-dependent changes in the mechanical system characteristics. The evaluation methodology further allows investigation of the degradation mechanisms of specific system failures and, thus, enables service life prediction by reproducing the performance of the complete system under realistic conditions. Constructional defects and material flaws can be investigated by this performance-related test methodology, thus allowing identification of possible improvements to material selection and application procedures.

Long-term weather resistance is an important factor to consider when selecting a sealant product for use in exterior weather-sealing applications. **Bull and Lucas** in their paper compare the long-term performance of construction sealant products based on silicone polymer, polyurethane polymer, and acrylic terpolymer after a 22-year exposure to outdoor weathering in south Florida. The paper shows that changes in performance attributes such as the toughness, flexibility, and adhesion of the products are good indicators of the physical and chemical degradation (i.e., reversion, cracking, hardening, etc.) occurring in outdoor exposure.

Previous accelerated weathering methods for construction sealants, such as ASTM C1519 and RILEM TC139-DBS, investigated the durability of sealed specimen joints based on their ability to function in cyclic movement while maintaining adhesion and cohesion after repeated exposure to laboratory accelerated weathering procedures. In these test methods, accelerated weathering and mechanical cycling are sequentially imposed on the specimen, and the whole exposure cycle, consisting of weathering and enforcement movement, is repeated iteratively several times. Anecdotal evidence, however, suggests that degradation is substantially accelerated by simultaneously weathering and mechanically cycling the specimen. Recently, two novel test methods have been proposed by RILEM Technical Committee 190-SBJ that allow simultaneous exposure to mechanical cycling and either outdoor weathering or accelerated weathering. In their first paper, **Gorman** and **Klosowski** selectively review previous weathering studies and discuss their thoughts on the development of novel test concepts that involve simultaneous exposure to weathering and joint movement. In their second paper, the same authors explore an alternative sealant weathering test method that also expands on the existing test methodologies. Sealed joint specimens are simultaneously exposed to enforced mechanical movement and either to accelerated weathering or to outdoor weathering in four different climates within the USA. The paper reports on the specific test protocol and the progress of the testing. Correlations of the damage observed after exposure to outdoor climate and in the artificial weathering machines are explored.

Moisture in the form of humidity, condensation, rain, or water immersion is the most commonly encountered element of the service environment and must be considered a critical factor in determining the long-term reliability of sealed or bonded joints. Moreover, the effects of moisture are exacerbated by elevated temperature. For many polymeric systems, warm, moist environments can considerably weaken the bulk or interfacial performance properties of the jointing materials formulated with these polymers. The majority of joint failures in service environments that comprise water exposure occur by degradation of the interfaces between sealant or adhesive, primer, and substrate. Therefore, predicting the interfacial degradation in an actual service environment is of utmost importance. **Wolf** provides information in his paper on the current understanding of the role of water in the failures of adhesive and sealant joints and discusses the usefulness of the Arrhenius relation in predicting the lifetime of immersed sealed or bonded joints based on data generated at elevated temperatures. The paper also suggests some guidelines aimed at improving the reliability of accelerated test and prediction procedures used in the evaluation of the durability performance of sealed or adhered joints in immersed environments.

Historically, joints in glass construction have been bonded with one- and two-component silicones. Ultraviolet (UV) and visible (VIS) light curing acrylates provide further design potential in glass constructions due to their inherent transparency, their rapid bonding capability, and an inherently

higher material strength. In their paper, **Weller and Tasche** examine the aging behavior of acrylate adhesives by testing bonded joints made of annealed glass and metal substrates. As a first step, the authors investigate the influence of the different surfaces of float glass (atmospheric or tin-bath side) on the tensile strength of bonded joints. Then, adopting the test protocol defined in the European EOTA guideline, the aging resistance of acrylate bonds between untreated annealed glass and metal substrates is examined using seven metal surfaces, i.e., polished-chrome brass; matt-chrome brass; powder-coated brass; turned, polished, and sanded stainless steel; and anodized aluminum. The authors also study the effect of glass surface treatments (pyrolytic silane treatment, sandblast coating, and atmospheric plasma treatment) on the residual strength after water exposure of the acrylate-bonded joints. Furthermore, the study comprises tests on life-size samples (load-bearing capacity and post breakage behavior) according to the guidelines and standards applicable in Germany for safety glazing. These life-size specimens are exposed to outdoor weathering for a period of 5 years, after which their critical safety behavior will be tested again.

Longo and Vandereecken compare silicone sealants with newly developed Si-modified organic (polyether, polyurethane, and polyacrylate) polymer-based sealants in their resistance to weathering and thermo-mechanical movement. The sealants are exposed to alternating periods of UV radiation through glass and thermo-mechanical cycling for 1 year. The results of this study show that most Si-modified organic sealants have limited durability in weather-sealing applications. The newly developed silicon-acrylate-based sealants tested during this study show improved durability but still demonstrate poor elastic recovery after exposure to simulated weathering in combination with thermo-mechanical movement. This poor elastic recovery limits their long-term movement capability.

Nakagawa and Yukimoto in their paper study the durability and performance of a silyl-terminated (Si-modified) polyacrylate (STPA) based construction sealant in comparison to a typical silyl-terminated polyether (STPE) sealant and a silicone sealant in order to demonstrate the potential of the STPA sealant as a high durability, high performance construction sealant that is also suitable for glazing applications. The study reveals that the polyacrylate backbone of STPA polymer has higher durability, especially UV stability and heat resistance, than the polyether one of STPE polymer, as shown by accelerated weathering tests using carbon-arc or super high irradiance xenon-light sources. Adhesion of the STPA sealant on glass is retained even after 10,000 hours exposure to super high irradiance xenon-light. The authors also compare the performance of the STPA-based sealant to that of the STPE based sealant by testing according to several industrial ISO and JIS standards. The STPA based sealant consistently conforms to a higher durability class specification than the STPE sealant. Furthermore, a cyclic movement test of the STPA-based sealant in a compression-extension machine shows no damage to the sealant even after 200,000 cycles of $\pm 40\%$ movement at room temperature. While, in all likelihood, the sealant prod-

ucts studied by **Longo** and **Vandereecken** are not identical with those studied by **Nakagawa** and **Yukimoto**, the corresponding polymers (silicone and Si-modified polyacrylate) are and it is interesting to note the difference in the behavior of these sealants observed in the two studies. While in the **Nakagawa** and **Yukimoto** study, the Si-modified polyacrylate sealant shows excellent resistance to fatigue aging when exposed to cyclic movement at room temperature without any weathering, the combined weathering and thermo-mechanical cycling studied by **Longo** and **Vandereecken** yields noticeable degradation. Still, both evaluations and previous studies by **Nakagawa** suggest the potential of Si-modified polyacrylate as polymer for durable elastomeric glazing joint sealants, including their use on photocatalytic self-cleaning glass (SCG), if the sealants are not subjected to extreme movements.

Factors Influencing the Durability of Sealed Joints and Adhesive Fixations

Silicone structural glazing has been a proven method of glass attachment to metal curtainwalls for more than 30 years. With the advent of novel substrate materials it is important to note that structural sealant adhesion testing does not qualify a substrate as suitable for the intended use. Since any chain is only as strong as its weakest link, the durability of the substrates involved in structural glazing is of great importance. In his paper, **Carbary** suggests a procedure for evaluating the durability of substrates used in conjunction with structural silicone glazing (SSG). Lap shear and peel adhesion specimens are evaluated after exposures to various conditions. Conditions of exposure include water, sodium hypochlorite (bleach), acetic acid (vinegar), salt fog, UV fluorescent accelerated weathering device, UV exposure, and heat. Evaluation of substrates and their interfaces with the sealant are completed after tensile testing and visual surface analysis. Substrates evaluated include steel, anodized aluminum, galvanized steel, extruded rigid polyvinyl chloride (PVC), glass reinforced thermoplastic resin (fiberglass), and polyvinylidene fluoride (PVDF) coated aluminum. These substrates are tested according to the suggested procedure to show differences in performance and to determine a minimum time frame required for testing. The results and guidelines set forth in this paper provide the foundation for a practice or a substrate specification for use in conjunction with structural silicone attachment methods.

Changing weather conditions prior to the application of sealants on porous substrates, such as the wetting of concrete by unexpected rainfall, can lead to poor sealed joint durability due to adhesion loss. **Gubbels** and **Calvet** study the adhesion of sealants with different chemistries, i.e., silicone, urethane, acrylic, silyl-terminated polyether, and silyl-terminated polyurethane, on wet concrete, when applied at various stages of the drying process. In the first two hours of drying, a drastic reduction of the pH at the concrete surface is observed, which is concurrent with a reduction of the surface humidity. This initial drying period shows the strongest effect on adhesion du-

rability. Therefore, the authors suggest that alkalinity and surface moisture are the major factors responsible for the poor adhesion observed on wet porous alkaline substrates. The critical drying timing also affects the adhesion development of the primer on the wet concrete substrate.

Silicone sealants have been used widely in the waterproofing industry because they resist deterioration. However, residue from silicone sealants (or from pre-formed silicone seals) can be difficult to remove from adjacent surfaces, if it contacts these surfaces inadvertently from improper application or fluid run-down. The paper by **Klosowski, Breeze, and Nicastrò** focuses on the challenge of removing silicone residue from window glass. Several of the likely sources of the silicone residue are discussed, along with the difficulty of measuring the presence of the colorless and odorless thin residue film. The testing evaluates commercially available cleaners and digesters in their effectiveness of removing the silicone residue. The results obtained by the authors are mixed and largely inconclusive; however, the test methodology developed can be used for further evaluation by other laboratories.

The paper by **Krelaus, Wisner, Freisinger, Schmidt, Böhm, and Dilger** demonstrates that ultra-high performance concrete (UHPC), with its unique material properties, is a suitable substrate for adhesive bonding. The authors present results that were generated as part of a research project aimed at investigating the properties of UHPC adhesive joints in terms of reliability, safety, and load-bearing capacity. Information on strength and durability of 14 adhesives are presented considering varying conditions of substrate surface pretreatment and different UHPC compositions. Exposure conditions include hygrothermal, freezing, and salt spraying exposures. A great variation of fracture pattern is observed; however, the authors demonstrate that the most critical situation of adhesive failure at the interface to the substrate can be avoided by bonding on mechanically pretreated UHPC surfaces. The results emphasize the need for a pretreatment of the UHPC form surface prior to adhesive bonding.

In her paper, **Hagl** details some of the investigations currently occurring within Germany with regard to the application of complex bonding geometries for structural engineering purposes. The author reports information on silicone adhesive material behavior in various bonding geometries resulting from the use of L- and T-type steel elements. Tensile, compression and shear tests are performed on aged and unaged specimens in order to analyze the impact of an aggressive environment. Several degradation modes are induced into the specimens in order to evaluate the load-bearing capacities and failure mechanisms of the different bonding geometries and to assess their behavior in the view of partial failure. **Hagl** presents an overview of the experimental and finite element analysis (FEA) modeling results. Former results obtained for U-type bonding geometry are reviewed in the light of the new experimental findings. Finally, the paper concludes by di-

rectly comparing all investigated bonding geometries with respect to durability considerations.

Development of New Test Methods and Performance-Based Specifications

With the recent threat of terrorist attacks, there has been an increased use of windows designed to mitigate the impact of bomb blasts. Due to the high strength and durability characteristics of silicone sealants, structural silicone sealants have been utilized in new bomb blast mitigating window designs. Effective bomb blast mitigating window designs allow the window system to withstand a moderate bomb blast without causing substantial injury to building occupants from the blast itself or flying glass shards. The occupants are protected because laminated or filmed glass, which can withstand the blast, is attached in the framing with a silicone sealant. Silicone sealants provide unique benefits to these window designs due to their strength properties and their ability to anchor the laminated glass in the framing during a blast situation. In their paper, **Yarosh, Wolf, and Sitte** report on the evaluation of three commercially available high strength structural silicone sealants at applied load velocities (movement rates) up to 5.0 m/s. These elevated load velocities are intended to simulate loads encountered during a bomb blast. Sealant joints are fabricated to evaluate the sealant in tension, shear, and combined tension and shear loads. Sealant joints are also exposed to accelerated weathering (heat, water, and artificial light through glass). Results show that the sealant strength values increase substantially at elevated rates of applied load. The paper discusses the effect of joint configuration, load velocities, and accelerating weathering on the performance and durability of the silicone sealants tested. The results and test method discussed in this paper provide the foundation for a specification for structural silicone attachment methods in bomb blast mitigating glazing.

The paper by **Enomoto, Ito, and Tanaka** presents information on the weatherability of construction sealants based on a newly developed test specimen design that allows simultaneous exposure of the sealant to forced compression and extension movement in a single specimen. In their study, exposure to cyclic movement and weathering is carried out simultaneously. Furthermore, an evaluation method for surface cracks induced by weathering is presented that allows an assessment of the overall “degree of degradation”, a single number characterizing the state of degradation of the sealant surface. In order to study the effects of the amplitude of extension and compression as well as the regional exposure factors on the degree of degradation, 12 sealants are exposed to outdoor weathering for 4 years at three exposure sites, located in the northern, central, and southern areas of Japan. The evaluation of surface cracks is carried out according to the rating provided in ISO 4628-4, with the modification, that new rating criteria are introduced to evaluate minute cracks. A mathematical equation determining the “degree of degradation” is obtained for each sealant, which is based

on a component reflecting aging under static conditions and on another component reflecting the dynamic conditions induced by mechanical movement and regional exposure factors. This equation provides a reasonable relationship between the experimental observation and calculated degradation over the exposure period. Based on the results of this study, the novel test specimen design has already been adopted in the RILEM TC190-SBJ Technical Recommendations and the ISO TC59/SC8 committee intends to use this design in a future international standard on sealant durability testing.

Rheological instruments have the capability to characterize the dynamic mechanical behavior of elastomeric materials undergoing oscillatory (cyclic) deformation under controlled test conditions and, therefore, provide a laboratory tool for assessing durability. Cyclic testing can be conducted under controlled strain (deformation) conditions at frequencies that simulate joint movement due either to thermal expansion differentials or seismic events, or under controlled stress (load) that model hurricane-force wind loads or design pressures. **Gordon, Lower, and Carbery** report on a durability study of four condensation-cure silicone sealants using rheological methods. The test specimens are allowed to cure in situ to optimize material/substrate contact with the rheometer plate fixtures at ambient conditions for one week under static conditions. For future considerations the authors note that rheometers can also be used to cure specimens under dynamic conditions while simultaneously measuring the change in rheological properties over time. In the absence of other artificial degradation effects, the authors attribute the initial stress reduction observed in sealants undergoing controlled strain sinusoidal deformation to the Mullins effect. The stress-softening phenomenon occurs within the first 24 hours of cycling; however, three of the four sealants subsequently exhibit signs of recovery during the remainder of the testing period. Under controlled-load cyclic testing at their design load (0.138 MPa) the sealants exhibit an ultimate deformation within the test cycle well below their rated movement capability with no apparent signs of fatigue. Therefore, the sealant materials tested should be acceptable in an impact-resistant assembly, if the frame remains rigid and the stresses induced from the design wind pressures are transferred to the fully cured and adhered sealant joints. A next step to further characterize the sealants is to ascertain that the cyclic strains or stresses imposed upon the sealants in real systems are quantified properly so that the rheology test methods presented can better assess the performance and durability of an individual material. The paper demonstrates the potential of rheology test methods as a screening tool to isolate and evaluate the mechanical durability of elastomeric silicone sealants in building assemblies undergoing cyclic deformation.

White, Hunston, and Tan examine the effects of applied strain on sealants exposed to outdoor weathering for two sealant formulations. Both static and dynamic strains are applied to the sealants during the summer in an outdoor location. Both sealants exhibit a reversible change in equilibrium distance. Stress relaxation studies reveal differences in the mecha-

nisms that affect modulus changes in the sealants. For one sealant, exposure without applied strain increases the modulus, while additionally applied strain decreases the modulus; for the other sealant only one mechanism that decreases the modulus is observed.

To fully understand accelerated aging of externally bonded carbon fiber reinforced polymer (CFRP) applications without testing each resin individually, researchers must develop an understanding of the mechanical and chemical bond properties of the CFRP system and the influence of water content and temperature on bond. Presently the proposed strength reduction factor for durability is the strength ratio of specimens submerged in water at 60°C for 60 days, which provides a lower bound durability strength reduction factor for CFRP applications. The paper by **Deng, Tanner, Dolan, and Mukai** examines the development of test methodology and specimen for both flexure and direct tension behavior of bonded CFRP materials using a specimen submerged in a water bath subject to elevated temperature. Test results of three commercial CFRP systems are presented. A discussion of accelerated aging is included in the developmental effort. Further research may provide a logical categorization of CFRP composite systems based on better defined mechanical and chemical properties of adhesive materials and different environments.

Considerable work has focused on the deterioration of jointing compounds used to seal building joints, while less emphasis has been placed on understanding the consequences of seal failure, particularly in respect to watertightness. Water entry at sealed joint deficiencies may lead to a number of different deteriorating effects on the building fabric that may induce failure of other envelope components or premature failure of the joint sealant. Joints are also subjected to substantial wind-driven rain loads in particular atop multi-storey buildings. The approach taken in the study by **Lacasse, Miyauchi, and Hiemstra** focuses on determining the fault tolerance of joint systems of a simulated wall panel when subjected to watertightness tests that emulate heightened wind-driven rain loads. Vertical and horizontal joint seals in which cracks along the sealant to substrate interface have been introduced artificially are subjected to water spray and air pressure. Rates of water entry across the joint are determined for cracks of different lengths and size. Results on vertical joints indicate that water readily enters open cracks in relation to the crack size, quantity of water present at the crack, and pressure across the opening. The study demonstrates that water may also penetrate cracks of non-extended closed joints. If the crack length in a joint of an actual building is known or verified from a field inspection and the climate loads impinging on the façade have been established, an estimate of the rate of water leakage can be calculated by using the information provided in this paper.

Field Experience with Sealed Joints and Adhesive Fixation

The paper by **Demarest, Liss, Queenan, and Gorman** compares the outdoor weathering behavior of a laboratory prepared high performance

acrylic sealant to that of a commonly used, commercially available two-part polyurethane sealant. Both sealants are installed in alternating joints around the perimeter of a tilt-up warehouse located in El Paso, Texas, USA. Furthermore, the sealants are subjected to a range of laboratory tests, including tensile testing, sealant specification testing, paintability, and accelerated weathering in both xenon-arc light and fluorescent UV weathering devices. The 3-year El Paso exposure results, in combination with the laboratory, weathering, and application test results, demonstrate the performance advantages of the high performance acrylic sealant and highlight its inherent suitability for use in low rise industrial applications such as tilt-up warehouses. After 3 years of exterior exposure the polyurethane sealant continues to function as a sealant, with good adhesion and adequate joint movement capability for the application. However, the polyurethane sealant exhibits considerable crazing, chalking and softening as the result of exposure and the function of at least one sealant joint appears to have been compromised by crazing through to the underlying backer rod.

Closure

As we publish this volume, I look forward to the next Symposium on Durability of Building and Construction Sealants and Adhesives (2011-DBCASA) and the associated flurry of papers in this dynamic industry. I encourage all readers to participate in the work of the ASTM C24 committee, to attend the future symposia, and to contribute new papers. Your participation and feedback help to advance the industry and, as a result, we will all benefit from improvements to our built environment.

In closing, I would like to gratefully acknowledge the outstanding quality of the contributions made by the authors as well as the dedicated efforts of the 2008 session chairpersons, the peer reviewers, the staff of ASTM and AIP, and the associated editor of JAI, who all helped to make the 2008 symposium and the publication of the associated papers possible.

Andreas T. Wolf
Wiesbaden, Germany

AUTHOR INDEX

Index Terms

Links

A

Ausilio, A. 3–14

B

Böhm, S. 227–253

Breeze, E. S. 217–226

Bull, E. D. 38–72

C

Calvet, C. 200–216

Carbary, L. D. 185–199 313–327

Carcano, V. 3–14

D

Demarest, V. 391–412

Deng, J. 342–358

Dilger, K. 227–253

Dolan, C. W. 342–358

E

Enomoto, N. 302–312

Index Terms

Links

F

Freisinger-Schadow, S. 227–253

G

Gordon, G. V. 313–327

Gorman, P. 73–83 84–110 391–412

Gubbels, F. 200–216

H

Hagl, A. 254–274

Hiemstra, J. 359–387

Hunston, D. 328–341

I

Ito, A. 302–312

K

Klosowski, J. M. 73–83 217–226 84–110

Krelaus, R. 227–253

L

Lacasse, M. A. 359–387

Liss, A. 391–412

Longo, D. 157–164

Lower, L. D. 313–327

Lucas, G. M. 38–72

Index Terms

Links

M

Miyauchi, H. 359–387

Mukai, D. 342–358

N

Nakagawa, Y. 165–182

Nicastro, D. H. 217–226

P

Pirskawetz, S. 15–37

Pozzi, E. 3–14

Q

Queenan, R. 391–412

R

Recknagel, C. 15–37

S

Schmidt, M. 227–253

Sitte, S. 277–301

T

Tan, K. T. 328–341

Tanaka, K. 302–312

Tanner, J. E. 342–358

Tasche, S. 135–156

Index Terms

Links

V

Vandereecken, P. 157–164

W

Weller, B. 135–156

White, C. C. 328–341

Wisner, G. 227–253

Wolf, A. T. 277–301 111–134

Y

Yarosh, K. 277–301

Yukimoto, S. 165–182

SUBJECT INDEX

Index Terms

Links

A

accelerated aging	342–358	227–253
accelerated testing	73–83	84–110
accelerated weathering	391–412	3–14
acrylic	84–110	
acrylic sealant	391–412	
acrylic terpolymer	38–72	
adhesion	38–72	
adhesive attachment	135–156	
adhesive bonding	227–253	
adhesive failure	15–37	
aging resistance	135–156	
Arrhenius	111–134	
artificial weathering	73–83	84–110

B

bomb blast	277–301	
bond strength	342–358	
bonded	111–134	
bonding design	254–274	

C

capability evaluation	15–37	
-----------------------	-------	--

Index Terms

Links

CFRP	342–358		
characterization	328–341		
cohesive failure	15–37		
correlation	3–14		
crazing	391–412		
curtainwall	277–301		
cyclic climatic testing	227–253		
cycling	313–327		
D			
deformation	313–327		
dimensional stability	185–199		
durability	342–358	185–199	111–134
	391–412	38–72	157–164
	313–327		
durability design	254–274		
durability evaluation	15–37		
E			
elastic recovery	38–72		
elastomers	313–327		
expansion-compression cycle test	165–182		
F			
fatigue	73–83	84–110	
fault tolerance	359–387		
FE analysis	254–274		
flexibility	38–72		
flexural strength	342–358		

This page has been reformatted by Knovel to provide easier navigation.

Index Terms

Links

fluid migration 217–226

freeze-thaw testing 227–253

G

glass 217–226 135–156

H

hardness 38–72

high speed 277–301

hybrid 157–164

hygrothermal testing 227–253

J

joint 111–134

joint deficiencies 359–387

joint geometry 254–274

joint movement 302–312

L

lap shear 185–199

lifetime 111–134

light curing acrylates 135–156

loading rate 277–301

M

mechanical characteristics 15–37

metal 135–156

modulus 328–341

Index Terms

Links

movement	313–327		
movement rate	277–301		
O			
out-door exposure	302–312		
outdoor exposure	3–14		
outdoor weathering	73–83	328–341	38–72
	84–110		
P			
pavement joints	15–37		
peel adhesion	185–199		
performance	15–37		
polyurethane	38–72	3–14	
polyurethane sealant	391–412		
R			
regional factor	302–312		
resistance	157–164		
review	73–83		
rheology	313–327		
rheometry	313–327		
RILEM TC 139 DBS	3–14		
S			
sealant	302–312	277–301	328–341
	313–327		
sealant failure	359–387		

Index Terms

Links

sealant joint	217–226		
sealants	73–83	3–14	84–110
sealed	111–134		
service life	111–134		
silicone	277–301	217–226	38–72
	157–164	313–327	84–110
silyl terminated polyacrylate	165–182		
strain	328–341		
strength reduction factor	342–358		
structural bonds	135–156		
structural glazing	254–274		
structural silicone	185–199		
substrate suitability	185–199		
superimposed loading	15–37		
system evaluation	15–37		
system test method	15–37		

T

telechelic polyacrylate	165–182
tensile strength	342–358
testing	359–387
thermo-mechanical	157–164
tilt-up	391–412
toughness	38–72

U

UHPC	227–253
UHPFRC	227–253
Ultra-High Performance Concrete	227–253

Index Terms

Links

urethane

84–110

W

water immersion

111–134

water penetration

359–387

watertightness

359–387

weatherability

302–312

weathering

157–164

weatherseal

157–164

window

277–301